Lecture Notes in Civil Engineering

Ravi Sundaram
Jagdish Telangrao Shahu
Vasant Havanagi *Editors*

Geotechnics for Transportation Infrastructure

Recent Developments, Upcoming Technologies and New Concepts, Volume 2

Springer

Lecture Notes in Civil Engineering

Volume 29

Lecture Notes in Civil Engineering (LNCE) publishes the latest developments in Civil Engineering—quickly, informally and in top quality. Though original research reported in proceedings and post-proceedings represents the core of LNCE, edited volumes of exceptionally high quality and interest may also be considered for publication. Volumes published in LNCE embrace all aspects and subfields of, as well as new challenges in, Civil Engineering. Topics in the series include:

- Construction and Structural Mechanics
- Building Materials
- Concrete, Steel and Timber Structures
- Geotechnical Engineering
- Earthquake Engineering
- Coastal Engineering
- Hydraulics, Hydrology and Water Resources Engineering
- Environmental Engineering and Sustainability
- Structural Health and Monitoring
- Surveying and Geographical Information Systems
- Heating, Ventilation and Air Conditioning (HVAC)
- Transportation and Traffic
- Risk Analysis
- Safety and Security

To submit a proposal or request further information, please contact the appropriate Springer Editor:

– Mr. Pierpaolo Riva at pierpaolo.riva@springer.com (Europe and Americas);
– Ms. Swati Meherishi at swati.meherishi@springer.com (India);
– Ms. Li Shen at li.shen@springer.com (China);
– Dr. Loyola D'Silva at loyola.dsilva@springer.com (Southeast Asia and Australia/NZ).

Indexed by Scopus

More information about this series at http://www.springer.com/series/15087

Ravi Sundaram · Jagdish Telangrao Shahu ·
Vasant Havanagi
Editors

Geotechnics for Transportation Infrastructure

Recent Developments, Upcoming Technologies and New Concepts, Volume 2

Springer

Editors
Ravi Sundaram
Cengrs Geotechnica Pvt. Ltd.
Noida, Uttar Pradesh, India

Vasant Havanagi
Geotechnical Engineering Division
CSIR Central Road Research Institute
New Delhi, Delhi, India

Jagdish Telangrao Shahu
Department of Civil Engineering
Indian Institute of Technology Delhi
New Delhi, Delhi, India

ISSN 2366-2557 ISSN 2366-2565 (electronic)
Lecture Notes in Civil Engineering
ISBN 978-981-13-6712-0 ISBN 978-981-13-6713-7 (eBook)
https://doi.org/10.1007/978-981-13-6713-7

Library of Congress Control Number: 2019931960

This Springer imprint is published by the registered company Springer Nature Singapore Pte Ltd.
The registered company address is: 152 Beach Road, #21-01/04 Gateway East, Singapore 189721, Singapore

Foreword

Transportation Geotechnics has evolved as an important discipline in geotechnical engineering contributing to design and construction of highways, railways, airports and metro-rail facilities. In order to strengthen and promote work in this area, the International Society of Soil Mechanics and Geotechnical Engineering (ISSMGE) has constituted a Technical Committee, designated as TC-202 on Transportation Geotechnics.

As a fast-growing economy, Indian developments in "Transportation Geotechnics" have been substantial. The accelerated pace of infrastructure construction, particularly highways, railways, metro-lines and airport runways has pushed up the need for advanced design and construction methodologies. In the design and construction of transportation infrastructure in urban areas, geotechnical engineers face many difficult problems related to ground conditions, geology, groundwater, the presence of adjacent structures, etc. In mountainous and hilly areas, construction of roads throws challenges of hill-slope stability, landslides and safety issues.

To strengthen and promote work on this subject, Indian Geotechnical Society (IGS) organized the *International Symposium on Geotechnics for Transportation Infrastructure (ISGTI 2018)* in April 2018 under the aegis of TC-202. While commemorating 70 years of Indian Geotechnical Society's accomplishments, ISGTI 2018 served as a significant platform for academic exploration, experience exchange and thought-inspiration amongst practitioners, researchers, academics and students. The goal was to apply broad engineering principles to bridge the gap between pavement and railway engineering and geotechnical engineering.

This publication, in two volumes, compiles the latest research and development on geotechnical aspects of design, construction, maintenance, monitoring and upgrading of roads, railways, metro-lines and other transportation infrastructure.

I congratulate the editors for the compilation of contributions from various authors, and I am sure that it will lead to a better understanding of the subject, making this publication a valuable treatise on Transportation Geotechnics.

Bengaluru, India

G. L. Sivakumar Babu
President, Indian Geotechnical Society

Professor, Indian Institute of Science

Preface

Transportation Geotechnics encompasses various disciplines of civil engineering such as pavement engineering, bridge engineering, hill area development, underground structures and geosynthetics. It is an important aspect in the construction of road and railway pavements and embankments, metro facilities, waterways, airports and pipelines.

To bring together professional experts including academicians, students, consultants and practising engineers on the subject on a common platform, Indian Geotechnical Society organized the International Symposium on Transportation Geotechnics in April 2018 at IIT Delhi.

Papers received from over 100 experts from 20 countries have been compiled in this publication to document the latest developments on the subject of Transportation Geotechnics. It covers nine parts as given below:

Part I: Challenges in Design and Construction of Pavements and Embankments.

Part II: Design and Construction of High-Speed Railway and Metro Track Substructures.

Part III: Advances in Waterways and Pipeline Geotechnics.

Part IV: Slope Stability, Landslides, Debris Flows and Avalanches on Hilly Roads and Remedial Measures.

Part V: Subsurface Sensing, Investigations and Monitoring in Transport Geotechnics.

Part VI: Use of Geosynthetics and Non-Traditional Materials in Transport Geotechnics.

Part VII: Transport Geotechnics in Underground Construction.

Part VIII: Ground Improvement Techniques for Transport Geotechnics.

Part IX: Emerging Trends in Transport Geotechnics—Unsaturated Soil Mechanics, Macro- and Nanotechnology, Climate Change and Sustainability.

This publication is presented in two volumes. Parts I–IV are covered in Volume 1, and Parts V–IX are included in Volume 2.

Volume 2 covering Parts V–IX includes 56 papers and includes the following expert lectures:

- Seasonal Variations in Properties of Expansive Soils along a Railway Corridor in Western India by Sanjay Gupta.
- Analyses and Design of the Highly Jointed Slopes on the Abutments of the World's Highest Railway Bridge Across the Chenab River in Jammu and Kashmir State, India, by T. G. Sitharam.
- Bridge Foundations in Strata with Potential of Liquefaction by Mahesh Tandon.
- Geotechnical Design of Underground Infrastructure—Outlining the Observational Approach by Florian Krenn.

All the articles were subjected to an extensive review. The peer review of the articles really helped to improve the quality of the research papers. We thankfully acknowledge the dedicated work of all the reviewers.

We deeply acknowledge the consistent efforts and the support provided by the publishers for bringing out a quality publication of this volume. We are also thankful to Maccaferri Environmental Solutions Pvt. Ltd., Strata Geosystems (India) Pvt. Ltd. and various other sponsors and exhibitors for their support and financial aid.

We hope that this volume, a storehouse of valuable information, will help to fast-track dissemination of knowledge so that students, researchers, practising structural, geotechnical and transportation engineers and other professionals definitely benefit from latest research and developments in this specialized subject. We hope the readers will find the proceedings very useful in their day-to-day research and professional life.

Noida, India — Ravi Sundaram
New Delhi, India — Jagdish Telangrao Shahu
New Delhi, India — Vasant Havanagi

About the International Symposium on Geotechnics for Transportation Infrastructure

This publication forms the proceedings of the first "International Symposium on Geotechnics of Transportation Infrastructure (ISGTI 2018)". The Technical Committee TC-202 of International Society for Soil Mechanics and Geotechnical Engineering (ISSMGE) along with Indian Geotechnical Society (IGS) and Indian Institute of Technology Delhi (IIT Delhi) organized ISGTI 2018 at IIT Delhi, New Delhi, India, on 7–8 April 2018. The symposium was organized in commemoration of 70 years of formation of IGS. The main part of the symposium was Transportation Geotechnics for Infrastructure Development.

Around 230 delegates registered for the symposium, out of which 40 delegates were from abroad representing 28 countries. A total of 185 abstracts were submitted, out of which finally 115 papers were presented by the delegates. Every paper was reviewed by two experts, and the authors incorporated the reviewers' comments and submitted the final paper. The delegates deliberated upon emerging challenges in the field of transportation geotechnical engineering for 2 days of the symposium. Seven awards were given to outstanding papers by young geotechnical engineers sponsored by Centre for Geomechanics and Railway Engineering, University of Wollongong, Australia, and the Symposium Organizing Committee.

The symposium is comprised of 4 plenary sessions consisting of 10 keynote lectures and 2 corporate presentations, 12 parallel sessions consisting of 11 invited lectures and general paper presentations, and the technical exhibition. The exhibition had a total of 21 stalls put up by multinational and Indian organizations for showcasing their products and equipment. Overall, ISGTI was well supported by sponsors and exhibitors who played a crucial role in making the event a success.

The need for building a strong and stable transportation infrastructure has become more critical than ever for sustainable engineering practices. Transportation Geotechnics provide key knowledge to building sustainable pavement and railroad track infrastructure. With recent major investments expected in road construction

and high-speed railways in India and many other countries, this was an appropriate juncture for organizing ISGTI in India.

We would like to express our sincere gratitude to TC-202 of ISSMGE for their contribution in overall planning of the symposium. The organization of the symposium was managed by an Organizing Committee guided by National and International Advisory Committees. We express our deep appreciation to the members of Organizing and Advisory Committees. The paper reviewers went through 185 abstracts and 115 full-length papers. Their untiring efforts are gratefully acknowledged. The contributions made by the keynote and invited speakers and the authors of papers as well as of the session chairmen and coordinators are also gratefully acknowledged. The symposium proceedings have been published by Springer. Their efficient and high-quality work is appreciated.

Ravi Sundaram
Jagdish Telangrao Shahu
Vasant Havanagi

Contents

About the Editors

Mr. Ravi Sundaram did his B.Tech. (1978) and M.Tech. (1980) from IIT Delhi. He started his career with McClelland Suhaimi Ltd. at Saudi Arabia and Qatar. He has 38 years experience as practicing geotechnical engineer and is a founder director of Cengrs Geotechnica Pvt. Ltd. His expertise includes geotechnical investigations, geophysical surveys, ground improvement and bored piles. He has worked on problems of collapsible soils, soft clays, expansive soils, weak rocks, artesian conditions and liquefiable soils. His interests include foundations for bridges, high rise buildings, large-diameter tanks, power plants, etc. He has published over 60 technical papers that reflect his experience in geotechnical engineering practice. He was awarded the IGS Delhi Chapter Lifetime Achievement Award for the year 2014–2015. He delivered the prestigious Sixth Madhav Lecture at Hyderabad in October 2017. He received Indian Geotechnical Society's IGS-Prof. Dinesh Mohan Memorial Award for Excellence in Professional Practice for the years 2016–2017.

Dr. Jagdish Telangrao Shahu graduated in 1986 from Nagpur University, India and obtained his M.Tech. and Ph.D. degrees from IIT Kanpur, India in 1988 and 1994, respectively. He did his post doctoral research at Institute of Lowland Technology, Japan from 1996 to 1999 and again visited Japan in 2006–2007 as Visiting Professor. Dr. Shahu joined IIT Delhi in 2002 as Assistant Professor. Since 2012, he is Professor at IIT Delhi. His main research interests are geotechnology for roads and railway tracks, ground improvement and geosynthetic applications. He has more than 50 papers in journals. He has also co-edited four book volumes. He has guided 50 M.Tech. and 9 Ph.D. theses.

Dr. Vasant Havanagi did his M.Tech. in Highway Engineering in the year 1988, from IIT, Kharagpur and completed his Doctorate in Geotechnical Engineering from IIT, Delhi in the year 2000. Presently he is a Senior Principal Scientist at CSIR-Central Road Research Institute, New Delhi. He has over 27 years of experience in R&D activities related to Geotechnical investigations, Ground improvement, Waste material utilization, Pavement design, Quality supervision,

Audit of highway projects etc. He has published more than 65 Research papers in National and International Journals, Conferences and Seminars etc. Awards for his R&D contribution/achievements included; DAAD (German Academic Exchange), IRC, SKOCH order of merit, CIDC etc. He is also involved activities of Indian Roads Congress (IRC), Bureau of Indian Standards (BIS), and Indian Geotechnical Society, Delhi chapter.

Part I
Subsurface Sensing, Investigations and Monitoring in Transportation Geotechnics

Seasonal Variations in Properties of Expansive Soils Along a Railway Corridor in Western India

Sanjay Gupta, Ravi Sundaram and Sorabh Gupta

Abstract The properties of expansive soils at shallow depth are influenced by moisture variations due to seepage of water into the soils during rains. The paper presents a case study in western India along a railway freight corridor. Testing on samples collected from boreholes drilled in the pre-monsoon and post-monsoon periods indicates substantial variations in moisture content, undrained shear strength, and swell pressure to about 3–3.5 m depth. Below this depth, these properties show insignificant change. This confirms that the active zone, the geotechnically unstable zone in expansive soils that undergoes swelling shrinkage due to moisture variations extends to about 3.5 m depth.

Keywords Expansive soils · Seasonal variations · Active zone: moisture variations · Undrained shear strength · Swell pressure

1 Introduction

A major railway corridor covering a distance of 1483 km is planned which shall connect Dadri (near Delhi) to a port near Navi Mumbai. It is being built for the movement of heavy freight by rail.

The paper presents results of investigations in a 57-km stretch in the Vadodara-Bharuch section in Gujarat.

A vicinity map of the project area showing the alignment of the railway freight corridor in Gujarat is presented in Fig. 1.

S. Gupta (✉) · R. Sundaram · S. Gupta
Cengrs Geotechnica Pvt. Ltd., A-100 Sector 63, Noida, India
e-mail: sanjay@cengrs.com

R. Sundaram
e-mail: ravi@cengrs.com

S. Gupta
e-mail: sorabh@cengrs.com

R. Sundaram et al. (eds.), *Geotechnics for Transportation Infrastructure*,
Lecture Notes in Civil Engineering 29,
https://doi.org/10.1007/978-981-13-6713-7_1

Fig. 1 Vicinity map

2 Project Alignment

In general, the railway freight corridor runs parallel to the existing railway track with a few detours in areas where there were space constraints. A map showing the investigations done in the Vadodara-Bharuch section is presented on Fig. 2.

Expansive soils of the Deccan Trap are encountered in this section of the railway corridor. Due to the hot summer season typically experienced in western India, followed heavy rains during monsoon, there is substantial moisture content variation over the year.

To assess the seasonal variations in the soil properties, boreholes were drilled along the alignment in the pre-monsoon and post-monsoon periods. This paper is based on the work done by the authors in this stretch in the year 2012.

3 Meteorological Data

The climate in the area is sub-tropical and has three well defined seasons—summer from April to June, monsoon from July to December, and mild winter from October to March.

As per the meteorological department (Kaur and Purohit 2013), the rainfall during Jan–Dec 2012 was about 928 mm out of which nearly than 95% occurred during the monsoon period (July–Sep). The year experienced normal rainfall (within ±20% of the annualized average rainfall).

Fig. 2 Project alignment in the vicinity of Vadodara

The maximum temperature in the pre-monsoon period (May–June) is generally around 37–41 °C. In July–September period, the maximum temperature comes down to 31–33 °C. Post-monsoon temperatures are around 32–36 °C in October–December.

4 Geological Setting

The close of the Mesozoic Era was marked by the outpouring of enormous lava flows which spread over vast areas of western, central, and southern India (Krishnan 1982). They issued through long narrow fissures in the earth's crust from a large magma basin. The lavas spread out far and wide as nearly horizontal sheets. The flows are called "traps" because of their step-like or terraced appearance of the rock outcrops.

The Deccan Traps cover a large tract of central and western India, extending over large parts of Madhya Pradesh, Gujarat, and Maharashtra. The basalts, upon weathering, form a clay/loam which is deep gray to black in color to 2–3 m depth below which it is brown colored due to iron content. These clays are usually rich in the clay mineral montmorillonite. These clays exhibit swelling behavior on coming in contact with water and shrink upon drying.

5 Investigation Program

In the section between Vadodara and Mumbai (approx. 400 km), about 166 boreholes were drilled to 5–10 m depth in the pre-monsoon period (April–May 2012) to assess the distribution of expansive soils (black cotton soils) along the alignment. This was followed by 32 boreholes to 5 m depth in the post-monsoon season (September–October).

The boreholes drilled in the post-monsoon period were used to assess the change in properties due to the seepage of rainwater into the ground.

In the 57-km stretch between Chainage 74 and 131 km (0 km taken at the port), 22 boreholes were drilled in the pre-monsoon period and 9 boreholes were drilled post-monsoon. Data from these boreholes have been analyzed to assess the trend of variation in soil properties along the alignment in the pre-monsoon and post-monsoon periods.

6 Soil Characteristics Along the Alignment

6.1 Physiography

Geographically, the area belongs to the western coastlands of the Deccan Peninsula. In general, the area gently slopes toward the west. The topography is primarily plain with moderate to deep cutting river valleys and occasional hillocks.

6.2 Stratigraphy Along Alignment

In general, the soils along the corridor to about 10 m depth consist of expansive silty clay/clayey silt of high to medium plasticity. The clays are generally very stiff to hard in consistency. Typical borehole profiles for four boreholes along the alignment are presented on Fig. 3.

6.3 Soil Properties

In general, the soils are highly plastic at shallow depth and medium to highly plastic at deeper depths. To illustrate the soil properties along the corridor and with depth, plots of various soil properties have been prepared along the alignment at 2 m depth and at 5 m depth. Data from all boreholes drilled along the railway corridor have been considered in the analysis (22 boreholes pre-monsoon and 9 boreholes post-monsoon).

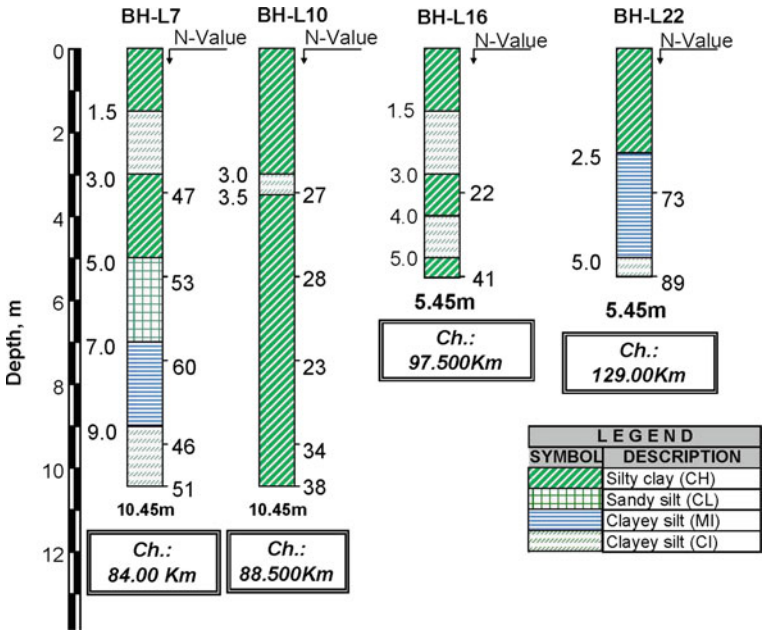

Fig. 3 Typical borehole profiles along the alignment (pre-monsoon)

Liquid Limit The liquid limit along the corridor determined in accordance with IS: 2720 (Part 5)-1985 ranges from 47 to 72% at about 2 m depth and from 35 to 70% at 5 m depth.

Plastic Limit The plastic limit determined as per IS 2720 (Part 5)-1985 ranges from 23 to 34% at 2 m depth and from 22 to 29% at 5 m depth. The liquid limit and plastic limit profiles along the alignment at 2 m depth and 5 m depth are presented on Figs. 4 and 5, respectively.

Clay Content The clay content [≤ 2 micron size particles (as determined by hydrometer analysis as per IS: 2720 (Part 4)-1985] along the alignment generally ranges from 24 to 40% at 2 m depth and from 16 to 32% at 5 m depth (see Figs. 6 and 7).

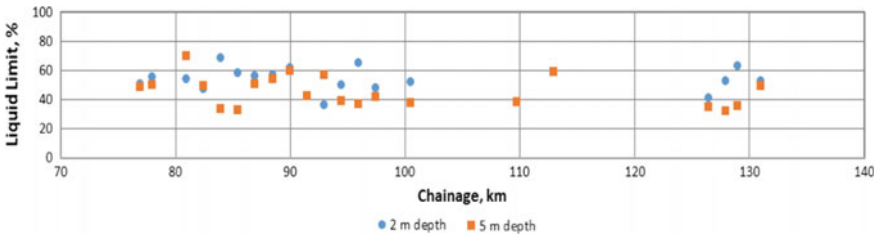

Fig. 4 Variation of liquid limit along the railway corridor at 2 and 5 m depths

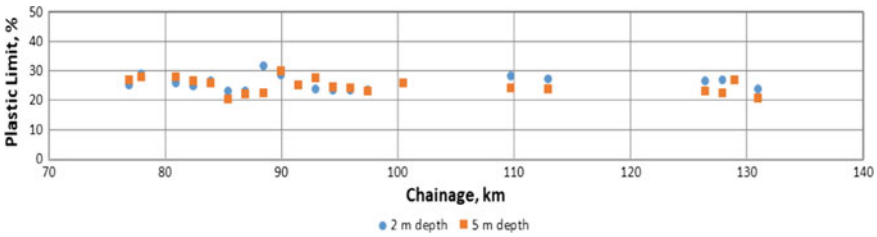

Fig. 5 Variation of plastic limit along the railway corridor at 2 and 5 m depths

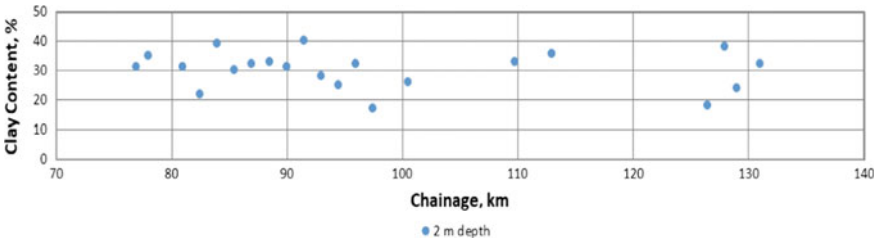

Fig. 6 Clay content (particle size ≤ 2 μm) along the railway corridor at 2 m depth

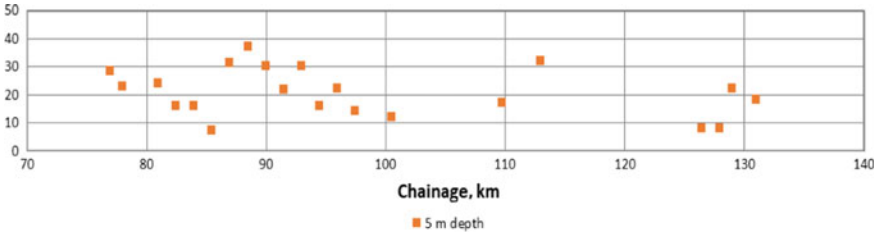

Fig. 7 Clay content (particle size ≤ 2 μm) along the railway corridor at 5 m depth

Free Swell Index The free swell index computed as the difference in volume of 10 g of soil soaked in water and in kerosene for 48–72 h (till volume change in water stabilizes) is an indicator of the swelling nature of the soil. The free swell index, determined in accordance with IS: 2720 (Part-40)-1977, ranges from 41 to 92 at 2 m depth and is generally below 30 at 5 m depth. The profile along the alignment is illustrated at 2 m depth and 5 m depth on Fig. 8.

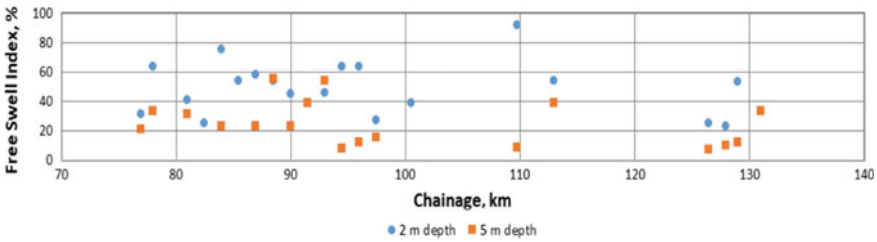

Fig. 8 Variation of free swell index along the railway corridor at 2 and 5 m depths

7 Seasonal Variations

The rainy season in most parts of India usually lasts for three months (June/July to August/September) followed by generally dry season for the balance nine months. During the summer months (April–June), moisture content in the top few meters reduces substantially due to evaporation and transpiration. The moisture lost is replenished during the rains in the monsoons.

To assess the variations in soil properties before and after monsoon, boreholes were drilled before monsoon during April–May (pre-monsoon) and later in September–October (post-monsoon). Undisturbed samples collected from the boreholes were tested in the laboratory to determine moisture content, undrained shear strength (q_u), and swell pressure. These post-monsoon parameters were compared with the pre-monsoon values to assess the change in soil properties with depth.

Figures 9, 10, 11, and 12 present the profile of moisture content, undrained shear strength (q_u), and swell pressure with depth at four typical boreholes along the alignment. All these tests were conducted on undisturbed samples. These four boreholes, widely spaced along the alignment, have been selected to demonstrate the overall trend of variation in the soil properties.

The above plots clearly illustrate the influence of water seepage during the rainy season and variation of the properties with depth. These are explained below:

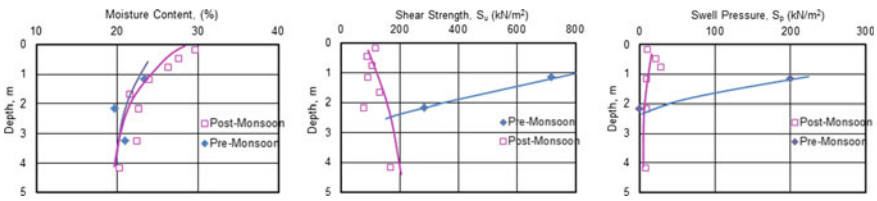

Fig. 9 Moisture content, undrained shear strength and swell pressure versus depth—Borehole L7 at Chainage 84.0 km

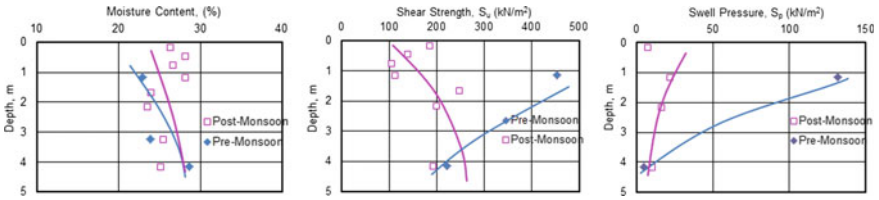

Fig. 10 Moisture content, undrained shear strength and swell pressure versus depth—Borehole L10 at Chainage 88.5 km

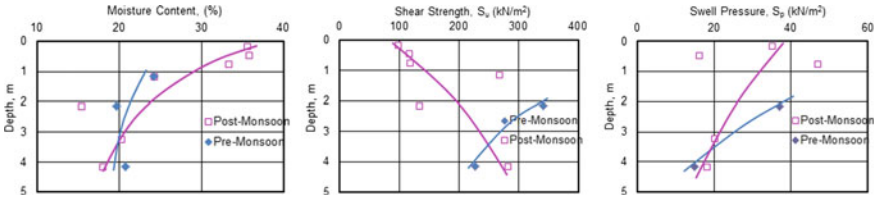

Fig. 11 Moisture content, undrained shear strength and swell pressure versus depth—Borehole L16 at Chainage 97.5 km

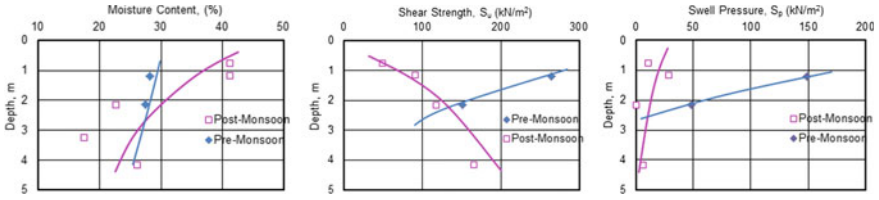

Fig. 12 Moisture content, undrained shear strength and swell pressure versus depth—Borehole L22 at Chainage 129 km

Moisture Content The moisture content, determined in accordance with IS: 2720 (Part 2)-1973, increases post-monsoon at shallow depth. The maximum increase is near the ground surface and the change in moisture content decreases with increasing depth. The increase at 2 m depth is about 40–55%. The change in moisture content is insignificant below about 3.2–3.5 m depth. The pre-monsoon and post-monsoon moisture content profile along the corridor at 2 and 5 m depths are presented on Figs. 13 and 14, respectively.

Undrained Shear Strength The undrained shear strength [IS: 2720 (Part 11)-1995] on undisturbed soil samples reduces post-monsoon at shallow depth with insignificant change below 3–3.5 m depth. The reduction in undrained shear strength at 2 m depth is about 55–65%. The variation of undrained shear strength in the pre-monsoon and post-monsoon periods along the corridor at 2 and 5 m depths are presented on Figs. 15 and 16, respectively.

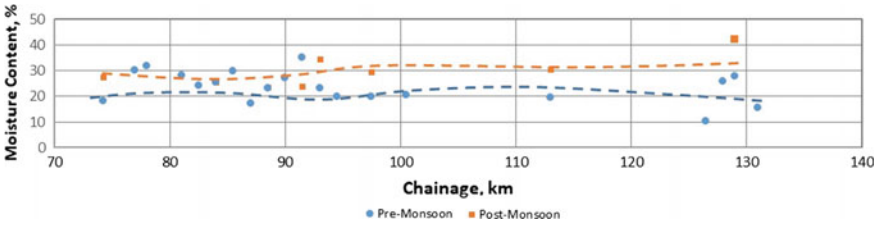

Fig. 13 Pre-monsoon and post-monsoon change in moisture content along the alignment at 2 m depth

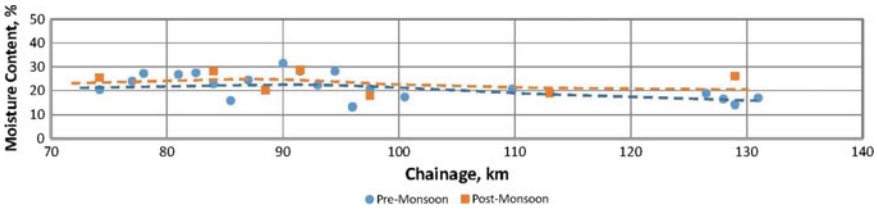

Fig. 14 Pre-monsoon and post-monsoon change in moisture content along the alignment at 5 m depth

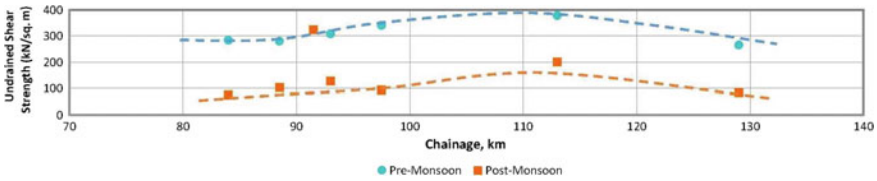

Fig. 15 Pre-monsoon and post-monsoon change in undrained shear strength along the alignment at 2 m depth

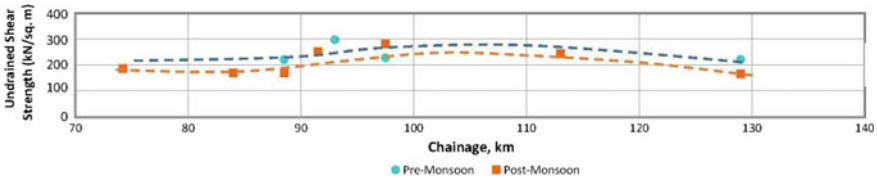

Fig. 16 Pre-monsoon and post-monsoon change in undrained shear strength along the alignment at 2 m depth

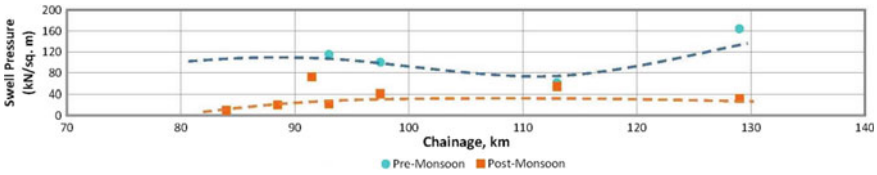

Fig. 17 Pre-monsoon and post-monsoon change swell pressure along the alignment at 2 m depth

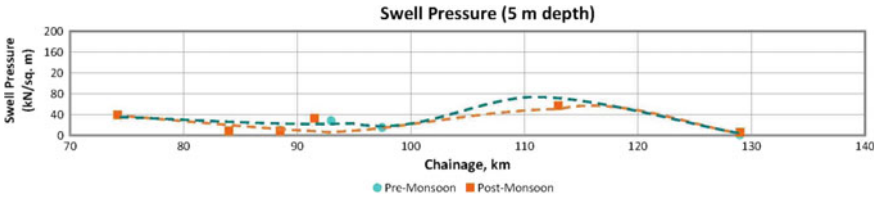

Fig. 18 Pre-monsoon and post-monsoon change in swell pressure along the alignment at 5 m depth

Swell Pressure The change of swell pressure in the pre-monsoon and post-monsoon periods along the corridor at 2 and 5 m depths are presented on Figs. 17 and 18, respectively. From Fig. 17, it can be seen that the swell pressure determined in accordance with IS: 2720 (Part 41)-1977 at 2 m depth on undisturbed soil samples at in situ moisture content samples decreases during the rainy season, largely on account of the increase in moisture content at shallow depths (Fig. 13). The swell pressure values at 5 m depth (Fig. 18) are typically low on account of the lower void ratios and higher moisture content values. The change in swell pressure below 2.5–3.5 is insignificant. The pre-monsoon swell pressure at 2 m depth is about 75–115 kPa and less than 35 kPa in the post-monsoon period. At 5 m depth, the swell pressure post-monsoon is generally low.

8 Active Zone

The active zone (Chen 1975; Katti 1978) in a deposit of expansive soil is the zone which is subject to swelling and shrinkage on account of variations in moisture content. In the active zone, there is a potential for variation in moisture content due to seepage from surface sources, precipitation, evaporation, variations in ground-water level, etc.

The seasonal moisture changes in these expansive soils lead to volume changes and vertical movements of the soil mass in the active zone. The moisture content is usually constant throughout the year at some depth below the ground level.

Thus, the active zone is a geotechnically unstable zone in which foundations may experience heave/settlement due to swelling/shrinkage of the soils.

The moisture changes in these soils occur due to the capillary forces setup by evaporation. Due to the extremely low permeability of the soils, the hydraulic gradient caused by the groundwater level fluctuations is insufficient to reduce or increase the moisture content of such clays. The change in moisture content is mainly due to the suction forces created by thermal gradients (Ramaswamy 1986).

In general, shrinkage/expansion below the groundwater level is negligible. However, all along the stretch investigated, water table is below 10 m depth.

Based on the data collected by various researchers in different parts of India (Mohan and Rao 1965; Ramaswamy and Abu Nasser 1984), the active zone in most areas of India is usually on the order of 2.5–3.5 m below the ground surface.

The current study reconfirms the trends reported in literature. As per the data collected, the active zone in this stretch of the railway corridor is about 3–3.5 m deep.

9 Conclusions

Geotechnical investigation was performed along a 57-km-long stretch along a railway corridor in Gujarat in western part of India. To investigate the seasonal variation in soil properties, boreholes were drilled in the pre-monsoon period (May–June) followed by boreholes in the post-monsoon period (September–October).

The study revealed that the moisture content of the soils increases in the top 3–3.5 m depth, below which the change in moisture content is insignificant. There are corresponding reductions in undrained shear strength and swell pressure in the top 3–3.5 m depth zone.

The active zone in which the soil properties are sensitive to moisture content variations extends to about 3.5 m depth in this part of Gujarat. Foundations in the active zone may experience swell/shrink behavior.

It is essential to assess the extent of the active zone so as to take adequate precautions in the design of the railway track and foundations constructed along the route.

Acknowledgements The authors are thankful to M/s. Nippon Koei Ltd. for giving Cengrs Geotechnica Pvt. Ltd. the opportunity to perform this investigation.

References

Chen FH (1975) Foundations on expansive soils. Elsevier Publishing Co.

IS: 2720 (Part 2)-1973, Determination of water content. Method of test for soils. Bureau of Indian Standards, New Delhi, Reaffirmed 2015

IS: 2720 (Part-4)-1985, Grain size analysis. Method of test for soils. Bureau of Indian Standards, New Delhi, Reaffirmed 2010

IS: 2720 (Part-5)-1985, Determination of liquid and plastic limit. Method of test for soils. Bureau of Indian Standards, New Delhi, Reaffirmed 2010

IS: 2720 (Part-11)-1993, Determination of shear strength parameters of specimen tested in unconsolidated undrained triaxial compression without the measurement of pore water pressure. Method of test for soils. Bureau of Indian Standards, Reaffirmed 2011

IS: 2720 (Part-40)-1977, Determination of free swell index of soils. Method of test for soils. Bureau of Indian Standards, Reaffirmed 2011

IS: 2720 (Part-41)-1977, Measurement of swelling pressure of soils. Method of test for soils, Bureau of Indian Standards, Reaffirmed 2011

Katti RK (1978) Search for solutions for problems in black cotton soils. In: First IGS annual lecture, Indian geotechnical conference-1978, New Delhi

Kaur S, Purohit MK (2013) Rainfall statistics of India-2012. Indian Meteorological Department, Hydromet Division, New Delhi

Krishnan MS (1986) Geology of India and Burma. CBS Publishers, New Delhi

Mohan D, Rao BG (1965) Moisture variations and performance of foundations in black cotton soils in India. In: Proceedings, international symposium on moisture equilibria and moisture changes in soils beneath covered areas. Butterworth publication, pp 175–183

Ramaswamy SV (1986) For which soil conditions are under-reamed pile foundations superior to other foundation systems. In: Proceedings Indian geotechnical conference, IGC-86, vol II, pp 121–125

Ramaswamy, Abu Nasser (1984) Heave predictions on water content profiles. In: Proceedings, first national conference on science and technology of buildings. Kaartom, Sudan

Analyses and Design of the Highly Jointed Slopes on the Abutments of the World's Highest Railway Bridge Across the Chenab River in Jammu and Kashmir State, India

T. G. Sitharam, Srinivas Mantrala and A. K. Verma

Abstract Indian Railways have embarked on the construction of world's highest railway bridge as a part of Udhampur–Srinagar–Baramulla Rail Link Project, a major infrastructure project in India. The bridge is being constructed across the river Chenab. The bridge consists of a main span of 467 m arch bridge on the steep slopes on the banks of the river Chenab. The bridge is about 359 m above the high flood level of the Chenab River. The bridge is located in highly seismic area characterized with maximum credible earthquake with a peak horizontal acceleration of 0.36 g. Considering the iconic nature of the bridge and highly jointed rock mass, a variety of tests were conducted to assess bearing capacity of the foundations and stability of the slopes. Continuum analyses using Slide and FLAC softwares were carried out. The slopes were also checked for wedge failure and toppling failure considering the joint characteristics. The slope stabilization measures against wedge failure consist of using passive rock bolts and active prestressed rock anchors. The methodology for the design of these rock bolts and prestressed rock anchors for wedge failures is described briefly. The slopes have been successfully stabilized using the methodology discussed in this paper.

Keywords Slope stability · Railway bridge · Earthquake

T. G. Sitharam (✉)
Department of Civil Engineering, Indian Institute of Science,
Bengaluru 560012, India
e-mail: sitharam@civil.iisc.ernet.in

S. Mantrala
Afcons Infrastructure Limited, Mumbai 400053, India
e-mail: srinivas.mantrala@afcons.com

A. K. Verma
Department of Mining Engineering, Indian Institute of Technology (ISM),
Dhanbad 826004, India
e-mail: akverma@iitism.ac.in

R. Sundaram et al. (eds.), *Geotechnics for Transportation Infrastructure*,
Lecture Notes in Civil Engineering 29,
https://doi.org/10.1007/978-981-13-6713-7_2

1 Introduction

The evaluation of stability of the natural rock slopes becomes very essential for the safe design especially when the slopes are situated close to structures which are built on these slopes. The stability of a natural slope becomes more critical if the slope is situated in earthquake prone areas (Kumsar et al. 2000). Slope failures are the most common natural hazards and are mainly caused due to the additional forces due to foundations of the structures on them or rainfall induced or earthquake-induced ground shaking and associated inertial forces. Earthquakes of even a very small magnitude may trigger failure in slopes in jointed rock masses which are perfectly stable otherwise. Hence, the study of the behaviour of rock slopes in order to have a safe design of structures built on them. Though the strength of the rock plays an important role in the slope stability, geological structure of the rock often governs the stability of slopes in jointed rock masses. Geological characteristics of rock mass include location and number of joint sets, joint spacing, joint orientations, joint material and seepage pressure (Wyllie and Mah 2004). The dynamic analysis of slopes in rock masses is studied by several earlier researchers using different techniques (Kumsar et al. 2000; Hatzor et al. 2004).

Indian Railways are building the iconic Chenab bridge across the river Chenab which will be world's highest railway bridge once completed. The bridge is located in young Himalayan Mountains, which are active. The general arrangement of the bridge is indicated in Fig. 1. Out of eighteen foundations, seven foundations are coming on the slopes. The founding strata consists of highly jointed dolomite with three joint sets. The joints are closely spaced. Since the foundations are coming on the slopes, the slopes need to be designed very carefully considering the long-term stability requirements. The photograph taken at the proposed site before the commencement of the excavation of the slopes is presented in Fig. 2.

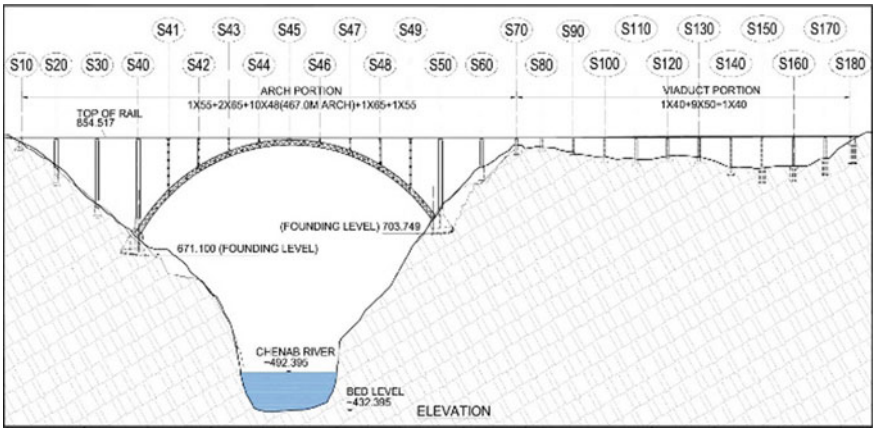

Fig. 1 The general arrangement of the bridge

Fig. 2 Left and right banks of Chenab Bridge before commencement of work

Figure 3 shows the photograph of the completed viaduct portion from S80 to S180. The portion from S130 to S180 is on transition and circular curves. For the first time in the world, the deck was launched incrementally on a combined circular and transition curves. The photograph of the deck is shown in Fig. 4. The stabilization of the slopes on both left and right banks was completed and the construction of foundations on the slopes has been completed. The photographs showing the stabilized slopes on the left and right banks are placed at Fig. 5 and Fig. 6 respectively.

Fig. 3 Completed viaduct on the right bank

Fig. 4 Incrementally launched deck on combined circular and transition curves

Fig. 5 Stabilized slopes on the left bank

Fig. 6 Stabilized slopes on the right bank

2 Rock Mass Characteristics

2.1 Joint Characteristics

The rocks present at the bridge site are heavily jointed. The subsurface at the extent of the bridge site considered for slope stability analysis essentially consists of Dolomitic limestone with different degrees of weathering and fracturing. The main discontinuities at the site are one sub-horizontal foliation joint dipping about 20°–30° in North-East (NE) direction and two sub-vertical joints. Figure 7 shows the rock mass exposed at the bridge site. The figure also depicts the intensity and spacing of the prevailing joint sets at the bridge site. Figure 8 shows the joint orientations at two drift locations.

2.2 Rock Mass Properties

After detailed analyses of geotechnical properties and in situ test results in drifts the properties for the slopes have been selected as two sets of properties, out of which one is very conservative estimate. Analyses have also been carried out treating the entire slope material as a single layer and in the other case with top disintegrated soil as a two-layer model. Tables 1 and 2 show the two sets of properties of rock mass for the continuum analyses of slope on the left bank and right bank respectively.

Fig. 7 Rock mass exposed at the bridge site

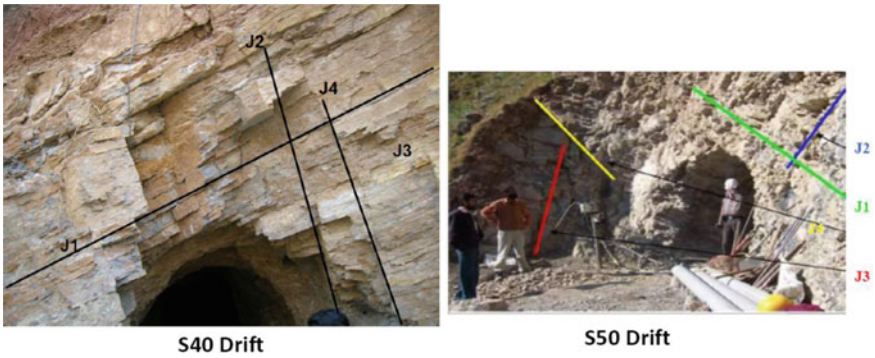

Fig. 8 Joint orientations at drift locations

Table 1 Two sets of properties of rock mass for left bank

Rock mass	Set 1	Set 2
Dry unit weight (kN/m^3)	27.095	26.752
Cohesion (c, MPa)	1.40	0.531
Friction angle (ϕ) degrees	44.42	49.10
Hoek and Brown parameter (m and s)	4.70 and 0.00127	0.793 and 0.0005
Bulk modulus (GPa)	50.55	6.31
Shear modulus (GPa)	37.92	4.73
RQD/RMR	49/48	10/37

Table 2 Two sets of properties of rock mass for right bank

Rock mass	Set 1	Set 2
Dry unit weight (kN/m^3)	27.095	27.095
Cohesion (c, MPa)	1.41	0.525
Friction angle (ϕ) degrees	42.61	49.06
Bulk modulus (GPa)	50.55	5.64
Shear modulus (GPa)	37.92	4.23
Hoek and Brown parameter (m and s)	4.706 and 0.00127	0.766 and 0.0005
RQD/RMR	49/48	10/36

3 Slope Stability Analyses

The detailed study carried out considers all possible failure modes such as global failure, wedge failure, planar failure and toppling failure. The analyses have been carried out for abutment slopes and many cross sections at both these abutment slopes. Final profile was arrived considering all the necessary alternatives, construction methodology and accessibility to the foundation locations on the slopes. The numerical programs used for the detailed slope stability analyses are as follows: Wedge failure analyses were carried out using SWEDGE (RocScience 2002); Global failure analyses using continuum approach using FLAC (Itasca 2002) and SLIDE (from Roc Science) programs; Planar failure analyses using DIPS (Roc Science 2002) and Toppling analyses using Hoek and Bray Analysis.

Analyses were carried out using two sets of rock mass properties which were decided based on large number of tests, borehole data and tests at drift locations. For the right abutment slopes, variation in rock mass properties along the slope was also considered in the continuum analyses. Lower values of moduli were considered for quartzite in the upper part of the slope. Sensitivity analyses were also done for the possible variations in shear strength parameters. There was no ground water reported during geotechnical investigations. Piezometers installed on the slope showed no head of water indicating that the water quickly drains off through the joints. However, pore pressure ratio (r_u) value of 0.3 was considered for the wedge failure analysis as decided in the design basis note. Allowable bearing pressures on foundations determined as 1 MPa (determined by several methods and after detailed deliberations) was applied at all foundations in the continuum analyses. Initially seismic analyses were done using PHA values of 0.31 g and 0.155 g for MCE and DBE cases, respectively. However, these values were increased later to 0.36 g and 0.18 g, respectively, considering the importance of the project. The earthquake response spectrum was derived for dynamic analyses using site-specific studies carried out by IIT Roorkee by multiplying a factor of 0.36 to obtain a peak horizontal acceleration of 0.36 g keeping the frequency contents and duration of the seismic event unchanged. The dynamic input is applied at the base of the slope.

Design factors of safety adopted for the slopes are as follows: FS = 1.5 with static loads; FS = 1.2 with static loads and DBE seismic loads; and FS = 1.0 with static loads and MCE seismic loads.

Using SLIDE software continuum analyses, both with circular and non-circular slip surfaces were carried out using two sets of properties as decided by the entire team and as per Design basis note. Static analyses, pseudostatic analyses with MCE loading, and pseudostatic analysis with DBE loading conditions were carried out with two sets of properties for all the slopes. Sensitivity analyses were also carried out with subset properties. Further, analyses with two-layer model considering pore water pressures were also done. Figures 9, 10, and 11 show the typical results from SLIDE analyses for some of the cases. Figures also show the factor of safety obtained for a circular slip analyses using Bishop's simplified approach for an equivalent continuum material.

Further, continuum analyses were carried out using FLAC. In this case also, static analyses, pseudostatic analyses with MCE and DBE conditions were carried out. Typical results from FLAC analyses have been presented in Figs. 12 and 13.

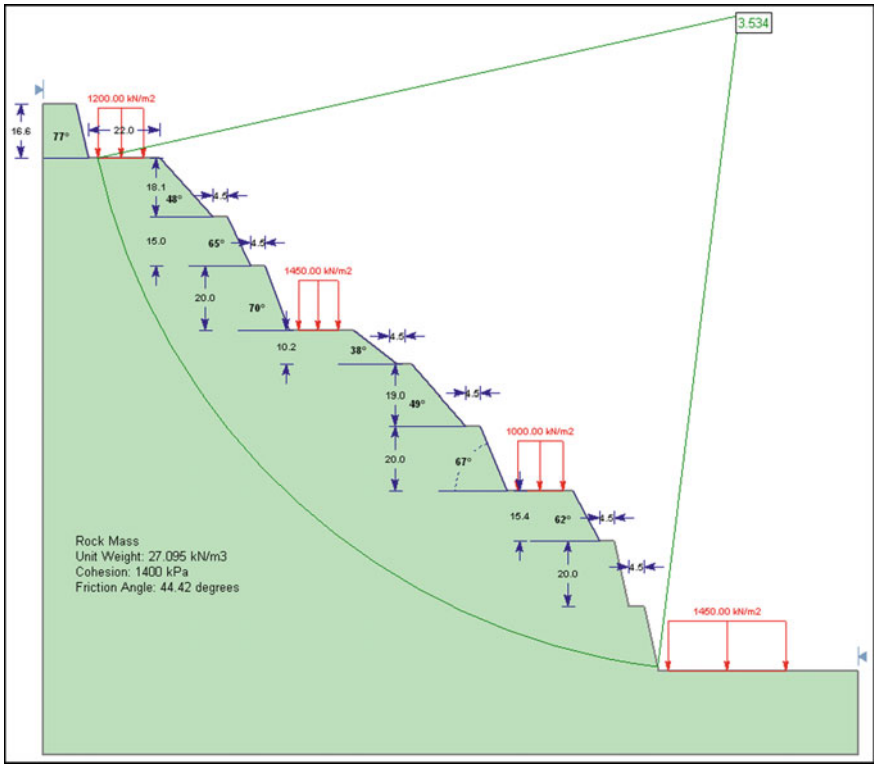

Fig. 9 Static analysis: circular global failure (FS = 3.534) using set 1 values

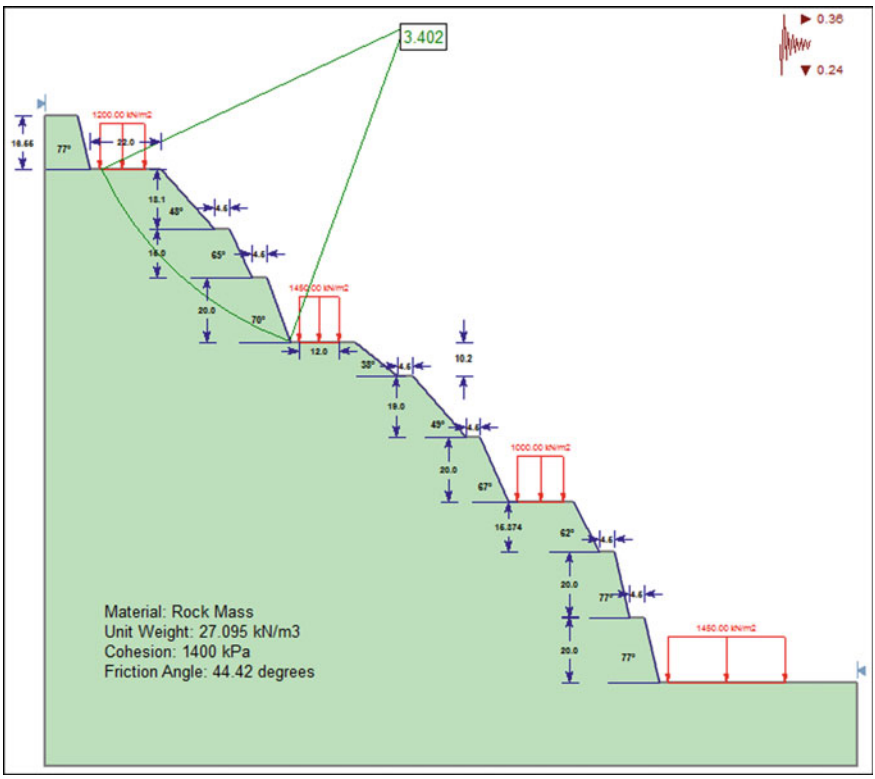

Fig. 10 Pseudostatic analysis: shallow slip failure (top), MCE condition ($\alpha h = 0.36$, $\alpha v = 0.24$) with set 1 values

From the displacement contours, the possible displacements at each founding level are tabulated and presented below in Table 3.

In addition, a dynamic analysis with MCE and DBE conditions was also carried out. Typical acceleration time history plot for MCE of the site is given in Fig. 14.

Global stability analyses with rock bolts and anchors were done to check the abutment slope up to river bed in one case and in other case 100 m below the arch foundation locations (S40 and S50).

Further for local stability considerations, a complete 3D wedge failure analysis of central and side slopes using SWEDGE was done without seismic force, and, with seismic force corresponding to MCE, with seismic force corresponding to DBE. Wedge failure analysis at different locations for different earthquake scenarios and with different friction parameters of the gouge material was analysed. Further, sensitivity analyses with three different friction angles were carried out along with

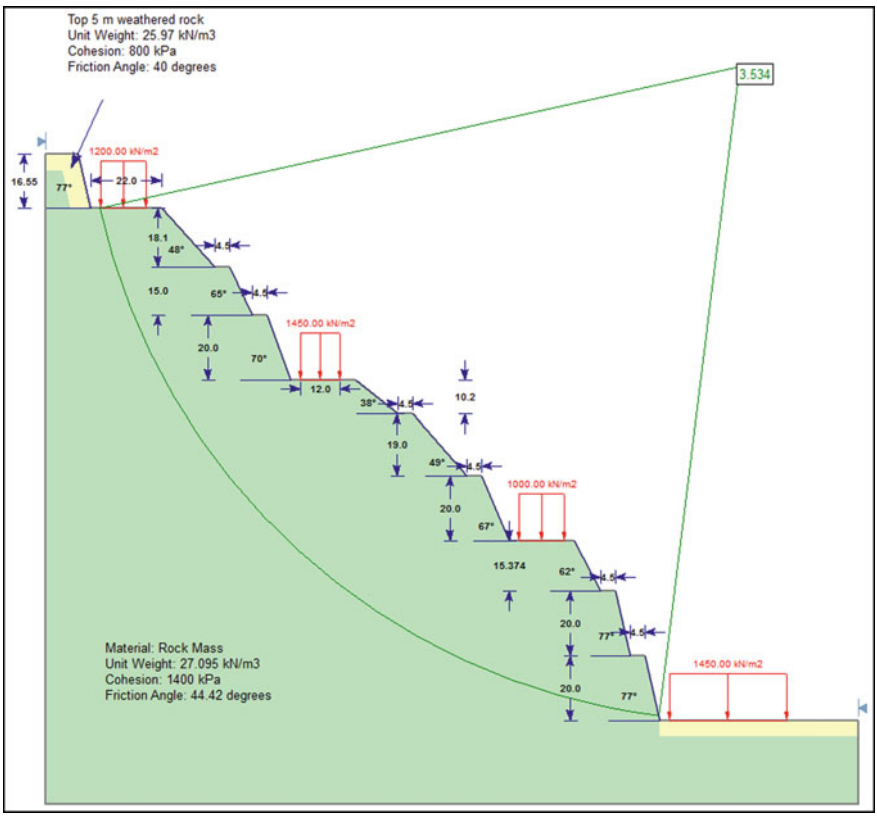

Fig. 11 Two-layered model: static analysis, circular global failure Ru coefficient = 0.3, FS = 3.534

flattened slopes to avoid any wedge failures and also analyses of slopes with rock anchors. Based on detailed analyses, appropriate strengthening measures were suggested using rock bolts and prestressed rock anchors which was executed at site.

4 Installation of Rock Bolts

4.1 Geological Logging of the Excavated Slope

After the slope is excavated, the surface is cleaned with water jet as shown in Fig. 15 and the geological log of the slope is prepared. Typical geological log is placed at Fig. 16. The data from the geological log are used for the validation of the design of slope stabilization measures.

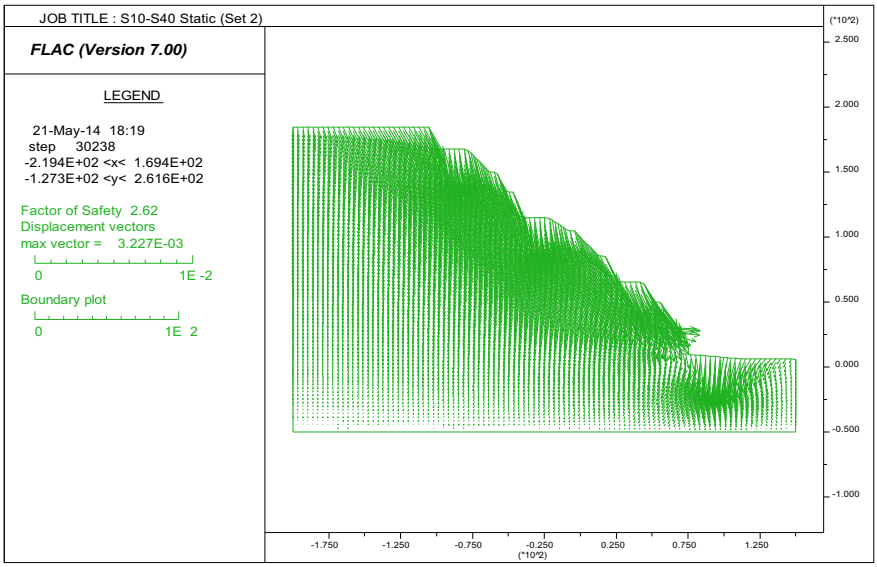

Fig. 12 Displacement vectors (FOS: 2.62, maximum displacement: 3.22 mm)

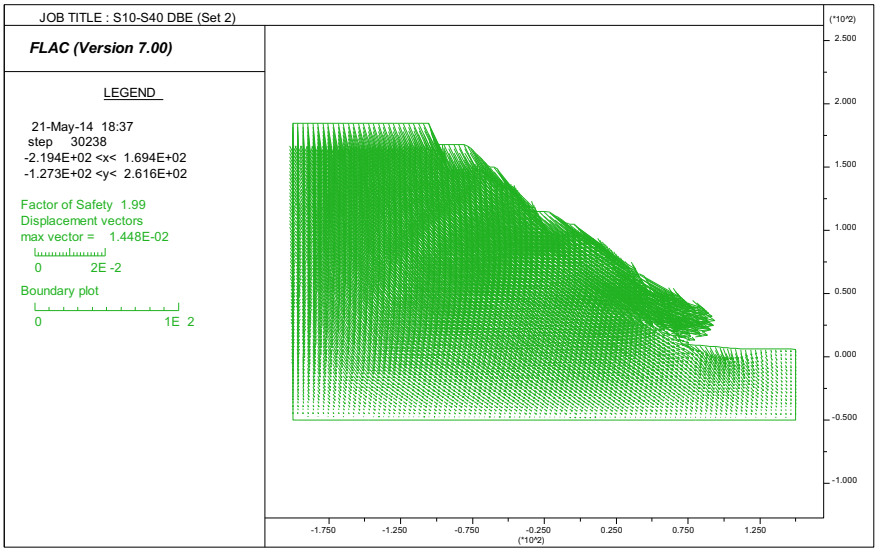

Fig. 13 Displacement vectors (FOS: 1.99, maximum displacement: 14.48 mm)—DBE CASE (seismic force coefficients: ah = 0.18; av = 0.12)

Table 3 Displacements at each founding level from FLAC analyses for foundations on Bakkal side

S.No.	Load case	Displacement type	Displacement in mm (magnitude)			
			S10	S20	S30	S40
1	Static	Lateral	0.5	0.5	1.0	−0.75
2	Static	Vertical	−3	−3	−2.5	−3.5
3	Design basis earthquake (DBE)	Lateral	2.5	7.5	10	2.5
4	Design basis earthquake (DBE)	Vertical	−9	−8	−8	−4
5	Maximum considered earthquake (MCE)	Lateral	15	20	25	5
6	Maximum considered earthquake (MCE)	Vertical	−17.5	−15	−15	−5

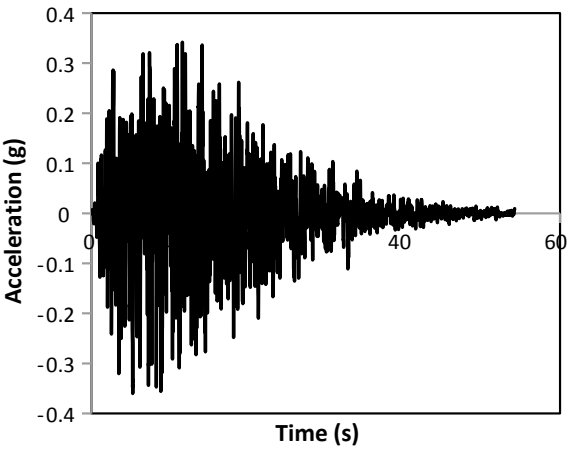

Fig. 14 Acceleration time history of the MCE for the site

4.2 Application of the First Layer of Shotcrete and Marking of Layout of Rock Bolts

After the geological logging is completed, the first layer of 50-mm-thick steel fibre reinforced shotcrete was applied as shown in Fig. 17. Later the location of rock bolt was marked on slope in accordance with the approved layout drawing.

Fig. 15 Cleaning of excavated slope with water jet

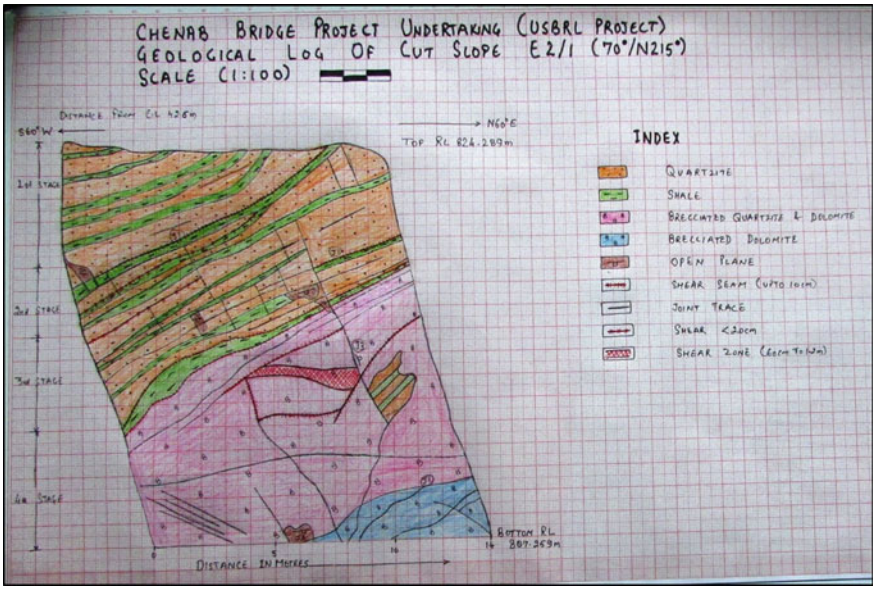

Fig. 16 Typical geological log of the excavated slope

Fig. 17 Application of 50 mm thick steel fibre-reinforced shotcrete

4.3 Drilling of Holes

Drilling of holes was done by air percussion drilling. The diameter of drilled hole was 100 mm, and the diameter of the rock bolt was 32 mm. The depth of drill hole was 300 mm more than the designed length of rock bolt. The inclination of the hole for rock bolt was perpendicular to slope. After drilling of holes, the holes were filled with neat cement grout. After the grout sets, the hole was again re-drilled.

4.4 Fabrication of Rock Bolt

Ribbed bars of 32 mm dia. of grade Fe 500 were used as rock bolts. Length of rock bolt was as per the approved drawing. The top 100 mm portion of the was threaded for fixing of M30 nut. Suitable centralizer was being fixed on the bar at spacing of 1.5 m to 2.0 m c/c to maintain clear cover to avoid bar coming in contact with ground. A mild steel plate of size 150 mm $\times$ 150 mm $\times$ 12 mm with central hole of 40 mm diameter was used as bearing plate. All rock bolts and bearing plates were coated with two coats of truncated inhibitor cement slurry to protect from corrosion.

4.5 Installation of Rock Bolts

The drilled holes were flushed by means of air jet to remove any loose materials. The rock bolt was inserted into the hole carefully along with centralizers and grout pipe. A photograph indicating the installation of rock bolts is placed at Fig. 18.

4.6 Grouting of Drill Holes

The hole was cleaned with jet of air for a period of 5 min (approx.) prior to commencement of grouting. A neat water cement grout was prepared with OPC 43/53 grade with water cement ratio of 1:0.45 as per approved grout mix design. Chemical admixture such as superplasticizer was being added to make the grout flowable; the dosages of superplasticizer will be as per grout design mix. Another chemical admixture was mixed in the grout mix to reduce shrinkage, and dosages was as per manufacturer's recommendation. The grout was mixed in high speed or colloidal mixer for about 2 min to get homogeneous and consistent mix. The flowability of grout was checked by standard flow cone of volume 1725 ml and orifice dia. 12.5 mm. The flow time of grout should be between 25 and 30 s. The minimum 28-day compressive strength of grout should be 30 MPa.

Fig. 18 Installation of rock bolts in progress

Grout mix will be pumped into hole by grout injector through grout pipe. Grouting will be done from bottom of the hole to top and grout pipe will be gradually removed as grouting progressed till fresh grout returns from the hole. After waiting for about 15–20 min, the depth of grout inside the grouted rock bolt will be checked. If there is loss of grout due to existing joints, this will be compensated by injecting additional grout inside the rock bolt hole. Once it is ensured that there is no loss of grout, the top surface of rock bolt hole will be neatly sealed with grout.

4.7 Tightening of Rock Bolt

The mild steel bearing plate of size 150 mm × 150 mm × 12 mm with central hole of dia. 40 mm was installed for the rock bolt. A 4-mm-thick plane washer was fixed on the rock bolt over base plate and tightened with M30 Nut using torque wrench to develop an axial tension equivalent to 25% design capacity of rock bolt as provided in approved drawing. Torque was applied on the rock bolts after grout attains 75% of required compressive strength which will be ascertained by conducting tests for compressive strength of grout cubes. After tightening of rock bolt, the second layer of steel fibre reinforced shotcrete is applied. The exposed portion of the rock bolt was covered by shotcrete.

4.8 Testing of Rock Bolts

The pull-out capacity of the rock bolts was ascertained by conducting pull-out tests on 1% of the working bolts. Pull-out tests were conducted up to 110% of the design capacity of the rock bolt. In the pull-out tests, there was no appreciable movement of the bolt indicating the adequacy of the design.

5 Installation of Prestressed Rock Anchors

Detailed slope stabilization analyses suggested providing prestressed bar anchors of capacity 640 kN below the foundation at S60 and prestressed cable anchors of capacity 1000 kN below the foundation S50. The finished slope below S60 foundation is shown in Fig. 19. The installation of prestressed cable anchors is in progress.

Fig. 19 Slope stabilized with prestressed bar anchors

6 Conclusions

Results from the continuum analyses using SLIDE software for both abutment slopes showed that factors of safety for all sets of properties with the are more than the required factors of safety for all the conditions considered. Similarly, the factors of safety obtained from the continuum analyses using FLAC are more than the required factors of safety for both static and pseudostatic and dynamic cases. The estimated displacements are well within the permissible limits and did not indicate any slope stabilization measures. Under dynamic loading conditions, all the displacements are less than 20 mm. Thus, differential displacements between each foundation will be far less than 20 mm which satisfies the structural design of the arch.

However, the results from the wedge failure analyses showed clearly that the factor of safety is less than required for MCE condition and warranted elaborate stabilization measures. The slopes were stabilized using both passive rock bolts and active prestressed rock anchors using both double corrosion protected prestressed bar anchors and cable anchors.

References

Hatzor YH, Arzi AA, Zaslavsky Y, Shapira A (2004) Dynamic stability analysis of jointed rock slopes using the DDA method: King Herod's Palace, Masada, Israel. Int J Rock Mech Min Sci 41(5):813–832

Itasca FLAC (2002) Fast Lagrangian Analysis of Continua, version 4.0 user's guide. Itasca Consulting Group. Inc., Thrasher Square East, p 708

Kumsar H, Aydan Ö, Ulusay R (2000) Dynamic and static stability assessment of rock slopes against wedge failures. Rock Mech Rock Eng 33(1):31–51

RocScience R (2002) Rocscience Inc. Toronto, Canada

Wyllie DC, Mah C (2004) Rock slope engineering. CRC Press

Bridge Foundations in Strata with Potential of Liquefaction

Mahesh Tandon

Abstract When liquefaction occurs, the soil loses its stiffness and strength and can not only deform but also flow laterally. In-situ testing is relied upon to assess the liquefaction potential of soils due to the difficulties in obtaining and laboratory testing of undisturbed samples. The standard penetration test (SPT) and the cone penetration test (CPT) are the two most frequently used field investigations for determining the characteristics of soils. In this paper, SPT values have been used as they remain by far the most popular and economical method of subsurface investigation in India. The methods suitable for design offices in the Indian context have received special attention in this paper which examines the effects of liquefaction on piled bridge foundations.

Keywords Liquefaction · Inertial effects · Kinematic effects · Evaluation

1 Introduction

IS 1893 Part 1 (2016) defines liquefaction as a state primarily in saturated cohesionless soils, wherein the effective shear strength is reduced to negligible value for all engineering purposes when the pore pressure approaches the total confining pressure during earthquake shaking. In this condition, the soil tends to behave like a fluid mass.

IS 1893 Part 1 (2016) stipulates the types of strata that should be investigated to evaluate its potential for liquefaction.

The Caltrans Geotechnical Manual (2014) suggests that soils with the characteristics shown in Table 1 are not liquefiable. $(N_1)_{60}$ is defined in a subsequent section of this paper.

Empirical and semi-empirical approaches for determining potential of liquefaction used in design offices cannot account for all the effects attributable to the

M. Tandon (✉)
Tandon Consultants Pvt. Ltd., New Delhi 110014, India
e-mail: mahesh.tandon@tcpl.com

R. Sundaram et al. (eds.), *Geotechnics for Transportation Infrastructure*,
Lecture Notes in Civil Engineering 29,
https://doi.org/10.1007/978-981-13-6713-7_3

Table 1 Soil not Liquefiable

$(N_1)_{60}$	% Fines
>30	≥ 5
>25	≥ 15
>21	≥ 35

characteristics of the soil, the topography, the ground motion and the structural arrangement. Nevertheless, for design office applications such approaches are invaluable especially if there is a consensus in a large body of experts and investigators that a particular approach is acceptable with the present state of knowledge.

A review of the design codes applicable to piles in liquefiable soils is available at Ghosh et al. (2012).

A comprehensive compilation of the SPT-based procedures including case history databases is recorded by Idriss and Boulanger (2010).

Wells (caissons) and piles are the most common types of foundations used in bridge structures. They have the advantage of transmitting loads to competent strata below when the upper strata have been subjected to liquefaction during strong ground shaking. Liquefaction results in loss of surface friction and stabilising support of the surrounding soil over the depth affected by the phenomenon. Well foundations, due to their large size and stiffness, are able to better cope with the effects of liquefaction.

2 Liquefaction Basics

The shear strength of cohesionless soil, τ, depends mainly on the angle of internal friction and the effective stress acting on the soil grains and can be expressed as

$$\tau = \sigma' \tan \varphi \tag{1}$$

$$\sigma' = \sigma - u \tag{2}$$

where

τ shear strength
σ' effective normal stress
σ total normal stress
u pore pressure
φ angle of internal friction.

When saturated loose cohesionless soils are subjected to earthquake loading, they tend to settle due to the densification of soil. The duration of the cyclic stress application is so short compared to the time required for water to drain that excess pore pressure progressively builds up. When the pore pressure equals the total stress, thereby reducing the effective stress to zero, the soil will experience a sudden degradation of strength and stiffness.

The most popular and accepted method of analysis of soil substrata for liquefaction potential is available at Youd et al. (2001). This method is suited up to a depth of 23 m below ground. Extrapolation beyond this depth could be of uncertain validity, AASHTO (2012).

The earthquake magnitude to be considered for liquefaction potential analysis is slightly different in international codes. AASHTO (2012) stipulates the basis as a 975-year return period (i.e. 5% possibility of exceedance in 50 years). IS 1893 Part 1 (2016) is not based on Probabilistic Seismic Hazard Analysis at present but stipulates specific values of horizontal ground accelerations to be adopted in the four seismic zones of the country.

3 Piled Bridge Foundations

The diameter of piles in bridge foundations is usually restricted to the range 800–1500 mm for reasons of economy and construction convenience, though occasionally large diameter (2000–2500 mm) or raked piles have been adopted in India. As a matter of interest, for the 6.15 km long rail-cum-road Padma Bridge in Bangladesh, some foundations consist of racked (inclination 1+1: 6V) steel tubular driven piles, 6 nos, each of 3 m diameter and 128 m depth. These were necessitated by the susceptibility to deep sour and high seismicity of the area. Since the surrounding soil over the liquefied height can no longer be depended upon to provide lateral support to the pile, the resulting deformations (including *P*-delta effects) and bending effects can be quite significant. Example of a bridge foundation on piles is shown in Fig. 1. This part of the analytical process relates to the "inertial effects" of liquefaction.

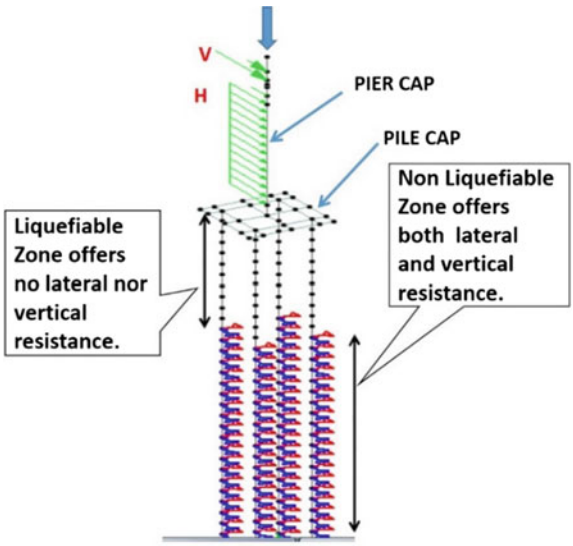

Fig. 1 Three-dimensional model of bridge pier and piled foundation

The diameter of pile must be selected with care so that apart from its vertical load carrying capacity the serviceability of the structure is not affected. The potential consequences of liquefaction associated with pile foundations include loss of vertical load capacity, loss of lateral stiffness and capacity, lateral loading due to lateral soil displacements and down-drag on piles due to post-liquefaction reconsolidation of soil.

Figure 2 from Bhattacharya et al. (2005) depicts deflected shapes of pile and pier in some structural configurations.

The problems concerning liquefaction have another dimension. Lateral spreading arises if soils subject to liquefaction are situated on a slope or near a river channel or sea which may cause movement of the liquefied soil perpendicular to the waterfront, thereby aggravating the induced effects further. In these conditions, the presence of non-liquefied soil strata overlying the liquefiable soil makes the situation even more onerous. The non-liquefied crust would exert passive earth pressure on the foundation. For shallow slopes, a simplified prescriptive approach is indicated in JRA (1996, 2002) based on back calculations from the observed damages in the Kobe earthquake of 1995. The equivalent static forces acting on the bridge foundations due to the ground flow can be estimated as (a) passive earth pressure of the upper non-liquefiable layer, plus (b) 30% of the overburden pressure of the lower liquefiable layer, as shown in Fig. 3. This part of the analytical process relates to the "kinematic effects" of liquefaction.

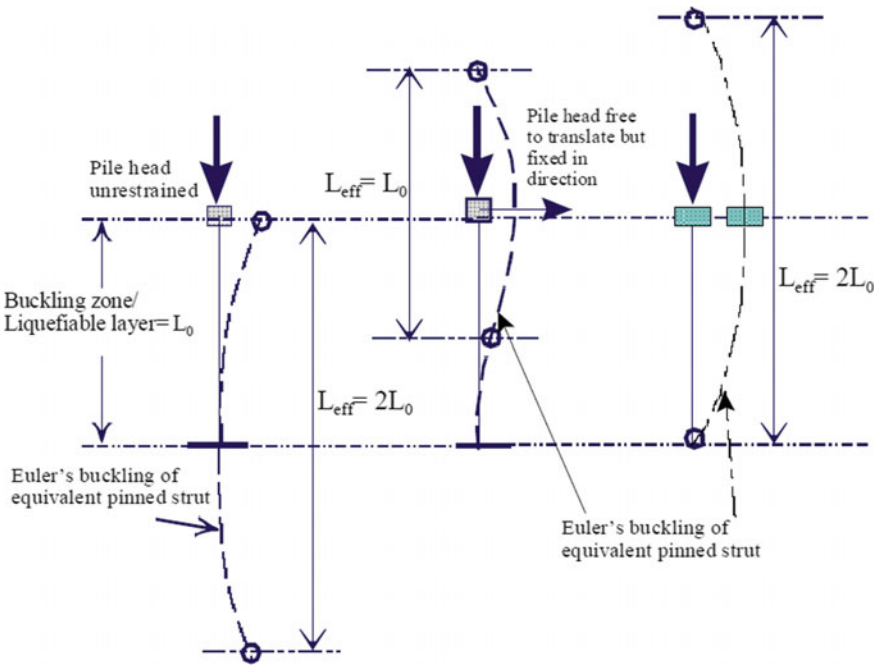

Fig. 2 Effective lengths for buckling considerations

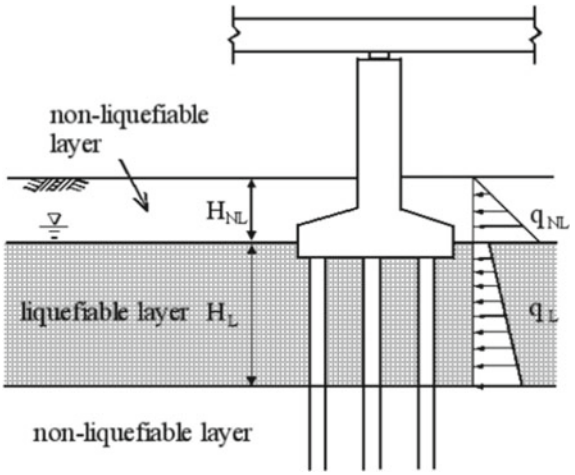

Fig. 3 JRA (1996) code of practice showing the idealisation for seismic design of bridge foundation

Showa Bridge, Fig. 4, is an example of failure due to lateral spreading, resulting in drag down the slope in the 1964 Niigata Earthquake. The bridge has a 24.8 m wide deck and a total length of 303.9 m (13.75 m + 10@ 27.64 m + 13.75 m). Each of the pier foundations consists of nine piles in a single row. One of the investigators, Bhattacharya et al. (2005), identified buckling as a possible failure mechanism of the piled foundations.

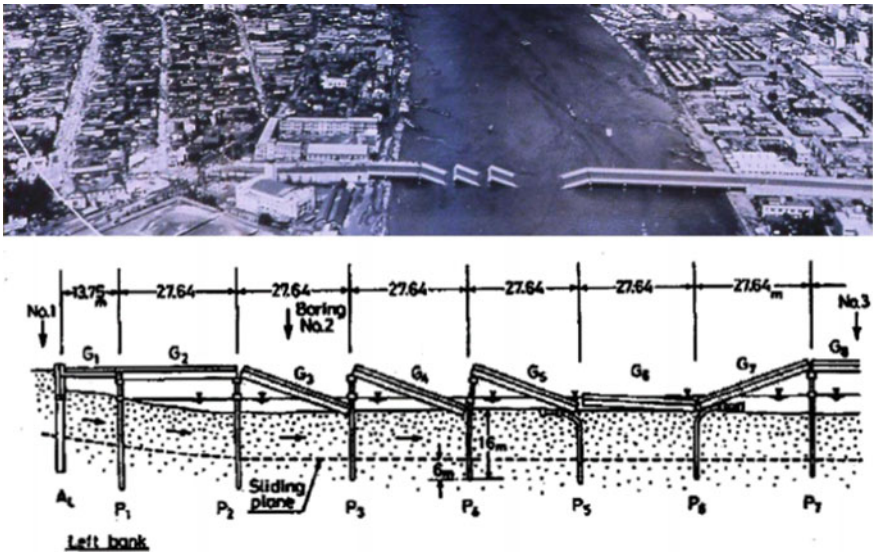

Fig. 4 Schematic diagram of the fall of the girder in Showa Bridge, Bhattacharya et al. (2005)

Following the 1964 collapse, a law was passed to prevent bridge piers being founded on a single row of piles, Bhattacharya et al. (2005).

The centrifuge test results of Haigh (2002) suggest that the pressure distribution in Fig. 3 is under-conservative in the transient phase but gives reasonable predictions for residual sliding.

The existing simplified methods cannot account for the "inertial effects" and the "kinematic effects" of liquefaction as coupled phenomena. This is justified by the fact that peak "inertial" loads are likely to occur before ground flow, Kavazanjian et al. (2011). The response of the structure to liquefaction is checked separately for the peak inertial load and the kinematic load (where applicable) without superimposing or adding the two.

Piles must be checked for buckling instability due to both inertial and kinematic effects as well as out-of-straightness which would increase lateral deflections, thereby reducing the buckling load. As per JRA (1996, 2002), the effective length of the pile should in no case exceed 50.

In the case of stiff piers including plate piers, it becomes difficult to avoid plastic hinging in the piles. Pile integrity and ductile behaviour should be ensured in such cases. The potential hinge locations should be provided with proper ductile reinforcement, for instance, in accordance with IS 13920 (2016) at the following locations: (a) at the pile heads just below the pile cap, (b) at the depth where maximum bending moments develop in the pile and (c) at the interfaces of soil layers having markedly different shear deformability. For the locations (b) and (c), longitudinal as well as confining reinforcement of the same amount as that required at the pile head should be provided.

The above issues should find specific provisions in IS 1893 Part 1 (2016) and RDSO Guidelines (2015).

4 Quantification of Liquefaction Potential

The quantification of liquefaction potential is carried out in accordance with Youd et al. (2001). The estimation of two parameters is required to evaluate liquefaction potential:

(A) CSR or critical (or cyclic) stress ratio—demand on soil layers during the seismic event
(B) CRR or critical (or cyclic) resistance ratio—capacity of the soil to resist liquefaction.

A factor of safety, FOS (= CRR/CSR), of greater than 1 is usually associated with non-liquefiable soil. A higher FOS may be warranted if uncertainty exists about the quality of data. The Indian code IS 1893 Part 1 (2016) recommends a value of 1.2.

Sample calculations in accordance with RDSO Guidelines (2015) of a real-life project by use of worksheets are shown in Tandon et al. (2015).

The evaluation is done in the following steps.

4.1 Determination of Design Groundwater Level

Caltrans (2014) suggests that if the groundwater table is at a level greater than 15 m, the site should be considered non-liquefiable.

It is usual to decide this on the basis of water table in the area as per local records. Since the water table in the area at the time of carrying out subsurface investigations could be at a lower level, it is recommended that the values obtained (e.g. soil density) should be modified to take this into account while evaluating CSR. The groundwater table affects the soil density, and hence, σ'_V, the effective vertical stress in the evaluation of CSR. IS 1983 Part 1 (2016) and RDSO Guidelines (2015) are silent on the subject. Eurocode 5 (2004) suggests that free-field site conditions (ground surface elevation and water table elevation) prevailing during the lifetime of the structure should be adopted.

4.2 Making a Realistic Stratification of the Soil from the Subsurface Investigation Data

The soil characteristics such as SPT values, unit weight and fines content (passing IS standard sieve no: 75 microns in the India context) are identified.

4.3 Normalisation of Field SPT Values

First, we must normalise the field SPT values, N, to (N_{60}) and then to $(N_1)_{60}$ for further processing, where

(N_{60}) SPT blow count of same soil for hammer with efficiency of 60%.

$(N_1)_{60}$ Value of (N_{60}) normalised for effective overburden pressure at ground level, i.e atmospheric pressure, 98 kPa.

The observed field test blow count values N need correction factor C_{60} to be applied to enable them to be converted to (N_{60}).

$$(N_1)_{60} = C_N C_{60} \tag{3}$$

C_{60} C_{HT} C_{Hw} C_{SS} C_{RL} C_{BD}, where
C_{HT} Energy ratio correction
C_{Hw} Hammer weight correction
C_{SS} Sampling method correction
C_{RL} Rod length correction
C_{BD} Borehole diameter correction and

$$C_N = \left(P_a/\sigma'_V\right)^{1/2} = 9.79\left(1/\sigma'_V\right)^{1/2} \tag{4}$$

where P_a is the atmospheric pressure.

A total of six numbers of corrections are applied on observed N value to arrive at $(N_1)_{60}$. There is no provision in the Indian codes for these corrections based on SPT equipment and methods employed in the country. Brief specification of the SPT equipment and methods is available in IS 2131 (1981).

The standard specifications for the SPT equipment recommended in Youd et al. (2001) is as per ASTM D1586 (2011), which is summarised in Table 1, and which is also included in RDSO Guidelines (2015).

In IS 1893 Part 1 (2016), it has been suggested that if the SPT values have been conducted as per IS 2131 (1981), the value of C_{60} may be taken as 1.

The RDSO Guidelines (2015), however, suggest that in the absence of test-specific energy measurement, the corrections, C_{60}, should in fact be carried out.

4.4 Evaluation of Cyclic Stress Ratio (CSR)

$$\mathrm{CSR} = 0.65(a_{max}/g)\left(\sigma_V/\sigma'_V\right)r_d \tag{5}$$

r_d Stress reduction factor which depends on depth below ground level.
a_{max}/g (Ratio of peak horizontal ground acceleration/acceleration due to gravity). For Zone IV, for instance, MCE = 0.24, IS 1893 which is suggested for liquefaction in case PGA is not available. Some codes like AASHTO (2012) recommend a value corresponding to a 975-year return period (5% probability in 50 years).
σ_V/σ_V' (Total vertical stress/effective vertical stress) should be evaluated for all the potentially liquefiable layers in the substrate. It would vary from approximately 2–1 depending upon where groundwater table is considered. It would be equal to 2 for groundwater table at ground level and equal to 1 if groundwater table is considered at the level lower than that where liquefaction is to be determined.

In Eq. (5), the flexibility of the soil profile is accounted for by r_d which can be calculated from Eqs. (6) and (6a).

$$r_d = 1 - 0.00765\,z \text{ for } z < 9.15 \text{ m} \tag{6}$$

$$r_d = 1.174 - 0.0267\,z \text{ for } 9.15 < z < 23 \text{ m} \tag{6a}$$

The depth z below the ground surface should be measured up to the centre of the concerned layer.

4.5 Making Correction for Fines

Seed and Idriss (1982) concluded that liquefaction potential in a soil layer increases with decreasing fines content and plasticity of the soil.

In accordance with IS 1893 Part 1 (2016), fines are defined as per cent by weight passing the IS Standard Sieve No. 75μ.

The corrections for fines content can be done following the equations developed by Idriss with the assistance of Seed for correction of $(N_1)_{60}$ to an equivalent clean sand value, $(N_1)_{60cs}$:

$$(N_1)_{60cs} = \alpha + \beta (N_1)_{60} \tag{7}$$

where $(N_1)_{60cs}$ is the blow count corrected for fines content, and α and β are coefficients that depend on the fines content.

$$(N_1)_{60cs} = \alpha + \beta (N_1)_{60} \tag{7a}$$

where α and β = coefficients determined from the following relationships:

$$\alpha = 0 \text{ for FC } \leq 5\% \tag{8a}$$

$$\alpha = \exp\left[1.76 - \left(190/\text{FC}^2\right)\right] \text{ for } 5\% < \text{FC} < 35\% \tag{8b}$$

$$\alpha = 5.0 \text{ for FC} \geq 35\% \tag{8c}$$

$$\beta = 1.0 \text{ for FC} \leq 5\% \tag{9a}$$

$$\beta = \left[0.99 + \left(\text{FC}^{1.5}/1.00\right)\right] \text{ for } 5\% < \text{FC} < 35\% \tag{9b}$$

$$\beta = 1.2 \text{ for FC} \geq 35\% \tag{9c}$$

4.6 Calculation of Cyclic Resistance Ratio $(CRR)_{7.5}$

The database from sites where liquefaction effects were or were not observed, a base curve for "clean sand" for magnitude 7.5 earthquakes, was arrived. The curve

was approximated to Eq. (10)—credited to AF Rauch of the University of Texas (1998)—which can be used more conveniently in worksheets.

$$\mathrm{CRR}_{7.5} = \frac{1}{34 - (N_1)_{60\mathrm{cs}}} + \frac{(N_1)_{60\mathrm{cs}}}{135} + \frac{50}{\left[10(N_1)_{60\mathrm{cs}} + 45\right]^2} - \frac{1}{200} \tag{10}$$

4.7 Calculation of the Magnitude Scaling Factor (MSF)

The next step is to calculate the CRR for the particular site by evaluating the magnitude scaling factor (MSF) for the particular site.

The data available for various parts of India for past earthquakes have been plotted in IS 1893 Part 1 (2016) which is shown in Fig. 5. If site-specific investigations have not been carried out, Fig. 5 can be used for determining the earthquake magnitude, (M_w), applicable to the site.

MSF is determined from Eq. (11).

$$\mathrm{MSF} = 10^{2.24}/M_w^{2.56} \tag{11}$$

4.8 Calculation of CRR

The CRR for the particular site is evaluated by multiplying $\mathrm{CRR}_{7.5}$ with MSF as shown in Eq. (12).

$$\mathrm{CRR} = \mathrm{CRR}_{7.5}(\mathrm{MSF}) \tag{12}$$

4.9 Evaluation of Factor of Safety, FOS

The factor of safety with respect to potential of liquefaction is finally arrived at by using Eq. (13).

$$\mathrm{FOS} = \frac{\mathrm{CRR}}{\mathrm{CSR}} \tag{13}$$

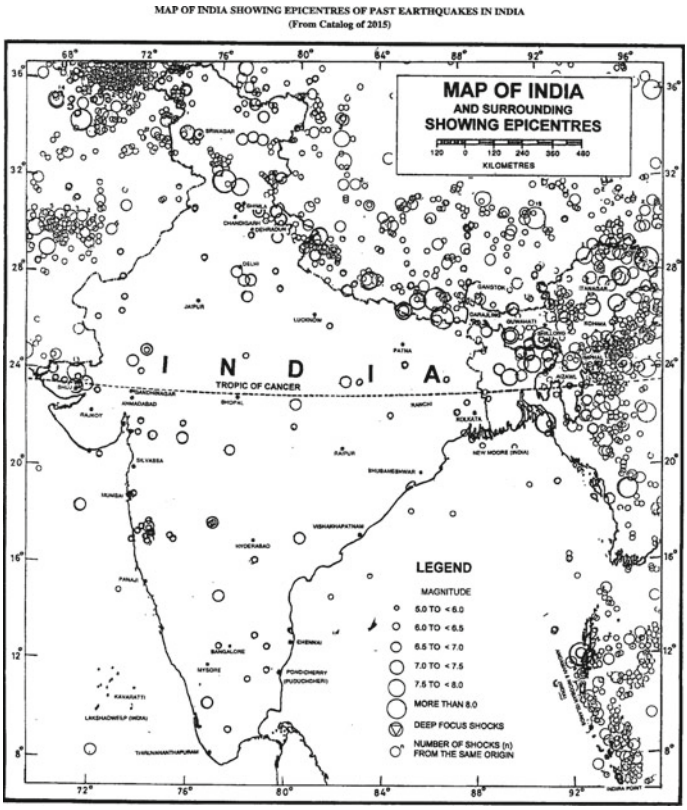

Fig. 5 Epicentres of past earthquakes (from IS 1893)

5 Conclusions

The paper highlights the methodology that should be employed in bridge design offices in the Indian context while determining the potential of liquefaction using SPT field tests. The frequently used code provisions have been reviewed. Some differences between the two codes/guidelines, i.e. IS 1893 Part 1 (2016) and RDSO Guidelines (2015), have been highlighted. Some of the missing provisions in these codes have been discussed.

In many situations, the liquefied layer is overlain by non-liquefied strata. The bridge site may be located on sloping ground or near a waterfront, in which case lateral spreading would occur creating significant lateral forces on the piles. A simplified approach to account for the same has been identified. Both inertial effects and kinematic effects of liquefaction have been discussed in the paper.

References

AASHTO LRFD Bridge Design Specifications (2012)

ASTM D1586 (2011) Standard test method for standard penetration test (SPT) and split-barrel sampling of soils

Bhattacharya S, Bolton MD, Madabhushi SPG (2005) A reconsideration of the safety of piled bridge foundations in liquefiable soils, soils and foundations. Jpn Geotech Soc 45(4):13–25

Caltrans Geotechnical Manual (2014) Liquefaction evaluation, Dec

Eurocode 8: Design of structures for earthquake resistance—Part 5: foundations, retaining structures and geotechnical aspects. The European Standard EN 1998-5:2004 has the status of a British Standard

Ghosh B, Mian J, Lubkowski ZA (2012) Design of piles in liquefiable soil: a review of design codes and methodologies. 15 WCEE LISBOA

Haigh SK (2002) Effects of earthquake-induced liquefaction on pile foundations in sloping ground. Ph.D. dissertation, Cambridge University, UK

Idriss IM, Boulanger RW (2010) SPT-based liquefaction triggering procedures, Department of Civil & Environmental Engineering. Report no. Center for Geotechnical Modeling UCD/CGM-10/02, Dec

IS 13920 (2016) Ductile design and detailing of reinforced concrete structures subjected to seismic forces—code of practice

IS 1893-Part 1 (2016) Criteria for earthquake resistant design of structures. Bureau of Indian Standards, Delhi

IS 2131 (1981) Method for standard penetrations test for soil. Bureau of Indian Standards, Delhi

JRA (1996) Specifications for highway bridges in Japan

JRA (2002) Specifications for highway bridges Japan Road Association, Preliminary English Version. Prepared by Public Works Research Institute (PWRI) and Civil Engineering Research Laboratory (CRL), Japan, Nov

Kavazanjian E, Martin GR, Dickenson SE, Hung CJ, Lam I, Shamsabadi A (2011) LRFD seismic analysis and design of transportation geotechnical features and structural foundations. NHI Course no. 130094, Reference Manual Geotechnical Engineering Circular No. 3, Aug

RDSO Guidelines on Seismic Design of Railway Bridges (2015) Research Design and Standards Organisation, Lucknow

Seed HB, Idriss IM (1982) Ground motions and soil liquefaction during earthquakes. Earthquake Engineering Research Institute Monograph, Oakland, CA

Tandon M, Gupta N, Grewal HS (2015) Evaluation of liquefaction potential of design of deep foundation. Indian National Group of The International Association for Bridge and Structural Engineering

Youd T, Idriss I, Andrus R, Arango I, Castro G, Christian J, Dobry R, Finn W, Harder L Jr, Hynes M, Ishihara K, Koester J, Liao S, Marcuson III W, Martin G, Mitchell J, Moriwaki Y, Power M, Robertson P, Seed R, Stokoe II K (2001) Liquefaction resistance of soils. Summary report from the 1996 NCEER and 1998 NCEER/NSF workshops on evaluation of liquefaction resistance of soils. ASCE J Geotech Geoenviron Eng

Evaluation of Performance of the Roadmesh Reinforcement Pavement at Trial Stretch on Chita-Khabarovsk Autoroad

Ushakov Victor and Inshakov Aleksander

Abstract An experimental section of asphalt concrete reinforced with Roadmesh metal mesh was constructed at Chita-Khabarovsk road in August 2008. It was with the participation of specialists from MADI (Moscow), Dorstroykontrol Research and Development Center (Chita), Maccaferri CIS and Zhireken branch of Trud CJSC (Irkutsk). In order to validate and elaborate the asphalt concrete reinforcement technology and for the evaluation of the mesh impact on the bearing capacity of the road pavement, cracking resistance and evenness of the asphalt concrete covering studies were carried out in 2009, 2010, and 2011. The paper presents the studies were carried out during 3 years of the pavement service under severe climatic and permafrost conditions and the results obtained.

Keywords Roadmesh · Asphalt reinforcement · Maccaferri CIS · Road pavement · Cracking resistance

1 Introduction

An experimental section of asphalt concrete reinforced with Roadmesh metal mesh was constructed at Chita-Khabarovsk autoroad in August 2008. It was with the participation of specialists from MADI (Moscow), Dorstroykontrol Research and Development Center (Chita), Maccaferri CIS and Zhireken branch of Trud CJSC (Irkutsk). In order to validate and elaborate the asphalt concrete reinforcement technology and for the evaluation of the mesh impact on the bearing capacity of the road pavement, cracking resistance and evenness of the asphalt concrete covering studies were carried out in 2009, 2010, and 2011. The studies were carried out

U. Victor
Moscow Automobile and Road Institute (MADI), Moscow, Russia
e-mail: ushakov@madi.ru

I. Aleksander (✉)
Maccaferri CIS, Moscow, Russia
e-mail: inshakov@maccaferri.ru

R. Sundaram et al. (eds.), *Geotechnics for Transportation Infrastructure*,
Lecture Notes in Civil Engineering 29,
https://doi.org/10.1007/978-981-13-6713-7_4

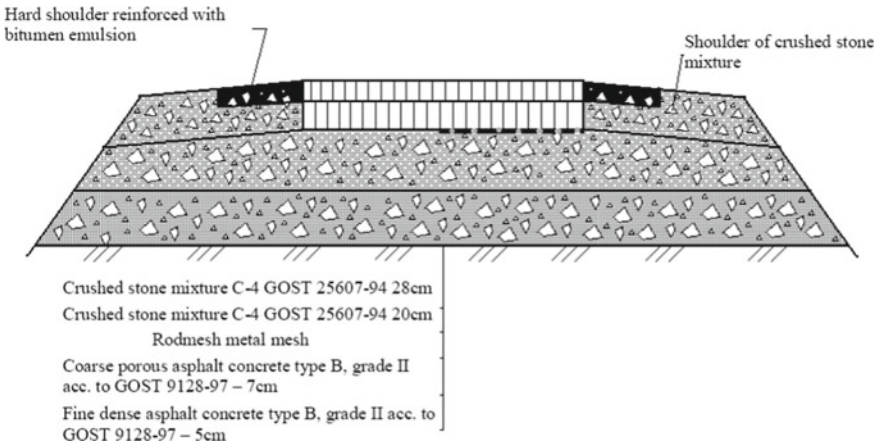

Fig. 1 Road pavement structure of Chita-Khabarovsk autoroad experimental section

during 3 years of the pavement service under severe climatic and permafrost conditions.

The experimental section is located at km 365 (ПК 143+02–ПК 144+02, left driving lane) of Chita-Khabarovsk autoroad. The section is in the valley of the Shirga River in Zabaykalye territory which is characterized by continuous permafrost and weak soils of the seasonally active layer of the roadbed foundation. The road pavement structure of Chita-Khabarovsk autoroad experimental section is shown in Fig. 1.

2 Evaluation of the Impact of the Road Pavement Reinforcement with Roadmesh—The General Condition of the Asphalt Concrete Covering Surface

The patterns of transverse and longitudinal cracks propagation at km 365 section of Chita-Khabarovsk autoroad (ПК 141+96–ПК 144+02) are shown in Figs. 2 and 3. Studies and monitoring of the experimental sections showed that cracks propagation at the unreinforced section (ПК 141+96–ПК 143+02), adjacent to the reinforced one (ПК 143+02–ПК 144+02, left driving lane) was more intense and they were irregular on the covering surface. In general, it should be pointed out that laying of Roadmesh metal mesh between the crushed stone foundation and asphalt concrete layers had a certain impact on formation and propagation of cracks in the asphalt concrete (Figs. 4 and 5).

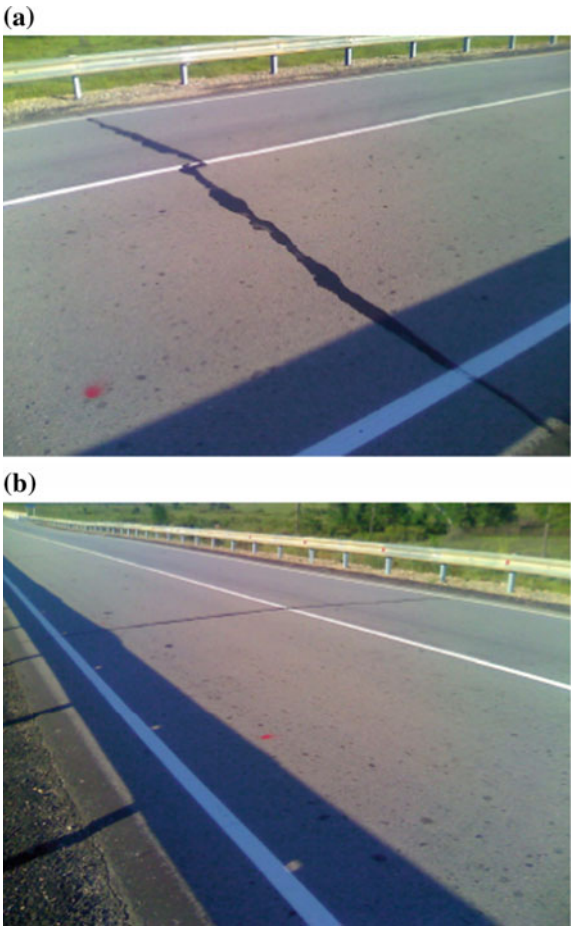

Fig. 2 **a** Transverse crack on experimental section ПК 143 +39 **b** Transverse crack on experimental section ПК 143 +50

Studies and monitoring of the experimental sections showed that cracks propagation at the unreinforced section (ПК 141+96–ПК 143+02), adjacent to the reinforced one (ПК 143+02–ПК 144+02, left driving lane) was more intense and they were irregular on the covering surface. In general, it should be pointed out that laying of Roadmesh metal mesh between the crushed stone foundation and asphalt concrete layers had a certain impact on formation and propagation of cracks in the asphalt concrete (refer Fig. 6).

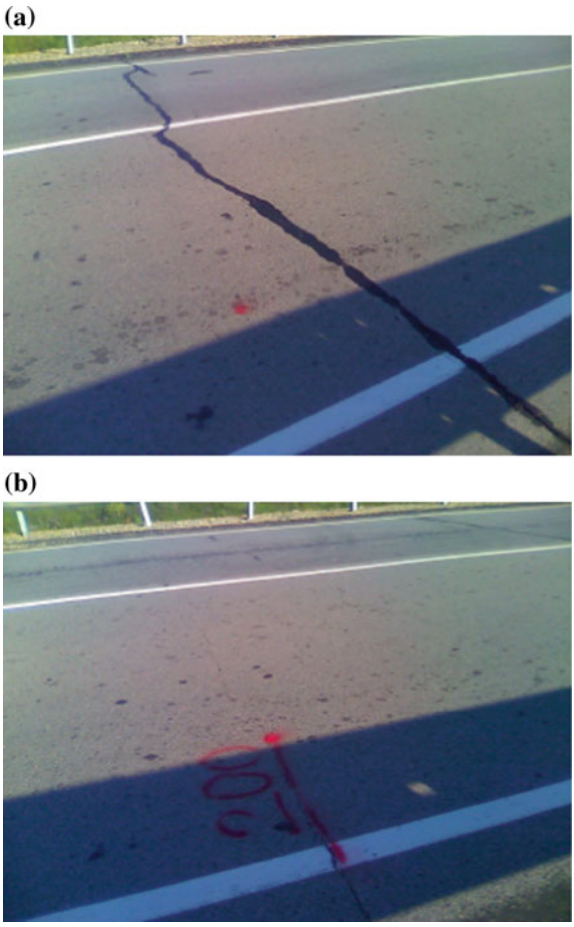

Fig. 3 **a** Transverse crack on experimental section ПК 143 +85 **b** Transverse crack at the end of experimental section ПК 144+00

3 Evaluation of Reinforcement Impact on the Pavement Surface Evenness

The evenness of the asphalt concrete covering surface of Chita-Khabarovsk autoroad was determined by the "amplitude method", by profile leveling at driving lanes at 5 m intervals. Results of surface evenness determination of asphalt concrete covering at Chita-Khabarovsk autoroad at km 365 (Пк 142+00–Пк 144+05) as of 2008 is shown in Table 1. The following are the observations from the study (refer Table 1).

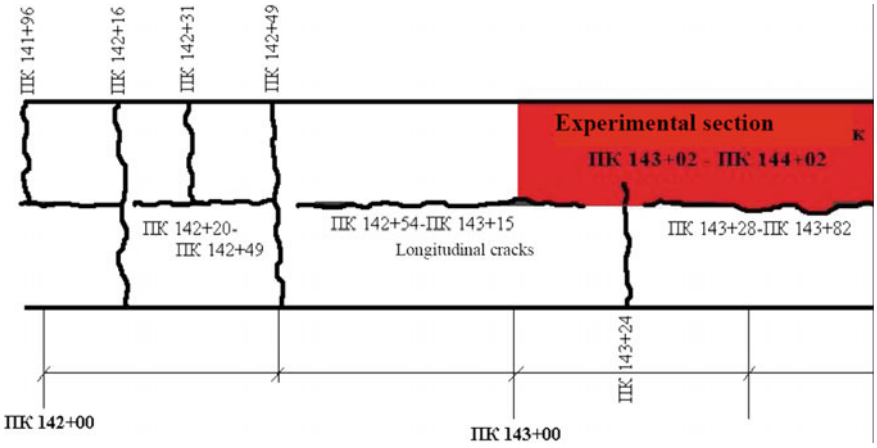

Fig. 4 Transverse and longitudinal cracks propagation pattern at Chita-Khabarovsk autoroad section at km 365 (ПК 142+00–ПК 144+02), revealed in 2009

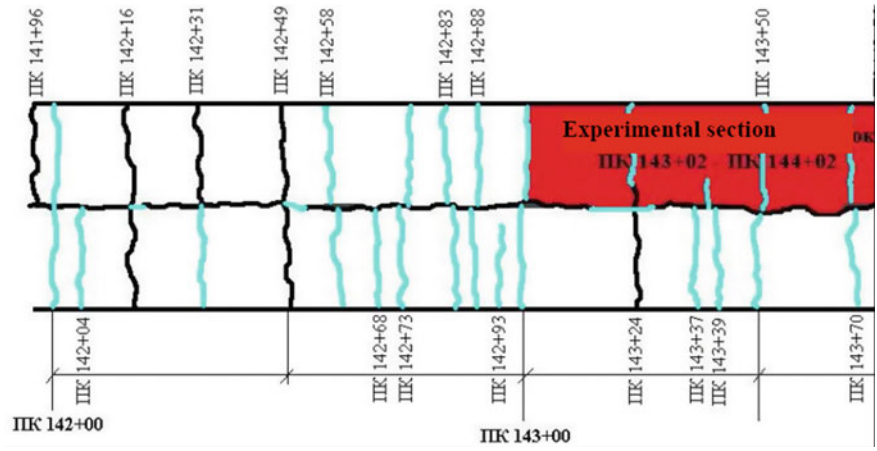

Fig. 5 Transverse and longitudinal cracks propagation pattern at Chita-Khabarovsk autoroad section at km 365 (ПК 142+00–ПК 144+02), revealed in 2011

1. At reinforced section ПК 143+02–ПК 144+02 (left driving lane), 95% of evenness determination results have amplitude values of up to 7 mm and 5%—up to 10.5 mm;
2. At unreinforced section Пк 143+02–Пк 144+02 (right driving lane), adjacent to the experimental one on the adjacent driving lane, 70% of evenness determination results have amplitude values of up to 7 mm, 25%—up to 10.5 mm, and 5%—over 10.5 mm;

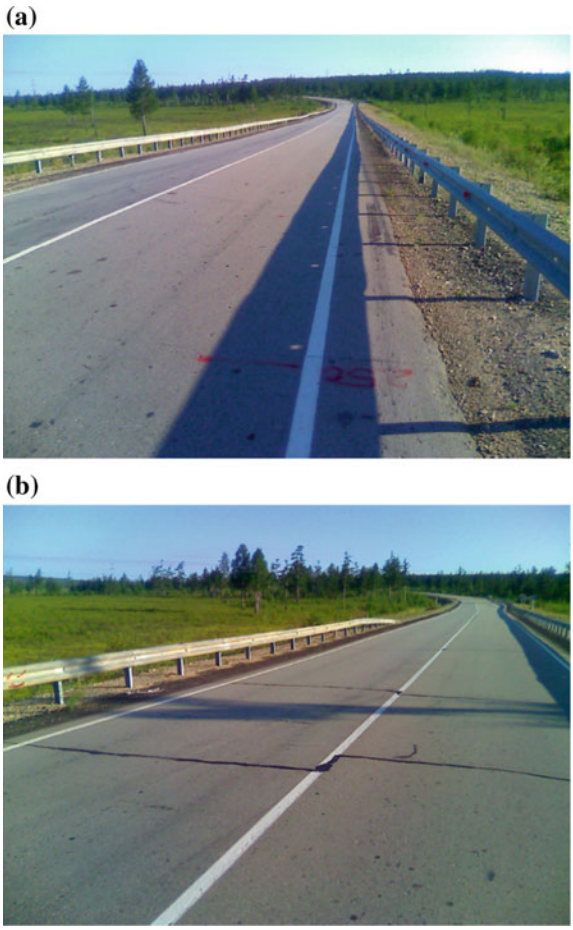

Fig. 6 **a** General view of the autoroad experimental section at km 365 (ПК 142+00–ПК 144+50)—July 2011 **b** General view of the section of Amur autoroad (Chita-Khabarovsk) at km 365 (ПК 142+00–ПК 143 +00)—July 2011

3. At unreinforced section Пк 142+00–Пк 143+02, adjacent to the experimental one, 77.5% of evenness determination results have amplitude values of up to 7 mm, 20%—up to 10.5 mm, and 2.5%—over 10.5 mm.

Similarly, the following are the conclusion drawn from the results of the test conducted on asphalt concrete at Chita-Khabarovsk autoroad at km 365 (Пк 142 +00–Пк 144+05) as of 2010.

1. At reinforced section ПК 143+02–ПкК144+02 (left driving lane), 90% of evenness determination results have amplitude values of up to 7 mm and 10%—up to 10.5 mm;

Table 1 Results of surface evenness determination of asphalt concrete covering at Chita-Khabarovsk autoroad at km 365 (Пк 142+00–Пк 144+05) as of 2008

Measurement point, ПК +	Left driving lane		Right driving lane	
	Reference hi, m marks	Amplitudes hi, m	Reference hi, m marks	Amplitudes hi, m
142+00	2.776	–	2.795	–
142+05	2.648	10.5	2.673	10
142+10	2.541	5.5	2.571	1
142+15	2.445	−6	2.471	−6.5
142+20	2.337	1.5	2.358	−5.5
142+25	2.232	−4	2.234	0.5
142+30	2.119	7	2.111	7
142+35	2.020	3.5	2.002	9.5
142+40	1.928	−2.5	1.912	−1
142+45	1.831	−6.5	1.82	−6.5
142+50	1.721	1	1.715	0
142+55	1.613	7	1.610	4
142+60	1.519	5	1.513	−0.5
142+65	1.435	−6	1.415	
142+70	1.339	−2	1.309	−0.5
142+75	1.239	10.5	1.202	11.5
142+80	1.6	7	1.118	9.5
142+85	1.095	−8	1.053	−1
142+90	1.014	−7	0.986	−10.5
142+95	0.919	1.5	0.898	4
143+00	0.827	10.5	0.818	2
143+05	0.756	8	0.742	10.5
143+10	0.701	2	0.687	4
143+15	0.650	2.5	0.640	4
143+20	0.604	6.5	0.601	6
143+25	0.571	−5.5	0.574	−2
143+30	0.527	−1	0.543	−8
143+35	0.481	3	0.496	−7
143+40	0.441	−2	0.435	−5.5
143+45	0.397	−6.5	0.363	4.5
143+50	0.340	−2	0.300	−8.5
143+55	0.279	2	0.220	19
143+60	0.222	4.5	0.178	10.5
143+65	0.174	6.5	0.157	−6
143+70	0.139	4	0.124	6
143+75	0.112	2	0.103	10.5
143+80	0.089	7	0.103	1.5

(continued)

Table 1 (continued)

Measurement point, ПК +	Left driving lane		Right driving lane	
	Reference hi, m marks	Amplitudes hi, m	Reference hi, m marks	Amplitudes hi, m
143+85	0.08	−3.5	0.106	−4
143+90	0.064	6	0.101	−2
143+95	0.060	−7	0.092	−7
144+00	0.042	−4	0.069	1
144+05	0.016	–	0.048	–

2. At unreinforced section ПК 143+02–ПК 144+02 (right driving lane), adjacent to the experimental one on the adjacent driving lane, 65% of evenness determination results have amplitude values of up to 7 mm, 15%—up to 10.5 mm, and 20%—over 10.5 mm;
3. At unreinforced section ПК 142+00–ПК 143+02, adjacent to the experimental one, 65% of evenness determination results have amplitude values of up to 7 mm, 15%—up to 10.5 mm, and 20%—over 10.5 mm.

Similarly, the following are the conclusion drawn from the results of the test conducted on asphalt concrete at Chita-Khabarovsk autoroad at km 365 (Пк 142 +00–Пк 144+05) as of 2011.

1. At reinforced section ПК 143+02–ПК 144+02 (left driving lane), 85% of evenness determination results have amplitude values of up to 7 mm, 10%—up to 10.5 mm, and 5%—over 10.5 mm;
2. At unreinforced section ПК 143+02–ПК 144+02 (right driving lane), adjacent to the experimental one on the adjacent driving lane, 50% of evenness determination results have amplitude values of up to 7 mm, 30%—up to 10.5 mm, and 20%—over 10.5 mm;
3. At unreinforced section ПК 142+00–Пк 14К+02, adjacent to the experimental one, 55% of evenness determination results have amplitude values of up to 7 mm, 20%—up to 10.5 mm, and 25%—over 10.5 mm.

On the basis of the evenness evaluation of the pavement experimental sections during the period of its service, we can draw a conclusion that reinforcement of the road pavement with Roadmesh metal mesh contributes to higher evenness of the asphalt concrete covering during a long period of service. The reinforcement protects the pavement from irregular deformation, especially under the permafrost conditions.

4 Evaluation of Reinforcement Impact on the Bearing Capacity of the Road Pavement

Evaluation of the impact of metal mesh on the bearing capacity of the road pavement was carried out in several steps. At the first stage, the relative variation in the road pavement strength when reinforced with Roadmesh metal mesh was determined directly upon the upper layer of the asphalt concrete covering. At each subsequent stage, the bearing capacity of the road structure in the period of its most weak condition was determined yearly for three years of service (refer Table 2). The MADI-TsNIL lever-type Benkelman beam was used for road pavement

Table 2 Results of determination of the road pavement strength at Chita-Khabarovsk autoroad section at km 365 (ПК 142+00–ПК 144+02) as of the day of commissioning upon completion of the road construction (October 2008)

Number of points	Elastic modulus, MPa					
	Left			Right		
	General	On the surface of the pavement lower layer	Difference of values	General	On the surface of the pavement lower layer	Difference of values
Adjacent section at km 365 (ПК 142+00–ПК 143+02)						
1	311	165	146	327	304	24
2	272	249	23	343	330	13
3	259	223	36	400	253	147
4	351	205	146	360	316	44
5	327	171	157	343	262	81
6	320	195	125	400	266	134
7	320	197	123	327	266	61
8	302	161	141	400	345	55
9	330	165	165	343	316	27
10	286	195	92	379	361	18
11	360	183	177	400	370	30
Experimental section at km 365 (ПК 143+02–ПК 144+02)						
12	351	165	186	351	330	21
13	300	177	124	379	361	18
14	320	183	137	369	266	103
15	343	217	126	343	304	39
16	306	253	53	327	310	18
17	360	276	84	327	316	11
18	313	192	121	379	323	56
19	300	167	133	369	316	53
20	343	185	158	400	330	70

strength trials. At the section of Chita-Khabarovsk autoroad, the load was applied using different vehicles—ATZ refueler on the basis of MAZ-53370-24 two-axle vehicle with 11.5 t (112.82 kN) load on the back axle and KDM-130V on the basis of ZIL-130 with 6.3 t (61.8 кН) load on the back axle. The wheel print areas amounted to 1456 and 1020 $cm^{2,}$ respectively.

The road pavement elastic modulus was determined using the following formula:

$$E = \frac{p \times D \times (1 - \mu^2)}{I_y}, \text{MPa}$$

where p—specific wheel pressure on the pavement, MPa; D—diameter of the circle equal to the wheel print, mm; Poisson's ratio—0.3; I_y—elastic deflection of the road pavement, mm.

From Table 2, it can be observed that the average values of the road pavement elastic modulus on the surface of the upper layer of the asphalt concrete are the following: at reinforced section ПК 143+02–ПК 144+02 (left driving lane)

Table 3 Results of the road pavement strength at Chita-Khabarovsk autoroad section at km 365 (Пк 142 +00–Пк 144+02)

No of points	Elastic modulus, MPa	
	Right	Left
Adjacent section at km 365 (ПК 142+00–ПК 143 +02)		
1	207	199
2	237	199
3	199	237
4	195	261
5	207	248
6	221	269
7	195	242
8	191	199
9	231	231
10	181	221
11	177	226
Experimental section at km 365 (ПК 143+02–ПК 144+02)		
12	221	181
13	221	216
14	231	248
15	191	203
16	216	216
17	187	248
18	191	199
19	199	216
20	207	216

—326 MPa; at unreinforced section ПК 142+00–ПК 143+02, adjacent to the experimental one—313 MPa, with average strength of the road pavement foundation of 196 MPa. The difference of values of elastic modulus of the road pavement on the asphalt concrete covering surface and the crushed stone foundation are the following: at the experimental section—130 MPa; at the section adjacent to the experimental one—117 MPa. Hence, laying Roadmesh metal mesh on the crushed stone foundation under a two-layer asphalt concrete covering provides a relative strength enhancement of 11.1%.

Results of the road pavement strength at Chita-Khabarovsk autoroad section at km 365 (Пк 142+00–Пк 144+02) are enlisted in Table 3. The average values of the elastic modulus on the surface of the upper layer of the asphalt concrete road pavement are 207 and 204 MPa at reinforced section (ПК 143+02–ПК 144+02) (left driving lane) and at unreinforced section (ПК 142+00–ПК 143+02), adjacent to the experimental one, respectively.

5 Conclusion

The following are the results found out from the trials of the experimental sections conducted at Chita-Khabarovsk autoroad, reinforced with Roadmesh mesh from 2008 to 2011.

1. Laying Roadmesh metal mesh between the crushed stone foundation and the asphalt concrete covering has a positive impact on the propagation of cracks in the asphalt concrete during the service period. At unreinforced sections of the asphalt concrete covering cracks, propagation is more intense and they are irregular on the covering surface as compared to the covering section reinforced with Roadmesh metal mesh.
2. Reinforcement with Roadmesh metal mesh protects the pavement from irregular deformation, especially under permafrost conditions. Reinforcement of the road pavement contributes to the preservation of the asphalt concrete covering surface evenness for a long period of service.
3. Reinforcement of flexible road pavement with Roadmesh metal mesh contributes to pavement strength enhancement by 10% at the average.
4. It is recommended to reinforce flexible road pavements with Roadmesh metal mesh at the sections with weak soils, at locations under permafrost conditions, at the locations where an even asphalt concrete covering is required for a long period of time.

Geotechnical Design Parameters for a Metro Tunnel from Pressuremeter Tests

Ravi Sundaram, Sanjay Gupta, Sorabh Gupta and Bhajan Lal

Abstract Being an in situ test, the pressuremeter provides a reliable assessment of soil parameters, eliminating the influence of sample disturbance. The paper outlines the analysis of pressuremeter data to interpret parameters such as undrained shear strength, pre-consolidation pressure, over-consolidation ratio, and in situ horizontal stress. The test was used effectively in conjunction with borehole data to assess the geotechnical parameters for the design of a metro tunnel. Data from two locations along the metro tunnel alignment are presented here.

Keywords Pressuremeter · Tests · Undrained shear strength · Pre-consolidation pressure · In situ horizontal stress · Metro tunnel

1 Introduction

The alignment of a tunnel of the Delhi Metro in old Delhi area is in the vicinity of a heritage structure. The stratigraphy along the alignment is primarily medium-dense Delhi Silt.

Geotechnical investigation for the design of tunnel included pressuremeter tests in addition to boreholes. The pressuremeter data were used to generate important design parameters such as undrained shear strength, pre-consolidation pressure, and in situ horizontal stress.

R. Sundaram (✉) · S. Gupta · S. Gupta · B. Lal
Cengrs Geotechnica Pvt. Ltd., A-100 Sector 63, Noida, India
e-mail: ravi@cengrs.com

S. Gupta
e-mail: sanjay@cengrs.com

S. Gupta
e-mail: sorabh@cengrs.com

B. Lal
e-mail: bhajan@cengrs.com

R. Sundaram et al. (eds.), *Geotechnics for Transportation Infrastructure*,
Lecture Notes in Civil Engineering 29,
https://doi.org/10.1007/978-981-13-6713-7_5

The parameters have been correlated with various laboratory tests such as triaxial tests and consolidation tests.

The paper presents data from two borehole locations along the alignment. A layout plan showing the locations investigated along the metro alignment is illustrated on Fig. 1.

2 Site Conditions

2.1 Geology

The deposits along the alignment belong to the "Indo-Gangetic Alluvium" and are river deposits of the Yamuna and its tributaries (Krishnan 1986). The Pleistocene and Recent deposits of the Indo-Gangetic Basin are composed of gravels, sands, silts, and clays with remains of animal and plants.

The older alluvium is rather dark colored (locally called "Bhanger") and consists primarily of silts and clays of low to medium plasticity and silty sands. It is generally rich in concretions or nodules of impure calcium carbonate. The age of the "Bhanger" alluvium is Middle to Upper Pleistocene.

The newer alluvium (locally called "Khadar") is light colored and poor in concretions. It contains lenticular beds of sand and gravel. It is merged by insensible gradations into the Recent or deltaic alluvia, and its age is Upper Pleistocene to Recent.

2.2 Stratigraphy

Based on the boreholes drilled (see Fig. 2 illustrating drilling in progress), sandy silt of low plasticity is encountered from ground level to 30 m depth with intermediate minor zones of clayey silt and silty sand.

Groundwater was met at 3.3–4.6 depth during the investigation.

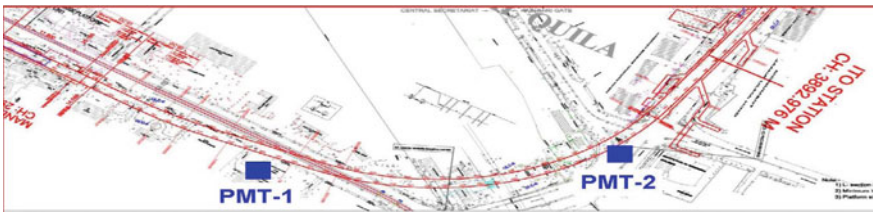

Fig. 1 Metro alignment showing test locations

Fig. 2 Geotechnical investigation in progress

SPT values range from 12 to 22 to about 6–9 m depth, from 26 to 38 to 18–22 m depth, and from 36 to 53 to 30 m depth.

2.3 Soil Properties

The soil properties based on laboratory tests conducted on the soil samples collected from the boreholes are presented in Table 1.

Table 1 Properties of Delhi Silt in project area

Parameter	Typical range of values
Gradation	
Gravel	0–4%
Sand	21–44%
Silt	49–70%
Clay	4–13%
Liquid limit	27–32%
Plastic limit	15–19%
Plasticity index	10–13%
Moisture content	16–21%
UU triaxial test (undrained)	c = 60–90 kPa ϕ = 5°–7°
CU triaxial test Effective stress parameters	c' = 25–30 kPa ϕ = 29°–30°
Consolidation test OCR	2–3

The soils are locally called Delhi Silt and are classified as clays of low plasticity (CL).

3 Pressuremeter Tests

Pressuremeter tests were done at 5-m depth intervals in NX diameter boreholes. The pressure versus volume change was recorded to assess the limit pressure and deformation modulus. A photograph of the test in progress is presented on Fig. 3.

Typical result of the test is illustrated on Fig. 4.

The limit pressure and deformation modulus interpreted from the test results are plotted in Figs. 5 and 6.

Fig. 3 Pressuremeter test in progress

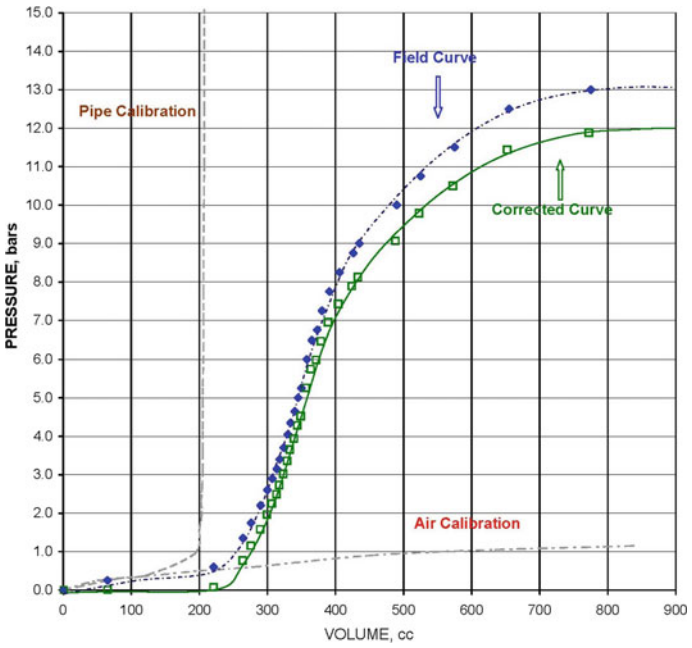

Fig. 4 Typical pressuremeter test result

4 Strength and Consolidation Parameters

Various correlations are available in the literature to calculate the undrained shear strength and pre-consolidation pressure of cohesive soils using the pressuremeter results. The values from different correlations vary by ±20% and may be moderated based on data from laboratory test results.

Based on the cavity expansion theory, Baguelin et al. (1978) proposed the following correlation to assess the undrained shear strength of cohesive soils:

$$s_u = \frac{(p_L - p_0)}{N_p}$$

where

s_u undrained shear strength (=2c)
p_L limit pressure

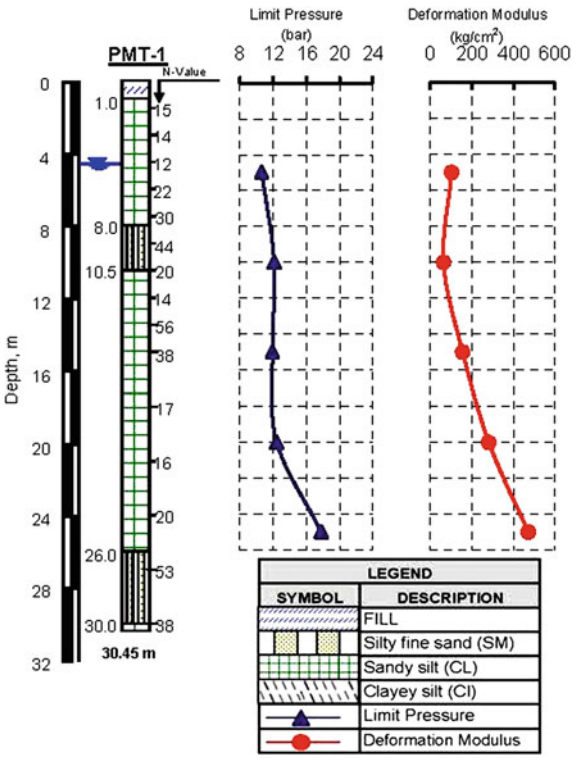

Fig. 5 Limit pressure and deformation modulus versus depth—PMT-1

p_0 in situ horizontal stress

$$N_p = 1 + \ell n(E_m/3s_u)$$

E_m pressuremeter deformation modulus.

Typical values of N_p range from 5 to 12. The authors have used an average value of 8.5 in the calculations.

Figure 7 presents plot of undrained shear strength (s_u) interpreted from the pressuremeter tests versus depth for one typical borehole. The s_u values from UU triaxial tests are plotted alongside for comparison.

Clarke (1995) has combined the theory of critical state concept with the cavity expansion theory to develop the following correlation between pre-consolidation pressure and undrained shear strength of clays:

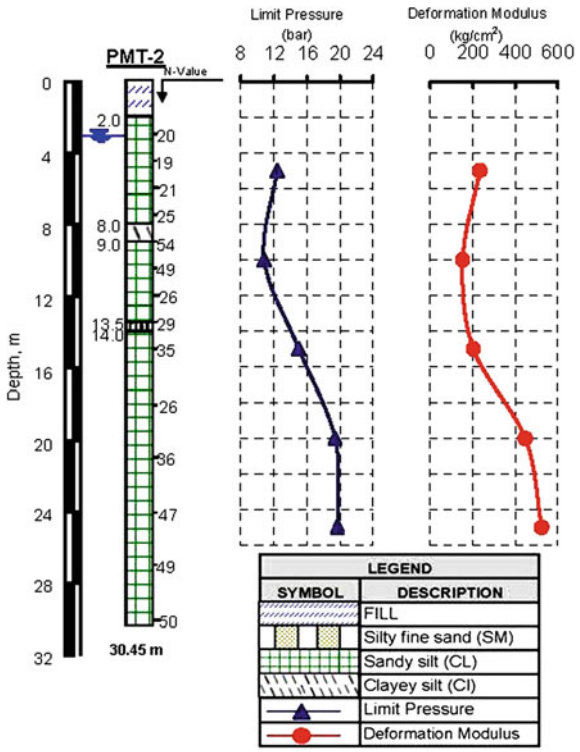

Fig. 6 Limit pressure and deformation modulus versus depth—PMT-2

$$p_c = \frac{4s_u}{M}$$

where

p_c pre-consolidation pressure
s_u undrained shear strength
M critical state parameter = 6 sin ϕ/(3 − sin ϕ)
ϕ effective angle of shearing resistance, taken from CU triaxial tests.

Figure 8 presents plot of p_c and OCR versus depth.

It may be seen that the undrained shear strength from the pressuremeter test compares well with the laboratory values.

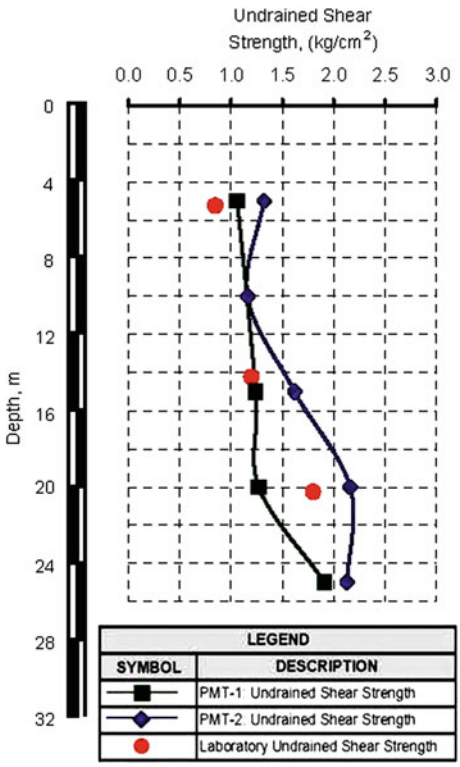

Fig. 7 Undrained shear strength versus depth

The pre-consolidation pressure assessed laboratory tests is about 20% lower than that interpreted from pressuremeter data. Over-consolidation ratios interpreted from laboratory data are also somewhat lower than those obtained from pressure.

4.1 In Situ Horizontal Stress

The in situ horizontal stress may be assessed by plotting the creep volume (volume change between 30 and 60 s under constant pressure in the pressuremeter test) versus the corrected pressure. The point where the creep volume is minimum

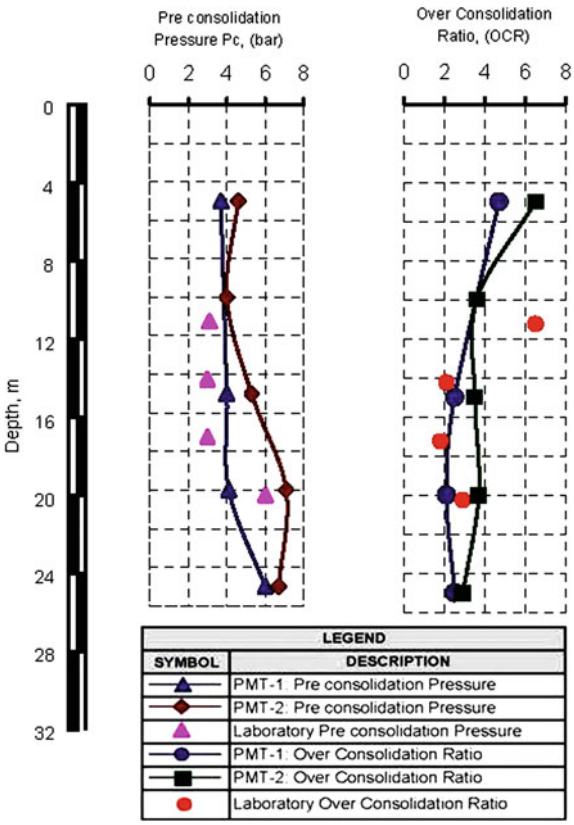

Fig. 8 Consolidation parameters versus depth

corresponds to the in situ horizontal stress. The value also corresponds to the liftoff point on the pressure versus volume curve (Clarke 1995).

Figure 9 presents a typical plot of creep volume versus pressure.

At the point of contact of the pressuremeter probe with the soil and expansion of cavity after overcoming the in situ horizontal stress, the creep volume is small. The creep volume again increases as the pressure in the soil approaches failure.

Plots of in situ horizontal stress versus depth as interpreted from the pressuremeter tests at the two test locations are presented on Figs. 10 and 11.

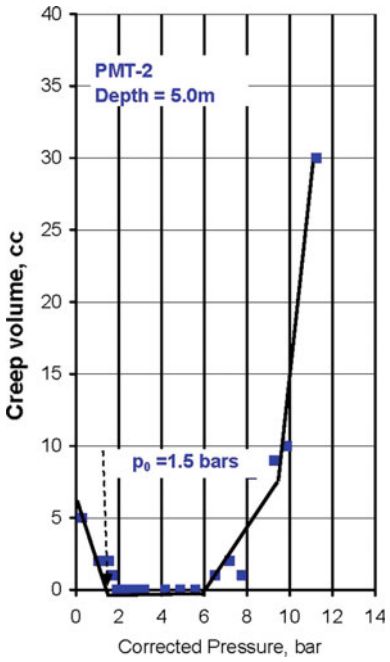

Fig. 9 Creep volume versus pressure

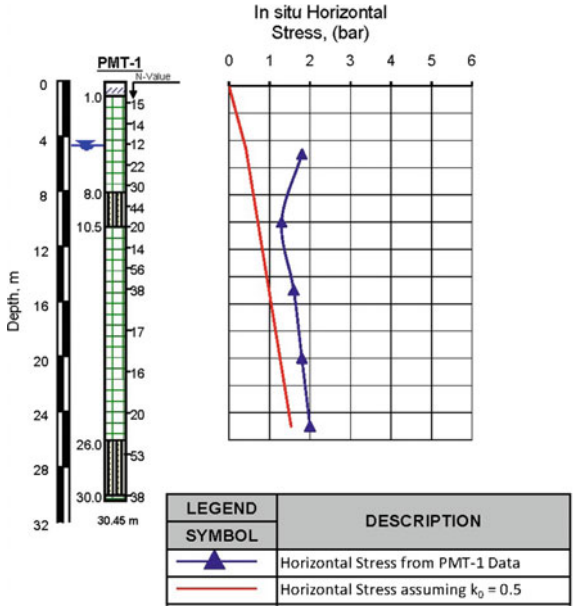

Fig. 10 In situ horizontal stress—PMT-1

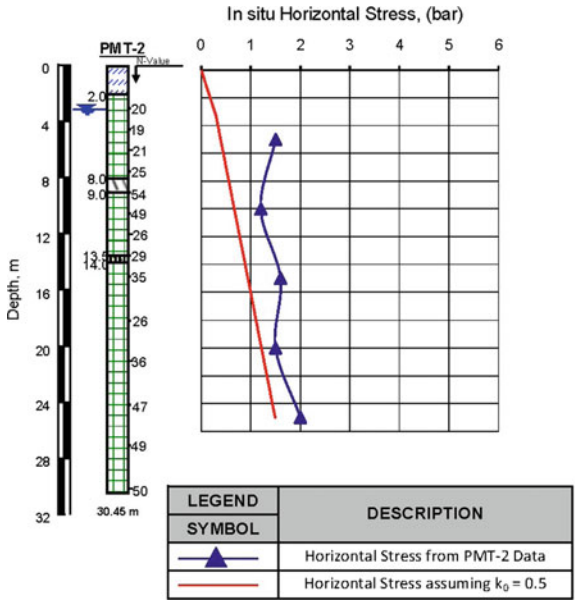

Fig. 11 In situ horizontal stress—PMT-2

The in situ horizontal stress computed as equal to overburden pressure multiplied by the coefficient of earth pressure at rest, k_0 (taken as equal to 0.5), is also presented on these graphs.

It may be seen that the in situ horizontal stress interpreted from pressuremeter is substantially higher than that conventionally computed considering k_0 as 0.5. k_0 from the pressuremeter is in the range of 2.2–2.5 at 5 m depth, 0.90–0.93 at 10 m depth below which k_0 is in the range of 0.63–0.68.

Table 2 summarizes the results of analysis.

5 Concluding Remarks

Pressuremeter test is a reliable in situ test to assess the geotechnical parameters for design. The interpreted shear strength and consolidation parameters for Delhi Silts (clay of low plasticity) show a good match with laboratory tests. The metro tunnel was designed effectively using these parameters.

Table 2 Pressuremeter data analysis for shear strength, consolidation parameters, and in situ horizontal stress

Test designation	Test depth, m	Soil classification	*N* values	Limit pressure (bars)	Deformation modulus (kg/cm^2)	Undrained shear strength (kg/cm^2)	Pre-consolidation pressure, p_c, (bar)	Over-consolidation ratio, (OCR)	In situ horizontal stress, (bar)
PMT-1	5.0	Sandy silt	12	10.6	102.6	1.06	3.7	4.7	1.8
	10.0	Silty sand	20	12.1	63.5	–	–	–	1.3
	15.0	Sandy silt	38	11.9	156.1	1.24	4.0	2.5	1.6
	20.0	Clayey silt	16	12.4	281.8	1.27	4.1	2.1	1.8
	25.0	Sandy silt	20	17.8	472.3	1.91	6.0	2.5	2.0
PMT-2	5.0	Sandy silt	20	12.4	234.1	1.32	4.6	6.5	1.5
	10.0	Sandy silt	14	10.8	152.8	1.16	4.0	3.6	1.2
	15.0	Sandy silt	27	15.0	203.4	1.62	5.3	3.5	1.6
	20.0	Sandy silt	30	19.4	446.5	2.16	7.1	3.7	1.5
	25.0	Sandy silt	36	19.7	524.4	2.13	6.7	2.9	2.0

References

Baguelin F, Jezequel JF, Shields DH (1978) The pressuremeter and foundation engineering. Trans Tech Publications, Clausthal

Clarke BG (1995) Pressuremeters in geotechnical design. Blackie Academic and Professional

Krishnan MS (1986) Geology of India and Burma. CBS Publishers, New Delhi

Non-destructive Intrinsic Self-sensing Method for Health Monitoring of Sub- and Superstructures

M. Vinothkumar and R. Malathy

Abstract Origination of cracks, deterioration and damages of structures such as bridges and tunnels has become a common problem. The loss of design strength due to the internal and external factors will lead to the origination of defects and cracks, and so continuous use of these structure results in collapse. The cracks and defects are repaired by implementing the rehabilitation methods at the right time, and the structures can be saved. Here, an effective monitoring technique to detect damage in concrete structures is discussed. Utilization of sensors for monitoring is not very appropriate because of the lifespan, economic aspect, and maintenance and sensitivity problems. Instead of using the sensors, a new technique, which uses self-diagnosing conductive material (the material which identifies the defects by itself), is adopted for monitoring the health of the structure. The stress–strain behaviour under loading condition is monitored using the sensing ability. The sensing ability of the diagnosing material was evaluated through the electrical conductivity test. The defect identification was done by uniaxial electrical test. The mechanical strength properties were evaluated through the compression test. The incorporation of diagnosing material enhances both the mechanical and sensing properties. The monitoring can be done periodically through the self-sensing ability.

Keywords Origination of cracks · Sensing ability · Stress–strain behaviour · Diagnosing material

M. Vinothkumar (✉) · R. Malathy
Department of Civil Engineering, Sona College of Technology,
Salem 636005, Tamil Nadu, India
e-mail: vinothkumarksr29@gmail.com

R. Malathy
e-mail: malathycivil@sonatech.ac.in

R. Sundaram et al. (eds.), *Geotechnics for Transportation Infrastructure*,
Lecture Notes in Civil Engineering 29,
https://doi.org/10.1007/978-981-13-6713-7_6

1 Introduction

The identification of origination of microcracks is one of the major critical works in the sub- and superstructures, especially in the underground tunnel and bridge structures. Identifying the origination of defects in concrete structures is most important and essential for ensuring the safety and stability of a particular sub- and superstructure. The process of establishing a method of damage prediction is generally known as a structural health-monitoring system (Farrar Ch 2007). Imparting the ability to the concrete to identify the origination of the cracks, defects and strain is known as intrinsic self-sensing method; the introduced concrete is called as self-sensing concrete (Han et al. 2015). The intrinsic self-sensing method is one of the innocuous methods to monitor the behaviour of concrete with respect to loading by itself without the requirement of any in-built, enclosed, or remote sensors (Chung 1998; Ou and Han 2009; Han et al. 2014a). The stress, strain, cracks and damages can be monitored by measuring the electrical resistivity of the intrinsic self-sensing concrete (Han et al. 2014a). The electrical resistivity measurement is one of the methods to recognize the defects, to conduct durability assessment, and to implement quality control of the concrete (Nadelman and Kurtis 2014; Claisse 2014). The origination and expansion of microcracks in concrete under loading condition were precisely identified by Ranade et al. (2014). Two kinds of phase are formed in intrinsic self-sensing concrete; one is formed by diagnosing material phase. The diagnosing material phase acts as conductive network, another phase is the aggregate phase which is used to provide the support to hold the functional filler. Han et al. (2014b, c) obtained a stable sensing response for concrete with nickel conductive powder and stated that concrete can serve as stress–strain sensors and the ordinary concrete is converted into self-sensing concrete by making use of the improved sensing ability of the concrete. Inada et al. (2005) evaluated the health of the structure by using self-diagnosing materials through the experimental studies.

In the present study, self-diagnosing conductive powder was used in the concrete as functional filler during the mixing stage of concrete. This conductive powder increased the sensing ability of the ordinary concrete. The conductive powder acted as functional fillers inside the concrete. An extensive conductive network was formed by the functional filler. The electrical behaviour of concrete is changed due to change of conductive network because of deformation of composites due to external loading. By measuring the variation in the electrical properties, the origination of the strain, cracks and damages due to static and dynamic loading can be monitored (Mao et al. 1996). Microseismic effect of these structures can be monitored by using these diagnosing materials through the electrical conductivity behaviour (Han et al. 2015; Chung 1998). In this research, three kinds of conductive powder, namely graphite, steel slag and coke breeze were tried, and their electrical conductivity behaviour was measured by electrical resistivity measurements. The origination of cracks could be identified by performing the electrical resistivity method. Different proportions of diagnosing materials were used in the concrete, and their sensing ability was identified in hardened concrete. Dielectric conductivity test was carried out to identify the

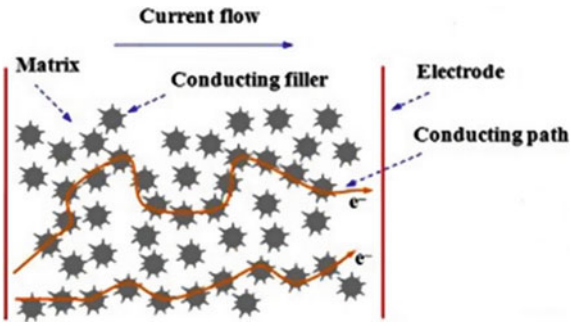

Fig. 1 Microstructure of concrete with filler diagnosing powder for sensing measurement

conductivity level of the diagnosing powder. Uniaxial electrical resistivity test was conducted for hardened concrete for defect identification. Compression test was conducted for M20 concrete with different mix proportions of conductive-powder-incorporated concrete as well as normal concrete to ensure the strength improvement. From Han et al. (2014a), Figure 1 depicts the conductive mechanism that takes place inside the structure.

2 Materials Used

In this study, the three kinds of diagnosing material were used to form the conductive network inside the concrete, i.e., steel slag, graphite powder, coke breeze. The physical properties of these materials are presented in Table 1, and the details of the material and their diagnosing abilities are described below.

2.1 Graphite Powder

Natural graphite is used as one of the diagnosing conductive materials. It occurs in metamorphic rocks, and also in igneous rocks (Anthony et al. 1990). It is a mineral consisting 5–40% of carbon (Kopeliovich 1982). Carbon imparts piezoelectric property to the concrete (Shi and Chung 1999). In the present study, flake type of graphite powder was used. The melting point of graphite is higher (3650 °C). Hence, it is used in experiments involving a wide range of temperatures.

Table 1 Properties of the diagnosing material

Properties	Steel slag	Graphite powder	Coke breeze
Specific gravity	3.4	2.46	3.26
Density (kg/m^3)	1663	1362	1532
Electrical resistivity (Ω cm)	5×10^{-3}	3×10^{-3}	1×10^{-3}

2.1.1 Diagnosing Ability of the Graphite Powder

Natural graphite exhibits higher conductivity for heat and electricity (Deprez and McLachlan 1998). The higher conductivity property enhances the diagnosing capacity. The diagnosing property is used to enhance the sensitivity of the functional filler. The electrical conductivity property of the graphite is used in the concrete to identify the defects and cracks through the electric field and electrical resistivity measurements. This conductive powder acts as a diagnosing material to pinpoint the origination of cracks. The graphite structure consists of hexagonal rings forming plates. The covalent bond is maintained between the carbon atoms and other three atoms in the plate. The outermost electron contains four valance electrons, out of the four three atoms from the covalent bonds. Remaining one electron does not constitute the covalent bond, and it is displaced from electron to electric field. These electrons attribute electrical conductivity to the graphite (Deprez and McLachlan 1998).

2.2 Steel Slag

It is a by-product of steel-manufacturing process. It is the one which is formed during depuration of the liquefied steel from contaminants in steel-manufacturing furnances. Initially, the slag occurs in the form of molten liquid melt which is a combined solution of silicates and oxides on cooling, and it becomes solidified. $4Fe + 3O_2 \rightarrow 2Fe_2O_3$ (Iron oxide), the Iron oxide mineral offers lower electrical resistivity to electrical and thermal. The addition of steel slag powder increases the density of the concrete. The increased density will be used to enrich the mechanical and durability property of the concrete (Arivoli and Malathy 2017; Collins and Ciesielski 1994).

2.2.1 Diagnosing Ability of the Steel Slag

The steel slag contains the content of Fe1-o, and other metal oxide which includes FeO, Fe_2O_3 and Fe_2O_4. The electrical resistivity of the FeO and Fe_2O_4 is 4×10^{-3} Ω cm which is nearly same as carbon fibre. As a result, the steel slag has also good electrical conductive property (Jia 2009). So, the presence of Iron oxide in the steel slag is used to enhance the electrical conductivity. The addition of steel slag to the concrete improves the electrical property of the concrete. Ordinary concrete will be converted into electrical conductive one by using the steel slag as one of the ingredients.

2.3 Coke Breeze

During the process of burning the coke or charcoal, a kind of light-weight powder is produced. It is known as coke breeze. Coke breeze can be used as filler in breeze concrete.

2.3.1 Diagnosing Ability of the Coke Breeze

Coke breeze is a common backfill material which is used for the cathodic production. It is one of the best carbonaceous materials. Coke breeze has high conductivity and very low resistivity. It has excellent mechanical strength enhancement property (Mohamed et al. 2002). When impressed current-type cathodic protection systems are used to mitigate corrosion on underground steel structures, the auxiliary anodes often are surrounded by a carbonaceous backfill. Backfill materials commonly used include coke breeze. The objective of the provision of backfill is to create the electron path for current flow, low resistivity and particle size. Low resistivity facilitates faster movement of electrons and the lower size of the particle will give the higher density of the concrete (Mohamed et al. 2002). Table 1 shows that the properties of the diagnosing material used in this study.

3 Experimental Programme

The different types of experiments were carried out to study the properties of the materials, sensing ability of the concrete and defect identification. The conducted experiments are explained below.

3.1 Dielectric Conductivity Test

This test was carried to determine the conductivity property of the diagnosing materials (Steel slag, graphite powder, coke breeze). Based on the conductivity value, the diagnosing capacity was confirmed. The conductive, diagnosing powder was taken in a crucible and subjected to compression. It was turned into pellets. The pellets were placed in between dielectric conductivity test setup plates. The test was carried out to determine the conductivity property of the diagnosing materials (steel slag, graphite powder, coke breeze). The conductive diagnosing powder was placed in the console of pelletizer equipment, and it was compressed and transformed into pellets. The pellets were placed in between the pair of dielectric conductive plates. The conductivity of the diagnosing substance in pellet forms was measured using the dielectric two-point conductivity test apparatus (Figs. 2 and 3).

Fig. 2 Pelletizer equipment for sample preparation

Fig. 3 Dielectric conductivity test arrangement

3.2 Uniaxial Electrical Test

The uniaxial technique is a more reliable method for evaluating the bulk electrical resistivity (Layssi et al. 2015). In this method, the voltmeter, Ammeter is connected with the root mean square (RMS), and the closed circuit is formed. The prepared concrete specimen is kept between the two parallel iron electrodes. The voltage

drop between the fixed electrodes is measured while applying the AC. Equation 1 describes the geometrical factor utilized in the method based on the cross section of the sample. The voltage drop was measured during the various loading conditions. Using the measured voltage drop, the resistivity was calculated using the Eq. 2.

$$k = A/L \tag{1}$$

where A is the cross-sectional area, and L is the length of the sample. The resistivity of the sample was calculated using the Eq. 2

$$R = V/I \tag{2}$$

The resistivity was determined by using the Eq. 3

$$\rho = k \times R \tag{3}$$

where R is a resistance, K is the geometrical factor, Eq. 3 shows the relation between resistance and resistivity. The geometrical factor depends on the size and shape of the sample, and the electrical resistivity was directly measured by using the above relation along with the voltage drop value. The prepared samples with different proportions (10, 20, 30 and 40% Replacement) and the normal concrete specimen were tested using this method. The electrical resistivity behaviour and the sensing ability were analysed. Figure 4 shows the test arrangement of uniaxial electrical test.

Fig. 4 Uniaxial electrical test arrangement

3.3 Compressive Strength Test

As per IS 516:1959, compression strength test was carried out to determine the mechanical strength of the prepared concrete specimen. Universal testing machine was employed for conducting this experiment.

4 Results and Discussion

The results of the conducted tests are discussed below.

4.1 Uniaxial Electrical Test

The uniaxial test was conducted to identify the ability of the sample to predict the damages which means through this test, and the change in electrical resistivity of the sample with respect to the gradual increase of compressive stress was found at different proportions of replacement for fine aggregate (10, 20, 30 and 40%). The change of resistivity value was noted at each level of loading for all the prepared samples. The initial electrical resistivity was decreased compared to the normal concrete while utilizing the diagnosing material and further the resistivity keeps on decreasing with application of load which shows that the formation of functional filler by diagnosing material inside the concrete is effectively working with good conductivity property. The different loads vs. electrical resistivity values were taken for all samples and given below.

4.1.1 Results of Graphite-Powder-Incorporated Concrete Sample

The following Fig. 5 shows the change of electrical resistivity of graphite-powder-incorporated concrete sample with respect to the applied compressive stress.

From the above observation, it is observed that the gradual increase of compressive stress leads to the gradual decrease of electrical resistance of graphite-powder-incorporated sample. Initially, the 10% replacement of graphite powder gives the higher electrical resistivity to the sample compared to the other replacements. But it is less compared to the normal concrete's resistivity. It means that the conductivity of the concrete is improved from the normal stage. At the particular level of compressive stress, the electrical resistivity starts to increase which indicate that the creak is originated. The replacement levels of graphite powder, i.e. 10, 20, 30 and 40% are reducing the initial electrical resistivity of the sample by 31, 36, 40 and 44%, respectively, from the normal stage.

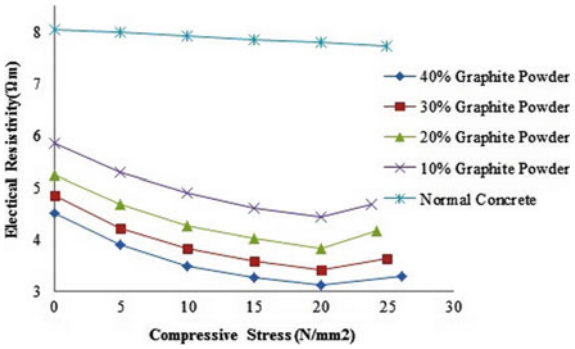

Fig. 5 Relationship between the electrical resistivity and compressive load for graphite-powder-incorporated concrete sample

4.1.2 Results of Steel-Slag-Incorporated Concrete Sample

Figure 6 shows the change in electrical resistivity of graphite with respect to applied compressive load.

From the electrical behaviour of the steel slag, it is observed that the increase in replacement level of steel slag leads to the decrease of electrical resistance of the sample. The initial-level replacement of 10% of steel slag gives a very less reduction of electrical resistivity of 4% compared to the normal stage. It means that the conductivity improvement is less compared to other diagnosing materials. For compressive stress of 25 N/mm^2, the resistivity of the concrete gets increased which indicates that the sample starts to get cracking. The replacement levels of steel slag, i.e. 10, 20, 30 and 40% to the fine aggregate, reduce the electrical resistivity of the sample by 4, 18, 24 and 32%, respectively, from the normal stage.

4.1.3 Results of Coke-Breeze-Incorporated Concrete Sample

Figure 7 shows the change in electrical resistivity of coke-breeze-incorporated concrete with respect to applied compressive stress.

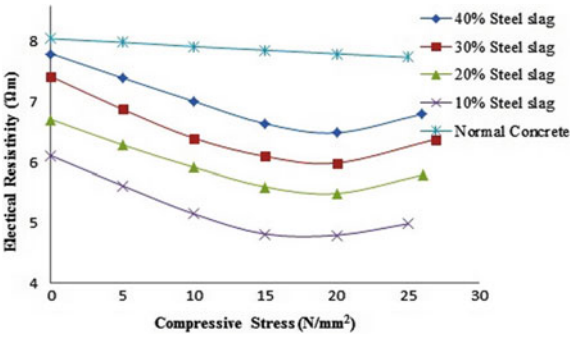

Fig. 6 Relationship between the electrical resistivity and compressive load for steel-slag-incorporated concrete sample

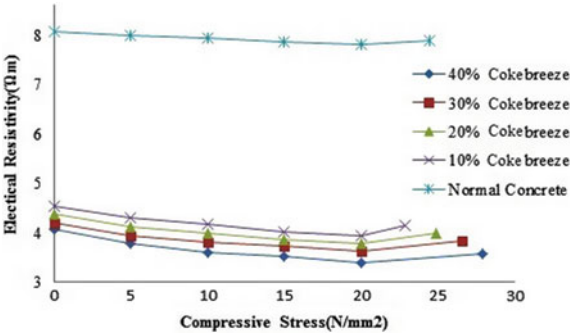

Fig. 7 Relationship between the electrical resistivity and compressive load for coke-breeze-incorporated concrete sample

From the above observation, the electrical resistivity behaviour of coke breeze was observed under loading condition. It is observed that the increase of compressive loading leads to the decrease of electrical resistance of the sample. It means that the conductivity of the concrete is improved from the normal stage. In this, the sudden increase of electrical resistivity occurs between the compressive stress increment of 20–25 N/mm^2, which shows that the above-said range. The replacement levels of coke breeze, i.e. 10, 20, 30 and 40% reduce the electrical resistivity of the sample by 42.6, 44.4, 46 and 49.3%, respectively, from the normal stage.

4.2 Compression Test Results

From the compression test, it is observed that the different diagnosing-material-mixed samples attain the peak strength at different proportions. The peak level of the strength was considered and charted as below. The steel slag mixture attains the peak value at 30% of replacement, and the graphite powder attains the peak strength for the replacement of 40%. The coke breeze attains the peak strength for the replacement of 30%. The following Fig. 8 shows the comparative result of diagnosing-material-incorporated concrete with normal concrete. The compressive strength of each diagnosing-material-incorporated concrete is varying due to the variation of the density level of the diagnosing powder.

5 Discussion

From the above tests, it is observed that the compressive strength of the samples attains the peak value at 30, 40 and 30% for the diagnosing material of steel slag, graphite and coke breeze, respectively. With respect to the compressive strength, the proportion of diagnosing material was fixed as below. Figure 9 shows the appropriate proportion of diagnosing material that can be used in the concrete for effective enhancement of the sensing ability as well as the mechanical property.

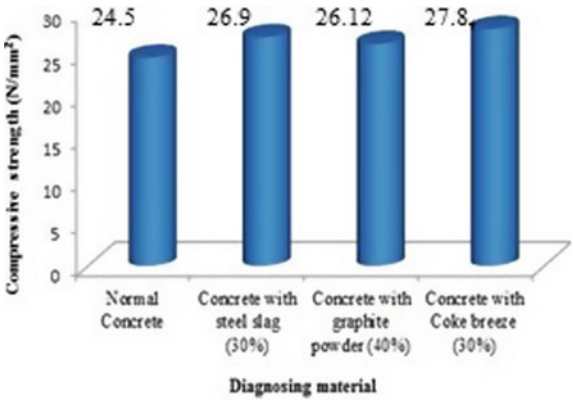

Fig. 8 Comparison chart for compressive strength of diagnosing-material-incorporated concrete and normal concrete

Fig. 9 Appropriate proportion of diagnosing material

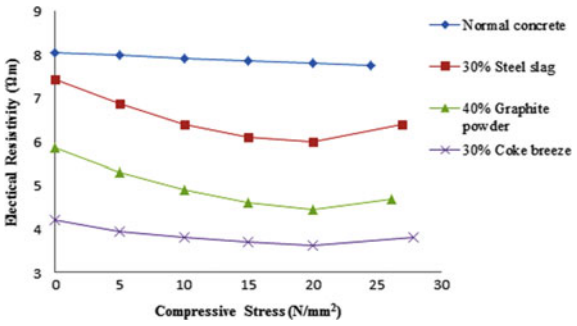

5.1 Application in Sub- and SuperStructures

The major sensitive structures like bridge, underground structure (tunnel, sewer pipes) and nuclear power plants need to be installed with proper health-monitoring system. The utilization of sensor for the health monitoring sometimes leads to failure because of the lifespan of the sensor, economic aspect, maintenance problem and missing homogeneity in the concrete, if it is embedded inside. Hence, instead of using the sensors, diagnosing conductive powder is used to study the stress–strain behaviour of the concrete under loading condition and the concrete homogeneous is also highly improved. The improved sensing ability, mechanical strength was obtained by this method. The origination of microcracks can be easily identified by making use of the change of electrical behaviour with respect to compressive stress. The subsequent studies recommend that an appropriate method needs to be implemented to assess the self-sensing ability. The self-sensing method is eco-friendly; because, it utilizes the industry waste products such as steel slag and coke breeze as it is components.

6 Conclusion

From the above results, it is observed that the increase of content of the diagnosing material is improving the conductivity property of the filler matrix in concrete; especially, the coke breeze reduces the initial electrical resistivity highly compared to other diagnosing materials. The different proportions of the conductive powder replacement by fine aggregate were tried like 10, 20, 30 and 40%. In each increment of the conductive powder, the electrical conductivity of the filler matrix is improved. The initial and subsequent resistivity of the concrete is comparatively decreased from the normal concrete. But the compressive strength of each proportion was tested and compared to the normal concrete. The higher strength improvement was attained for the particular proportion only like 30, 40 and 30% for steel slag, graphite, coke breeze, respectively. This proportion is prescribable for the final replacement of diagnosing materials. Finalization of the proportion of the conductive powder is based on the compression strength criteria as well as the sensing ability criteria. At the particular compressive stress, the gradual decrease of electrical resistivity starts to increase due to the gradual increase of loading which states that the crack is originated. In each loading condition, it is monitored that the electrical resistivity of the concrete is decreasing during the loading stage and it is increasing during unloading stage, which states that the concrete can serve as stress–strain sensors. The incorporation of diagnosing conductive materials with the concrete is improving the sensing ability, mechanical property and homogeneity of the concrete. The novelty of this paper is the appropriate method for health monitoring of concrete structures without using any sensors have been discussed. The appropriate method was identified and selected for conducting the electrical resistivity measurement. The appropriate diagnosing materials were selected based on the sensitivity and electrical behaviour, mechanical strength property eco-friendly and sustainability for the formation of the filler matrix inside the concrete. The relative application areas were identified and prescribed.

References

Anthony JW, Bideaux RA, Bladh KN, Monte C (eds) (1990) Handbook of mineralogy (PDF). "Graphite"

Arivoli M, Malathy R (2017) Optimization of packing density of M20 concrete with steel slag as coarse aggregate using fuzzy logic. Arch Metall 3:1903–1913

Ch Farrar R, Worder K (2007) An introduction to structural health monitoring. Philos Trans R Soc A 365:303–315

Chung DDL (1998) Self-monitoring structural materials. Mater Sci Eng Rep 57–78

Claisse PA (2014) Letter: using electrical testes as durability indicator. Concr Int 36:10

Collins RJ, Ciesielski SK (1994) Recycling and use of waste materials and by products in Highway construction. National cooperative highway Research Program synthesis of highway practices 199, Transportation Research board, Washington

Deprez N, McLachlan DS (1998) The analysis of the electrical conductivity of graphite powder during compaction. J Phys D Appl Phys 101–107 (Institute of physics)
Han BG, Yu X, Ou JP (2014a) Multifunctional and smart nanotube reinforced cement based materials, Chapter 1. In: Gopalakrishna K, Bergeson B, Taylor P, Attoh-Okine NO (eds)
Han B, Yu X, Ou J (2014b) Nickel powder based self-sensing concrete, Chapter 9. In: Self-sensing concrete in smart structures. Elsevier Publications, pp 271–313
Han B, Ding S, Yu X (2014c) Challenges of self-sensing concrete, Chapter 11. In: Self-sensing concrete in smart structures, vol 59. Elsevier Publications, pp 361–376
Han B, Ding S, Yu X (2015) Intrinsic self-sensing concrete and structures: a review, vol 59. Elsevier Publications, pp 110–128
Inada H, Okuhara Y, Kumagai H (2005) Health monitoring of concrete using self-diagnosing materials. In: Sensing issues in civil structural health monitoring. Springer, Berlin, pp 239–248
Jia XW (2009) Electrical conductivity and smart properties of $Fe_{1-\sigma}$ o waste mortar. Dissertation for the doctor degree in engineering, Chongqing University, China
Kopeliovich D (1982) Substances and technologies. Knowledge sources on material science. www.subtech.com
Layssi H, Ghods P, Alizadeh AR, Saleehi M (2015) Electrical resistivity of concrete-concepts, applications, and measurement techniques. Concr Int
Mao QZ, Zhao BY, Sheng R, Li ZQ (1996) Resistance changement of compression sensible cement specimen under different stresses. J Wuhan Univ Technol 11:41–45
Mohamed FM, EI Hussiny NA, Shalabhi MEH (2002) Granulation of coke breeze fine for using sintering process. Sci Sinter 42:193–202
Nadelman EI, Kurtis KE (2014) A resistivity-based approach to optimizing concrete performance. Concr Int 36:50–54
Ou JP, Han BG (2009) Pezoresistive cement based strain sensors and self-sensing concrete components. J Intell Mater Syst Struct
Ranade R, Zhang J, Lynch JP (2014) Influence of micro cracking on the composite resistivity of engineered cementaneous composites. Cem Compos Res 58:1–12
Shi ZQ, Chung DDL (1999) Carbon fiber-reinforced concrete for traffic monitoring and weighing in motion. Cem Concr Res 29:435–439

Use of Ground-Penetrating Radar (GPR) as an Effective Tool in Assessing Pavements—A Review

Ruchita Salvi, Ajinkya Ramdasi, Yashwant A. Kolekar and Lata V. Bhandarkar

Abstract In recent times, the road network in India is increasing rapidly and has become main route of transportation for goods and people. This has led to the boom in economic activities leading to greater tonnage being carried by the road. Further, this is assisted with the increase in road network by constructing new highways and increasing the traffic capacity of the existing highways/roads. The quality of roads and the thickness of each layer need to be designed properly to cater to this increased traffic movement and the tonnage too. GPR assists in quality assessment and interpretation of pavement conditions more precisely. With the use, the pavements generally tend to have problems, viz. cracking, roughness, rutting, and raveling over a period of time. To enhance the life of pavement, improve its riding quality, and minimize the maintenance requires thorough investigations of the existing pavements. Previously, investigations were carried out using visual observation of base course, core extraction, and its examination in the laboratory for which the core is extracted from the rutted section of roads. The methods used conventionally are time consuming, difficult to perform, and also not economical. So geophysical method such as ground-penetrating radar (GPR) is an alternative to the conventional methods, and being nondestructive, it is less difficult, time consuming, and also economical to use which gives detailed information about the

R. Salvi · A. Ramdasi · Y. A. Kolekar (✉)
Department of Civil Engineering, College of Engineering Pune, Pune, India
e-mail: yashwantkolekar@gmail.com

R. Salvi
e-mail: ruchitassalvi456@gmail.com

A. Ramdasi
e-mail: ramdasi.ajinkya@gmail.com

L. V. Bhandarkar
Department of Physics, College of Engineering Pune, Pune, India
e-mail: blv.physics@coep.ac.in

R. Sundaram et al. (eds.), *Geotechnics for Transportation Infrastructure*,
Lecture Notes in Civil Engineering 29,
https://doi.org/10.1007/978-981-13-6713-7_7

pavement layer thickness, measurement of depth of rebar, dowel, etc., without much disturbance to the existing traffic movement. Thus, GPR can be used effectively in estimating total deteriorated sections and repair estimates.

Keyword Ground-penetrating radar (GPR)

1 Introduction

This paper describes the various studies carried out to understand the usage of GPR for assessing the quality of pavement and provide useful information to the engineer. The applications and problems discussed by various authors guide us to understand the recent developments in the GPR technique. This paper provides an insight into the applicability, limitations, and future scope for development of GPR as an effective tool in assessing the quality of the pavement and its improved understanding.

2 Ground-Penetrating Radar (GPR)

The ground-penetrating radar (GPR) is based on principle of radar where the source transmits electromagnetic (EM) waves with frequency varying from 10 MHz to 2.5 GHz into pavements. These EM waves reflect some of the waves through layer of material having different EM characteristics. EM waves which reflect back are received by receiver of GPR system which is shown as a plot of amplitude and time.

The passing speed of EM wave through a particular material is under the influence of its relative dielectric constant (ε_r). Surface reflection method is used for asphalt pavement materials, and relative dielectric constants are calculated.

The values of materials' relative dielectric constants are calculated, and the thickness of the particular layers (h_i) is found using equation:

$$h_i = \frac{c\Delta t_i}{\sqrt{\varepsilon_r}} \tag{1}$$

where c—speed of EM wave through vacuum

1. Δt_i—time between amplitudes A_i and A_{i+1}
2. ε_r—relative dielectric constant of the material.

EM signal can be sent up to 1000 scans/second.

3 GPR Principle

The reflected energy is collected and displayed as a waveform showing amplitudes and time elapsed between wave transmission and reflection (Fig. 1).

The determination of the pavement layer thickness is most successful application of the GPR. By "picking" the first peak of the reflected electromagnetic wave and knowing the layer dielectric constant (μ) and travel time (t) in nanoseconds, the thickness is determined (Al-Haddad and Abed 2013).

$$h(\text{in}) = 11.8 * t/\sqrt{\varepsilon} \tag{2}$$

Generally, the amplitude of the reflected pulses is used. With the help of the dielectric constant in air which is equal to (1), the subsurface layer dielectric constant can be calculated from

$$\sqrt{\varepsilon_1} = \frac{A_\text{m} + A_0}{A_\text{m} - A_0} \tag{3}$$

where

A_0 and A_m are the reflected amplitudes from the top of surface layer and the metal plate, respectively.

The dielectric constant of the subsequent layer is calculated from

$$\sqrt{\varepsilon_2} = \sqrt{\varepsilon_1}\frac{1 - \left(\frac{A_0}{A_\text{m}}\right)^2 + \frac{A_1}{A_\text{m}}}{1 - \left(\frac{A_0}{A_\text{m}}\right)^2 - \frac{A_1}{A_\text{m}}} \tag{4}$$

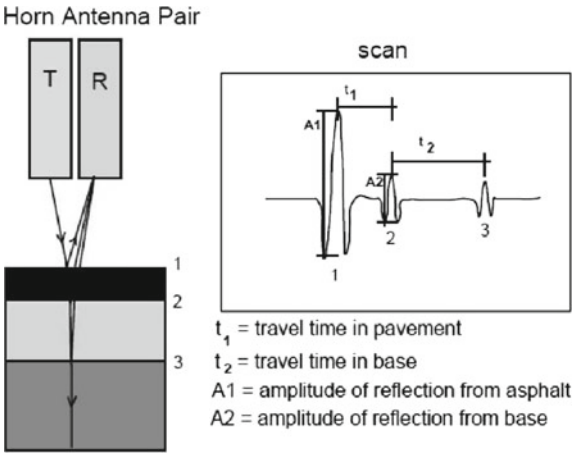

Fig. 1 Basic principle of GPR technique with horn antenna for pavement examination; T represents the transmitting antenna and R the receiver antenna. Interface 1 presents the air–asphalt interface, 2 presents the asphalt–base course interface, and 3 presents the base–sub-base interface (Al-Haddad and Abed 2013)

where A_1 is the reflected amplitude from the top of subsequent layer; moreover, a similar formula can be recursively obtained for the nth layer

$$\sqrt{\varepsilon_n} = \sqrt{\varepsilon_{n-1}} \frac{1 - \left(\frac{A_0}{A_m}\right)^2 + \sum_{i=1}^{n-2} y_i * \frac{A_i}{A_m} + \frac{A_{n-1}}{A_m}}{1 - \left(\frac{A_0}{A_m}\right)^2 - \sum_{i=1}^{n-2} y_i * \frac{A_i}{A_m} + \frac{A_{n-1}}{A_m}} \tag{5}$$

where

A_i is the reflected amplitude from the top of ith layer, and y_i is the reflection coefficient between the ith and $i + 1$th layers and can be calculated using the following equation:

$$y_i = \frac{\sqrt{\varepsilon_i} + \sqrt{\varepsilon_{i-1}}}{\sqrt{\varepsilon_i} - \sqrt{\varepsilon_{i-1}}} \tag{6}$$

The ranges of propagation velocities and dielectric constants for the pavement materials are given in Table 1.

4 Types of GPR

GPR is available in various types depending on the nature of work and application required. The principle of physics involved in GPR is based on the principles of propagation of electromagnetic waves, but different hardware and data processing

Table 1 Dielectric constants and propagation velocities for various pavement materials (Cao et. al 2011)

Material	Dielectric constant	Propagation velocities (m/ns)
Air	1	0.3
Ice (Frozen soil)	4	0.15
Granite	9	0.1
Limestone	6	0.12
Sandstone	4	0.15
Dry sand	4–6	0.12–0.15
Wet sand	30	0.055
Dry clay	8	0.11
Wet clay	33	0.052
Asphalt	3–6	0.12–0.17
Concrete	9–12	0.087–0.10
Water	81	0.033
Metal	∞	0

procedures are employed in different GPRs. The commercial and the most commonly used is "Impulse" GPR system, which transmits a short pulse of electromagnetic energy and records the time taken for reflections of the pulse to return to a receiver. Other varieties of GPR have different engineering applications, and these varieties are not suitable for assessing the quality of pavements.

Antennas are available in various ranges for GPR, and the most commonly used for impulse systems are "dipole" antenna which acquire data in time domain, requiring contact with the pavement surface (ground coupled) and "horn" antenna, are capable to operate while suspended at a short distance above the pavement surface (air coupled).

The greater depth of penetration (for a given signal frequency) is accomplished by the ground-coupled dipole antennas, whereas for higher data acquisition rates, air-coupled horn antennas facilitate higher speed surveys.

Horn antennas are more suitable, when the top layers of a pavement are to be evaluated for quality assessment, whereas ground-coupled dipole antennas are designed to be used near the surface so that the power radiated into the surface or medium is maximum possible and hence more suitable for thicker pavements (e.g., airports) or where information about the pavement foundation too is also required.

The purpose of this paper is to get data for land development, site selection, and other related activities using nondestructive modern sophisticated technology, in economical way. Greater accurate results in shorter time frame are achieved using these techniques.

The GPR type used in the field work is RAMAC GPR produced by MALA Company for geosciences as shown in Figs. 2 and 3.

Fig. 2 GPR setup

Fig. 3 Working of GPR

5 Methodology

- A grid will be generated on the ground manually at a suitable interval using paint/chalk.
- GPR antennas of different frequencies will be dragged on the grid lines by the GPR operator, who will be carrying the machine along with one laptop computer on his shoulder. Electromagnetic waves will be penetrated and received through the antenna. Acquired data will be stored in the laptop computer as soft files, and laptop will have a digital display of the GPR profile at the site itself.
- GPR antennas of different frequencies will be dragged on the grid lines by the GPR operator, who will be carrying the machine along with one laptop computer on his shoulder. Electromagnetic waves will be penetrated and received through the antenna.
- Acquired data will be stored in the laptop computer as soft files, and laptop will have a digital display of the GPR profile at the site itself.

6 Application of the Technique (Evans et al. 2008)

Different types of information can be extracted using GPR depending upon techniques used. The site needs to be decided to work upon so that the engineer and the GPR specialist can think upon the methodologies to be incorporated to obtain the optimum information from the site. Although GPR is self-sufficient equipment to provide information regarding pavements, various pavement investigations such as FWD or coring of pavements are done along with GPR testing so that the data obtained at site by GPR and pavement investigations can complement each other.

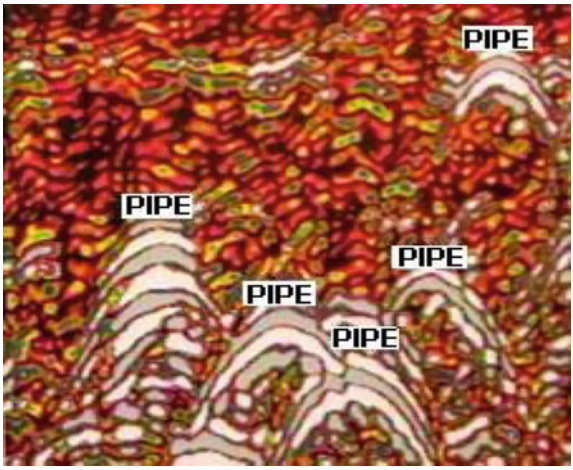

Fig. 4 Raw data showing signature of pipes by GPR (Geomodel)

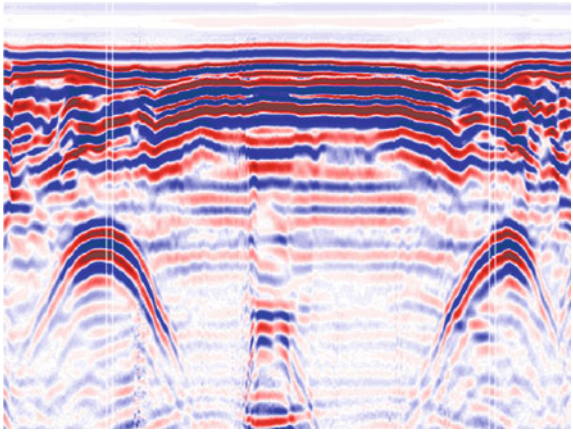

Fig. 5 Processed image of signature of pipes (Parsan)

6.1 To Find Underground Utilities

Deeper depths are reached using antennas with low frequencies from 25 to 200 MHz obtain subsurface reflections from (about 10–30 m or more), at the cost of low resolution. But with higher frequencies from 300 to 1000 MHz obtain shallow depths reflection (0 to about 30 feet), with have high resolution. These high-frequency antennas are used to investigate surface soils and to locate small or large, shallow buried objects in concrete (Figs. 4 and 5).

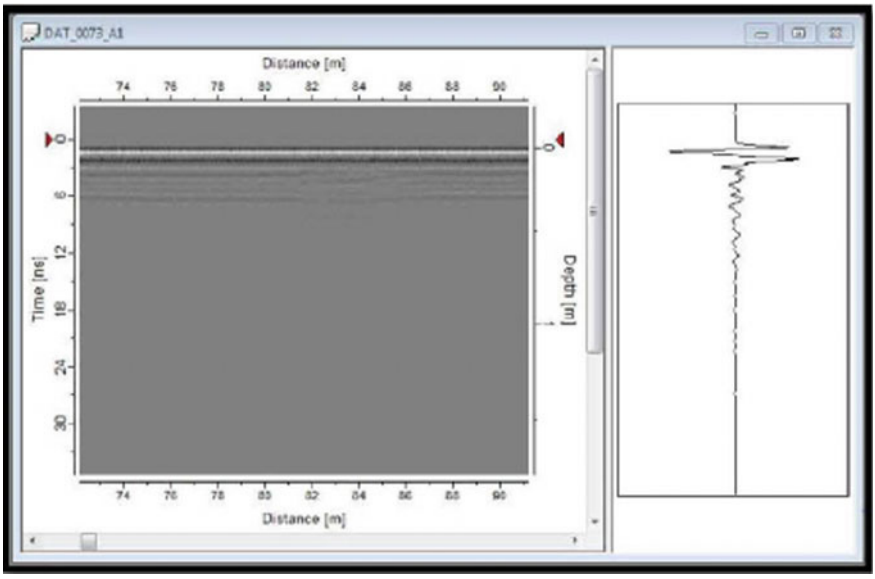

Fig. 6 Raw data of pavement (Al-Haddad and Abed 2013)

6.2 *Pavement Thicknesses*

GPR is used in calculating pavement thickness of a freshly laid pavement or an existing worn-out pavement. The different strata are identified based on the contrast in the dielectric properties at material interfaces. The interface between asphalt roads and subgrade is easily identified as compared to the interface between concrete pavement and subgrade; this is due to the similarity in the dielectric properties of the cement-bound material with the granular subgrade (Figs. 6 and 7).

6.3 *Quality Control*

GPR plays a vital role is assessing the quality of the newly laid pavement. They are used effectively to assess air-void content (i.e., percentage of air in the material mix), segregation of aggregates (which can be identified from the localized areas of low density material), which can be the result from poor mixing or unfair construction practices), and density of bound materials in addition to quality control of pavements that involves determination of layer thicknesses. The density and compaction of bituminous material are greatly affected by the presence of air voids, which is an important factor affecting the life and deformation properties of the pavements.

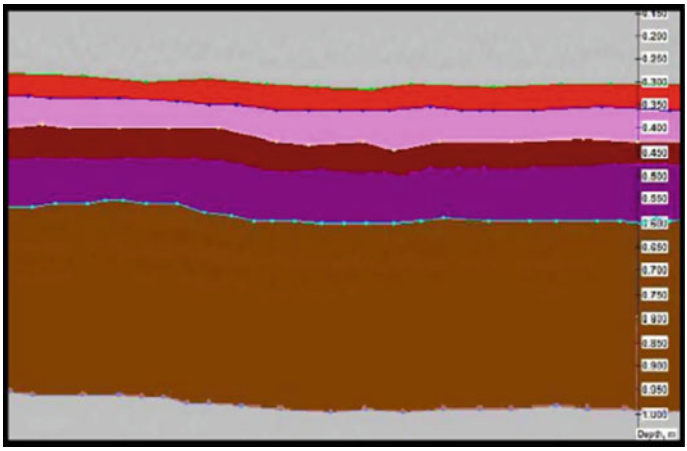

Fig. 7 Pavement profile after processing (Al-Haddad and Abed 2013)

6.4 Voids

GPR offers a useful tool for the detection of voids in the pavements of subgrade. The study shows the potential of a ground-coupled dipole antenna which is a relatively low-frequency (400 MHz) antenna used in GPR to locate voids as small as 50 mm in depth and locate other voids beneath reinforcement, although drilling and coring are recommended to determine the extent and depth of the void.

7 Accuracy and Limitation

(a) The accuracy of depth is normally within ±15%, while *X*–*Y* accuracy would be within ±5%. Accuracy in position can be improved by deploying positioning system.
(b) Georadar method cannot differentiate between a power cable (live or dead)/ telephone cable or OFC, metallic/nonmetallic/concrete utility. Hence, it is always essential to have all the background information like information on expected cables or pipes.
(c) It can give very tentative idea about the d out the diameter of the utility.
(d) The measurements of the Georadar are based on the returning signals reflected by a dielectric constant change. The signal penetration (maximum depth at which utility can be detected) depends on the dispersion of the signal in the soil. Hence, in clay, the depth of penetration would be least, while in sand it would be high.

(e) To detect larger objects, such as sewer lines, usually buried at greater depths, a low-frequency antenna (300 MHz) is used (depth range 2–10 m), while to detect smaller objects usually at lesser depths, a high-frequency antenna (500 MHz) is used (depth range 0.5–5 m).
(f) The minimum size that can be detected is related to antenna frequency and is limited to 1/8th of the signal wavelength. Hence, a 500-MHz antenna will detect objects larger than 30 mm dia. And a 100-MHz antenna will detect objects larger than 150 mm.
(g) While Georadar is the most efficient method for utility mapping, some objects can elude detection for various reasons, as mentioned below: Two objects very close to each other can be perceived as only one object.

  (i) An object located under another object/utility may not be seen.
  (ii) In a small boulder-type filling, a branch-off pipe or cable could be missed as confused with the surrounding rocks.
  (iii) A utility coming in and leaving the corridor between two survey lines could be missed, particularly if its presence is not expected.
  (iv) A highly conductive soil and or landfill areas could limit the penetration to the desired depths.

Similarly pavements covered with RCC slabs can also limit the signal penetration. A small corridor width under investigation could elude detection of a large diameter utility as confused with the soil bedrock interface.

8 Conclusion

As a part of geotechnical engineering, pavements have large number of uncertainties which could limit the use of nondestructive testing methods in respective field areas, but introduction of GPR has contributed to predict the uncertainties likes voids, thickness, and quality control analysis to ease and also to provide a solution more precisely. Though it is nondestructive, it yields more information and accurate data because of its precision which has helped to solve various problems of fields specifically related to pavements.

References

Al-Haddad AHA, Abed AA (2013) Evaluation of pavement layer thickness for Al-Kut-Baghdad rural highway using ground penetrating radar. Int J Struct Civil Eng Res 2(3). ISSN 2319 – 6009

Cao Y, Labuz J, Guzina B (2011) Evaluating a pavement system based on GPR full-waveform simulation. In: TRB 2011 annual meeting

Dai S, Yan Q (2014) Pavement evaluation using ground penetrating radar. In: Pavement materials, structures, and performance, ASCE 2014 GSP 239

Domitrović J, Rukavina T (2013) Application of GPR and FWD in assessing pavement bearing capacity. Rom J Transp Infrastruct 2(2)

Evans R, Frost M, Stonecliffe-Jones M, Dixon N (2008) A review of pavement assessment using ground penetrating radar (GPR). In: 12th international conference on ground penetrating radar, Birmingham, UK, 16–19 June 2008

Scullion T, Saarenketo T (1998) Applications of ground penetrating radar technology for network and project level management systems. In: 4th international conference on managing pavements

Part II
Use of Geosynthetics, and Non-Traditional Materials in Transportation Geotechnics

Analytical Modeling of Indian-Made Biodegradable Jute Drains for Soft Soil Stabilization: Progress and Challenges

Kirti Choudhary, Cholachat Rujikiatkamjorn, Buddhima Indraratna and P. K. Choudhury

Abstract Installation of vertical drains in soft soil is probably the most popular preloading method of ground improvement today. These drains reduce the consolidation time of the soil by providing alternative pathways to relieve the pore water pressure in the soil quickly thus reducing construction time. Jute drains have been introduced as an environmentally friendly alternative to synthetic drains in recent times. However, owing to higher absorption capacity of jute and their tendency to degrade in soil their consolidation behavior can be vastly different from that of synthetic drains. In this review, the paper provides in detail the properties of jute drains along with significant developments that have been achieved over the years in understanding their consolidation behavior. The clogging and degradation behavior in these drains is investigated in relation to the limitations in analytical modeling. This article aimed to discuss not only the challenges associated with modeling this phenomenon but also suggests approaches by which this problem can be solved.

Keywords Analytical modeling · Ground improvement · Jute drains · Preloading · Soft soil stabilization

K. Choudhary · C. Rujikiatkamjorn (✉) · B. Indraratna
Ph.D. Candidate, Centre for Geomechanics and Railway Engineering, School of Civil Engineering, University of Wollongong, NSW, Australia
e-mail: cholacha@uow.edu.au

K. Choudhary
e-mail: kc966@uowmail.edu.au

B. Indraratna
e-mail: indra@uow.edu.au

P. K. Choudhury
National Jute Board, Calcutta, India
e-mail: jutegeotech@gmail.com

R. Sundaram et al. (eds.), *Geotechnics for Transportation Infrastructure*,
Lecture Notes in Civil Engineering 29,
https://doi.org/10.1007/978-981-13-6713-7_8

1 Introduction

Prefabricated vertical drains (PVDs) remain one of the most popular methods of ground improvement for soft clays (Walker et al. 2012; Geng et al. 2012). These drains relieve pore pressure in the ground by providing a horizontal pathway to water by taking advantage of the anisotropy of soil permeability (Indraratna et al. 2014). Although a number of models have been proposed over the years to simulate the consolidation behavior aided by synthetic drains, a number of challenges exist in analytical modeling for natural drains such as those made of Jute. These challenges primarily occur due to higher absorption capacity of jute and their tendency to degrade in soil. Natural fibers such as jute are typically composed of α cellulose, hemicellulose, and lignin which make the fiber highly hygroscopic. This is in contrast to synthetic drains which are typically made of polyester or polyethylene and are hydrophobic in nature. Cellulose typically breaks down into smaller compounds in the presence of extreme chemical environments. Saha et al. (2012) reported that the degradation of jute fibers is extremely rapid outside the pH range of 4–9. Since soils are typically acidic in nature, these fibers start to degrade after a period of about 6–9 months depending on the acidity of the soil. This phenomenon of degradation tends to reduce the efficiency of natural drains overtime as compared to synthetic drains which are known to last in soil for a period of 12–15 years (Mininger et al. 2011).

Extensive testing to understand the effect of degradation was performed at University of Wollongong (on jute drains provided by National Jute Board of India, NJBI) which includes large scale consolidometer testing of different types of jute drains as well as wick drains at different stages of consolidation and post-processing tests to ascertain the degree of consolidation. To the authors' knowledge, large-scale consolidometer testing in natural prefabricated vertical drains was only carried out once by Asha and Mandal (2015) but that study was largely focused on the effect of compressive stress on the consolidation efficiency of jute drains. Some of the aspects of the study were discussed in this article. A summary of the drains tested in the experimentation program is provided in Fig. 1 and Table 1.

Fig. 1 Jute drains used in the study (drain 1, 2 and 3 from left to right as per Table 1)

Table 1 List of prefabricated jute drain (PVJDs) tested

Sample No.	Type of PVJD
1	Inter-woven with jute wick 145 g/m
2	Inter-woven with jute wick 92 g/m
3	Inter-woven with coconut coir 115 g/m

Figure 2 shows the differences of settlements for all the cases. It can clearly be seen that Drain 3 performs the best among all the jute drains, and its performance is nearly identical to that of the synthetic drain. Apart from the three types of jute drains mentioned here, a fourth type (PVJD with jute filter coconut coir) was used in the successive consolidation test mentioned later. Based on consolidation test up to 24 months, jute drains perform well considering the fact that degradation happens in these drains.

A review of the challenges associated with modeling consolidation in natural drain sis discussed, and it is suggested the approaches by clogging and degradation can be taken into account. This can significantly improve the modeling accuracy of these drains as most of the existing theoretical or numerical models tend to overestimate the reduction in pore pressure with time as compared to field data.

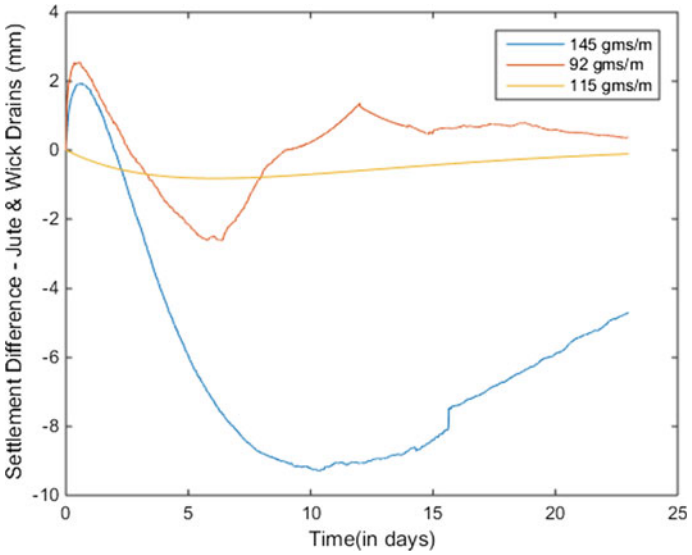

Fig. 2 Differences in settlements of PBJDs that of synthetic wick drain

2 Clogging in Vertical Drains

The drain filter surrounding the core primarily serves two functions during the consolidation process: (1) prevent soil particles from entering the core and (2) allow maximum flow of water inside the core so as to allow for maximum possible drainage through the core. For an effective drainage system, a soil filtration system should develop around the drain filter so that any further transport of particles to the core is prevented. The development of such a filtration system is critical to the long-term performance of the drain.

The ability of development of such a filtration system is dependent upon a number of factors such as (McGown 1976):

- Physical and chemical characteristics of the filter jacket
- Soil Characteristics
- Magnitude of external loads or stresses applied on the system
- Hydraulic conditions in and around the filter jacket.

To achieve the required filtration system, a number of criteria were proposed as to what should be the ideal ratio of filter opening to that of the particle size distribution of the soil. One such criteria was given by Carroll (1983) which states that the O_{95} value of the filter AOS should be less than approximately 2–3 times the D_{85} of the soil. Here O_{95} refers to the 95% of the opening size of the geotextile and D_{85} refers to the soil grain diameter at 85% passing based on particle size analysis.

$$\frac{O_{95}}{D_{85}} \leq 2 - 3 \tag{1}$$

A number of such criteria were summarized and reported by Bergado et al. (1996).

When the effective filter is unable to develop, finer particles in the soil can flow with the water and permeate the filter jacket of the drain to reach the core. This deposition of particles on the filter and in the core leads to the development of an adverse hydraulic potential in the soil near the filter which is detrimental to the flow of water inside the core leading to a reduction in the rate of the consolidation process.

3 Theory of Radial Consolidation

3.1 Barron's Theory of Consolidation

Barron (1948) gave the solutions for both the equal strain case and the free strain case based on the work of Terzaghi (1925) by considering the flow profiles into and out of an infinitesimally small cylindrical element. The generalized three-dimensional equation of consolidation is given by:

$$\frac{\partial \bar{u}}{\partial t} = C_{\mathrm{v}}\left(\frac{\partial^2 u}{\partial z^2}\right) + C_{\mathrm{h}}\left(\frac{\partial^2 u}{\partial r^2} + \frac{1}{r}\frac{\partial u}{\partial r}\right) \tag{2}$$

For radial flow only, this equation becomes:

$$\frac{\partial \bar{u}}{\partial t} = C_{\mathrm{h}}\left(\frac{\partial^2 u}{\partial r^2} + \frac{1}{r}\frac{\partial u}{\partial r}\right) \tag{3}$$

where $\bar{u}$ is the average excess pore water pressure, t is time, r and z are the cylindrical coordinates, C_{v} and C_{h} are vertical and horizontal coefficient of consolidation, respectively, and u is the excess pore water pressure at a given location.

The solution of this equation is obtained using method of separation of variables which results into complicated expressions of u dependent on Bessel functions of the first and second kind similar to the solutions of the heat transfer equation in cylindrical coordinates. Solutions were also given for the cases where smear and well resistance were included. However, the solutions are cumbersome to compute, and hence for brevity, the mathematical analysis was not discussed here.

3.2 Approximate Equal Strain Solution Proposed by Hansbo (1981)

Another equal strain solution was developed by Hansbo (1981) using the equal strain theory, the approximate degree of consolidation (U_{h}) of a soil cylinder consolidated by a vertical drain can be expressed as,

$$U_{\mathrm{h}} = 1 - \exp\left(-\frac{8T_{\mathrm{h}}}{\mu}\right)$$

where the time factor (T_{h}) is given by,

$$T_{\mathrm{h}} = \frac{C_{\mathrm{h}} t}{d_{\mathrm{e}}^2}$$

where C_h is the horizontal coefficient of consolidation, t is time and d_{e} is the diameter of the influenced zone. The parameter μ is given by the following expression:

$$\mu = \ln\left(\frac{n}{s}\right) + \left(\frac{k_{\mathrm{h}}}{k_{\mathrm{s}}}\right)\ln(s) + \pi z(2l - z)\frac{k_{\mathrm{h}}}{q_{\mathrm{w}}} - 0.75 \tag{6}$$

Here k_{h} and k_{s} are the permeability of the undisturbed zone and smear zone, respectively, q_{w} is the discharge capacity of the drain, l is the height of the vertical

drain, n is the ratio of the diameter of the influenced zone to that of the drain and s is the ratio of the diameter of the smear zone to that of the drain.

The second and the third terms in the equation represent the effect of smear and well resistance of the drain, respectively. If these effects are ignored, the value of μ simplifies to

$$\mu = \ln(n) - 0.75 \tag{7}$$

4 Incorporating Clogging in Modeling of Vertical Drains

Clogging in vertical drains is a time-dependent phenomenon that significantly reduces the efficiency of vertical drains in dissipating excess pore water pressure at the soil–drain interface. In the past, analysis of clogging was restricted to a physical modeling of the particle interface interactions and migration. Considering mass and momentum conservation principles, one can relate properties such as particle size distribution, mass flow rate, and filter capacity to changes in permittivity of the filter medium (Xiao and Reddi 2000). Since it is difficult to model the random arrangement of voids in the filter, assumptions regarding its structure are made and they are usually modeled as a cubic or tetrahedral arrangement. The most fundamental analysis is probably the Kozeny-Carman and the Ergun equations (McCabe et al. 2005; Akgiray and Saatçi 2001)

$$\Delta P = \frac{kV_s\mu(1-\epsilon)^2 L}{\phi_s^2 D_p^2 \epsilon^3} \tag{8}$$

$$\Delta P = \frac{150V_s\mu(1-\epsilon)^2 L}{D_p^2\epsilon^3} + \frac{1.75\rho V_s^2(1-\epsilon)L}{D_p\varepsilon^3} \tag{9}$$

where D_p is the diameter of the particle, ϕ_s is the sphericity of the particles in bed, ϵ is the porosity of the filter bed, V_s is the superficial velocity, μ is the viscosity of the fluid, L is the height of the filter bed, k is a numerical constant, and ΔP is the pressure drop across the bed.

Another approach of assessing the permeability of the filter as a function of time is to assume the probabilistic deposition of soil particles in nature. Xiao and Reddi (2000) developed a clogging model based on the assumption that the pores in the filter are long cylinders and asserted that the deposition process of a particle inside these cylinders is a probabilistic process controlled by a lumped parameter. However, the determination of the parameters for different geotextiles is challenging. The lumped parameter for synthetic geotextiles might be different by an order of magnitude in comparison with natural geotextiles.

A similar argument can be given for physical models such as those developed by Locke et al. (2001), these models usually deploy empirically derived equations for

determining viscosity interactions. Such empirical models are usually relevant for a very narrow domain and cannot be generalized for different categories of soils and geotextiles encountered in real engineering problems.

5 Degradation Modeling of Jute Vertical Drains

Indraratna et al. (2016) show that there are two parameters affected by degradation of vertical drains; one relates to the discharge capacity, q_w and others relating to the drain length l and its equivalent diameter d_w. While traditional theory applied to radial consolidation (e.g., Hansbo 1981) assumes these parameters to be unchanged or constant during the period of consolidation, in situ degradation makes these parameters time-dependent, hence, adversely affecting the rate of soil consolidation.

The approach elucidated hereinto incorporate degradation of natural jute drains was proposed earlier by Indraratna et al. (2016). The assumption of time invariance of the discharge capacity during consolidation is ignored. Although the reduction in discharge capacity may be influenced by a number of factors, e.g., the characteristics of natural fibers and the soil pH (Kim and Cho 2009), it is further assumed that the degradation process starts immediately upon drain installation. In this context, Indraratna et al. (2016) modeled the rate of degradation of jute drains as an exponential function with time.

In the long term, due to complete degradation, the jute drain simply becomes a tube of concentrated organic matter whose discharge capacity is practically undefined. Therefore, q_w becomes synonymous with soil permeability. Again, for a simplified solution, constant geometric parameters for the jute drain are assumed over time; thence by geometrically integrating the flow through the whole unit cell, one should be able to obtain the same results as those obtained for a conventional synthetic (prefabricated) vertical drain, PVD. As suggested earlier by Indraratna et al. (2015), the average excess pore pressure of the unit cell u can be written as:

$$u = \frac{\int_0^l \int_{r_w}^{r_s} u_s(2\pi r)\mathrm{d}r\mathrm{d}z + \int_0^l \int_{r_s}^{r_e} u_u(2\pi r)\mathrm{d}r\mathrm{d}z}{V} \tag{10}$$

In Eq. (10), u_s and u_u are the excess pore pressures in the disturbed zone and the undisturbed zone, respectively; the geometric quantities r_w, r_s and r_e are the radii of the vertical drain, the disturbed zone, and influence zone, respectively; V is the volume of a unit cell having a radius r_e and a length, l, to determine its magnitude by $V = \pi\left(r_e^2 - r_w^2\right)l$.

Having integrated and re-arranged Eq. (10), the time-dependent average excess pore pressure $u(t)$ is then given by (Indraratna et al. 2016):

$$u(t) = \frac{\gamma_w}{2k_{h,a}} \frac{d_e^2}{4} \left(\mu_{n,s,a} + \mu_{q,a}\right) \frac{\partial \varepsilon}{\partial t} \tag{11}$$

In the above, ε is the vertical strain of the unit cell; $\mu_{n,s,a}$ captures the effects of the smear (disturbed) zone and the drain influence zone, $\mu_{q,a}$ represents the role of reduced discharge capacity, and γ_w is the unit weight of water in the ground (can be brackish in floodplains). As proposed by Indraratna et al. (2016), the magnitudes of $\mu_{n,s,a}$ and $\mu_{q,a}$ can be determined algebraically as:

$$\begin{aligned} \mu_{n,s,a} &= \frac{n^2}{n^2-1}\left[\ln\left(\frac{n}{s}\right) + \frac{k_{h,a}}{k_{s,a}}\ln(s) - \frac{3}{4}\right] \\ &\quad + \frac{s^2}{n^2-1}\left[1 - \frac{s^2}{4n^2}\right] + \frac{k_{h,a}}{k_{s,a}}\left(\frac{1}{n^2-1}\right)\left[\frac{s^4-1}{4n^2} - s^2 + 1\right] \\ \mu_{q,a} &= \frac{2}{3}\pi\frac{k_{h,a}}{q_{w,a}(t)}l^2\left(1 - \frac{1}{n^2}\right) \approx \frac{2}{3}\pi\frac{k_{h,a}}{q_{w,a}(t)}l^2 \end{aligned} \tag{12}$$

In the above, $q_{w,a}(t)$, is a function that captures the decrease of the drain discharge capacity over time, and its introduction by Indraratna et al. (2016) here makes the solution different to traditional methods.

The well-known relationship between the dissipation of excess pore water pressure (EPP) and the compressibility of soil can also be written as shown below:

$$\frac{d\varepsilon}{dt} = -m_v \frac{du}{dt} \tag{13}$$

where m_v is the coefficient of volume compressibility for one-dimensional compression. By substituting (13) into (11) and re-arranging, the following expression can be obtained:

$$u + \frac{\gamma_w m_v}{2k_{h,a}} \frac{d_e^2}{4} \left(\mu_{n,s,a} + \mu_{q,a}\right) \frac{du}{dt} = 0 \tag{14}$$

As shown by Indraratna et al. (2016), Eq. (14) is an ordinary differential equation with variable time t and it can be generalized as follows.

$$u + f(t)\frac{du}{dt} = 0 \tag{15}$$

In the above, the general function $f(t)$ is written as:

$$f(t) = \chi_a\left(\mu_{n,s,a} + \frac{\lambda_a}{q_{w,a}(t)}\right) \tag{16}$$

where

$$\chi_{\mathrm{a}} = \frac{\gamma_{\mathrm{w}} m_{\mathrm{v}} d_{\mathrm{e}}^2}{8k_{\mathrm{h,a}}} = \frac{d_{\mathrm{e}}^2}{8c_{\mathrm{h,a}}}$$

$$\lambda_{\mathrm{a}} = \frac{2}{3}\pi k_{\mathrm{h,a}} l^2$$

The general solution for Eq. (15) yielding the average EPP u_{a} at time t with a given form of discharge capacity reduction $q_{w,a}(t)$, can then be represented by:

$$u_{\mathrm{a}}(t) = u_{\mathrm{o}} \exp\left(- \int_0^t \frac{1}{f(t)} \mathrm{d}t \right) \tag{17}$$

Further details of the model derivation and discussion can be found elsewhere in Indraratna et al. (2016).

6 Behavior of Jute Drains in Comparison with Synthetic Drain: Field Study

The National Soft Soil Field Testing Facility has been established at Ballina, NSW and is managed by the Australian Research Council Centre of Excellence for Geotechnical Science and Engineering (ARC-CGSE) for conducting various geotechnical trials and soil property investigations (Pineda et al. 2016). A trial embankment: 3 m high, 80 m long, and 15 m wide crest with a side slope set to be 1.5H: 1V was constructed. A working platform, 95 m long, 25 m wide, and 1 m thick, was laid on the existing ground surface to provide drainage. The embankment is divided into 3 sections: two sections are 30 m long and consist of conventional PVD and Jute PVD (biodegradable drain); the third section is 20 m long and consists of conventional PVD with a synthetic drain, but no sand drainage layer. Jute drains were installed in one of the sections to compare its performance with synthetic drains. Vertical drains were installed on a nominally 1.2 m square grid.

As shown in Fig. 3, irrespective of the different properties of jute drains compared to polymeric wick drains, the measured settlement, excess pore water pressure for both drains are very similar to each other. Although the performance of jute drains can be affected by the pyritic (acidic) soil conditions at shallow depths (1–2), the jute drains used in this embankment have more than adequate discharge capacity; hence, the pore pressure dissipation rates between the two types of PVD are expected to be similar, albeit some biodegradation of the jute drains is expected after about 6 months as shown in the recent laboratory experiments at the University of Wollongong, and also verified by examining a jute drain recovered from the Ballina site.

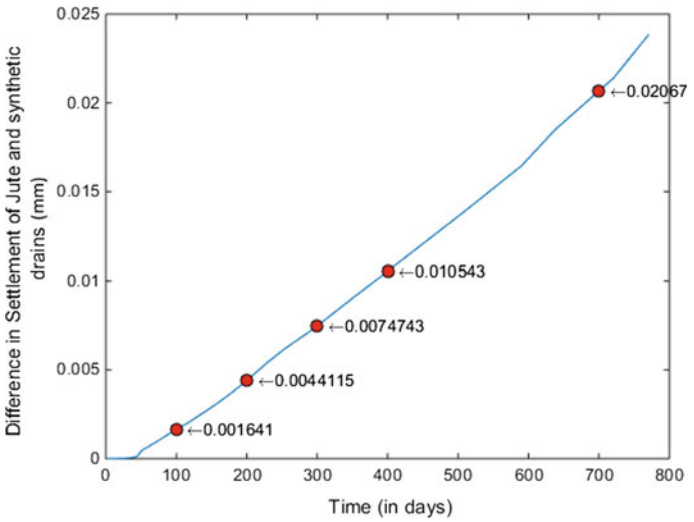

Fig. 3 Comparison of jute and synthetic drain data in terms of settlement

7 Conclusion

A number of analytical models proposed in the literature were reviewed and their limitations with respect to modeling natural drains were discussed in detail. The primary issue that limits these numerical models is the lack of provision for modeling clogging and degradation in natural vertical drains and even if such provisions are available their applicability to real-world data is highly limited. Although the applicability of these models to synthetic drains was verified consistently, very few field studies of Jute drains were reported in the literature and hence their verification becomes difficult. It was to bridge this gap that the Ballina field study was carried out incorporating the study of consolidation behavior of both synthetic and jute drains supplied by the National Jute Board of India. Highly acidic soil and groundwater conditions can exacerbate biodegradation in the presence of acidophilic bacteria. Even then, the rate of biodegradation of jute drains may become seriously significant only after about 1.5–2 years upon installation. However, by this time, the consolidation of soft soils would most likely attain a high level of degree of consolidation (i.e. say >95% of primary consolidation). Ballina field trial shows that the degradation of jute drains does not affect the consolidation efficiency even after a year.

Acknowledgment This research was supported (partially) by the Australian Government through the Australian Research Council's Linkage Projects funding scheme (project LP140100065). The authors also acknowledge the National Jute Board of India (NJBI), Coffey, Douglas Partners, Soilwicks, and Menard Oceania for funding of this research. The Authors would to acknowledge kind permission from Elsevier to reuse some excerpts obtained from Indraratna et al. (2016) in this paper.

References

Akgiray Ö, Saatçı AM (2001) A new look at filter backwash hydraulics. Water Sci Tech: Water Supply 1(2):65–72

Asha BS, Mandal JN (2015) Laboratory performance tests on natural prefabricated vertical drains in marine clay. Proc Inst Civil Eng Ground Improv 168(1):45–65

Barron RA (1948) Consolidation of fine-grained soils by drainwells. Trans ASCE 113(2346): 718–724

Bergado DT, Anderson LR, Miura N, Balasubramaniam AS (1996) Soft ground improvement in lowland and other environments. ASCE Press, ASCE, New York, USA, p 427p

Carroll RG Jr (1983) Geotextile filter criteria. Transp Res Rec 916:46–53

Geng XY, Indraratna B, Rujikiatkamjorn C (2012) Analytical solutions for a single vertical drain with vacuum and time-dependent surcharge preloading in membrane and membraneless systems. Int J Geomech 12(1):27–42

Hansbo S (1981) Consolidation of fine-grained soils by prefabricated drains. In: Proceedings of the 10th international conference on soil mechanics and foundations engineering, Stockholm, Sweden, pp 677–682

Indraratna B, Nimbalkar S, Rujikiatkamjorn C (2014) From theory to practice in track geomechanics —Australian perspective for synthetic inclusions. Transp Geotechn 1(4):171–187

Indraratna B, Nguyen TT, Carter J, Rujikiatkamjorn C (2016) Influence of biodegradable natural fibre drains on the radial consolidation of soft soil. Comput Geotech 78:171–180

Indraratna B, Sathananthan I, Rujikiatkamjorn C, Balasubramaniam AS (2015) Analytical and numerical modeling of soft soil stabilized by prefabricated vertical drains incorporating vacuum preloading. Int J Geomech 5(2):114–124

Kim JH, Cho SD (2009) Pilot scale field test for natural fiberdrain. In: Li G, Chen Y, Tang X (eds) Geosynthetics in Civil and Environmental Engineering. Springer, New York, pp 409–414

Locke M, Indraratna B, Adikari G (2001) Time-dependent particle transport through granular filters. J Geotech Geoenviron Eng 127(6):521–528

McCabe WL, Smith JC, Harriot P (2005) Unit operations of chemical engineering, 7th edn. McGraw-Hill, New York, pp 163–165

McGown A (1976) The properties and uses of permeable fabric membranes. In: Lee, Ingles, Yeaman (eds) Proceedings of the workshop on materials and methods for low cost road, rail and reclamation works. University of New South Wales, Australia, pp 663–710

Mininger KT, Santi PM, Richard D (2011) Life span of horizontal Wick drains used for landslide drainage. Environ Eng Geosci 17(2):103–121

Pineda J, Suwal L, Kelly R, Bates L, Sloan S (2016) Characterization of Ballina Clay. Geotechnique 66(7):1–22

Saha P, Roy D, Manna S, Adhikari B, Sen R, Roy S (2012) Durability of transesterified jute geotextiles. Geotext Geomembr 35:69–75

Terzaghi K (1925). Erdbaumechanik auf Bodenphysikalischer Grundlage. Franz Deuticke, Liepzig-Vienna

Walker R, Indraratna B, Rujikiatkamjorn C (2012) Vertical drain consolidation with non-Darcian flow and void ratio dependent compressibility and permeability. Géotechnique 62(11):985–997

Xiao M, Reddi LN (2000) Comparison of fine particle clogging in soil and geotextile filters. Proc Geo-Denver 2000. https://doi.org/10.1061/40515(291)12

Characterization of Cement Stabilised Flyash for Use as Structural Layer in Rural Road Pavements

Anusree Bhowmik and Umesh Chandra Sahoo

Abstract Though flyash has been used as a fill material and stabilizing material in road construction, studies on its use in bulk quantity for construction structural layers (i.e. subbase and base) are very limited. In the present study, an attempt has been made to use flyash and stone dust mixture (70:30 ratio) and stabilized with cement as a structural layer material for use in rural road pavements. To address the brittleness of the stabilized material, polypropylene fibers were also added as reinforcing material. Mechanical properties of the stabilized material, in terms of unconfined compressive strength, flexural strength, indirect tensile strength, flexural modulus (E_{flx}), Poisson's ratio (μ) were evaluated to assess the suitability of the material. Durability tests were also conducted on the samples to meet the specifications. Results indicate that, cement stabilized flyash-stonedust mix can be suitably used for construction of subbase and base layers of rural road pavements.

Keywords Flyash · Cement · Stabilization · Rural roads · Pavement

1 Introduction

In India, power supply mostly comes from thermal power plants where coal is feed into the boiler and as a residue in this process huge amount of flyash is generated. This flyash is usually dumped on wastelands and leachates generated from it have been polluting the surrounding area and water bodies. Fly ash, with an estimated production of about 200 MT per year and maximum usage of 60% is demanding our attention to explore suitable methods for bulk usage of flyash as a construction material.

A. Bhowmik (✉) · U. C. Sahoo
School of Infrastructure, Indian Institute of Technology, Bhubaneswar 752050, Odisha, India
e-mail: ab28@iitbbs.ac.in

U. C. Sahoo
e-mail: ucsahoo@iitbbs.ac.in

R. Sundaram et al. (eds.), *Geotechnics for Transportation Infrastructure*,
Lecture Notes in Civil Engineering 29,
https://doi.org/10.1007/978-981-13-6713-7_9

In India, class F flyash is mostly generated, which contains less than 10% calcium oxide and requires an activator like cement, lime, gypsum or other alkali activators (like NaOH, KOH, Na_2O) for cementing action. These activators create an environment of minimum pH 13, which is desired for the dissolution of flyash. Cement or lime present in mixture provide ample supply of $Ca(OH)_2$ which reacts with the dissolved silicates and aluminates (SiO_2, Al_2O_3) in the fly ash to form the C–S–H gel. This pozzolanic property of flyash makes it an excellent material for use as a soil stabilizer. Many researched carried out investigations on use of flyash stabilized with lime or cement for use in subgrade and some cases in subbase (Ghosh and Subbarao 2006; Kumar and Singh 2008; Poran and Ahtchi-Ali 1998). Xu and Sarkar (1991) observed that gypsum activated cement stabilized flyash has more densified structure compared to unstabilized one.

Researchers pointed out the long term strength gain of lime stabilized flyash. A significant increase in UCS values of lime stabilized flyash compared to unstabilized one after 90 days curing was reported by Ghosh and Subbarao (2007). Fraay et al. (1990) established a threshold pH value of 13 to dissolve the silicates and aluminates in flyash. Attempts were also made to determine tensile strength, modulus of rupture and durability aspects of lime stabilized flyash (Sobhan and Mashnad 2002; Behera and Mishra 2012). Kumar and Singh (2008) successfully used fiber reinforced cement stabilised flyash in rural road sub-base. They studied the effect of randomly reinforced polypropylene fiber on UCS, CBR, modulus of elasticity and on permanent-resilient strains. Shear strength parameters of fiber reinforced soil flyash samples were studied by Kaniraj and Havanagi (2009). Performance evaluation of soil stabilized with fly ash were conducted by various researchers (Kaniraj and Havanagi 2009; Lav and Lav 2001), which reported good performance.

Studies on use of flyash in bulk quantity for construction of pavement structural layers (i.e. subbase and base) are limited. Considering the huge length of rural roads are being constructed under PMGSY, an attempt has been made in the present study to use cement stabilized flyash-stone dust mixture (70:30) as a structural layer material in rural road pavements. Cement stabilised flyash layer does not come under conventional stabilised granular layer and it does not satisfy gradation and material characteristics required for cement stabilization as per IRC: SP 89. To use this unconventional inferior material in structural layers of low volume roads reinforcing I done with fiber and then stabilizing with cement. After that mechanical properties of the stabilized material, in terms of unconfined compressive strength, flexural strength, indirect tensile strength, flexural modulus (E), Poisson's ratio (μ) were evaluated to assess the suitability of the material.

2 Material and Methodology

2.1 Materials

As flyash is of very low unit weight, stone dust was added in certain proportion. This composite material was then mixed with different percentage of cement to improve its mechanical properties. Polypropylene fibers were incorporated to address the brittle behaviour of cement stabilized flyash samples. So the main inputs are flyash, stone dust, cement and polypropylene fibers.

Composition	Representation
80% Flyash + 20% Stone dust, without fiber	80 FA-20 SD-0 PP
70% Flyash + 30% Stone dust, without fiber	70 FA-30 SD-0 PP
60% Flyash + 40% Stone dust, without fiber	60 FA-40 SD-0 PP
70% Flyash + 30% Stone dust, with 12 mm fiber	70 FA-30 SD-12 PP

The details of ingredients used in this study are given below:

2.1.1 Flyash (FA)

Fly ash was collected from National Aluminium Corporation (NALCO) Angul, Odisha. This flyash is classified as class F according to ASTM C 618. Particle size distribution of the flyash is given in Table 1. Based on the gradation, it may be classified as MLN-MIN (combination of Non-plastic inorganic coarse silt sized fractions and non-plastic inorganic medium silt sized fractions). Flyash is a cohesionless material. Liquid limit and plastic limit of flyash could not be found out. As per standard plastic limit test flyash could not be rolled into thread and sample disintegrated while cutting groove for liquid limit determination. So plasticity index could not be determined.

Table 1 Physical properties of NALCO flyash. Adapted from Sridharan and Prakash (2007)

Properties	% fraction by total weight	
Sand sized fraction	16.67	
Silt sized fraction	Fine silt	4.73
	Medium silt	5.91
	Coarse silt	69
Clay sized fraction	3.70	

2.1.2 Stone Dust (SD)

Stonedust used in the present study were basically granite dust obtained from crusher with maximum particle size of 4.75 mm. Based on gradation, it can be designated as poorly graded sand (SP).

2.1.3 Cement

Ordinary Portland Cement (OPC) 43 grade confirming to IS 8112 (1989) has been used in this study.

2.1.4 Polypropylene Fiber (PP)

Non-water absorbent high density polypropylene fibers, resistant to alkalis, acids and chemicals was used in this study. Aspect ratios (AR = length/diameter) of fiber is 500 and the fiber content was taken to be 0.5% by weight of mix.

2.2 Methodology

2.2.1 Compaction Test

Standard Proctor compaction tests were conducted in accordance with ASTM D 698-92 (1992). The samples were compacted in a 1000 cc mould in 3 layers and with compaction energy of 600 kN m/m^3. Flyash is a cohesionless material and we are intending it to use in low volume roads, so modified compaction test is not performed in this study.

2.2.2 pH Test

The measurement of pH was carried out using pH meter (make: Systronics, India) with an accuracy up to ± 0.02 units. As suggested by several researchers (Fraay et al. 1990; Alexander et al. 1954) a minimum pH of 13 was considered in this study.

2.2.3 Unconfined Compressive Strength (UCS)

The specimens prepared for UCS test were of 38 mm diameter and 76 mm long. Two series of sample were prepared. In series 1, FA to SD ratio varied among 80:20, 70:30 and 60:40 with 0% fiber and with 2, 4 and 6% cement by total weight

of mix. In series 2 PP fiber @0.5% of total was added to series 1. Samples prepared in OMC-MDD were kept wrapped in polyethylene sheets to prevent moisture loss. The tests were conducted as per ASTM D 2166-85 at a strain rate of 1.25 mm/min.

2.2.4 Indirect Tensile Strength (ITS)

Indirect diametral tensile tests (IDT) were carried out with 100 mm dia. samples Loading rate of 1 mm/min was used.

2.2.5 Poisson's Ratio

In this study Poisson's ratio was determined by ITS test samples in accordance with the study by Paul and Gnanendran (2016). Cyclic haversine loading at 30% of failure load (as load deformation response of the material was linear up to 40% of failure load) obtained from monolithic ITS on frequency of 1 Hz at 25 °C has been used. Specimen was conditioned for first 1000 cycles to eliminate possible permanent deformation accumulation (Allen 1973). A thin hard iron strip of width 12 mm was used for uniform distribution of load over entire depth of sample. Two LVDT's on surface of specimen along horizontal and vertical diameter, as shown in Fig. 1, are placed to measure deformation of horizontal and vertical diameters.

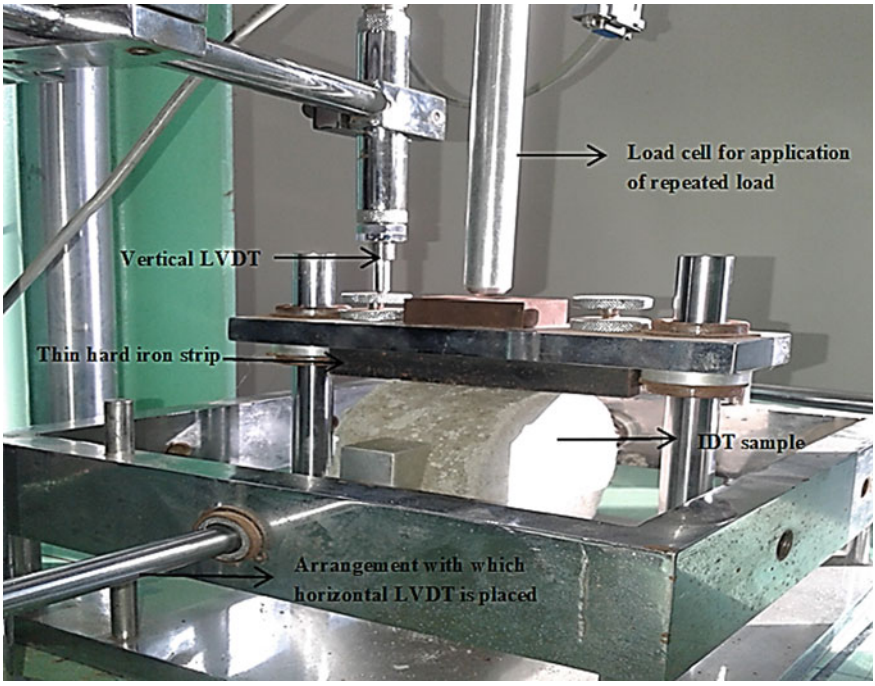

Fig. 1 IDT test set up for determination of Poisson's ratio

Poisson's ratio was calculated using relationship (Eq. 1) developed by Paul and Gnanendran (2016). Dynamic stiffness modulus from IDT was also found out using Eq. (2) in order to investigate the differences of various moduli values.

$$\mu = \frac{-c_g - a_g \frac{\delta v}{\delta h}}{d_g + b_g \frac{\delta v}{\delta h}} \tag{1}$$

$$E_{IDT} = \frac{p}{t\delta h}\left(a_g + b_g \mu\right) \tag{2}$$

where, P = Cyclic load applied in N (30% of failure load at ITS), t = thickness of the sample (60 mm), μ = Poisson's ratio, E_{IDT} = dynamic stiffness modulus from ITS testing (MPa), δv and δh are deformation along vertical and horizontal diameter in mm. a_g, b_g, c_g and d_g are constant values which are dependent on gauge length (distance between gauge points at which Linear variable differential transformers (LVDT) are placed) to diameter ratio of sample. In our test condition this ratio is 1, and therefore, constant values are chosen accordingly.

2.2.6 Flexural Modulus

Bottom up cracks are the primary mode of failure for stabilised layers. General of bottom up cracks are controlled by flexural modulus of the layer. So flexural modulus (E_{flx}) will be used for design purpose. Determination of flexural modulus was done according to the method described in NCHRP report 789 (2014). Figure 2 shows the flexural modulus test setup used in the present study. Beam specimens (75 mm × 75 mm × 285 mm) were subjected to haversine cyclic load of 100 cycles with a peak load which is equal to 30% of failure load of beam samples determined from flexural strength test. The load was applied at 1 Hz frequency at 25 °C. A contact load of 1 N was applied on the specimen to prevent rocking action. A linear variable differential transformer (LVDT) was placed at center of beam to measure the central deflection. The first 50 cycles are considered as pre-conditioning. The flexural modulus of the specimen was determined by averaging data from the second 50 consecutive cycles. Flexural modulus (E_{flx}) was calculated as follows:

$$E_{flx} = \frac{23PL^3}{108bd^3\delta h} \tag{3}$$

where, E_{flx}= flexural modulus in MPa, P = Cyclic load given to specimen (N), L = length of beam (mm), b = average width of beam (mm), d = average depth of beam (mm), and δh = peak displacement at mid-span (mm).

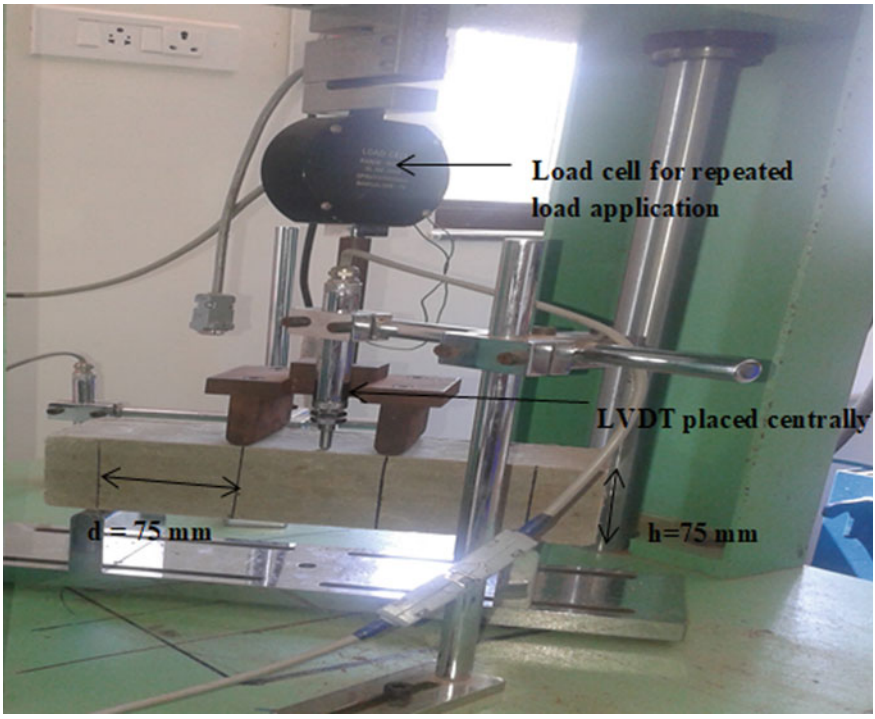

Fig. 2 Flexural modulus test setup

2.2.7 Durability Test

The Wetting-Ddying (W-D) durability of any material primarily depends on its pore structure. As water moves in and out of pore network of the specimen during W-D cycling, the pore walls experience capillary pressure and may collapse. Mechanical brushing was found to be inadequate for finer materials like flyash. In absence of any standard test for checking the performance of cement stabilized flyash, durability tests as given by Usmen and John (1990) was adopted. After 10 cycles of alternate wetting-drying, residual UCS values were found out after 7 days and 28 days of curing. One cycle consisted of 5 h soaking (at 25 °C) then 42 h oven drying at 72 °C. To simulate more destructive effect (Kampala et al. 2008) the samples were immerged in water at room temperature for 2 h before UCS testing.

3 Results and Discussion

The following section present the results obtained through various investigations carried out on cement stabilized FA-SD mixture. Figure 3 shows compaction curve with and without fiber (excluding cement variation as addition of small % of cement will not vary OMC-MDD much) for different FA-SD composition. Inclusion of fibers at 0.5% ratio had little impact on OMC of mixes as the fibers are non-water absorbent. Moreover, tests were conducted to check whether the composition is maintaining a minimum pH of 13 or not; else, other alkali activator would have been used. From Fig. 4, it can be observed that OPC cement satisfies the criterion whereas Portland slag cement (PSC) needs 1% NaOH to be added to satisfy the criteria.

Based on UCS test results of series 1 samples (Fig. 5), highest values were recorded with FA:SD ratio of 70:30 composition was found to deliver highest strength. This may be attributed to the particle size distribution of 70FA:30SD curve, which was a typical well graded curve. The particle packing will be better compared to other compositions. As per MORD guidelines a material is suitable for the use in low volume roads if the 7-day UCS value is more than 1.76 MPa for subbase and 3.0 MPa for base course. Here, for 70FA:30SD, it satisfies the condition for stabilized base with 6% cement.

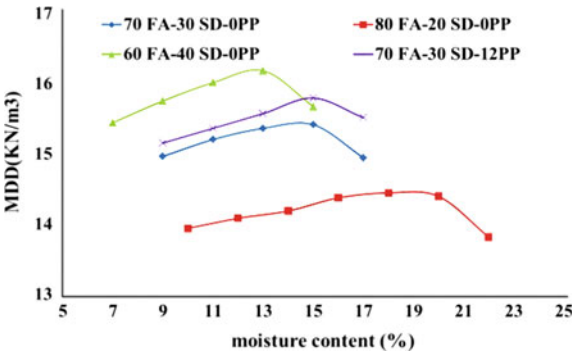

Fig. 3 Compaction curves for different FA-SD mixtures (without cement)

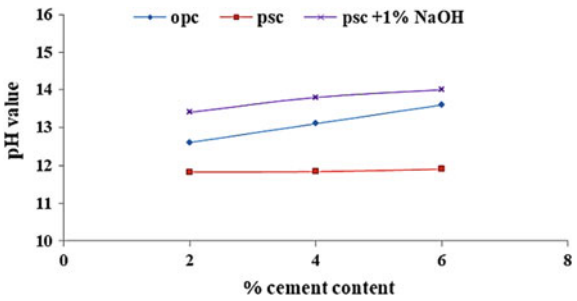

Fig. 4 pH variation with different composition

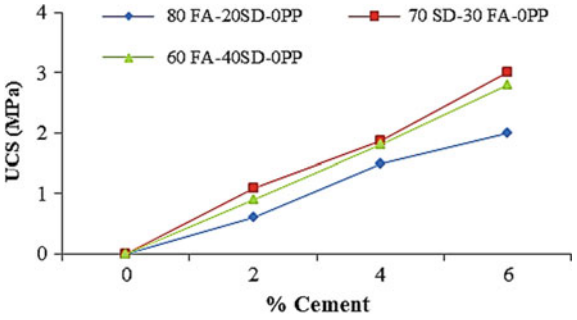

Fig. 5 7-day UCS for different FA-SD composition

From the observation of failure pattern of UCS samples it was realized that the composite material is very brittle in nature. This material may not be suitable for use as base layer as large tensile stresses are experienced by the stabilized bases at the bottom of the layer.

Therefore, polypropylene fibers of 12 mm length with aspect ratio of 500 was used in the study. Though there is no significant strength gain, fiber inclusion showed the improvement in brittle behaviour of the material. A representative (for 2 and 4% are not shown) stress—strain graph for 6% cement stabilised samples is shown in Fig. 6 to emphasize the effect of fiber inclusion.

Samples without fibers show a sudden drop in stress at a constant strain rate of about 3%. However, after inclusion of fibers, these characteristics of the material changed and an elongated stress strain curve depicts the ductile nature of the material. Therefore, all further investigations were carried out on 70FA-30SD-12PP composition (with addition of 2, 4 and 6% cement). 7 day, 28 days and 56 days UCS values for this composition are presented in Fig. 7. It may be observed that, at higher curing period (56 days) the strength reaches as high as 4.93 MPa and the strength gain over time follows an exponential curve. Kumar and Singh (2008) also

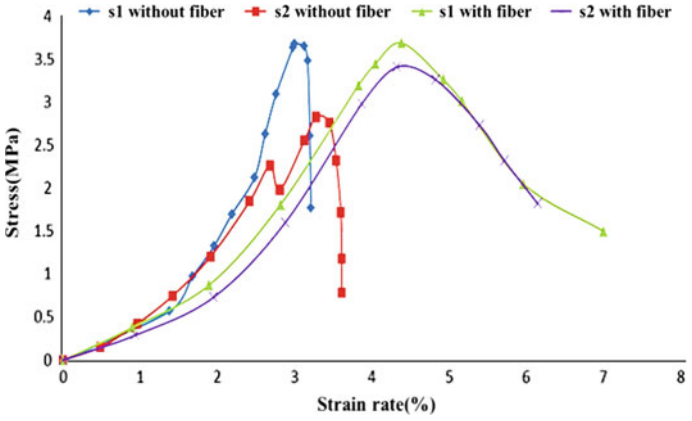

Fig. 6 Representative stress-strain curve for 6% cement stabilised samples

reported a significant gain of UCS after inclusion of randomly oriented fibers in flyash soil mixture which was not observed in the present case.

In addition, flexural strength values for 28 and 45 day cured reinforced and unreinforced beam samples were determined. From Fig. 8 it can be noted that fiber reinforcement has improved flexural strength of the material. Highest flexural strength improvement could be seen for 6% cement stabilised-fiber reinforced sample; an increase of 105 and 107% (base sample is 6% cement stabilised—without fiber reinforcement) for 28 and 45 day cured sample was reported.

According to Vutukur et al. (1974), IDT test is only valid when primary failure occurs along the loading diameter. Therefore, only those results were considered which primary fracture had occurred along the loading diameter (Fig. 9). Test results also showed that IDT strength increases linearly with increase in cement content at both 28 day and 45 day curing (Fig. 10) Cumberledge et al. (1976) mentioned that for road bases to resist freeze–thaw cycles a tensile strength of 0.46 MPa or above is required. It may be observed that, for 6% cement after 28 days curing and for 4 and 6% cement after 45 days curing, ITS values are satisfying the criteria for road base.

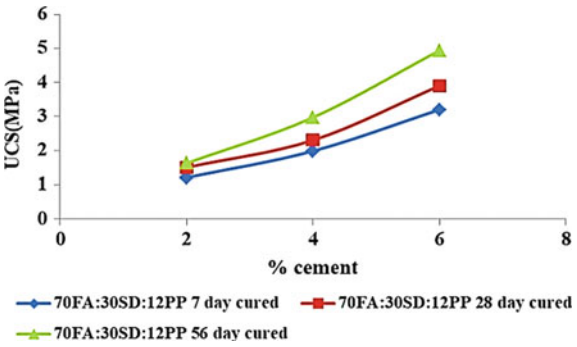

Fig. 7 UCS value for different curing periods

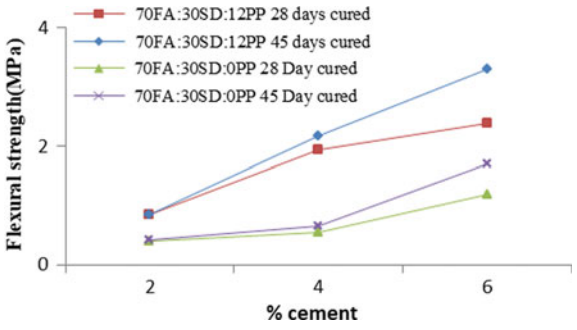

Fig. 8 Flexural strength of 70FA-30SD with and without reinforcement

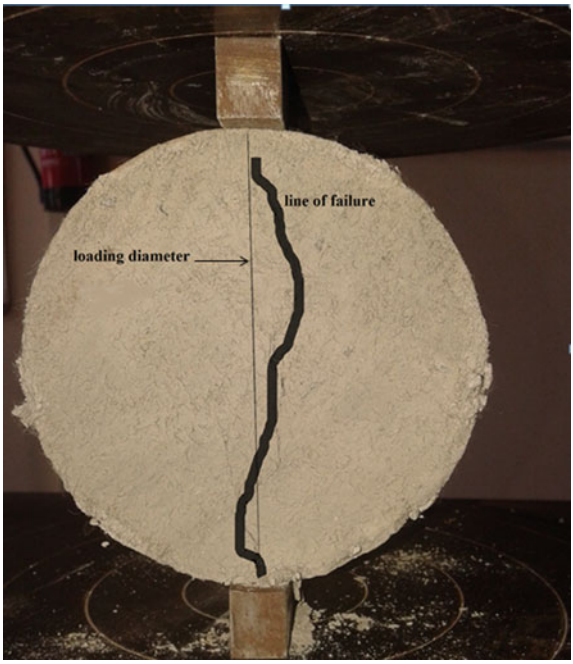

Fig. 9 Failure in sample of IDT test

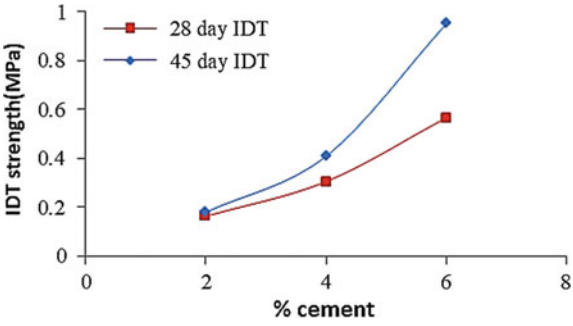

Fig. 10 Variation of IDT strength with cement content

From load-deformation response of monotonic load IDT test, it was found that up to 40% of failure load the material was in elastic region. So, Poisson's ratio was found at 30% of failure load using Eq. (1). Due to inability of the experimental setup at low cement content a worthy horizontal deflection curve could not be found out (as the horizontal and vertical deflection values were something less than 0.015 mm, this was not accurately detectable by LVDTs). AUSTROADS (2010)

Table 2 Poisson's ratio at various cement content

Binder content	28 days cured	45 days cured
2% cement	–	–
4% cement	–	0.14
6% cement	0.21	0.12

recommended range of Poisson's ratio for cementitiously stabilised materials is 0.1–0.3 and values for Poisson's ratio from our study fall in between this range (Table 2). With increase in curing period a significant decrease in Poisson's ratio could be seen which indicates rapid strength gain over time.

In field, a pavement is subjected to dynamic traffic loading, therefore we need to characterize the material under dynamic loading rather than static. Flexural modulus and tensile modulus determined from IDT test are reported in Table 3. For 6% cement stabilized samples, the modulus is more than 6000 MPa at 28 day curing (as flyash is a slow strength gaining material so very less flexural strength values at 7 day curing was identified. So 28 days flexural modulus values will be used for design purpose).

In the durability test, after 10 cycles of wetting-drying, residual UCS values were determined for 7-day and 28-day cured samples. After completing targeted W-D cycles, the samples were kept in water for 2 h before conducting the UCS tests. Table 4 shows the percentage decrease in UCS values after different W-D cycles.

Table 3 Different tensile modulus of the cement stabilized fiber reinforced FA-SD

Binder content	Flexural modulus at 28 days (MPa)	Dynamic stiffness modulus from IDT at 28 days (MPa)
2% cement	3595	1755
4% cement	5935	3291
6% cement	7729	6118

Table 4 Percentage decrease of strength after wetting-drying cycles

Binder content	Percentage decrease of UCS for 7-day cured samples	Percentage decrease of UCS for 28-day cured samples
2% cement	15	11.7
4% cement	11	10.1
6% cement	9.4	7.6

4 Conclusion

The applicability of stabilized FA-SD composite mixed with polypropylene fiber as a structural layer in rural road was studied through unconfined compressive strength, indirect tensile test, flexural strength and durability aspects. Two major input parameters for design flexural modulus and Poisson's ratio have also been worked out.

The following conclusions can be drawn from the test results

1. Addition of stone dust increased the unit weight of the composite material. Inclusion of polypropylene fiber did not significantly affect the compaction characteristics of the mix (1.97% increase in MDD with no visible change in OMC for 70FA:30SD composition).
2. Stabilization with cement is an effective way to enhance the unconfined compressive strength of flyash. FA and SD in 70:30 was found to be optimum UCS result. UCS increased with increase in cement percentage. A maximum of 17% increase in UCS values for increase in 1% cement could be seen from results. Strength values have increased exponentially for increase in curing time.
3. No significant strength gain in UCS was observed after inclusion of 0.5% PP fiber, however inclusion of fiber changed the brittle behavior to ductile.
4. Due to fiber reinforcement, 105 and 107% increase in flexural strength for 28 day and 45 day cured sample respectively was observed with fiber reinforced 6% cement stabilization (base sample—without reinforcement with 6% cement stabilisation).
5. An increase in 75% in the value of IDT strength of 45 days cured sample for fiber reinforced-6% cement stabilisation (base sample is 28 days cured fiber reinforced-6% cement stabilised).
6. Poisson's ratio was found to be in the range of 0.1–0.2, which is within well accepted range for stabilised layer.
7. Due to inclusion of fiber very high tensile modulus value could be seen. With 6% cement, the flexural modulus at loading rate of 1 Hz was found to be more than 6000 MPa.
8. Durability of the samples against W-D cycles increased with increase in curing period and cement content for stabilization, though no specific value could be found for the increase in durability with percentage increase in cement content.

After analyzing the results, it may be stated that stabilization of FA-SD with cement and reinforcing with polypropylene fiber is a potential material for the use in base layers of rural road pavements.

References

Alekgender GB, Heston Wm, Iler RK (1954) The solubility of amorphous silica in water. Grasselli Chem Dept 58:453

Allen J (1973) The effect of non-constant lateral pressures of the resilient response of granular materials. Ph.D. thesis, University of Illinois at Urbana-Champaign, Urbana, IL

ASTM (1985) ASTM standard test method for unconfined compressive strength of soil. ASTM D 2166, Philadelphia, USA

ASTM (1989) ASTM standard test method for flexural strength of soil cement using simple beam with three point loading. ASTM D1635, Philadelphia, USA

ASTM (2003) Standard test method for wetting and drying compacted soil cement mixtures. ASTM D 559-03, Philadelphia, USA

AUSTROADS (2010) Guide to pavement technology part 2 (2012): Pavement structural design. AUSTROADS, Sydney, Australia

Behera B, Mishra MK (2012) Strength assessment and compositional analysis of lime stabilized flyash and mine overburden mixes upon curing. Int J Solid Waste Tech Manag 38(3):211–221

Characterization of cementitiously stabilized layers for use in pavement design and analysis. NCHRP Report 789

Cumberledge G, Hoffman GL, Bhajandas AC (1976) Curing and tensile strength characteristics of aggregate-lime-pozzolan. Transportation Research Record 559, Transportation Research Board, Washington, D.C., pp 21–29

Fraay A, Bijen JM, Vogelaar P (1990) Cement-stabilized fly ash base courses. Cem Concr Compos 45:279–291

Ghosh A, Subbarao C (2006) Tensile strength bearing ratio and slake durability of class F fly ash stabilized with lime and gypsum. J Mat Civil Engg ASCE 18:18–27

Ghosh A, Subbarao C (2007) Strength characteristics of class F fly ash modified with lime and gypsum. J Geotech Geoenviron Engg, ASCE 133:757–766

Indian Standard 2720 (Part 26). Methods for test of soils—laboratory determination of pH value, New Delhi, India

Kampala A, Horpibulsuk S, Prongmanee K, Chinkulkijniwat A (2008) Influence of wet-dry cycles on compressive strength of calcium carbide residue-fly ash stabilized clay. J Mater Civil Engg, ASCE 12:151–163

Kaniraj SR, Havanagi VG (2009) Compressive strength of cement stabilized fly ash soil mixtures. J Mater Civil Engg, ASCE 29:673–677

Kumar P, Singh SP (2008) Utilization of fiber reinforced fly ash in road sub-bases. J Mater Civil Engg, ASCE 134:171–180

Lav AH, Lav MA (2001) Microstructural development of stabilized fly ash pavement base material. J Mater Civil Engg, ASCE 12:157–163

Paul DK, Gnanendran CT (2016) Determination of stiffness modulus and Poisson's ratio of lightly stabilised granular materials from indirect diametral tensile testing. Geotech Test J, ASTM 39:582–595

Poran CJ, Ahtchi-Ali F (1998) Properties of solid waste incinerator flyash. J Geotech Engg, ASCE 115:1119–1133

Sobhan K, Mashnad M (2002) Tensile strength and toughness of soil-cement-fly-ash composite reinforced with recycled high-density polyethylene strips. J Mater Civ Eng ASCE 14:177–184

Sridharan A, Prakash K (2007) Geotechnical engineering characterization of coal ashes, CBS Publishers Ltd.

Usmen MA, John B (1990) Stabilization characteristics of class F fly ash. Transp Res Rec 1288:59–69

Vutukur VS, Lama RD, Saluja SS (1974) Handbook on mechanical properties of rocks: testing techniques and results. Trans Tech Publications, Clausthal

Xu A, Sarkar SL (1991) Microstructural study of gypsum activated fly ash hydration in cement paste. Cement Concr Res 21(6):1137–1147

Effects of Stabilization on Engineering Characteristics of Fly Ash as Pavement Subbase Material

Deepti Patel, Rakesh Kumar, Krupesh Chauhan and Satyajit Patel

Abstract Scarcity of natural resources is increasingly encountered around the world because of the increasing population. Fly ash is one of the problematic waste materials being generated in very large quantity in India by thermal power plants. The use of fly ash in road base, subbase, and subgrade layer provides an opportunity to use high volumes of the materials. In this study, engineering properties of different fly ash-lime (FAL) mixes and fly ash-cement (FAC) mixes were investigated for their effective use as subbase material for flexible pavements. The effect of binder content and curing period on unconfined compressive strength (UCS), CBR, and resilient modulus for all the mixes was studied. Fly ash with minimum 6% lime content and fly ash with minimum 6% cement content satisfy the minimum strength criteria recommended by Indian Road Congress (IRC) for their use in subbase layer. The resilient modulus of these mixes was found to be higher than that of conventional granular subbase (GSB). Finite element analyses of a five-layer flexible pavement system are carried out and the service life ratio of FAL and FAC mixes in relation to the conventional GSB layer is evaluated.

Keywords Unconfined compressive strength · CBR · Resilient modulus · Fly ash · Lime · Cement

D. Patel · R. Kumar · K. Chauhan · S. Patel (✉)
Department of Civil Engineering, S V National Institute of Technology, Surat 395007, India
e-mail: spatel@amd.svnit.ac.in; satya24may@gmail.com

D. Patel
e-mail: deepti82svnit@gmail.com

R. Kumar
e-mail: krakesh@ced.svnit.ac.in

K. Chauhan
e-mail: kac@ced.svnit.ac.in

R. Sundaram et al. (eds.), *Geotechnics for Transportation Infrastructure*,
Lecture Notes in Civil Engineering 29,
https://doi.org/10.1007/978-981-13-6713-7_10

1 Introduction

Expeditious industrialization in India has resulted in the scarcity of naturally available construction materials. Investigating the feasibility of industrial wastes as a compatible construction material has become a vital area because of fast depleting natural construction resources. Industrial waste like fly ash can be effectively used in construction of highways and embankments, ensuing to the preservation of valuable land from colossal waste disposal subsequently averting the concomitant environmental problems. The annual generation of fly ash in India was reported to be 180 million tons in the year 2015–16 with a utilization rate of 60%. At the present generation rate, in the year 2025 fly ash generation will reach around 300 million tons. Fly ash is a waste material generated from thermal power plants which exhibit moderate pozzolanic characteristics. Fly ash utilization for stabilization purposes is always encouraged at locations where it is easily available. Class F fly ash is the least commonly used ash, mainly due to its self-cementations properties. It consists of siliceous and aluminous materials and usually being activated by lime or cement to create a stabilized mixture with augmented pozzolanic characteristics.

Kolias et al (2004) evaluated the mechanical properties of class C fly ash stabilized with cement, to avoid cracking of the stabilized layer and maintain the high modulus values and reduced the thickness of pavement layers. Kaniraj and Gayathri (2003) investigated the UCS strength till increased a certain curing period and then tended to decrease. The rate of increase in strength was high till about 14 days, decreased significantly during 28–90 days and became very small beyond 90 days. The role of lime and gypsum addition on strength behavior of fly ash was studied by Ghosh and Subbarao (2007), Consoli et al (2011) evaluated the strength parameters of sandy soil treated with fly ash and lime mixed for used in bases under pavements. UCS increased linearly with the amount of lime for soil–fly ash–lime mixtures (Sivapullaiah and Moghal 2011). Ghosh and Subbarao (2007) reported the UCS value of 6307 kPa at curing period of 3 months for fly ash stabilized with 10% lime and 1% gypsum. They developed the correlation of deviator stress at failure and cohesion with UCS values.

The resilient modulus in a repeated load test is defined as the ratio of the maximum deviator stress (σ_d) and the recoverable elastic strain (ε_r) as follows:

$$M_r = \frac{\sigma_d}{\varepsilon_r} \tag{1}$$

The resilient modulus (M_r) of cemented stone aggregates for use as road material and their estimation using different empirical models is reported by Peerapong and Hamid (2009); and Puppala et al. (2011). M_r values increase with deviator stress due to strain-hardening phenomenon for unbound aggregates (Arulrajah et al. 2013) and stabilized base materials (Puppala et al. 2011; Patel and Shahu 2016).

The objective of this study is to investigate the beneficial use of Class F fly ash mixed with lime and cement in subbase layer of flexible pavement system. A series of tests, namely UCS, CBR, durability, resilient modulus tests, were conducted on different fly ash-lime mixes and fly ash-cement mixes. Finite element analyses of a five-layer flexible pavement system are carried out and the service life ratio of FAL and FAC mixes in relation to the conventional GSB layer is evaluated.

2 Experimental Program

2.1 Materials

Fly ash was collected from Hindalco Industries Ltd. (Unit: Birla Copper) Dahej, Gujarat. Fly ash satisfies all the physical requirements for use as a pozzolana in lime-fly ash concrete as per IRC: SP 20 (2002). In accordance with ASTM C 618 (1999), this fly ash belongs to Class F type. Hydrated lime with 64% CaO content was used for the present study. Cement used in the research work is 53 Grade Ordinary Portland cement.

2.2 Mix Proportions

In the present study, different percentages of lime (3, 6, 9, and 12%) and cement (4, 6, 8, and 10%) were mixed separately with fly ash to prepare fly ash-lime (FAL) mixes and fly ash-cement (FAC) mixes, respectively. The mix proportions and their designations are given in Table 1.

Table 1 Mix proportions and their designations

Mix proportions	Mix designations
Fly ash + 3% lime	FA3L
Fly ash + 6% lime	FA6L
Fly ash + 9% lime	FA9L
Fly ash + 12% lime	FA12L
Fly ash + 4% cement	FA4C
Fly ash + 6% cement	FA6C
Fly ash + 8% cement	FA8C
Fly ash + 10% cement	FA10C

2.3 Tests Performed

For the determination of UCS, lime and cement were mixed separately with fly ash in a required proportion in dry condition. A right amount of water (close to optimum moisture content) was added to give proper consistency to the mixture for easy molding. Cylindrical samples of 50-mm-diameter and 100 mm height were then prepared by compacting the mix at their corresponding maximum dry density. The samples were sealed in an airtight polythene bag and kept at a temperature of 27 ± 2 °C for different curing period. The unconfined compressive strength of these cured samples was then determined using a conventional compression testing machine at a constant strain rate of 0.6 mm/min as per IS: 2720 (Part X)-1991.

CBR value of a material is an important parameter to study its feasibility for the utilization in the subbase course of flexible pavements as per IRC: 37 (2012). Therefore, CBR tests were carried out on different fly ash-lime mixes and fly ash-cement mixes in accordance with IS: 2720 (Part-16) 1987. CBR specimens were first cured for 7 days and then soaked for 4 days prior to testing.

Durability tests adopted in the present study are applicable for the stabilized pavement materials. The tests were carried out in accordance with ASTM D 559 (2003). The specimens were first cured for 28 days and then subjected to several wetting and drying cycles. One wetting and drying cycle consists of 5 h soaking in water and 42 h of heating at a temperature of 72 °C in a thermostatically controlled oven. The weight loss of the specimens was determined after 12 such cycles of alternate wetting and drying.

Resilient modulus (M_r) of different fly ash-lime mixes and fly ash-cement mixes was determined using a repeated load triaxial (RLT) test apparatus (Make: Geotechnical Digital System, UK) as per AASHTO T-307 (2000). Specimen preparation and curing procedure for RLT tests were similar to that for UCS tests. A haversine-shaped load pulse was applied to simulate the traffic wheel loading condition (Puppla et al. 2011). At each loading sequence, 100 repetitions of the corresponding cyclic load were applied using a haversine-shaped load (loading pulse of 0.1 s with a resting period of 0.9 s). Resilient modulus was calculated for 15 different stress combinations applicable for subbase materials as per AASHTO T-307 (2000).

3 Results and Discussion

3.1 Unconfined Compressive Strength

Specimens prepared for UCS test were cured for 7 and 28 days before the test. UCS values of different fly ash-lime mixes and fly ash-cement mixes are shown in Fig. 1. Compressive strength increases with the binder (lime and cement) content. The UCS values at 28 days curing were found to be 16–43% higher than that at 7 days curing.

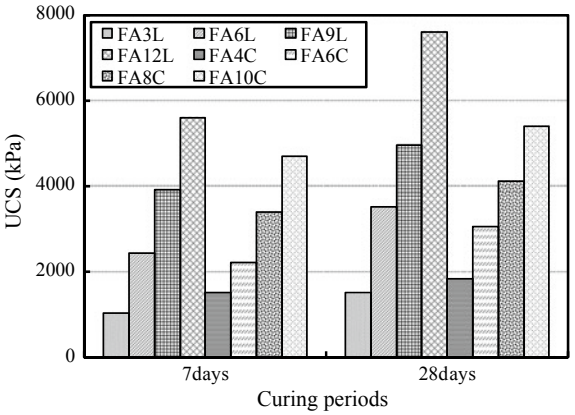

Fig. 1 Variation of UCS with binder (lime and cement) content for 7 and 28 days of curing period

The strength development in fly ash-lime and fly ash-cement mixes happens mainly due to pozzolanic reaction of fly ash with lime and cement. In this reaction, calcium silicate hydrate (C–H–S) and calcium aluminosilicate hydrate (C–A–S–H), collectively called binding gels, are formed which bind the fly ash particles together resulting in a hardened mass. With an increase in binder (lime and cement) content, the quantity of gel formation increases which bind the particles more efficiently leading to an increase in the compressive strength. The pozzolanic reaction is a slow process. Therefore, the formation of binding gel and hence the compressive strength increases with an increase in curing period.

For a given binder content, the UCS values of fly ash-lime mix were found to be higher than that of fly ash-cement mix owing to the higher specific surface area of lime as compared to that of cement.

In accordance with IRC 20 (2002), the minimum laboratory UCS value of fly ash-lime mix after 28 days and fly ash-cement mix after 7 days should be 1.5 and 1.7 MPa, respectively, for their use as a subbase material in flexible pavements. Figure 1 shows that fly ash with minimum 6% lime content and fly ash with minimum 6% cement content satisfy the IRC criteria.

3.2 California Bearing Ratio (CBR)

The soaked CBR values obtained for different FAL mixes and FAC mixes after 7 days curing and 4 days soaking are given in Table 2. The broad trends observed for CBR values and the reasons for these trends are similar to those described earlier for UCS values.

Table 2 CBR values of different mixes

Mixes	CBR (%)	Mixes	CBR (%)
FA6L	64	FA6C	58
FA9L	89	FA8C	73

The minimum CBR value recommended by IRC: 37 (2012) is 30% for subbase course of flexible pavements. Hence, all the four mixes adopted in the present study with a minimum curing period of 7 days satisfy this criterion.

3.3 Durability

The loss of dry weight for FA6L, FA9L, FA6C, and FA8C mixes are obtained as 17.1, 16.2, 17.8, and 16.6%, respectively. Hence, all the four mixes satisfy the criterion for the maximum permissible percentage loss in weight (=30%) recommended by IRC: 89 (2010) for the stabilized mix to be used in pavement subbase course.

3.4 Resilient Modulus

Repeated load triaxial tests conducted on different FAL and FAC mixes to simulate the traffic wheel loading under different confining pressure. Figure 2 illustrates the resilient modulus of the mixes after 28 days curing period for six different stress combinations. M_r value increases with the confining pressure and deviator stress. This behavior is in consistent with the previous (Arulrajah et al. 2013; Puppala et al. 2011; Patel and Shahu 2016). Also, M_r increases with an increase in binder content. The broad trends observed for M_r values with binder content and curing period, and the reasons for these trends are similar to those described earlier for UCS values.

Figure 3 shows the effect of curing period on resilient modulus of various mixes and also compares their M_r values with those of conventional granular subbase layer. The resilient modulus of all the mixes after 28 days curing periods was found to be higher than that of GSB. This shows that the thickness of the subbase layer can be reduced if GSB is replaced by FAL and FAC mixes.

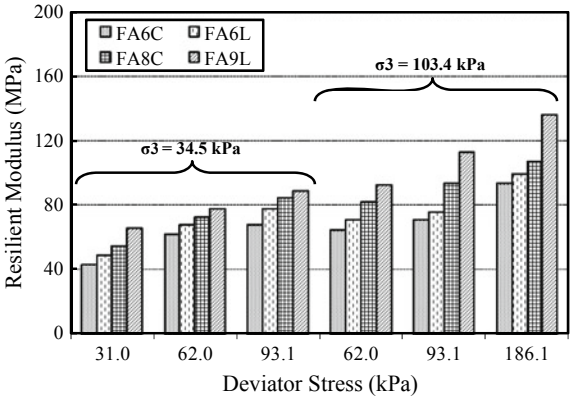

Fig. 2 Variation of resilient modulus with deviator stress and confining pressure at 28 days curing period

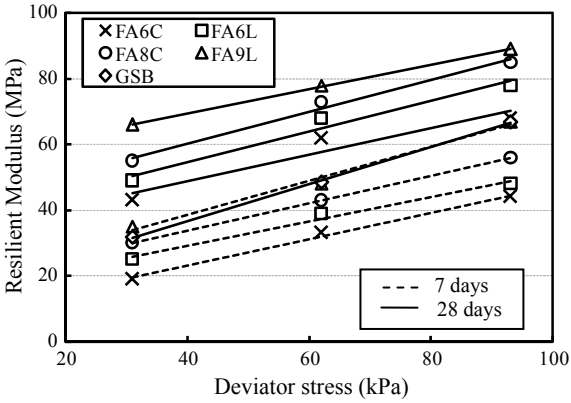

Fig. 3 Effect of deviator stress and confining pressure on resilient modulus of fly ash-lime and fly ash-cement mixes for 7 and 28 days curing period

3.5 *Modeling of Resilient Modulus*

In the present study, the performance of three stress-dependent models is compared to predict the resilient modulus of FAL and FAC mixes.

i. **Model 1**—The following two-parameter model is suggested by Witczak and Uzan (1988):

$$M_{\mathrm{r}} = k_1 \times \sigma_{\mathrm{d}}^{k_2} \tag{2}$$

ii. **Model 2**—The following two-parameter model, commonly known as $k - \theta$ model:

$$M_{\mathrm{r}} = k_3 \times \sigma_{\mathrm{d}}^{k_4} \tag{3}$$

iii. **Model 3**—The following three-parameter model is proposed by Puppala et al. (2011) and Patel and Shahu (2016) for stabilized specimens:

$$\frac{M_{\mathrm{r}}}{P_{\mathrm{a}}} = k_5 \times \left(\frac{\sigma_3}{P_a}\right)^{k_6} \times \left(\frac{\sigma_{\mathrm{d}}}{P_{\mathrm{a}}}\right)^{k_7} \tag{4}$$

where θ = bulk stress; σ_3 = confining stress; σ_{d} cyclic deviator stress; P_{a} = atmospheric pressure; and k_1 to k_7 = model constant.

The model constants k_1 to k_7 were obtained from the regression statistical analysis. The predicted M_{r} values were compared with the measured M_{r} values, and the coefficient of determination (R^2) for Model 1, Model 2, and Model 3 were determined as 0.93, 0.87 and 0.98, respectively, for FAL mixes; and 0.91, 0.86 and 0.95, respectively, for FAC mixes.

The highest R^2 values are obtained for Model 3, indicating three-parameter model provides the best prediction of resilient modulus for both FAL mixes and

FAC mixes. The advantage of the models lies in separating the effects of deviator stress and confining pressure on M_r values (Patel and Shahu 2016).

The plot between predicted and measured M_r values for all FAL and FAC mixes for Model 3 is shown in Figs. 4 and 5. The model constants (k_5, k_6, and k_7) obtained for all FAL and FAC mixes are presented in Table 3.

3.6 Service Life of Flexible Pavements

Service life of pavement was evaluated through finite element analysis of a five-layer flexible pavement system using a commercial finite element code, Plaxis. The thickness of different layers of the pavements was adopted as per IRC: 37 (2012) for traffic intensity of 100 million standard axles (MSA) and subgrade CBR of 3%. A linear elastic model is used for all the layers, such as Bituminus Concrete

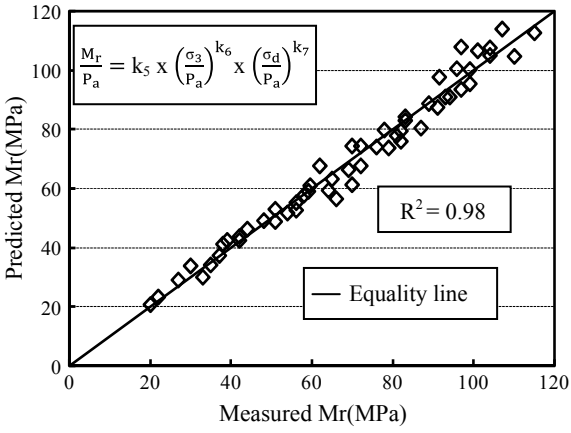

Fig. 4 Measured resilient modulus versus predicted resilient modulus using Model 3 for fly ash-lime mixes

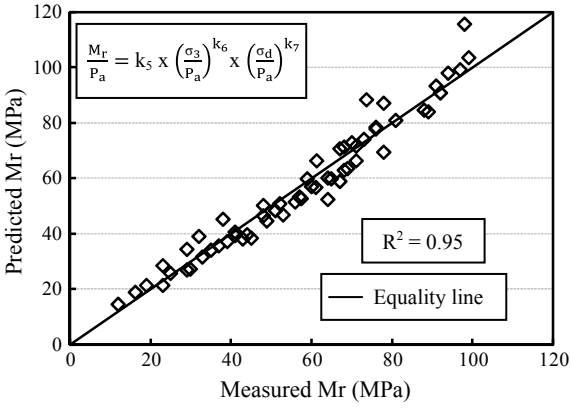

Fig. 5 Measured resilient modulus versus predicted resilient modulus using Model 3 for fly ash-cement mixes

Table 3 Model constants of FAL and FAC mixes after 7 and 28 days of curing period

Mixes	Curing days	$M_R = k_5 \times \left(\frac{\sigma_3}{P_a}\right)^{k_6} \times \left(\frac{\sigma_d}{P_a}\right)^{k_7}$		
		k_5	k_6	k_7
FA6L	7	0.629	0.129	0.545
	28	0.925	0.164	0.328
FA9L	7	0.764	0.174	0.541
	28	0.999	0.101	0.396
FA6C	7	0.500	0.179	0.565
	28	0.738	0.121	0.451
FA8C	7	0.523	0.075	0.535
	28	0.804	0.109	0.404

(BC), Dense Bituminous Macadam (DBM), base, subbase, and subgrade layers. The input parameters of different layers other than FAL and FAC mixes are taken from Patel and Shahu (2016). M_r values of FA6L, FA9L, FA6C, and FA8C mixes are adopted as 82, 91, 68, and 78 MPa, respectively, as determined experimentally corresponding to deviator stress of 93.1 kPa and confining pressure of 34.5 kPa. A uniform pressure of 575 kPa was applied on a circular contact area with radius of 150 mm, which is equivalent to the pressure caused by a single-axle wheel load of 40.80 kN (Fig. 6).

The service life ratio (SLR) of pavements with FAL and FAC mixes in the subbase course vis-a-vis the conventional GSB layer based on fatigue failure criteria is determined by the following equation:

$$\text{SLR} = (\varepsilon_{t1} / \varepsilon_{t2})^{3.89} \tag{5}$$

where ε_{t1} and ε_{t2} are the maximum horizontal tensile strains developed at the bottom of DBM layer made up of conventional GSB and that of stabilized fly ash, respectively. The values of ε_{t1}, $\varepsilon_{t2,}$ and maximum deformation δ at the pavement surface as obtained from the finite element analyses and service life ratios for various materials are given in Table 4. The pavement with FAL and FAC mixes in subbase layer has higher service life compared to the pavement with GSB layer.

The construction cost per cubic meter of FA6L, FA9L, FA6C, FA8C, and GSB subbase layer as per the current schedule of rates of Public Work Department (PWD) in Gujarat are obtained as 729, 843, 898, 1016, and 985 Indian Rupees, respectively. Hence, the construction cost can be saved up to 26% by replacing the conventional GSB with fly ash + 6% lime (FA6L) mix.

4 Conclusion

From the present study on engineering properties of fly ash-lime mix and fly ash-cement mix, the following conclusions are drawn.

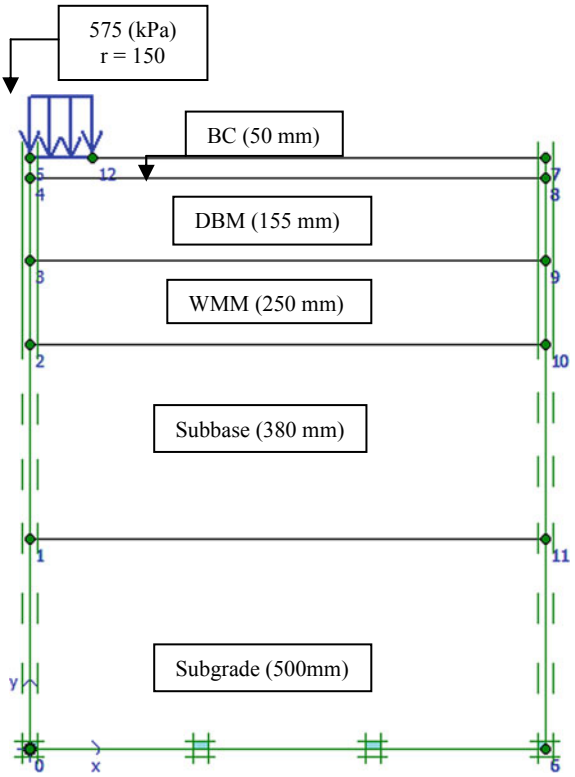

Fig. 6 Finite element analysis of flexible pavement system using plaxis for traffic intensity of 100 MSA and subgrade CBR of 3%

Table 4 Service life ratio (SLR) for various subbase materials for 3% subgrade CBR

Subbase material	δ (mm)	ε_{t1} or ε_{t2} (micron)	SLR	Construction cost per m^3 in INR
GSB	418	261.2	1.000	985
FA6L	405	255.4	1.107	729
FA9L	402	254.2	1.131	843
FA6C	413	257.5	1.067	898
FA8C	409	256.5	1.086	1016

δ = maximum deformation at the pavement surface

- UCS and resilient modulus increase with binder content and curing period for all the mixes. Fly ash with minimum 6% lime content and fly ash with minimum 6% cement content satisfy the IRC strength criteria for use in subbase course of flexible pavement.
- Durability test results showed the weight loss in the range of 16% to 18% for stabilized fly ash mixes. Hence, these mixes satisfied the durability criteria as per IRC: SP: 89-2010.

- The CBR value of only fly ash is 12. As per IRC: 37 (2012), the subbase materials should have minimum CBR value of 30% for traffic exceeding 2 MSA. The CBR value was found up to 89 and 73% for FAL and FAC mixes, respectively.
- A three-parameter model provides the best fit for the effects of both confining pressure and deviator stress on resilient modulus of FAL and FAC mixes.
- The pavement with FAL and FAC mixes in subbase layer has higher service life compared to the pavement with GSB layer. Construction cost can be saved up to 26% by replacing the conventional GSB with fly ash + 6% lime (FA6L) mix.

References

AASHTO T 307-99 (2000) Determining the resilient modulus of soils and aggregate materials

Arulrajah A, Piratheepan J, Disfani MM, Bo MW (2013) Resilient moduli response of recycled construction and demolition materials in pavement subbase applications. J Mater Civ Eng 25 (12):1920–1928

ASTM C 618 (1999) Standard methods for coal fly ash and raw or calcined natural pozzolana for use as amineral admixture in concrete. American Society for Testing Materials, Philadelphia

ASTM D 559 (2003) Standard methods for wetting and drying compacted soil-cement mixtures. American Society for Testing Materials, Philadelphia

Consoli NC, Rosa AD, Saldanha RB (2011) Variables governing strength of compacted soil-fly ash-lime mixtures. J Mater Civ Eng 23(4):432–440

Ghosh A, Subbarao C (2007) Strength characteristics of class F fly ash modified with lime and gypsum. J Geotech Geoenviron Eng 133(7):757–766

IRC 37 (2012) Tentative guidelines for the design of flexible pavements. Indian Roads Congress, New Delhi

IRC SP 20 (2002) Rural road manual. Indian Roads Congress, special Publication, New Delhi

IRC 89 (2010) Guidelines for soil and granular material stabilization using cement, lime and fly ash. Indian road congress, special publication, New Delhi

IS 2720 (Part 16) (1987) Laboratory determination of CBR, Indian Standard, New Delhi

IS 2720 (Part 10) (1991) Determination of unconfined compressive strength, Indian Standard, New Delhi

Kaniraj SR, Gayathri V (2003) Factors influencing the strength of cement fly ash base courses. J Transp Eng 127(7):574–584

Kolias S, Rigopoulou VK, Karahalios A (2004) Stabilisation of clayey soils with high calcium fly ash and cement. Cement Concr Compos 27(2005):301–313

Patel S, Shahu JT (2016) Resilient response and permanent strain of steel slag-fly ash-dolime mix. J Mater Civ Eng 28(10):04016106

Peerapong J, Hamid N (2009) Mechanical behaviours of hydrated cement treated crushed rock base as a road base material in Western Australia. Int J Pavement Eng 10(1):39–47

Puppala AJ, Hoyos LR, Potturi AK (2011) Resilient moduli response of moderately cement-treated reclaimed asphalt pavement aggregates. J Mater Civ Eng 23(7):990–998

Sivapullaiah PV, Moghal AAB (2011) Role of Gypsum in the strength development of fly ashes with lime. J Mater Civ Eng 23(2):197–206

Witczak M, Uzan J (1988) The universal airport design system, "Rep. I of IV: Granular material characterization. Department of Civil Engineering, University of Maryland, College Park, MD

Experimental Study on Geocell and of Fibre Reinforced Soil Sub-grade Under Static and Repetitive Load

A. Ramesh, Ch. Nageshwar Rao and M. Kumar

Abstract Development of transportation infrastructure will provide an overall development of country's economy. This is achieved by providing better quality and longevity of roads. To improve the quality of pavement structure, soil sub-grade properties play a vital role. As known fact that soil sub-grade handles the vehicular wheel load transmitted from the pavement structure. A few soils when used in pavement construction do not provide desirable properties. The performance of such soils can be improved with reinforcement of non-traditional materials. In this paper, an attempt is made to enhance the properties of silty soil in two stages. In the first stage of study, soil is reinforced with basalt fibre (non-traditional material) with varying length (i.e. 25, 50 and 75 mm) and percentages (0.2, 0.4 and 0.6). CBR, resilient modulus (M_R) and UCS values were enhanced with reinforcement of basalt fibre for 50 mm length and 0.4%, when compared with natural soil. In the second stage of study, lateral confinement is achieved by providing plastic PET bottles of varying diameter of 50, 80 and 100 mm in the form of geocell. These PET bottles are provided at 1/3H and 1/2H. CBR and resilient modulus (M_R) values were observed to be higher for 80 mm diameter PET bottles provided at 1/3H.

Keywords Resilient modulus · CBR · Fibres · Plastics · PET bottles

A. Ramesh (✉) · Ch. Nageshwar Rao
Department of Civil Engineering, VNR Vignana Jyothi Institute of Engineering and Technology, Hyderabad, Telangana, India
e-mail: ramesh_a@vnrvjiet.in

Ch. Nageshwar Rao
e-mail: nageshwarrao_ch@vnrvjiet.in

M. Kumar
Department of Civil Engineering, University College of Engineering Osmania University, Hyderabad, Telangana, India
e-mail: kumartrans@gmail.com

R. Sundaram et al. (eds.), *Geotechnics for Transportation Infrastructure*,
Lecture Notes in Civil Engineering 29,
https://doi.org/10.1007/978-981-13-6713-7_11

(a) Chopped Basalt fiber (b) PET Bottle of different diameter

Fig. 1 Fibre PET bottle used in the study

1 Introduction

Developing countries like India is curtailed for providing complete road network system due to limited financial constraints. Predominately pavements are constructed in layers as sub-grade, sub-base, base and are greatly influenced on quality and life of pavement. One of the most important materials among the other is nature of sub-grade soil materials. The real challenge lies in construction flexible pavements over a weak sub-grade having low California bearing ratio (CBR). Constructing pavements on such weak sub-grade requires more thickness. In order to improve the engineering soil properties of such weak soil, replacement of existing soil might not be a challenging solution. On the other hand, if the stability of the local soil is not adequate for supporting the vehicular wheel loads, the properties of existing soil can be improved by soil stabilization/modification techniques. Randomly, distributed fibre when used at regular intervals on highway pavements will produce better performance in the stabilization process of weak soil sub-grade. Polyethylene terephthalate (PET) plastic wastes are destroying the societal environment.

The current study focuses on improving local soil using basalt fibre and PET bottle as confinement in the form of geocell. Optimum fibre content and influence of PET bottle as confinement in local soil are assessed in the laboratory. Figure 1 provides fibre and PET bottle used in the study.

2 Background of Study

Many studies have been conducted by researchers for investigating the behaviour of weak soil when reinforced with different types of fibre and providing confinement through laboratory experimental tests. Consoli et al. (2003) conducted response studies on thick homogenous stratum of compacted sandy soil with polypropylene

(PP) fibres. The PP-reinforced fibre exhibited axial strains greater than 20%, than unreinforced soil specimens. Kumar et al (2006) tested on highly compressible clay in unconfined compressive strength with varying percentages of flat and crimped polyester fibre. The test results indicate that as the fibre length and/or fibre content increases, there is an improvement in UCS value. Chegenizadeh (2013) studied the effect of fibre inclusion on CBR ratio. The test results indicate that the CBR ratio for reinforced clay increased by two times as fibre content and length increased.

Tang et al. (2006), Akbulut et al. (2007), Sadek et al. (2010), Babu & Chouksey (2011) conducted studies on reinforcing soil with plastic waste. Their findings on reinforcing soil with plastic waste increase the strength, CBR and reduce the compressibility. In this study, the authors have focused on the analysis of engineering behaviour of soil reinforced with polyethylene terephthalate (PET) plastic waste (Athanasopoulos 1993) and addition of varying length and proportion of fibre. From the literature, most of the authors have attempted in fibre reinforcement and soil confinement. In this paper, we have made an attempt in understanding the effect of reinforcement and confinement on CBR, M_R and UCS parameters.

3 Methodology and Experimental Programme

In the present investigation, a methodology is proposed for evaluation of natural soil when reinforced with basalt fibre and provided lateral confinement with plastic PET bottle of different diameter at different heights. Table 1 provides details of study methodology.

The soil was collected from site near forest training academy, Dulapally village, Hyderabad city, and fibre is collected from HDM, New Delhi, and plastic PET bottles collected from local shredding yard in Hyderabad city. The initial properties of soil are determined in the laboratory, and particle size distribution is shown in Fig. 2. The physical properties of basalt fibre are obtained from the supplier. Table 2 provides the properties of soil, Table 3 provides properties of fibre and Table 4 provides properties of PET bottle.

Table 1 Methodology adopted for study

Stage No.	Description
1.	Literature survey and collection of materials
2.	Physical properties of material used in the study
3.	Estimation of index properties, dry density, OMC, CBR, resilient characteristics (M_R) and UCS for natural soil
4.	Assessment of CBR, resilient characteristics (M_R) and UCS parameters for soil reinforced with fibre of varying length and providing lateral confinement with different diameter and heights
5.	Discussion on above laboratory results and conclusions

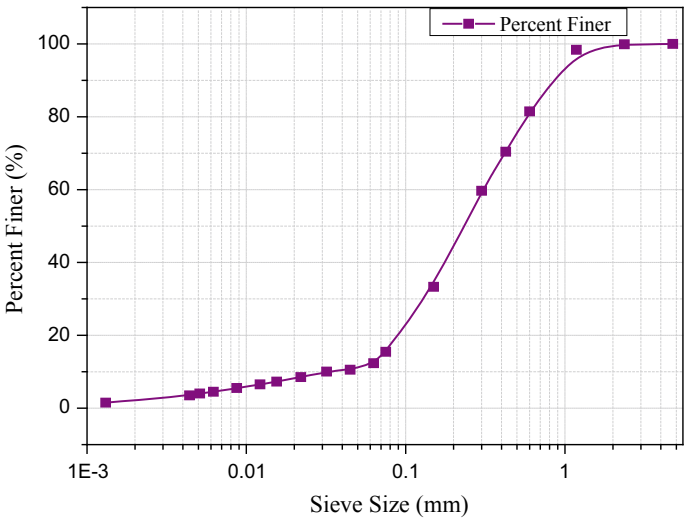

Fig. 2 Particle size distribution

Table 2 Properties of silty sand

Properties	Test results	IS Test specifications
Liquid limit (%)	35	IS 2720 (Part V) 1985
Plastic limit (%)	18	IS 2720 (Part V) 1985
Plasticity index (%)	17	–
Specific gravity	2.6	IS 2720 (Part III/Sec 1) 1980
Maximum dry density (g/cc)	1.95	IS 2720 (Part VIII) 1983
Optimum moisture content (%)	12	IS 2720 (Part VIII) 1983
IS Classification	Silty sand	IS 2720 (Part IV) 1985
Unconfined compressive strength (kPa)	356	IS 2720 (Part X) 1973
Particle size distribution		
Percentage of sand (%)	46	IS 2720 (Part IV) 1985
Percentage of silt (%)	47.5	
Percentage of clay (%)	6.5	

Table 3 Properties of basalt fibre

Properties	Limits
Tensile strength (MPa)	2800–4800
Elastic modulus (GPa)	86–90
Strain at break (mm/mm)	0.0315
Specific gravity	2.7

Table 4 Properties of polyethylene terephthalate (PET bottle)

Properties	Limits
Tensile strength (MPa)	450
Elastic modulus (N/mm^2)	3100
Ultimate elongation (%)	11.2
Density kg/m^3	1380

Source Chowdhury et al. (2013)

In the present study, the improvement of sub-grade soil when treated with fibre and plastic PET bottles placed at 1/3H and 1/2H (H is the height of mould from top) of CBR mould is determined by conducting soaked test as per IS 2720: (Part XVI) 1987. Basalt fibre of 25, 50 and 75 mm length is mixed at OMC with careful monitoring and after visual satisfaction in uniformity of fibre when reinforced in soil. As the length and percentage of fibre are less, segregation has not observed during the process of sample preparation. The soil in CBR mould is compacted at modified proctor density. The penetration and load were observed from load cell and LVDT arrangement through online DAQ connected to CBR instrument (Fig. 3). Soil samples are tested after 4 days of soaking in water. PET bottles are provided as geocells for different diameters and varying height.

Resilient modulus (AASHTO 2007) (M_R) is an important mechanical property widely used for the analysis and design of pavements. A repeated axial cyclic stress of fixed magnitude with load duration of 0.1 s and rest period of 0.9 s rest is applied to cylindrical test specimen. Total period of loading and unloading (rest period) together constitutes one loading cycle (1 s) which amounts to 1 Hz frequency. The stress pulse shape was haversine in nature. The repeated load tests were performed on CBR mould. Each combination is applied in 100 cycles after preconditioning of 500 cycles. The total resilient or recoverable axial deformation response of the specimens is used to calculate resilient modulus. The tests were terminated when the total vertical permanent strain exceeds 5%. Figure 4 provides the set-up of repeated load test for determining resilient modulus (M_R).

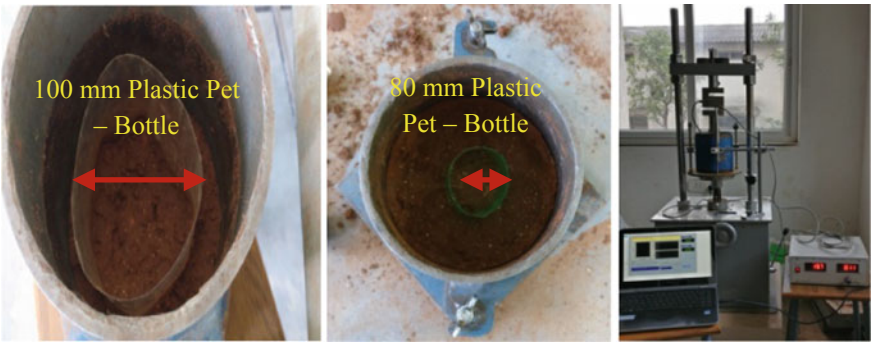

Fig. 3 Plastic confinement preparation and CBR test performed through online DAQ

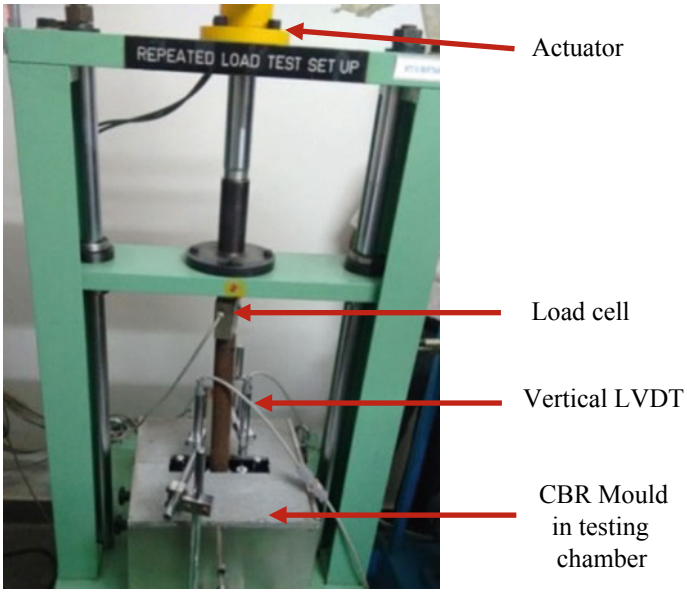

Fig. 4 Repeated load test set-up for M_R determination

4 Results and Discussion

The CBR values of soaked soil with and without fibre reinforcement and lateral confinement by plastic PET bottles were determined in the laboratory. The fibre reinforcement is provided by varying length of 25, 50 and 75 mm and percentages of 0.2, 0.4 and 0.6, respectively. Lateral confinement is provided at 1/3H and 1/2H from top of the mould. The maximum CBR value is 14.67%, obtained with the inclusion of fibre of 50 mm length of 0.4%. Natural soil when confined with PET bottle of 80 mm diameter has enhanced its CBR value by 13.33% at H/3 and is more because it is within the pressure bulb, whereas when placed at 1/2H as it is away from the pressure bulb the CBR value observed is 10.56%. The CBR value of fibre-reinforced soil in soaked condition also observed to be improved from 6.3% to 14.67% for the fibre length of 50 mm with 0.4%. Table 5 provides test results for fibre-reinforced soil mixes, and Table 6 provides PET bottle confinement for soil mixes, respectively.

Similar trend of increase in CBR, resilient modulus and UCS for the fibre percentage 0.4 and length 50 mm, respectively, are shown in Figs. 5, 6 and 7.

Resilient modulus (M_R) test was carried on CBR mould for defined number of passes and to achieve deformation of 2.5 mm. It is observed that 50 mm length and 0.4% fibre reinforcement has improved the resilient characteristics from 67 to 250 MPa when compared with natural soil. Similar trend was observed for lateral confinement of soil when provided with plastic PET bottle at H/3 and 80 mm diameter. Figure 8 provides variation in resilient characteristics for lateral confinement.

Table 5 Comparison of CBR, M_R and UCS values for soaked specimens treated with fibre

Basalt fibre length (mm)	Per cent fibre (%)	CBR Value (%)	M_R (kPa) × 10^3	UCS (kPa)
0	**0**	**6.30**	**67**	**356**
25	0.2	10.30	118	395
	0.4	10.50	121	410
	0.6	10.10	112	382
50	0.2	14.40	242	501
	0.4	14.67	250	512
	0.6	13.91	232	498
75	0.2	12.55	182	472
	0.4	13.22	189	481
	0.6	11.63	178	465

Table 6 CBR values for soaked specimens with lateral confinement

PET bottle confinement dia. mm	Test No.	CBR			
		(@ H/3)	Average (@H/3)	@ H/2	Average (@H/2)
0	1	7.0	6.3	7.0	6.33
	2	6.1		6.0	
	3	5.9		6.0	
50	1	8.8	9.0	8.0	7.83
	2	8.9		7.5	
	3	9.3		8	
80	1	12.9	13.33	10.0	10.56
	2	14.2		10.5	
	3	12.9		11.2	
100	1	11.8	12.63	9.1	9.56
	2	13.2		9.9	
	3	12.9		9.7	

It is observed from Table 5 that unconfined compressive strength (UCS) is increased from 356 to 512 kPa for fibre length of 50 mm and 0.4%, and thereafter, UCS values reduced. This is because more length of fibre induces lubrication effect and resulted in decreased trend. Similarly at 25 mm fibre length, the UCS value observed to be lesser than 50 mm, and this is because of insufficient length of fibre for development of friction from surrounding soil. From Table 5, similar inferences can be drawn in case of M_R values for respective fibre length, percentages and in

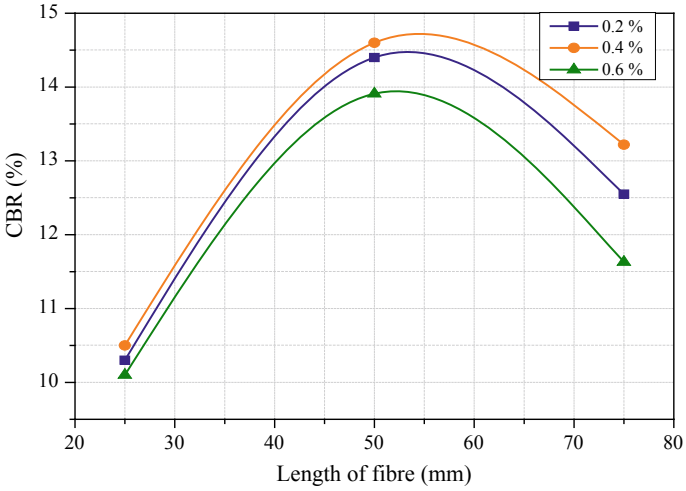

Fig. 5 Variation of CBR value with reference to length of fibre and percentage

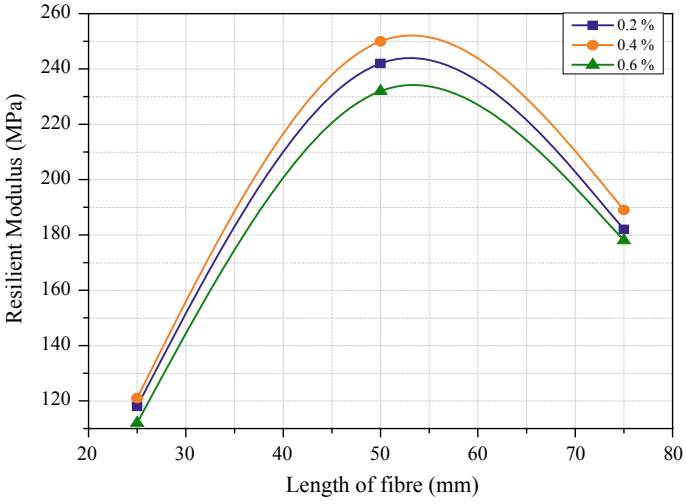

Fig. 6 Variation of resilient modulus with reference to length of fibre and percentage

case of lateral confinement too. In the field, the same concept can be implemented wherever week soils zones are met with during pavement constructions. However, the waste PET bottles can be reused in the form of geocells by moulding process. Further investigations are required in test tracks before implementation in the field.

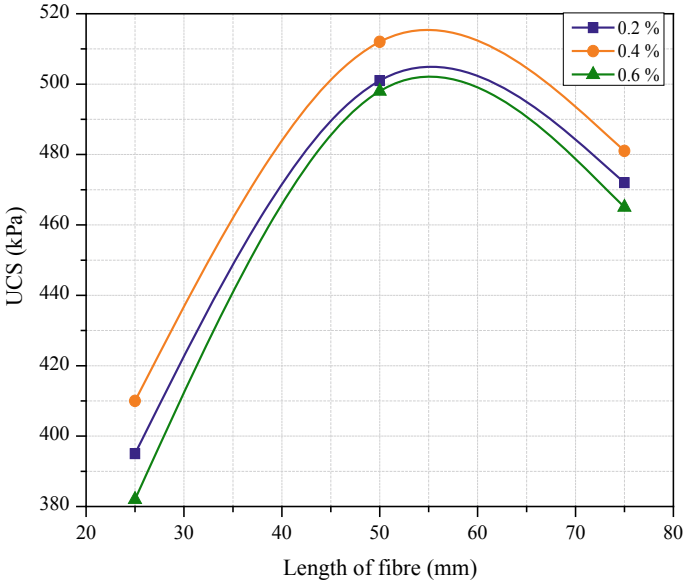

Fig. 7 Variation of UCS value with reference to length of fibre and percentage

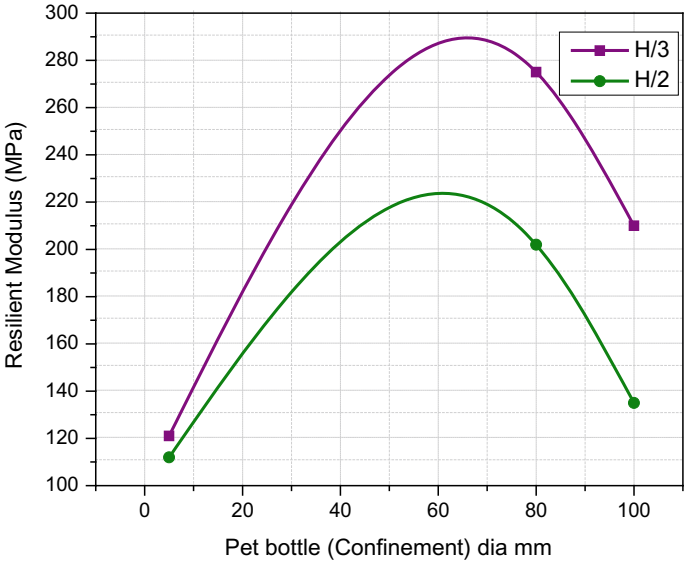

Fig. 8 Variation of resilient characteristics for lateral confinement

5 Conclusions

The strength development in terms of CBR value, UCS and modulus of resilient measured soil reinforced with basalt and PET—bottle confinement on silty soils. Based on the results, the following conclusions are drawn.

(a) The addition of basalt fibre is effecting in enhancing the CBR, UCS and M_R values. This could be due to the mobilization of frictional resistance between fibre and surrounding soil.
(b) Confinement with PET—Bottle enhanced the CBR and M_R by offering soil resistance to lateral yield due to confinement.
(c) UCS value increased by addition of fibre by offering resistance to strain developed in the soil by fibre when compared to natural soil.
(d) CBR, resilient modulus and UCS for the fibre percentage of 0.4 and length 50 mm increased. At 0.2 and 0.6%, of lengths 25 and 75 mm, respectively, are shown decreased trend due to obvious reason that at 0.2% and 25 mm length has insufficient frictional resistance, whereas at 0.6% and 75 mm length slip might have occurred between fibre and surrounding soil, respectively.

References

Akbulut S, Arasan S, Kalkan E (2007) Modification of clayey soils using scrap tire rubber and synthetic fibers. J Appl Clay Sci 38(1–2):23–32

Consoli NC, Vendruscolo JP, Prietto PDM, Pasa GS (2003) Behavior of plate load tests on soil layers improved with cement & fiber. J Geotech Geoenvironmental Eng 129(1):96–101

Chegenizadeh Amin, Nikraz Hamid (2013) Silty clay and fibre interaction. J Adv Mater Res 690–693:415–420

Kumar A, Walia BS, Mohan J (2006) Compressive strength of fibre reinforced highly compressible clay. J Constr Build Mater 20:1063–1068

Sadek S, Najjar S, Freiha F (2010) Shear strength of fiber-reinforced sands. J Geotech J Geoenvironmental Eng 136(3):490–499

Chowdhury S, Maniar AT, Suganya O (2013) Polyethylene terephthalate (PET) waste as building solution. Int J Chem Environ Biol Sci 1(2):308–312

Tang C et al (2006) Strength and mechanical behavior of short polypropylene fiber reinforced and cement stabilized clayey soil. J Geotext Geomembr 25(3):194–202

Books & Codes

AASHTO T 307–99 (2007) Standard method of test for determining the resilient modulus of soils and aggregate materials. American Association of State Highway and Transportation Officials, Washington, DC

Athanasopoulos GA (1993) Effect of particle size on the mechanical behaviour of sand-geotextile composites. Geotext Geomembr 12(3):255–273

Babu GLS, Chouksey SK (2011) Stress-strain response of plastic waste mixed soil. Waste Manag 31(3):481–8. (New York, N.Y.)

IS 2720: Part III: Sec 1: (1980) Methods of test for soils: determination of specific gravity Section 1 fine grained soils
IS 2720: Part IV: (1985) Methods of test for soils: grain size analysis
IS 2720: Part V: (1985) Method of test for soils: determination of liquid and plastic limit
IS 2720: Part VIII: (1983) Methods of test for soils: determination of water content-dry density relation using heavy compaction
IS 2720: Part XVI: (1987) Methods of test for soil: laboratory determination of CBR

Improved Performance of Railroad Ballast Using Geogrids

Chuhao Liu, Ngoc Trung Ngo and Buddhima Indraratna

Abstract Geogrids are commonly used to stabilise and reinforce ballast, and over the various laboratory tests have been carried out to determine how geogrids affect the interface between geogrid and ballast aggregates. This paper presents a critical review and interpretation of the results of large-scale direct shear tests and cyclic tests on key parameters such as the interlocking effects of aperture size and the location of geogrids. Field investigations from sites at Bulli and Singleton as well as findings from Discrete Element Modelling, including the influence zone of geogrid and the linear relationship between geometric anisotropy and stress ratio, are examined and discussed. It also includes a presentation and discussion of analytical modelling for quantifying the geogrid reinforcing effect (pullout tests).

Keywords Geogrid · Ballast · Rail transport · Discrete element modelling

1 Introduction

Ballasted rail tracks are the major infrastructure catering for public and freight transport in many countries. Ballast is a free-draining granular medium designed as a load-bearing layer in rail tracks; its main functions are as follows: (i) transmitting induced train loads to the underneath layers at a reduced and acceptable level of stress, (ii) providing lateral resistance, and (iii) facilitating drainage for tracks (Selig and Waters 1994; Indraratna et al. 2011a). Upon repeated train passage, ballast particles are almost free to move laterally and this leads to the settlement of sub-

C. Liu · N. T. Ngo · B. Indraratna (✉)
Centre for Geomechanics and Railway Engineering, University of Wollongong, Wollongong, NSW 2500, Australia
e-mail: indra@uow.edu.au

C. Liu
e-mail: cl751@uowmail.edu.au

N. T. Ngo
e-mail: trung@uow.edu.au

R. Sundaram et al. (eds.), *Geotechnics for Transportation Infrastructure*, Lecture Notes in Civil Engineering 29,
https://doi.org/10.1007/978-981-13-6713-7_13

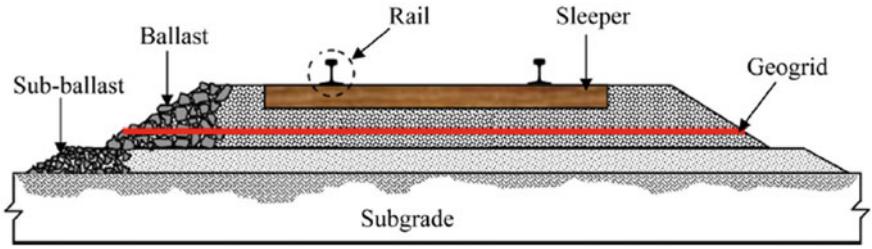

Fig. 1 Geogrid reinforced railway Indraratna et al. (2011a, b)

grade soil (foundation). Significant degradation of ballast due to track substructures subjected to large cyclic stresses causes the ballast to become fouled, less angular, and its shear strength decreases (Indraratna et al. 2011a). These issues result in excessive track settlement and instability, as well as high maintenance costs.

These problems can be mitigated by utilising planer geosynthetics; three-dimensional cellular reinforcement (geocells) and energy absorbing rubber mats. The ability of geosynthetics to improve track stability has been the subject of numerous experimental and numerical investigations (e.g. Kwon and Penman 2009; Biabani et al. 2016a; Bathurst and Raymond 1987; Rujikiatkamjorn et al. 2013), among others, all of whom conclude that geosynthetics could stabilise ballast and thus reducing maintenance costs. Figure 1 shows a schematic diagram where geogrid is used in ballasted tracks. Much research has been carried out on geogrid reinforced ballast in order to understand how geogrids interact with particles and how to optimise it as reinforcement. This paper will critically examine how geogrids improve the performance of ballasted tracks. The Authors' assessment is categorised into three main parts: laboratory testing, field investigations and computational analysis (theoretical aspects and DEM simulations).

2 Laboratory Testing

Brown et al. (2007) carried out several full-scale experiments on geogrid reinforced ballast to determine some key factors (aperture size, stiffness, profile of the rib cross section and location) that influence geosynthetic reinforcement. They find that the aspect ratio (size of aperture to the mean ballast size) helps to quantify the effectiveness of geogrid reinforcement. With 50-mm ballast, 65-mm aperture has the smallest settlement after 3000 cycles loading, which means the optimum aspect ratio is 1.3. Hussaini (2013) also carried out large-scale direct shear tests for geogrids with different size apertures; he used the interface efficiency factor (α) previously defined by Koerner (1998) to quantify the degree of reinforcement. This factor is equal to the ratio of the apparent shear strength of the geogrid/ballast interface to the internal shear strength of the ballast, hence:

$$\alpha = \frac{\tan \delta}{\tan \phi} \tag{1}$$

where δ is the apparent friction angle of the geogrid/ballast interface and ϕ is the internal friction angle of the ballast. Hussaini (2013) reports that with 35-mm ballast the optimum size aperture of geogrid is 42.5 mm, which means the optimum aspect ratio is 1.2 in this case. Although the optimum aspect ratio between these two references is different, they both conclude that the reinforcement became more effective as the aspect ratio increased, but after reaching its optimum point it became less effective as the aspect ratio increased further (Indraratna et al. 2017).

Brown et al. (2007) report that in experiments with a lighter overburden, as the geogrid became stiffer, the extent of reinforcement decreased, but in tests with a higher overburden, stiffer grids showed better reinforcement. They thus concluded that the overburden load needs to be high enough to mobilise the better reinforcement provided by stiffer geogrid because with a lower overburden load, stiffer grids will not deform and will not form good interlocks.

Hussaini et al. (2016) carried out several large-scale cyclic tests that were instrumented by fibre bragg grating (FBG). They find that the lateral and vertical deformation decreased using geogrids, as was the breakage of ballast. They also report that the optimum location of geogrid for reducing breakage is 130 mm above the sub-ballast. However, Brown et al. (2007) carried out two tests with geogrids at the bottom and mid-depth of the ballast layer and one test with two geogrids at the bottom and mid-depth, respectively. Their results indicate that the optimum location is at the bottom of the ballast layer, the usual position used in the field, and two geogrid installations did not provide more effective reinforcement. However, Raymond and Ismail (2003) reported that the geogrid should be as close as possible to the bottom of the sleeper and two geogrid layers give better reinforcement than one. Hussaini (2013) reported that the friction angle of the grid/ballast interface decreased with increasing normal stress, as expected.

Indraratna et al. (2011b) carried out several large-scale direct shear tests under different normal stress for ballast and geogrid reinforced ballast. Shear stress–strain results measured in the laboratory are shown in Fig. 2. They report that the peak shear stress of geogrid reinforced ballast is higher than unreinforced ballast for all normal stresses due to the interlocking effect between geogrid and ballast. They also report that while geogrids reduce dilation they have no effect on compression, so they conclude that geogrids restrict the movement of ballast, and reduce dilation (Tutumluer et al. 2012; Biabani et al. 2016b). As for compression, since the geogrids are thin and flexible, they will not have very much influence on compression. They then carried out tests for ballast with different degrees of fouling and report that the peak shear stress continues to increase as the normal stress increases, but it decreases as the degree of fouling increases. The reason why coal fines reduce the peak stress is because they fill the voids between particles and reduce the particle to particle friction. They said the fines lubricate the ballast and facilitate the particle's rolling and sliding. Therefore, fouling will increase the effect of dilation.

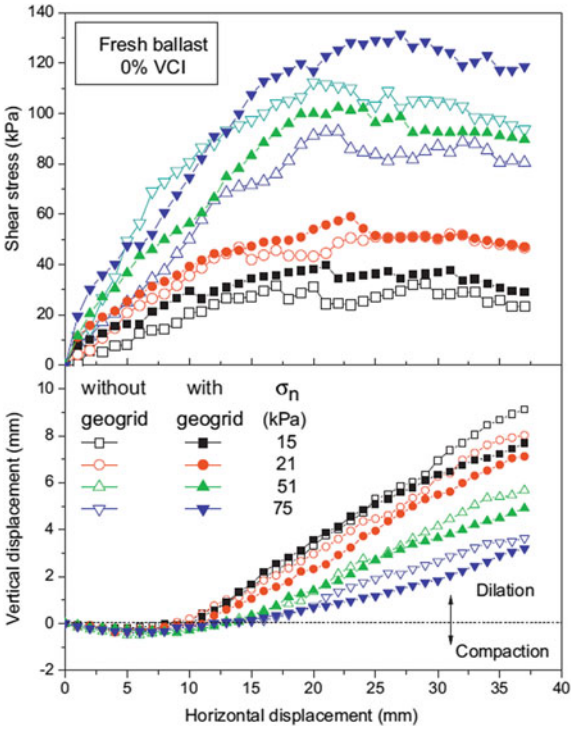

Fig. 2 Direct Shear Test Results (Indraratna et al. 2011b)

Indraratna et al. (2013) used a novel track process simulation apparatus (TPSA) to investigate the deformation of fouled ballast reinforced with geogrid. The TPSA was modified based on the design of Indraratna and Salim (2003), and the lateral stress ratio used in TPSA was justified by field measurements at the Bulli and Singleton tracks in Australia. As Fig. 3 shows, there are three key parts: the horizontal and vertical displacement measure system, the confining stress controlling system, the axial load system and the prismoidal triaxial chamber. The void contaminant index (VCI) proposed by Indraratna et al. (2010a) is used to quantify the degree of fouling, as shown below

$$\mathrm{VCI} = \frac{1+e_\mathrm{f}}{e_\mathrm{b}} \times \frac{G_\mathrm{sb}}{G_\mathrm{sf}} \times \frac{M_\mathrm{f}}{M_\mathrm{b}} \times 100 \tag{2}$$

where, e_f is the void ratio of fouling material, e_b is the void ratio of the fresh material, G_sb is the specific gravity of the fresh material, G_sf is the specific gravity of the fouling material, M_f is the dry mass of fouling material, and M_b is the dry mass of fresh material.

The lateral and vertical displacement of fresh and fouled ballast with and without geogrid inclusion were measured during the test and revealed that the geogrid reduced the lateral and vertical displacement because the particles over geogrid are

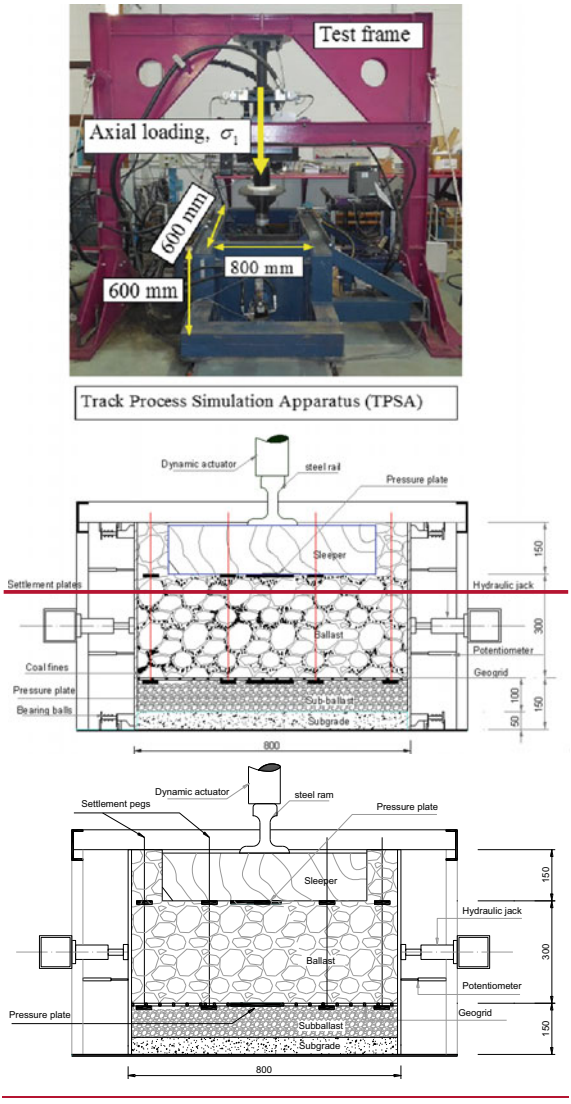

Fig. 3 View of TPSA. Modified after Indraratna et al. (2013) with permission from ASCE

compressed and penetrated partially into apertures to create an interlock between ballast and geogrid. This interlock acts as an internal non-horizontal deformed boundary that stops the particles from moving freely (Ngo et al. 2017a; Indraratna et al. 2016). This increase in the VCI leads to an increase in lateral displacement as the coal fines coat the particles and inhibit surface contact between them. These fouling materials could provide a lubricating effect that helps the particles roll and slide over each other. They also measured the vertical displacement via the linear variable differential transformer (LVDT) and settlements pegs and found that

geogrid reduced the settlement of fresh ballast while all the fouled ballast and fresh ballast reinforced with geogrid had the smallest settlement. They also reported that all the samples settled rapidly during the initial 100,000 cycles, began to gradually deform within 300,000 cycles, and then reached relatively stable settlement towards the end of cyclic loading (500,000 cycles). They believe this phenomenon indicates that in the first range of cyclic loading, the ballast is rearranged and becomes denser, but after reaching a certain degree of compression, any further loading cannot cause further settlement, it only promotes dilation. They also report that in terms of the effect of the VCI, the geogrid reduced the settlement of the fresh ballast quite significantly (a 52 and 32% decrease in terms of lateral and vertical deformation). However, an increase in the VCI decreases this reduction because when the VCI equals 40%, the reduction in lateral and vertical displacement decreased by 12 and 5%, respectively. Beyond this point of fouling, the effect of geogrid can be omitted so they concluded that 40% VCI is the threshold value, beyond which geogrid has almost no reinforcing effect on ballast and will cause premature dilation. They therefore recommended this value as a guide for track maintenance. They also carried out a DEM simulation to further understand the deformation of fouled ballast and then compare it with the laboratory results.

3 Field Investigations

Indraratna et al. (2010a) carried out a field investigation at Bulli, New South Wales, Australia to study the benefit of installing a layer of geosynthetics at the interface between ballast and sub-ballast and also compare the behaviour of recycled graded ballast and uniform fresh ballast. They installed settlement pegs, displacement transducers and pressure cells to measure the lateral and vertical displacement, as shown in Fig. 4. Since the settlement of graded recycled ballast is less than uniform fresh ballast, their field measurements show that geosynthetics can reduce the lateral displacement of fresh ballast by a large amount and recycled ballast reinforced with geosynthetics performed as well as fresh ballast without geosynthetic reinforcement. They also concluded that installing a geocomposite layer at the interface between ballast and capping can provide internal confinement and thus reduce the maintenance costs.

Indraratna et al. (2014a) reported their field investigations at Singleton where they measured the vertical strains of ballast reinforced by three types of geogrids and the long term and transient strain of geogrids against time with strain gauges. Their measurements indicate that the reinforcing effect of geogrids is mainly controlled by their geometric and mechanical properties and the type of subgrade. They also find that geogrids reduced vertical settlement by around 35%, thus indicating the apparent benefits of reducing maintenance costs. They conclude that the optimum size of geogrids with the smallest amount of ballast deformation is 1.1 D_{50}.

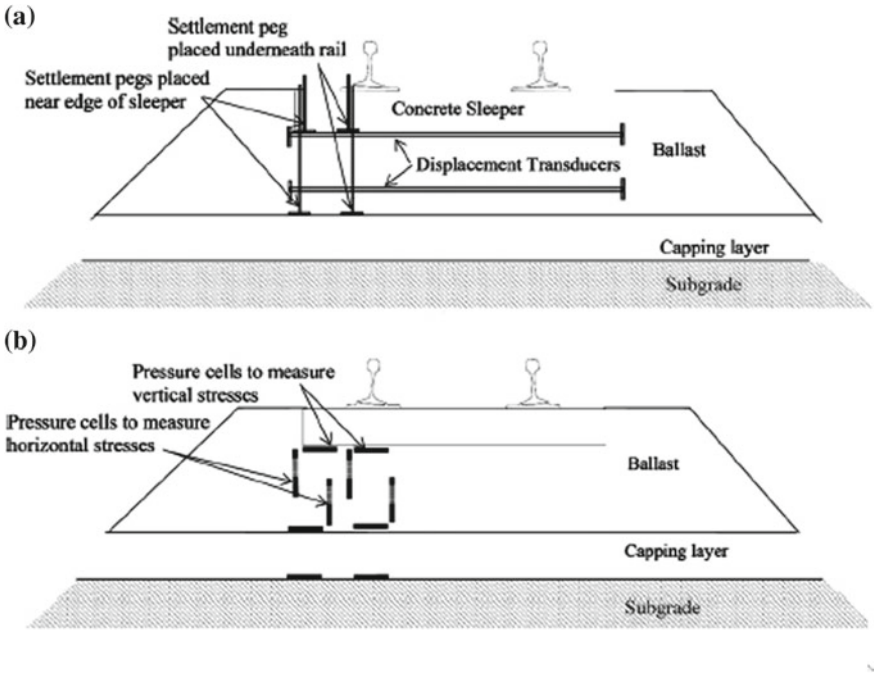

Fig. 4 **a** Placement of settlement pegs and displacement transducers; **b** placement of pressure cells. Indraratna et al. (2010a) with permission from ASCE

4 Discrete Element Modelling

Cundall and Strack (1979) proposed a distinct element method to model the mechanical behaviour of the particles assemblies. They developed this method by modelling the interaction between particles in contact and the motion of each particle. They then validated this method by comparing the force vector plots from this simulation from a program called BALL with those from a photoelastic analysis, and concluded that this method predicts the behaviour of these assemblies very well. DEM has been used by Lim and McDowell (2005), Ngo et al. (2017b), Huang et al. (2009), Indraratna et al. (2014b), among others to model the behaviour of ballast. McDowell et al. (2006) developed a discrete element model to simulate the pull-out test and cyclic triaxial test for ballast reinforced by geogrid. They began by simulating unreinforced ballast in a large-scale triaxial test and then validating the results using reported by Indraratna et al. (1998). They considered angularity by using clumps consisting of several overlapping spheres to model the real shapes of ballast. After comparing the DEM results and the results from the experiments, they found that 0.8 was the value of inter-particle friction that matched the real shear strength of ballast in the experiments. However, dilation did occur in some cases, which conflicted with compression in the experiments, but they said this is probably

caused by the ballast not breaking in DEM. They carried out several DEM simulations with four aspect ratios (1.6, 1.4, 1.1 and 0.9) in the pull-out tests under the same 0.5 kN surcharge and found the simulation with an aspect ratio of 1.4 had the highest pull-out force at the smallest strain; they concluded that 1.4 is the optimum aspect ratio for this case. They also found that the average shear contact force reached its maximum point at the geogrid and then disappeared 20 cm above and below it, and thus concluded that the maximum reinforcing effect provided by geogrid is 20 cm above and below it. Finally, they simulated a cyclic triaxial test with three layers of geogrid and then developed a force ratio β to quantify the effect of reinforcement. It is defined as the ratio of the average contact force in a cuboid 1 cm above and below the four intact apertures in the geogrid to the average contact force in the cuboid 2 cm above and below the entire cross section. Therefore, according to the variation of β, there were strong contacts in the middle of two geogrids during unloading.

Ngo et al. (2014) used DEM to simulate large-scale direct shear tests for fresh and foul ballast reinforced with geogrid. They also used the Void Contaminant Index (VCI) defined by Indraratna et al. (2010b) to quantify the degree of fouling and found that fouled ballast will reduce the number of broken bonds, which agrees with the experiment. Ngo et al. (2014) reported that the DEM simulations show that the maximum strain of the geogrid with a 40% VCI of fouled ballast is less than in the fresh ballast because the coal fines increase the amount of contacts between particles and geogrid, thus reducing the interlocking effect between ballast and geogrid.

Chen et al. (2014) used DEM to simulate large box pull-out tests, but unlike McDowell et al. (2006) they modelled geogrids by bonding several small balls together with contact and parallel bonds, and also developed a new model to combine two layers of small balls by parallel bonds. They used four types of clumps (2-ball, 4-ball, 8-ball tetrahedral, and 8-ball flaky) to simulate the disposal angle. This approached was also used by Ngo et al. (2016), and Hang et al. (2010). The critical state angle for the disposal of ballast should be a function of the inter-particle friction angle and angularity. According to Kwan (2006), they chose 0.6 as the particle–particle coefficient of friction and also simulated 20-mm-diameter spheres for comparison. The disposal angle in the DEM simulations showed that the disposal angles of the 2-ball and 4-ball clumps are consistent with the real disposal angle of around 40°. The disposal angles of 8-ball tetrahedral and 8-ball flaky are greater than 40° because there are some large voids in the ballast caused by the extra interlock of the complex shape. The simulation results agree with the results of the experiments, especially for the initial 20-mm displacement. They also deduced from the DEM simulations that the shape factor has almost no influence on the initial 20-mm displacement.

Sufian et al. (2017) used DEM to study how the anisotropy of the contact networks influence the internal friction angle. They divided all the contact networks into four sub-networks; strong and non-sliding, strong and sliding, weak and non-sliding, and weak and sliding. The strong and weak contacts are defined by the mean inter-particle contact force (Radjai et al. 1998; Thornton and Antony 1998;

Han et al. 2011). If the contact force of this contact is higher than the mean inter-particle contact force it belongs to the strong contact, but according to Alonso-Marroquín et al. (2005), the contact with the friction force that equals the product of the inter-particle coefficient of friction times the normal contact force belongs to the sliding contact. So by calculating the contribution made by four kinds of contact sub-networks, they found that the shear resistance comes mainly from the geometric anisotropy of the strong and non-sliding contact sub-networks, denoted as $a_c^{s\eta}$. They therefore concluded that the strong and non-sliding sub-networks formed an almost solid structure that forms the main shear resistance, while other three contact networks formed a fluidic structure to form the mean stress. They also found that a unique linear relationship between the geometric anisotropy of the strong and non-sliding sub-networks and the macroscopic stress ratio, as follows:

$$\frac{q}{p} = 0.4a_c^{s\eta} \tag{3}$$

5 Theoretical Analysis

Teixeira et al. (2007) reported that the pull-out resistance has two parts, where one is passive resistance from the transverse ribs and another is the shear resistance between the soil and the surface of the longitudinal and transverse ribs.

Jewell et al. (1984) developed an analytical model to calculate the pull-out force; their theory has two parts, the skin friction between the soil and the reinforcement plan and the other is the bearing force mobilised by the transvers ribs in grids. They assumed that these two parts are independent and additive, and the maximum reinforcement is equal to a fully rough sheet where the friction angle is equal to soil's friction angle. Thus, the pull-out force can be calculated as:

$$P = 2LW\sigma_n' f_b \tan\phi \tag{4}$$

where, L the length of the geogrid, W is the length of the geogrid, σ_n' is the effective normal stress at the geogrids surface, f_b is the bond coefficient which is limited between 0 and 1. When it is equal to 1, the pull-out force will reach its maximum, and the skin friction part of the pull-out force is described as:

$$P_{sf} = 2\alpha_s LW\sigma_n' \tan\xi \tag{5}$$

where α_s is a fraction of the area of the reinforcement plan, ξ is the friction angle between the surface of the geogrid and the soil. The bearing stress part is determined as:

$$P_{bs} = \left(\frac{L}{S}\right) W \alpha_b B \sigma_b' \tag{6}$$

where S is the size of the geogrid aperture, so $\frac{L}{S}$ means the number of bearing surfaces in one strip, B is the thickness of the grids, α_b is the fraction of available bearing area in the total area WB, and σ_b' is the effective stress normal to the bearing surface of the ribs. Jewell et al. (1984) developed an equation of a lower estimate of this stress, as given by:

$$\frac{\sigma_b'}{\sigma_n'} = \tan\left(\frac{\pi}{4} + \frac{\phi}{2}\right) \exp\left[\left(\frac{\pi}{2} + \phi\right) \tan\phi\right] \tag{7}$$

Equation 7 shows that σ_b' depends solely on the friction angle of soil, which is unreasonable so Jewell (1990) said the particle size is also an important factor that will influence this parameter. He found out that when $B/D_{50} < 10$, D_{50} is the mean particle size of soil and σ_b' will decrease with increasing B/D_{50}, so when $B/D_{50} > 10$, it will remain constant, as defined by:

if $B/D_{50} < 10$

$$\frac{\sigma_b'}{\sigma_n'} = \left(\frac{\sigma_b'}{\sigma_n'}\right)_{\infty} \left(\frac{20 - B/D_{50}}{10}\right) \tag{8a}$$

and if $B/D_{50} > 10$

$$\frac{\sigma_b'}{\sigma_n'} = \left(\frac{\sigma_b'}{\sigma_n'}\right)_{\infty} \tag{8b}$$

Palmeria and Milligan (1989) reported that reducing the space between the bearing ribs decreased the maximum pull-out force due to interference between thee bearing members. They therefore defined a term called the degree of interference which is quantified by comparing the pull-out force of the geogrid and the ideal maximum pull-out force upon which each grid acts as an isolated grid without interacting with each other, hence

$$\mathrm{DI} = 1 - \left(P_p / nP_0\right) \tag{9}$$

where DI is the degree of interference, P_p is the maximum pull-out force for geogrid, n is the number of grids, P_0 is the maximum pull-out force for a single aperture. They then suggested the probable empirical equation to calculate DI should consider the number of bearing members in the geogrid, and the size and thickness of the apertures. Jewell (1990) developed the following equation

$$\mathrm{DI} = \left(1 - \frac{1}{n}\right)\left(1 - \frac{(S/\alpha_b B)}{(S/\alpha_b B)_\phi}\right) \tag{10}$$

where, $(S/\alpha_b B)_\phi$ means the ideal condition that makes f_b reach its maximum limit, which is 1. Note that DI increases with an increasing number of ribs, so where there are more ribs, there will be a greater difference between one of apertures in the geogrids and an isolated aperture. According to the second part of Eq. (9), DI decreases as the size of the aperture increases, and increases as the geogrid becomes thicker. Because of the degree of interference, Palmeria and Milligan (1989) modified the equation of calculating bond coefficient as below

$$f_b = (\tan \xi_{sr} / \tan \phi)$$

$$f_b = (1 - \mathrm{DI})(B/S)\left(\sigma_b^{'}/2\sigma_n^{'} \tan \phi\right) \tag{11}$$

where ξ_{sr} is the equivalent friction angle between soil and geogrid, ϕ is the friction angle of soil.

6 Conclusions

This paper reviewed how geogrids improved the performance of ballast, as carried out in the laboratory, in field investigations, in DEM simulations and by theoretical analysis. The laboratory experiments revealed several results of large-scale direct shear tests and cyclic triaxial tests, where the key parameters that influence the reinforcing effect were discussed from recent literature. In the second part, several studies on using DEM simulate pull-out tests and direct shear tests were reviewed, and the new findings of a correlation between anisotropic geometry and the stress ratio were reviewed and discussed. This approach is a promising way to do research on the interaction between geogrid and particles. In the last part, theoretical analysis of pull-out tests was presented and improvements to the original analytical equation were also introduced. This analytical model is very important for understanding and quantifying the mechanism of geogrid/soil interaction.

Acknowledgements The authors greatly appreciate the financial support from the Rail Manufacturing Cooperative Research Centre (funded jointly by participating rail organisations and the Australian Federal Government's Business Cooperative Research Centres Program) through Project R2.7.1. The performance of stabilised ballast in rail tracks. The author would also like to thank A/Prof Cholachat Rujikiatkamjorn for his guidance and support at various times. The Authors are also grateful to UOW technical staff, namely, Mr. Alan Grant, and Mr. Cameron Neilson for their assistance during the laboratory study.

References

Alonso-Marroquín F, Luding S, Herrmann HJ, Vardoulakis I (2005) Role of anisotropy in the elastoplastic response of a polygonal packing. Phys Rev E 71(5):1–18

Bathurst RJ, Raymond GP (1987) Geogrid reinforcement of ballasted track. Transp Res Rec 1153:8–14

Biabani, Indraratna, Ngo NT (2016a) Modelling of geocell-reinforced subballast subjected to cyclic loading. Geotext Geomembr 44(4):489–503

Biabani MM, Ngo NT, Indraratna B (2016b) Performance evaluation of railway subballast stabilised with geocell based on pull-out testing. Geotext Geomembr 44(4):579–591

Brown SF, Kwan J, Thom NH (2007) Identifying the key parameters that influence geogrid reinforcement of railway ballast. Geotext Geomembr 25(6):326–335

Chen C, McDowell GR, Thom NH (2014) Investigating geogrid-reinforced ballast: experimental pull-out tests and discrete element modelling. Soils Found 54(1):1–11

Cundall P, Strack (1979) A discrete numerical model for granular assemblies. Geotechnique 29(1):47–65

Han J, Bhandari A, Wang F (2011) DEM analysis of stresses and deformations of geogrid-reinforced embankments over piles. Int J Geomech ASCE 12(4):340–350

Huang H, Tutumluer E, Hashash YMA, Ghaboussi J (2009) Discrete element modeling of aggregate behavior in fouled railroad ballast. Geotech Spec Publ 192:33–41

Huang H, Tutumluer E, Hashash YMA, Ghaboussi J (2010) Discrete element modeling of coal dust fouled railroad ballast behavior. In: The 89th annual meeting DVD of the transportation research board, Washington, DC

Hussaini SKK (2013) An experimental study on the deformation behaviour of geosynthetically reinforced ballast. Ph.D. thesis, University of Wollongong

Hussaini SKK, Indraratna B, Vinod JS (2016) A laboratory investigation to assess the functioning of railway ballast with and without geogrids. Transp Geotech 6:45–54

Indraratna, Salim (2003) Deformation and degradation mechanics of recycled ballast stabilised with geosynthetics. Soils Found 43(4):35–46

Indraratna B, Ionescu D, Christie HD (1998) Shear behavior of railway ballast based on large-scale triaxial tests. J Geotech Geoenviron Eng 124(5):439–449

Indraratna B, Nimbalkar S, Christie D, Rujikiatkamjorn C, Vinod J (2010a) Field assessment of the performance of a ballasted rail track with and without geosynthetics. J Geotech Geoenviron Eng 136(7):907–917

Indraratna, Nimbalkar, Tennakoon (2010b) The behaviour of ballasted track foundations: track drainage and geosynthetic reinforcement. In: GeoFlorida 2010: advances in analysis, modeling and design, pp 2378–2387

Indraratna B, Ngo NT, Rujikiatkamjorn C (2011a) Behavior of geogrid-reinforced ballast under various levels of fouling. Geotext Geomembr 29(3):313–322

Indraratna B, Salim W, Rujikiatkamjorn C (2011b) Advanced rail geotechnology—ballasted Track. CRC Press, Taylor & Francis Group, London, UK

Indraratna B, Ngo NT, Rujikiatkamjorn C (2013) Deformation of coal fouled ballast stabilized with geogrid under cyclic load. J Geotech Geoenviron Eng 139(8):1275–1289

Indraratna B, Ngo NT, Rujikiatkamjorn C, Vinod J (2014a) Behaviour of fresh and fouled railway ballast subjected to direct shear testing—a discrete element simulation. Int J Geomech ASCE 14(1):34–44

Indraratna B, Nimbalkar S, Rujikiatkamjorn C (2014b) Enhancement of rail track performance through utilisation of geosynthetic inclusions. Geotech Eng J SEAGS AGSSEA 45(1):17–27

Indraratna B, Nimbalkar, Ngo NT, Neville (2016) Performance improvement of rail track substructure using artificial inclusions—experimental and numerical studies. Transp Geotech 8:69–85

Indraratna B, Sun Q, Ngo NT, Rujikiatkamjorn C (2017) Current research into ballasted rail tracks: model tests and their practical implications. Aust J Struct Eng 1–17

Jewell RA (1990) Reinforcement bond capacity. Geotechnique 40(3):513–518
Jewell RA, Milligan GWE, Sarsby RW, DuBois D (1984) Interaction between soil and grids. Polymer grid reinforcement. Thomas Telford, pp 18–30
Koerner RM (1998) Designing with geosynthetics, 4th edn. Prentice Hall, New Jersey
Kwan CC (2006) Geogrid reinforcement of railway ballast. Ph.D. thesis, University of Nottingham
Kwon J, Penman J (2009) The use of biaxial geogrids for enhancing the performance of sub-ballast and ballast layers-previous experience and research. In: Bearing capacity of road, railways and airfields, Taylor & Francis Group, London
Lim, McDowell (2005) Discrete element modelling of railway ballast. Granular Matter 7(1):19–29
McDowell GR, Harireche O, Konietzky H, Brown SF, Thom NH (2006) Discrete element modelling of geogrid-reinforced aggregates. Proc Inst Civil Eng-Geotech Eng 159(1):35–48
Ngo NT, Indraratna B, Rujikiatkamjorn C (2014) DEM simulation of the behaviour of geogrid stabilised ballast fouled with coal. Comput Geotech 55:224–231
Ngo NT, Indraratna B, Rujikiatkamjorn C (2016) Modelling geogrid-reinforced railway ballast using the discrete element method. Transp Geotech 8(2016):86–102
Ngo NT, Indraratna B, Rujikiatkamjorn C (2017a) A study of the geogrid–subballast interface via experimental evaluation and discrete element modelling. Granular Matter 19(3):54–70
Ngo NT, Indraratna B, Rujikiatkamjorn C (2017b) Simulation ballasted track behavior: numerical treatment and field application. Int J Geomech 17(6):04016130
Palmeria EM, Milligan GWE (1989) Scale and other factors affecting the results of pull-out tests of grids buried in sand. Geotechnique 39(3):511–542
Radjai F, Wolf DE, Jean M, Moreau JJ (1998) Bimodal character of stress transmission in granular packings. Phys Rev Lett 80(1):61
Raymond G, Ismail I (2003) The effect of geogrid reinforcement on unbound aggregates. Geotext Geomembr 21(6):355–380
Rujikiatkamjorn C, Ngo NT, Indraratna B, Vinod J, Coop M (2013) Simulation of fresh and fouled ballast behavior using discrete element method. In: Proceedings of the international conference on ground improvement and ground control, Research Publishing, Singapore, pp 1585–1592
Selig ET, Waters JM (1994) Track geotechnology and substructure management. Thomas Telford, London
Sufian A, Russell, Whittle AJ (2017) Anisotropy of contact networks in granular media and its influence on mobilised internal friction. Géotechnique 1–14
Teixeira SH, Bueno BS, Zornberg JG (2007) Pullout resistance of individual longitudinal and transverse geogrid ribs. J Geotech Geoenviron Eng 133(1):37–50
Thornton C, Antony J (1998) Quasi-static deformation of particulate media. Phil Trans R Soc London A: Math Phys Eng Sci 356(1747):2763–2782
Tutumluer E, Huang H Bian (2012) Geogrid-aggregate interlock mechanism investigated through aggregate imaging-based discrete element modeling approach. Int J Geomech 12(4):391–398

Incorporation of the Influence of Hexagonal Stabilisation Geogrids into Mechanistic-Empirical Pavement Design Method

Mike Horton, Piotr Mazurowski and Timothy Oliver

Abstract Since their introduction to civil engineering almost 40 years ago, geogrids have become one of the standard solutions for constructing roads over soft soils. However, traditionally geogrids are used for the primary purpose of reaching a required bearing capacity of the road foundation, and they are not considered as providing benefit to the final pavement structure itself and their influence is not taken into account in the whole pavement design. In recent years, a new approach has been introduced to use geogrids to stabilise the unbound aggregate base of the whole pavement structure. Stabilisation of an aggregate layer with a suitable geogrid can improve the mechanical properties of this layer, which results in substantial increase of final pavement performance. This can be utilised either to increase pavement life or to reduce the thickness of the pavement or a combination of the two, including thickness of asphalt layers, leading to reduced construction costs. This way of incorporating geogrids can be used in pavements constructed both on weak and firm soils. This paper describes the process of developing a modification of Mechanistic-Empirical Pavement Design Method (MEPDM) which allows for incorporation of the influence of one type of stiff hexagonal geogrid on the performance of a whole pavement construction. Results of full-scale accelerated pavement tests of non-stabilised and geogrid stabilised sections are presented, as well as other tests and studies which confirm that geogrid can increase the stiffness of an unbound aggregate layer, limit deformations and retain higher stiffness for longer period of time. Based on analysis of data from these tests, a modification of MEPDM has been developed in the form of special algorithms for calculation of the factors enhancing the pavement life.

Keywords Geogrid · MEPDM · Mechanical stabilisation · Pavement optimisation

M. Horton · T. Oliver
Tensar International, Cunningham Court, BB12QX Blackburn, UK
e-mail: mhorton@tensar.co.uk

T. Oliver
e-mail: TOliver@tensar.co.uk

P. Mazurowski (✉)
Tensar Polska, Azymutalna 9, 80-298 Gdańsk, Poland
e-mail: PMazurowski@tensar.pl

R. Sundaram et al. (eds.), *Geotechnics for Transportation Infrastructure*,
Lecture Notes in Civil Engineering 29,
https://doi.org/10.1007/978-981-13-6713-7_14

1 Introduction

Geogrids have been introduced to civil engineering almost 40 years ago. They have been successfully used in a great number of applications, especially in transportation infrastructure projects, such as roads and railways. During that time, geogrids have been constantly developed to create more efficient products, the latest significant development being the introduction of hexagonal structure stabilisation geogrids in 2007. Geogrids can be used in many quite different applications, from reinforced earth structures like retaining walls and steep slopes, through reinforcement of embankment base on weak soils, asphalt reinforcement, to stabilisation of aggregate capping layer, sub-base or base in pavement structures on weak soils. This paper focuses on the use of stabilisation geogrids in pavement structures, but not limited to applications on weak soils only. A modification of Mechanistic-Empirical Pavement Design Method (M-EPDM) developed for one type of hexagonal geogrid is presented here, which allows for incorporation of the benefits of aggregate base stabilisation with geogrid into pavement design procedure.

2 The Concept of Mechanical Stabilisation

When unbound well-graded aggregate is placed and compacted on a layer of stiff geogrid, aggregate particles interlock within the geogrid apertures and are confined by its stiff ribs. A geogrid/aggregate composite is created, in which lateral restraint provided by the geogrid reduces strain and thereby increases the stiffness of the layer compared to the same layer without geogrid. Stiff geogrid ribs resist particle movement, even under cyclic loadings (Liu et al 2017), preventing layer deformation. A geogrid/aggregate composite is often referred to as "Mechanically Stabilised Layer" (MSL) (Fig. 1).

Stabilisation of aggregate with a geogrid increases the stiffness or modulus of a layer. The modulus of unbound aggregate is a function of the stress state (Θ) and is given by the relation (AASHTO (1993)):

$$E = k_1 \Theta^{k_2} \tag{1}$$

where:

Θ—a sum of principal stresses ($\sigma_1 + \sigma_2 + \sigma_3$)

k_1, k_2—constants depending on material type (Fig. 2).

When a load is applied to a layer, the stiff ribs of a geogrid react preventing aggregate particles from moving laterally, thus horizontal principal stresses σ_2 and σ_3 increase. When the sum of principal stresses increases, the modulus of a layer increases, and so the layer has higher bearing capacity compared to the same layer without geogrid.

Fig. 1 Aggregate particles interlocked within geogrid

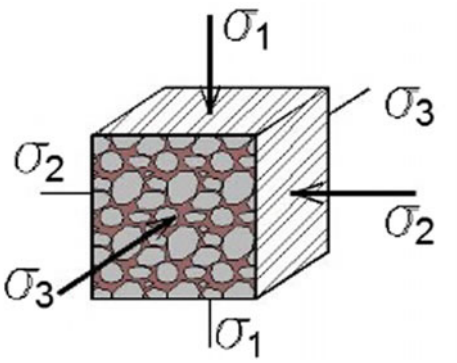

Fig. 2 Principal stresses acting on aggregate

The stiffness increase in stabilised aggregate has been confirmed by laboratory tests. Kwon et al. (2012) used a test combination of AASHTO T307 (Determining the Resilient Modulus of Soils and Aggregates) and NCHRP 598 (Repeated Load Permanent Deformation) to test both stabilised and non-stabilised poorly graded silty gravel samples. A modulus increase of 5–20% has been observed in stabilised samples. Also field tests of in situ resilient modulus conducted with Automated Plate Load Tests (APLT) exhibited 5–30% modulus increase of geogrid stabilised sections compared to non-stabilised control sections (White 2014a, b).

3 The Concept of Pavement Optimisation

The use of geosynthetics in an aggregate base to increase pavement design life or to decrease its thickness for a given design life can assist with "pavement optimisation." Pavement optimisation can be described as delivering the primary design objectives of a pavement at the most economic cost. The design objectives are likely to be a minimum traffic life, but may also include construction time or

meeting environmental needs. In USA, the use of geosynthetics for pavement optimisation has been acknowledged and adopted for common use, and it is described in AASHTO R50-09 Standard (2009). According to it: "Geosynthetics are used in the pavement structure for structural support of traffic loads over the design life of the pavement. The geosynthetic is expected to provide one or both of these benefits: (1) improved or extended service life of the pavement, or (2) reduced thickness of the structural section." This document outlines the procedure that should be undertaken in order to incorporate geosynthetics in pavement design. Although it describes a procedure which is applicable to empirical pavement design methods, the procedure may be adopted for use in mechanistic-empirical pavement design methods as well.

An important requirement stated in the AASHTOR50-09 standard, which should be met no matter which design method is to be used, is the necessity to perform full-scale pavement testing for any geosynthetic being considered. AASHTO R50-09 states: "Because the benefits of geosynthetic reinforced pavement structures may not be derived theoretically, test sections are necessary to obtain benefit quantification." This is important because of differences in performance of different types of geosynthetics, and even different types and grades of geogrids. Physical characteristics, such as tensile strength, are not a reliable indicator of performance in a given application. Strong evidence exists (Jenner et al. (2002)), including full-scale trafficking tests, confirming that geogrids with similar tensile strength characteristics can have quite different performance levels. AASHTO R50-09 recognises that design methods based upon performance testing of one type of geosynthetic may only be applied to use of that specific geosynthetic: "Design procedures use experimentally derived input parameters that are often geosynthetic specific. Thus, computed engineering designs and economic benefits are not easily translated to other geosynthetics."

4 Full-Scale Trafficking Tests

In line with AASHTO R50-09 requirements a series of trafficking tests have been performed in order to quantify benefits of using hexagonal stabilisation geogrid in flexible pavements. Testing consisted of three stages, in which multiple full-scale pavement sections have been constructed and trafficked at the US Army Engineer Research and Development Center (ERDC). Details of test sections arrangement, instrumentation, trafficking and results are available in reports (Jersey et al. 2012; Norwood and Tingle 2014; Robinson et al. 2017); the most important information is summarised below.

Test sections consisted of 2.44 m (8 ft) by 15.2 m (50 ft) areas, build-up is shown on Fig. 3. All sections were constructed using typical construction equipment and technologies inside a hangar, so the potential influence of variable environmental factors has been eliminated. The subgrade was prepared to achieve a bearing capacity of either 3 or 6% CBR. The granular base layer consisted of either

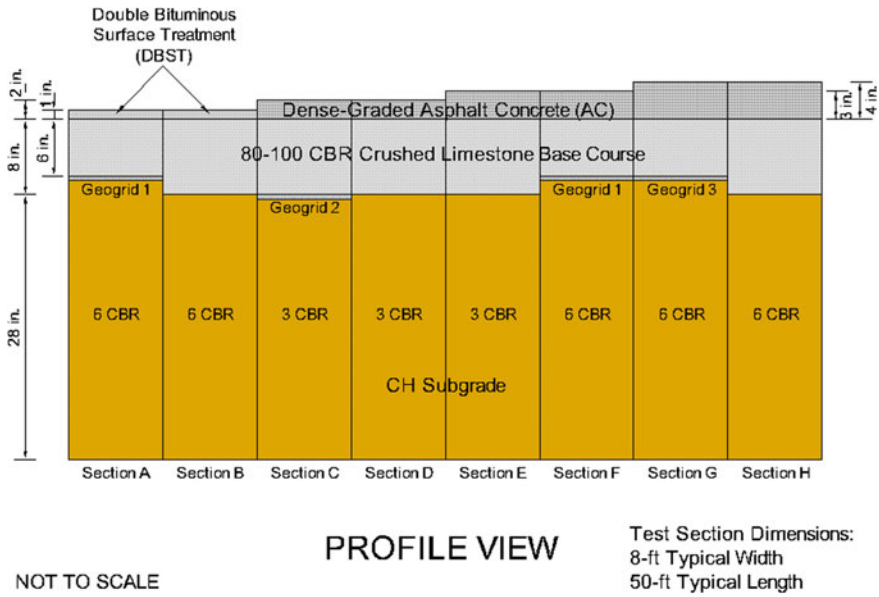

Fig. 3 ERDC test sections build-up

15 or 20 cm of crushed limestone of 90.5–100% CBR compacted at an optimum moisture content. Four of the sections had a base layer stabilised with hexagonal geogrids. Two sections had a double bituminous surface treatment (DBST), and six had surfacing of 5, 7, 5 or 10 cm of dense-graded hot mix asphalt (HMA). Only results for sections with HMA surfacing are discussed within this paper.

The test sections were trafficked with the Heavy Vehicle Simulator (HVS). The HVS is capable of simulating typical heavy highway traffic for accelerated pavement testing (APT). The configuration consisted of tandem-axle dual wheel gear loaded to a load of 20, 000 lb (∼90 kN) and set to deliver a normally distributed bi-directional traffic pattern with a lateral wander of 3 ft (0.9 m). The HVS was equipped with an environmental chamber surrounding the trafficking gear, maintaining a constant temperature of 77 ± 10 °F (25 ± 5.5 °C) in, to minimise the temperature change influence on the asphalt modulus. Throughout the tests, rut depth measurements were collected on all test sections. Rutting was the decisive failure mechanism of all sections tested. Figures 6 and 7 present results from the trafficking of test sections constructed on 3 and 6% CBR subgrade, respectively (Figs. 4 and 5).

All sections with an aggregate base layer stabilised with hexagonal geogrids significantly outperformed the non-stabilised control section. Even stabilised sections with thinner asphalt and/or base layers, performed better than the non-stabilised sections.

Fig. 4 HVS in hangar at ERDC facility

Fig. 5 Tandem-axle dual wheel gear used in ERDC tests

These tests also show one additional aspect of base layer stabilisation with hexagonal geogrids, which is an important novelty in geogrids applications. Geogrids have traditionally been associated with construction on weak and very weak soils. A subgrade of 6% CBR ($\sim Ev2 = 60$ MPa) is a relatively firm subgrade, for which the use of geogrid would be not even considered. Tests completed at ERDC proved that use of hexagonal geogrids in base stabilisation is fully justified and beneficial also in the case of pavements constructed on firm subgrade.

The trafficking tests described above proved that use of hexagonal geogrids to stabilise unbound aggregate base layers provides substantial benefits to pavement structures. These benefits can be utilised either by increasing the life of a pavement without changing its thickness, or by decreasing the thickness of pavement layers while maintaining required life.

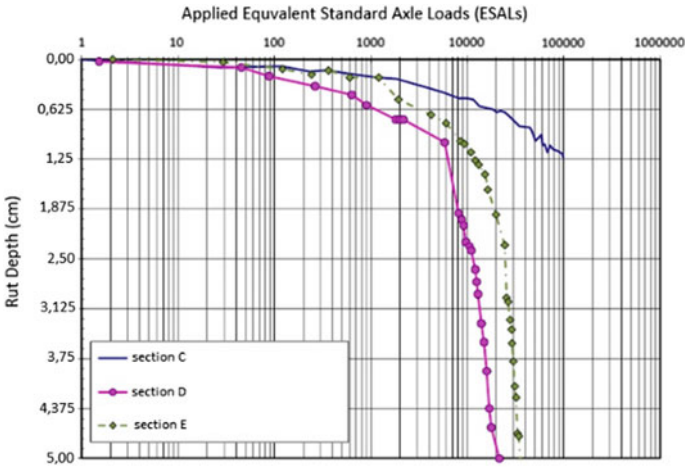

Fig. 6 Trafficking results for sections on 3% CBR subgrade (Jersey et al. 2012)

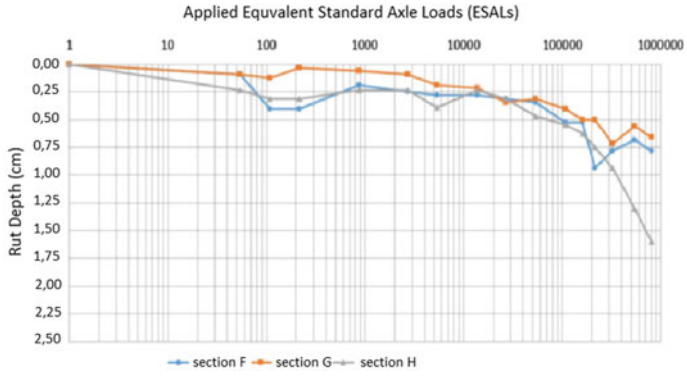

Fig. 7 Trafficking results for sections on 6% CBR subgrade (Robinson et al. 2017)

5 Back-Calculation of Layer Modulus

Data gathered during APT tests have been a basis for modification of mechanistic-empirical pavement design methods (M-EPDM) which incorporates the influence of hexagonal geogrid on a pavement life.

The initial route to modifying M-EPDM was to assume an increase in the modulus of the aggregate layer as a result of stabilisation. To estimate the necessary modulus increase that would deliver the observed life of geogrid stabilised pavement sections from APT tests, back calculations were made.

Of the two main flexible pavements failure mechanisms—permanent deformation and asphalt fatigue cracking—only data for deformation are available from the APT tests. Data on asphalt fatigue cracking have not been collected; however, from

observations of test sections after the tests have been completed, it was clearly seen that pavement permanent deformation was the decisive failure mechanism of all tested sections. In four out of six test sections described above, rut depth has reached at least 0.5 inch ($\sim$12.5 mm). In the remaining two sections, the number of axle loads needed to reach the same rut depth can be extrapolated. 12–12.5 mm rut depth is considered a pavement failure point in many Transfer Functions used throughout the world. Knowing the number of axle loads applied to test sections to reach this rut depth, it is possible to estimate the magnitude of aggregate modulus increase in the geogrid stabilised sections compared to non-stabilised sections.

Pavement sections have been modelled in Bisar 3.0 Layered Elastic Analysis software. A standard axle load of 80 kN with 650 kPa contact pressure has been applied. Pavement layers have been modelled with following parameters:

- asphalt layers: E = 3000 MPa, v = 0.30
- crushed aggregate base: E = 200 MPa, v = 0.30
- subgrade: E = 30 MPa (for 3% CBR subgrade) and 60 MPa (for 6% CBR subgrade), v = 0,35

First, the appropriate Transfer Function (TF) had to be chosen. The resulting life of the same pavement can vary substantially if calculated with different TFs. For the purpose of back calculations described here, the following permanent deformation TFs has been tried:

– Asphalt Institute 12.5 mm subgrade rutting
– Shell 95% 12 mm subgrade rutting
– Austroads
– Nottingham University

In the first stage, results from three non-stabilised sections have been compared with calculations. The best match between calculation results and test results has been obtained using the Shell 95% 12 mm subgrade rutting Transfer Function, and this TF has been used in all subsequent calculations. The TF is given by the relation (Shell (1978)):

$$\varepsilon = k\left(\frac{1}{N}\right)^{m} \tag{2}$$

where:

ε—vertical compressive strain at the top of the subgrade
N—number of axle loads to reach 12 mm rut depth
k = 0.028
m = 0.25

M-E pavement design methods are not able to perfectly predict the life of a pavement. It is almost impossible to get an exact match between calculation results and the actual life of the pavements observed in tests; however, it can be noted that calculated results are in the same order of magnitude as results from tests (Table 1).

Table 1 Calculated and measured pavement life

Test section	No. of ESALs to 0.5″ rut APT	Vertical strain on top of the subgrade[microstrain]	No. of ESALs to 12 mm rut depth—Shell TF
A	6351	2576	13,959
B	11,960	1954	42,163
D	500,000	1075	460,255

Table 2 Pavement life for different UG modulus

Test section	No. of ESALs to 0.5″ rut in APT	No. of ESALs to reach 12 mm rut depth calculated with Shell TF for UG modulus value of:			
		200 MPa	400 MPa	600 MPa	2000 MPa
C	104,000	13,959	50,915	118,543	1,546,501
E&F	2,000,000 (extrapol.)	65,386	132,712	238,520	1,984,617

In the second stage of calculations, stabilised pavement sections have been analysed. A series of calculations have been carried out with different values of unbound aggregate modulus in order to match, as closely as possible, the results obtained in APT tests. Given the relatively similar results of sections E and F, and the fact that for these sections the number of axle loads to reach 0.5″ rut depth had to be extrapolated, both these sections have been analysed together. The results of these calculations are summarised in Table 2.

The above comparison shows that in order to obtain results from an M-E analysis similar to real-life results from testing, the modulus of an aggregate layer stabilised with geogrid should be increased three to ten times. As discussed earlier, it is confirmed that the modulus of a geogrid stabilised aggregate layer is increased. However, no evidence exists to support an increase as high as three to ten times the initial value. This magnitude of increase has to be considered unrealistic and should not be used in pavement design.

This analysis shows that an aggregate modulus increase should not be the only way to incorporate geogrid benefits into M-E pavement design procedure. In the M-E method modification discussed in this paper, a second way of incorporating these benefits has been introduced, in the form of so-called life Shift Factors.

6 Unbound Aggregate Modulus Enhancement Factor

A special algorithm has been developed for calculation of aggregate modulus Enhancement Factor (EF). EF depends on:

- Subgrade modulus
- Thickness of the stabilised layer divided into fully confined, partially confined and unconfined zones

Fig. 8 Multi-level shear box

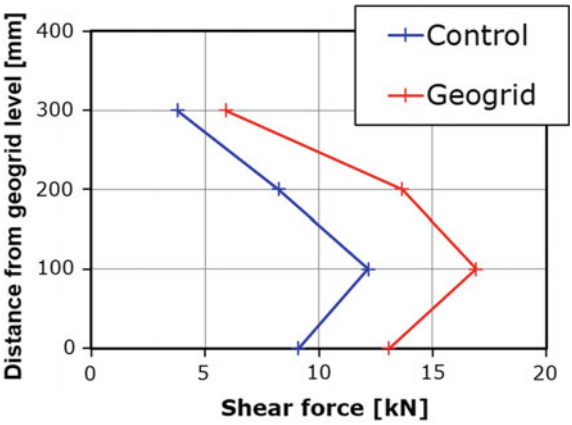

Fig. 9 Shear resistance results

The stabilised layer can be divided into three zones of different confinement effect because the confinement effect diminishes as the distance from a geogrid increases. This phenomenon has been confirmed by the shear tests with multi-level shear box by Horvat et al. (2013). A specially designed 1 × 1 × 1 m shear box, in which the position of shear plane can be varied, was used (Fig. 8). Both a geogrid stabilised aggregate sample and a control sample have been tested. Shear resistance has been significantly higher in the stabilised sample compared to non-stabilised. The difference has been high in a 15–20 cm zone directly above the level of geogrid, and diminished as the distance from geogrid increased (Fig. 9).

Data from this test and others have been used to determine the thickness of fully confined and partially confined zones to be used in algorithm for calculation of aggregate modulus EF.

7 Pavement Life Shift Factors

Shift factors reflect the hexagonal geogrid's ability to not only increase initial parameters and performance of flexible pavements, but also to retain these parameters and performance over longer period of time, compared to non-stabilised pavements. Aggregate layer modulus is retained due to a reduction in deformation by controlling particle movement due to confinement. Strong evidence confirming this effect exists, starting from observation of many roads sections for more than ten years, to numerous laboratory and field tests. NCHRP 598 tests (Kwon et al. (2012)) confirmed greater resistance to permanent deformation at higher number of load cycles of stabilised sample compared to non-stabilised. DEM wheel load simulation confirmed substantial reduction of aggregate particle displacement in stabilised layers under a moving wheel. In situ automated plate load tests (APLT) (Wayne et al. (2014)) demonstrated a 50% reduction in permanent deformation of stabilised sections compared to non-stabilised sections. The APT tests described above are of course also a confirmation of this ability.

Life Shift Factors are not constants, as the geogrids influence on pavement life depends on several factors. Based on detailed analysis of APT tests results, algorithms for calculation of life Shift Factors have been developed, both for asphalt life and for subgrade life. These algorithms take into account:

For asphalt life Shift Factor:

- thickness of asphalt layer
- distance from geogrid to the bottom of lowest asphalt layer
- stabilised layer thickness
- type of hexagonal geogrid

For subgrade life Shift Factor:

- thickness of asphalt layer
- distance from geogrid to the top of the subgrade
- stabilised layer thickness
- type of hexagonal geogrid.

8 Modified M-EPDM Procedure

Standard M-EPDM procedure for flexible pavements design—in simplified form—is shown on a scheme on Fig. 10.

A modified M-EPDM procedure for flexible pavements with unbound granular base layer stabilised with hexagonal geogrid is shown on Fig. 11. As described earlier, there are two separate factors reflecting the beneficial effects of a geogrid which are taken into account simultaneously in the design. First, the modulus of the aggregate layer stabilised with geogrid is increased by multiplying the initial value by a modulus enhancement factor. This is done in the pre-linear elastic analysis

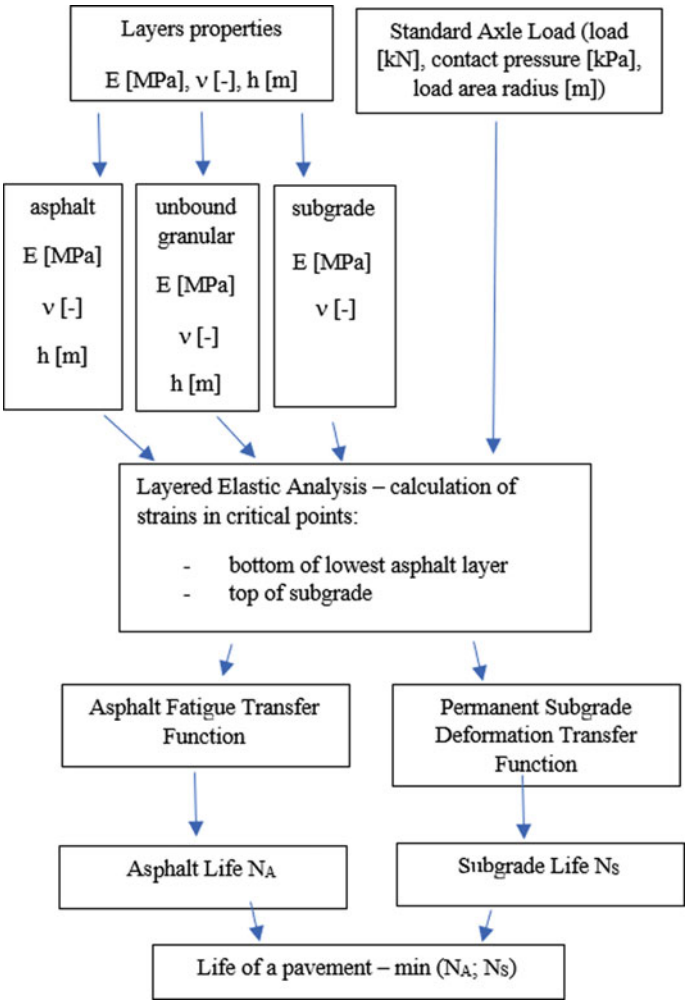

Fig. 10 Standard M-EPDM procedure

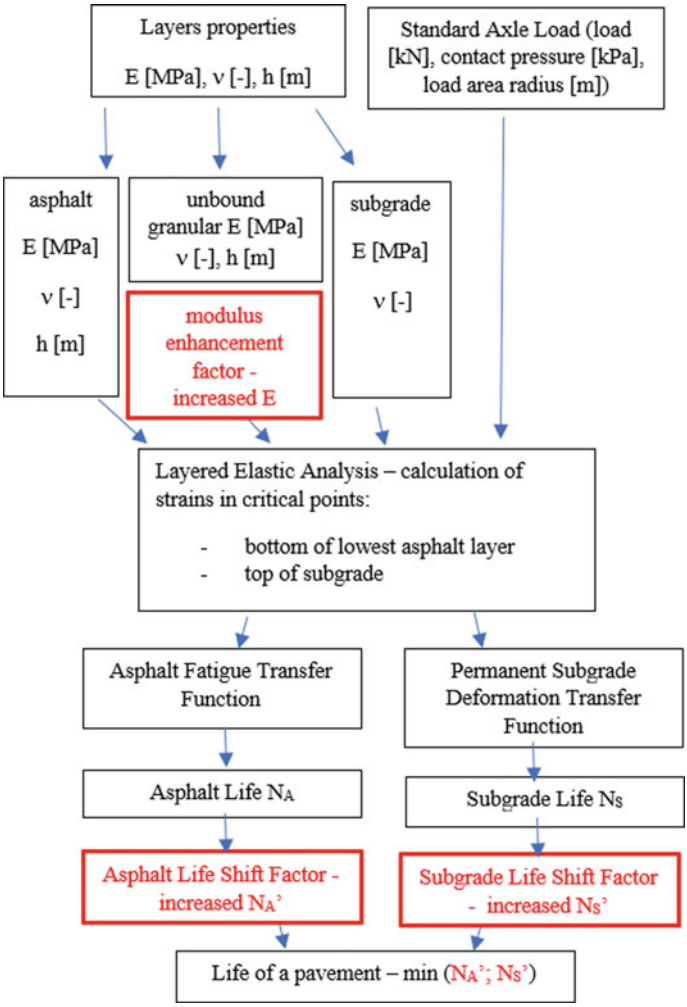

Fig. 11 Modified M-EPDM procedure

(LEA) stage, when material parameters are entered in software. Then, strains in the asphalt layers and the subgrade at critical points and life are calculated, as in standard M-EPDM procedures. Finally, Life Shift Factors are applied to the calculated life, both for asphalt and subgrade, to determine the final life of pavement being designed.

A new M-E pavement design software tool (SPECTRA M-E) has been developed by one producer of hexagonal stabilisation geogrids. This software includes algorithms for the modulus EF and life Shift Factors described above. It is believed to be the first M-EPDM software to incorporate the geogrid effect. Both the methodology behind the algorithms and the software have been validated by a third-party independent reviewer (Applied Research Associates (2015)).

9 Conclusions

Flexible pavements design can by optimised by the inclusion of hexagonal stabilisation geogrids in the unbound aggregate base. Tests described in this paper have confirmed that stabilisation can result in an increase in the life of the pavements or enable a decrease in pavement layers thickness, including asphalt layers, for a given target life. This opens up a range of economic opportunities for the Contractor and Client, not discussed in this paper. These will include construction cost and time savings, reduces construction traffic and associated damage to access roads, or substantial savings in greenhouse gas emission.

Stabilisation geogrids in this application can be used both on weak and firm soils, which is a new approach to geogrids use.

Pavements with base layer stabilised with hexagonal geogrids can be designed with the use of modified Mechanistic-Empirical design methods. The methodology applied to develop the geogrid effect in the form of modulus Enhancement Factors and life Shift Factors included in the SPECTRA M-E modified M-EPDM has been presented in this paper. It is believed to be the first M-EPDM to incorporate stabilisation geogrids in whole pavement analysis.

References

American Association of State Highway and Transportation Officials (1993) AASHTO guide for design of pavement structures, Washington, USA

American Association of State Highway and Transportation Officials (2009) Standard practice for geosynthetic reinforcement of the aggregate base course of flexible pavement structures AASHTO R 50-09, Washington, USA

Applied Research Associates (2015) Independent review of spectra M-E pavement design software, Champaign, USA

Horvat F, Szabolcs F, Zoltan M (2013) Evaluation of railway track geometry stabilisation effect of geogrid layers under ballast on the basis of laboratory multi-level shear box tests, Acta Technical Jaurinensis

Jenner CG, Watts GRA, Blackman DI (2002) Trafficking of reinforced, unpaved subbases over a controlled subgrade. In: Proceedings of 7th international conference on geosynthetics, Nice, France

Jersey SR, Tingle JS, Norwood GJ, Kwon J, Wayne M (2012) Full-scale evaluation of geogrid-reinforced thin flexible pavements. Transport Res Rec, J Transport Res Board, No. 2310, TRB of the National Academies, Washington, USA

Kwon J, Wayne M, Norwood GJ, Tingle JS (2012) The implementation of findings from accelerated pavement testing in pavement design and construction practice, in advances in pavement design through full-scale accelerated pavement testing. In: Jones, Harvey, Mateos, Al-Quadi (eds), Taylor & Francis Group, London, UK

Liu S, Huang H, Qui T, Kwon J (2017) Comparative evaluation of particle movement in a ballast track structure stabilized with biaxial and multiaxial geogrids. Transport Res Rec: J Transport Res Board, No. 2607

Norwood GJ, Tingle JS (2014) Performance of geogrid-stabilized flexible pavements. Final report. EDRC/GSL TR-14-28. U.S. Army ERDC, USA

Robinson WJ, Tingle JS, Norwood GJ (2017) Full-scale accelerated testing of multi-axial geogrid stabilized flexible pavements. Draft final report EDRC/GSL TR-17-X. U.S. Army ERDC, USA

Shell Pavement Design Manual—asphalt pavements and overlays for road traffic (1978) Shell Ltd, London, UK

Wayne M, Kwon J, White D (2014) Assessment of pavement foundation stiffness using cyclic plate load test. In: Proceedings of 10th international conference on geosynthetics, Berlin, Germany

White JD (2014a) In situ performance verifiaction of geogrid-stabilized aggregate layers. Dewitt County, Cuero, Texas—Schlinke Rd., Geomatters Technologies Inc., Ames, USA

White JD (2014b) Preliminary APLT comparision of Ev strain modulus and in-situ resilient modulus/permanent deformation. Geomatters Technologies Inc., Ames, USA

Influence of Crack Depth on Performance of Geosynthetic-Reinforced Asphalt Overlays

V. Vinay Kumar and Sireesh Saride

Abstract The influence of crack depth in the existing pavement layer on the performance of geosynthetic-reinforced asphalt overlays against reflective cracking is evaluated in this study. The two-layered asphalt beam specimens having a crack depth of 40, and 25 mm in the bottom layer are tested under repeated load four-point bending test to understand the influence of crack depth on the performance of geosynthetic-reinforced asphalt overlays. A digital image analysis technique was incorporated to study the failure modes of unreinforced and geosynthetic-reinforced specimen. Two different types of geosynthetic interlayers, namely woven geo-jute mat (GJ) and a biaxial polypropylene grid with a square aperture size of 40 mm (PP), are used in the study. The repeated loading tests were conducted on all the specimens under four-point bending configuration in a load-controlled mode at a frequency of 1 Hz. The performances of reinforced specimens were compared with the unreinforced specimen (CS), and the improvement in fatigue life was estimated. Fatigue test and DIC results indicate that the reinforced specimens improved the fatigue life of overlays, irrespective of crack depth and among them, the performance of PP specimens is superior. A superior performance of geosynthetic interlayers is witnessed at a larger crack depth (40 mm), irrespective of the interlayer type.

Keywords Geosynthetic interlayers · Crack depth · Asphalt overlays · Digital image correlation

V. Vinay Kumar · S. Saride (✉)
Department of Civil Engineering, Indian Institute of Technology Hyderabad, Kandi, Sangareddy 502285, Telangana, India
e-mail: sireesh@iith.ac.in

V. Vinay Kumar
e-mail: christite.vinay@gmail.com

R. Sundaram et al. (eds.), *Geotechnics for Transportation Infrastructure*, Lecture Notes in Civil Engineering 29,
https://doi.org/10.1007/978-981-13-6713-7_15

1 Introduction and Background

The flexible pavements over a period of their service life develop various types of distress due to innumerous detrimental factors such as varying weather conditions, high traffic wheel loads and weak subgrade, and other pavement layer conditions. These distresses result in the reduction in the pavement serviceability and necessitate an immediate need for a rehabilitation program to restore the pavement serviceability. The most common and convenient technique employed to restore the serviceability of deteriorated pavements is by providing an hot mix asphalt overlay of sufficient thickness (Kumar et al. 2017; Kumar and Saride 2017). The HMA overlays are believed to improve the ride quality by reducing the roughness of pavement surface. However, the incorporation of HMA overlays on an existing distressed pavement surface is witnessed to be an interim solution, as the distress from the existing pavement reflects onto the new overlays within a transient duration. This phenomenon of reflection of cracks and distress into and through the new overlays is known as reflective cracking (Kumar and Saride 2018). The major factors influencing the rate of reflective cracking in asphalt overlays are temperature variations and repeated traffic loads (Cleveland et al. 2002). Further, the reflection cracks are often observed to result in the premature failure of the pavement system, as they allow moisture ingression into the layers below through the cracks (Elseifi and Al-Qadi 2003).

Reflective cracking phenomenon is regarded as a complex phenomenon, due to the innumerous influencing factors and hence cannot be completely arrested. Besides, there are a number of possible treatment techniques to retard the rate of cracking in asphalt overlays. Among the various treatment techniques available to restrict the crack growth into the overlays, the inclusion of a geosynthetic interlayer below the asphalt overlay is found to be effective, due to their stress absorbing and reinforcing effects (Elseifi 2003; Saride and Kumar 2017).

There are numerous test methods such as TTI overlay test (Cleveland et al. 2002), Wheel reflective cracking device (Prieto et al. 2007), UGR-FACT (Moreno-Navarro and Rubio-Gamez 2014) available to evaluate the effectiveness of various geosynthetic interlayers as an anti-reflective cracking system. Besides, researchers (Caltabiano 1990; Brown et al. 2001; Virgili et al. 2009; Ferrotti et al. 2012; Kumar and Saride 2017; Saride and Kumar 2017) have studied the effectiveness of various geosynthetic interlayers as an anti-reflective cracking system under flexural fatigue tests.

Based on the existing literature, it can be summarized that the geosynthetics are placed between the new asphalt layers. However, in general, the interlayers will be placed at the interface of old and new pavement layers, to restrict the reflection cracking. Hence, in the current study, the unreinforced and geosynthetic-reinforced asphalt overlays are placed on an old deteriorated pavement extruded during a highway rehabilitation project. The main objective of the study was to evaluate the influence of crack depth on the performance of geosynthetic-reinforced asphalt overlays using repeated four-point bending tests and digital image analysis.

2 Materials and Methods

2.1 Geosynthetic Interlayers

Two different types of geosynthetic interlayers, namely woven geo-jute mat (GJ) and biaxial polypropylene grid (PP), have been considered in the current study to understand the influence of crack depth on the performance of geosynthetic-reinforced asphalt overlays. To understand the working mechanical and tensile properties of the geosynthetic interlayers, wide width tensile strength tests were performed on both machine (MD) and cross-machine (CMD) directions as per ASTM D4595 (2009). The tensile strength characteristics of the interlayers are discussed in detail in the subsequent paragraphs to follow.

Woven geo-jute (GJ) mat comprises of natural jute fibers and threads. Figure 1 presents the geo-jute mat prepared by machine weaving. The GJ interlayer has an ultimate tensile strength of 25 kN/m (MD) at a strain of 5% and 20 kN/m (CMD) at a strain of 13%. The biaxial polypropylene grid (PP) is manufactured by extending the polypropylene material along the machine and cross-machine directions (MD and CMD) to obtain a square aperture of 40 mm. The biaxial grid has a rib thickness of 2 mm along both the MD and CMD as shown in Fig. 2. The PP interlayer has an ultimate tensile strength of 30 kN/m at a strain of 10–12%.

2.2 Binder Tack Coat and Asphalt Concrete

The binder tack coat adopted in the study is a penetration grade (PG) 60/70 bitumen. The binder has a penetration value of 66 and a specific gravity of 1.01. The binder has a softening point, flash point, and fire points of 52, 340, and 360 °C,

Fig. 1 Woven geo-jute (GJ) mat interlayer

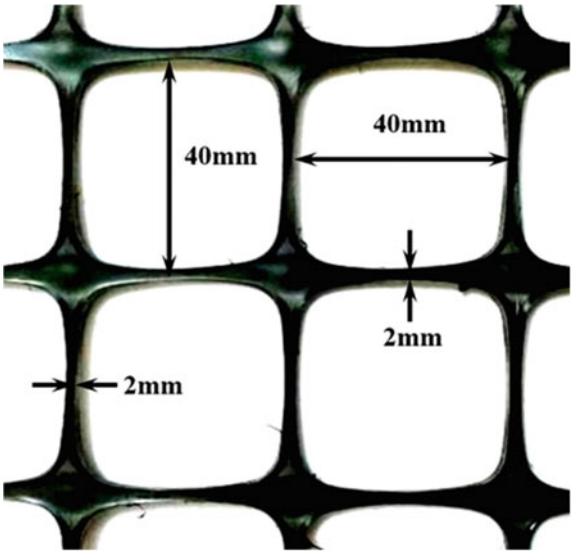

Fig. 2 Biaxial polypropylene grid (PP)

respectively. In addition, a binder viscosity of 400 cP has been reported. The adopted asphalt concrete mix consists of a PG-60/70 binder and a maximum aggregate of 25 mm size. Marshall Stability tests were performed on the asphalt concrete mix, and the optimum binder content of the mix was found to be 5.5% by weight of the aggregates. The asphalt concrete mix with an optimum bitumen content has a strength and flow values of 14.25 kN and 2.5 mm, respectively.

2.3 Two-Layered Asphalt Specimen Preparation

The two-layered asphalt slab of 400 mm length, 300 mm width, and 90 mm thickness consists of a 45-mm-thick old pavement layer, a binder tack coat, a geosynthetic interlayer and a 45-mm-thick HMA overlay. The old distressed pavement block was extruded from an existing highway during rehabilitation project and cut into a dimension of 400 mm length, 300 mm width, and 45 mm thickness. A PG-60/70 binder tack coat is applied on the old pavement layer at a residual rate of 0.25 kg/cm^2 and then the geosynthetic interlayers as per experimental program. Further, the asphalt concrete mix is compacted with the help of a 5-kg static weight compactor having a height of fall of 500 mm. The two-layered asphalt slabs (Fig. 3) with and without geosynthetic interlayers were then cut into the beam specimens of 400 mm length, 50 mm width, and 90 mm thickness. To understand the influence of crack depth on the performance of geosynthetic-reinforced asphalt overlays, a notch was created in the old pavement layer. The notch depths were of two sizes, i.e., 40 and 25 mm. These depths correspond to about 90 and 55% of the bottom layer thickness, respectively.

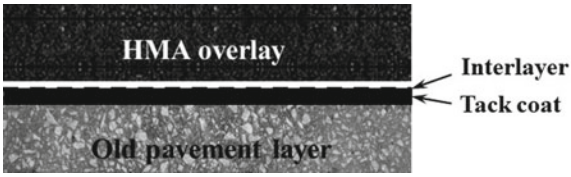

Fig. 3 Schematic of two-layered asphalt slab

Further, the specimens were prepared for the digital image analysis by completely painting one of the specimen faces with white color and spraying a black paint under controlled pressure to create a uniform random speckle pattern. The random speckle pattern on the specimens helps to understand the displacement and strain fields in the specimens. The detailed specimen preparation procedure is explained by Saride and Kumar (2017), Kumar and Saride (2017), and Kumar and Saride (2018).

3 Experimental Program

3.1 Flexural Fatigue Test

The flexural fatigue tests were performed on the asphalt beam specimens with different notch depths, under load-controlled mode. Figure 4 presents the schematic of flexural fatigue test setup, and the load was applied with the help of a computer-controlled servo-hydraulic actuator system. A continuous haversine-type loading pattern was applied at a frequency of 1 Hz with an intention to create a live moving traffic (single-axle contact pressure of 550 kPa). In this regard, the maximum load to be applied was calculated using Eq. 1 (ASTM D7460 2010) and it was determined to be 0.6 kN.

$$\sigma_{\mathrm{f}} = \frac{Pl}{bh^2} \tag{1}$$

where σ_{f} is the maximum flexural stress in kPa, P is the maximum load applied in kN, l is the span length of beam in m, b and h are the width and thickness of the beam in m.

A maximum load of 0.6 kN and a seating load of 0.06 kN was applied continuously on the notched beam specimens until complete fracture, and the corresponding vertical deformations at the mid-span length were recorded at the end of every load cycle. These vertical deformations could be adopted in the maximum strain equation to estimate the maximum tensile strains based on the bending theory as per ASTM D7460 (2010).

Further, to understand the crack growth characteristics in the two-layered asphalt beam specimens, a two-dimensional, non-contact optical technique has been employed.

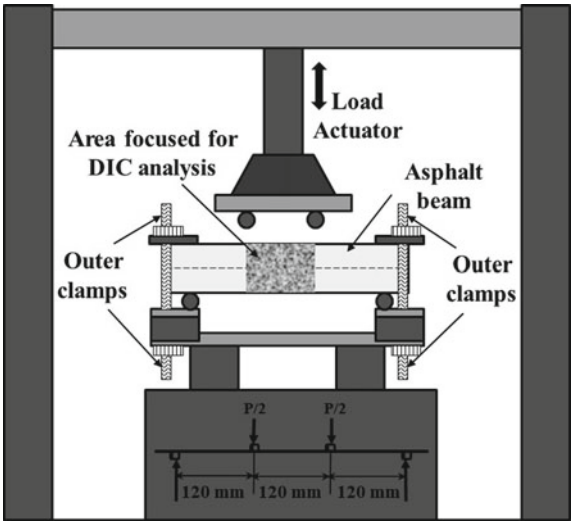

Fig. 4 Schematic of flexural fatigue test setup

3.2 Digital Image Correlation (DIC) Technique

Digital image correlation is a non-contact, optical technique based on the image processing and numerical computing generally employed to measure the full-field displacements effectively. Further, based on the displacement field, the corresponding strains mobilized in the specimen can be determined. The basic principle of the DIC technique is to identify the changes in speckle pattern of the deformed images with respect to that of an undeformed reference image. The process of image recording consists of recording an undeformed reference image and a calibration image before applying the repeated loads. The calibration image is recorded in order to convert the image scale from pixel units to millimeters unit. The images are recorded continuously during the testing at different number of load cycles and are analyzed with the help of commercial software tool (VIC-2D) to study the crack growth characteristics along with the corresponding deformations and strains mobilized in the two-layered asphalt beam specimens.

4 Results and Discussion

4.1 Flexural Fatigue Test Results

The load-controlled notched beam fatigue tests help to understand the impact of different crack depths on the performance of geosynthetic-reinforced asphalt overlays placed on an old distressed pavement layer. The repeated load was applied continuously on the two-layered notched asphalt beam specimen resulting in an

increase in the vertical deformation of the specimen, with an increase in the number of load repetitions. The increase in vertical deformation causes the dissipation of energy from the specimen and reduces the specimen stiffness, which further results in complete fracture (failure) of the specimen (Kumar and Saride 2017).

The flexural fatigue test results of two-layered asphalt beam specimens with 40 and 25 mm notch depths are presented in Fig. 5, in the form of variation of vertical deformation, as a function of number of load cycles (*N*). It is observed that, the control specimen (CS) could not successfully resist a large number of load repetitions in both the configurations, i.e., cracks propagated into the overlays at a very less number of load cycles (*N*). However, as expected, the specimens with 25-mm notch depth were capable of resisting a large number of load cycles, in comparison with the specimens with 40 mm notch depth. For instance, the fatigue life (*N*) of specimens with 25 mm notch depth is 66, 115, and 674 for CS, GJ, and PP specimens, respectively.

However, the specimens with 40-mm notch depth possess a fatigue life of 14, 33, and 323, for control, GJ, and PP specimens, respectively. The variation in fatigue life of beam specimens with different notch depths may be attributed to their flexural stiffness, which is higher for 25 mm notched specimens followed by 40 mm notched specimens.

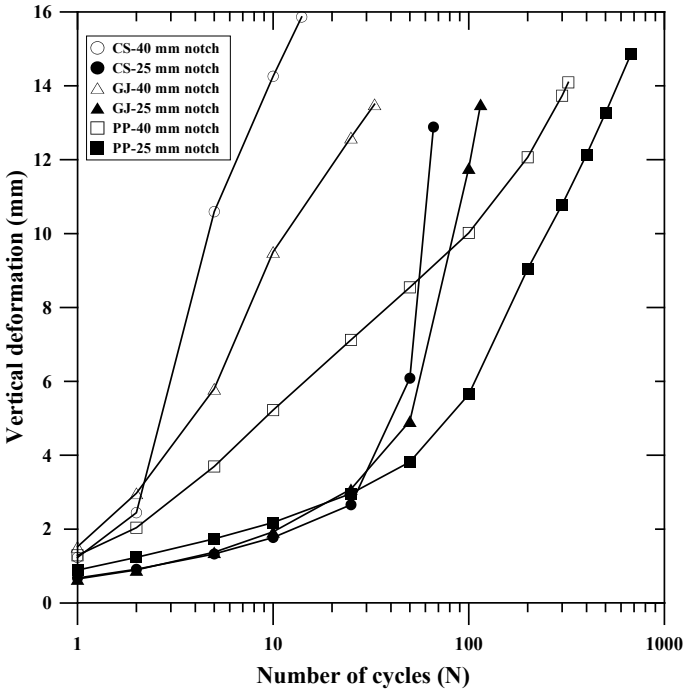

Fig. 5 Variation of vertical deformation with number of cycles

From Fig. 5, it can also be visualized that the specimens with geosynthetic interlayers have shown higher fatigue life, irrespective of the notch depths in the bottom layer. This finding suggests that the geosynthetic reinforcements incorporated in the notched asphalt beam specimens have restricted the vertical deformations and cracks, in turn, enhancing the performance life. Among the specimens with geosynthetic interlayers, the fatigue life of PP specimens is superior to that of GJ specimens, irrespective of the notch depth. Besides, the fatigue life of GJ specimen is observed to be slightly better than that of control specimens. The superior performance of PP specimens may be attributed to their high initial stiffness and their ability to induce an ultimate tensile strength of 36 kN/m at a strain of 10%.

Overall, the geosynthetic interlayers incorporated at the interface of old and new asphalt layers intervene with the crack growth in the vertical direction, by absorbing the crack energy (tensile). In addition, the crack growth is dissipated in the lateral direction at the interface zone by the geosynthetic interlayers. Hence, an improvement in the fatigue life is witnessed.

Further, to quantify the rate of improvement in the geosynthetic-reinforced asphalt beam specimens, a performance indicator is introduced. The performance indicator, improvement ratio is denoted by the term I_{NF} and is defined as a ratio of number of load repetitions sustained by a geosynthetic-reinforced beam specimen to that sustained by a control specimen, at same vertical deformation level, and mathematically expressed as presented in Eq. 2.

$$I_{\mathrm{NF}} = \frac{N_{\mathrm{R}}}{N_{\mathrm{U}}} \tag{2}$$

where N_{R} and N_{U} are the fatigue lives of geosynthetic-reinforced and unreinforced specimens, respectively.

Figure 6 presents the variation of fatigue life improvement ratio with vertical deformation for all the notched asphalt beam specimens. It can be visualized that the I_{NF} has increased with an increase in the vertical deformation, irrespective of the notch depth and the geosynthetic-interlayer type. Besides, a prominent performance improvement can be witnessed in asphalt specimens with 40 mm notch depth against the specimens with 25 mm notch depth. This finding can be attributed to the stiffness of the asphalt beam specimens, as the control specimen with a 25-mm notch depth has resisted a large number of load cycles in comparison with the control specimen with a 40-mm notch depth. Hence, a reduction in the improvement ratio can be witnessed. In this regard, it is also clear that, the PP specimen with a 40-mm crack depth had achieved an improvement ratio of about 5.4 against an improvement ratio of 2.2 in PP specimen with a 25-mm notch depth, at 6-mm vertical deformation. Further, an important observation to be noted is that, the improvement ratios of PP specimen with a 40-mm notch depth have been increased after a vertical deformation of 4 mm is reached. It is believed that, at about 4-mm deformation, the crack would have reached the interlayer, and hence, a smooth transfer of strain energy from the cracks takes place and the specimen can resist a higher number of load repetitions.

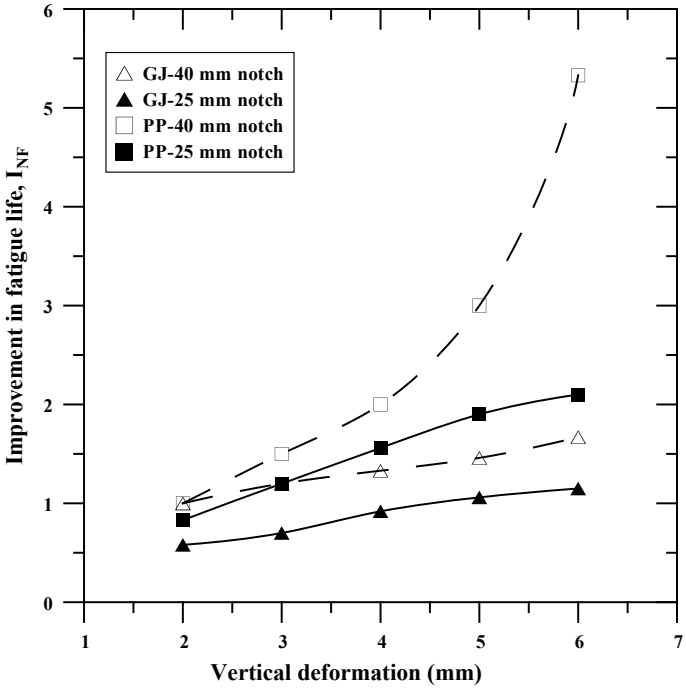

Fig. 6 Variation of fatigue life improvement ratio with vertical deformation

However, a detailed information about the crack growth characteristics in unreinforced and geosynthetic-reinforced asphalt beam specimens with 40 and 25 mm notch depths can be obtained by using the DIC technique, as presented in the following section.

4.2 DIC Analysis

The digital image correlation technique was adopted during the flexural fatigue test program with an intention to understand the crack evolution and the propagation patterns. The deformed images after different load cycles are compared with that of undeformed image and the variation in deformation is obtained in the form of vertical deformation bands. Figure 7 presents the variation of vertical deformation bands for all the specimens at failure. The downward deformation is considered to be negative for the analysis, and it can be visualized that each vertical bands represent a uniform deformation in that vertical strip along the specimen. Further, it is to be noted that in the control specimens, the deformation bands are continuous, whereas they are found discontinuous in the specimens with geosynthetic interlayers. This condition may be attributed to the incorporation of geosynthetics at the interface of old and new

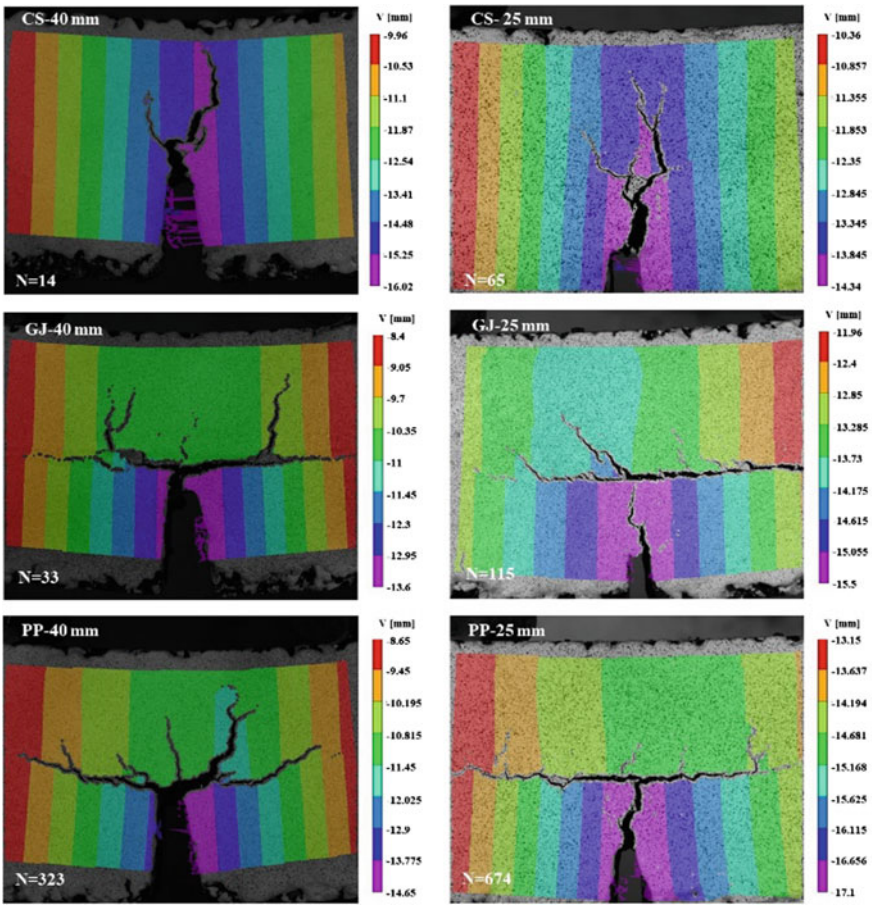

Fig. 7 Variation of vertical deformation bands for all the specimens at failure

pavement layers. The geosynthetic interlayers restrict the vertical deformation and in turn the crack propagations effectively. Hence, maximum vertical deformations are observed in the bottom layer, below the interlayer zone.

The geosynthetic interlayer incorporated below the asphalt overlay effectively restricts the vertical crack growth by minimizing the maximum tensile strains mobilized in the specimen. Figure 8 presents the tensile strain contours at failure condition for all the specimen configurations. It is clear that the tensile strain for the control specimen is consistently higher, irrespective of crack depth. A tensile strain as high as 74 and 33% in control specimens with 40 and 25 mm notch depths, respectively. Besides, low tensile strains are witnessed in the geosynthetic-reinforced notched asphalt beam specimens, irrespective of crack depth. In addition, a maximum tensile strain is witnessed consistently, in the asphalt beam specimens with 40-mm notch depth, irrespective of the geosynthetic-interlayer type.

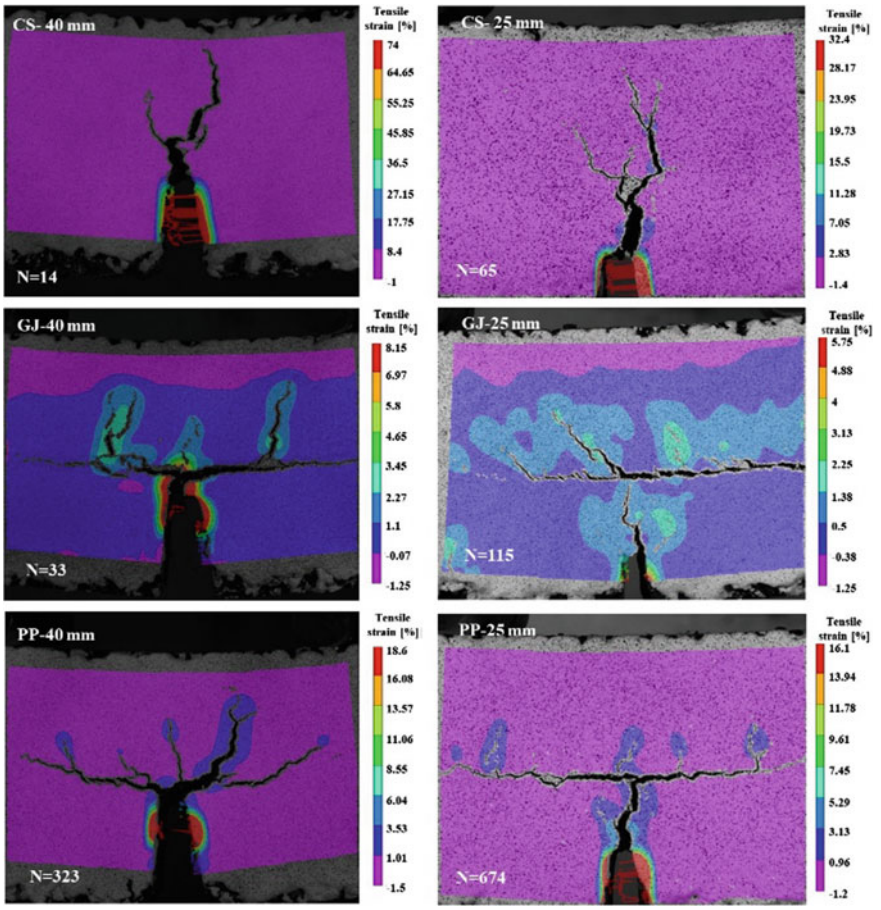

Fig. 8 Variation of tensile strain contours for all the specimens at failure

Further, the maximum tensile stress responsible for vertical crack growth is effectively absorbed by the geosynthetic reinforcements incorporated at the interface zone. Besides, this mechanism of geosynthetic reinforcements often results in a horizontal crack growth below the geosynthetics interlayer, at the interface zone. This condition can be clearly witnessed from Figs. 7 and 8. The crack growth in horizontal direction leads to the accumulation of vertical strains at the interface zone resulting in a possible delamination of pavement layers at the interface zone.

Overall, it can be incurred that there is an enhancement in the performance life of asphalt overlays with the incorporation of geosynthetic reinforcements. Among the notched beam specimens, a maximum improvement is witnessed in asphalt beam specimens with 40-mm notch depth, irrespective of geosynthetics type. Besides, among the geosynthetic-reinforced asphalt beam specimens, a superior performance was witnessed in PP specimens, irrespective of notch depth.

5 Conclusions

The influence of crack depth on the performance of geosynthetic-reinforced asphalt overlays placed on a pre-cracked pavement layer was studied under flexural fatigue tests with the help of digital image analyses, and the following conclusions can be drawn:

- All the geosynthetic interlayers improved the fatigue lives of two-layered asphalt beam specimens, irrespective of notch depth in the bottom layer. Among them, the performance of PP specimens is superior to the GJ specimens.
- The performance improvement of specimens with a larger crack depth (40 mm) is found to be superior to that with a lesser crack depth (25 mm), irrespective of the geosynthetic-interlayer type. Owing to the fact that the reinforcing and membrane effects of geosynthetic interlayers are completely mobilized in specimens with larger crack depths, due to the high deformations witnessed at very few load repetitions.
- The DIC analysis suggested that the tensile strains at the crack tip were very high in CS compared to the specimens with geosynthetic-interlayers, irrespective of notch depth in the bottom layer. An average reduction in tensile strain of about 35–70% was noticed in specimens with geosynthetic interlayers.
- The maximum vertical strains are mobilized at the interface zone in the geosynthetic-reinforced asphalt specimens, as a result of horizontal crack growth in that zone. This condition leads to a possible delamination between the pavement layers.

References

ASTM D4595 (2009) Standard test method for determining tensile properties of geotextiles by the wide-width strip method. Annual book of ASTM standards. ASTM International, West Conshohocken, PA

ASTM D7460 (2010) Standard test method for determining fatigue failure of compacted asphalt concrete subjected to repeated flexural bending. Annual book of ASTM standards. ASTM International, West Conshohocken, PA

Brown SF, Thom NH, Sanders PJ (2001) A study of grid reinforced asphalt to combat reflection cracking. J Ass Asph Paving Technol 70:543–569

Caltabiano MA (1990) Reflection cracking in asphalt overlays. Thesis submitted to University of Nottingham for the Degree of Master of Philosophy

Cleveland GS, Button JW, Lytton RL (2002) Geosynthetic in flexible and rigid pavement overlay. Report 1777-1. Texas Transport Institute, Texas A&M University System

Elseifi MA (2003) Performance quantification of interlayer systems in flexible pavements using finite element analysis. Instrument response and non destructive testing. Ph.D. thesis submitted to Virginia Polytechnic Institute and State University

Elseifi MA, Al-Qadi IL (2003) A simplified overlay design model against reflective cracking utilizing service life prediction. Transp. Res. Rec. J. Transp. Res. Board No 3285

Ferrotti G, Canestrari F, Pasquini E, Virgili A (2012) Experimental evaluation of the influence of surface coating on fiberglass geogrid performance in asphalt pavements. Geotext Geomemb 34:11–18

Kumar VV, Saride S (2017) Use of digital image correlation for the evaluation of flexural fatigue behavior of asphalt beams with geosynthetic interlayers. Transport Res Rec: J Transport Res Board 2631:55–64

Kumar VV, Saride S (2018) Evaluation of cracking resistance potential of geosynthetic reinforced asphalt overlays using direct tensile strength tests. Constr Build Mater 162:37–47

Kumar VV, Saride S, Peddinti PRT (2017) Interfacial shear properties of geosynthetic interlayered asphalt overlays. In: Proceedings of geotechnical frontiers-2017, Orlando, USA

Moreno-Navarro F, Rubio-Gamez MC (2014) UGR-FACT test for the study of fatigue cracking in bituminous mixes. Constr Build Mater 53:182–189

Prieto JN, Gallego J, Perez I (2007) Application of the wheel reflective cracking test for assessing geosynthetics in anti-reflection pavement cracking systems. Geosynth Int 14(5):287–297

Saride S, Kumar VV (2017) Influence of geosynthetic-interlayers on the performance of asphalt overlays placed on pre-cracked pavements. Geotext Geomembr 45:184–196

Virgili A, Canestrari F, Grilli A, Santagata FA (2009) Repeated load test on bituminous systems reinforced by geosynthetics. Geotext Geomemb 27:187–195

Interface Behavior of Geogrid-Reinforced Sub-ballast: Laboratory and Discrete Element Modeling

Ngoc Trung Ngo and Buddhima Indraratna

Abstract This paper shows a study on the interface behavior of biaxial geogrids and sub-ballast using a direct shear box and computational modeling. A series of large-scale direct shear tests are performed on sub-ballast (capping layer) with and without geogrid inclusions. The laboratory test data indicate that the interface shear strength is mainly decided by applied normal stresses and types of geosynthetics tested. Discrete element modeling approach is used to investigate the interface shear behavior of the sub-ballast subjected to direct shear loads. Irregular-shaped sub-ballast particles are modeled by clumping of many spheres together in pre-determined sizes and positions. Biaxial geogrids are simulated in the DEM by bonding small balls together to build desired geogrid shapes and opening apertures. The numerical results reasonably match with the measured test data, showing that the introduced DEM model can simulate the interface behavior of sub-ballast stabilized by the geogrids. In addition, the triaxial geogrid presents the highest interface shear strength compared to the biaxial geogrids; and this can be associated with the symmetric geometry of grids' apertures that can distribute load in all directions. Evolutions of contact forces of unreinforced/reinforced sub-ballast specimens and contour strain distributions during shear tests are also investigated.

Keywords Transport geotechnics · Geogrid · Sub-ballast · Interface behavior · Discrete element method

N. T. Ngo (✉) · B. Indraratna
Faculty of Engineering and Information Sciences, Center for Geomechanics and Railway Engineering, University of Wollongong, Wollongong 2522, NSW, Australia
e-mail: trung@uow.edu.au

B. Indraratna
e-mail: indra@uow.edu.au

R. Sundaram et al. (eds.), *Geotechnics for Transportation Infrastructure*,
Lecture Notes in Civil Engineering 29,
https://doi.org/10.1007/978-981-13-6713-7_16

1 Introduction

With the rapid urbanization is ongoing across Australia, the need for appropriate ground improvement techniques is mandatory to build road and rail networks over soft subgrade having low shear strength. A typical ballasted track sub-structure commonly has a compacted layer of sub-ballast (capping layer) aving commonly broadly graded mixtures of sand and gravel placed above a subgrade. A ballast layer (i.e., 300–500 mm thick) placed over the sub-ballast (Selig and Waters 1994; Indraratna et al. 2011a). The typical functions of sub-ballast are to: (i) transmit and distribute the applied moving loads to the underneath layers at a decreased stress level (Powrie et al. 2007; Indraratna et al. 2013); (ii) to protect ballast particles from penetrating downward to the formation soil and to prevent subgrade fines from pumping up the upper ballast layer (Trani and Indraratna 2010); and (iii) to decrease the building up excess pore pressure under repeated train loads and to facilitate the drainage capacity of ballasted tracks (Indraratna et al. 2011a).During train operations, ballast aggregates become degraded and starts to lessen its shear strength and drainage capacity (Tutumluer et al. 2008; Rujikiatkamjorn et al. 2012; Ngo et al. 2017a, b, c), among others. Deterioration of track geometry due to excessive differential settlements and lateral displacements as a result of the localized failure of formations (sub-ballast and subgrade layers) often lead to the reduction in track stability and longevity. There have been an increasing use of planer geosynthetics (i.e., geogrids, geotextiles, or geo-composites) in ballasted tracks to decrease excessive settlements (differential settlements) and lateral deformations under dynamic train loading (Ngo and Indraratna 2016).

There have been numerous studies on soils stabilized by geosynthetics, but very few studies have been performed to investigate sub-ballast stabilized by geogrids using the experiment or via numerical modeling approaches (Ngo et al. 2016). In addition, these studies on sub-ballast were often limited by only using the continuum-modeling approach; and therefore, the discrete nature and angularly shaped particles of sub-ballast have not been modeled properly (Biabani et al. 2016; Indraratna et al. 2017), among others. It is found that these studies did not consider the possibility of using geogrids in reducing the thickness of the sub-ballast. Despite some attempts to study granular materials stabilized by geogrids, where the interaction mechanism and the interface responses between the sub-ballast(capping) and geogrid which is mainly governed by the interlocking among particles and geogrids are not modeled precisely in view of micro-mechanical aspects (Ngo et al. 2017a, b, c). In this paper, large-scale direct shear tests are performed, and discrete element method (DEM) is utilized to model geogrid-reinforced sub-ballast, investigating the shear stress–strain responses and corresponding contact force distributions of this composite assembly.

2 Laboratory Study

2.1 Large-Scale Direct Shear Test

A large-scale direct shear apparatus having typical dimension of 300 mm long 300 mm wide × 200 mm was used to investigate interface responses of the geogrid-stabilized sub-ballast, as illustrated in Fig. 1. The sub-ballast (capping) was collected from Bombo quarry, New South Wales, Australia. Prior to every test, ballast aggregates were cleaned and sieved, following to the Australian Standards, AS 2758.7 (1996). The particle size distribution characteristics of the sub-ballast tested in laboratory is identical to one often exercised in Australia (i.e., D_{max} = 19 mm, D_{min} = 0.075 mm, C_u = 16.3, C_c = 1.3, γ_d = 18.5 kN/m^3). Three different geogrids having varied shapes and opening apertures, as shown in Fig. 1, were used to study the influences of different types of geogrids' geometry on the shear strength of the composite specimens (Fig. 1).

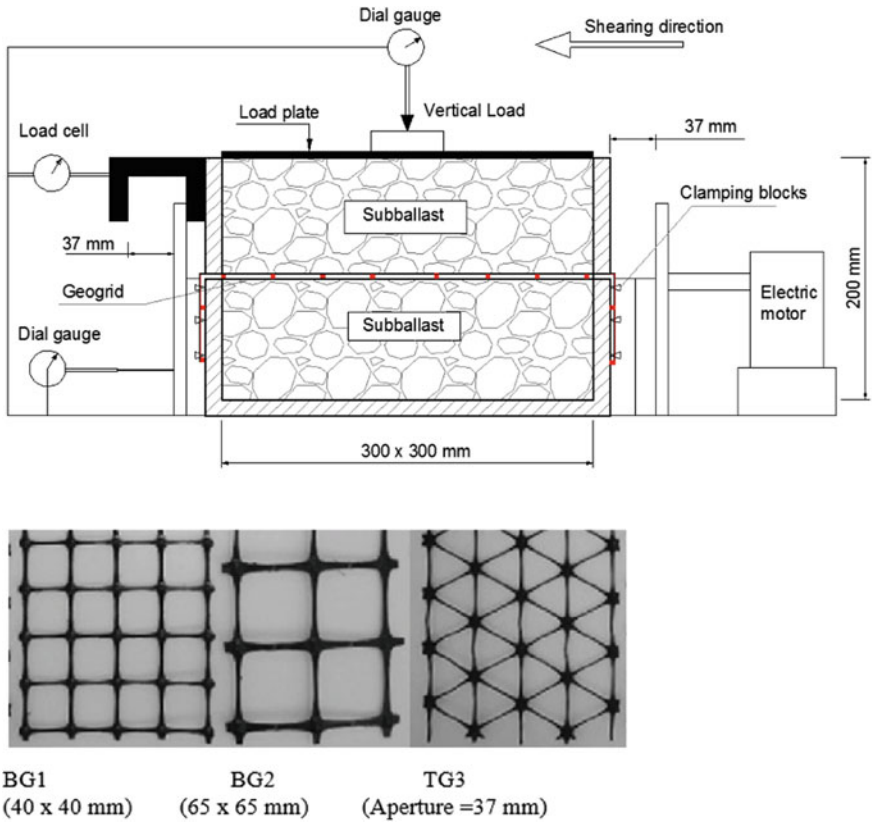

Fig. 1 Large-scale direct shear box and geogrids used

The sub-ballast was filled into the direct shear apparatus and compacted into every 100-mm-thick layer to attain an approximate field density of γ_d = 18.5 kN/m^3. A layer of geogrid was then embedded and secured at the middle of the upper and lower shear boxes. The upper part of the shear apparatus was then poured with remaining capping aggregates and compacted to the pre-determined density. It is noted that there is a small gap (around 1.5–2 mm) between the geogrid and the upper box so that the friction between them can be ignored during the shearing progress. A loading plate was sit on the top surface of the upper box and that allows the sub-ballast aggregates to move in vertical direction during shearing. This loading plate was also utilized to apply vertical normal loads to the ballast specimen and to record vertical displacements (i.e., normal strain) during the testing. Direct shear tests were sheared under low normal stresses of σ_n = 6.7–45 kPa, mimicking actual low confinements in real track conditions (Indraratna et al. 2013).The composite geogrid sub-ballast specimen was sheared to a given horizontal displacement of Δh = 30 mm (ε_s = 10%). During shearing progress, shear forces, vertical, and horizontal displacements were recorded at every 1 mm of lateral displacements by a load transducer and displacement potentiometer, respectively.

3 Discrete Element Modeling

The discrete element method (DEM) was first introduced by Cundall and Strack (1979), and it has been increasingly adopted to study load-deformation responses of ballast particles (McDowell et al. 2006; Huang and Tutumluer 2011; Rujikiatkamjorn et al. 2013; Indraratna et al. 2014; Ngo et al. 2014; Ngo et al. 2017a, b, c), among others. Recently, the discrete element method (DEM) has been increasingly adopted in the recent past decades as promising alternatives to the continuum-based method for the study of granular materials. The DEM enables deeper insight into the micro-mechanical characteristics of granular materials such as contact force distributions, fabric anisotropy, and particle breakage that are almost impossible or unlikely to be measured in the laboratory (McDowell and Bolton 1998; O'Sullivan and Cui 2009; Huang et al. 2009b; Ngo et al. 2017a, b, c), among others.

3.1 Modeling Sub-Ballast Aggregates in DEM

Irregularly shaped sub-ballast particles having varied angularities (i.e., varying shapes and sizes) were simulated in the DEM by connecting and overlapping a number of spherical balls together at suitable positions (Ngo et al. 2017a, b, c). In this study, a library of nine sub-ballast particles was simulated by connecting 25–50 balls together, as illustrated in Fig. 2a. These simulated aggregates range from 2.5 to 19 mm and mimic the particle size distribution conducted experimentally. It is noted that small-sized particles were not used in these simulations is to reduce

required excessively calculation time. Ngo et al. (2014) and Lim and McDowell (2005) also adopted this approach to study the micro-mechanical behavior of granular materials, and they indicated that the absence of miniature aggregates has no significant affect on the results provided that the relative density of the specimen is identical as the one conducted in the laboratory.

The simulated sub-ballast particles were then placed inside the simulated shear box without any overlapping within the specified constrains of the simulated shear box and were further compacted to a given density of γ_d = 18.5 kN/m^3 that is identical to that conducted in the laboratory (Fig. 2b).

3.2 *Modeling of Geogrids*

Three types of geogrids were examined in the current analysis. Geogrids having different shapes and openings (i.e., apertures) was modeled by connecting a number of small balls together (i.e., balls having diameters of around 1.5–3 mm), as presented

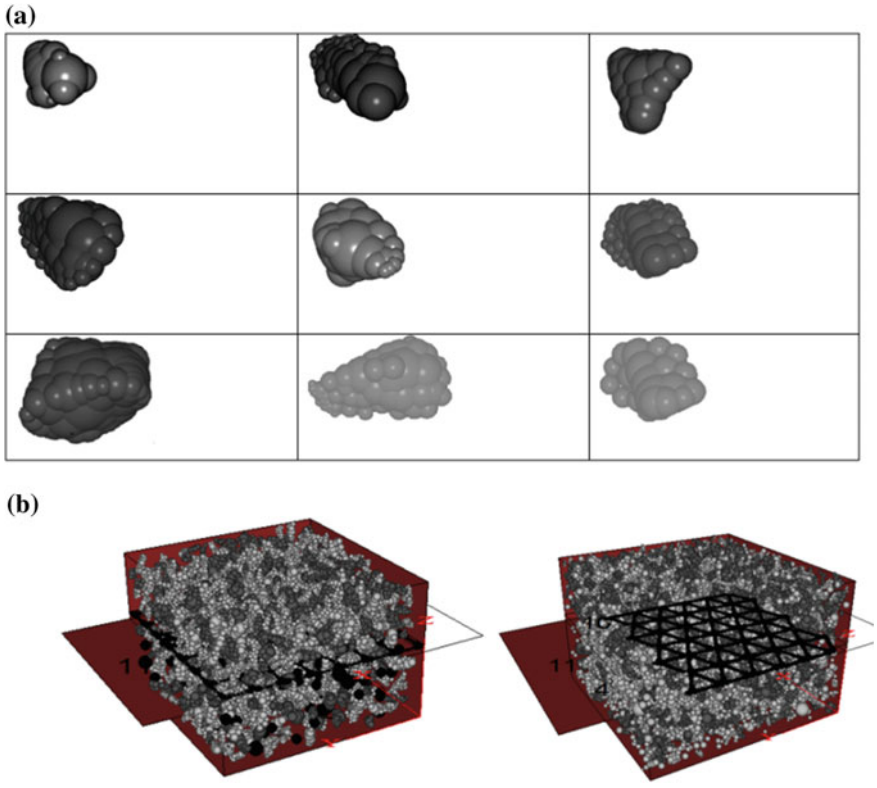

Fig. 2 Modeling sub-ballast aggregates and shear box in DEM After Ngo et al. (2017a, b, c)

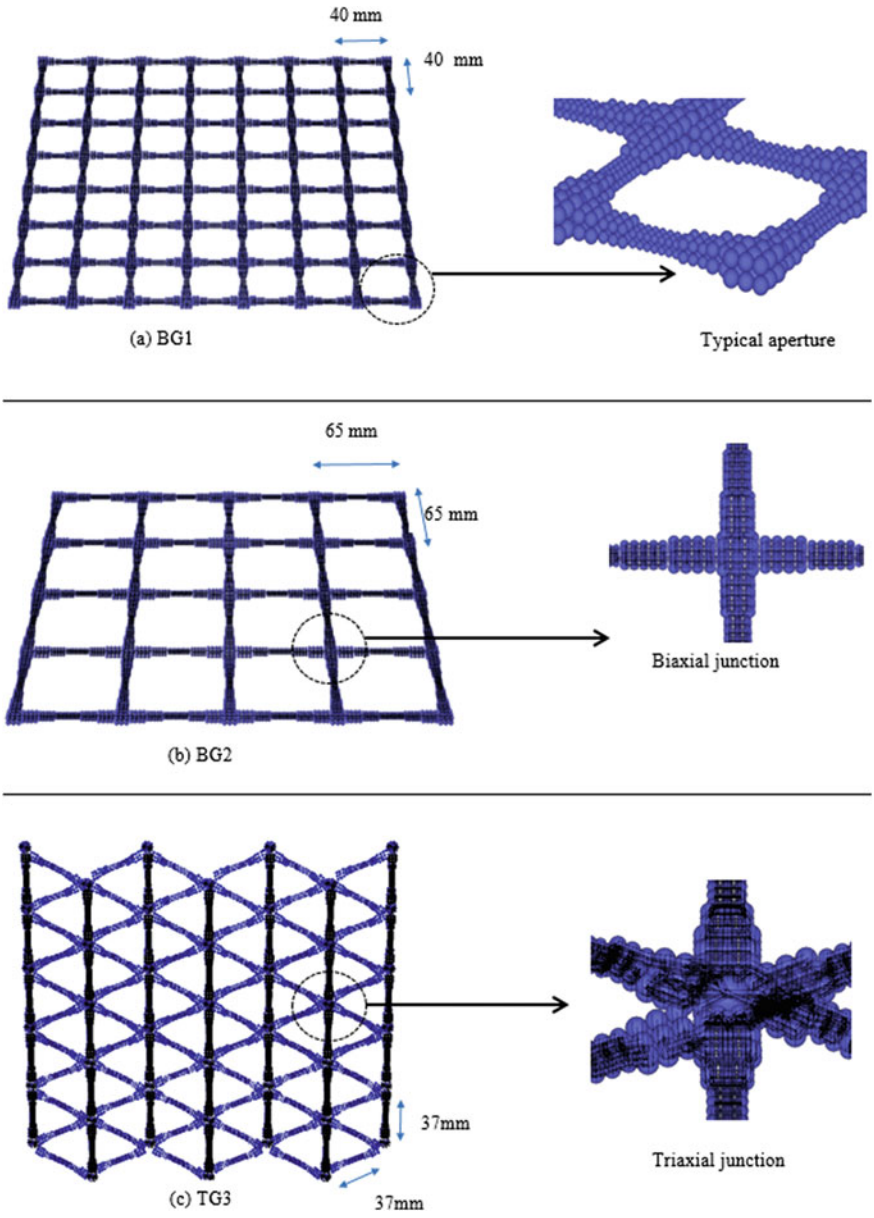

Fig. 3 Simulated geogrids in DEM: **a** Biaxial geogrid—BG1, 40 mm × 40 mm; **b** Biaxial geogrid—BG2, 65 mm × 65 mm; and **c** Triaxial geogrid—TG3 After Ngo et al. (2017a, b, c)

in Fig. 3. The geogrids comprise of spheres of varying sizes was modeled, where the bigger spheres were utilized to simulate the junctions of geogrids and the small spheres used for the middle of the geogrid ribs. Spheres were bonded together using

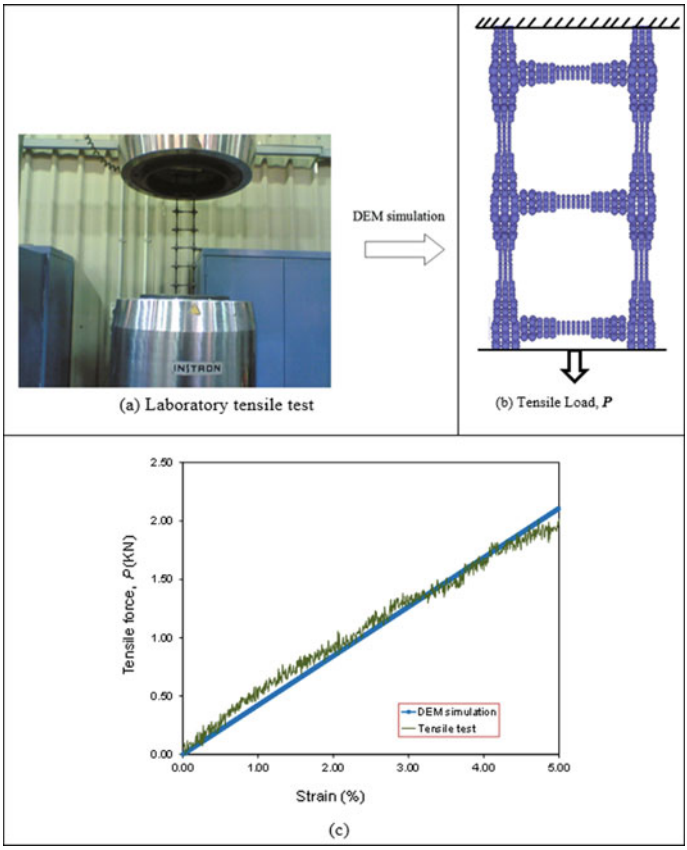

Fig. 4 **a** Tensile test for geogrids: **b** Predicted load-displacement from DEM; and **c** Comparison of DEM and laboratory test data *Data source* Ngo et al. (2017a, b, c)

parallel bonds corresponding to the measured tensile strength (i.e., within the geogrid's elastic range of up to 5%) and were determined by calibrating with test data measured from tensile tests (Fig. 4). Each bond can represent the force–displacement responses of a finite-sized piece of cementation materials placed between two balls in contact and are able to carry both tensile forces and moments. Once the geogrid was generated and secured in the compacted sub-ballast, the model was cycled (i.e., iteration)to enable the simulated geogrid freely interact with the surrounding aggregates. Normal forces were applied to the loading plate of the shear box and were kept constantly by modifying the positions and displacements of the top plate via a servo-control mechanism developed by Itasca (2016). The composite assembly was then iterated to equilibrium state where a ratio of maximum un-balanced forces to the average contact forces was less than a set threshold of 1.15×10^{-4}. This condition applied to facilitate the interlock among sub-ballast aggregates and the geogrids and also enables the sub-ballast grains to build contacts with each other. This process also

ensured the unit weight (i.e., density) of the composite assembly unchanged. The shear box was then forced to shear horizontally at a speed of 8.35×10^{-5} mm/time step to a maximum lateral displacement of $\Delta h = 30$ mm.

3.3 Determination of Micro-Mechanical Parameters

Selecting the input micro-mechanical parameters (i.e., stiffness, parallel bond radius, parallel bond stiffness, etc.) can be complicated considering different parameters, i.e., stiffness k_n and k_s, friction coefficient f, and parameters for the bonding strength that governs the flexibility and tensile strength of geogrids. In this study, the input micro-mechanical parameters were selected by back-calculation of tensile load-displacement behavior with measured laboratory test data using an INSTRON tensile testing machine, as illustrated in Fig. 4. Simulations of tensile tests subject to varied normal and shear stiffness were then implemented. The tensile force–strain responses predicted from the DEM compared to those obtained in laboratory are presented in Fig. 4c. The calibration procedure was described elsewhere by Ngo et al. (2017a, b, c). Selected input parameters for simulating the geogrids and sub-ballast adopted in this study are presented in Table 1.

Input parameters of sub-ballast were also determined by calibrating the shear stress–strain behavior given by DEM modeling with those measured experimentally (Ngo et al. 2015; Biabani et al. 2016b). Contact stiffness (k_n, k_s) and inter-particle coefficient of friction (μ) to model sub-ballast were determined by direct shear tests of sub-ballast where these parameters were changed gradually until the predicted results agreed well with those measured in laboratory(i.e., similar technique used for the geogrids). It is noted that this approach is time-consuming and starting values of input parameters were selected from available literature. Figure 5 shows comparison of shear stress-displacement responses of sub-ballast with different values of μ; and it shows that when $\mu = 0.85$ exhibits a reasonable match with test data.

Table 1 Selected input parameters for geogrids and sub-ballast

Input parameters	Geogrid	Sub-ballast
Particle density (kg/m^3)	972	2350
Coefficient of friction	0.47	0.85
Contact normal stiffness, k_n (N/m)	5.91 × 106	4.82 E8
Contact shear stiffness, k_s (N/m)	5.91 × 106	2.41 E8
Contact normal stiffness of wall-particle, $k_{n\text{-wall}}$ (N/m)	3.25 × 109	3.25 E9
Shear stiffness of wall of wall-particle, $k_{s\text{-wall}}$ (N/m)	3.25 × 109	3.25 E9
normal strength, ϕ_n(kN)	56.8	
Parameters for contact bonds shear strength, ϕ_s (kN)	56.8	
Parallel bond radius multiplier	6.27 E7	
Parallel bond normal stiffness, k_{np} (kPa/m)	6.27 E7	
	0.5	
	297 E7	

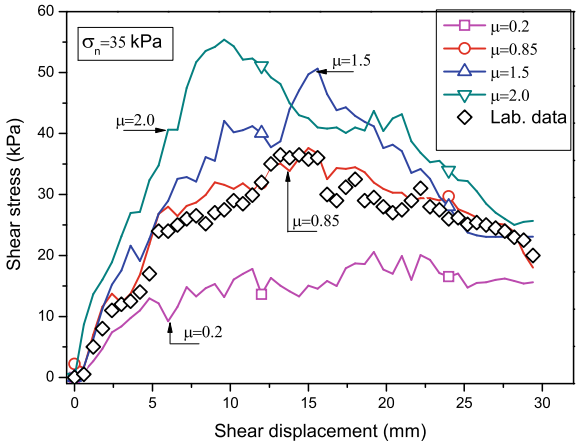

Fig. 5 Influences of the friction coefficient, μ on the shear stress–strain behavior of sub-ballast

4 Results and Discussion

4.1 Shear Stress–Strain Responses

DEM modeling of large-scale shear tests for unreinforced sub-ballast were subjected to three different normal stresses of $\sigma_n = 6.7, 20.5,$ and 45 kPa. The shear stress ratio (τ/σ_n) and the normal strain (ε_n) at a corresponding shear strain(ε_s) predicted by the DEM and compared with data measured in the laboratory are presented in Fig. 6. It is clearly seen that the DEM predictions match reasonably well with those measured experimentally under given normal stresses. The strain softening behavior of sub-ballast and its volumetric dilation were obtained in all DEM simulations; and it shows that the higher the normal stress (σ_n), the lower the shear stress ratio, τ/σ_n.

The introduced DEM model was then adopted to simulate sub-ballast reinforced by different geogrids (biaxial grids—BG1, BG2; and triaxial grid—TG3) subject to a low normal stress of 6.7 kPa, simulating small confinement in a real ballasted track. Figure 7 presents comparisons of the shear stress–strain responses predicted by DEM with those measured in the laboratory. It is observed that the predicted results agree well with the laboratory test data, implying that the proposed DEM model is able to predict the interface behavior of sub-ballast stabilized by the geogrids. The triaxial geogrid-reinforced sub-ballast shows the lowest volumetric dilation; and this is probably due to the symmetric geometry of the grid that can transfer the applied loads more uniformly and can also facilitate better interlock with the surrounding aggregates than the other types of geogrids. The enhanced performance provided by the triaxial grid (TG3) can also be associated with the isotropic-radial stiffness that is nearly constant in all direction, and that can restrain the sub-ballast particles better at their interfaces.

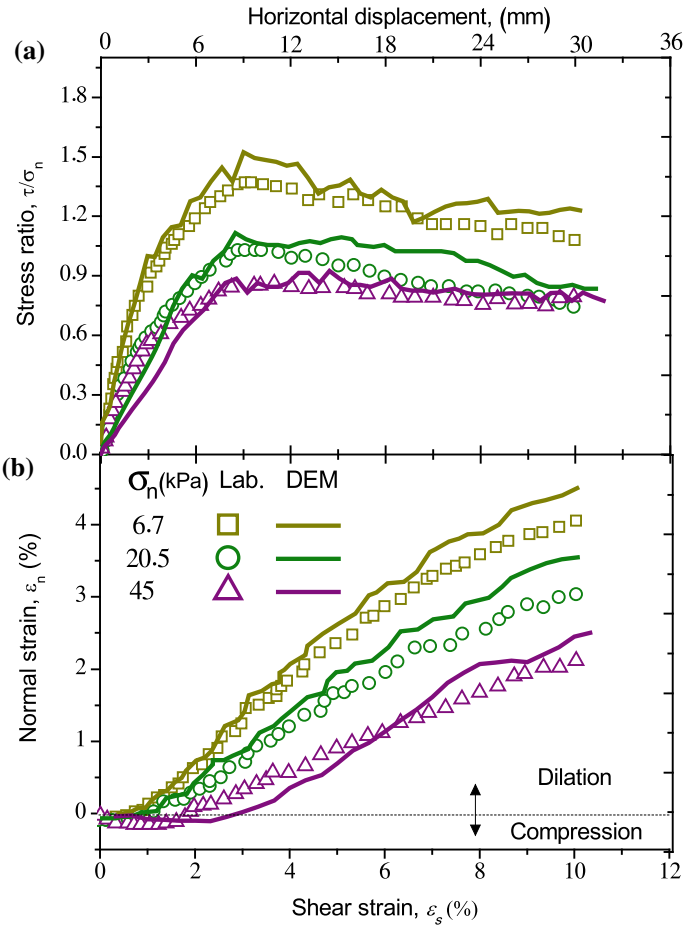

Fig. 6 **a** Shear stress ratio (τ/σ_n) plotted with shear strain, **b** normal strain plotted with shear strain *Data source* Ngo et al. (2017a, b, c)

4.2 Responses of the Geogrids

Figure 8 shows the distributions of mean contact forces plotted along the depth of the shear box for sub-ballast specimen sat a given shear strain of $\varepsilon_s = 5\%$ and a given normal stress of $\sigma_n = 6.7$ kPa. It is seen that the unreinforced sub-ballast shows the smallest induced contact forces compared to those for the reinforced specimens. The sub-ballast stabilized by the triaxial geogrid (TG3) exhibits the highest mobilized contact forces, approximately of 71 N (for TG3) compared to 53 and 39 N for biaxial grids BG1 and BG2, respectively. A confinement zone can be found in a depth of about 50 mm from the interface of geogrid and sub-ballast where the inclusion of geogrid results in a significant increase in induced contact

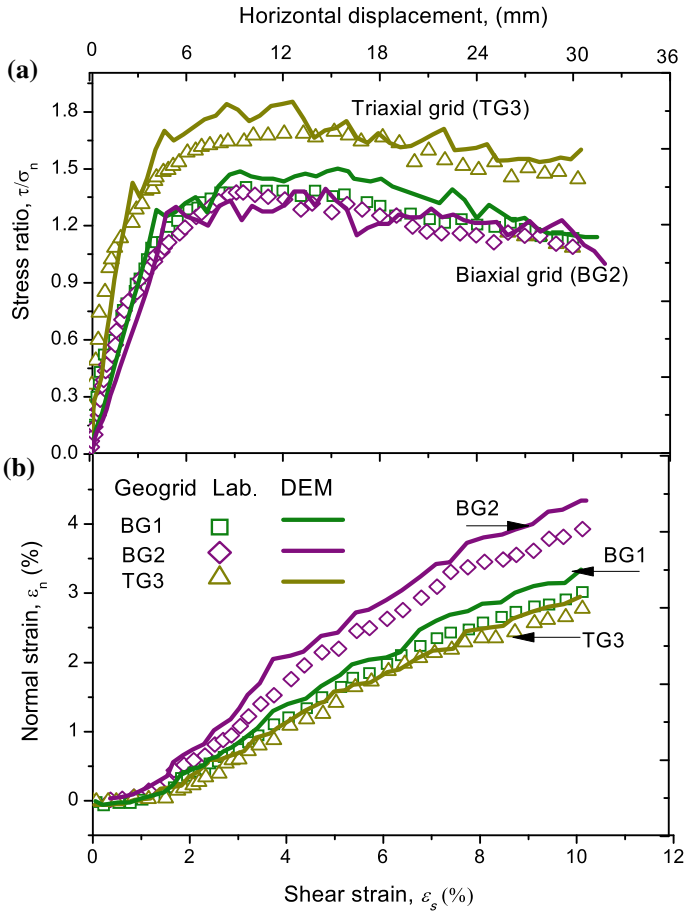

Fig. 7 **a** Shear stress ratio (τ/σ_n) plotted with shear strain, **b** normal strain plotted with shear strain After Ngo et al. (2017a, b, c)

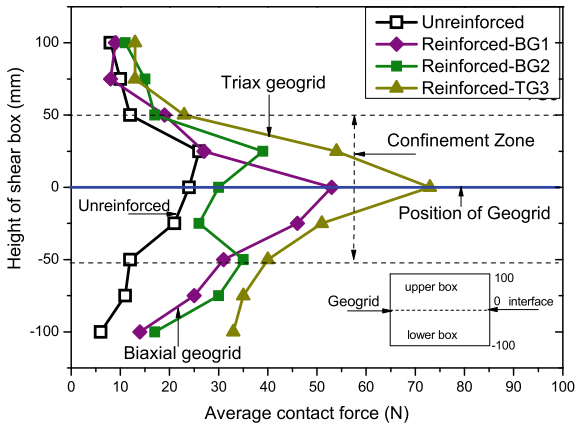

Fig. 8 Mean contact forces of sub-ballast with and without geogrid subject to a shear strain of $\varepsilon_s = 5\%$

forces. The mean contact forces measured at the interface reach a value of approximately three times compared to those that are near to the top loading plate and bottom boundary of the shear box. This mobilization of large magnitude forces inside the confinement zone of grids was a result of the strong mechanical interlock occurred between them (e.g., Indraratna et al. 2011a; Ngo et al. 2014).

Figure 9 shows contour strains induces in the geogrids in lateral shearing direction (ε_{xx}measured at a given shear strain of $\varepsilon_s = 5\%$ (i.e., approximately measured at the peak shear strength) for a biaxial grid (BG1) and a triaxial grid (TG3). It is observed that strains develop non-uniformly across the geogrids where the mobilized strains may depend on the degree of interlock that occurs between the

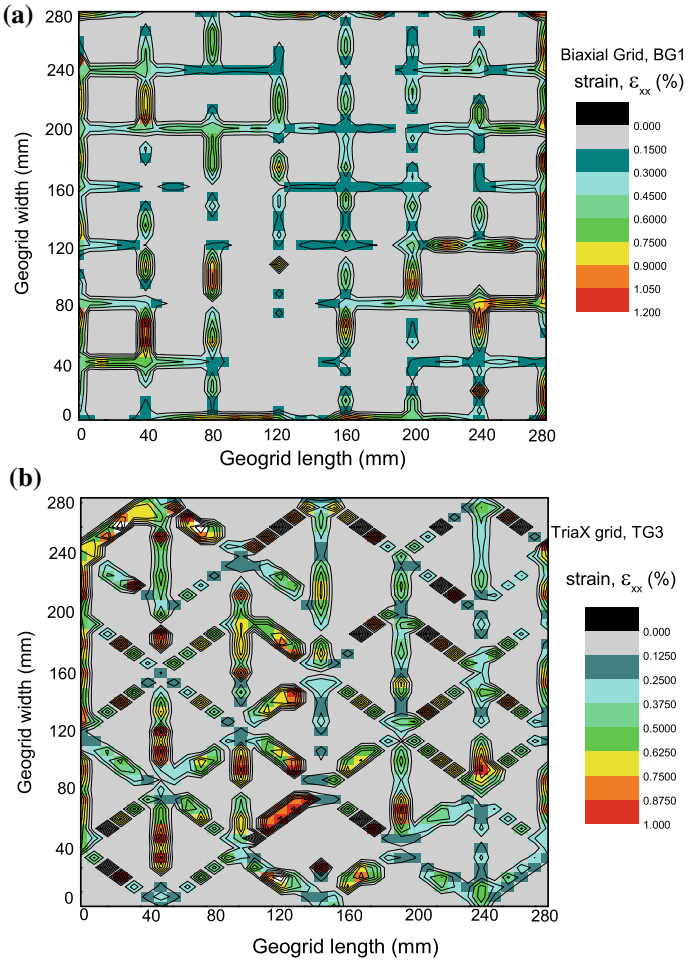

Fig. 9 Predicted contour strains induced across the geogrid: **a** Biaxial grid (BG1); and **b** Triaxial grid (TG3) *Data source* Ngo et al. (2017a, b, c)

geogrid and sub-ballast particles. It is noted that the triaxial grid (TG3) exhibits slightly smaller mobilized strains compared to the biaxial grid (BG1), approximately of 1.0% for the triaxial grid compared to 1.2% strain for biaxial grid, BG1. This can be justified by the symmetric shape of the triaxial grid that would provide better stress distribution than the square apertures.

5 Conclusions

Large-scale direct shear tests were performed on sub-ballast aggregates with and without the inclusion of different types of geogrid. The laboratory test results were used to calibrate and verify the proposed DEM models. DEM simulations for geogrids with varied shapes and opening apertures were simulated by connecting many spherical balls together.

The shear stress–strain responses predicted by the DEM analysis agreed well with experimental data, showing that the introduced DEM model can simulate the interface behavior of sub-ballast aggregates stabilized by different types of geogrids. Triaxial grid had the largest ratio of τ/σ_n while it exhibited the smallest volumetric dilation. This was due to the symmetrical shape of triangular apertures that can transfer applied loads across the geogrid and can provide a better interlock with granular particles. Taking advantages of DEM simulation, the variations of mean contact forces along the depth of the shear apparatus were presented for both unreinforced/reinforced sub-ballast specimens. The triaxial geogrid-stabilized sub-ballast experienced the largest mobilized contact forces at their interfaces. Contour strains mobilized across the geogrids in the lateral shearing direction were also analyzed.

Acknowledgements The authors greatly appreciate the financial support from the Rail Manufacturing Cooperative Research Centre (funded jointly by participating rail organizations and the Australian Federal Government's Business Cooperative Research Centres Program) through Project R2.5.1—Performance of recycled rubber inclusions for improved stability of railways. The Authors would like to thank the Australasian Centre for Rail Innovation (ACRI) Limited, and Tyre Stewardship Australia Limited for providing the financial support needed to undertake this research. Some research outcome is reproduced in this paper with kind permission from the Granular Matter. The Authors are thankful to Mr. Alan Grant, Duncan Best, and Mr. Ritchie McLean for their help in the laboratory.

References

AS 2758.7 (1996) Aggragates and rocks for engineering purposes; Part 7: Railway ballast, Sydney, NSW, Australia

Biabani MM, Indraratna B, Ngo NT (2016a) Modelling of geocell-reinforced subballast subjected to cyclic loading. Geotext Geomembr 44(4):489–503

Biabani MM, Ngo NT, Indraratna B (2016b) Performance evaluation of railway subballast stabilised with geocell based on pull-out testing. Geotext Geomembr 44(4):579–591

Cundall PA, Strack ODL (1979) A discrete numerical model for granular assemblies. Geotechnique 29(1):47–65

Huang H, Tutumluer E (2011) Discrete Element Modeling for fouled railroad ballast. Constr Build Mater 25:3306–3312

Huang H, Tutumluer E, Hashash YMA, Ghaboussi J (2009b) Discrete element modelling of aggregate behaviour in fouled railroad ballast. In: Geotechnical Special Publication, 192, pp 33–41

Indraratna B, Ngo NT, Rujikiatkamjorn C (2013) Deformation of coal fouled ballast stabilized with geogrid under cyclic load. J Geotech Geoenviron Eng 139(8):1275–1289

Indraratna B, Ngo NT, Rujikiatkamjorn C, Vinod J (2014) Behaviour of fresh and fouled railway ballast subjected to direct shear testing - a discrete element simulation. Int J Geomech ASCE 14 (1):34–44

Indraratna B, Salim W, Rujikiatkamjorn C (2011) Advanced rail geotechnology - ballasted track., CRC Press, Taylor & Francis Group, London, UK

Indraratna B, Sun Q, Ngo NT, Rujikiatkamjorn C (2017) Current research into ballasted rail tracks: model tests and their practical implications. Aust J Struct Eng 18(3):204–220

Itasca (2016) Particle flow code in three dimensions (PFC3D). Itasca Consulting Group Inc, Minnesota

Lim WL, McDowell GR (2005) Discrete element modelling of railway ballast. Granular Matter 7 (1):19–29

McDowell GR, Bolton M (1998) On the micromechanics of crushable aggregates. Geotechnique 48(5):667–679

McDowell GR, Harireche O, Konietzky H, Brown SF, Thom NH (2006) Discrete element modelling of geogrid-reinforced aggregates. Proc ICE - Geotech Eng 159(1):35–48

Ngo NT, Indraratna B (2016) Improved performance of rail track substructure using synthetic inclusions: experimental and numerical investigations. Int J Geosynthetics Ground Eng 2(3): 1–16

Ngo NT, Indraratna B, Rujikiatkamjorn C (2014) DEM simulation of the behaviour of geogrid stabilised ballast fouled with coal. Comput Geotech 55:224–231

Ngo NT, Indraratna B, Rujikiatkamjorn C (2015) A study of the behaviour of fresh and coal fouled ballast reinforced by geogrid using the discrete element method. In: Geomechanics from micro to macro - proceedings of the TC105 ISSMGE international symposium on geomechanics from micro to macro, IS-Cambridge 2014

Ngo NT, Indraratna B, Rujikiatkamjorn C (2016) Modelling geogrid-reinforced railway ballast using the discrete element method. Transport Geotech 8(2016):86–102

Ngo NT, Indraratna B, Rujikiatkamjorn C (2017a) Micromechanics-based investigation of fouled ballast using large-scale triaxial tests and discrete element modeling. J Geotech Geoenviron Eng 134 (2): pp 04016089

Ngo NT, Indraratna B, Rujikiatkamjorn C (2017b) Stabilisation of track substructure with geo-inclusions – experimental evidence and DEM simulation. Int J Rail Transport 5 (2): 63–86

Ngo NT, Indraratna B, Rujikiatkamjorn C (2017c) A study of the geogrid–subballast interface via experimental evaluation and discrete element modelling. Granular Matter 19 (3): 54, 51–16

O'Sullivan C, Cui L (2009) Micromechanics of granular material response during load reversals: combined DEM and experimental study. Powder Technol 193(3):289–302

Powrie W, Yang LA, Clayton CR (2007) Stress changes in the ground below ballasted railway track during train passage. In: Proceedings of the institution of mechanical engineers: part F: J of rail rapid transit, pp 247–261

Rujikiatkamjorn C, Indraratna B, Ngo NT, Coop M (2012) A laboratory study of railway ballast behaviour under various fouling degree. In: The 5th Asian regional conference on geosynthetics, pp 507–514

Rujikiatkamjorn C, Ngo NT, Indraratna B, Vinod J, Coop M (2013) Simulation of fresh and fouled ballast behavior using discrete element method. In: Proceedings of the international conference on ground improvement and ground control, pp 1585–1592. Singapore, Research Publishing

Selig ET, Waters JM (1994) Track geotechnology and substructure management. Thomas Telford, London

Trani LDO, Indraratna B (2010) Assessment of subballast filtration under cyclic loading. J Geotech Geoenviron Eng 136(11):1519–1528

Tutumluer E, Dombrow W, Huang H (2008) Laboratory characterization of coal dust fouled ballast behaviour. In: AREMA 2008 annual conference and exposition, Salt Lake City, UT, USA

Jarofix Waste Material in Embankment Construction

A. K. Sinha and V. G. Havanagi

Abstract Due to the large-scale road infrastructural development in India, conventional soil is depleting very fast while different industries are producing a huge amount of waste materials as by-products. Utilization of such waste materials leads to sustainable road construction. Jarofix is one of the waste materials generated during the extraction of zinc from its ore. At present, the accumulated jarofix is about 35 lakh tons, while the annual production is about 6 lakh tons in India. Detailed R & D study was carried out to study the feasibility of jarofix in the construction of embankment. Jarofix sample was collected from Chittorgarh, Rajasthan and its geotechnical characteristics were investigated. Design and slope stability analysis of jarofix embankment of varying heights (1–10 m) and slopes (19°–45° or 1V:3H to 1V:1H) was carried out to decide its practical applicability in the field construction. The factor of safety was determined by numerical analysis under different water conditions, viz. partially saturation, steady flow, sudden draw down with, and without seismic factor. Results of variation of factor of safety with height, saturation, and slope are presented. Multiple linear regression analysis was carried out to evaluate the effect of different design parameters on the factor of safety of the embankment. A typical settlement analysis of jarofix embankment is also presented in this paper. It is concluded that jarofix waste material has a good potential for construction of embankment.

Keywords Jarofix · Waste · Material · Embankment · Construction · Stability

A. K. Sinha (✉) · V. G. Havanagi
Geotechnical Engineering Division, CSIR-Central Road Research Institute,
New Delhi 110025, India
e-mail: sinha.crri@nic.in

V. G. Havanagi
e-mail: vasant.crri@nic.in

R. Sundaram et al. (eds.), *Geotechnics for Transportation Infrastructure*,
Lecture Notes in Civil Engineering 29,
https://doi.org/10.1007/978-981-13-6713-7_17

1 Introduction

India is a major zinc producer country in the world. Indian zinc industry consists of primarily two private industries, namely Hindustan Zinc Limited (HZL), Rajasthan and Binani Zinc Ltd., Ernakulam, Kerala. Hindustan Zinc has a market share of 60% of total zinc production. Hindustan Zinc Ltd. operates zinc smelters at Chanderiya (Rajasthan) by hydro-process has annual capacity of 3 lakh ton; Debari (Rajasthan) has a hydro-process with an annual capacity of 1 lakh ton; the Binani zinc smelter limited operates by hydro-process and has annual capacity of 0.3 lakh ton at Ernakulum (Kerala). This industry has approximately 4.3% share in the total zinc smelter capacity in the Asia Pacific region. Figure 1 shows the flowchart of jarofix production by hydrometallurgical process.

Zinc ores are extracted from zinc mines. The lumpy (rocky) ores are crushed and grounded into particles of size smaller than 0.1 mm. By flotation process, zinc concentrate ores are prepared which has zinc content of 40–60%. During the extraction of zinc from its ore by hydro-process, jarosite waste material is produced as a by-product. It is mixed with 2% lime and 10% cement, to make a stable material which is called jarofix. At present, the accumulated jarofix is about 35 million tons, while the annual production is about 6 million tons in India (Sinha et al. 2012). Figure 2 shows the typical jarofix mound at Chittorgarh, Rajasthan. It is occupying about 100 acres of costly land near the plant. Different researchers advocated that this material has potential for road construction (Pappu et al. 2006; Sinha et al. 2012; Arora et al. 2013).

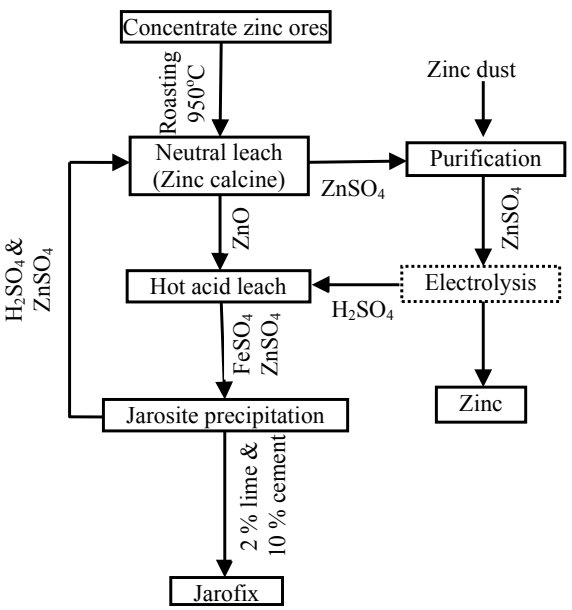

Fig. 1 Flowchart of jarofix production by hydro-process (Sinha et al. 2012)

Fig. 2 Typical view of jarofix mound at Chittorgarh

Chen and Dutrizac (2000) stabilized jarosite material with Portland cement for safe disposal. Seyer et al. (2001) studied the mineralogical behavior of jarosite mixed with lime/Portland cement which resulted in stabilized mix. Demers and Haile (2003) advocated that cured/aged jarofix is easy to excavate, compact and is chemically stable. It makes an excellent fill material. Vsevolod et al. (2005) stabilized the jarosite waste material with small percentage of cement/lime and concluded that the stabilized mix has potential for use in base and sub-bases of road, airfields and dams, manufacturing of tiles and bricks, etc. Reddy et al. (2011) studied the geotechnical characteristics of jarosite waste and concluded that it is suitable for the utilization as a landfill material. In India at present, jarofix has no application and is dumped haphazardly on the costly land available near the plant.

In the present study, jarofix was collected from Hindustan zinc limited, Chittorgarh and local soil from nearby area. Geotechnical characterization of both materials was carried out in the laboratory. Based on geotechnical characteristics, stability analysis of jarofix and jarofix-soil embankments of varying height (1–10 m) and slopes (19°–45° or 1V:3H to 1V:1H) was carried out to decide its practical applicability in the field construction. The factor of safety was determined by numerical analysis under different water conditions, viz. partially saturation, steady flow, sudden draw down with and without seismic factor. The effect of different water conditions on stability of jarofix embankment has been discussed. Variation of factor of safety with height, saturation, and slope is presented. Multiple linear regression analysis was carried out to evaluate the effect of different parameters, viz. height, slope and jarofix content on the factor of safety of the embankment.

2 Characterization of Jarofix and Soil

Geotechnical investigation was carried out on jarofix and local soil samples considering the possible application in the construction of embankment. Different laboratory tests that were carried out includes specific gravity test, free swelling index test, grain size analysis, liquid limit and plastic limit tests, Proctor compaction test, and direct shear test. The results are discussed in the following sections.

2.1 Specific Gravity Test

The specific gravity values of jarofix and soil were obtained as 2.60 and 2.75, respectively (IS 2720-Part 3/Sec 2, 2002). The lower specific gravity value of jarofix particles may be due to polycrystalline structure of jarofix particles. Demers and Haile (2003) and Pappu et al. (2006) have reported that value of specific gravity of jarofix in the range of 2.65–2.89.

2.2 Free Swelling Index Test

It was observed that both jarofix and soil have low free swelling index values of 10 and 7%, respectively (IS 2720-Part 40, 2002). Results indicate that both materials have a low degree of expansion/swelling nature. The low FSI of jarofix is due to the presence of lime and cement after addition to jarosite.

2.3 Grain Size Analysis

Grain size distribution of jarofix and soil was evaluated by Indian standard procedure (IS 2720-Part 4, 2006). The coefficient of uniformity (C_u) and coefficient of curvature (C_c) were determined as 5 and 4 for jarofix. As the value of C_u is less than 6; C_c value is out of range (1–3), jarofix is classified as gap graded silt size fine grained material with 75% of its particles passing 75-μm sieve. Soil is observed to be coarse-grained material with 52% of its particles retained on 75-μm sieve. It is composed of 8% gravel, 44% sand, 30% silt, and 18% clay size particles. The coefficient of uniformity (C_u) and coefficient of curvature (C_c) were determined as 300 and 0.04 for soil, respectively.

2.4 Liquid Limit and Plastic Limit Tests

Liquid limit (LL) and plastic limit (PL) of the jarofix were observed to be 59 and 43%, respectively. The plasticity index of the jarofix is calculated as 16%. According to Indian standard classification (IS 2720-part 5, 2006), jarofix is classified as MH, i.e., inorganic silt of high compressibility (IS 1498, 1970). The liquid limit and plastic limit of the soil were determined as 34% and 16, respectively. The plasticity index of the soil is calculated as 18% and classified as SC, i.e., sand with clay content.

2.5 Modified Proctor Compaction Test

The values of maximum dry density (MDD) and optimum moisture content (OMC) for jarofix and soil were obtained as 13.5 kN/m^3 and 35%; 20 kN/m^3 and 9%, respectively (IS 2720-Part 8, 2006). Compaction curves for different jarofix-soil mixes (J-100% jarofix; J3S1-75% jarofix + 25% soil; J2S2-50% jarofix + 50% soil; J1S3-25% jarofix + 75% soil and S-100% soil) along with zero air void lines are shown in Fig. 3.

It was observed that increase in soil content in the jarofix-soil mixes, there is an increase in dry density with the corresponding decrease in optimum moisture content. This may be due to higher unit weight of soil as compared to jarofix. Similar trend was also observed by Pappu et al. (2010) for mixes of jarosite-clay and jarosite-coal combustion residues. Shahu et al. (2013) also observed similar increase in density on mix of copper slag and fly ash specimens (Havanagi et al. 2012).

2.6 Direct Shear Test

Slope stability of jarofix embankment depends on its shear strength and is evaluated by carrying out direct shear test as per IS 2720, part–13 (2002). The jarofix samples were prepared at 95% density as per MORTH (2013). Each layer of 200 mm thickness of embankment is specified to be compacted at 95% of the maximum dry density. The test was carried out under partially (UU test) saturated condition at different normal stresses varying in the range of 25–150 kPa. The specimens were then sheared at the rate of 1.25 mm/min. The normal stress was held constant throughout the test. For each normal stress, the variation in shear stress with horizontal displacement was recorded.

Shear stress ~ displacement curves for jarofix specimens at different normal stresses are shown in Fig. 4. It was observed that shear stress increases with horizontal displacement and reaches a distinct peak value and then decreases to a

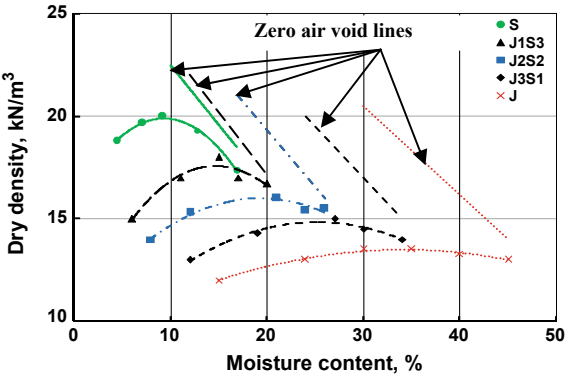

Fig. 3 Proctor compaction curves of jarofix-soil mixes

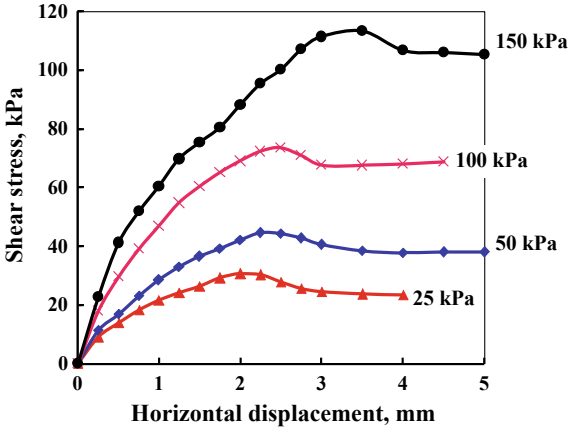

Fig. 4 Variation of shear stress with displacement of jarofix

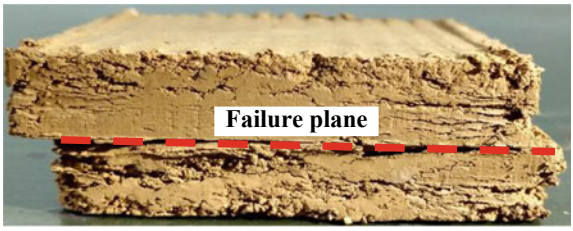

Fig. 5 Typical view of failed jarofix specimen in direct shear test

constant ultimate or critical state stress value. The peak shear stress was observed to be reached at a horizontal displacement of 2–3.5 mm. Shear strength parameters (cohesion and angle of internal friction) were determined corresponding to peak shear stress of jarofix and obtained as c = 14 kPa and ϕ = 22°, respectively. It was observed that stress $\sim$ displacement behavior of jarofix material is similar to silty soil (Kaniraj and Havanagi 2001), fly ash (Kaniraj and Havanagi 1999), sandy soil (Bakker et al. 2005) and Ottawa sand (Taylor 1948).Similarly, cohesion and angle of internal friction of selected soil were determined as c = 7 kPa and ϕ = 30°, respectively.

A typical view of failure pattern from direct shear test is shown in Fig. 5. Ductile failure pattern was observed at optimum moisture content.

3 Stability Analysis of Jarofix Embankment

The different geotechnical characteristics, viz. shear strength parameters, bulk and saturated densities of different jarofix-soil mixes, were used for slope stability analysis of the jarofix embankment.

Table 1 Cross-sectional details and factors considered for stability analysis

Parameters	Values
Height of embankment, (*H*), *m*	1, 2, 4, 6, 8, 10
Slope of embankment (β), V:H	1:1; 1:2; 1:3
Seismic coefficient	Horizontal coefficient, $\alpha_h = 0.05$ Vertical coefficient, $\alpha_v = 0.025$
Water condition	Partially saturation, steady flow (fully saturation), sudden draw down

Stability analysis was carried out using computer software (Geo 5, 2012). The software uses the simplified Bishop's method (1955). The analysis was carried out using limit equilibrium method where only minimum factor of safety (FoS) was determined by optimizing critical slip circle. The height of the embankment was assumed as 1, 2, 4, 6, 8, and 10 m while slope was assumed to vary as 1V:1H, 1V:2H, and 1V:3H. The surcharge loading due to pavement crust thickness and traffic is taken as total 24 kN/m^2 (IRC-113, 2013; and MDT 2008). The soil used for stabilization of jarofix was considered as subsoil for the analysis. Stability analysis was carried out under different saturation conditions, viz. partially saturated, fully saturated, and sudden drawdown. Seismic effect was considered by using seismic factors $\alpha_h = 0.05$ and $\alpha_v = 0.025$ where α_h and α_v are horizontal and vertical acceleration coefficients, respectively (IRC 6, 2014) based on earthquake zone. Details of cross section of embankment, seismic and saturation conditions considered for stability analysis are given in Table 1.

3.1 Result and Discussions

The effect of different parameters on factor of safety of embankment has been discussed below.

3.1.1 Effect of Height

The factor of safety of different embankment heights (1–10 m) was observed to be in the range of 2.32–0.58 for jarofix (J), 2.28–0.55 for J3S1, 2.30–0.53 for J2S2 and 2.33–0.52 for J1S3, respectively. It was observed that embankment is in general stable up to the height of 2 m for all considered slope, water saturation condition, and seismic factor. However, it was also observed that factor of safety decreases with increase in the height of embankment for a particular slope, water saturation,

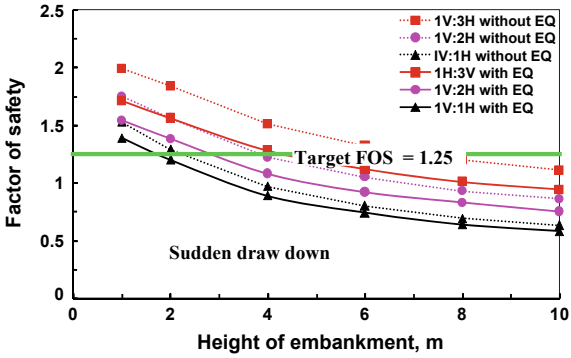

Fig. 6 Factor of safety ~ height of jarofix embankment

and seismic condition. The variation of factor of safety with height of jarofix embankment is shown in Fig. 6 with or without earth quake (E.Q.) factor.

Considering the target factor of safety of 1.25 (IRC 75, 2015), jarofix and their mixes are stable up to the height of 5 m for slope of 1V:3H and 2 m for slope of 1V:2H under all considered water saturation conditions and seismic factor.

3.1.2 Effect of Saturation

It was observed that the factor of safety of embankment drastically reduces from partially saturation condition to sudden drawdown condition. However, the decrease is marginal from partially saturation condition to steady seepage flow.

3.1.3 Effect of Slope

The variation of factor of safety values with slope of the jarofix embankment is graphically plotted as shown in Fig. 7. It is observed that factor of safety decreases with increase in the slope of embankment under different saturation and seismic conditions. It was also observed that rate of decrease of factor of safety is more for slope from 3H:1V to 2H:1V than for 2H:1V to 1H:1V. It was concluded that jarofix, jarofix-soil embankment of different height with slope 1H:1V in general are unstable under different saturation and seismic conditions.

3.1.4 Effect of Jarofix Content

The factor of safety marginally increases with increase in content of jarofix in jarofix-soil mixes under specific saturation and seismic condition. Variation of FoS with jarofix content for different heights of embankment under sudden drawdown and seismic conditions is shown in Fig. 8.

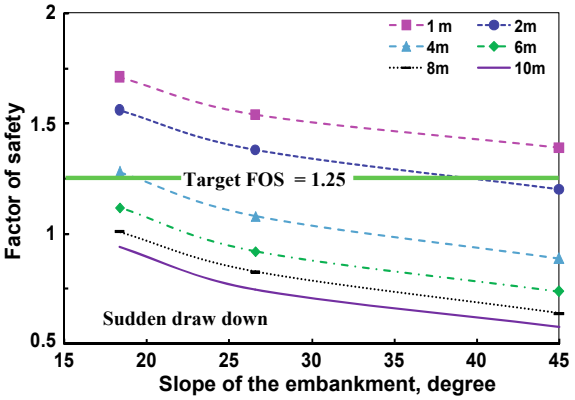

Fig. 7 Factor of safety ~ slope of jarofix embankment

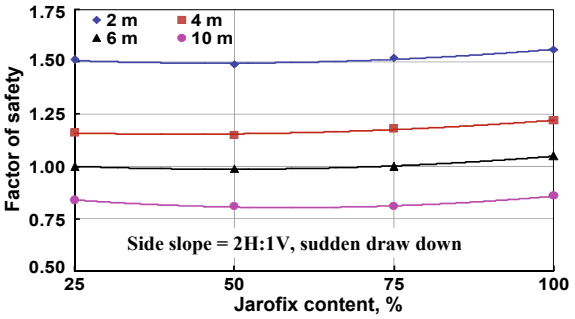

Fig. 8 Variation of factor of safety with jarofix content

3.1.5 Multiple Linear Regression Analysis

Multiple Linear Regression (MLR) analysis was carried out under sudden draw down, steady seepage and partially saturated conditions with seismic factor.

(a) *For sudden drawdown condition:* From the analysis, the obtained high R^2 value (0.96) indicates that this model is capable to explain 96% of variation in the model. It was observed that the t-stat values of explanatory variables, namely height (H) and slope (β), are significant at 5% level of significance. This indicates that these model coefficients of H, β, and jarofix content are more appropriate parameters in estimating the FoS.

(b) *For steady seepage flow condition:* From the analysis, the obtained high R^2 value (0.95) indicates that this model is capable to explain 95% of variation in the model. The t-stat values of explanatory variables namely H, β and jarofix content are significant at 5% level of significance. This indicates that model coefficients of H, β and jarofix content are more appropriate parameters for estimating the FoS (Table 2).

Table 2 Estimated model coefficients for jarofix-soil embankment under sudden drawdown condition

Parameters	Coefficients	Standard error	t-Stat	*P*-value
Intercept	1.887	0.045	41.642	0.000
H, *m*	−0.086	0.003	−24.320	0.000
β, degrees	−0.013	0.001	−13.687	0.000
Jarofix content, %	0.001	0.000	1.382	0.171

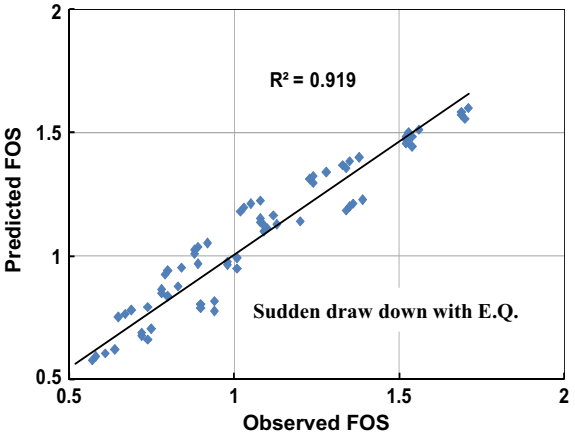

Fig. 9 Predicted FoS ~ Observed FoS

c) *For partially saturated condition:* From the analysis, the obtained high R^2 value (0.93) indicates that this model is capable to explain 93% of variation in the model. It was observed that the t-stat values of explanatory variables namely *H*, β and jarofix content are significant at 5% level of significance. This indicates that these model coefficients of *H*, β and jarofix content are more appropriate parameters for estimating the FoS.

The observed FoS values with respect to predicted FoS values is shown in Fig. 9 for sudden drawdown for jarofix-soil embankment. It was observed that there is insignificant variation in between observed and predicted FoS.

4 Conclusions

- Low specific gravity value of jarofix is due to crystalline structure of jarofix particles. The material was observed to be non-expansive in nature. Jarofix and soil are fine- and coarse-grained materials, respectively.

- The moisture density curve of jarofix is in general flat indicating in-sensitiveness of dry density with moisture content. The material has low maximum dry density as compared to conventional soil.
- At 95% compacted specimens, shear stress increases with horizontal displacement and reaches the distinct peak value and then decreases to a constant ultimate or critical/residual state stress value. Jarofix and soil were observed to be cohesive-frictional material.
- Jarofix embankment in general is stable up to the height of 2 m for all considered slope, water saturation condition, and seismic factor. The factor of safety decreases with increase in the height of embankment for a particular slope and seismic condition. Considering the target factor of safety of 1.25, jarofix and their mixes are stable up to the height of 5 m for slope of 1V:3H under all the considered conditions.
- Factor of safety marginally increases with increase in content of jarofix in jarofix-soil mixes under specific saturation and seismic condition. It drastically reduces from partially saturation condition to sudden drawdown condition. The factor of safety decreases with increase in the slope of embankment under different saturation and seismic conditions. The rate of decrease of factor of safety is more for increase of slope from 3H:1V to 2H:1V than from 2H:1V to 1H:1V. It is also concluded that jarofix and jarofix-soil embankment of different heights with slope 1H:1V are in general, unstable under different saturation and seismic conditions.
- Multiple linear regression analysis indicated that factor of safety values of jarofix-soil embankment under different saturation conditions depend on the height, slope and jarofix content. FoS value is more affected by the height of the embankment in the case of sudden drawdown condition while the slope of the embankment is dominant factor in the case of partially saturated and steady seepage flow conditions. However, jarofix content is the least affecting factor.

Acknowledgements The kind approval of Director, CSIR-Central Road Research Institute, New Delhi, India 110 025 to publish the research paper is acknowledged. The project was sponsored by Hindustan zinc limited is also acknowledged.

References

Arora VK, Havanagi VG, Sinha AK (2013) Characterization of copper slag and jarofix waste materials for road construction. In: Proceedings of international conference on world academy of science and technology. Int. science index issue 84, Melbourne, Australia, pp 1353–1358

Bakker KJ, Bezuijan A, Broere W, Kwast EA (2005) Geotechnical aspects of underground constriction in soft ground. In: Proceedings of 5th International Symposium TC28, Amsterdam, Netherland

Bishop AW (1955) The use of the slip circle in the stability analysis of slopes. Geotechnique 5 (1):7–17

Chen TT, Dutrizac JE (2000) A mineralogical study of jarofix products for the stabilization of jarosite for disposal. J Miner Metals Mater Soc (TMS), pp 917–933
Demers B, Haile G (2003) Management of tailings stabilized by lime and cement at Canadian electrolytic zinc, Valleyfield, Québec. In: Proceedings of mining and the environ, Sudbury, Ontario, Canada, 25–28 May
Geo 5 (2012) Fine spol. S r. o. Zaverka 12, 169 00 Praha 6, Czech Republic. www.finesoftware.eu/geotechnical -software
Havanagi VG, Sinha AK, Arora VK, Mathur S (2012) Design and Stability analysis of copper slag embankment. J Indian Highways 40(10):17–23
IRC 6 (2014) Standard specifications and code of practice for road bridges, section II – loads and stresses, Indian Road Congress, New Delhi, India
IRC SP 75 (2015) Design of high embankment, Indian Road Congress, New Delhi, India
IRC-113 (2013) Guidelines for the design and construction of geosynthetic reinforced embankment on soft sub-soils, Indian Road Congress, New Delhi, India
IS 1498 (1970) Classification and identification of soils for general engineering purposes, published by Bureau of Indian standard, New Delhi, India
IS 2720 (Part 3/ Sec 2-2002) Methods of test for soils: part 3 determination of specific gravity, section 2 fine, medium and coarse grained soils, published by Beauro of Indian Standard, New Delhi
IS 2720 (Part 4-2006) Methods of test for soils: part 4 grain size analysis, published by Beauro of Indian Standard, New Delhi
IS 2720 (Part 5-2006) Methods of test for soils: part 5 determination of liquid and plastic limit, published by Beauro of Indian Standard, New Delhi
IS 2720 (Part 8-2006) Methods of test for soils: part 8 determination of water content- dry density relation using heavy compaction, published by Beauro of Indian Standard, New Delhi
IS 2720 (Part 13-2002) Methods of test for soils: part 13 direct shear test, published by Beauro of Indian Standard, New Delhi
IS 2720 (Part 40-2002), Methods of test for soils: part 40 determination of free swell index of soils, published by Beauro of Indian Standard, New Delhi
Kaniraj SR, Havanagi VG (1999) Compressive strength of cement stabilized fly ash soil mixture. Cement Concr Res 29:673–677
Kaniraj SR, Havanagi VG (2001) Correlation analysis of laboratory compaction of fly ashes. Pract Periodical Hazard, Toxic Radioact Waste Manag, ASCE 5(1):25–32
MDT Geotechnical Manual (2008) Roadway slopes and embankments. Montana Department of Transportation, MDT, USA
MORTH (2013) Specifications for road and bridge works, Ministry of Road and Highway Transport, New Delhi, India
Pappu A, Mohini S, Shyam RA (2006) Jarosite characteristics and its utilisation potentials. Sci Total Environ 359:232–243
Pappu A, Mohini S, Shyam RA (2010) Recycling hazardous jarosite waste using coal combustion residues. J Mater Charact 6:1342–1355
Reddy CNVS, Sanghamitra B. and Angel, R. V. (2011) A study on properties of jarosite waste for landfill capping design. In: Proceedings of Indian geotechnical conference, Kochi, India
Seyer S, Chen TT, Dutrizec JE (2001) Jarofix: Addressing iron disposal in the zinc industry. J Mineral 53(12):32–35
Shahu JT, Patel S, Senapati A (2013) Engineering properties of copper slag-fly ash- dolime mix and its utilization in the base course of flexible pavement. J Mater Civil Eng ASCE 25 (12):1871–1879
Sinha, A.K., Havanagi, V.G., Arora, V.K., Ranjan, A. and Mathur, S. (2012) Recycling Jarofix waste as a construction material for embankment and sub grade, Inter. J. of Solid Waste Technology and Management, vol. 38(3), pp 169–181
Taylor DW (1948) Fundamental of soil mechanics. John Wiley and Sons, New York
Vsevolod AM, Haroldo AP, Patricio RI (2005) Potential application of acid jarosite wastes as the main component of construction materials. Constr Build Mater 19:141–146

Model Study on RE Wall Using Municipal Solid Waste as Backfill Material

Kinjal H. Gajjar, Manish V. Shah and Alpa J. Shah

Abstract In Western India, Ahmedabad city generates more than 4000 TPD waste including 300 MT of construction and demolition debris waste, which is dumped at Pirana site. Such a huge mound of garbage has become a complex problem due to its environmental impact. Over conventional RCC rigid retaining wall, reinforced earth wall is preferred because of ease of construction, reduced cost, and better performance. If a naturally occurring deposit of acceptable granular soil material is not available abundantly near the site for the reinforced zone, then the cost may rise significantly. Initial geotechnical investigation carried out on municipal solid waste of Pirana site shows that it is non-plastic in nature having a higher angle of internal friction. The main objective of this research is to evaluate the suitability of providing municipal solid waste as an alternative backfill material in RE wall by performing load–displacement and load–settlement test and to reduce the burden on the existing Pirana landfills. From this study, municipal solid waste depicted better results in terms of lateral displacement of modeled RE wall as compared to sand, but contrary to it municipal solid waste showed greater vertical settlement than sand.

Keywords RE wall · Backfill material · MSW

K. H. Gajjar (✉) · M. V. Shah · A. J. Shah
Applied Mechanics Department, LD College of Engineering, Ahmedabad 380015, India
e-mail: gajjarkinjal1@hotmail.com

M. V. Shah
e-mail: mvs2212@yahoo.co.in

A. J. Shah
e-mail: alpa.jogin@gmail.com

R. Sundaram et al. (eds.), *Geotechnics for Transportation Infrastructure*,
Lecture Notes in Civil Engineering 29,
https://doi.org/10.1007/978-981-13-6713-7_18

1 Introduction

Reinforced earth is a composite material formed by the interaction between a frictional soil and reinforcing strips/sheets. In concept, it is like reinforced concrete; that is, reinforced earth is an economical means of improving the mechanical properties of basic material, earth, by reinforcing it. The earth and the reinforcement are combined through friction. The result is a monolithic mass that acts cohesively, supporting its own weight and applied loads. The reinforcing strips/layers resist stresses produced within the soil mass; stresses are transferred to the strips/layers via friction. Modern use of soil reinforcing for retaining wall construction was pioneered by French architect and engineer Henri Vidal in the 1960s. As per Vashi et al. (2011) comparing with the traditional gravity earth retaining structure, geosynthetic reinforced earth retaining structures have better engineering characteristics of light deadweight, beautiful shape, construction convenience, etc. Mostly, granular material is used in the construction of reinforced earth, but nowadays there is a scarcity of granular material because of huge quantity of sand mining for various construction purposes. According to Hyun et al. (2011), soil is probably the most extensively used construction material in the world. Sufficient amount of free soil of required quality and quantity is not easily available. For that reason, a large amount of trees are cut now for obtaining more soil for road construction which causes great environmental danger. Due to rapid economic growth and urbanization, a huge quantity of municipal solid waste is being generated and creating a tremendous harmful effect on public health. Disposal of municipal solid waste is not only wasteful, but costly because of the lack of landfill space and stringent environmental policy. Shah and Jose (2017) concluded from leachate studies that municipal solid waste of Pirana landfill is a non-hazardous material as the concentration of heavy metals is within the permissible limits. According to Patil et al. (2016), beneficial use of municipal solid waste ash in road construction is the preferable option for safe and economical utilization of million tons of municipal solid waste ash. Though the beneficial use of municipal solid waste ash in road construction material has been known for many decades, it is still not yet fully utilized. The major obstacles to further use of municipal solid waste are the large variation in physical and chemical properties. Because of non-plastic nature and high value of angle of internal friction, municipal solid waste may be a better option to be used as a backfill material in reinforced earth wall. The utilization of a huge volume of municipal solid waste will increase with increasing realization of the environmental benefits associated with such use. The present challenge of finding an alternative backfill material economically as well as having similar characteristics to that of soil may be achieved by using municipal solid waste.

2 Materials Used

2.1 Sand

Sand to be used as a backfill material in reinforced earth wall model has the following index and engineering properties given in Table 1.

2.2 MSW

MSW to be used as a backfill material in reinforced earth wall model was procured from Pirana site, Ahmedabad, after sieving it from 4.75 mm IS sieve having properties given in Tables 2, 3, and 4.

Table 1 Index and engineering properties of sand

Test	IS code	Symbol	Value
Grain-size analysis	IS: 2720-4:1985	C_u	2.90
		C_c	1.117
Soil classification	IS: 1498-1970		SP
Specific gravity	IS: 2720-3:1980	G	2.66
Relative density	IS: 2720-14:1983	Υ_{max} (kN/m^3)	18.70
		Υ_{min} (kN/m^3)	15.20
Direct box shear	IS 2720-13:1986	c (kN/m^2)	0
		ϕ	32.29°

Table 2 Physical properties of MSW

Test	IS code	Symbol	Value
Grain-size analysis	IS: 2720-4:1985	C_u	3.428
		C_c	1.166
Specific gravity	IS: 2720-3:1980	G	2.25
Relative density	IS: 2720-14:1983	Υ_{max} (kN/m^3)	13.94
		Υ_{min} (kN/m^3)	10.98
Direct box shear	IS 2720-13:1986	c (kN/m^2)	3.471
		ϕ	34.76°

Table 3 Proximate analysis of municipal solid waste

Parameter	Value (%)
Moisture	0.80
Volatile matters	11.60
Ash	10.55
Fixed carbon	14.83

Table 4 EDAX test results of municipal solid waste

Element	Value (% weight)
Oxygen (O)	60.56
Magnesium (Mg)	1.7
Aluminum (Al)	5.32
Silicon (Si)	19.54
Potassium (K)	1.45
Calcium (Ca)	5.80
Iron (Fe)	5.73
Sodium (Na)	–

2.3 Geogrid

Geogrid used as reinforcement was constructed of high molecular weight and high tenacity knitted polyester yarns with a proprietary coating. Mechanical properties of geogrid are given in Table 5.

3 Test Setup

Model tests were performed in a steel tank of size 700 mm × 990 mm × 750 mm. Both sides of the tank were provided with perspex sheet to observe the rupture surface. The wooden facing panel of 30-mm thickness was fixed to the open face of the tank model. The panel was made up of eight no. of blocks having a size of

Table 5 Mechanical properties of geogrid

Parameter	Value
Tensile strength—MD (kN/m)	60
Tensile strength—CMD (kN/m)	20
Creep reduction factor	1.47
Partial factor—installation damage	1.07
Partial factor—environmental effects	1.10

300 mm × 175 mm and four no. of blocks having a size of 150 mm × 175 mm. According to BS 8006:2010, five layers of geogrid having a length of 525 mm and a spacing of 150 mm were fixed to the facing panel by means of clamps. To carry out the tests on reinforced earth wall model, the vertical downward load was applied by means of mechanical jack. To measure the displacements, totally six dial gauges were set up in RE wall model, out of which two dial gauges were set up in order to measure vertical settlement of backfill material and four dial gauges, viz. H_1, H_2, H_3, and H_4, were set up in a way to measure the horizontal displacement of RE wall (Table 6 and Figs. 1, 2).

Table 6 Location of dial gauges

Designation (mm)	H_1	H_2	H_3	H_4
Horizontal distance (left to right)	85	260	435	610
Vertical distance (bottom to top)	690	540	390	60

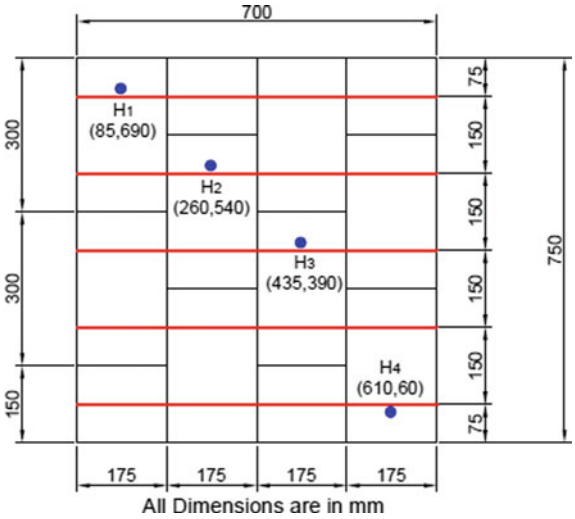

Fig. 1 Schematic diagram of facing panel

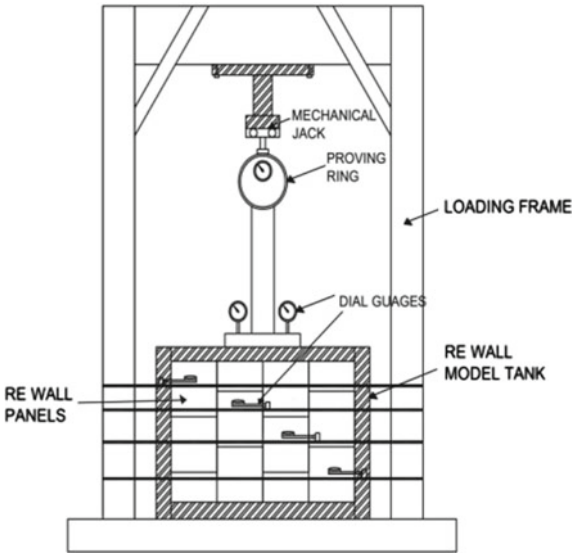

Fig. 2 Schematic diagram of reinforced earth wall test model

4 Test Procedure

A load–displacement and load–settlement test was performed on RE wall model in order to know the displacement characteristics of RE wall and also the settlement characteristics of backfill material. For this, the following procedure was performed on RE wall model.

The tank was filled in layers by compacting the backfill material to achieve the relative density of 80% as per IRC SP 102-2014 along with providing geogrid at a spacing of 150 mm.

A plate of size 250 × 250 mm having 25-mm thickness was placed on RE wall model having firm contact with backfill material, in order to have uniform transfer of load. The loads were applied in Rankine's failure wedge.

A seating load of 6.86 kN/m^2 was applied in the plate using mechanical jack.

The load is then applied in multiple uniform increments of 1.96 kN. When there is no perceptible increase in settlement or when the rate of settlement reduces to 0.02 mm per minute as given in IS 1888-1982 and the deformation rate becomes nearly constant, the dial gauge readings were noted. The readings were noted until the wall displaces to a greater extent or when the proving ring rebounds.

Load versus displacement graph and load versus settlement graph were then plotted to know the load–displacement characteristics of RE wall and settlement characteristics of backfill material (Figs. 3 and 4).

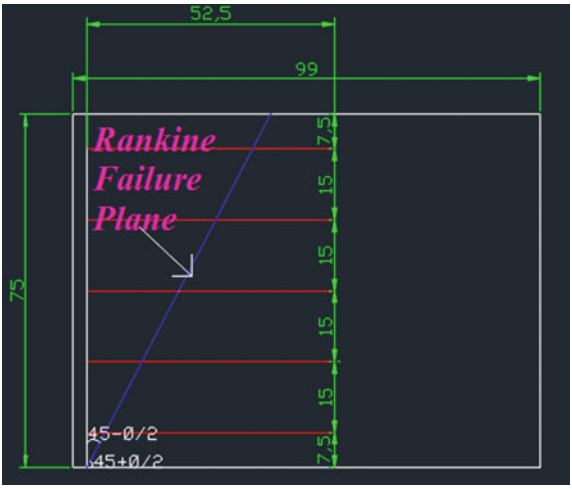

Fig. 3 Rankine's failure wedge

Fig. 4 Reinforced earth wall test model

5 Results and Discussion

The test was performed on reinforced earth wall model using sand and MSW as a backfill material. The backfill material was deposited at 80% of relative density. The results obtained for settlement and displacement at particular dial gauge location, viz. H_1, H_2, H_3, and H_4, for each load increment are shown in the following graphs.

5.1 Load–Displacement Curve

5.1.1 At H_1 Dial Gauge Location

See Fig. 5.

5.1.2 At H_2 Dial Gauge Location

See Fig. 6.

5.1.3 At H_3 Dial Gauge Location

See Fig. 7.

5.1.4 At H_4 Dial Gauge Location

See Fig. 8.

Graphs 5, 6, 7, and 8 show the displacement behavior of RE wall at particular dial gauge locations, i.e., H_1, H_2, H_3, H_4, for both backfill materials, sand and

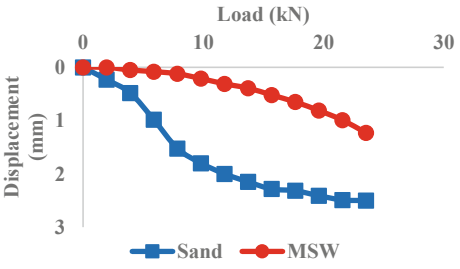

Fig. 5 Load versus displacement characteristics for sand and MSW at H_1 dial gauge location

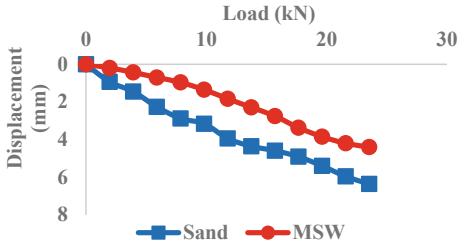

Fig. 6 Load versus displacement characteristics for sand and MSW at H_2 dial gauge location

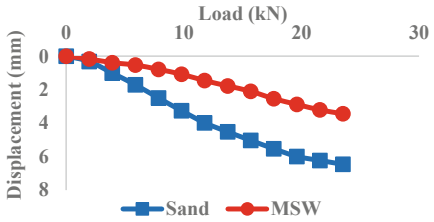

Fig. 7 Load versus displacement characteristics for sand and MSW at H_3 dial gauge location

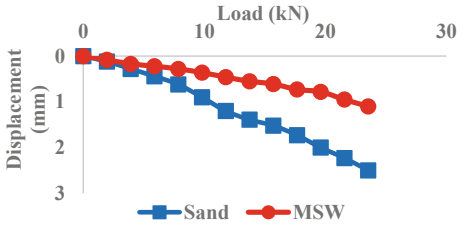

Fig. 8 Load versus displacement characteristics for sand and MSW at H_4 dial gauge location

MSW. From the graph, it can be observed that the displacement of RE wall at each particular load with MSW as a backfill material is less than that obtained with the sand as a backfill material. The total displacement of RE wall at 23.54 kN load with MSW and sand as a backfill material is 1.23, 4.40, 3.44, 1.10 mm and 2.50, 6.46, 6.36, 2.50 mm, respectively. Displacement of RE wall is more prominent at H_2 dial gauge location (260 and 540 mm from the left and bottom of the wall, respectively). Sand is dense, and hence the lateral soil pressure on the facing will be high. Thus at higher loads, the active earth pressure on facing was larger and hence the steep increases in facing displacement. As the density of the MSW is less, the lateral earth pressure on the facing panel also reduces. Hence, the facing displacements were reduced.

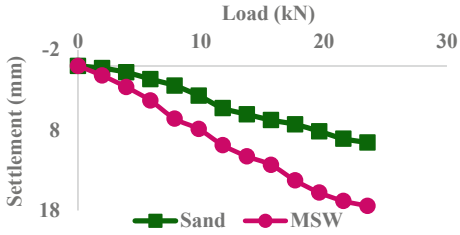

Fig. 9 Load versus settlement characteristics for sand and MSW

5.2 Load–Settlement Curve

See Fig. 9.

Graph 9 shows the settlement behavior of both sand and MSW. From the graph, it can be observed that the settlement at each particular load in MSW is more than the settlement in sand. The total settlement at 23.54 kN load in MSW and sand is 17.425 and 9.535 mm, respectively.

6 Conclusions

The important conclusions from this study are summarized below:

For both backfill materials, maximum displacement was observed in the center part while minimum in the top and bottom parts which may be due to end constraints. Angle of internal friction has a significant influence on RE wall displacement behavior. Owing to the higher angle of internal friction of MSW than that of sand, the amount of displacement of wall is less.

The settlement of MSW is nearly double than that of sand.

References

BS 8006:2010 Strengthened/reinforced soils and other fills

Hyun P, Borinara P, Hong KD (2011) Geotechnical considerations for end-use of old municipal solid waste landfills. Int J Environ Res 5(3):573–584

IS 1888-1982 Method of load test on soils

IRC SP 102-2014 guidelines for design and construction of reinforced soil walls

Patil S, Bachhav SS, Kshirsagar DY (2016) Beneficial use of municipal solid waste ash in sub base in road costruction. Int J Eng Invent 5(3):24–28

Shah MV, Jose J (2017) MSW-leachate-soil-interactions and its effect on shear parameters using admixture. In: Proceeding of geotechnical issues and practices on deltaic deposits and highly compressible soils, 19th international conference on soil mechanics and geotechnical engineering (ICSMGE), Korea, pp 9–12

Vashi JM, Desai AK, Solanki CH (2011) Mixture of soil and flyash as reinforced earth wall backfill. Aust Geomech 46(4):103–106

Numerical Study on Cyclic Shear Behavior of Soil–Geosynthetics Interface

R. Roy, H. Venkateswarlu and A. Hegde

Abstract Geosynthetics are being widely used as a reinforcement material in the construction of mechanically stabilized earth (MSE) walls. The strength and stability of these walls are depending upon the interface behavior between soil and reinforcement material. It is understood from the literature review that the dynamic interface properties of soil and geosynthetics are not well explored yet, as in the case of static loading conditions. The present study investigates the cyclic behavior of the interface between sand and non-woven geotextile material. The objective was achieved by simulating the cyclic direct shear test using finite element-based package PLAXIS^{2D}. The behavior of interface shear stiffness, and damping ratio were studied with increase in number of cycles and displacement amplitude. In addition, the interface behavior of geotextile with the sand having different fines content was also studied. The results revealed that the increase in the fines content causes the reduction in the interface shear stiffness. The interface shear strength properties obtained from the cyclic direct shear test were compared with the static shear test. The friction angle obtained from the cyclic shear test was 6% higher than that obtained from the static direct shear test.

Keywords Sand–geotextile interface · Cyclic interface behavior · Interface shear stiffness · Damping ratio · PLAXIS^{2D}

R. Roy · H. Venkateswarlu · A. Hegde (✉)
Department of Civil and Environmental Engineering, Indian Institute of Technology Patna, Patna 801103, India
e-mail: ahegde@iitp.ac.in

R. Roy
e-mail: ratance01@gmail.com

H. Venkateswarlu
e-mail: hasthi.pce16@iitp.ac.in

R. Sundaram et al. (eds.), *Geotechnics for Transportation Infrastructure*,
Lecture Notes in Civil Engineering 29,
https://doi.org/10.1007/978-981-13-6713-7_19

1 Introduction

Geotextile is one of the popular reinforcing materials used in the soil to increase the tensile resistance. The general applications of geotextile include pavements, foundations, retaining walls, and the slope stabilization, etc. Generally, the geotextile is embedded in the soil. The performance of the geotextile is largely influenced by its interaction with surrounding soil at the interface. The interface behavior of soil–geosynthetics material varies under static and cyclic loading conditions. In practice, the structures are often subjected to dynamic loads in addition to the static loads due to earthquakes, blasting operations, and transit systems, etc. For the safe design, it is important to consider the response of the soil–geosynthetics interface under dynamic loading also.

Compared to the studies performed in static loading, fewer investigations have been carried out under cyclic loading conditions (Desai et al. 1985; O'Rourke et al. 1990; De and Zimmie 1998; Mayer et al. 2004; Kim et al. 2005). Most of the previous studies are experimental in nature. Experimental studies followed the direct shear and cyclic shear test (Silver and Seed 1971; Koutsourais et al. 1991; Swan et al. 1991; Murthy and Sridharan 1993; Izgin et al. 1998; Lee and Manjunath 2000; Abu-Farsakh et al. 2007; Nye and Fox 2007; Ling et al. 2008; Soroush and Soltani-Jigheh 2009; Kwak et al. 2013; Wang et al. 2016). These laboratory studies can quantify the frictional resistance of the soil–geosynthetics interface. The laboratory results significantly depend on several factors. It includes the boundary effects, variation in the testing procedure, soil placement, and type of compaction (Juran et al. 1988). Due to these reasons, there is a wide scatter in the reported results of the direct shear test (Bakeer et al. 1998). Hence, the finite element analysis is widely being used to understand the mechanism of soil–geosynthetics interaction (Sugimoto and Alagiyawanna 2003; Khedkar and Mandal 2009; Basudhar 2010; Roy and Hegde 2017; Hegde and Roy 2018). The major advantage of using numerical simulations is time saving, and one can visualize the distribution of the stresses and strains within a system. The advancement in computer science and technology, the current numerical packages are well equipped to handle the complexities involved in the problems.

In the present study, an attempt has been made to simulate the dynamic response of sand–geotextile interface using finite element package PLAXIS^{2D}. The response of sand–geosynthetics interface was also studied with varying fines content. Further, the results of direct shear test and cyclic shear test were also compared.

2 Numerical Analysis

2.1 Materials Used

In this study, totally three types of sands, namely sand *A*, sand *B,* and sand *C,* have been used. Sand *A* was locally available, with no fines content. The density and shear strength properties were determined from the laboratory tests. The Young's

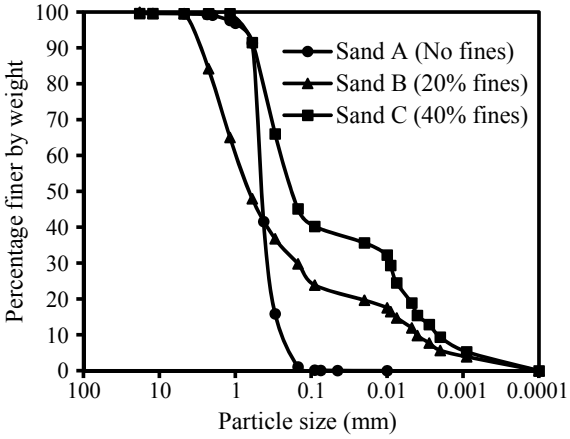

Fig. 1 Grain size distribution of the different sands is used in the study. *Courtesy* Sukmak et al. (2016) for sand *B* and S and *C*

modulus of the sand *A* was determined from the consolidated undrained triaxial test. The properties of sand *B* and sand *C* were borrowed from the study, reported by Sukmak et al. (2016). Figure 1 represents the particle size distribution for different sands used in this study. Table 1 represents the different properties of three sands.

A non-woven geotextile was used in the present study. Though non-woven geotextiles are known for drainage applications, there are instances where these materials were also used as reinforcement (e.g., Portelinha et al. 2013). Tensile strength of the geotextile material was determined from the tensile strength test as per the codal provision of ASTM D-4632 (2008). Figure 2 represents the stress–strain behavior of the geotextile material. The other properties of the geotextile used in this study have been summarized in Table 2.

2.2 Modeling Details

In the present study, PLAXIS^{2D} was chosen for the analysis by considering its ability to model a wide range of geotechnical problems. It uses a finite element solution to solve the initial and boundary value problems. It has several built-in material models and structural elements to model the variety of geomaterials and the reinforcements. The program is inbuilt with convenient and easy-to-use

Table 1 Properties of different sands

Properties	Sand *A*	Sand *B*	Sand *C*
Dry unit weight, γ (kN/m^3)	16.5	20.1	18.9
Young's modulus, E (kN/m^2)	13000	10000	5000
Porosity, (n)	0.3	0.4	0.4
Cohesion, c (kN/m^2)	0	20	25
Friction angle, φ (°)	35°	35°	32°

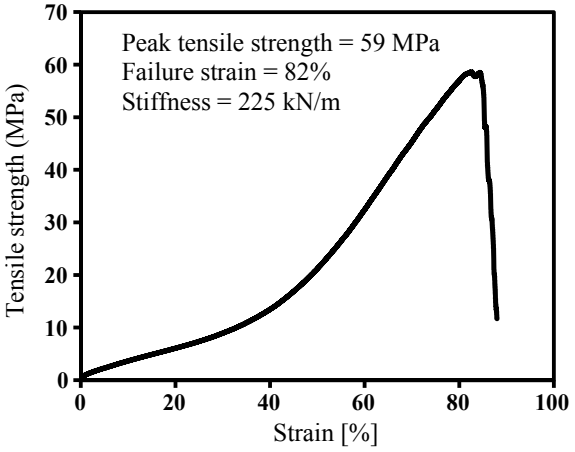

Fig. 2 Stress–strain curve of geotextile material

Table 2 Properties of geotextile

Parameters	Values
Polymer	Polypropylene
Thickness (mm)	1.1
Aperture opening size (mm)	0.2
Mass per unit area (g/m^2)	295
Secant modulus at 2% strain (kN/m)	225

graphical user interfaces, which facilitates the quick generation of the model geometry. In addition, it is also equipped with wide range of advanced features to analyze the complex and cyclic behavior of the systems.

In this study, the dimensions of the cyclic direct shear test numerical model were considered as per the guidelines of ASTM D-5321 (2008). The plan dimensions of the direct shear test were considered as 300 mm × 300 mm. The soil was used to fill the lower container of the model. The geotextile was placed between the upper and lower boxes. Prescribed line displacement was applied on both sides of the upper half box, while the lower box was restrained for the horizontal and vertical movements. The interface was assigned to the upper surface of geotextile. The interface was modeled using the interface structural element and it was assumed to follow the elasto-plastic behavior. The behavior of the sand was simulated to follow the Mohr–Coulomb failure yield criterion. The geotextile was modeled using the geogrid structural element. The behavior of geotextile was assumed to follow linear elastic law. Geotextile was modeled as an elastic material.

Figure 3 represents the numerical model of large direct shear test. The similar codal provision was followed for modeling the cyclic shear and direct shear test conditions. Cyclic direct shear test was modeled under displacement control method as suggested by Wang et al. (2016). The numerical model of cyclic direct shear test was same as large direct shear test as shown in Fig. 3. However, the displacement

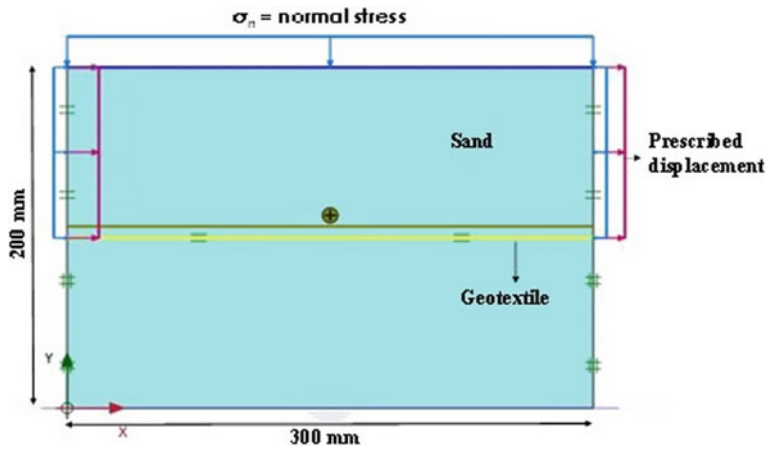

Fig. 3 Numerical model of large direct shear test

arrangement was differed slightly. The stepwise procedure for conducting the cyclic direct shear test is presented schematically in Fig. 4. The analysis was carried out under three different normal stresses, 100, 150, and 200 kPa. Preliminary analyses revealed that the results were free from boundary effects, the deformations and stresses were contained well within the boundaries. Based on the findings of the sensitivity analyses, the medium mesh was chosen for the analysis. Before performing the actual simulations, the numerical models were validated with the results reported in the literature.

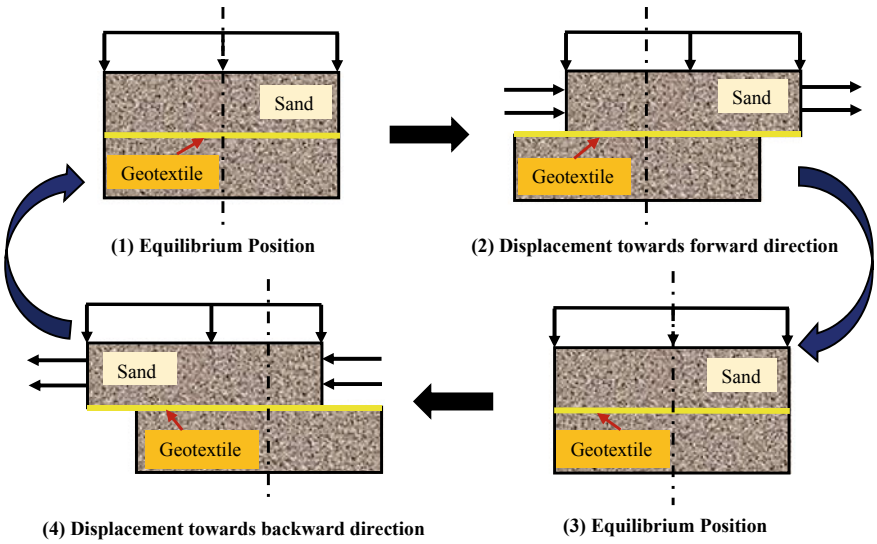

Fig. 4 Schematic representation about the mechanism of cyclic direct shear test

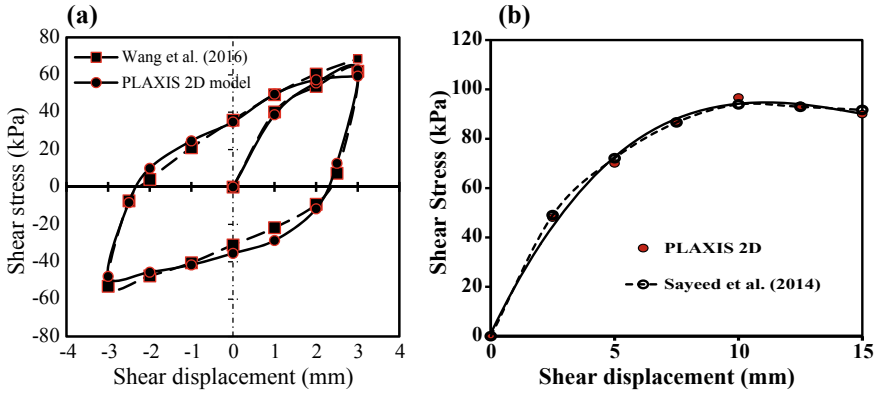

Fig. 5 Validation of the numerical model: **a** cyclic direct shear test and **b** direct shear test

2.3 Validation

The numerical model of cyclic direct shear test was validated with the experimental results reported by Wang et al. (2016). Similarly, the large-scale direct shear test was validated with experiment results of Sayeed et al. (2014). In the validation process, the dimensions of the model, material properties, and the constitutive model behavior similar to the experimental studies were used. Figure 5a, b shows the comparison of numerical results with the findings of experimental study, for both the cases. A good match was obtained between the experimental and numerical studies. After the completion of validation, the model was further modified and utilized to investigate the sand–geotextile interface behavior.

3 Results and Discussions

To study the effect of fines content on interface behavior, three different sands, namely sand *A* (0% fines content), sand *B* (20% fines content), and sand *C* (40% fines content), have been used. The variation of shear stiffness and damping ratio was studied with increase in number of cycles (*N*) and normal stress. The present analysis was carried out under three different normal stresses and displacement amplitude conditions. Figure 6 shows the schematic representation of hysteresis loop obtained from the cyclic direct shear test. From the hysteresis loop, the interface shear stiffness (*K*) and damping ratio (*D*) were calculated using Eqs. (1) and (2). The interface shear stiffness can be defined as the slope of the line joining the maximum and minimum peaks of the shear stresses. It indicates the state of interface response between soil and geosynthetics material.

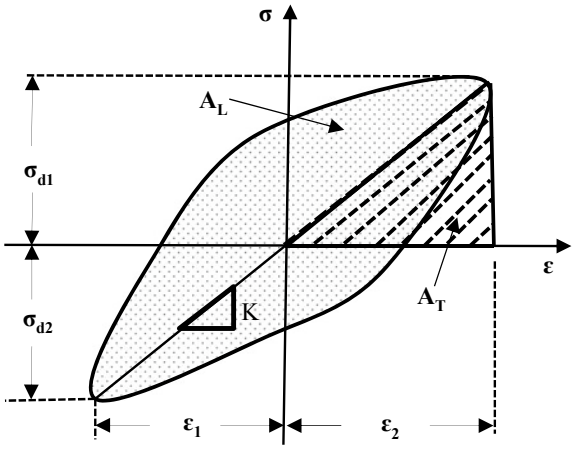

Fig. 6 Schematic representation of stress–strain hysteresis loop

$$K = \frac{\sigma_{d1} + \sigma_{d2}}{\varepsilon_1 + \varepsilon_2} \tag{1}$$

where σ_{d1} and σ_{d2} are the maximum shear stresses in compression and tension, respectively. Similarly, ε_1 and ε_2 are maximum strains in compression and tension, respectively.

$$D = \frac{A_L}{4\pi A_T} \tag{2}$$

where A_L is the area enclosed by the hysteresis loop and A_T is the area of the shaded triangle.

Figure 7 represents the variation of interface shear stiffness with increase in fines content and number of cycles. The shear stiffness corresponding to 200 kPa normal stress was used for the comparison in the figure. From Fig. 7, the increment in shear stiffness with increase in number of cycles at the initial stages is observed.

It is due to the increase in the interface resistance with the number of cycles. The densification of sand takes place due to the repeated movement of box. Ferreira et al. (2016) also reported the similar behavior. In addition, the interface shear stiffness decreases with increase in the fines content. With the increase in fines content, there was a reduction in interaction between the sand and geotextile material. The fines content reduces the contact between sand particles and geosynthetics. It leads to a reduction in the interface shear stiffness. The similar observations were also reported by Kenney (1997), Mitchell (1993), and Thevanayagam (1997). Figure 8a, b represents the variation of the damping ratio with increase in number of cycles and the displacement amplitude. The presented results in the Fig. 8a, b are corresponding to the Sand *A* (no fines content). The damping ratio (*D*) is the parameter, used to find out the dynamic response of

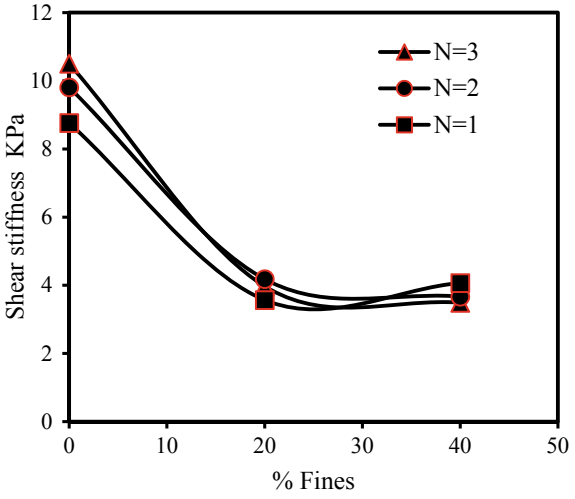

Fig. 7 Effect of fines content on interface shear stiffness

interface behavior. It indicates the dissipation of energy within a soil system under cyclic loading conditions. Vieira et al. (2013) also used this parameter to characterize the dynamic response of sand–geotextile interface.

From Fig. 8a, it was observed that the damping ratio was decreased with increase in number of cycles. The increase in stiffness at the interface zone due to less energy dissipation might be the cause of this variation. Wang et al. (2016) also reported the similar variation. Similarly, the variation of damping ratio with increase in displacement amplitude is shown in Fig. 8b. From the figure, the damping ratio was found to increase with the increase in displacement amplitude. It was attributed due to the increment of shear area with increase in the displacement amplitude. It leads to increase in dissipation of energy as well as damping ratio for each cycle. The similar variation has also reported by Dobry and Vucetic (1988).

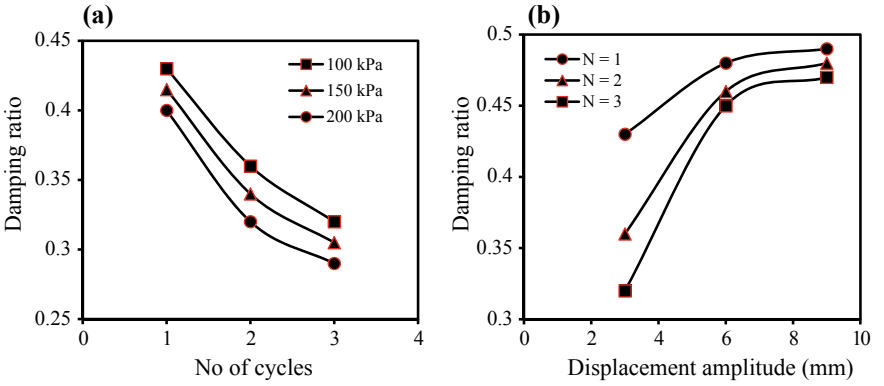

Fig. 8 Variation of damping ratio with **a** number of cycles and **b** displacement amplitude

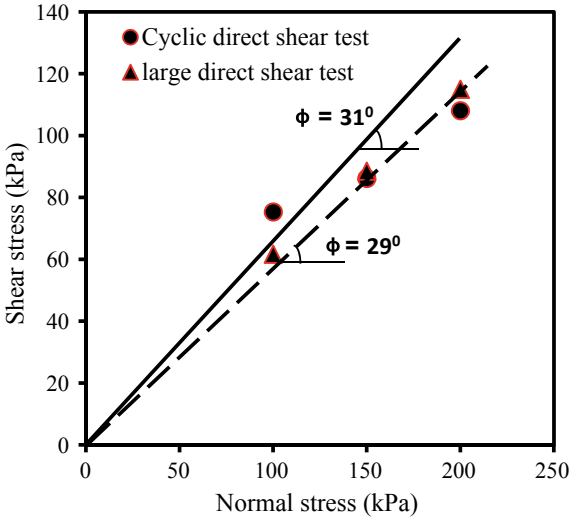

Fig. 9 Comparison of interface friction angle under static and dynamic conditions

Figure 9 represents the comparison of Mohr–Coulomb failure envelopes obtained from the cyclic direct shear test and the direct shear test. The relationship between the interface shear stress and the normal stress can be defined using the Mohr–Coulomb failure criteria (Bakeer et al. 1998). Based on the Mohr–Coulomb criteria, the interface shear strength properties were calculated. From the figure, it was observed that the interface friction angle obtained from cyclic direct shear test was about 6% greater than that of large direct shear test. The Improvement in the compactness of sand at interface zone due to cyclic displacement might be the reason for this marginal variation. The similar trend of variation was also observed by Ling et al. (2008) and Wang et al. (2016).

4 Conclusions

In the present study, the numerical modeling approach was demonstrated to study the interface behavior between sand and geotextile material. The interface behavior was studied for both in static and cyclic loading conditions. The cyclic and static response was analyzed through cyclic direct shear test and large-scale direct shear test. In addition, the effect of fines content on interface behavior of sand and geotextile was also studied. The following inferences can be drawn from the study.

i. Maximum interface shear stress of sand–geotextile interface totally depends on number of cycles, displacement amplitude, and normal stress.
ii. The interface friction properties obtained from the direct shear test and the cyclic direct shear tests vary minimally. The interface friction angle obtained from cyclic direct shear test was about 6% greater than that of large direct shear test.

iii. The interface shear stiffness decreases with increasing fines content. This is due to reduction of sand–geotextile interaction.
iv. Damping ratio was found to be decreased with increase in number of cycles and increased with the increase in displacement amplitude.

The findings from the study are useful in the design of the reinforced earth walls and steep slopes in the highway sections. The study has few limitations. Only one type of geotextile was used in this study. Hence, the results are applicable to limited cases. Further, the experimental studies are recommended to ascertain the numerical findings.

References

ASTM D-4632 (2008) Standard test method for grab breaking load and elongation of geotextiles. American Society for Testing and Materials, West Conshohocken, PA, USA

ASTM D-5321 (2008) Standard test method for determining the coefficient of soil and geosynthetic or geosynthetic and geosynthetic friction by the direct shear method. American Society for Testing and Materials, West Conshohocken, PA, USA

Abu-Farsakh M, Coronel J, Tao M (2007) Effect of soil moisture content and dry density on cohesive soil-geosynthetic interactions using large direct shear tests. J Mater Civ Eng 19 (7):540–549

Bakeer RM, Abdel-Rahman AH, Napolitano PJ (1998) Geotextile friction mobilization during field pullout test. Geotext Geomembr 16(2):73–85

Basudhar PK (2010) Modeling of soil–woven geotextile interface behavior from direct shear test results. Geotext Geomembr 28(4):403–408

De A, Zimmie TF (1998) Estimation of dynamic interfacial properties of geosynthetics. Geosynth Int (Special Issue on Geosynthetics in Earthquake Engineering) 5(1–2):17–39

Desai CS, Drumm EC, Zaman MM (1985) Cyclic testing and modelling of interfaces. J Geotech Eng ASCE 111(6):793–815

Dobry R, Vucetic M (1988) Dynamic properties and seismic response of soft clay deposits. Department of Civil Engineering, Rensselaer Polytechnic Institute

Ferreira F, Vieira C, de Lurdes Lopes M (2016) Cyclic and post-cyclic shear behaviour of a granite residual soil-geogrid interface. Procedia Eng 143:379–386

Hegde A, Roy R (2018) A comparative numerical study on soil–geosynthetic interactions using large scale direct shear test and pullout test. Int J Geosyn Ground Eng 4(1):1–11

Izgin M, Wasti Y, Silver (1998) Geomembrane–sand interface frictional properties as determined by inclined board and shear box tests. Geotext Geomembr 16(4):207–219

Juran I, Knochenmus G, Acar YB, Arman A (1988) Pullout response of geotextiles and geogrids. In: Proceedings of symposium on geotextiles for soil improvement. ASCE, Geotech. Special Publication. 18, pp 92–111

Kenney TC (1997) Residual strength of mineral mixtures. In: Soils and foundations. Proceedings of 9th international conference on soil mechanics and foundation engineering, vol 1, pp 155–160

Khedkar MS, Mandal JN (2009) Pullout behaviour of cellular reinforcements. Geotext Geomembr 27(4):262–271

Kim J, Riemer M, Bray JD (2005) Dynamic properties of geosynthetic interfaces. Geotech Test J 28(3):1–9

Koutsourais MM, Sprague CJ, Pucetas RC (1991) Interfacial friction study of cap and liner components for landfill design. Geotext Geomembr 10(5–6):531–548

Kwak CW, Park IJ, Park JB (2013) Evaluation of disturbance function for geosynthetic–soil interface considering chemical reactions based on cyclic direct shear tests. Soils Found 53 (5):720–734

Lee KM, Manjunath VR (2000) Soil-geotextile interface friction by direct shear tests. Can Geotech J 37(1):238–252

Ling HI, Wang JP, Leshchinsky D (2008) Cyclic behaviour of soil-structure interfaces associated with modular-block reinforced soil-retaining walls. Geosynth. Int. 15(1):14–21

Mayer N, Nernheim A, Kohler U (2004) Geosynthetic–soil interaction under cyclic loading. In: 3rd European geosynthetics conference, Munich, Germany, 1–3 Mar 2004, pp 635–639

Mitchell JK (1993) Fundamentals of soil behavior, 2nd edn. Wiley, New York

Murthy BS, Sridharan A (1993) Evaluation of interfacial frictional resistance. Geotext Geomembr 12(3):235–253

Nye CJ, Fox PJ (2007) Dynamic shear behaviour of a needle-punched geosynthetic clay liner. J Geotech Geoenviron Eng 133(8):973–983

O'Rourke TD, Druschel SJ, Netravali AN (1990) Shear strength characteristics of sandpolymer interfaces. J Geotech Eng ASCE 116(3):451–469

Portelinha FHM, Bueno BS, Zornberg JG (2013) Performance of nonwoven geotextile-reinforced walls under wetting conditions: laboratory and field investigations. Geosyn Int 20(2):90–104

Roy R, Hegde A (2017) Numerical simulation of geotextile-sand interface using box shear test and pullout test: a comparison. In: Proceedings of sixth Indian Young geotechnical engineers conference (6IYGEC) 2017, 10–11 Mar, Trichy, pp 514–519

Sayeed MMA, Ramaiah BJ, Rawal A (2014) Interface shear characteristics of jute/polypropylene hybrid nonwoven geotextiles and sand using large size direct shear test. Geotext Geomembr 42 (1):63–68

Silver ML, Seed HB (1971) Deformation characteristics of sands under cyclic loading. J Soil Mech Found Div

Soroush A, Soltani-Jigheh H (2009) Pre-and post-cyclic behavior of mixed clayey soils. Can Geotech J 46(2):115–128

Sugimoto M, Alagiyawanna AMN (2003) Pullout behavior of geogrid by test and numerical analysis. J Geotech Geoenviron Eng 129(4):361–371

Sukmak K, Han J, Sukmak P, Horpibulsuk S (2016) Numerical parametric study on behavior of bearing reinforcement earth walls with different backfill material properties. Geosynth Int, pp 1–17

Swan RH, Bonaparte R, Bachus RC, Rivette CA, Spikula DR (1991) Effect of soil compaction conditions on geomembrane-soil interface strength. Geotext Geomembr 10(5–6):523–529

Thevanayagam S (1997) Dielectric dispersion of porous media as a fractal phenomenon. J Apply Phys 82(5):2538–2547

Vieira CS, Lopes ML, Caldeira LM (2013) Sand-geotextile interface characterisation through monotonic and cyclic direct shear tests. Geosynth Int 20(1):26–38

Wang J, Liu FY, Wang P, Cai YQ (2016) Particle size effects on coarse soil-geogrid interface response in cyclic and post-cyclic direct shear tests. Geotext Geomembr 44(6):854–861

Red Mud-Fly Ash Mix as an Embankment Fill Material

Parvathi Geetha Sreekantan, A. K. Sinha and Vasant G. Havangi

Abstract Red mud is an industrial waste which is being generated by Bayer's process of alumina production. It is generally dumped near the plant in a pond without any usage, occupying costly land. However, it has the potential for application in the construction of road embankment. It has also the potential for application in raising embankment height for the disposal of industrial waste pond itself. Thus, capacity augmentation of waste pond is also possible by mass recycling of red mud which leads to conserve the conventional soil. Considering this, red mud sample was collected from Hindalco, Muri, Jharkhand. Chemical and geotechnical characterization was carried out for its application in embankment construction. As its natural moisture content is very high due to disposal in a lean slurry form, with solid concentration in the range of 25–50%, it is very difficult to use in the field for the construction of embankment. Accordingly, it was blended with fly ash in the different proportion varying from 5 to 50% which is abundantly available near the plant. Detailed laboratory investigation was carried out on red mud-fly ash mixes, viz. modified proctor, permeability and triaxial shear tests. Suitability of red mud and its mixes as an embankment material was derived as per Indian standard specifications. This paper presents the geotechnical characterization of red mud and its mixes with fly ash. Design and stability analysis were also presented for a typical red mud embankment with or without fly ash mix. It was inferred that red mud alone and mixes with fly ash are suitable for the embankment construction.

Keywords Red mud · Fly ash · Embankment · Construction · Characterization

P. G. Sreekantan (✉) · A. K. Sinha · V. G. Havangi
Geotechnical Engineering Department, CSIR-Central Road Research Institute, New Delhi 110025, India
e-mail: parvathi.crri@nic.in

A. K. Sinha
e-mail: sinha.crri@nic.in

V. G. Havangi
e-mail: vasant.crri@nic.in

R. Sundaram et al. (eds.), *Geotechnics for Transportation Infrastructure*, Lecture Notes in Civil Engineering 29,
https://doi.org/10.1007/978-981-13-6713-7_20

1 Introduction

Rapid growth of population and industrialization during the last few decades has resulted in generation of huge quantity of industrial wastes all around the world. Geotechnical engineers and researchers are in high demand for using these industrial wastes in construction industry, as mass utilization is possible through these uses, rather than commercial ones. It is a great challenge to make quality construction products out of these industrial wastes without compromising the construction standards or living conditions of public. The first step towards this is to check their basic feasibility as a construction material. One of such challenges was to make use of red mud to construct raising height of embankments for the red mud pond itself.

Red mud is a waste formed from the refining of bauxite that produces alumina as raw material for the production of aluminium. There are two processes for alumina production, namely Bayer's and sintering processes. In India, alumina is generally produced from Bayer's process. This process generates red mud with a very high water content (about 50%) and is again mixed with water to dispose off in lean slurry form to the ponds. This long-term dumping in ponds would not only occupy scarce land resources, but also create pollution problems. Red mud is composed of a mixture of solid and metallic oxides. The red colour arises from iron oxides, which comprise up to 60% of the mass of the red mud (Wang and Liu 2012). The mud is highly basic with a pH ranging from 10 to 13. In addition to iron, the other dominant components include silica, unleached residual alumina and titanium oxide. A typical bauxite plant produces one to two times as much red mud as alumina (Atun and Hisarli 2000). This ratio is dependent on the type of bauxite used in the refining process and the extraction conditions.

Number of researchers had characterized the red mud for various applications such as Barrow (1982), Kumar et al. (1989), Atun and Hisarli (2000), Jiang and Ning (2003), Zhang and Pan (2005) and Liu et al. (2011). It has been observed from these studies that the characteristics of red mud such as physical, chemical, mechanical performances, particle, morphology and structure vary widely and depend on the bauxite ore quality and the process of refining and extraction. There is no guideline available for the utilization of red mud as construction material including FHWA (2012), due to its lack of proper characterization as well as presence of heavy metals in some of the red mud. Very limited basic study on geotechnical characterization as well as utilization of red mud in construction works has been carried out, such as Wang and Liu (2012), Parvathi and Ghosh (2016), Gangadhara Reddy and Hanumantha (2016) and Kushwaha and Kishan (2016).

Both the freshly dumped red mud contain very high water content; practically, old and it is very difficult to dry it during embankment construction process. So fly ash, which is another potential industrial waste, can be mixed to it before compaction. This can be practically done by spreading two materials in layers and then mixing using soil mixing ploughs. Field trials of mixing and compaction may be required to design the layer thickness and frequency of plough. The paper presents

the geotechnical characterization of red mud, fly ash and their mixes as well as design and stability analysis for a typical red mud embankment with or without fly ash mix.

2 Materials and Their Characterization—Physical and Chemical

The materials for the study, red mud and fly ash, were collected from Hindalco plant at Muri, Jharkhand, and were investigated for their basic physical and chemical characterizations. The morphological characteristics red mud obtained from SEM image taken in X100-200 nm at 5 kV are shown in Fig. 1 and that of fly ash, taken in X500-50 μm range at 15 kV, is shown in Fig. 2. The SEM image of red mud reveals its irregular size and shape, but largely circular-shaped particles, closely associated, non-porous microstructure of silt- and clay-sized particles. The SEM image of fly ash reveals isotropic, spherical shaped particles, even though some irregular-shaped particles are also present.

Different tests, namely specific gravity, grain size analysis, pH and salt contents, were tested as per Bureau of Indian Standards (IS 2720-Part 3 2002; Part 4 2006; Part 26 1997 and Part 27 2006, respectively).

Specific gravity value was obtained as 2.87 for red mud and 2.08 for fly ash. From the grain size analysis, it was observed that red mud and fly ash are fine-grained materials. Red mud has 27% clay and 70% silt-sized particles, whereas fly ash has around 4% sand and 96% silt-sized particles. The estimated pH and salt contents of red mud and fly ash are given in Table 1.

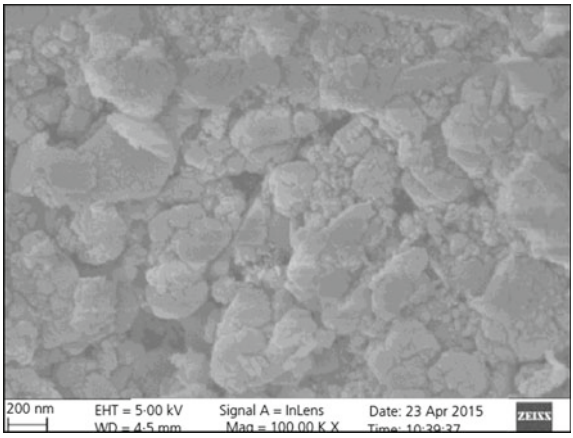

Fig. 1 SEM image showing the irregular particle shape [Ref: Gangadhara Reddy and Hanumantha (2016)]

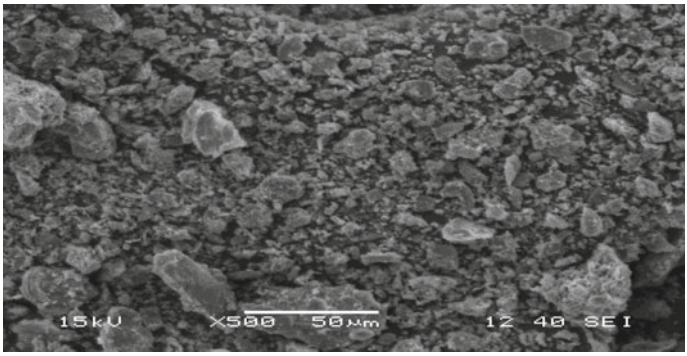

Fig. 2 SEM image of fly ash samples taken in X500-50 µm [Ref: Prasad (2013)]

Table 1 Chemical test results

Property	Red mud	Fly ash
pH at 32 °C	10.5	8.37
Chloride (ppm)	395	–
Sulphate (ppm)	274	116

3 Geotechnical Characterization

The main parameters which govern the use of fill material are its particle size distribution, plasticity characteristics and density. But, if the material is to be used for high embankments or other specialized constructions, undrained shear strength parameters and permeability also become important. Different geotechnical tests, namely Atterberg limits, permeability, modified proctor, unconfined compressive strength and direct shear tests, were conducted on red mud and fly ash samples as per Bureau of Indian Standards (IS 2720-Part 5 2006; Part 17 2002; Part 7 2011; Part 10 2006 and Part 13 2002, respectively).

3.1 Red Mud

It was observed from the Atterberg test that the liquid limit and plastic limit of red mud are 40% and 22%, respectively. As per Indian standards classification (IS 1498 2007), red mud is classified as medium compressible clayey silt (CI).

The maximum dry density (MDD) and optimum moisture content (OMC) of red mud were observed to be 15.2 kN/m^3 and 32%, respectively.

Unconfined compressive test was conducted on red mud samples with 97% of MDD and OMC, and the values were obtained as 72 kPa. Direct shear test and falling head permeability tests were also conducted for the fully saturated specimen at 97% of MDD and OMC, and the results have been summarized in Table 2.

Table 2 Geotechnical properties of red mud and fly ash

Property		Red mud	Fly ash
Liquid limit (%)		40	–
Plasticity index (%)		22	NP
Maximum dry density (kN/m^3)		15.2	11.7
Optimum moisture content (%)		32	36
Unconfined compressive strength (kPa)		72	–
Shear strength parameters	C (kPa)	3.48	4.5
	Φ (°)	32	33.77
Permeability (m/s)		2.9×10^{-9}	8.12×10^{-8}

3.2 *Fly Ash*

It was observed from the Atterberg test that fly ash is a non-plastic material. As per Indian standards classification (IS 1498 2007), fly ash is classified as sandy silt (ML).

The maximum dry density (MDD) and optimum moisture content (OMC) of fly ash were observed to be 11.7 kN/m^3 and 36%, respectively.

Direct shear test and falling head permeability tests were also conducted for the fully saturated specimen at 97% of MDD and OMC, and the results have been summarized in Table 2.

3.3 *Red Mud-Fly Ash Mixes*

Red mud contains very high water content which makes it practically difficult for drying during construction process. To overcome this problem, fly ash was mixed with red mud for reducing the moisture and improve the engineering properties of red mud. Accordingly, red mud was blended with fly ash in the different proportion varying from 5 to 50%. Geotechnical characterization of different red mud-fly ash mixes was studied to evaluate the suitability in embankment construction, as detailed below.

3.3.1 Modified Proctor Test

Modified proctor tests were conducted on red mud-fly ash mix with different proportions as per IS 2720-Part 7 (2011). The variation of dry density with respect to moisture content of different red mud-fly ash mixes is shown in the Fig. 3. The results are shown in Table 3.

The variation of maximum dry density with respect to the percentage of fly ash added to the mix is shown in Fig. 4.

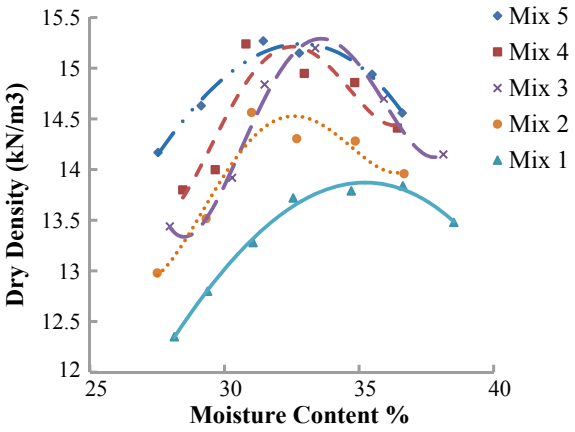

Fig. 3 Variation of dry density with respect to moisture content of different red mud-fly ash mixes

Table 3 Modified proctor test results of mixes

Material	Fly ash content (%)	Red mud content (%)	OMC (%)	MDD (kN/m^3)
Mix 1	50	50	36.2	13.85
Mix 2	40	60	31.2	14.60
Mix 3	20	80	32	15.20
Mix 4	15	85	31.1	15.25
Mix 5	10	90	31.7	15.30
Mix 6	5	95	32	15.2
Red Mud	0	100	32	15.2

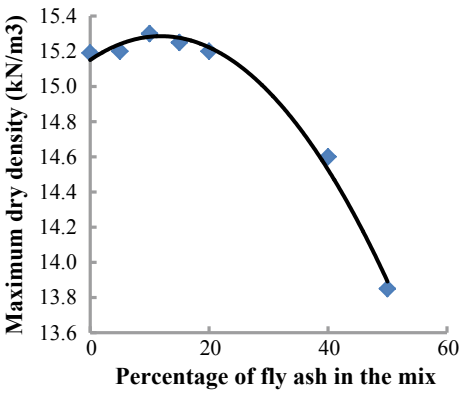

Fig. 4 Variation of maximum dry density with respect to the percentage of fly ash added to the mix

3.3.2 Triaxial Test

Consolidated undrained triaxial tests were conducted on some of the red mud-fly ash mixes as per IS 2720-Part 12 (1981).The specimen was first consolidated at 200 kPa confining pressure before shearing. Pore pressures were also measured to determine the effective stress parameters. The stress–strain behaviour for different mixes is shown in Figs. 5, 6 and 7. Shear strength parameters were obtained from the p-q failure envelope as shown in Fig. 8, and the results for different mixes are summarized in Table 4.

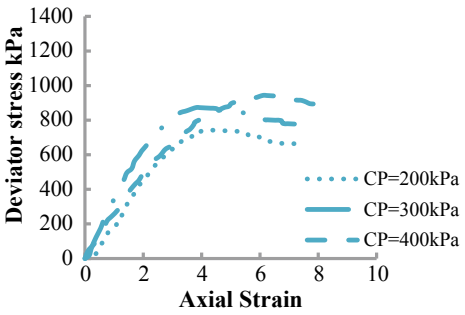

Fig. 5 Consolidated undrained test results for the mix 1

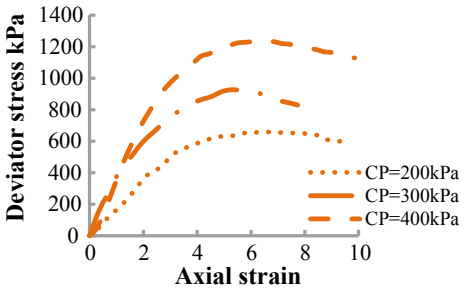

Fig. 6 Consolidated undrained test results for the mix 2

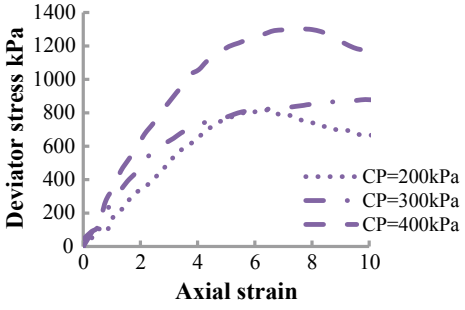

Fig. 7 Consolidated undrained test results for the mix 3

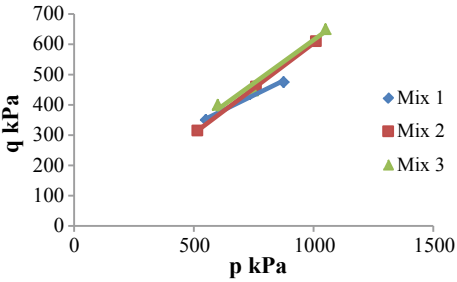

Fig. 8 Failure envelope (total stresses) for different mixes

Table 4 Shear strength parameters for different mixes

Parameters		Mix 1	Mix 2	Mix 3
Total stress parameters	Φ (°)	21	34	31
	C (kPa)	18	4	11
Effective stress parameters	Φ′ (°)	20.6	35	34
	C′ (kPa)	16	4	9

4 Discussions on Test Results

It was observed that the specific gravity values of red mud and fly ash are higher and lower, respectively, compared to conventional soil. This may be due to the different mineral composition in these materials. It is also concluded that red mud from Hindalco plant has much lower maximum density compared to other red mud from most of other plants in the country (Gangadhara Reddy and Hanumantha 2016).

Fly ash, which is a lighter material compared to red mud, will improve the soil gradation, thus a slight improvement in the density and shear strength. The results from modified proctor tests show that when the percentage of fly ash increases, the density also slightly improves till 20% and then decreases rapidly. As per the MORTH (2013), embankments up to 3 m height can be constructed with a material density of 15.2 kN/m^3. Thus, a mix having a maximum percentage between 10% and 20% of fly ash qualifies as an embankment material.

It is to be noted that the when the percentage of fly ash increases, the failure occurs at a smaller strain. The failure curve of Mix 3 shows a brittle type of failure, thus denser packing. This is complemented by the proctor test results as well. From the consolidated undrained shear test result, a generalized conclusion for shear strength improvement cannot be drawn, as both red mud and fly ash are having comparable shear strength. But this data can be used for the design of embankments which is provided in the next section.

5 Stability Analysis of a Typical Embankment

The analysis and design of an embankment using red mud-fly ash mixes have been done. A typical section of embankment using local soil in the nearby area, Jharkhand, was also analysed for comparison. The subsoil profile considered for the analysis is shown in Table 5. Typical stability analysis of embankment made of red mud and its mixes is shown in Fig. 9. The groundwater table has been encountered on the site between 0.55 and 7.5 m below the ground level. A critical groundwater level of 0.55 m has been chosen for the analysis. Thus, the shear strength properties (Total Stress) of fully saturated embankment material are considered. Stability analysis was carried out using Bishop's simplified method for static condition as well as for seismic (pseudo-static) condition, considering earthquake data for Zone 1 V. Computer software was used for this limit equilibrium analysis.

Result of the stability analysis is given in Table 6. The variation of factor of safety with percentage of fly ash content in the mix is shown in Fig. 10.

Table 5 Soil profile considered for the analysis

Soil layer	Depth (m)	N	Υ_{bulk}(kN/m^3)	Shear strength parameters (total stress)	
				C (kPa)	Φ (°)
Residual soil (sandy clay)	0–5	15–35	21	54	3
Sandy silt	5–7	33–34	21	10	32
Weathered rock	>7	>100			

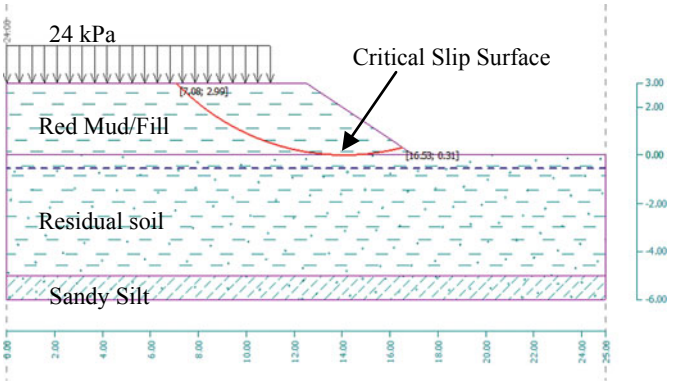

Fig. 9 Typical stability analysis of embankment

Table 6 Analysis results

Embankment material	Factor of safety-static	Factor of safety-seismic
Silty clay	2.3	1.72
Red mud	3.06	2.3
Mix 3	2.44	1.84
Mix 2	1.9	1.41
Mix 1	2.6	2.0

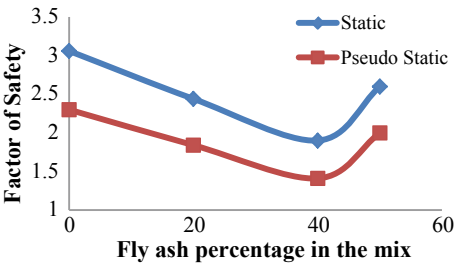

Fig. 10 Variation of factor of safety with respect to percentage of fly ash in the mix

It is observed that the factor of safety for static and seismic conditions keeps on gradually decreases as the percentage of fly ash increases till 40% and then increases. This is because the net reduction in the weight of embankment. The sudden dip in the curve is due to the fact that cohesion intercept for mix 2 is very low. Thus, the red mud and its mixes with fly ash, except mix 2, show an improved factor of safety compared to soil.

A typical cross section for the construction of embankment as well as pavement layers is shown in Fig. 11. A cover soil layer of 2 m with locally available soil is recommended to avoid any erosion of underlying red mud and fly ash material. To aid sufficient permeability of the embankment material, an intermediate soil layer of 0.4 m thickness is also recommended.

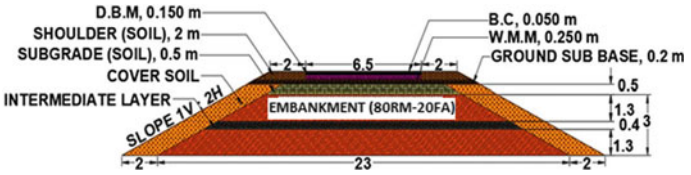

Fig. 11 Typical cross section of road embankment with red mud-fly ash mix

6 Conclusion

This paper presents the geotechnical characterization of red mud, fly ash and their mixes in different proportions obtained from Hindalco plant, Jharkhand, as well as the stability analysis of a typical embankment made out of those materials.

- Both the materials are fine-grained soil like material, with red mud having higher density compared to fly ash. Red mud is a plastic soil with plasticity index of 22%, while fly ash is a non-plastic material.
- Red mud from Hindalco plant has much lower maximum density compared to other red mud from most of other plants in the country.
- Red mud and fly ash were mixed at different proportions varying from 5% to 50%, and the result shows that the maximum dry density of mixes having percentage between 10% and 20% exhibits higher densities.
- The shear strength and permeability of red mud and fly ash have comparable values.
- There is no significant improvement in shear strength parameters of red mud after adding fly ash.
- A typical embankment stability analysis shows that the factor of safety for static and seismic condition shows that the red mud and all it mixes with fly ash, except mix 2, shows an improved factor of safety compared to soil.
- Considering the maximum dry density and shear strength characteristics, red mud-fly ash mix (80:20) may be the best suited for embankment construction.

Acknowledgements The authors are thankful to the Director, CSIR-Central Road Research Institute, for giving permission to publish this paper.

References

Atun G, Hisarli G (2000) A study of surface properties of red mud by potentiometric method. J Colloids Interf Sci 228:40–45

Barrow NJ (1982) Possibility of using caustic residue from bauxite for improving the chemical and physical properties of sandy soils. Aust J Agric Res 33:275–285

FHWA-RD-97-148 (2012) User guidelines for waste and byproduct materials in pavement construction, Federal Highway Administration, U.S. Department of Transportation

Gangadhara Reddy N, Hanumantha Rao B (2016) Evaluation of the compaction characteristics of untreated and treated red mud. Geo-Chicago Chicago, Illinois

IS 1498 (2007) Classification and identification of soils for general engineering purposes, Bureau of Indian Standards (BIS)

IS 2720—Part 3 (2002) Methods of test for soils—Part 3 determination of specific gravity Section 1: fine grained soils, Bureau of Indian Standards (BIS)

IS 2720—Part 4 (2006) Methods of test for soils—Part 4: grain size analysis, Bureau of Indian Standards (BIS)

IS 2720—Part 5 (2006) Methods of test for soils—Part 5: determination of liquid and plastic limit, Bureau of Indian Standards (BIS)

IS 2720—Part 7 (2011) Methods of test for soils—Part 7: determination of water content-dry density relation using light compaction, Bureau of Indian Standards (BIS)
IS 2720—Part 10 (2006) Methods of test for soils—Part 10: determination of unconfined compressive strength, Bureau of Indian Standards (BIS)
IS 2720—Part 12 (1981) Methods of test for soils: Part 12 determination of shear strength parameters of soil from consolidated undrained triaxial compression test with measurement of pore water pressure, Bureau of Indian Standards (BIS)
IS 2720—Part 13 (2002) Methods of test for soils—Part 13: direct shear test, Bureau of Indian Standards (BIS)
IS 2720—Part 17 (2002) Methods of test for soils—Part 17: laboratory determination of permeability, Bureau of Indian Standards (BIS)
IS 2720—Part 26 (1997), Determination of pH value, Bureau of Indian Standards (BIS)
IS 2720—Part 27 (2006) Determination of total soluble sulphates, Bureau of Indian Standards (BIS)
Jiang Y, Ning P (2003) Comprehensive utilization of red mud from alumina plant. Environ Sci Technol 26:40–44
Kumar V, Nautiyal BD, KJha A (1989) Use of neutralized red mud in concrete. Indian Concr J 4:505–507
Kushwaha SS, Kishan D (2016) Stabilization of red mud by lime and gypsum and investigating its possible use in geoenvironmental engineering. Geo-Chicago, Chicago, Illinois
Liu W, Zhang X, Jiang W (2011) Study on particle-size separation pretreatment of Bayer red mud. Chin J Environ Eng 5:921–924
MORTH (2013) Specification for road and bridge works, ministry of road transport and Highway Indian Roads Congress, New Delhi, India
Parvathi GS, Ghosh A (2016) Capacity augmentation of red mud pond using industrial waste. In: International geotechnical engineering conference on sustainability in geotechnical engineering practices and related urban issues, Mumbai, India
Prasad A. (2013) Production and utilization of fly ash based biofertillizers in plant growth, B. Tech thesis report, National Institute of Technology, Rourkela
Wang P, Liu D-Y (2012) Physical and chemical properties of sintering red mud and bayer red mud and the implications for beneficial utilization. Materials 5:1800–1810
Zhang Y, Pan Z (2005) Characterization of red mud thermally treated at different temperatures. J Jinan Univ Sci Tech 19:293–297

Review on Compaction and Shearing-Induced Breakage of Granular Material

Miriam Tawk, Buddhima Indraratna, Cholachat Rujikiatkamjorn and Ana Heitor

Abstract With ongoing expansion of the transport infrastructure to accommodate the need of growing population, the stress on natural construction resources, such as quarried aggregates, has been increasing. Hence, the use of alternative non-traditional waste material is becoming more popular. Coal wash, a by-product of coal mining, has been recently suggested as a substitute to traditional quarried materials. However, recent research showed that these waste aggregates have a weaker structure than conventional materials, which translates into significant potential for breakage upon compaction and loading. Therefore, it is important to quantify breakage and evaluate its influence on the final structure of the soil body and the associated geotechnical properties. This paper presents a critical literature review on compaction and shearing-induced breakage of granular material. The review addresses the available breakage indices developed in the literature to quantify breakage and their limitations. The factors affecting the degree of breakage and the influence of the latter on the different geotechnical properties of compacted granular materials is also discussed. The findings of this review could be

M. Tawk · C. Rujikiatkamjorn · A. Heitor
School of Civil, Mining and Environmental Engineering, Faculty of Engineering and Information Sciences, University of Wollongong, Wollongong, NSW 2522, Australia
e-mail: mst055@uowmail.edu.au

C. Rujikiatkamjorn
e-mail: Cholacha@uow.edu.au

A. Heitor
e-mail: aheitor@uow.edu.au

B. Indraratna (✉)
Centre for Geomechanics and Railway Engineering, School of Civil, Mining and Environmental Engineering, Faculty of Engineering and Information Sciences, University of Wollongong, Wollongong, NSW 2522, Australia
e-mail: indra@uow.edu.au

R. Sundaram et al. (eds.), *Geotechnics for Transportation Infrastructure*,
Lecture Notes in Civil Engineering 29,
https://doi.org/10.1007/978-981-13-6713-7_21

extrapolated to waste materials and corresponding treatment methods could be developed to reduce their breakage potential, so they can be more confidently accepted as substitutes to traditional materials in transport infrastructure.

Keywords Breakage · Compaction · Shearing · Non-traditional materials

1 Introduction

Breakage can have a significant effect on the behaviour of granular materials as it induces critical changes in the properties of the material body. Investigations on particle breakage in the literature were driven by different geotechnical concerns, and this paper attempts to (a) define and quantify particle crushing, (b) identify the factors that favour this mechanism as well as (c) its effect on the geotechnical behaviour of soils in different applications (Sowers et al. 1965; Lee and Farhoomand 1967; Marsal 1967, 1973; Hardin 1985; Lade and Yamamuro 1996; Lade et al. 1996; Indraratna et al. 2005; Hossain et al. 2007; Lade and Karimpour 2010; Bandini and Coop 2011; Rujikiatkamjorn et al. 2013; Indraratna et al. 2015; Wang et al. 2015; Gupta 2016; Heitor et al. 2016; Yaghoubi et al. 2017). Sowers et al. (1965) analysed settlement data for 14 rockfill dams and conducted laboratory confined compression tests on rockfills to identify a relationship between continuing settlements of rockfill dams and crushing over time. Lee and Farhoomand (1967) conducted anisotropic compression triaxial tests on granular soil to assess the effect of particle breakage on the design of gravel drains and soil filters in dams. Marsal (1967) tested the behaviour of coarse granular material using large-scale triaxial apparatus and assessed the effect of particle breakage on shear strength and compressibility of rockfill specimens. Lade and Yamamuro (1996) assessed the effect of particle breakage on the strength behaviour of sand through triaxial drained and undrained compression and extension tests. Lade et al. (1996) proposed a measure to quantify particle breakage in an attempt to assess the associated changes in permeability. Hardin (1985) analysed data for single mineral soils as well as rockfill-like material to determine the variables that affect breakage and define the extent of particle crushing during loading. Indraratna et al. (2005) evaluated the effect of confining pressure on the degradation of ballast and identified and optimum zone for minimum particle breakage. Indraratna et al. (2015) studied the effects of particle breakage on the critical state line of ballast under monotonic loading using large-scale triaxial apparatus and developed constitutive models incorporating particle breakage. Wang et al. (2015) conducted an experimental study on sandstone–mudstone mixtures and assessed the effect of particle size on compaction and associated particle breakage. In their study, Gupta (2016) investigated the effect of particle size and confining pressure on the breakage of rockfill material in medium triaxial tests.

All of these studies considered conventional quarried materials that are traditionally used in most civil engineering applications. Recent studies on the potential

use of non-traditional material have also assessed particle breakage and its effect on the behaviour of such material (Rujikiatkamjorn et al. 2013; Heitor et al. 2016; Yaghoubi et al. 2017). Rujikiatkamjorn et al. (2013) evaluated the potential use of coal wash as a water-front reclamation fill in terms of compaction characteristics, shear strength and collapse potential and quantified the degree of breakage of the waste material induced by compaction. Also, Heitor et al. (2016) studied the influence of particle breakage on the drained and undrained shear behaviour of coal wash. Yaghoubi et al. (2017) assessed the effect of compaction method on the geotechnical characteristics, including breakage, soil–water properties, stiffness and resilient modulus, of recycled crushed bricks and recycled concrete aggregates.

With the emergent need to expand the existing infrastructure, stresses on natural resources are increasing and the use of waste material as a substitute to quarried aggregates has become crucial now more than ever. However, some waste materials, such as coal wash, are weaker than traditional aggregates and higher degrees of breakage could occur when these materials are subject to loading. For these materials to be more confidently accepted as construction materials, their behaviour must be thoroughly investigated under different conditions. In this paper, a critical review of the findings of some investigations on particle breakage in the literature is presented. The review addresses the factors that influence breakage, the effect of breakage on the geotechnical behaviour of materials and the existing breakage indices that could be used to quantify particle degradation. The applicability of these findings to non-traditional materials given the differences in structure and properties are examined.

2 Particle Breakage Indices

Tailored to certain geotechnical applications, breakage indices have been defined differently to quantify the degree of breakage and its effects on the geotechnical properties of soil bodies such as permeability, shear strength, settlements, critical state line, etc. were evaluated (Lee and Farhoomand 1967; Marsal 1967; Hardin 1985; Lade et al. 1996; Indraratna et al. 2005).

Lee and Farhoomand (1967) investigated the compressibility of granular soils and focused on the effects of particle breakage on the design of high earth dams in terms of gravel drains and soil filters. They defined a term to quantitatively assess particle breakage which is based on D_{15}, a key grain size used in the design of drains and filters for dams:

$$\text{relative crushing} = \frac{D_{15i}}{D_{15a}} \tag{1}$$

where D_{15i} is the grain size corresponding to 15% of the material finer in the initial grain size distribution, and D_{15a} that in the grain size distribution after testing.

Marsal (1967) studied particle breakage of rockfill materials and defined a quantitative breakage measure, B_g, as the percentage by weight of the solid phase that has undergone breakage:

$$B_g = \sum (\Delta W_k > 0) \tag{2}$$

and,

$$\Delta W_k = W_{ki} - W_{kf} \tag{3}$$

where W_{ki} and W_{kf} represent the percentage of the total sample weight retained in each grain size of the particle size distribution before and after testing, respectively (Marsal 1973).

Hardin (1985) investigated the effect of particle breakage on the strength and stress–strain behaviour of soils. The author defined the potential for breakage b_p of a given particle size D with reference to the maximum silt size, 0.074 mm, assuming that silt size particle do not crush or require a very large amount of stress to break:

$$\begin{aligned} b_p &= \log_{10}\left(\frac{D}{0.074}\right) \quad \text{for} \quad D \geq 0.074 \text{ mm} \\ b_p &= 1 \quad \text{for} \quad D < 0.074 \text{ mm} \end{aligned} \tag{4}$$

Then, breakage potential B_p for a soil element is defined as:

$$B_p = \int_0^1 b_p \cdot \mathrm{d}f \tag{5}$$

where df is a differential of per cent passing divided by 100. Hence, total breakage after loading is given by:

$$B_t = \int_0^1 \left(b_{po} - b_{pl}\right) \cdot \mathrm{d}f \tag{6}$$

where b_{po} is the original value of b_p before loading and b_{pl} is the value of b_p after loading. Based on the observations that B_t is proportional to B_p when the only variable is particle size distribution, the author defined another term, relative breakage, that is independent of particle size distribution as follows:

$$B_r = \frac{B_t}{B_p} \tag{7}$$

Lade et al. (1996) proposed a particle breakage that reflects the effect of breakage on permeability built upon Hazen's formula for permeability (Hazen 1911)and designed to have a lower limit of zero when no breakage occurs and an upper limit of one for infinite breakage:

$$B_{10} = 1 - \frac{D_{10f}}{D_{10i}} \tag{8}$$

where B_{10} is particle breakage factor, D_{10f} is the effective grain size (the grain size corresponding to 10% of the material smaller by weight) of the final gradation and D_{10i} that of the initial grain size distribution. Drained and undrained triaxial compression tests showed that shearing-induced particle breakage increases with increased confining pressures and increased mean normal stress at failure. For the same confining pressure, samples under drained tests showed more particle breakage than those under undrained tests. However, for the same mean normal stress at failure, the trend is vice versa mainly because of the difference in stress path. The proposed breakage index shows an excellent correlation with the total energy input per unit volume in one unique curve for drained and undrained triaxial compression and extension tests which is described by a hyperbolic function:

$$B_{10} = \frac{E_t}{a + bE_t} \tag{9}$$

where a and b are curve fitting parameters. Consequently B_{10} can be used to determine D_{10f} and calculate permeability k based on Hazen (1911) formula:

$$k = 100\left(D_{10f}\right)^2 \tag{10}$$

Indraratna et al. (2005) proposed a Ballast Breakage Index, BBI, based on the shift in the particle size distribution. Instead of assuming that all particle have the potential to be broken into silt size particles as proposed by Hardin (1985), an arbitrary boundary of maximum breakage extending from the smallest ballast particle (2.36 mm) to an upper limit defined by the maximum particle size $d_{\max}$ and d_{95} is used as shown in Fig. 1 and BBI is defined as:

$$\mathrm{BBI} = \frac{A}{A + B} \tag{11}$$

where A is the area between the initial and final particle size distribution and B is the area between the final particle size distribution and the arbitrary boundary of maximum breakage. BBI has a lower limit of 0 when no breakage occurs and 1 for maximum breakage.

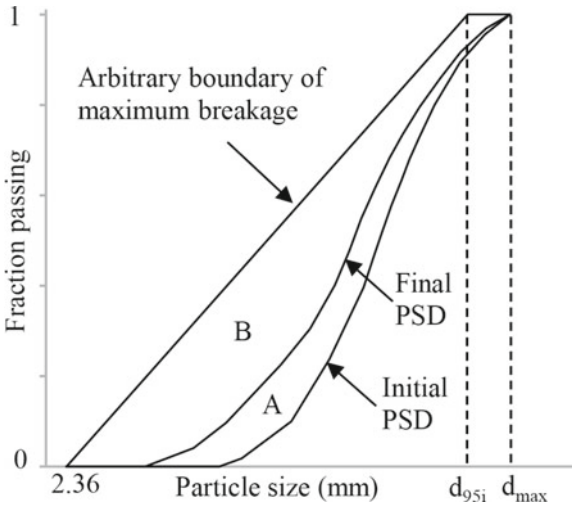

Fig. 1 Breakage index for ballast degradation (after Indraratna et al. 2005)

3 Effects of Particle Breakage

The main concern of geotechnical studies on particle breakage is to predict its effects on the behaviour of granular material when the latter is subject to changes in stress state. A high degree of breakage could lead to catastrophic unexpected failures if its effects are unaccounted for in geotechnical design as the shear strength and compressibility of granular material are highly affected by breakage (Marsal 1967).

Sowers et al. (1965) found that the rate of settlement in dams decreases over time. This phenomenon can be attributed to a decrease in the rate of crushing with time. At each contact point, grains are crushed and stresses are redistributed, the points subject to crushing are less, and hence the rate of crushing-induced settlement is less. Besides induced settlement, crushing of particles in soil filters in dams may result in decreased permeability and increased fine content and the filters would cease to meet the design requirements (Lee and Farhoomand 1967). The strength of rockfill materials is also altered by particle breakage. Through the correlation between the principal stress ratio and particle breakage for different materials, Marsal (1967) concluded that the strength of rockfills decreased with increasing particle breakage.

Lade et al. (1996) found a direct relationship between void ratio at failure and particle breakage for sand; the void ratio at failure is higher for lower levels of particle breakage. This suggests that breakage constitutes a major component of the volumetric change occurring during shearing. Based on their triaxial tests on sand incorporating creep and stress relaxation, Lade and Karimpour (2010) concluded that particle crushing and particle rearrangement play an important role in the time dependency of the stress–strain relationship observed in granular material where the strain rate and load rate are not of significant influence. Moreover, Bandini and

Coop (2011) reported a shift in the critical state line (CSL) location of sands as a result of particle breakage. However, a high degree of breakage is required for such behaviour to be observed.

Indraratna et al. (2005) established a correlation between particle breakage and volumetric strains for ballast under cyclic loading:

$$\ln \varepsilon_v = \alpha e^{\beta(\mathrm{BBI})} \tag{12}$$

where ε_v is the volumetric strain, α and β are empirical constants and BBI is the Ballast Breakage Index defined in (11). Hossain et al. (2007) evaluated the effect of particle breakage on permanent deformations of ballast under cyclic loading through a 2D discrete element method (DEM) and also found that particle crushing has a significant effect on settlements and volumetric strains. Particle breakage may also influence the critical state of ballast under monotonic loading (Indraratna et al. 2015). As particle breakage becomes significant at high confining pressures, the location of the CSL is shifted in the q-lnp′ and v-lnp′ planes. Also, when particle breakage increases, the critical stress ratio M_c decreases, the CSL is no longer linear in the v-lnp′ plane.

Degradation can also have a detrimental effect on the shear strength parameters of non-traditional materials such as coal refuse. The friction angle of the mining waste may decrease from 29°–32° to 13° when the material undergoes breakage (Taylor 1978). In addition, Heitor et al. (2016) showed that compaction-induced breakage for different compaction efforts of coal wash has a significant effect on the stress–strain properties of the material and the critical state line in the e-lnp′ plane.

4 Factors Affecting Particle Breakage

When a granular material is subjected to loading, particles tend to form a more stable arrangement resulting in the breakage of their angular corners (Indraratna et al. 2005). In practice, breakage could be induced by compaction or by shearing, i.e. loading. In this context, breakage of a soil body is highly dependent on external factors, such as compaction effort and loading conditions, and on the properties of the soil body itself.

4.1 Compaction-Induced Particle Breakage

Compaction is one of the most employed soil improvement techniques. During compaction, the sharp angularities of particles can be broken causing a shift in the particle size distribution towards smaller sizes (Rujikiatkamjorn et al. 2013; Wang et al. 2015). Few studies have assessed breakage induced by compaction prior to

loading (Rujikiatkamjorn et al. 2013; Wang et al. 2014, 2015; Heitor et al. 2016; Yaghoubi et al. 2017). Studies show that the degree of particle breakage depends on moisture content, compaction effort, compaction method and initial particle size distribution.

Rujikiatkamjorn et al. (2013) found that compaction-induced breakage decreases by 25–5% when coal wash is compacted at the dry side of OMC, then starts to increase again when the moisture content increases beyond the OMC. On the other hand, Wang et al. (2014) reported similar particle size distribution of sandstone–mudstone mixtures after compaction for different water contents. This suggests that the sensitivity of compaction-induced breakage to water content is dependent on the type of granular materials. However, sandstone–mudstone mixtures exhibited an increase in breakage with increasing compaction effort (Wang et al. 2014). Heitor et al. (2016) reported a similar trend for compacted coal wash. In their study on the effect of particle size on the compaction behaviour of sandstone–mudstone mixtures, Wang et al. (2015) showed that breakage increases when the median particle diameter d_{50} and gravel content increases. Yaghoubi (2017) study on compaction of recycled concrete showed that breakage associated with impact compaction (modified proctor) is slightly larger than that for static compaction.

4.2 Shearing-Induced Particle Breakage

Unlike compaction-induced breakage, many studies in the literature have focused on the breakage of granular material after loading in one-dimensional and triaxial compression tests and shearing tests (Sowers et al. 1965; Lee and Farhoomand 1967; Hardin 1985; Lade and Yamamuro 1996; Lade et al. 1996; Indraratna et al. 2005; Hossain et al. 2007; Gupta 2016; Heitor et al. 2016).

Sowers et al. (1965) studied the effect of wetting on crushing of rockfills and found that initially dry rocks experienced lower breakage levels than wet samples and dry samples developed additional breakage when wetted. They also found that adding an agent to water that reduces surface tension increased the additional breakage induced by wetting. It is suggested that this phenomenon resulted from a local increase in stress when water entered the microfissures at highly stressed contact points.

The study conducted by Lee and Farhoomand (1967) showed that crushing increases with increasing coarseness and angularity under the same stress conditions. Also, uniform soil showed higher compression, hence higher crushing, than graded soils with the same maximum particle size. For the same ratio between major and minor stresses K_c, crushing was found to increase with confining pressure and when K_c increased, i.e. shear stress increased, the relative crushing of tested samples also increased.

Hardin (1985) studied the effect of six different variables, namely particle size distribution, state of effective stress and effective stress path, initial void ratio, particle shape, and particle hardness on breakage of different soils. Consequently, he defined three relationships that could be used to predict particle breakage during

loading incorporating the effect of the six variables (i.e. particle size distribution, particle shape, state of effective stress, effective stress path, void ratio and particle hardness).

High pressure triaxial tests on sand (Lade et al. 1996) also showed that breakage increases with confining pressure and that drained triaxial tests exhibited more particle breakage than undrained tests. Such behaviour is attributed to lower mean normal effective stress due to the development of high pore pressures in undrained tests.

On the other hand, Indraratna et al. (2005) found that breakage of ballast under cyclic loading is greatest at low confining pressures (< 30 kPa). Minimum breakage was observed at confining pressures between 30 and 75 kPa which can be attributed to better particle arrangement, lower contact forces, and hence lower stress concentration. Breakage increased again with increasing confining pressures due to higher contact stresses and the inability of particles to move. Hossain et al. (2007) reported similar trends from DEM analysis.

Gupta (2016) observed an increase in particle breakage with increasing particle size of rockfills. Such behaviour is associated with a decrease in the number of contact points and consequently an increase in contact pressures. The study also showed that higher confining pressures lead to higher degrees of breakage in rockfill materials for all confining pressures which is also attributed to higher contact pressures between particles.

A similar increase in breakage with confining pressures for compacted coal wash is reported by Heitor et al. (2016) where shearing-induced breakage prevails at high confining pressures and compaction-induced breakage is greater at lower pressures.

5 Discussion

5.1 Volumetric Behaviour and Particle Breakage

Lee and Farhoomand (1967) test results showed that volume change is highly dependent on the major principal stress and independent of the shear stress or the minor principal stress where a unique relationship was observed between volume change and vertical stress for different K_c ratios. In other words, under the same vertical stress, volume change is the same for increasing confining pressure. However, crushing is highly dependent on the confining pressure, i.e. for the same vertical stress, particle breakage increases with increasing confining pressure.

One could argue that volume change can be split between shearing effects and particle breakage. For the same vertical stress, shearing-induced volume change decreases with increased confining pressure because the shear stress is decreasing. At the same time, particle breakage-induced volume change increases with increasing confining pressure keeping the overall volume change constant. A new model could be developed to describe the volumetric behaviour of soils incorporating particle breakage.

5.2 Applicability of Breakage Indices

Theories for particle breakage have been developed for dam rockfills, which capture large particles and do not have a significant amount of fines. In transport infrastructure, base and subbase material may contain up to 17% fines. Therefore, these indices might not be appropriate to quantify breakage after compaction or shearing.

Lade et al. (1996) used linear extrapolation to get D_{10f} when more than 10% of particles passed the No. 200 sieve. However, for materials with a relatively high fines content, extrapolated values of D_{10f} would be very small and erroneous. Similarly, the use of D_{15} would give unrealistic results in certain circumstances. Plus, because breakage usually occurs in larger particles, D_{10} and D_{15} values after compaction and loading are insensitive to variations in moisture content, compaction methods, state of stress and other factors that are shown to influence particle degradation in the literature. Therefore, the corresponding breakage indices could not be used to assess improvement methods that would minimize particle breakage during compaction and loading. On the other hand, breakage indices proposed by Marsal (1967), Hardin (1985) and Indraratna et al. (2005) incorporate the full PSD curve before and after compaction and not only a specific particle size. However, these indices might also require modifications that are tailored to specific materials and corresponding breakage behaviour.

5.3 Numerical Modelling of Particle Breakage

Besides experimental investigations and empirical equations developed to evaluate particle breakage and its effect on the behaviour of granular materials, numerical models have also been established in the literature (McDowell and Harireche 2002; Indraratna et al. 2005; Lu and McDowell 2010; Ngo et al. 2017).

McDowell and Harireche (2002) studied the fracture of soil particles compressed between flat platens through discrete element modelling to evaluate the effect of particle size on strength. They modelled a sand particle of a given size as an agglomerate of balls bonded together and flaws are simulated by the removal of balls. They found that particle size did not affect strength when 0–25% balls are removed from the agglomerate. This is attributed to a difference in geometry between agglomerates of different sizes. To correctly model the degradation of particles under stress, regular geometry could be removed and flaws could be introduced by initially removing 30% of the balls.

Hossain et al. (2007) developed a numerical model based on a 2D DEM analysis to simulate ballast breakage under different confining pressures. They modelled the angularity of ballast particles by clumping two to nine circular particles together to form particle of different sizes. To simulate breakage, each particle is assigned a tensile strength value, and when the tensile stress induced by contact forces exceed

the tensile strength of the ballast particles, the particle is released from the clump. Breakage is then quantified from the shift in the particle size distribution (Indraratna et al. 2005).

Lu and McDowell (2010) also modelled the mechanical behaviour of railway ballast and particle degradation under monotonic and cyclic loading using a DEM model. A ballast particle is modelled as a clump of ten balls in a tetrahedral shape and asperities are simulated by bonding eight small balls to the clump. Breakage of small asperities is simulated by the breakage of parallel bonds between clumps and that of larger asperities is simulated by the breakage of the small balls bonded to the clump. The results of the model were found to be in good agreement with the experimental results of large-scale tests (Lackenby et al. 2007).

Ngo et al. (2017) developed a coupled numerical model based on a DEM and a finite difference method (FDM) to simulate the load–deformation relationship of ballast under cyclic loading incorporating particle degradation. Breakage is simulated by the degradation of contact bonds between particles. When compared to the change in BBI (Indraratna et al. 2005) measured in the laboratory, the evolution of bond breakage with load cycles and load frequency showed similar trends.

6 Conclusion

The problem of particle breakage was investigated in the literature. The findings of these studies are reviewed in this paper,and the following conclusions are made:

1. Breakage indices were developed to target a certain problem such as the effect of breakage on permeability, shear strength, settlements, etc., and due caution must be taken when selecting a certain index to quantify breakage.
2. Breakage is highly dependent on external as well as internal factors. During compaction, the moulding moisture content, the compaction effort applied, and the compaction method employed are shown to affect the extent of breakage. The state of stress, as well as the properties of the soil, such as particle size distribution and particle strength, also highly influence breakage during compression/shearing.
3. It is crucial to account for breakage, in geotechnical design as it could significantly affect the behaviour of soil bodies and yield unexpected settlements or failures.
4. DEM models incorporating particle breakage could be developed to aid in evaluating the effect of breakage on the behaviour of granular materials and investigate improvement methods to minimize particle degradation in practice.

Acknowledgements The first author's Ph.D. scholarship is supported by the Australian Research Council (ARC) Linkage Project (LP160100280).

References

Bandini V, Coop MR (2011) The influence of particle breakage on the location of the critical state line of sands. Soils Found 51(4):591–600

Gupta AK (2016) Effects of particle size and confining pressure on breakage factor of rockfill materials using medium triaxial test. J Rock Mech Geotech Eng 8(3):378–388

Hardin BO (1985) Crushing of soil particles. J Geotech Eng 111(10):1177–1192

Hazen A (1911) Discussion of "Dams on sand foundations", by AC Koenig. Trans Am Soc Civil Eng 73(3):199–203

Heitor A, Indraratna B, Kaliboullah CI, Rujikiatkamjorn C, McIntosh GW (2016) Drained and undrained shear behavior of compacted coal wash. J Geotech Geoenviron Eng 142(5): 04016006-1-04016006-10

Hossain Z, Indraratna B, Darve F, Thakur PK (2007) DEM analysis of angular ballast breakage under cyclic loading. Geomech Geoeng 2(3):175–181

Indraratna B, Lackenby J, Christie D (2005) Effect of confining pressure on the degradation of ballast under cyclic loading. Géotechnique 55(4):325–328

Indraratna B, Sun QD, Nimbalkar S (2015) Observed and predicted behaviour of rail ballast under monotonic loading capturing particle breakage. Can Geotech J 52(1):73–86

Lackenby J, Indraratna B, McDowell G, Christie D (2007) Effect of confining pressure on ballast degradation and deformation under cyclic triaxial loading. Geotechnique 57(6):527–536

Lade PV, Karimpour H (2010) Static fatigue controls particle crushing and time effects in granular materials. Soils Found 50(5):573–583

Lade PV, Yamamuro JA (1996) Undrained sand behavior in axisymmetric tests at high pressures. J Geotech Eng 122(2):120–129

Lade PV, Yamamuro JA, Bopp PA (1996) Significance of particle crushing in granular materials. J Geotech Eng 122(4):309–316

Lee KL, Farhoomand I (1967) Compressibility and crushing of granular soil in anisotropic triaxial compression. Can Geotech J 4(1):68–86

Lu M, McDowell GR (2010) Discrete element modelling of railway ballast under monotonic and cyclic triaxial loading. Geotechnique 60(6):459–467

Marsal RJ (1967) Large-scale testing of rockfill materials. J Soil Mech Found Div 93(2):27–43

Marsal RJ (1973) Particle breakage. In: Casagrande A, Hirschfeld RC, Poulos SJ (eds) Embankment dam engineering: Casagrande volume. Wiley, New York, pp 130–141

McDowell GR, Harireche O (2002) Discrete element modelling of soil particle fracture. Géotechnique 52(2):131–135

Ngo NT, Indraratna B, Rujikiatkamjorn C (2017) Simulation ballasted track behavior: numerical treatment and field application. Int J Geomech 17(6):1–12

Rujikiatkamjorn C, Indraratna B, Chiaro G (2013) Compaction of coal wash to optimise its utilisation as water-front reclamation fill. Geomech Geoeng 8(1):36–45

Sowers GF, Williams RC, Wallace TS (1965) Compressibility of broken rock and the settlement of rockfills. In: 6th international conference on soil mechanics and foundation engineering, Montréal, Canada

Taylor R (1978) Properties of mining wastes with respect to foundations. In: Bell F (ed) Foundation engineering in difficult ground. Butterworths, London, pp 175–203

Wang JJ, Cheng YZ, Zhang HP, Deng DP (2015) Effects of particle size on compaction behavior and particle crushing of crushed sandstone-mudstone particle mixture. Environ Earth Sci 73 (12):8053–8059

Wang JJ, Zhang HP, Deng DP (2014) Effects of compaction effort on compaction behavior and particle crushing of a crushed sandstone-mudstone particle mixture. Soil Mech Found Eng 51 (2):67–71

Yaghoubi E, Disfani MM, Arulrajah A, Kodikara J (2017) Impact of compaction method on mechanical characteristics of unbound granular recycled materials. Road Mater Pavement Des 18(2):1–23

The Influence of Rubber Crumbs on the Energy Absorbing Property of Waste Mixtures

Yujie Qi, Buddhima Indraratna, Ana Heitor and Jayan S. Vinod

Abstract The practical application of waste materials such as steel furnace slag (SFS) and coal wash (CW) is becoming more prevalent in civil engineering. While the addition of rubber crumbs (RC) derived from waste tyres can influence the geotechnical properties of the mixtures of SFS and CW significantly, especially the energy absorbing property. In this paper, the energy absorbing property of the SFS + CW + RC mixtures under static loading has been evaluated by the strain energy density. As expected, the energy absorbing capacity of the waste mixture increases with the addition of RC. To further illustrate the influence of rubber crumbs on the energy absorbing property of the waste mixtures, particle degradation has also be examined after finishing the triaxial tests. It has been found that the addition of RC can significantly reduce the particle breakage of the waste mixtures. Therefore, with high energy absorbing property, the SFS + CW + RC mixtures can be further extended to dynamic loading projects, such as railway capping layer.

Y. Qi
School of Civil, Mining and Environmental Engineering, Centre for Geomechanics and Railway Engineering, Australian Research Council Training Centre for Advanced Technologies in Rail Track Infrastructure, University of Wollongong, Wollongong, NSW 2522, Australia
e-mail: yq346@uowmail.edu.au

B. Indraratna (✉)
Civil Engineering, Faculty of Engineering and Information Sciences, Centre for Geomechanics and Railway Engineering, Australian Research Council Training Centre for Advanced Technologies in Rail Track Infrastructure, University of Wollongong, Wollongong, NSW 2522, Australia
e-mail: indra@uow.edu.au

A. Heitor · J. S. Vinod
Faculty of Engineering and Information Sciences, Centre for Geomechanics and Railway Engineering, Australian Research Council Training Centre for Advanced Technologies in Rail Track Infrastructure, University of Wollongong, Wollongong, NSW 2522, Australia
e-mail: aheitor@uow.edu.au

J. S. Vinod
e-mail: vinod@uow.edu.au

R. Sundaram et al. (eds.), *Geotechnics for Transportation Infrastructure*,
Lecture Notes in Civil Engineering 29,
https://doi.org/10.1007/978-981-13-6713-7_22

Keywords Waste mixtures · Rubber crumbs · Energy absorbing property · Strain energy density

1 Introduction

CW and SFS are very common granular by-products of the coal mining and steel industries in Australia, respectively. The production of these wastes in Wollongong (Australia) alone can amount to several millions of tons per year (Leventhal and de Ambrosis 1985). To prevent the adverse geotechnical properties of these waste materials (i.e. the volumetric expansion for SFS and the breakage potential for CW; Indraratna 1994; Heitor et al. 2016; Wang 2010), SFS and CW can be mixed in selected ratios and have been successfully employed as a structural fill for Port Kembla Outer Harbour reclamation (Chiaro et al. 2013; Tasalloti et al. 2015a, b). However, the application of SFS + CW is only limited to static loading as more breakage of coal wash may be generated by dynamic loading. Therefore, the energy absorbing property of the waste mixture needs to be improved before applying it as capping layer to major rail projects.

Due to the rapidly increasing number of vehicles worldwide every year, waste tyres has become a critical environmental problem in many urban cities, and in Australia alone, 500,000 tons of tyres are replaced every year (Mashiri et al. 2015). Recycled tyres are typically granulated or shredded and exhibit low shear strength, low unit weight of solids (the specific gravity generally ranges from 1.00 to 1.36), high compressibility, high hydraulic conductivity and high energy absorbing capacity (Senetakis et al. 2012; Zheng and Kevin 2000; Edil and Bosscher 1994). However, as the low shear strength and high deformation properties, granulated rubber materials cannot be used alone in civil engineering, but their geotechnical properties boost their usage in rubber–soil mixtures.

It has been reported that the inclusion of scrap tyres can increase the hydraulic conductivity, reduce the swelling of soil–rubber mixtures (Racichandran et al. 2016; Indraratna et al. 2018; Qi et al. 2017a). Moreover, in recent years, the high energy absorbing capacity of RC has been well applied in civil works for the purpose of vibration isolation and anti-seismic construction in the form of soil–rubber blends. Tsang et al. (2012) found using rubber–soil mixture as an alternative seismic isolation material could significantly reduce the horizontal and vertical acceleration and displacements. The cyclic loading tests on rubber–waste mixtures conducted by Qi et al. (2017b) reveal that the inclusion of RC could increase the damping ratio of the waste mixtures.

Therefore, with the high energy absorbing capacity, the inclusion of RC into the SFS + CW blends will promote enhanced strain energy absorption and reduce particle breakage of the blended mix. The aim of this study was to investigate the effect of RC content (R_b, %) on the energy absorbing property of the waste mixtures by evaluating the strain energy density and the particle breakage of the SFS + CW + RC mixtures. To further prove the high energy absorbing property improved by adding RC, comparison between the waste materials and traditional capping layer materials will also be provided.

2 Materials

The SFS and CW used in this study were provided by Illawarra Coal and ASMS (Australia Steel Milling Services), respectively. RC was from waste tyres, and three different sizes (0–2.3, 0.3–3, and 1–7 mm) of RC were used. The traditional capping layer materials (sub-ballast) which is crushed rock was obtained from Bombo quarry near Wollongong, New South Wales, Australia.

The specific gravity (G_s) of SFS, CW, RC and traditional sub-ballast used in this study is 3.43, 2.11, 1.15 and 2.7, respectively. Figure 1 presents the particle size distribution (PSD) curves of SFS, CW, RC and traditional sub-ballast. The dry method was used to sieve oven-dried SFS, traditional sub-ballast and air-dried rubber crumbs, whereas the wet method was used for CW. According to the unified soil classification system (USCS), SFS and CW can be classified as well-graded gravel with silty-sand (GW-GM), and well-graded sand with gravel (SW), respectively, while RC can be referred to as granulated rubber.

3 Testing Program

To exclude the influence of the gradation, all the waste mixtures are prepared with the same gradation, and the target PSD for the SFS + CW + RC mixtures is shown in Fig. 1, and the target PSD is kept similar to traditional sub-ballast. To achieve the target PSD, all the waste materials were sieved and separated into different particle sizes (6.7, 4.75, 2.36, 1.18, 0.6, 0.425, 0.3, 0.212 and <0.212 mm), and then, the exact mass according to a given size range provided by the target PSD was weighed and blended thoroughly until a uniform appearance of the waste mixture was obtained. In this study, the blending ratio of SFS:CW is kept at 7:3 as with blending ratio (by weight), the SFS + CW + RC mixtures present low volume expansion

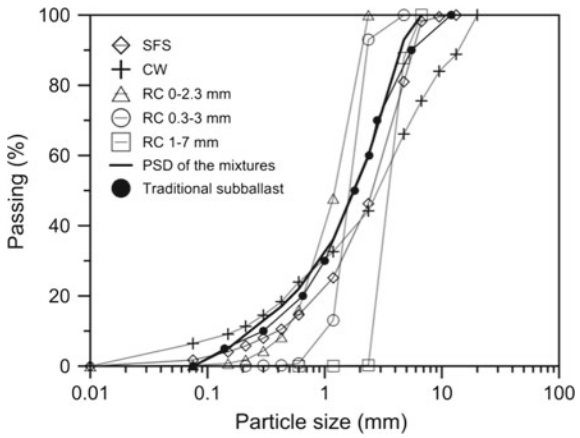

Fig. 1 The particle size distribution of SFS, CW, RC and the target PSD for the SFS + CW + RC

Table 1 Geotechnial properties of SFS + CW + RC mixtures and traditional sub-ballast

Mixtures	R_b (%)	G_s	$\gamma_{d\max}$ (kN/m^3)	OMC (%)
SFS70 + CW30	0	2.89	20.30	11.5
SFS63 + CW27 + RC10	10	2.51	17.57	12.5
SFS56 + CW24 + RC20	20	2.22	15.50	13
SFS49 + CW21 + RC30	30	1.99	13.83	14
SFS42 + CW18 + RC40	40	1.80	12.40	15
Traditional sub-ballast	–	–	18.5	4.6

while maintain enough shear strength for a capping layer material (Indraratna et al. 2018). To investigate the influence of RC content (R_b, %) on the energy absorbing property of the waste mixtures, R_b in the blended mixtures varied from 0 to 40% (Table 1, by weight).

All the specimens for the monotonic triaxial tests and swell potential tests were prepared with the optimum moisture content (OMC, %) and compacted to achieve the initial dry unit weight equal to 95% of their maximum dry density ($\gamma_{d\max}$, kN/m^3). The specific gravity, optimum moisture content, and the maximum dry density of SFS + CW + RC mixtures and traditional sub-ballast are shown in Table 1. It can be observed that the specific gravity of the mixtures decreases with the inclusion of RC, which is because of the low unit weight of rubber materials (Table 1). When $R_b \geq 10\%$, the dry unit weight of the SFS + CW + RC mixtures is lower than traditional sub-ballast. This will assist in reducing the surcharge load applied to the subgrade layer. The optimum moisture content for traditional sub-ballast is much lower than that of SFS + CW + RC mixtures.

The mixtures are expressed as SFS + CW + RC, and the numbers after SFS, CW and RC are the percentages of steel furnace slag, coal wash and rubber crumbs by weight.

The static consolidated drained triaxial tests were carried out in accordance with ASTM D7181 (2011) following three stages, i.e. saturation, consolidation and shearing. During the saturation stage, the air was firstly expelled by flooding deaired water from the bottom of the specimen (50 mm in diameter and 100 mm in height), then back pressure was applied at a rate of 1 kPa/minute until 500 kPa was achieved. This stage was completed when the Skempton's B-value exceeded 0.98, and then, isotropic consolidation was conducted until the desired mean effective confining pressure achieved the target value (e.g. 10, 40, or 70 kPa). To simulate the practical condition of railway sub-base and sub-ballast, a low confining pressure was adopted. After consolidation, monotonic shearing was conducted with a relatively slow constant strain rate of 0.2 mm/min to ensure fully drained conditions. The triaxial tests were completed when 25% axial strain was achieved. Once the tests were completed, sieving procedure was repeated so that particle breakage arising from the shearing process could be evaluated.

4 Results and Discussion

4.1 Stress–Strain Behaviour

Figure 2a shows the typical stress–strain behaviour of the waste mixtures with different amounts of RC and tested at $\sigma'_3 = 70$ kPa. It can be observed that the peak deviator stress decreases as the amount of RC increases, which is not surprising considering that rubber has very low shear strength compared to SFS and CW materials. All the specimens exhibited a predominantly strain softening behaviour accompanied by a contractive–dilative response. However, as RC contents increased, the strain softening behaviour was weakened and the axial strain corresponding to the peak deviator stress also increased. This indicates that the stress–strain response changes from brittle to ductile, likely due to an increase in the rubber-to-rubber interaction in the skeleton of the mixtures. Similar observations were also reported by Kim and Santamarina (2008) for sand–rubber mixtures.

The curves of axial strain versus volumetric strain of the waste mixtures are presented in Fig. 2b. It is evident that all specimens were compressed initially, and then dilated until a certain axial strain was achieved. As expected, greater inclusion of RC results in larger compression, which is due to the high compressibility of

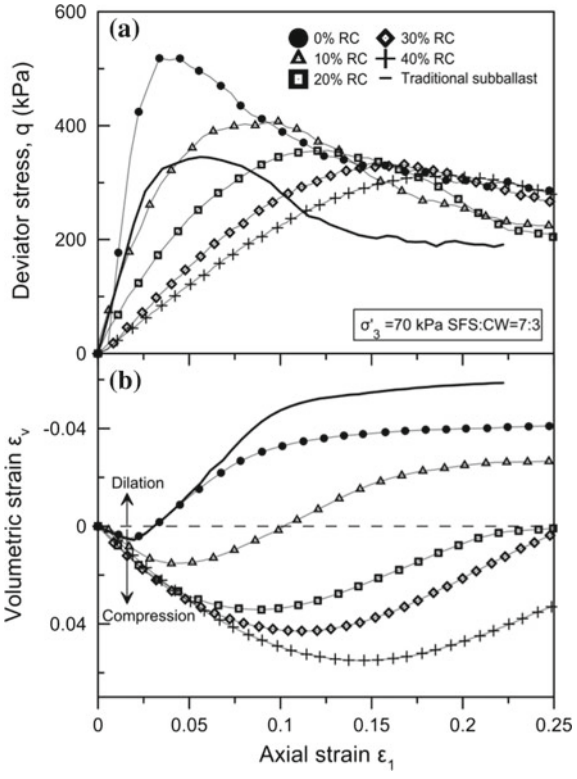

Fig. 2 Stress–strain curves of SFS + CW + RC mixtures and traditional sub-ballast under $\sigma'_3 = 70$ kPa

rubber materials. For the SFS + CW + RC mixtures having 40% RC, the volumetric strain is around 6% in compression.

The stress–strain curves of traditional sub-ballast are also shown in Fig. 2. It can be observed that the peak deviator stress of traditional sub-ballast is lower than the waste mixture with 0 and 10% of RC while similar to the waste mixture with 20% of RC. Strain softening is obvious after attaining the peak deviator stress. The volumetric strain–axial strain curve of the traditional sub-ballast shows that the contractive part of the volumetric strain is similar to SFS + CW + RC mixture having 0% RC, but the traditional sub-ballast exhibits more dilation when the axial strain increases. All the waste mixtures with $R_b \geq 10\%$ are more contractive than the traditional sub-ballast. This is because of the high deformation property of rubber materials.

The peak frictional angle ($\emptyset'_{peak}$) of SFS + CW + RC mixtures and traditional sub-ballast is shown in Table 2. It is noted that the peak shear strength decreases as the effective confining pressure increases, which is in agreement Chiaro et al. (2013) for SFS + CW mixtures. Moreover, with $R_b < 10\%$, the SFS + CW + RC mixtures (SFS:CW = 7:3) have sufficient shear strength to serve as capping layer materials.

4.2 Energy Absorption

The strain energy density is adopted to evaluate the energy absorbed in shearing triaxial tests, and it can be computed considering the area under the shear stress–strain curve up to failure (Fig. 3), as represented by Eq. (1)

$$E = \int_0^{\gamma_f} \tau \mathrm{d}\gamma \tag{1}$$

where E is the strain energy density (kPa), γ_f represents the shear strain (dimensionless) up to failure, and τ is the shear strength (kPa). Failure is defined as the point when the specimen reaches the peak deviator stress, under the static triaxial

Table 2 Peak friction angle ($\emptyset'_{peak}$) of SFS + CW + RC mixtures and traditional sub-ballast

Mixtures	R_b (%)	$\emptyset'_{peak}$ (°) at $\sigma'_3 = 10$ kPa	$\emptyset'_{peak}$ (°) at $\sigma'_3 = 40$ kPa	$\emptyset'_{peak}$ (°) at $\sigma'_3 = 70$ kPa
SFS70 + CW30	0	62.5	54.4	51.9
SFS63 + CW27 + RC10	10	60.6	50.8	48.1
SFS56 + CW24 + RC20	20	58.1	49.5	45.9
SFS49 + CW21 + RC30	30	53.9	47.9	44.7
SFS42 + CW18 + RC40	40	52.7	45.9	43.7
Traditional sub-ballast	–	58.9	49.4	45.4

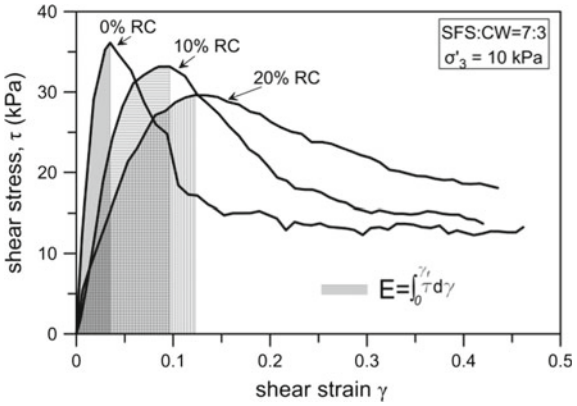

Fig. 3 Shear stain–stress curve of SFS + CW + RC mixtures with 0–20% RC under $\sigma'_3 = 10\,\text{kPa}$

conditions, which is in agreement with Kim and Santamarina (2008) for sand–rubber mixtures.

Figure 4 presents the strain energy density of the SFS + CW + RC mixtures having different RC contents computed based on the drained triaxial shearing results. It can be seen that the strain energy density of the waste mixtures increases with the effective confining pressure as the peak shear stress increases with the confining pressure. Clearly, it can be observed that the strain energy density of SFS + CW + RC mixtures with $R_b = 10\%$ is around 2 folds greater than the mixtures without rubber indicating the high energy absorbing capacity of rubber materials.

Furthermore, when RC > 10%, with more RC is included the increase in strain energy density is marginal, especially at lower effective confining pressures (i.e. $\sigma'_3 = 10$ and 40 kPa). This is likely related to the decrease in shear strength and

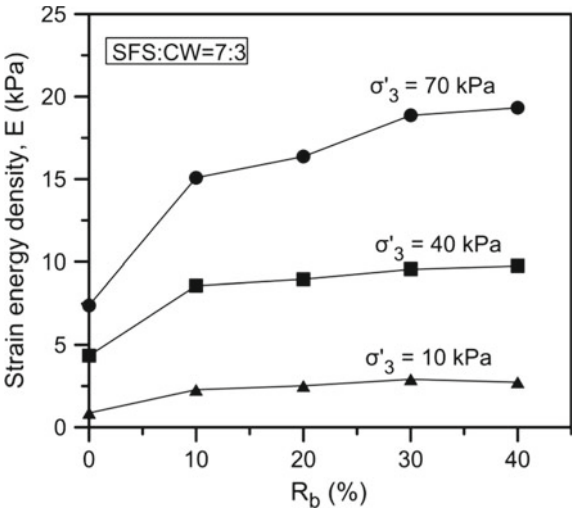

Fig. 4 Strain energy density of SFS + CW + RC mixtures varying with RC contents

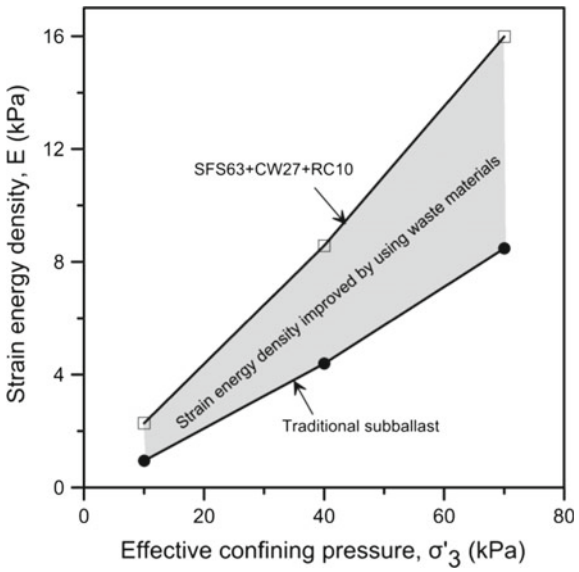

Fig. 5 The strain energy density of traditional sub-ballast and the SFS + CW + RC mixtures with 10% RC

particle breakage when more RC included, which can be further proved by comparing the shade area under the shear strain curve of the waste mixtures with 10 and 20% RC (Fig. 3). On this basis, it seems that 10% RC is sufficient for the mixture to serve as an energy absorbing layer while tolerating an acceptable reduction in shear strength.

In Fig. 5, the comparison between the strain energy density of traditional sub-ballast and the waste mixture with 10% RC is depicted. It is obvious that using the SFS + CW + RC mixture (SFS:CW = 7:3) with 10% RC can significantly improve the energy absorbing capacity of the capping layer materials. This is even more significant as the effective confining pressure increases, as evidenced by a larger gap between the strain energy density of the traditional sub-ballast and the waste mixture with $R_b = 10\%$.

4.3 Particle Breakage

Another important method to examine the effect of the RC content on the energy absorbing property of the SFS + CW + RC mixtures is to check the particle breakage after compaction and shearing. Particle breakage is also a very important parameter that should be evaluated to quantify the level of degradation that a granular material undergoes when subjected to impact loading and shearing. Typically the incidence of particle breakage can be quantified considering the breakage index (BI) that relies on the evaluation of the initial and final gradations (Indraratna et al. 2005) shown in Fig. 6a. In this study, the BI index was determined

for the waste mixtures with different RC contents upon compacting and shearing at $\sigma'_3 = 10, 40,$ and 70 kPa, and the test results are shown in Fig. 6b.

As expected, the addition of rubber crumbs significantly reduced particle breakage in the waste mixtures, and BI of the waste mixtures having 30 and 40% RC is negligible. This is because of the high energy absorbing property of rubber materials the loads can be buffered as the rubber crumbs deform, which then reduces breakage of CW and SFS.

Moreover, BI increases as the confining pressure increases. For the waste mixtures having 0% RC, it seems that the majority of particle breakage induced by shearing occurs at low confining pressures (σ'_3 = 10 kPa), and only 1% increase in BI when σ'_3 increases from 40 to 70 kPa. To ensure less deformation and less particle degradation, the SFS + CW + RC mixtures with <2% BI under $\sigma'_3 =$

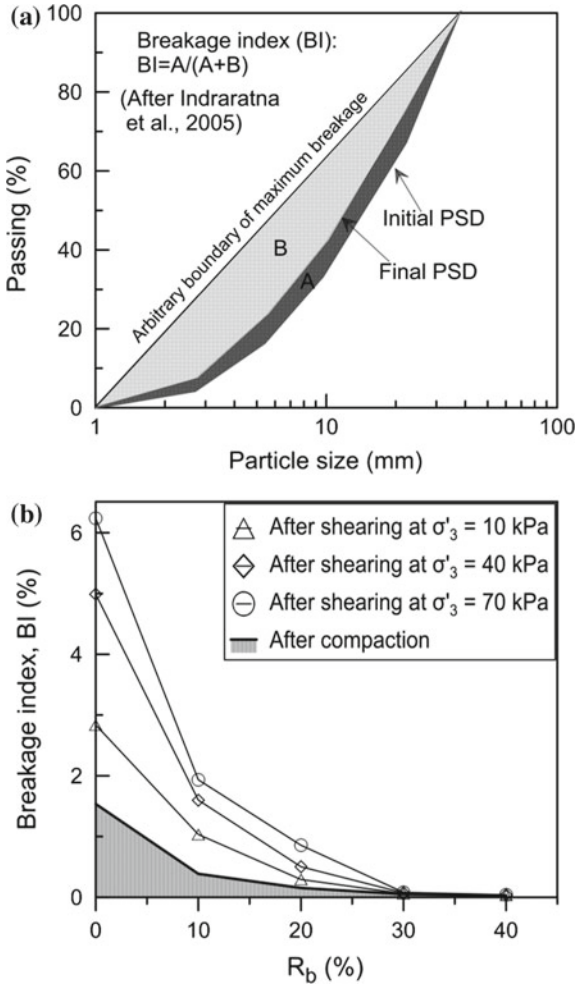

Fig. 6 **a** The definition of the breakage index (after Indraratna et al. 2005), **b** BI of the SFS + CW + RC mixtures under different effective confining pressures

40 kPa are recommended (Indraratna et al. 2018; Qi et al. 2017a). Therefore, in the waste mixtures, RC contents should not be less than 10% to reduce the particle breakage.

5 Conclusions

In this study, rubber crumbs (0–40%) were mixed into the SFS + CW blends (with SFS:CW = 7:3) in the aim of increasing the energy absorbing property of the waste mixtures. Consolidated drained triaxial tests were conducted on the waste mixtures to examine the stress–strain behaviour, strain energy density and the particle breakage of the SFS + CW + RC mixtures. The test results reveal that the inclusion of RC can significantly increase the energy absorbing capacity and reduce the particle breakage of the waste mixtures, albeit a reduction of the shear strength was observed. Therefore, with the high energy absorbing capacity, the SFS + CW + RC mixtures can be extended to dynamic loading projects, such as railway capping layer. Overall, for the SFS + CW + RC mixtures with the blending ratio of SFS: CW = 7:3, 10% was suggested as the optimal RC content as with this RC content the waste mixture has sufficient energy absorbing capacity, shear strength and acceptable particle breakage.

Acknowledgements The first author would like to acknowledge the financial assistance provided by the China Scholarship Council, Australian Research Council Discovery Project (ARC-DP), and the Australian Research Council funded Industrial Transformation Training Centre for Advancement of Rail Infrastructure (ITTC-Rail). The assistance provided by industry (ASMS and South 32) in relation to the procurement of material used in this study is gratefully acknowledged. The assistance in the laboratory from Mr. Richard Berndt and the occasional technical feedback from A/Prof. Cholachat Rujikiatkamjorn are appreciated.

References

ASTM D7181, American Society for Testing and Materials (2011), Standard method for consolidated drained triaxial compression test for soils, ASTM International, West Conshohocken PA, USA

Chiaro G, Indraratna B, Tasalloti SMA, Rujikiatkamjorn C (2013) Optimisation of coal wash-slag blend as a structural fill. Ground Improv 168(GI1):33–44

Edil T, Bosscher P (1994) Engineering properties of tyre chips and soil mixtures. Geotech Test J 17(4):453–464

Heitor A, Indraratna B, Kaliboullah CI, Rujikiatkamjorn C, McIntosh G (2016) A study on the drained and undrained shearing behaviour of compacted coal wash. J Geoenviron Eng, Geotech. https://doi.org/10.1061/(ASCE)GT.1943-5606.0001422

Indraratna B (1994) Geotechnical characterization of blended coals tailings for construction and rehabilitation work. Q J Eng Geol Hydrogeol 27:353–361

Indraratna B, Lackenby J, Christie D (2005) Effect of confining pressure on the degradation of ballast under cyclic loading. Geotechnique 55(4):325–328

Indraratna B, Qi YJ, Heitor A (2018) Evaluating the properties of mixtures of steel furnace slag, coal wash, and rubber crumbs used as subballast. J Mater Civ Eng 30(1):04017251

Kim HK, Santamarina JC (2008) Sand-rubber mixtures (large rubber chips). Can Geotech J 45:1457–1466

Leventhal AR, de Ambrosis LP (1985) Waste disposal in coal mining—a geotechnical analysis. Eng Geol 22(1):83–96

Mashiri M, Vinod JS, Sheikh MN, Tsang HH (2015) Shear strength and dilatancy behaviour of sand–tyre chip mixtures. Soil Found 55(3):517–528

Qi YJ, Indraratna B, Heitor A, Vinod JS (2017a) Developing an energy absorbing layer using waste materials. In: International conference of ground improvement (ICGI2017), Hangzhou, China, 27–29 Oct 2017, pp 26–33

Qi YJ, Indraratna B, Heitor A, Vinod JS (2017b) The role of rubber crumbs on the cyclic behaviour of steel furnace slag and coal wash mixtures. J Geotech Geoenviron Eng 144 (2):04017107

Racichandran PT, Prasad AS, Krishnan KD, Rajkumar PRK (2016) Effect of addition of waste tyre crumb rubber on weak soil stabilisation. Indian J Sci Technol 9(5):1–5

Senetakis K, Anastasiadis A, Pitilakis K (2012) Dynamic properties of dry sand/rubber (SRM) and gravel/rubber (GRM) mixtures in a wide range of shearing strain amplitudes. Soil Dyn Earthq Eng 33(1):38–53

Tasalloti SMA, Indraratna B, Rujikiatkamjorn C, Heitor A, Chiaro G (2015a) A laboratory study on the shear behaviour of mixtures of coal wash and steel furnace slag as potential structural fill. ASTM Geotech Test J 38(4):361–372

Tasalloti SMA, Indraratna B, Chiaro G, Heitor A (2015b) Field investigation on compaction and strength performance of two coal wash-BOS slag mixtures. In: International foundations congress and equipment Expo 2015, IFCEE 2015, San Antonio, United States, Geotechnical Special Publication, vol 256, pp 2359–2368

Tsang HH, Lo SH, Xu X, Sheikh MN (2012) Seismic isolation for low-to-medium-rise buildings using granulated rubber-soil mixtures: numerical study. Earthq Eng Struct Dynam 41 (14):2009–2024

Wang G (2010) Determination of the expansion force of coarse steel slag aggregate. Constr Build Mater 24(10):1961–1966

Zheng YF, Kevin SG (2000) Dynamic properties of granulated rubber/sand mixtures. Geotech Test J 23(3):338–344

Use of Glass Grid and SAMI as Reinforced Interlayer System in Runway

Satyajit Roy and Mahabir Dixit

Abstract Runways are made of rigid as well as flexible pavement. Generally, flexible pavement is sandwiched between two rigid ends. Traffic loading, age hardening, or temperature cycling typically cause fatigue and reflective cracking in flexible pavement. When cracking is present, the traditional remedy has been to apply thicker asphalt overlays. Reinforcement using an interlayer system has been demonstrated as a multipurpose solution to improve the performance, extend service life and thus to reduce maintenance cost of runway pavement. Among a large number of existing interlayer systems, glass grid along with SAMI (Stress Absorbing Membrane Interlayer) have shown effective use in pavement reinforcement with a hot mix asphalt overlay. Glass grids are composed of series of fiberglass strands coated with an elastomeric polymer and formed into a grid structure. However, SAMI is a layer of PMB (polymer-modified bitumen), which shall be laid over glass grid surface, together with a covering of aggregate chips, spread, and rolled to retard reflection cracking. This paper presents the characteristics (physical properties) of glass grid fiber and SAMI layer, methodology of laying of the layers, their theoretical aspects, field tests for checking their adhesiveness, etc.

Keywords Glass grid · SAMI · Reflection cracking · PMB

1 Introduction

A reflection crack is a one of the most common types of failure in asphalt pavement, which is impacted by traffic and thermal loading. As per Plug and de Bondt (2010), reflective cracking is due to the inability of the overlay to withstand shear and tensile actions induced by the old pavement. Reflection cracking can also happen in

S. Roy (✉) · M. Dixit
Central Soil and Materials Research Station, New Delhi 110016, Delhi, India
e-mail: satyajit_wow@yahoo.com

M. Dixit
e-mail: mdixit64@gmail.com

R. Sundaram et al. (eds.), *Geotechnics for Transportation Infrastructure*,
Lecture Notes in Civil Engineering 29,
https://doi.org/10.1007/978-981-13-6713-7_23

overlays placed on joints or cracks in concrete pavement. The pavement can be maintained by overlay. Cracks under the overlay cause stress concentration at the bottom of the overlay. Due to the repeated stress concentration, a crack starts in the overlay that has similar shape to the crack in the old pavement. Interlayer systems have been receiving increasing attention from the pavement community as efficient reinforcement solutions for pavements, to delay crack initiation and propagation. However, the mechanisms underlying the mechanical behavior of these interlayer systems are not fully understood, and the most appropriate interlayer systems and their optimal location in the pavement system are still a subject of discussion.

As per Nguyen et al. (2013), although the range of commercially available interlayer products is very wide, the large varieties of products can be classified in a limited number of categories.

They include:

- Sand asphalt,
- SAMIs (Stress Absorbing Membrane Interlayer),
- Paving fabrics or geotextiles,
- Paving grids (steel, glass fiber, and polymeric),
- Composites thereof.

In this paper, use of glass grid and SAMI as reinforced interlayer system in runways constructed and maintained by Military Engineering Services will be discussed.

1.1 Definition of Glass Grid and SAMI

Glass grids are made of series of fiber glass strands coated with an elastomeric polymer and formed into a grid structure having remarkably high tensile strength and high modulus of elasticity. It is self-adhesive material, whose bonding with existing surface mainly depends on surface cleanliness, wrinkle-free laying and accurate rolling with pneumatic tire roller. A polymer coating generally soaks glass grids. The polymer coating helps higher compatibility and adhesion with existing bituminous surface. Polymer increases mechanical performance and protection against various chemicals and abrasive materials. Glass fiber grids have a square or rectangular open mesh form. The open structure helps in aggregate interlock between paving courses, restrains lateral movement of the aggregate, and decreases shear potential of pavement layers. Glass fiber grids are generally used with a tack coat of PMB 70 to enhance their performance. As per Plug and de Bondt (2010), a polymer-modified bond coat will generate improved (initial) shear strength. It will also have higher shear energy than a standard tack coat during service life of the pavement.

However, SAMI is a layer of PMB (polymer-modified bitumen), which shall be laid over glass grid surfaces, together with a covering of aggregate chips, spread and rolled to retard reflection cracking, having 6 mm average thickness. Cross section of a typical SAMI layer is shown in Fig. 1.

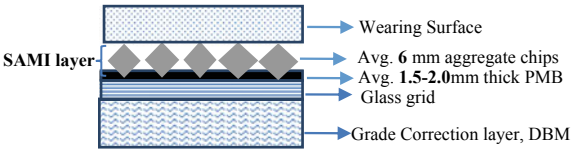

Fig. 1 Cross section of SAMI

In SAMI, PMB and aggregate chips are not mixed together before application, rather bitumen @11 kg/10 m^2 and chips of average thickness 6.00 mm are applied separately as different activities. As a result, chips do not get fully coated with bitumen, only up to height of 1.5–2.00 mm depth of aggregate from bottom it remain filled with bitumen as shown in Fig. 1. Over this uncoated part of aggregates, final wearing layers are laid. Therefore, from the above discussion, one can easily conclude that SAMI got poor adhesion with final wearing surface, i.e. dense asphaltic concrete.

The ability of asphalt to withstand tensile stresses is limited. This reflective cracking is due to the inability of the overlay to withstand shear and tensile actions induced by the old pavement. In order to delay, if not completely eliminate the possibility of reflection cracks, state-of-the-art fiber reinforced glass grids along with SAMI (Stress absorbing Membrane Interlayer) are used over grade correction layer of DBM (Dense Bituminous Macadam) to redirect the crack energy.

Glass grid and SAMI are used in asphalt layers, for reinforcement of a deteriorated pavement, or between new asphalt layers. Glass grid and SAMI shall not be used directly on existing old cracked and undulated surface. First cracks are to be repaired, and grade correction layer shall be laid before putting Glass grid and SAMI as interlayer system in existing surface of runway resurfacing. There are other purposes for which interlayer system can be used, i.e. moisture barriers, stress relieving interlayer, and reinforcement. Glass grid and SAMI reduce reflective cracking, water infiltration and development of fatigue cracking; prolong the maintenance life of runway and increases stability as well as structural integrity of runway. Poor bonding with the asphalt material and difficulties to recycle the reinforced asphalt materials are only disadvantages with glass grid. The close view of glass grid and SAMI layer is presented in Fig. 2.

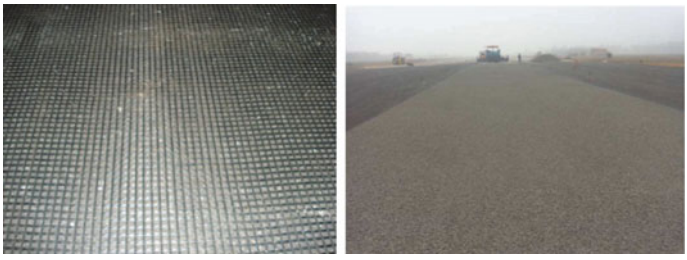

Fig. 2 Close view of glass grid and SAMI

2 Details of Fiber Glass Grid

The glass grids having grid size of 12.5 mm × 12.5 mm c/c are of self-adhesive type which come in the package of 100 m × 3 m and laid with a transverse lap of 100 mm and longitudinal lap of 50 mm. No movement of men and machineries is allowed on the laid glass grid.

2.1 Material Characteristics

As per Tensar International (2008), there are various types of glass grid, viz. type 8501, 8502, 8522, 8512, 8550, CG 50, and CG 100. Varity of products of glass grid system ensure optimum reinforcement benefits as the product is matched to the specific needs and material characteristics of a project. The most important considerations when selecting a product are aperture size, tensile strength, and grid coverage and moisture barrier. The typical materials that are used in airfield pavements are glass grid Type 8501. These materials are consisting of glass fiber strands arranged in a grid structure of mesh size 12.5 mm × 12.5 mm (Fig. 1) covered with a polymer (PMB 70) coating and a pressure sensitive adhesive. It is also important to mention that there is no loss of strength at paving temperatures, and the material is characterized by very high tensile strength, low elongation with high asphalt compatibility, physical durability, and thermal and chemical stability. The physical properties of fiber reinforced glass grids are presented in Table 1.

2.2 Workmanship and Laying Methodology

Glass grid is to be laid as per section 703 of MoRT&H (2005) specification and IRC SP 59 (2002). Laying of glass grid needs high attention as the main important factor in laying is its adhesion with existing pavement surface. The pavement surface where it is

Table 1 Physical properties of glass grid (type 8501)

Physical property	Unit	Requirement	Remarks (ASTM)
Tensile strength (longitudinal and transverse direction)	kN/m	100 (min)	D6637-01 Method A
Elongation at break (longitudinal and transverse direction)	%	Less than 5	D6637-01
Mass/unit area	g/m^2	370 (min)	D5261-92
Melting point	°C	218 (min)	D276
Young's modulus	Gpa	69	C1557

to laid shall be free of oil, vegetation, sand, dirt, water, gravel, and other debris. It is laid by a mechanical device (typically with a tractor that has been modified so that the glass grid material can be front-mounted) under the supervision of manufacturer. The favorable surface temperature before laying the glass grid shall be between 5 and 60 ° C. The glass grid laid should be free from ripples, if present, then these must be removed by pulling the grid tight or in extreme cases (on tight radial), by cutting and laying flat. Overlapping is another important factor at the time of laying and lapping shall be provided both longitudinally and in transverse direction. In transverse direction, lapping shall be of 100 mm and in longitudinal direction it shall be 50 mm. After laying, glass grid shall be rolled with pneumatic tyred roller or with rubber coated roller to activate its adhesive properties. During rolling, one supervisor shall be deputed for cleaning of tyres of roller to avoid pickup of grid. After rolling and satisfactory bonding with existing surface, construction and emergency traffic may run on glass grid mesh; however, turning and braking of vehicles must be avoided on glass grid surface. Glass grid laid shall not be kept open for more than 24 h, and it shall be covered with pavement layers within same day. The minimum compacted thickness layer shall be 40 mm. Glass grid mesh must be stored in dry covered conditions free from dust, sunlight, and stocked vertically to avoid misshaped rolls. The laying of glass grids is presented in Fig. 3.

2.3 *Test of Proper Adhesion*

As per Tensar international (2008), 1 m^2 of glass grid is placed on the area to be paved and to be rolled by rubber tyred roller in order to activate self-adhesive glue. In next step, hook of spring balance to be inserted under the center of grid piece and pull to be applied upwards until grid starts to pull from the surface. If reading of spring balance comes 5 kg (11 LBS) or more than the grids are fit for paving. One has to stop the laying of glass grid immediately if grid moves or ripples. If reading of spring balance during pulling comes, less than 5 kg (11 LBS), then paving of material not be done due to poor adhesion. The rolling and adhesive testing of glass grid is presented in Fig. 4.

Fig. 3 Laying of glass grid

Fig. 4 Rolling and adhesive testing of glass grid

3 Stress Absorbing Membrane Interlayer

SAMI (Stress Absorbing Membrane Interlayer) is laid as per clause No. 522 of MoRT&H (2005) specification. It can be laid as single coat or double coat depending on type and width of crack as per table 500-47 of MoRT&H (2005). As military airfields are FOD (Foreign object disposal), sensitive and crack width beyond 1–2 mm are not acceptable, so for crack width of 1–2 mm, a single surface treatment consisting of sprayed application of polymer-modified bitumen (PMB-70) @11 kg/10 m^2 followed by application of dry stone chips of avg. thickness 6 mm have found effective. So the average thickness of SAMI layer comes out as 6 mm, where aggregate up to depth of 1.5–2.0 mm in bottom generally remains filled with polymer-modified bitumen, which is already shown in Fig. 1. Moreover, thickness and specification of SAMI are chosen keeping in mind the requirement of PCN value of airfield. The modern day's airfields require PCN-70 as their strength criteria to cope up with landing and takeoff of latest heavy aircrafts. As per Khanna and Justo (1992), Khanna and Arora (1999), Saxena (1999), Rangwala and Rangwala (2012), the pavement classification number (PCN) is an International Civil Aviation Organization standard used in combination with the aircraft classification number (ACN) to indicate the strength of a runway, taxiway, or airport apron (or ramp). This helps to ensure that the airport runway, taxiway, and apron (or ramp) are not subjected to excessive wear and tear, thus prolonging the usable life of the runway while promoting safe operations of the aircraft landing thereon. The value is calculated based on a number of factors, such as aircraft geometry, pavement's traffic patterns, bearing strength of the each pavement layer, etc. There is no method available for direct measurement of PCN, and it can be determined by combining analysis with measurement. In modern days design, the airfields where requirement of airfield strength is PCN-70, there use of 6-mm-thick SAMI layer along with glass grid are common as well as very effective for prolonging the life of runway.

3.1 Workmanship and Laying Methodology

The aggregate shall consist of crushed rock or other hard material in accordance with clause 510.2.2 of MoRT&H (2005) specification. The chips shall be single sized, clean, hard, durable, of cubical shape, free from dust and soft or friable matter, organic or other deleterious matter and conforming to grading as presented. The grading requirement of chips is presented in Table 2.

The properties of aggregate are presented in Table 3.

The requirement of PMB as per IRC SP 53 (2002) is presented in Table 4.

3.2 Rate of Spread of Binder and Aggregate

The quantity of materials required for 10 m^2 of surface for stress absorbing membrane interlayer is as per Table No. 500-47, MoRT&H (2005) and presented in Table 5.

Table 2 Grading requirement of chips

Sieve designation (mm)	Cumulative percent by weight of total aggregate passing for the nominal size 6 (mm)
10	100
6.3	85–100
3.35	0–35
1.18	0–10
0.425	0–2
0.075	0–1.5
Minimum 65% by weight of aggregate	Passing 6.3 mm, retained 3.35 mm

Table 3 Properties of aggregate

Properties	Requirement (value)	Test method
Aggregate impact value %	Not exceeding 30%	IS: 2386 (Part IV)
Flakiness index, %	Not exceeding 25%	IS: 2386 (Part I)
Water absorption, %	Not exceeding 1%	IS: 2386 (Part III)
Soundness, percent with sodium sulfate	Not exceeding 12%	IS: 2386 (Part V)
Coating test for stripping	More than 95% coating	AASHTO T-AASHTO T-182

Table 4 Requirement of PMB as per IRC SP 53 (2002)

Designation	Grade and requirement PMB-70	Method of test
Penetration at 25 °C 0.1 mm, 100 gm, 5 s	50–90	IS: 1203-1978
Softening point (R&B) °C, minimum	55	IS: 1205-1978
Ductility at 27 °C, cm	+60	IS: 1208-1978
Flash point, by COC, °C, minimum	220	IS: 1209-1978
Elastic recovery of half thread in ductilometer at 15 °C, %, minimum	75	ASTM-D-5976 1996 Appendix-I
Separation, difference in softening point, R&B, C, maximum	3	ASTM-D-5976 1996 Appendix-II
Viscosity at 150 °C, Poise	2–6	IS: 1206-1978
Thin film oven test on residue, (TIOT) (IS: 9382-1992)		
Loss in weight, % maximum	1.00	IS: 9382-1982
Increase in softening point, °C, maximum	6.00	IS: 1205-1978
Reduction in penetration of residue at 25 °C, %, maximum	35	IS: 1205-1978
Elastic recovery of half thread in ductilometer at 25 °C, % minimum	50	ASTM-D-5976 1996 Appendix-I

Table 5 Quantity of materials required for 10 m^2 of surface for stress absorbing membrane interlayer

Type/width of crack	Specification	Quantity of binder kg/10 m^2	Quantity of chipping
1–3 mm	Single coat	11	0.11 cm of 6 mm size chips

3.3 Workmanship and Laying Methodology

SAMI is laid as per clause no. 522 of MoRT&H (2005) specification.

Weather and seasonal Limitations: Spreading of SAMI require water free surface, i.e. dry surface. SAMI shall not be laid in rains, dust storms, and fogs. Temporary arrangement for covering the surface shall be made to protect the surface in case of partial rainy days. After rains, air jets shall be used for speedy drying of surface.

Aggregates, which are to be used as SAMI layer shall be absolutely, dry for proper adhesion with PMB-70. So to get absolute dry materials, aggregates shall be dry heated in hot mix plant.

Preparation of surface: Here glass grid and SAMI are used as a reinforced interlayer. First glass grid shall be laid which is already discussed in para 2.2, after that SAMI laid over glass grid. The glass grid and SAMI layer shall not be laid directly on existing surface. Due to prolong use and repeated load application on runway, longitudinal as well transverse gradient of runway gets disturbed and it

develops different types of cracks. Therefore, before laying cracks are to be repaired first, then grade correction layer is to be applied to bring back the surface in proper gradient as per ICAO norms. Dense bituminous macadam (DBM) can be used as grade correction layer. Over that grade correction layer, glass grid and SAMI shall be laid. If cracks and gradient of existing surface are not corrected before application of glass grid and SAMI, then the adhesion of interlayer system with existing surface will not be proper, as a result, effectiveness of interlayer system will be reduced. Therefore, repair of cracks and correction of gradient is vital activity for proper functioning of interlayer system.

Application of modified bitumen: After preparation of surface, first polymer-modified bitumen shall be heated to 160–170 °C. It will be sprayed on the clean and dry surface in a uniform manner @11 kg/10 m^2 with the help of pressure sprayer having self-heating arrangement and spray nozzle bar capable of spraying modified bitumen uniformly at specified rate. At the time of spraying of hot PMB, precautions shall be taken to avoid excessive deposits of binder, which may be caused by stoppage or staring of sprayer or through leakage. Excessive deposit of bitumen if found in localized points shall be corrected before application of cover material.

Application of Cover material: Spreading of chips shall start within few minutes of spraying of polymer-modified bitumen. After spreading of chips, manual sweeping of chips to be ensured for uniform spreading of material.

Rolling: The next activity is rolling with rubber tyred self-propelled rollers. The roller shall have a minimum operating weight 8–10 tones. Due to rolling, aggregates get partially immersed in PMB as shown in Fig. 1. Rolling shall be continued until the chips are firmly embedded in modified bituminous material. Excessive rolling leading to crushing of aggregate shall be avoided. The laying of glass grid, SAMI, and DBM is presented in Fig. 5.

Fig. 5 Laying of glass grid, SAMI, and DBM

4 Reinforcement Mechanism

With passage of time, due to extensive use of runway, severe distresses like spalling of joints/edges, localized depressions, dislodging of aggregates and extensive cracks develops in pavement, which results in poor riding quality and severe FOD (Foreign object disposal) hazards. In addition, longitudinal and transverse gradient of runway get disturbed badly to the extent beyond the limit of ICAO norms. For the above-mentioned reasons, resurfacing of runways becomes necessary for good quality flying of latest heavy aircrafts. In the earlier times, the concept of interlayer system was not there in runway resurfacing works; moreover, aircraft specifications and number of flying hours were not also similar compared to present-day scenario. Nowadays aviation industry has started getting momentum and government is also giving special attention in this area. The specification as well as types of passenger/defense-related aircrafts also changed. Moreover, number of flying hours (take off/landing) has also increased considerably to cope with the requirement of public as well as defense requirement. It has seen resurfacing with conventional method, i.e. without using interlayer system only sustain for 2–3 years, but on the other hand, resurfacing using inter layer system can give good quality surface for flying up to 8–10 years. It is believed that stress develops from existing old surface/cracks due to application heavy aircrafts loads (which is known as reflection cracks) started to move upward until and unless it reaches reinforcement layer. As soon as it touches interlayer system and if the interlayer is stiff enough compared to surrounding materials, the crack will turn horizontally and will move along with interlayer system until its energy exhausted. However, this is an assumption; detail analysis of function of interlayer system is still a subject of research. As per Nguyen et al. (2013), glass fiber grids and SAMI act principally as a reinforcement interlayer system helping to delay reflective cracking. The process of energy dissipation is presented in Fig. 6.

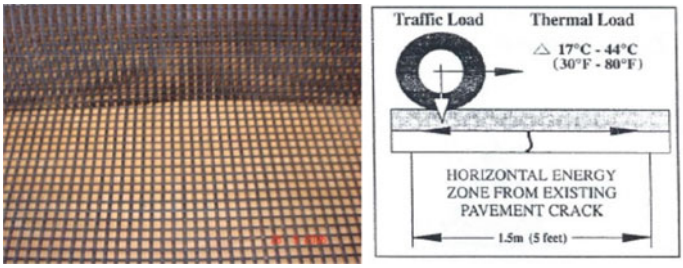

Fig. 6 Energy dissipation

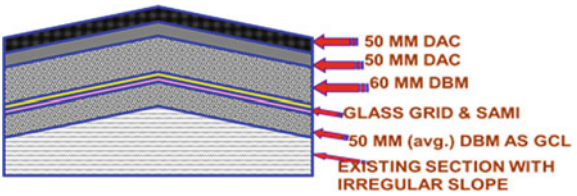

Fig. 7 Cross section of flexible overlay

5 Cost Comparison with Conventional Method

General cross section of resurfacing of flexible pavement of airfield taken from one of the project of runway in North East is presented in Fig. 7.

Designed cross sections of flexible overlays may vary from place to place depending on existing PCN value of runway where repair to be carried out, requirement of new PCN value of flexible overlay, physical properties of materials to be used for construction, other environmental factors, etc. Conventional methods of repair of flexible overlay means repair without using interlayer system. As per the literature of Tensor International Corporation, conventional method of repairing was common some 30 years back. However, due to introduction of heavy modern aircrafts, increase of traffic loads, i.e. increase in number of landing and tack off operations of aircrafts, increase in temperature variations and other climatic factors, etc. it is observed that runway repaired by conventional method cannot provide the best surface for flying more than 1.5–2 years. On the other hand, repair involving glass grid and SAMI along with other asphaltic layers as shown in Fig. 7 prolong the life of airfield runway up to 8–10 years.

Analysis of rates: Rates of different layers as per Fig. 7 reflected below are taken form quoted rates of contractor in one of the runway project of North East.

For Conventional method: Cost in Rs. (Per 10 m^2)

(1) Preparation of surface and tack coat (7.5 kg) = 450.00
(2) DBM (Dense Bituminous macadam) 50 mm = 600.00
(3) Tack coat of VG-10 @5 kg = 250.00
(4) DBM (Dense Bituminous macadam) = 650.00
(5) DAC (Dense asphaltic concrete) 100 mm = 1200.00
(6) Tack coat of PMB-70 @3 kg = 160.00
Total (Per 10 m^2) = Rs. 3310.00

Method using glass grid and SAMI: Cost in Rs. (Per 10 m^2)

(1) Glass grid, its laying, rolling complete = 1900.00
(2) SAMI (including spreading PMB and chips) = 750.00
Total (Per 10 m^2) = Rs. 2650.00

From above analysis, it is clear that cost of repair almost become double when we use glass grid and SAMI. Already explained above, life of conventional repair is 1.5 to 2 years, whereas in interlayer system, life increases up to 10 years. So in case

of conventional repair, within periods of 10 years, few more additional repairs (3–4 times) have to be initiated for getting quality flying surface. Moreover, the involvement of time for repeated planning and execution as well as disturbance of flying operations during execution will cause more inconvenience to all.

6 Conclusions

Reinforcement using an interlayer system has been demonstrated as a multipurpose solution to improve the performance, extend service life, and thus to reduce maintenance cost of runway pavement. Among a large number of existing interlayer systems, glass grid along with SAMI (Stress Absorbing Membrane Interlayer) has shown effective use in pavement reinforcement with a hot mix asphalt overlay. The glass fiber-based reinforced system has been used for 30 years and subject of many studies. Two main features, which qualify the property of glass grid, are adhesion of grid to asphalt material and the resistance to cracking of grid reinforced asphalt layer. Out of these two, adhesive property can be tested at site only with procedure described above, and other test is laboratory method. Another important property of glass grid is their resistance to damage during construction. As per Nguyen et al. (2013), the mechanisms of action of these reinforcements are still not fully understood, and the design of reinforced pavements remains mainly empirical and this remains an important subject for research.

Acknowledgements We would like to express my thanks of gratitude to engineers of Military Engineering Services and special thanks to Col Sudeep Mishra who shared their experiences about challenges faced in resurfacing of runway in North East region and helped me a lot in writing this paper.

References

IRC SP 59 (2002) Guidelines for use of Geotextiles in road pavements and associated works, New Delhi, India

IRC SP 53 (2002) Guidelines for use of modified bitumen in road construction, New Delhi, India

Khanna SK, Arora MG (1999) Manual of airport planning and design. Nem Chand & Brothers, Roorkee

Khanna SK, Justo CEG (1992) Manual of highway engineering. Nem Chand & Brothers, Roorkee

MORT&H (2005) Road and bridges works. Specification, Indian Road Congress

Nguyen ML, Kerzreho JP, Hornych P (2013) Review of glass fiber grid use for pavement reinforcement and APT experiments at IFSTTAR. Editions Hermes 14(Supplement 1)

Plug CP, de Bondt AH (2010) Adhesion of reinforcement grids in asphalt overlays. Prepared for 5th world congress on emulsions held on Lyon, France

Rangwala SC, Rangwala PS (2012) Manual of airport planning and design, Charotar

Saxena SC (1999) Manual of airport engineering, Charotar

Tensar International Corporation Atlanta (2008) Manual of glass grid pavement reinforcement system, Georgia, USA

Use of Jute Geotextile in Strength Enhancement of Soft Subgrade Soil

Shalinee Shukla, R. P. Tiwari, Vaishali Rajbhar and Ayush Mittal

Abstract Construction of pavement on soft or weak soils is highly unsecure since such soils have low shear strength and California bearing ratio (CBR), high compressibility, liquefaction potential, and differential settlement. In India, more than 20% land area is covered with such type of soils. The pavement constructed over such soils will deteriorate significantly under heavy wheel loads, leading to substantial increase in construction and maintenance costs. In order to overcome such problems, some soil reinforcement technique has to be adopted because removal and replacement of soil will lead to heavy economic burden. Therefore, in the present investigation, open weave jute geotextile is chosen as the reinforcement material. The geotextile is placed in single and multiple layers at various depths from top of mold, and heavy compaction and soaked CBR tests are conducted. The test results indicate improvement in maximum dry density (MDD) for all reinforced cases as compared to virgin soil. Increase in CBR is observed for all single and double layer reinforced specimens and for one triple layer reinforced case. Maximum improvement of 54, 102, and 52%, respectively, is reported when geotextile is placed in single layer at 0.2H depth, double layer at 0.2H and 0.4H depths, and triple layer at 0.2H, 06H, and 0.8H depths from top of specimen, whereas it decreases even below to virgin soil value for four layers reinforcement. Thus, it can be concluded that jute geotextile can be effectively used as reinforcement material which not only boosts rural economy but also contributes in carbon foot print reduction to a great extent.

Keywords California bearing ratio · Compaction · Jute geotextile · Strength · Subgrade

S. Shukla · R. P. Tiwari · V. Rajbhar · A. Mittal (✉)
Department of Civil Engineering, MNNIT Allahabad, Allahabad 211004, UP, India
e-mail: ayushmittalce0012@gmail.com

S. Shukla
e-mail: sshukla@mnnit.ac.in

R. P. Tiwari
e-mail: rpt@mnnit.ac.in

R. Sundaram et al. (eds.), *Geotechnics for Transportation Infrastructure*,
Lecture Notes in Civil Engineering 29,
https://doi.org/10.1007/978-981-13-6713-7_24

1 Introduction

The need to set up more infrastructure projects to meet the demand of growing needs of population compels the engineers to make use of weak soils which were earlier left out. The pavement constructed over such soils will significantly increase the construction and maintenance costs due to increase in crust thickness and frequent failures. The pavement performance depends mainly on the properties of soil subgrade since it serves as its foundation. This brings the role of reinforced earth technique into picture which can be in the form of strips, rods, sheets, and fibers. Till now, conventional materials such as lime, cement, and fly ash are used for soil reinforcement but due to lack of strength isotropy, poor mixing, and health issues related to dust, the more and more use of geosynthetics are made nowadays.

Many studies have been conducted on use of synthetic geotextiles (Elshakankery et al. 2013; Nair and Latha 2009; Tuna and Altun 2012; Noorzad and Mirmoradi 2010; Ghazavi and Roustaei 2013; Rawal and Anaandjiwala 2007; Ghosh and Dey 2009), polymeric geogrids (Zornberg and Gupta 2009; Kuity and Roy 2013; Leshchinsky et al. 2016; Brown et al. 2007), and synthetic fibers (Chore et al. 2011; Tang et al. 2007; Consoli et al. 2010; Akbulut et al. 2007; Botero et al. 2015) on the strength improvement of soil. Prabakar and Sridhar (2002) used sisal fibers, Lekha et al. (2015) used Areca nut coir, Bera et al. (2009) studied the effect of jute geotextile on fly ash, Lekha and Kavitha (2006) used coir geotextiles for stabilizing waterfront clay dykes, Qu et al. (2013) used wheat straw fibers, Rao and Nasr (2012) used linen fibers, Anggraini et al. (2015) used coir fibers, Ahmad et al. (2010) studied the effect of using oil palm empty fruit bunch fiber, Marin et al. (2010) used sheep wool, Bouhicha et al. (2005) used barley straw, Estabragh et al. (2013) used palm fibers to study the various properties of coarse and fine grained soils.

In the present investigation, influence of open mesh woven jute geotextile on the strength behavior of poor subgrade soil is studied. The jute geotextile sheets are placed in single and multiple layers at various depths of soil subgrade, and heavy compaction and soaked CBR tests are conducted.

2 Materials Used

2.1 Soil

The soil used in this study is obtained from Meja (25.14°N, 81.97°E), Allahabad district, Uttar Pradesh, India. The area is largely covered with fine grained soils. The top soil is removed while sampling since it contains organic matter and other foreign materials and after reaching a depth of 1 m below ground surface, soil is collected. The soil is classified as silt of intermediate compressibility (MI) as per Indian Standard Classification System (IS 1498-1970). Table 1 shows the various geotechnical properties of soil. Grain size distribution curve of soil is shown in Fig. 1.

Table 1 Various properties of soil

Properties	Value
Atterberg's limits	
(a) Liquid limit (%)	36
(b) Plastic limit (%)	19
(c) Plasticity index (%)	17
Grain size distribution	
(a) Gravel (%)	0.03
(b) Sand (%)	9.40
(c) Silt (%)	67.57
(d) Clay (%)	23.00
Soil classification (ISCS)	Silt of intermediate compressibility (MI)
Water content (%)	16.80
Specific gravity	2.70
Free swell index (%)	32.50
pH value	7.54
Optimum moisture content (%)	13.60
Maximum dry density (kN/m^3)	18.80
Soaked CBR (%)	3.83

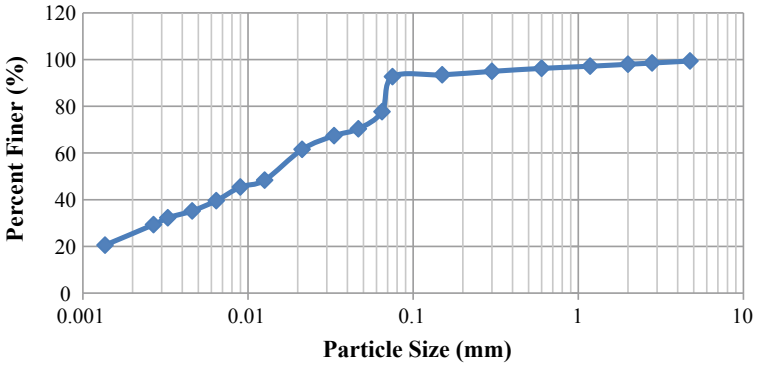

Fig. 1 Grain size distribution curve for soil

2.2 *Geotextile*

The geotextile used in this study is open mesh woven jute geotextile of 500 gsm (gram per square meter). The jute geotextile supplied by Indarsen Shamlal Pvt. Ltd., Kolkata is shown in Fig. 2. The index properties of jute geotextile as provided by manufacturer are shown in Table 2.

Fig. 2 Open mesh woven jute geotextile

Table 2 Index properties of jute geotextile

Particulars	Value
Mass per unit area (g/m^2) at 20% water content	500
Open area (%)	50
Strength (kN/m)	10/7.5 (MD/CD)
Thickness (mm)	4
Durability (years)	4
Water holding capacity on dry weight (%)	500

3 Experimental Details

A series of heavy compaction [IS 2720 (Part 8)-1983] and soaked CBR tests [IS 2720 (Part 16)-1987] have been carried out on soil sample reinforced with jute geotextile in single and multiple layers, placed at various depths of soil subgrade. Figure 3 illustrates the various positions of jute geotextile in soil specimen. The term H used is the total height of soil sample in testing mold which is 127.3 mm for both compaction and CBR test.

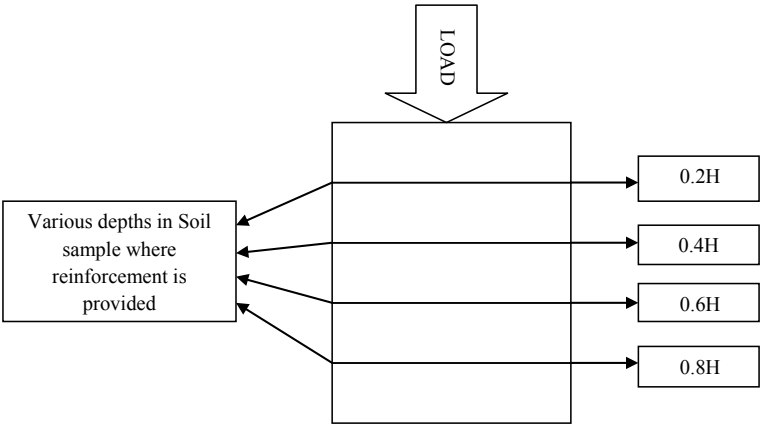

Fig. 3 Position of geotextile layer in soil

4 Results and Discussions

4.1 Heavy Compaction

The compaction results of soil reinforced with and without jute geotextile sheets are shown in Table 3. It is observed that MDD for all geotextile reinforced specimens are more as compared to virgin soil. The MDD for virgin soil is 18.60 kN/m^3 which increases to maximum of 19.95, 19.38, 19.31, and 18.73 kN/m^3, respectively, for single, double, triple, and four layers of reinforcement. This increase in MDD is due to greater compactness achieved with jute geotextile, resulting in reduction of voids with void spaces occupied by solid particles having greater specific gravity. The optimum moisture content (OMC) increased with increase in number of jute geotextile layer. The OMC for virgin soil is 13.60% which changes to 7.01, 11.76, 12.61, and 13.80%, respectively, for single, double, triple, and four layers of reinforcement. This increase in OMC is attributed to water absorption tendency of natural jute fiber.

4.2 California Bearing Ratio

The CBR results of soil specimen reinforced with and without jute geotextile sheets are shown in Table 4. Significant improvement in CBR is observed for soil specimen reinforced with geotextile in single and double layers. The CBR for

Table 3 OMC-MDD values of soil reinforced with jute geotextile

Position of jute geotextile from top of specimen	Experimental value	
	MDD (kN/m^3)	OMC (%)
Virgin soil	18.60	13.60
0.2H	19.45	12.49
0.4H	19.25	12.81
0.6H	19.95	7.01
0.8H	18.91	14.80
0.2H and 0.4H	19.33	14.05
0.4H and 0.6H	19.38	11.76
0.4H and 0.8H	19.28	12.51
0.6H and 0.8H	19.37	12.26
0.2H, 0.4H and 0.6H	19.31	13.43
0.2H, 0.4H and 0.8H	19.21	12.61
0.2H, 0.6H and 0.8H	18.73	14.42
0.4H, 0.6H and 0.8H	19.17	13.77
0.2H, 0.4H, 0.6H and 0.8H	18.73	13.80

Table 4 Soaked CBR values of soil specimen reinforced with Jute geotextile

Position of jute geotextile from top of specimen	CBR (%)
Virgin soil	3.83
0.2H	5.92
0.4H	5.42
0.6H	4.96
0.8H	4.86
0.2H and 0.4H	7.80
0.4H and 0.6H	5.60
0.4H and 0.8H	5.32
0.6H and 0.8H	5.23
0.2H, 0.4H and 0.6H	3.48
0.2H, 0.4H and 0.8H	3.42
0.2H, 0.6H and 0.8H	5.85
0.4H, 0.6H and 0.8H	3.33
0.2H, 0.4H, 0.6H and 0.8H	3.48

unreinforced soil is 3.83% which increases to 5.92, 5.42, 4.96, and 4.86%, respectively, for single layer of geotextile at 0.2H, 0.4H, 0.6H, and 0.8H depth from top of specimen. This value further increases to 7.80, 5.60, 5.32, and 5.23%, respectively, corresponding to double layer reinforcement at 0.2H and 0.4H, 0.4H and 0.6H, 0.4H and 0.8H and 0.6H and 0.8H depths from top of mold. However, with further increase in number of geotextile layers (triple and four), significant reduction in CBR is taking place except for one triple layer reinforcement condition (0.2H, 0.6H, and 0.8H depths) where CBR of 5.85% is reported. This increase in CBR is due to greater resistance offered by jute geotextile sheets to penetration of plunger. However, in triple and four layer reinforcement conditions, integrity of soil system is lost due to separation of all the soil layers completely from each other and it no longer behave as a single unit, causing reduction in strength.

5 Conclusions

Based on the laboratory results and discussions made the following conclusions are drawn:

Maximum improvement in dry density is observed for single layer reinforcement condition and as the number of reinforcing layer increases reduction in MDD is noticed, but it remains more than unreinforced soil sample indicating improvement in strength and stability. The pavement constructed over such stabilized subgrade will perform better under heavy wheel loads. OMC increases with decrease in MDD as the number of jute geotextile layer increases, indicating hydrophilic nature of jute. The CBR has increased to maximum of 5.92, 7.80, and 5.85%, respectively, for single, double, and triple layer of reinforcement as against 3.85% for

unreinforced soil. This increase in CBR will cause significant reduction in thickness requirement of pavement, thus saving costly base and sub-base aggregate materials. It is also concluded that improvement in geotechnical properties of soil with geotextile will occur up to certain number of reinforcing layers and with further increase in number of reinforcing layers, reduction in strength will start.

These conclusions can be used effectively in area of pavement construction on soft soils where some reinforced earth technique has to be adopted. It will also be a boon for jute industry since a new field of application will emerge as their traditional use in gunny bags are facing severe competition from synthetic products.

References

Ahmad F, Bateni F, Azmi M (2010) Performance evaluation of silty sand reinforced with fibers. Geotext Geomembr 28:93–99

Akbulut S, Arasan S, Kalkan E (2007) Modification of clayey soils using scrap tire rubber and synthetic fibers. Appl Clay Sci 38:23–32

Anggraini V, Asadi A, Haut BBK, Nahazanan H (2015) Effects of coir fibers on tensile and compressive strength of lime treated soft soil. Measurement 59:371–381

Bera AK, Chandra SN, Ghosh A, Ghosh A (2009) Unconfined compressive strength of fly ash reinforced with jute geotextiles. Geotext Geomembr 27:391–398

Botero E, Ossa A, Sherwell G, Shelley EO (2015) Stress-strain behavior of a silty soil reinforced with polypropylene terephthalate (PET). Geotext Geomembr 43:363–369

Bouhicha M, Aouissi F, Kenai S (2005) Performance of composite soil reinforced with barley straw. Cement Concr Compos 27:617–621

Brown SF, Kwan J, Thom NH (2007) Identifying the key parameters that influence geogrid reinforcement of railway ballast. Geotext Geomembr 25:326–335

Chore HS, Kumthe AA, Abnave SB, Shinde SS, Dhole SS, Kamerkar SG (2011) Performance evaluation of polypropylene fibers on sand-flyash mixtures in highways. J Civ Eng (IEB) 39 (1):91–102

Consoli NC, Bassani MAA, Festugato L (2010) Effect of fiber-reinforcement on the strength of cemented soils. Geotext Geomembr 28:344–351

Elshakankery MH, Almetwally AA, Tawfik KA (2013) Experimental study of bearing capacity for Egyptian soils reinforced by geotextiles. J Appl Sci Res 9(3):2378–2385

Estabragh AR, Bordbar AT, Javadi AA (2013) A study on the mechanical behavior of a fiber-clay composite with natural fiber. Geotech Geol Eng 31:501–510

Ghazavi M, Roustaei M (2013) Freeze-thaw performance of clayey soil reinforced with geotextile layer. Cold Reg Sci Technol 89:22–29

Ghosh A, Dey U (2009) Bearing ratio of reinforced fly ash overlaying soft soil and deformation modulus of flyash. Geotext Geomembr 27:313–320

Kuity A, Roy TK (2013) Utilization of geogrid mesh for improving the soft subgrade layer with waste material mix compositions. Procedia Soc Behav Sci 104:255–263

Lekha KR, Kavitha V (2006) Coir geotextile reinforced clay dikes for drainage of low-lying areas. Geotext Geomembr 24:38–51

Lekha BM, Goutham S, Shankar AUR (2015) Evaluation of lateritic soil stabilized with Areca nut coir for low volume pavements. Transp Geotech 2:20–29

Leshchinsky B, Evans TM, Vesper J (2016) Microgrid inclusions to increase the strength and stiffness of sand. Geotext Geomembr 44:170–177

Marin CG, Gomez CR, Petric J (2010) Clay-based composite stabilized with natural polymer and fiber. Constr Build Mater 24:1462–1468

Nair AM, Latha GM (2009) Bearing resistance of geosynthetic reinforced soil-aggregate systems. In: Indian geotechnical conference, Guntur, India, pp 185–188

Noorzad R, Mirmoradi SH (2010) Laboratory evaluation of the behaviour of a geotextile reinforced clay. Geotext Geomembr 28:386–392

Prabakar J, Sridhar RS (2002) Effect of random inclusion of sisal fiber on strength behaviour of soil. Constr Build Mater 16:123–131

Qu J, Li C, Liu B, Chen X, Li M, Yao Z (2013) Effect of random inclusion of wheat straw fibers on shear strength characteristics of Shanghai cohesive soil. Geotech Geol Eng 31:511–518

Rao SVK, Nasr AMA (2012) Laboratory study on the relative performance of silty-sand soils reinforced with linen fiber. Geotech Geol Eng 30:63–74

Rawal A, Anaandjiwala R (2007) Comparative study between needlepunched nonwoven geotextile structures made from flax and polyester fibers. Geotext Geomembr 25:61–65

Tang C, Shi B, Gao W, Chen F, Cai Y (2007) Strength and mechanical behavior of short polypropylene fiber reinforced and cement stabilized clayey soil. Geotext Geomembr 25:194–202

Tuna SC, Altun S (2012) Mechanical behaviour of sand-geotextile interface. Sci Iran Trans A: Civ Eng 19(4):1044–1051

Zornberg JG, Gupta R (2009) Reinforcement of pavements over expansive clay subgrades. In: 17th international conference on soil mechanics and geotechnical engineering, Alexandria, Egypt, pp 765–768

Part III
Transportation Geotechnics in Underground Construction

Geotechnical Design of Underground Infrastructure—Outlining the Observational Approach

Florian Krenn

Abstract Tunneling for infrastructure has got a long tradition, and has become more and more important in the last years in India. The topographical features of India—the Himalayas as the best example—and the growth of urban spaces make tunneling an important component in many infrastructure projects, thus putting geotechnics for underground works into a key role. Geotechnics for tunneling needs therefore to be approached in a comprehensive manner, from investigation, ground description, and subsequent design to the implementation. The observational approach is in the opinion of the author the first choice for economical geotechnical works, with different depths of application depending on the project boundary conditions and risk appreciation.

Keywords Tunneling · Observational approach · NATM · Risk management

1 Introduction

The economic development of countries is highly dependent on their infrastructure. Even in the information age, the transport of goods and persons is an inevitable prerequisite to get goods and services to the place where they are needed. It can be coined as infrastructure being the link between demand and supply. Any landbound means of transport has an inherent linear sphere of influence, whereas the shipping and air traffic are in principle pointwise connections, leading to concentration of people and goods in one place. The distribution from such points of concentration (harbors, airports) requires usually landbound, i.e., linear, means of transport.

Since landbound means land use and dependence on the landform configuration, it becomes inevitable to put infrastructure below the ground (tunnels) or above the ground (bridges). The main difference between tunnels and bridges as "artificial" structures for infrastructure—and infrastructure includes apart from rail and road-

F. Krenn (✉)
Geoconsult India Pvt. Ltd., Gurgaon 122016, India
e-mail: florian.krenn@geoconsult.co.in

R. Sundaram et al. (eds.), *Geotechnics for Transportation Infrastructure*,
Lecture Notes in Civil Engineering 29,
https://doi.org/10.1007/978-981-13-6713-7_25

ways also cables, water ducts, sewage ducts, air ducts, etc.—is that bridges by nature have limited points of contact to the ground, whereas tunnels are inside the ground and that means full interdependence with all existing structures and the ground in all respects, as well as influence onto the structures above the tunnel.

1.1 Geotechnical Design for Tunneling

Tunneling happens within the ground—be it through mountains or be it below the surface of a busy city. The main requirement for successful and economical tunneling is to understand the ground. The ground which a tunnel is developed through is load and building material at the same time. This stipulation has the consequence that the behavior (in the engineering sense) of the ground has to be described.

"Describing" the ground comprises the following activities

- Developing a Geological Model, through field and desk studies
- Geotechnical investigations with the objective to get the material properties for certain loading conditions (tests) and to confirm and refine the initial geological model
- Development of a Model to describe the behavior of the ground due to tunneling
- Assessment of the impact of support measures onto the ground behavior, with the objective of ensuring the stability of the opening, and of the behavior ground and support (system behavior)

The description of the ground behavior is part of a proper geotechnical design for tunnels; however, it is not the end of the process but the beginning.

1.2 Risk Management in Tunneling

In a linear infrastructure project of several hundreds of meters to tenths of kilometers describing every meter in detail is difficult, it is even in many tunnel projects hard to investigate the ground conditions throughout the length as overburden, accessibility, and other constraints make geotechnical investigations very costly or simply impossible.

In urban surroundings, it is also not possible to investigate everywhere, and in many places undocumented utilities, geometric deviations from original drawings, forgotten voids, and ancient structures are only encountered when the tunnel drive hits them.

So all the hazards associated with unforeseen ground conditions are there, from inadequate support, face instability, material inflow, excessive settlement to collapse. Comprehensive investigations and surveys reduce the risk substantially, also a geotechnical design which takes into account several possible forms of ground behavior, still a residual risk remains and the same has to be mitigated and brought under control.

Apart from the classical approach to risk management—identification of the risk and then developing mitigation measures the observational approach to tunneling allows a further reduction of risk.

1.3 The Observational Approach in Tunneling

The observational approach requires the following steps in addition to the steps outlined in Fig. 1:

- Putting down the expected ground conditions together with the proposed support and the expected system behavior ("Prediction")
- Development of a procedure to observe the prognosis and the behavior of the system ("Monitoring")
- Defining of actions and measures in case the monitoring highlights deviations from the Prediction
- Monitoring the impact of the measures

1.4 The New Austrian Tunneling Method (NATM)

The name "New Austrian Tunneling Method" was coined 1962 by Prof. Ladislaus van Rabcewicz; with his patent (1948) he prepared the grounds for the observational approach in tunneling, and since then it has been successfully applied in many projects and many countries, also in India. However, in some projects, NATM becomes a catchword, and the actual implementation contains only elements of NATM. This is highlighted in brief to stimulate the discussion on the actual implementation of NATM.

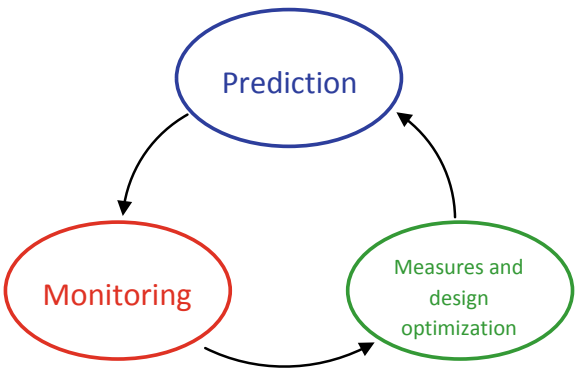

Fig. 1 Circular process of the observational approach

2 NATM—A Short Review on the Principles and the State of the Art

The "New Austrian Tunneling Method" or NATM has two peculiarities which are reflected in the name: on the one hand, it was developed mainly by Austrian engineers and miners, and this legacy is pointed out. On the other hand, the word "New"—to distinguish it from the so-called Austrian Tunneling Method, which was used up to the time the NATM came up.

Up to today, many engineers and tunneling experts worldwide have contributed to the progress of this approach to tunneling; however, the name remained NATM. NATM is employing the observational approach for tunneling and geotechnical monitoring is an integral part of NATM.

2.1 Historical Background

Prof. Rabcewicz filed a patent for a tunneling method which was based on a double concrete shell approach, where the inner (secondary) lining should be installed after the deformations have ceased. The (outer) primary lining should be installed quickly to avoid disintegration of the rock mass (loosening). The loosened rock mass is acting like a dead load onto the lining, a major shortcoming observed with the then traditional methods. Rabcewicz also proposed a waterproofing between primary and secondary lining. The point of time for installation of the inner lining should be determined based on monitoring results.

The combination of already existing materials like shotcrete (to prevent loosening of the ground) and rock bolts (now used in a systematic manner) made it possible to implement this tunneling method. The first application of a systematic support system consisting of rock bolts and shotcrete was successfully applied by Rabcewicz in 1956 in Venezuela. In 1962, Prof. Rabcewicz presented the new method during the Salzburg Colloquium and coined the name "New Austrian Tunneling Method." The breakthrough projects which were then executed were the Railway Tunnel in Schwaikheim (Germany, 1963–1965), the Massenbergtunnel in Leoben (Highway, Austria, 1964–1965). The international breakthrough of NATM came at the Tarbela project (Pakistan, 1968–1975), where the gate chambers were constructed according to NATM (Rabcewicz and Golser, 1974). The principles were successfully applied to shallow tunneling and tunneling with high overburden, and the method was adopted in other countries like Japan, India, Korea, etc. In India, the 11.2-km-long Pir Panjal (T80) railway tunnel, which is in operation since 2013, has been designed and constructed by applying NATM. The development of NATM has been dealt with in several publications (e.g. Schubert and Lauffer (2012), ITA-Austria (2012)).

2.2 Basic Principles of NATM

The following principles can be stated to be the basic principles of NATM:

- Prevent disintegration/detrimental loosening of the ground, thus keeping its strength
- Use the strength of the ground to take additional stresses resulting from the excavation
- Monitor the behavior of the system to observe stabilization process and allow for adjustments of construction measures to ground conditions

The following points need to be observed also:

- Rounded shapes to avoid stress concentrations
- Support shall ideally work as shell (support pressure to become normal forces in the lining)
- Only a closed cross section is a stiff cross section—ring closure must be obtained to activate the support pressure of the primary lining.

2.3 Further Developments and Current Status

The initial shortcomings of NATM were tackled by the tunneling community (mainly in Austria and neighboring states). Those shortcomings were the lack of accepted design rules, the missing specifications, the limited practice/training of miners, and the lack of appropriate contractual models. The quality assurance of the main support elements, rock bolts, and shotcrete had to be developed, and also the setup of the organization of a project had to be in line with the observational approach.

The issues of specifications, manpower training, and quality assurance in respect to shotcrete and rock bolts have been solved, also the contractual modalities in Austria have been brought in line, and the organizational setup was modified in a manner to take full advantage of the observational approach. Schubert (2008) outlines the development of the observational approach with emphasis on the geotechnical design.

The accepted design rules have been laid down in the "Guideline for the Geotechnical Design of Underground Structures with Conventional Excavation" (current revision dates from 2010) which has been developed by the Austrian Society for Geomechanics.

Monitoring of the system support—ground is considered very important, and the improvement of the monitoring process by developing new monitoring and evaluation methods was actively supported by the Clients and the Contractors; since more than 20 years, the monitoring of absolute displacements by electronic total stations is the standard procedure.

3 Guideline for the Geotechnical Design of Underground Structures with Conventional Excavation

The Guideline for the Geotechnical Design of Underground Structures with Conventional Excavation (Austrian Society for Geomechanics 2010a, b) has been published to standardize *the ground characterization* and give a *coherent procedure for the determination of excavation and support during design and construction*.

The objectives of the guideline are given as the *economic optimization of the construction considering the ground conditions as well as safety, long-term stability, and environmental requirements*.

The variability of the geological boundary conditions requires that a *consistent and specific procedure* be used during the design process.

The ground conditions and ground behavior determine the geotechnical design and need to be assessed in depth. This requires the application of a project and ground specific procedure, and a strategy allowing a *consistent and coherent design procedure* that is *traceable throughout the entire project*, and an *optimal adjustment of the construction to the actual ground conditions* encountered on site.

The guideline shall help to follow a systematic procedure. All concepts, considerations, and decisions shall be recorded in a way, that a review of the decision making process is possible.

The basic procedure outlined in this guideline covers 7 steps for the first phase (design):

1. Determination of Ground Types
2. Determination of Ground Behavior and Assignment to Ground Behavior Types
3. Selection of construction concept
4. Assessment of system behavior in the excavation area
5. Detailed determination of the excavation and support method and evaluation
6. Geotechnical report-framework plan
7. Determination of excavation classes (for the tender)

The stepwise procedure allows to identify hazards and aims at risk mitigation by tackling the cause of the hazard or appropriate measures to reduce the impact of any identified hazard.

The determination of the Ground Behavior Types defines the most common failure modes in tunneling and helps to identify the “main hazard” for a specific section according to the boundary conditions coming from the rock mass parameters, the hydrogeological conditions, and the stress conditions (overburden).

The work flow during the design phase is shown in Fig. 2.

The Phase 1 (Design) ends with issuance of the tender documents. Once the project has been awarded, the site organization is set up, and the Phase 2 (Construction) starts. This phase is broken down to 4 steps, namely

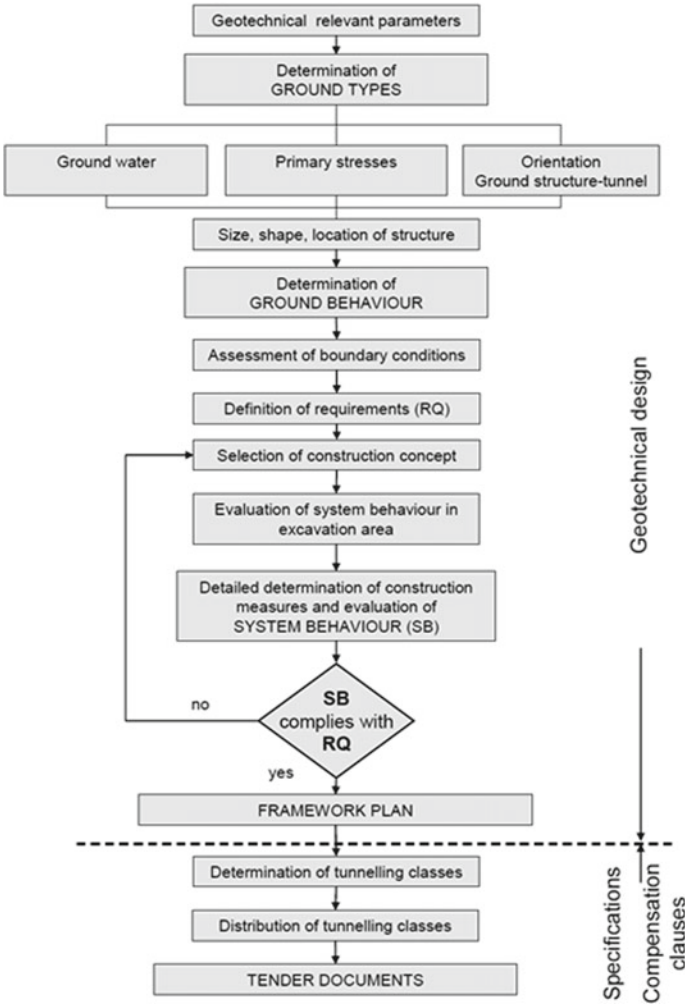

Fig. 2 Schematic procedure of the geomechanical design (Austrian Society for Geomechanics 2010a, b)

1. Determination of the encountered Ground Type and prediction of ground characteristics
2. Assessment of system behavior in excavation area
3. Determination of excavation and support measures and prediction of System
4. Verification of System Behavior

The associated work flow is shown in Fig. 3.

The most important point after the verification of the system behavior is the update of the design. As stated in the guideline, *Due to limited information*

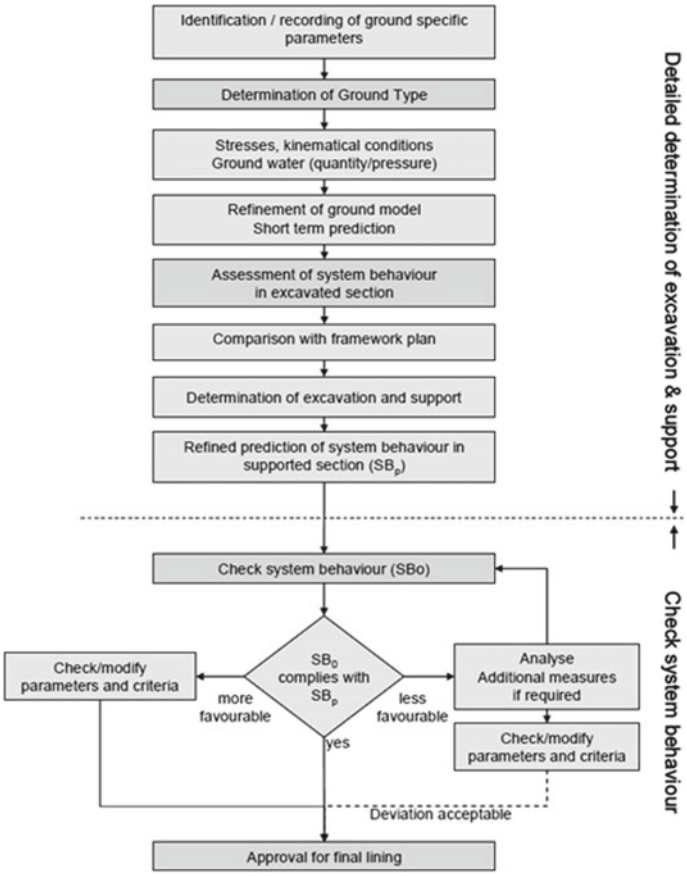

Fig. 3 Basic procedure of determination of construction measures and check of system behavior during construction (Austrian Society for Geomechanics 2010a, b)

available during design, the number of assumptions and simplified models has to be used to arrive at a design, which is the basis for the framework plan and the tender documents. To achieve the goal of a safe and economical construction, it is required to continuously update the geotechnical design with the increasing level of information.

This statement implies that the level of information is increasing during construction, and one means of getting information on the system behavior is regular geotechnical monitoring.

4 Monitoring and Risk Management

As outlined before, NATM has as central element the monitoring of the behavior of the system ground—support. Apart from being a tool for optimization the support system, the geotechnical monitoring is a valuable tool for risk management in tunneling.

The value of monitoring—not only the geotechnical monitoring of the system behavior—cannot be underestimated if and when the monitoring results are being analyzed, compared to the assumed conditions and behavior, and measures/actions are prepared.

Figure 4 shows the development of the level of risk in terms of point of time of recognition. The more promptly, precise, and systematic the monitoring cum analysis is done, the earlier deviations can be recognized and pro-actively mitigated/eliminated.

4.1 Geotechnical Monitoring in NATM

The application of NATM requires the development of a comprehensive geotechnical monitoring program, which is part of the daily operations and is one of the pillars of the geotechnical safety management.

The state of the art in (daily) monitoring is geodetic monitoring with precision bi-reflex targets and highly precise electronic total stations. Apart from the

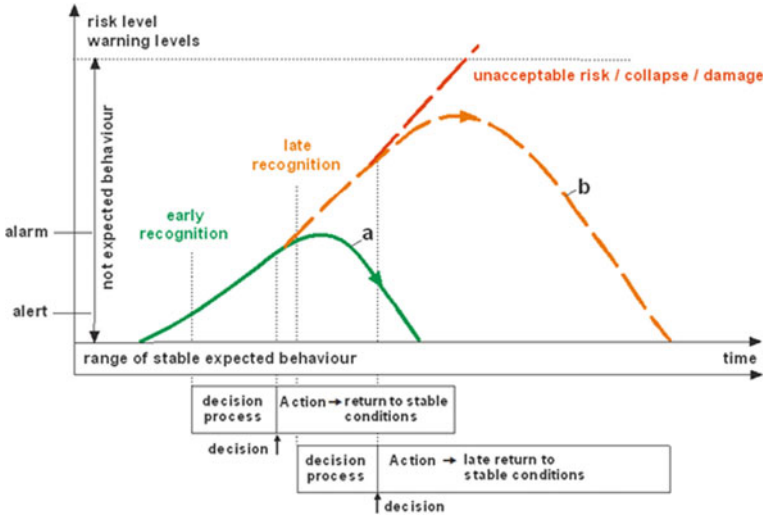

Fig. 4 Relation between risk level and point of recognition

displacement monitoring below and above ground, other instruments like extensometers, inclinometers, etc. are being monitored as per monitoring program, and the results are being reviewed daily.

It has to be added that it is good practice to review the face mappings (geological documentation) together with the monitoring results.

4.2 Overall Monitoring

It has to be pointed out here that "Monitoring" is not limited to Geotechnical Monitoring as it is understood by tunnel practitioners (displacement monitoring). Monitoring or better *Observations* can—and shall—cover the whole range of information and assumptions taken during the design, as well as other *observable* incidents.

E.g., the face mapping in Conventional Tunneling is a documentation tool, and many times it is used as the sole input for the support choice when support classes are linked to index values like RMR or Q. However, the procedure to compare the encountered rock mass vis-à-vis the information available at the design stage would be the proper implementation of the observational approach. The next step is the review of the monitored displacements for a certain rock mass against the values predicted in the design.

Also the observation of certain phenomena, e.g., sudden increase water ingress at a TBM face can be coined monitoring and needs to be introduced into a comprehensive risk management if it is regarded as a hazard or can be linked to one.

4.3 Monitoring Issues

Monitoring is an activity which is time critical when used for the observational approach, as decisions are made based on the monitoring results. It cannot be overemphasized that monitoring data which are not taken frequently and processed immediately for further interpretation will not be the information the engineer needs; they will be mere documentation.

The diagram shown in Fig. 4 is already defining the requirements:

- The time between data capture and results presentation must be as short as possible, to identify deviations from the predicted behavior as soon as possible.
- Once a deviation is recognized, the decision process must start
- The earlier measures are started, the more efficient they are
- Needless to say, the more choice of measures is there, the more accurate a deviation can be tackled

This all leads to the conclusion that on the one hand the possible ground behaviors (failure modes) need to be assessed in the design phase, and on the other hand, all the possible contingency measures need to be planned and must be ready for implementation on site. A measure which is proposed in the design but cannot be executed due to lack of preparation is useless.

5 Design Issues

It can be observed that in the design of infrastructure tunnels, some issues are of recurring nature, leading more than once to uneconomical and inappropriate designs.

The area of focus is around the description of the ground and subsequently, based on this description, the excavation and support design.

5.1 Ground Description

Describing the ground in Engineering terms, that is defining the model which formulates the behavior of the ground under different loading conditions, its reaction to stress changes, its strength under changed stress conditions and finally arriving at a "classification," is a challenging task. It is no surprise that the way ground is described has taken an evolution from the rock mass classification proposed by Terzaghi (1946), the introduction of the standup time as important criterium by Lauffer (1958), and the introduction of the Ground Behavior Types in the Guideline for Conventional Excavation by the Austrian Society for Geomechanics (2010a, b).

5.1.1 Index Classifications

For rock mass, several classification systems have been developed. All these classification systems take several geological, geometric, and design/engineering parameters or parameter ranges as input and give one index number as output. The most common rating/index approaches for tunneling are the Rock Mass Rating (RMR) introduced by Bieniawski (1973, modified 1989) and the Tunneling Quality Index Q proposed by Barton et al. (1974). The Geological Strength Index (GSI) was introduced by Hoek (1994) and Marinos et al. (2005) and is focusing on the engineering geological description of the rock mass.

The objective of all classification systems is to divide the rock mass along the alignment or in the project area into regions, which are separately classified and given one range of index values.

5.1.2 Procedure as Per Austrian Guideline (2010)

The Austrian Guideline (2010) gives the designer a structured process which first defines the ground types (geological formations with similar properties) and then overlays the ground types with the relevant boundary conditions as:

- Ground water regimen
- Initial stress state
- Orientation of the structures

Many of the mentioned boundary conditions are also considered in the before mentioned index values. The addition which is made now is to introduce the size, shape, and position of the planned structure and assess the stability of this structure without any support. This leads to the definition of the Behavior Types as shown in Table 1.

It is obvious that more effort will go into such a classification system, and that the description of the anticipated behavior including the range of displacements to be encountered is highly valuable for the observational approach; also the careful consideration of the probability of occurrence of each behavior type in a specific project already leads to more appropriate planning of contingency measures.

5.2 Choice of Excavation and Support

The ground description forms the basis of design of the excavation and support measures. As already outlined in the prior section, one approach is the direct linking of the support measures to the RMR or Q derived earlier. The other approach is to design the support measures including additional measures (e.g., pipe roofing) based on the behavior type.

Table 1 Categories of behavior types (OeGG 2010a, b)

Basic categories of behavior types (BT)	
1	Stable
2	Potential of discontinuity controlled block fall
3	Shallow failure
4	Voluminous stress induced failure
5	Rock burst
6	Buckling
7	Crown failure
8	Raveling ground
9	Flowing ground
10	Swelling ground
11	Ground with frequently changing deformation characteristics

5.2.1 Excavation and Support Design with Index Values

For the most commonly used classification systems, RMR and Q, correlations/guidelines have been developed to derive the appropriate support system as per index value. The definition of support classes for a project would flow out from the anticipated ranges of index values. Here it has to be mentioned that in these rock mass classification schemes different combinations of geological input parameters may result in the same value, and this might be misleading.

The Q system requires, apart from the Q-value derived from RQD and joint data, the so-called Equivalent Dimension which is the span or height of the structure over the excavation support ratio (ESR). The values for ESR are suggested by Barton et al. (1974), so the span remains as variable factor.

For the RMR system, Bieniawski (1989) gave guidelines for excavation and support of 10-m span horseshoe shaped rock tunnels, as per RMR value.

In both cases, a system as complex as excavation and support of a tunnel is based on one index value, which may not be appropriate at all. The Q system allows to consider the influence of the span, but there is no consideration of the shape of the structure, whereas the RMR system has predefined the shape and the span of the structure for its support guideline.

None of the index values—RMR or Q—allow/propose an estimate of the anticipated deformations/displacements, which is a shortcoming when the design needs to be verified by means of Geotechnical Monitoring.

5.2.2 Excavation and Support Design According to the Austrian Guideline (2010)

The analysis of excavation and support is based upon the behavior types defined earlier. This implies that the order of magnitude of deformations (unsupported structure) has been analyzed before, as well as the proposed cross section—shape and size (span). The support design is done with the objective to reach the requirements for the structure—support and ground. The requirements are depending on the project and may range from maintaining a defined factor of safety for the support to restricting the deformations to maintain the strength of the ground (e.g. in shallow tunneling).

The interaction between the ground and the support system is being analyzed, and the results are reviewed against the requirements. Once the requirements are met for a specific behavior type, an excavation and support class can be formalized. Apart from the geological boundary conditions also the anticipated range of displacements is part of the design and is a key parameter for the observation/monitoring during design.

5.3 Design of Contingencies

The application of an observational approach calls for a plan of contingency actions if the monitoring reveals behavior outside the acceptable limits.

One inherent contingency is that in case the ground changes, the excavation and support scheme may change. This is true for any design based upon classification systems (RMR, Q) as well as the design as per the Austrian Guideline (2010). Once the index range/behavior type has been covered in the initial excavation and support design, it can be implemented when needed.

The design of further contingencies requires to leave the framework of a classification system and directly model the anticipated risk/failure mode. The particular design risk is that originally the ground has been described in terms of a value only, which is not reflecting the actual situation in totality and might lead to wrong design assumptions for special support situations. This needs to be overcome by employing a comprehensive design approach for contingencies and employ more refined models than (single) index value rock mass classification schemes.

6 Implementation and Update of the Design

Once the design is being implemented, the validation and feedback process is started for an observational approach. Here we can identify the major difference between any design which is relying on a rock mass classification system only and the observational approach: within the chosen rock mass classification scheme, the face mapping is taken and the respective RMR or Q-value is being assessed. Based upon the calculated value, the support measures will be defined and implemented. In the observational approach, the similar procedure is applied, but in addition the geotechnical monitoring results are also taken into account on a daily basis. This way also mid-term and long-term stability issues can be identified and tackled, before the support develops overloading phenomena or even local failures occur.

Since the displacement measurements are connected to the geological conditions, the design assumptions are verified constantly and in case of systematic deviations the design assumptions can be reworked.

6.1 Monitoring Program

One of the key elements of the observational approach is the implementation of a comprehensive monitoring program. As discussed earlier, the time between taking the reading and getting the results must be as short as possible. In case of tunneling and the optical displacement monitoring employed there as standard procedure, this means that the time to take the readings should be as short as possible (electronic

data acquisition is a must), and the time to process the data to get the information must be kept as short as possible through automated data transfer and processing through appropriate software.

The state of the art is to have electronic total stations which connect directly to a geotechnical monitoring software which automatically stores the data, processes the same, and produces immediately diagrams for further use by the geotechnical/tunneling engineer.

In order to be able to interpret the data correctly, the construction activities around the monitoring sections needs to be plotted also.

7 General Implementation Issues

It has to be stated that with the most sophisticated design tools, and most advances construction materials, the Quality Assurance and Quality Control still remains paramount. It becomes even more important as with a more accurate modeling inherent factors of safety are reducing and a deviation from the design assumptions may prove fatal. At the same time, the observational approach helps to identify shortcomings in the models used for the design and improve the models to guarantee the required factors of safety.

8 Case Study

In order to show the advantages of the observational approach one case study will be given. It is an underground cavern project which was executed between 1998 and 2004.

8.1 Project Outline

The CERN LHC (Large Hadron Collider) project comprised apart from a complete exchange of the accelerator to supra conducting magnets the construction of new caverns for the ATLAS and CMS experiments. GIBB-SGI-GC JV was awarded the contract for the civil engineering consultancy services for the new Large Hadron Collider LHC, Package 02 in CERN, comprising the caverns and facilities for the CMS experiment.

The caverns UXC 55, with a height of 33 m and a width of 27 m, and USC 55 (height of 16 m and a width of 19 m) are the main underground structures which were excavated in the overconsolidated ground (see Fig. 5).

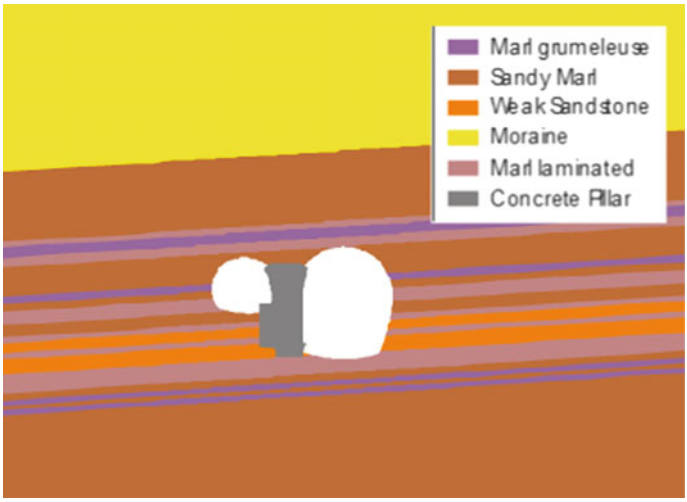

Fig. 5 Geological model—UXC55 and USC55 caverns

8.2 Construction Stages and Monitoring

The construction of the caverns happens in the following stages:

1. Excavation of the pillar between the two caverns
2. Backfilling of the pillar with concrete
3. Excavation of the caverns
4. Inner lining/water proofing and concrete works

During the excavation of the pillar in 2000 and 2001, the ground showed time-dependent behavior which was clearly monitored during a stop of excavation works due to a strike.

The monitoring data shown in Fig. 6 triggered a design review process in June 2001, as this behavior was not anticipated in the design.

8.3 Design Review and Model Calibration

The design review process started with runs to simulate the pillar excavation—as there were geotechnical monitoring data available. These back calculations were used to choose the material model employed and to establish the parameters by calibration against the monitored displacements. This task was concluded, and two parameter sets were chosen for the further design—the most probable behavior ("black line") and the worst probable behavior ("red line") as shown in Fig. 7.

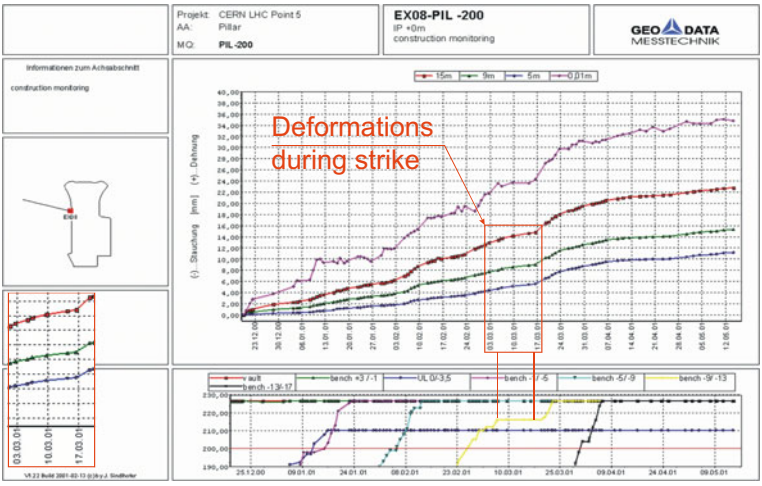

Fig. 6 Monitoring data—pillar excavation

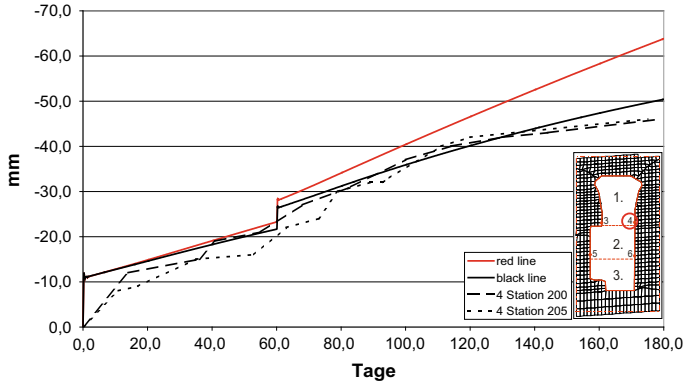

Fig. 7 Calibration results from pillar excavation

On the basis of the two parameter sets, the primary support was reviewed and subsequently re-designed. The initial support design was done for the most probable case, with clearly defined procedure of support increase in case the monitored behavior turning toward the "red line" prediction.

At the same time, the structural team prepared its estimates for the inner lining which under the given loading can fulfill the specifications and requirements, with the provision to take the most appropriate design after having reviewed the monitoring data after the excavation has been completed.

8.4 Monitoring Results—Cavern Excavations

The monitoring during construction showed that the most probable parameter set was the most appropriate choice as shown in Fig. 8.

The structural design of the inner lining was then continued and concluded, as were the other construction works.

The last CMS detector piece was lowered into the UXC55 cavern in 2008, and the LHC project was inaugurated on 10 October 2008.

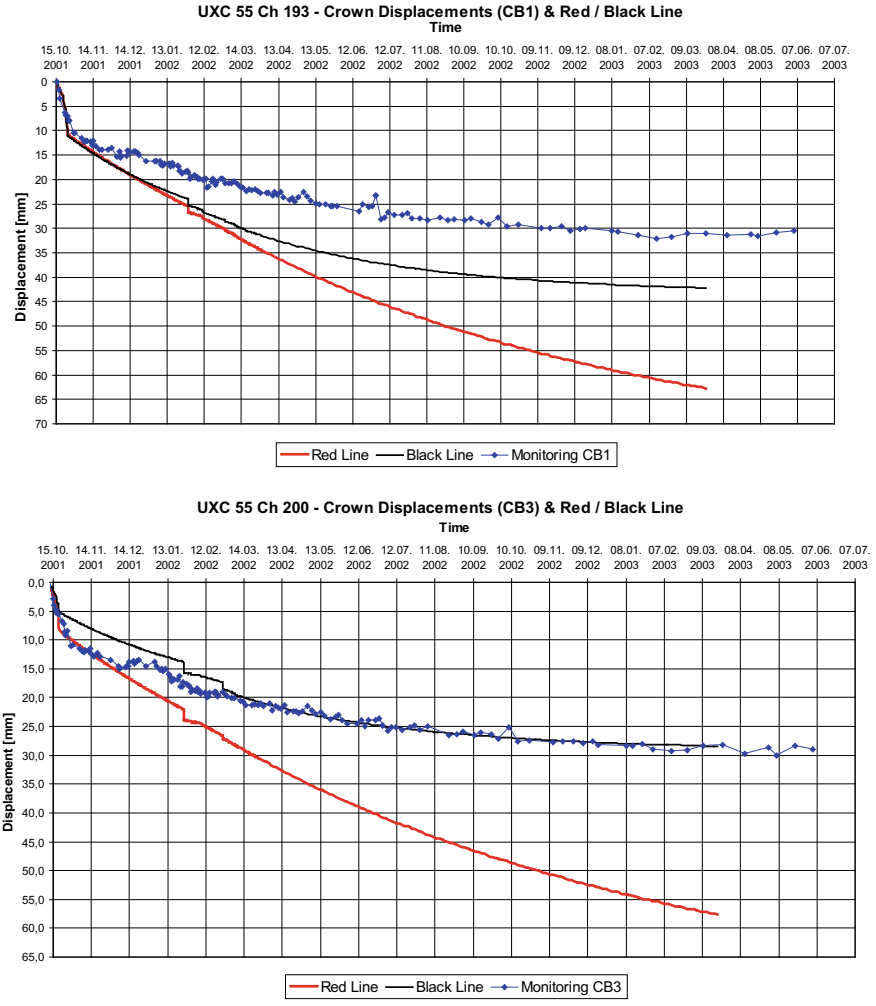

Fig. 8 Monitoring data and predictions for selected cavern displacement points

9 Conclusions

A brief overview over the observational approach and the New Austrian Tunneling Method (NATM) with specific emphasis on the Guideline for the Geotechnical Design of Underground Structures with Conventional Excavation (2010) was given. Some shortcomings which may arise in the application of Rock Classification schemes, namely RMR and Q, were highlighted and in parallel the procedure with an observational approach outlined.

Finally a case study of a cavern project is given, showing the advantages of the observational approach.

This paper shall stimulate the discussion and encourage the implementation of the observational approach, and the author is grateful to have been invited to give his views on the subject.

References

Barton NR, Lien R, Lunde J (1974) Engineering classification of rock masses for the design of tunnel support. Rock Mech 6(4):189–239

Bieniawski ZT (1973) Engineering classification of jointed rock masses. Trans S Afr Inst Civ Eng 15:335–344

Bieniawski ZT (1989) Engineering rock mass classifications. Wiley, New York

Hoek E (1994) Strength of rock and rock masses. ISRM News J 2(2):4–16

Lauffer H (1958) Gebirgsklassifizierung für den Stollenbau. Geol. Bauwesen 24(1):46–51

Marinos V, Marinos P, Hoek E (2005) The geological strength index—applications and limitations. Bull Eng Geol Environ 64:55–65

Terzaghi K (1946) Rock defects and loads on tunnel supports. In: Proctor RV, White TL (eds) Rock tunneling with steel supports, vol 1. Commercial Shearing and Stamping Company, Youngstown, pp 17–99

Due to the number of publications on NATM, selected references available in English are given below

Austrian Society for Geomechanics (OeGG) (2010a) Guideline for the geotechnical design of underground structures with conventional excavation. Austrian Society for Geomechanics, Salzburg, Austria

Austrian Society for Geomechanics (OeGG) (2010b) NATM—the Austrian practice of conventional tunnelling, Austrian Society for Geomechanics, Division "Tunnelling", Working Group "Conventional Tunnelling"

ITA-Austria (2012) 50 years of NATM—experience reports, ITA-Austria, Salzburg, October 2012 (Remark—contains an extensive list of references)

Rabcewicz LV, Golser J (1974) Application of the NATM to the underground works at Tarbela, water power, September and October 1974

Schubert W (2008) The development of the observational method. Geomechanik und Tunnelbau 1 (5):352–357

Schubert W, Lauffer H (2012) NATM—from a construction method to a system. Geomech Tunn 5 (5):455–463

Critical Evaluation on Retention of Fine Sand Through Soil Nailing for Construction of Rail Underpass by Box Jacking—A Case Study

Kanwar Singh, Satyendra Mittal, P. S. Prasad and Kishor Kumar

Abstract The scope of construction of rail underpass with precast concrete boxes and jack pushing technique has been increased tremendously to maintain uninterrupted flow of rail and road traffic in many Indian metropolitan cities. The project has become more challenging when the construction of one of such underpasses had to go through the two random 12 m high and 2 m thick rubble masonry walls with poorly graded fine sand as a backfilled material. The site is located in zero tolerance zone of Indian Railways where about 200–250 trains move everyday over the tracks. The challenging site conditions demanded a novel ground improvement technique which could have stabilised the box/tunnel face in controlled conditions during box jacking operation with live rail traffic. This paper describes an innovative stepwise de-stabilisation and stabilisation of soil nailing technique which was successfully used first time in the world for construction of three adjacent large size underpasses below the two rail tracks on Old Delhi–Shahadra section near Salimgarh Fort, Yamuna Bazaar, New Delhi, India.

Keywords Underpass · Box jacking · Soil nailing · Soil stabilisation

K. Singh (✉) · P. S. Prasad · K. Kumar
Geotechnical Engineering Division, CSIR-Central Road Research Institute, New Delhi 110025, India
e-mail: skanwar7777@gmail.com

P. S. Prasad
e-mail: pulikanti@gmail.com

K. Kumar
e-mail: kishornhrm@gmail.com

S. Mittal
Civil Engineering Department, IIT Roorkee, Roorkee 247667, Uttarakhand, India
e-mail: satyendramittal@gmail.com

R. Sundaram et al. (eds.), *Geotechnics for Transportation Infrastructure*, Lecture Notes in Civil Engineering 29,
https://doi.org/10.1007/978-981-13-6713-7_26

1 Introduction

Delhi being a city of 25 millions of population currently houses with one crore number of vehicles and 9.94% vehicles are added every year from year 2016. This demand completes rethinking of transportation network to avoid unprecedented time spent on roads due to unpredicted traffic jam. In one of such cases, to ease the pressure on the main road, Public Works Department of Delhi had planned a bypass, which was to undergo through a 140 years old railway bridge approach. The three road under bridge (RUB) planned (Fig. 1) by PWD in which two RUB of size 10.5 m × 5.75 m and one RUB was 9 m × 4 m as internal dimensions. The external dimensions of the two RUB's are 12 m × 7.45 m and one RUB is 10.5 m × 5.70 m. The locations of three RUB's (underpass) are shown in Fig. 1. The three RUB's were constructed at a location where existing rail level (RL 214.06 m) was above 5.58 m from natural ground level (NGL RL 208.48 m) while the required road level through RUB was set out to be at RL 206.01. The embankment of railway was confined in between two rubble stone masonry retaining walls. The general x-section of embankments is shown in Fig. 2.

The GPR results revealed that the retaining wall had over a 2 m thick battered face towards earth side. The RUB was to be constructed by box pushing method covering 22 m of pushing length for each underpass. The pushing was only possible after dismantling of RR wall and there was a fear of instability of cohesionless soil strata. The 8.5 m high earth face made up of this cohesionless soil would have collapsed, anyway, after the removal of masonry. The India railway has, therefore, anticipated the following problems during the removal of masonry retaining wall.

- Earth pressure due to dismantling of 2 m thick random rubble masonry wall leading to disruption of railway track.
- Serious disruption to the rail traffic in case of any failure leading to unprecedented impact on functioning of over 200–250 numbers of trains.
- Water supply line of 300 mm dia. passing through the embankment could also experience damage.

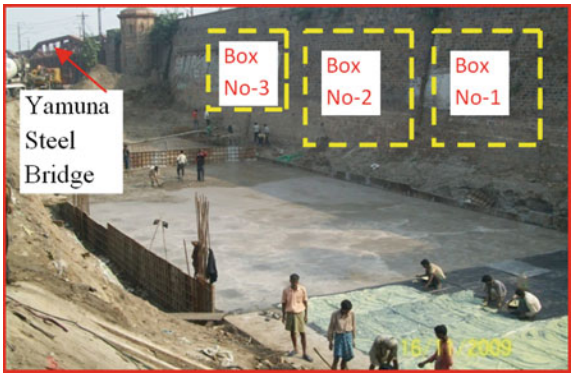

Fig. 1 Location of railway underpass

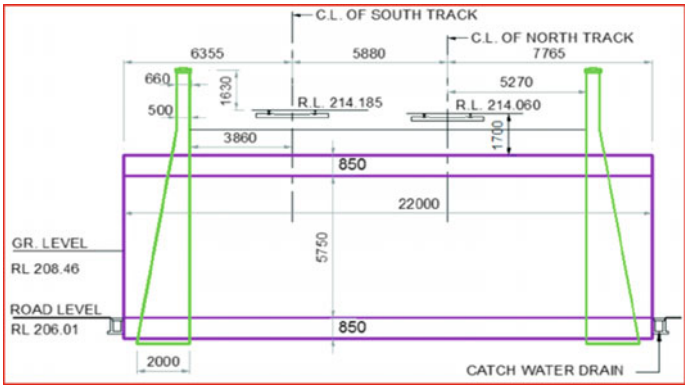

Fig. 2 X-section of embankments

- Rail signal transmission could also be affected, in case of any anticipated failure.
- Existing Retaining wall likely to be bulged due to box jacking leading to instability of the wall and track both.

Since 200–250 passengers and goods trains pass this section daily, there was no scope of any mistake during the construction of RUB as indicated by the railway authority. Ground improvement by pipe arch roofing, cement/bentonite and relieving girders below the rail sleepers was initially thought by railway and found not feasible due to inadequate vertical overburden height of 1.7 m. The soil nailing was finally thought of to stabilise the cohesionless soil tunnel face during box pushing operation when it cut to almost vertical profile for a height of about 8.5 m. The details of design and construction methodology of soil nailing for controlling stepwise vertical de-stabilisation and stabilisation for the construction of underpass below the live rail traffic are explained in this paper.

The geotechnical investigations report was provided by Indian Railways. However, just to cross check the soil profile at site, one confirmatory test bore hole was drilled in rail embankment. The properties of embankment soil fill material obtained from the laboratory investigations are given in Table 1.

2 Box Jacking Technique with Soil Nailing

In the last two decades, the scope of construction of underpass by jack pushing has increased manifold. Jacked box tunnelling provides planners and designers with a non-intrusive technique for creating underground space at shallow depth beneath existing infrastructure, where it is either impractical or inconvenient to undertake construction from the surface Clarkson and Ropkins (1977) and Ropkins (1998). To date the technique has been used to create underground space primarily for rail, road and pedestrian accesses together with a major river diversion culvert at

Table 1 Properties of embankment fill material

Parameters	Value	Units
Cohesion (c)	0	kN/m^2
Angle of internal friction (ϕ)	29.5	°
Specific gravity of sand (G)	2.65	
D_{60}	0.18	mm
D_{30}	0.12	mm
D_{10}	0.08	mm
Maximum dry density	17.0	kN/m^3
OMC	10.5	%
C_u	2.25	
C_c	1	
Soil classification as per Indian standards	SP-SM	

Dorney, Berkshire. It could equally well be used to create underground space for car parking and office access, archive and cold storage, machinery rooms, etc. In last two decades, as per the soil conditions, the construction of few underpasses with precast concrete segments using box jacking techniques below live rail tracks was executed at various places (Didcot, Oxfordshire UK; Thurrock, Essex, UK; Railway Station, London, UK; Lewisham Railway Station, London, UK; and Northamptonshire, UK) without any ground improvement technique. However some projects where, dewatering (Berkshire, UK, Boston, Massachusetts, USA) and ground freezing (Silver Street Station, London, UK) measures were used to stabilise the soil conditions and the same process of box jacking installation below road Allenby and Ropkins (2003, 2004).

In the similar projects elsewhere, the high stresses on the overburden soil have been experienced during jack pushing operations. At some of the sites, even sudden collapse of soil mass between live load and top of precast tunnel was noticed. Before year 2010, most of the box jacking projects were executed without any ground improvement technique by Indian Railways. During these projects, lot of difficulties like up heaving of soil, movement of rail track and sudden collapse of soils inside the box were noticed which resulted the delay in completion as well as construction cost was increased considerably. However, in order to prevent the sudden collapse of soil and to transfer the load at wider area, soil nailing technique has been applied in this study.

Soil nail has been increasingly utilised globally for the last few decades due to its technical and economic advantages. It is one of the effective techniques for soil stabilisation of natural and man-made steep cut slopes by inserting the metallic/anchor rods directly into the soil mass as a 'driven nails' or as grouted nails. In view of the development in the frictional and tensile strength characteristics, various types of soil nails (plain or ribbed) have been successfully implemented by the various researchers for controlling de-stabilisation in the field (Potyondy 1961; Schlosser and Guilloux 1981; Schlosser 1982; Cartier and Gigan 1983; Jewell

1990; Heymann et al. 1992; Luo et al. 2000; Patra et al. 2001; Junaideen et al. 2004; Chu and Yin 2005; Pradhan et al. 2006; Gosavi et al. 2006; Su et al. 2007; Mittal et al. 2008; Su et al. 2008; Yin and Zhou 2009; Zhang et al. 2009; Babu and Singh 2010).

In order to protect the sudden collapse behaviour of soil, up heaving and to transfer the high stresses at wider area, soil nailing was used by CSIR-CRRI, with which the factor of safety of underneath soil with live rail loads has increased considerably. The corresponding author has also been awarded national and international patent Singh et al. (2012, 2015), respectively, for underpass construction using soil nailing technique in the year 2012 and 2015. The soil nailing technique was designed on the basis of pull-out load capacity of nails.

2.1 In Situ *Soil Nail Pull-Out Tests*

In order to determine the apparent coefficient of friction (f^*) between in situ soil and nail for designing of nail network, in situ pull-out tests have been conducted at different levels on retaining wall in close vicinity to the smaller box. Seven initial pull-out tests were conducted at site. Out of seven, four tests were conducted on 100 mm diameter grouted nails. Perforated GI pipe of 89 mm dia. (perforation of 12 mm @ 50 mm c/c in staggered on periphery of pipe) was centrally installed, and the same was grouted with 1:1 (cement: sand mortar). Out of three driven nails, 32 mm and 28 mm diameter tor steel nails were tested at two and one location, respectively. The test nails were installed with the help of machine mounted on platform as shown in Fig. 3 and same nails were tested by jack assembly.

Fig. 3 Installation of test nail

3 Soil Nailing Design by GEO 4

Based on the results of the pull-out tests conducted in the field and after several iterations, the nailing scheme was designed using GEO 4 software. The length of the driven nails varied according to their location and site condition. The cross-sectional profile of the cut slope, external loads and nailing scheme are shown schematically in Fig. 4. The details of spacing of the nails as per designed requirement for stabilising the cut face at the RUB location is given in Table 2. The total length of the nails was kept 30 cm extra for facilitating in driving of nails. The complete designed soil nailing scheme was checked for external and internal stability similar to the conventional earth-retaining structures.

3.1 External Stability of Nailed Wall

3.1.1 Check for Overturning Stability

Resisting moment, M_{res} = 7911.34 kNm/m
Overturning moment, M_{ovr} = 466.96 kNm/m

Overturning of nailed wall is ACCEPTABLE

3.1.2 Check for Slip Failure

Resisting lateral force, H_{res} = 0.9 * 581.44 = 523.29 kN/m
Active lateral force, H_{act} = 163.63 kN/m

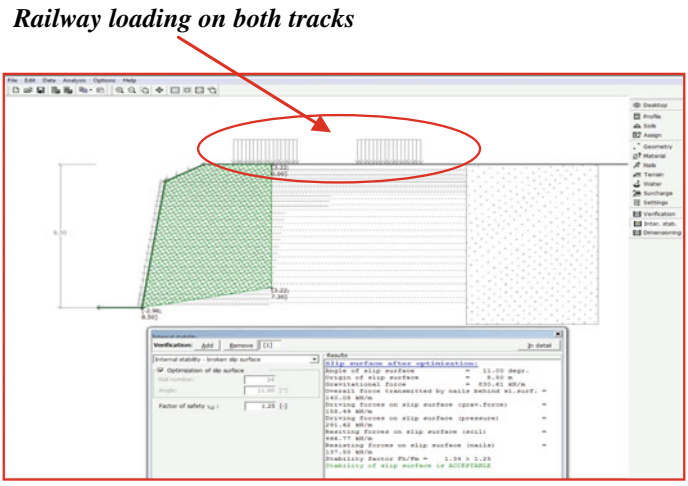

Fig. 4 Stability analysis with loading on both tracks

Table 2 Details of nails designed by GEO 4

S. No.	Dia. of nail (mm)	Depth from rail top (m)	Spacing (m)		Effective length of nails (m)
			Vert.	Horiz.	
1	100[a]	1.30	0.3	0.5	15
2	32	1.55	0.3	0.4	15
3	32	1.75	0.2	0.3	15
4	32	2.0	0.25	0.3	15
5	32	2.3	0.3	0.3	15
6	32	2.6	0.3	0.3	8
7	32	2.9	0.3	0.3	8
8	32	3.2	0.3	0.3	8
9	28	3.6	0.4	0.3	6
10	28	4.0	0.4	0.3	6
11	28	4.4	0.4	0.3	6
12	28	4.8	0.4	0.3	6
13	28	5.2	0.4	0.3	6
14	28	5.6	0.4	0.3	6
15	28	6.0	0.4	0.3	6
16	28	6.4	0.4	0.3	6
17	28	6.8	0.4	0.3	6
18	28	7.2	0.4	0.3	6
19	28	7.6	0.4	0.3	6
20	28	8.0	0.4	0.3	6
21	28	8.4	0.4	0.3	6
22	28	8.7	0.3	0.3	6
23	28	9.0	0.3	0.3	6

[a]Grouted nail (89 mm dia. perforated GI pipe nail)

Forces acting at the centre of the footing bottom

Overall moment M = 3607.29 kNm/m
Normal force N = 1173.17 kN/m
Shear force Q = 163.63 kN/m
Slip failure of wall is ACCEPTABLE

3.1.3 Check for Bearing Capacity of Foundation

Eccentricity of normal force (e) = 0.00 cm
Maximum allowable eccentricity (e_{allow}) = 265.32 cm

Eccentricity of the normal force is ACCEPTABLE

Stress at the footing bottom Sigma = 145.92 kPa
Bearing capacity of foundation soil Rd = 500.00 kPa

Bearing capacity of soil is ACCEPTABLE

3.2 *Internal Stability of Nailed Wall*

Internal stability of nails and tunnel face has been checked separately for three different loading conditions: (a) the train was considered on both the tracks (Delhi–Shahadra and Shahadra–Delhi); (b) train considered on single track (Delhi–Shahadra); (c) train on another single track (Shahadra–Delhi). A typical calculation of internal stability when the train load is considered on both tracks is shown in Fig. 4 and complete soil nailing design by GEO 4 software is shown in Fig. 5. The other possibility of the loading was also analysed and found acceptable.

3.2.1 Railway Loading on Both Tracks (Delhi–Shahadra and Shahadra–Delhi)

Resisting forces on slip surface (soil) = 466.77 kN/m
Resisting forces on slip surface (nails) = 137.50 kN/m
Stability factor Fh/Fm

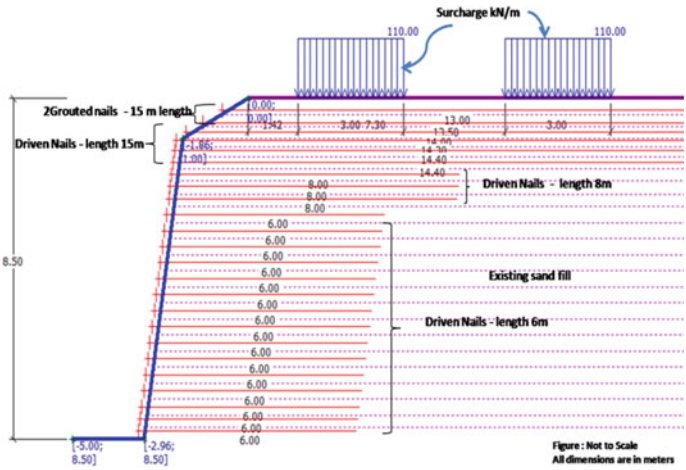

Fig. 5 Soil Nailing designed by GEO 4 software

$$\mathrm{Fh/Fm} = 466.77 + 137.5)/(158.49 + 291.62)$$

Stability factor = 1.34 > 1.25

Stability of slip surface is ACCEPTABLE

3.3 Stability Analysis of End Portion (4 m from Exit End)

Stability analysis of the embankment soil was checked with different loading condition and found safe after considering the nails in box tunnel overburden and inside the box tunnel face. It was also proposed in the design, when the nails would touch to the exit end of the retaining wall, these were to be cut off by 30 cm to create a space towards pushing end. In such cases, the effective length of the nails would have to be reduced in subsequent pushing for a constant height of excavation. However, instability was anticipated by reducing the effective length of the nails by 4 m before the exit end. To analyse the instability of the embankment at this end, the FOS was again computed with different surcharge loading and found inadequate. In order to increase the FOS, vertical driven nails of 28 mm diameter and 7 m length were applied and FOS analysed and found adequate. The stability analysis after considering the horizontal and vertical nails at the surface is shown in Fig. 6. The FOS values of embankment with horizontal and vertical nails are given in Table 3.

4 Underpass Construction Methodology

4.1 Stepwise Procedures for c/o RUB by Soil Nailing

The construction of underpass involved preparation of thrust bed, casting of RCC boxes, dismantling of RR wall and immediate installation of soil nailing system for stabilisation of cohesion less soil. The construction of boxes was done at the thrust bed, very close to site as shown in Fig. 7. In view of the safety and other execution problems, the railway authority had proposed to push the smaller box first. Accordingly, the construction methodology was planned to define step wise procedure.

I. In order to cater the load to the wider area heavy-duty (IS 200) girders were provided (Fig. 8) below rail track at every two sleepers. One end of the girders was rested on embankment and other end on the box with pulley arrangement.

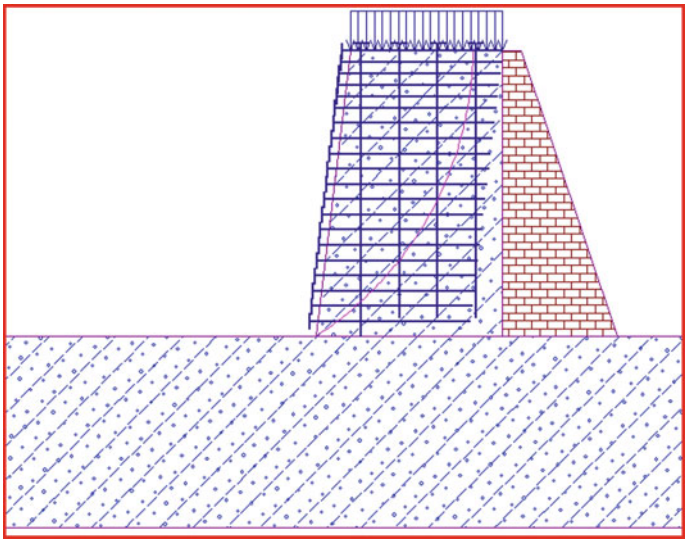

Fig. 6 Stability analysis with horizontal and vertical nails

Table 3 FOS with horizontal and vertical nails

Surcharge (kN/m)	F.O.S of an embankment	
	Horizontal nails	Horizontal and vertical nails
80	1.02	1.16
100	0.97	1.10
125	0.92	1.04

Fig. 7 Construction of boxes

II. The length of RR wall (width of box) was divided in two segments for each underpass to control the dismantling process.
III. Dismantle the wall face vertically about 40–50 cm (Fig. 9) till the soil strata appear and immediately shuttering plates were anchored to protect the soil erosion. The shuttering plates were placed in such a way that plates should not be touched with the boundary of box.
IV. One layer of 100 mm dia. (with perforated pipe) grouted nails were installed (Fig. 10) up to the entire width of embankment. One grouted nail was installed extra on either sides of box to protect the side slope.
V. One layer of driven nail (32 mm dia. Tor steel) with length of 15 m (width of embankment) was provided above the box.
VI. Repeat the process of dismantling of wall, placing of shuttering plates and installation of driven nails (Fig. 11) till the entire face of the wall is converted into nailed wall (Fig. 12) for smaller (first) box. Thereafter, the other boxes were taken up for installation of nails.
VII. In the mean time, the precast boxes became ready for pushing.
VIII. It was ensured and checked that all the driven nails should have an extra length of at least 300 mm outside the shuttering plate.
IX. A drag sheet made of 1.5 mm thick galvanised iron sheet was also provided at top of boxes to minimise the frication.
X. The cutting shoe of the box is inserted about 100 into embankment soil. A care is to be taken that shuttering plate should not be touched to the cutting shoe.
XI. The soil from the tunnel/box face (inside) was excavated about 50 mm thick after loosening of plates near the cutting shoe.
XII. The inclination (slope) angle of soil face was matched with angle of cutting shoe which also maintained the uniformity slopes. A care was taken that soil face was kept behind about 50 mm from the edge of cutting shoe.

Fig. 8 Installation of girder

Fig. 9 Dismantling of wall

Fig. 10 Grouted nail installation

Fig. 11 Driven nail installation

Fig. 12 Complete nailed wall

XIII. The process of loosening of plate, excavation of soil from the box tunnel face, tightening of shuttering plate and jack pushing of box was repeated under live train loads up to 300 mm.
XIV. Thereafter, the exposed nails pushed/drive further towards the embankment in the 300 mm segmental length till the remaining *H*/2 length.
XV. When the nails touched to the exit end of the retaining wall, the nails were cut up to length of 300 mm from the tunnel face to create a pushing space. The cutting of nails was taken place in segments of 300 mm.
XVI. When the box tunnel face was at a length of *H*/2 (remaining length), the vertical nails were provided as per design scheme.
XVII. Three boxes were pushed successfully (Fig. 13) after full retention of cohesionless soil by soil nailing. This technique proved that this could be viable solution for such projects. The traffic is plying through the RUB (Fig. 14).

Fig. 13 GI sheet installation

Fig. 14 Box pushing in progress

5 Conclusions

Due to large scale infrastructure projects, the need of providing box tunnel below the existing structures (road/rail track, etc.) cannot be ruled out. The provision of nails into the overburden and box tunnel face enhances the stability of overburden and tunnel face. As clearly evident from this study, the horizontal pushing of box tunnel plays a very vital role. The vertical nails were required to meet the stability requirement; therefore, the vertical nails were also provided for the 4 m width of the embankment (last portion of pushing length). The combination of horizontal and vertical nails finally enhanced the factor of safety up to the required level. It is evident from this project, the vertical nails are helpful when the underpass/boxes are to be pushed through a retaining wall otherwise the horizontal nails could be sufficient enough to maintain the stability.

Acknowledgements Authors thanks to Director, CSIR-Central Road Research Institute, New Delhi, India for approving and providing the financial support to carry out model study in CSIR-CRRI laboratory. Authors are also thankful to railway engineers Sh. Ajit Singh, Deputy Chief Engineer and Sh. M. K. Kinger, Executive Engineer and Sh. S. P. Singla & Company for assigning a Consulting Project No. CNP-1666.

References

Allenby D, Ropkins JWT (2003) Geotechnical aspects of large section jacked box tunnels. In: Proceedings of the transportation geotechnics symposium, 2003, Nottingham

Allenby D, Ropkins JWT (2004) The use of jacked-box tunnelling under a live motorway. Geotech Eng 157(Issue GE4):229–238. Thomas Telford Publishing, London

Babu G, Singh V (2010) Soil nails field pull-out testing: evaluation and applications. Int J Geotech Eng 4(1):13–21

Cartier G, Gigan JP (1983) Experiments and observations on soil nailing structures. In: Proceedings of 8th European conference on soil mechanics and foundation engineering, vol 1, Helsinki, 473–476

Chu LM, Yin JH (2005) Comparison of interface shear strength of soil nails measured by direct shear box tests and pull-out tests. J Geotech Geoenviron Eng 131(9):1097–1107

Clarkson TE, Ropkins JWT (1977) Pipe-jacking applied to large structures. Proc Inst Civ Eng 62 (1):539–561

Heymann G, Rohde AW, Schwartz K, Friedlaender E (1992) Soil nail pull-out resistance in residual soils. In: Proceedings of the international symposium on earth reinforcement practice, Balkema, 487–492

Jewell RA (1990) General report–soil nailing. In: Proceedings of the international reinforced soil conference, Thomas Telford, London, 197–202

Junaideen SM, Tham LG, Law KT, Lee CF, Yue ZQ (2004) Laboratory study of soil-nail interaction in loose completely decomposed granite. Can Geotech J 41(2):274–286

Luo SQ, Tan SA, Yong KY (2000) Pull-out resistance mechanism of a soil nail reinforcement in dilative soils. Soils Found 40(1):47–56

Meenal G, Saran S, Mittal S (2006) Model test for validation of model analysis of nailed cuts. Indian Geotech J 39(1):96–116

Mittal Satyendra, Singh Kanwar and Mathur S (2008) Behaviour of vertical cut using Soil Nailing Technique in saturated condition, Journal of the South East Geotechnical Society, June 2008, pp 113–120

Patra CR, Basudhar PK (2001) Nailed soil structure: an overview. Indian Geotech J 31(4):322–362

Potyondy JG (1961) Skin friction between various soils and construction materials. Geotechnique 11(4):339–353

Pradhan B, Tham LG, Yue ZQ, Junaideen SM, Lee CF (2006) Soil-nail pull-out interaction in loose fill materials. Int J Geomech 6(4):238–247

Ropkins JWT (1998) Jacked box tunnel design and construction. In: Proceedings of the Sessions of Geo-Congress 98, Special Publication No 87. American Society of Civil Engineers, Reston, Virginia, USA, 21–38

Schlosser F, Guilloux A (1981) Le frottement dens les sols. Rev Fr Geotech 16:65–77

Schlosser F (1982) Behaviour and design of soil nailing. In: Proc., Symp. on recent developments in ground improvement techniques, Bangkok, 399–413

Singh K, Prasad PS, Mathur S, Gangopadhyay S, Azad F (2012) National Patent on, stepwise vertical De-stabilization and stabilisation of compacted collapsible sandy soil for construction of Rail underpass (WO2014013508A2)

Singh K, Prasad PS, Mathur S, Gangopadhyay S, Azad F (2015) International Patent on stepwise vertical De-stabilization and stabilisation of compacted collapsible sandy soil for construction of Rail underpass (WO2014013508A2, US20150197895)

Su LJ, Chan TCF, Shiu YK, Cheung T, Yin JH (2007) Influence of degree of saturation on soil nails pull-out resistance in compacted completely decomposed granite fill. Can Geotech J 44 (11):1314–1328

Su LJ, Chan CFT, Yin JH, Shiu YK, Chiu SL (2008) Influence of overburden pressure on soil-nail pullout resistance in a compacted fill. J Geotech Geoenviron Eng 134(9):1339–1347

Yin JH, Zhou WH (2009) Influence of grouting pressure and overburden stress on the interface resistance of a soil nail. J Geotech Geoenviron Eng 135(9):1198–1208

Zhang LL, Zhang LM, Tang WH (2009) Uncertainties of field pull-out resistance of soil nails. J Geotech Geoenviron Eng 135(7):966–973

Finite Element Analysis of Ground Movements and Geotechnical Capacity Loss Induced Due to Shield Tunnels

Animesh Sharma

Abstract Due to an exponential increase in urbanization, there is a growing need for a systematic mass transportation system in developed and developing countries. A reasonable solution is underground transportation system like tunnels. An inevitable aspect of the construction of underground tunnel in urban locale is the ground movements associated with it. With that under consideration, the current study encases the assessment of settlements induced due to bored tunnels using finite element method. Current study undertakes a detailed analysis of the parameters affecting the ground movements and also investigates the geotechnical capacity loss associated with it. The observed results from finite element analysis are then compared with the conventional theoretical results. Based on observed trends, geotechnical parametric factors are proposed considering which a more precise range of settlements can be obtained. The study investigates the phenomenon of the associated geotechnical loss induced due to bored tunnels by simulating twin bored tunnels, i.e. two tunnels in close proximity, with one passing first, followed by the second bored tunnel. The results suggested that there was a considerable reduction in geotechnical capacity loss generated due to associated ground movements. The study concludes that upon accounting the geotechnical factors and loss associated, a more precise assessment of the ground movements can be arrived at and hence an even precise assessment of the impact upon the structures in proximity.

Keywords Urban tunnels · Ground movements · Geotechnical loss · Settlements · PLAXIS · Finite element analysis

A. Sharma (✉)
Geotechnical Engineer, Afcons Infrastructure Ltd, Kolkata East West Metro UG1, Kolkata, West Bengal, India
e-mail: animesharma009@yahoo.com

R. Sundaram et al. (eds.), *Geotechnics for Transportation Infrastructure*, Lecture Notes in Civil Engineering 29,
https://doi.org/10.1007/978-981-13-6713-7_27

1 Introduction

With the advent of growing need for providing a systematic mass transit system, using urban tunnels has substantially increased. Tunnelling basically can be termed as a form of excavation which events to change in existing stresses creating movements in the ground. These ground movements adversely impact the existing buildings and structures within close proximity to the tunnel. Accurate assessments of ground movements are vital, especially for urban tunnels because the assessment of impact of tunnelling on nearby structures and buildings relies particularly on the associated ground movements. The conventional approach for the determination of ground movement comprises of theoretical evaluations, which include the use of semi-empirical methods for assessment of ground movements due to bored tunnels.

Earliest methods for the assessment of ground movements due to tunnelling can be traced back to Peck (1969a, b) which was further developed by Attewell et al. (1986) and O'Reilly and New (1982) as a Gaussian or normal distribution curve which is the most commonly used empirical method for assessment of ground settlements. The empirical equations developed can be represented as:

$$s = S_{\max} . \exp\left(-\frac{y^2}{2i^2}\right) \tag{1}$$

$$V_s = \sqrt{2\pi} * k * z * S_{\max} \tag{2}$$

where

s	settlement at any horizontal distance, y
$S_{\max}$	maximum settlement
V_s	volume of settlement trough
Z	depth to tunnel axis
y	horizontal distance
i	point of inflexion
k	trough width parameter (assumed as 0.5 for clayey soils and 0.3 for sandy soils)

The equations were derived from numerous sets of physical model laboratory tests and case studies over time (Fig. 1).

Furthermore studies were put forward by Cording et al. (1975), Burland et al. (1977), Schmidt et al. (1989), O'Reilly and New (1982), Mair et al. (1996), whereby they conducted several reviews encasing multiple case studies in various soil conditions. Their findings confirmed the data and equation as suggested by O'Reilly and New (1982). Further Sagaseta (1987) presented boundary condition-based theory and equation on ground deformation, whereby he focused mainly on displacement parameter and eliminated the stress component. This theory was later further developed by Verruijt and Booker (1996). Several researchers like Loganathan and Poulos (1998) also presented equations based upon the closed form

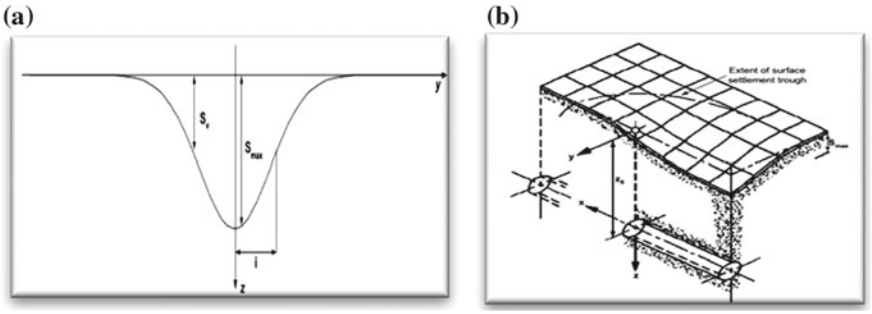

Fig. 1 Settlement Trough **a** Gaussian distribution curve for settlements due to tunnel, **b** 3D representation of generated settlement trough due to tunnel (Attewell and Yeates 1984)

solutions to predict the surface settlement. Several physical centrifugal model studies have been conducted by researchers like Atkinson et al. (1979), Mair et al. (1993) in order to study the ground movements and aspects such as face stability during tunnelling. From previous studies, it can be established that there is a clear trend of a Gaussian distribution curve being followed by the surface settlements above the tunnel. The factors over which the surface settlement depends are the *amount of volume loss generated due to tunnelling, depth of tunnel, diameter of tunnel, the type of soil*.

The current study compares the empirical theoretical approach to the finite element approach and considers the various factors effecting the ground movements. PLAXIS 2D, i.e. a finite element software, has been used for the analysis of the assessment of ground movements due to bored tunnels. Amongst the various factors affecting the ground movements, the current study mainly focuses on the geotechnical parameters and its corresponding effect on the ground movements. Various relevant geotechnical parameters are varied and their effect has been considered in this study.

Based on the obtained results, geotechnical factors have been proposed to the empirical correlations for precise assessments. The study also tries to investigate the propagation of sub-surface settlement from the surface to the tunnel crown and factors associated. Further, the study also emphasises on the geotechnical loss associated with the ground movements and are compared with the relevant literature.

2 Theoretical Approach for Assessment of Ground Movements

In the current study, comparisons have been made in order to attain correlations amongst the results obtained through theoretical assessments and finite element analyses. For the simplicity of forming the basis of the complex phenomenon of the

ground movements due to tunnelling, the factors effecting have been divided into 3 parts as:

Tunnel Geometrical Parameters include the *depth of tunnel* from the ground level and the dimensions of the tunnel like *inner and outer diameters*.

Geotechnical Parameters include the *geotechnical properties* of existing soil being tunnelled through.

Tunnel Construction Parameters can again be further divided into tunnel structural parameters and tunnel operational parameters. Tunnel structural parameters mainly includes the *stiffness of tunnel lining* used while operational parameters include the time response aspects like the *maintenance of face pressure* during construction for face stability and parameters related to *tail void grouting*. Operational parameters are implicitly considered in the theoretical evaluations and are not considered in the present study.

Amongst the factors affecting the ground movements, the geometrical and construction parameters of tunnel are important and are well epitomized in the empirical formula mentioned in Eq. 1. The equation implicitly considers the geometrical and tunnel construction parameters through parameters such as tunnel depth, diameter, trough width parameter and volume loss. The current study mainly emphasises on investigating the effects of variation of geotechnical parameters on the ground movements and thereby ascertaining the trend observed. For theoretical assessments of ground movements, the aforementioned Eqs. 1 and 2 have been used. Table 1 details the assumed default parameters considered for theoretical and finite element analysis. These default geotechnical parameters are further varied in order to study the corresponding effect on ground movements.

Table 1 Default geotechnical and tunnel lining parameters considered for PLAXIS analysis

Parameter	Symbol	Value	Unit
Cohesion	c’	0.5	kPa
Undrained cohesion	Cu	75	kPa
Angle of internal friction	Φ’	30	Degrees
Hardening soil model	E_{50}^{ref}	12,000	kPa
	E_{oed}^{ref}	8000	kPa
	E_{ur}^{ref}	25,000	kPa
Shear modulus	G_{ref}	4000	kPa
Co-efficient of earth pressure	k_0	0.5	
Bulk density	ϒ	19	kN/m^3
Dry density	$ϒ_d$	17	kN/m^3
Tunnel parameters			
Tunnel diameter	D	6	M
Axial stiffness	EA	9,000,000	kNm/m
Bending stiffness	EI	32,000	kNm^2/m
Segment thickness	T	0.3	M

3 Finite Element Modelling

In order to assess the effects of geotechnical parameters on ground settlements, finite element analysis was carried out using PLAXIS 2D. The analysis was carried out in plane strain model with 15-node elements. The mesh was considered fine. The geometry (40 × 80 m) considered was symmetrical in nature, and hence only half portion was considered for the analysis (Fig. 2). Standard fixities were considered for the model with full fixity at the bottom ($U_x = U_y = 0$) and roller condition at vertical sides ($U_x = 0$). Hardening soil model was used for the simulation citing the stress-dependent accounting of stiffness modulus in it. Tunnel lining has been simulated using the tunnel element provided in PLAXIS. For the analysis, 1% volume loss was assumed. Table 1 lists the default geotechnical and tunnel properties assumed for the analysis, which was varied to study the effect on ground deformations.

Tunnelling can basically be defined as a form of excavation which leads to changes in stresses. Different types of soil exhibit different behaviour, i.e. undrained and drained conditions during excavation process; hence, different soil types were considered to simulate different stress conditions during the excavation, i.e. total stress/undrained and effective stress/drained conditions. Corresponding parameters are then varied, and the consequent effects on the ground movements have been studied.

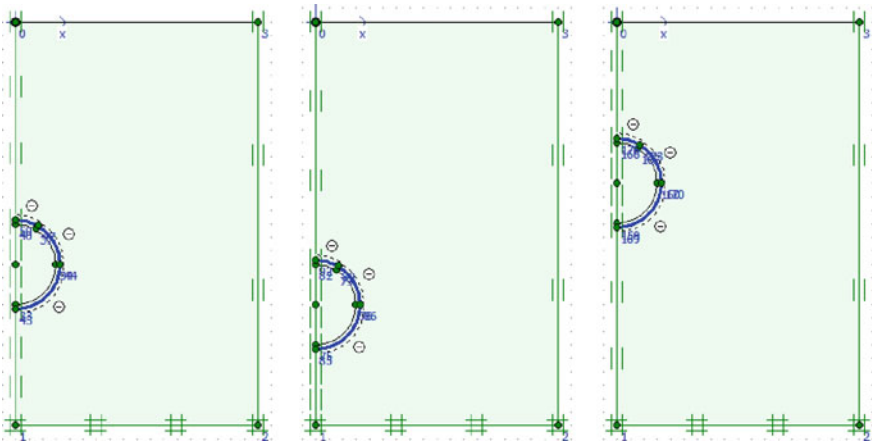

Fig. 2 Finite element model showing different depths of tunnel

4 Geotechnical Factors Effecting Ground Deformations

The geotechnical parameters of the existing soil have a profound effect on the observed surface ground movements. From the numerical analysis, it can be said that the following geotechnical parameters had an impact on the observed pattern of maximum ground settlements.

- Cohesion (Undrained/Effective)
- Friction Angle of soil
- Young's Modulus of Soil.

Following figures represent the observed trend of maximum settlement upon varying the respective geotechnical parameters.

It is quite evident from the observed trend in Fig. 3 that cohesion of soil and surface ground deformations generated are inversely proportional to each other. This can be explained as the cohesion of soil is directly proportional to the shear strength of soil and hence directly relates it to its attractive/bonding forces. Hence stronger the cohesion is, stronger will be the intermolecular bonding and attractive forces between them which will hold the soil particles to each other and reduce the ground movements. Several other parametric case studies conducted by Bahtiyar Unver et al. in 2013 and Houari Ouabel in 2014 have confirmed the observed trend, whereby the ground movements decreased with an increase in the cohesion of soil.

Figure 4 depicts the observed trend of variation of friction angles of soil. Since the friction angle of soil is again directly proportional to the shear strength of soil, it was observed that the ground settlements were indirectly proportional to the soils friction angle. The observed behaviour can be explained from the aspect that the friction angle of soil relates the soil to its interparticle arrangement of the soil and hence to its shear strength.

Young's modulus or modulus of elasticity of soil is a stiffness parameter. Therefore, a considerable reduction in ground movements was observed due to the increase in stiffness parameter of the soil, i.e. Young's modulus. From the

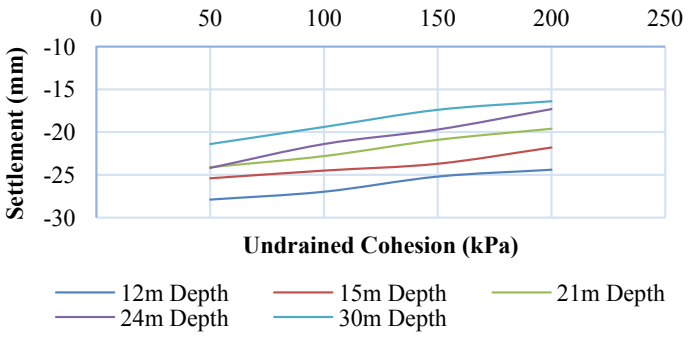

Fig. 3 Observed trends of settlements in FEM analysis upon varying cohesion and tunnel depth

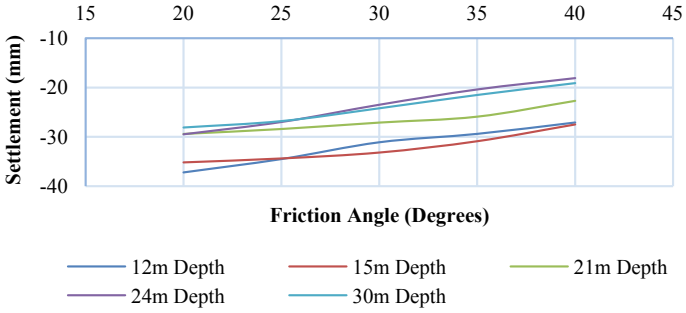

Fig. 4 Observed trends of settlements in FEM analysis upon variation of friction angle and tunnel depth

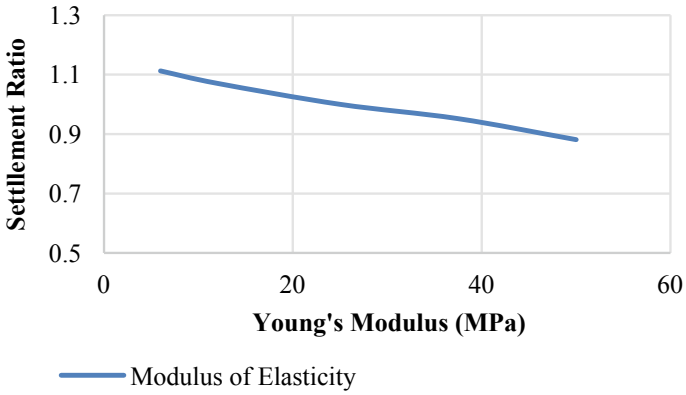

Fig. 5 Observed trends of settlements with respect to the modulus of elasticity of soil

mentioned results in Fig. 5, it can be clearly observed that the observed ground movements are a function of soil parameters on a great extent.

The observed variation has been expressed in the form of **parametric settlement ratio,** i.e. the ratio of maximum finite element settlements to maximum theoretical settlements. From the observed trend and pattern, geotechnical factors based upon the settlement ratio can be considered to represent the effect of existing geological and geotechnical conditions on ground movements. The values suggested for the corresponding geotechnical factors can be considered from the suggested figures (Figs. 6 and 7).

The observed trend of the settlements with respect to parametric variation was found to be in good agreement with several literatures. Bahtiyar Unver et al. in 2013 conducted a detailed study to assess the parametric trend of surface settlements due to tunnel. Field observations from various metro lines, i.e. Tehran Metro, Istanbul Metro and Mashhad Metro, were compared with the results from empirical and numerical approaches using finite element difference method. Since field

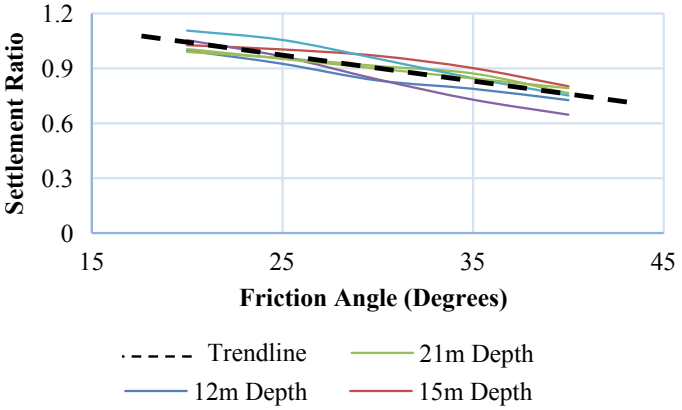

Fig. 6 Observed trend of settlements ratio with respect to the friction angle of soil

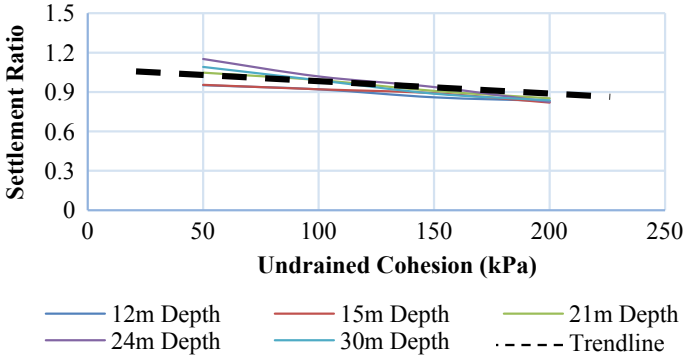

Fig. 7 Observed trends of settlements ratio with respect to the undrained cohesion of soil

observations covered vast geology, parametric studies were undertaken to assess the trend for the variation. The study concluded by suggesting a new equation with the incorporation of more parameters for assessment of settlements. The obtained trend of parametric variation is in good agreement and validates the results of the current study. Luis Miranda et al. studied the influence of geotechnical variability in tunnel excavation. Statistical variation was studied using two computational tools, i.e. FLAC and MATLAB. The numerical study was then compared to the field settlement observations from the Alfornelos tunnel. The results regarding the parametric variation were found to be comparable with the results of the current study. Houari Ouabel in 2014 conducted a parametric study of mechanical response around the tunnel. Numerical results were compared to the results of the Algiers Metro. The results suggested that geotechnical parameters had an obvious influence on the settlements. Poisson's ratio, Young's modulus and friction angle were found as the important influencing parameters.

Observed trend of ground movements with respect to parametric variation as depicted in several above-mentioned literatures and field observations concur with the results of the current study and thereby validate it. Considering the results, patterns, figures and correlations from the observed trend of current study, a more refined assessment of the anticipated ground movements and their anticipated response to the buildings and structures in close proximity can be done.

5 Pattern of Sub-surface Settlements

For the current study, since the soil conditions were assumed to be homogeneous and isotropic for the numerical analysis, the patterns of propagation of sub-surface settlements were studied for both total stress and effective stress conditions. The observed pattern of sub-surface settlements was further analysed for the parametric variation. The observed patterns suggested that the propagation of settlements or sub-surface settlements varied with different geotechnical conditions and properties. The propagation of maximum settlements along the sub-surface tunnel axis was found to incrementally increase with an increase in depth and reaching its maximum at its crown level. The observed trend of sub-surface settlements has been represented by **sub-surface settlement ratio,** i.e. ratio of surface settlements to sub-surface settlements along the tunnel axis. Parametric variations revealed the geotechnical factors affecting the pattern of propagation and were found to be similar to the factors affecting the ground movements on the surface as it can be observed in Figs. 9 and 10 that the propagation of settlements reduced with an increase in shear strength parameters or stiffness of soil. Although the theoretical assessments consider the effect of geometrical level of tunnel axis, the geotechnical aspects are worth to be accounted for. The results presented in Figs. 8, 9 and 10 suggest that in both total stress and effective stress conditions, the settlements increased incrementally with respect to depth and reached its maximum at tunnel crown level.

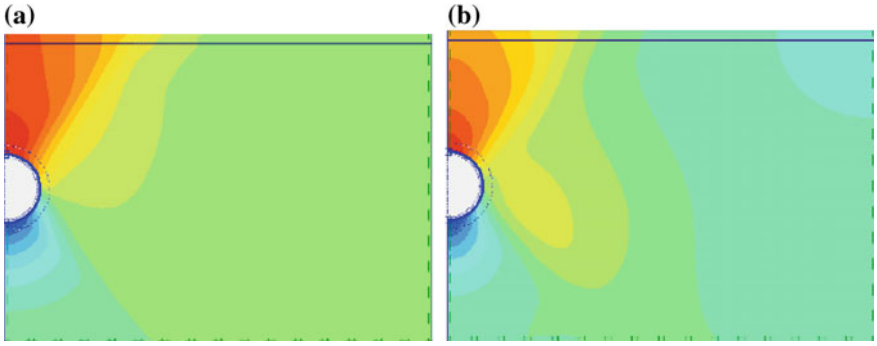

Fig. 8 Depiction of trend of settlement in **a** effective stress condition **b** total stress condition

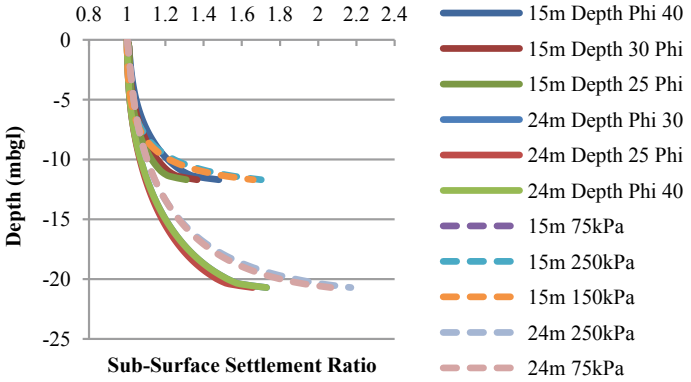

Fig. 9 Trend of propagation of maximum settlements (sub-surface settlements) in total and effective stress conditions with respect to depth

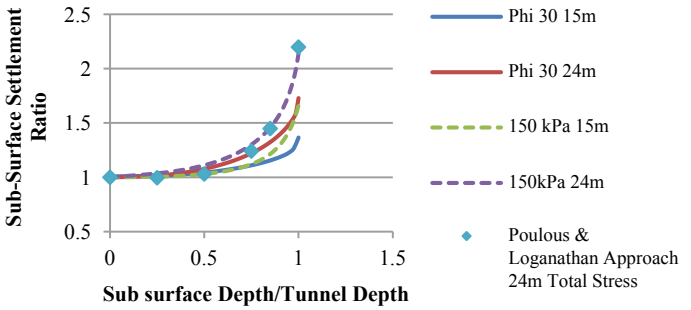

Fig. 10 Observed surface/sub surface settlement ratio in total/effective stress conditions with respect to settlement depth/tunnel depth

Figures 9 and 10 illustrate the sub–surface settlements in both effective and total stress conditions, whereby a parabolic trend with an increase in depth has been followed. The observed sub-surface settlement ratio, i.e. maximum surface/sub-surface ratio increased with depth with its maximum at tunnel crown. For effective stress/drained condition, the increment ratio of surface to sub-surface settlement was found to be 1.3:1.6, whereas in the case of total stress condition, a range of 1.7–2.3 (Fig. 9) was observed. Similar trend and range have been observed in empirical correlation suggested by Loganathan et al. The reason for the behavioural difference in the propagation pattern can be explained as the cohesion of soil or inter-particle bonding between soil particles. Due to inter-particle bonds amongst the soil particles, the same volume loss propagates as relatively smaller settlement at the surface. Another important factor worth attributing the behavioural difference in observed pattern of propagation in different soil conditions can be cited as the point of inflexion, i.e. i-value in aforementioned Eq. 1 which varies with different

soil conditions. The observed trends of propagation of settlements can find their possible application in assessing settlements for the construction of tunnels above or below tunnels, basements, pipelines, and underground utilities in close proximity of bored tunnel.

6 Geotechnical Capacity Loss Due to Induced Ground Movements

In order to assess the geotechnical capacity loss generated due to ground movements, the behaviour of ground movements during the simulation of twin tunnelling was studied. In the analysis, construction of a bored tunnel was simulated in proximity to an existing bored tunnel. For the simulation, both the bored tunnels were considered having same geotechnical and tunnel lining parameters, with the first tunnel being constructed a definite time interval before the second tunnel.

The analysis sequence can be briefly described: twin bored tunnel construction sequence has been simulated in PLAXIS. The parameters considered for the analysis were the same as aforementioned in this paper. In order to simulate the practical construction sequence, a definite time period has been considered between the construction sequences of both the tunnels, for simplicity, it has been assumed as 30 days. The finite element analysis results suggest that even upon keeping all the affecting parameters same, relatively higher magnitude of surface settlements were observed for the second/latter bored tunnel (Fig. 11). A suitable explanation for the phenomenon is the associated geotechnical capacity loss due to the ground movements produced due to the first tunnel. This can be explained as the construction of the first tunnel induces volume loss and exhibits ground movements/settlements. Now due to these induced settlements, the soil gets remoulded/disturbed and undergoes a certain degree of loss in its shear strength, i.e. the geotechnical capacity loss.

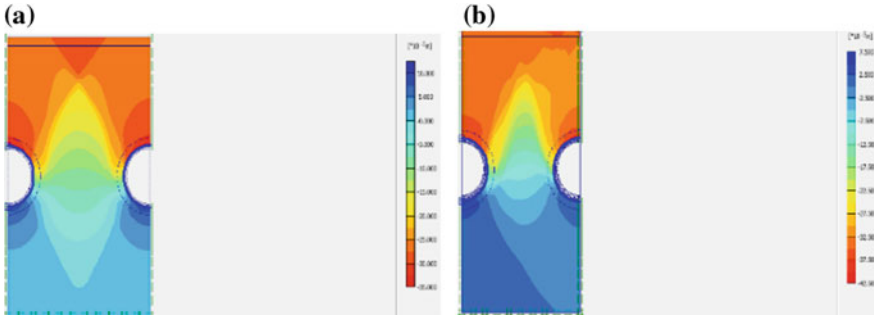

Fig. 11 Comparative settlements **a** both tunnels constructed at same time **b** Second tunnel constructed after some time interval

According to the results of the current study described in Sect. 5, the settlements generated are function of the shear strength of soil and are inversely proportional to it; therefore, when the second bored tunnel is constructed in proximity to the existing first tunnel, due to the reduced shear strength or geotechnical capacity, the observed settlements are relatively greater than the settlements in the first tunnel. For precise assessment of settlement due to the second tunnel, the geotechnical factors pertaining to the reduced shear strength must be accounted for.

From the analysis, it can be said that the degree of geotechnical loss is found to be in direct correlation with the induced settlements.

Figure 11 shows the comparative trend of settlements and geotechnical loss observed in the case of twin tunnels simulated simultaneously and with a definite time interval. It is evident from Fig. 11a that simulation of twin tunnels at the same time, i.e. with no time interval, leads to symmetrical settlements at both tunnel axes, whereas upon provision of a time lapse between the simulations of twin tunnels as shown in Fig. 11b, the latter tunnel yields a relatively greater settlement value. This aspect validates the phenomenon of geotechnical loss associated due to tunnelling. In order to ascertain the extents of the effects of geotechnical loss, centre-to-centre spacing of tunnel axes were varied and the **twin tunnel settlement ratio,** i.e. the ratio of maximum surface settlement observed at the axis of the first tunnel to the maximum surface settlement observed at the axis of the second/latter tunnel, was observed.

Figures 12 and 13 illustrate the effect observed upon varying the geotechnical parameters and horizontal centre-to-centre spacing between the tunnel axes in effective and total stress conditions. The effect of geotechnical capacity loss was found to be relatively more profound in effective stress conditions since the observed maximum settlement ratio was found to be in range of 1.1–1.2 and the effect was observed till a transverse distance of 2.0–2.5 times the diameter of tunnel

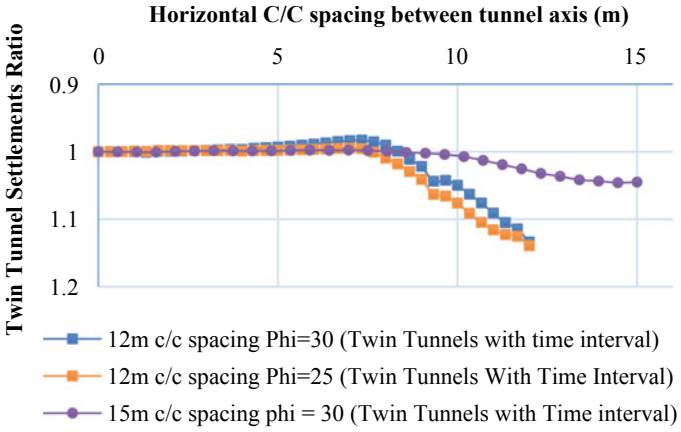

Fig. 12 Comparison of settlement ratio for twin tunnel simulation with time interval in effective stress condition

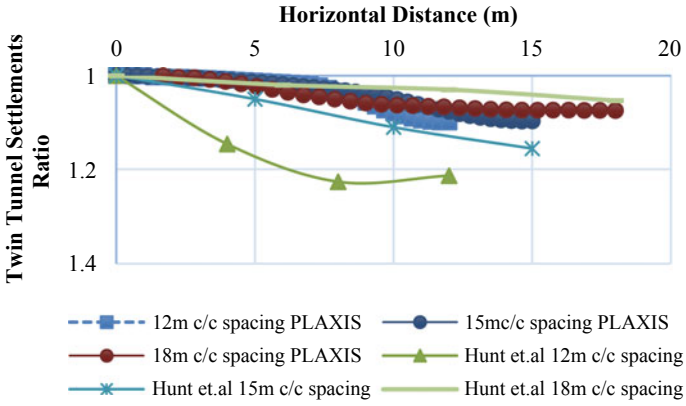

Fig. 13 Comparison of twin tunnel settlement ratio for twin tunnel simulation with time interval in total stress condition

(2–2.5 D) from the tunnel centre, after which the effects were reduced or were found to be negligible. Total stress conditions as the settlement ratio was found to be in the range of 1.06–1.1. The effect of geotechnical loss was observed for a transverse distance, i.e. 3.0–3.5 times the diameter of tunnel (3–3.5 D).

From the simulations and the results presented in Figs. 12 and 13, we can say that the trend of observed geotechnical capacity loss is in direct correlation to the observed trends of the settlements as described in Sect. 5. The reason for the occurrence of the observed trend could be explained by the pattern of settlements observed in respective soil types.

The observed occurrence has been documented in FHWA tunnel manual (FHWA Technical Manual for Design and Construction of Road Tunnels, ITA/AITES Report 2006), where the observed phenomenon of the higher degree of settlements in the second bored tunnel has been mentioned Burland (1995). In recent years, several case studies and literatures have been put forward citing the asymmetrical trend of settlements induced due to twin tunnel boring. In the year 2005, Hunt carried out a detailed study and proposed the modification factors for assessment of settlement due to second tunnel of twin tunnels Hunt (2005). Hunt also proposed the modification applicable to the vertical and horizontal displacements for the twin tunnelling. Figure 12 also compares the effect of variation of horizontal centre-to-centre distance in twin tunnelling in soft soil according to Hunt. The trends observed are similar to the results observed from the numerical simulation. In the year 2014, M. Molina et al. (2014) conducted a study encasing various case studies and various empirical theories put forward and compared the observed results Laver (2011). The results are in good agreement with the findings of the present study and validate the observed phenomenon of asymmetrical settlement produced due to twin tunnels.

The observed geotechnical loss due to twin tunnelling can be compared with the similar phenomenon observed in piles. During construction of group piles, it is a recommended practice that the spacing of piles be minimum 2.5–3.0 times the

diameter of pile in order to avoid the overlapping of the pressure bulbs generated or geotechnical capacity loss generated due to piling. The observed geotechnical loss can basically be termed as temporary in nature as the soil is likely to regain the geotechnical loss with time owing to its thixotropic nature.

7 Conclusion

Following points can be concluded from the study:

The results of the theoretical settlements and settlements obtained using the finite element method were found to be comparable, but upon varying the geotechnical parameters of the soil, an appreciable change was observed in the observed maximum settlement. Based on the observed set of results in total stress/undrained conditions and effective stress/drained conditions, corresponding strength and stiffness parameters such as cohesion, friction angle and Young's modulus of soil were found to be the important geotechnical parameters, since inverse correlation was observed between the cohesion/friction angle of soil and the observed maximum settlements observed.

The observed pattern of propagation of sub-surface settlement in homogeneous and isotropic soil suggested that the settlements increased incrementally with an increase in depth with its value reaching the maximum at the crown level of the tunnel. The settlements increased in a linear parabolic trend in both effective stress/drained and total stress/undrained condition. The ratio of incremental increase of maximum settlement at tunnel crown level with respect to surface settlements was observed to be considerably high in total stress condition/clayey soils (1.7–2.3) as compared with effective stress condition/sandy soils (1.3–1.6).

The study investigated the associated geotechnical loss/loss in shear strength generated due to ground movements by simulation of twin tunnelling operation; it was observed that simulation of second or latter tunnel of the twin tunnel produced a relatively larger magnitude settlement. The reason for the observed phenomenon was assessed to be the geotechnical loss or loss in shear strength of soil generated due to the ground movements produced due to the simulation of the first/existing tunnel. To study the extent of the geotechnical loss observed due to twin tunnelling, the horizontal centre-to-centre spacing between the tunnels was considered as a varying parameter. In total stress condition, the effect of geotechnical loss on the second tunnel was found to be in the range of 1.06–1.1 times the effect on first tunnel, and the effect was found to be till the distance of 3.0–3.5 D, whereas in effective stress condition the effect was in the range of 1.1–1.2 times the effect in the first tunnel was extended to 2.0–2.5 D in transverse direction.

The results suggest that a precise range of settlements can be assessed considering the effect of geotechnical parameters and by considering the associated loss due to twin tunnelling. The precise evaluation of ground movement will further lead to even accurate assessments of the impact on the structures in proximity.

References

Atkinson JH, Potts DM (1979) Subsidence above shallow tunnels in soft ground. J Geotech Engin, Am Socie Civil Engin GT4:307–325

Attewell PB, Yeates J (1984) Tunnelling in soil. In: Attewell PB, Taylor RK (eds) Ground movements and their effects on structures, Surrey University Press, London, pp 132–215

Attewell PB, Yeates J, Selby AR (1986) Soil movements induced by tunnelling and their effects on pipelines and structures. Blackies and Sons Ltd, London

Boscardin MD and Cording EJ (1989) Building response to excavation-induced settlement. ASCE, J Geotech Eng 115(1):1–21

Burland JB (1995) Assessment of risk of damage to buildings due to tunnelling and excavations. In: Invited Special Lecture to IS-Tokyo'95: 1st international conference on Earthquake Geotechnical Engineering

Burland JB, Broms BB, de Mello VF (1977) Behaviour of foundations and structures. In: 9th International Conference on Soil Mechanics and Foundation Engineering. Tokyo, State-of-the-Art Report, pp 495–546

Cording EJ, Hansmire WH (1975) Displacements around soft ground tunnels—General Report. In: 5th Pan American Conference on Soil Mechanics and Foundation Engineering, Buenos Aires, Session IV, pp 571–632. French translation by J. Ke´risel, Les de´placements autour des tunnels en terrain tendre (1977, AFTES-TOS, no. 8 et 12)

El Houari, N et.al (2011) Numerical simulation of the mechanical response of the tunnels in the saturated soils by Plaxis Jordan. J Civ Eng 5(1):9–31

FHWA Technical Manual for Design and Construction of Road Tunnels—Civil Elements Publication No. FHWA-NHI-10-034

Hunt DVL (2005) Predicting the ground movements above twin tunnels constructed in London Clay. Ph.D. Thesis—University of Birmingham. Birmingham, 302

ITA/AITES Report (2006) On Settlement induced by tunnelling in Soft Ground. Tunn Undergr Space Technol 22(2007):119–149

Laver R (2011) Long-term behaviour of twin tunnels in London Clay. Ph.D. Thesis by Richard Laver. University of Cambridge

Loganathan N, Poulos HG (1998) Analytical predictions of tunnelling induced ground movements. Geotech Engin J, Am Socie Civil Engin 124(9)

Mair RJ, Taylor RN, Burland JB (1996) Prediction of ground movements and assessment of building damage due to bored tunnelling. In: Mair RJ, Taylor RN (eds) International Symposium on Geotechnical Aspects of Underground Construction in Soft Ground, Balkema, pp 713–718

Mair R, Taylor R and Bracegirdle A (1993) Sub-surface settlement profiles above tunnels in clay. Geotechnique 43(2):315–320

Molina Rodriquez M et.al (2014) Twin tunnels and asymmetrical settlement troughs in soft soils. Proceedings of the world tunnel congress 2014—tunnels for a better Life. Foz do Iguaçu, Brazil

O'Reilly MP and New BM (1982) Settlements above tunnels in the United Kingdom—their magnitude and prediction. In: Proceedings of Tunnelling '82. IMM, London

Peck RB (1969) Deep excavations and tunnelling in soft ground, Proc. 7th Int. Conf. On Soil Mechanics and Foundation Engineering, Mexico City, State-of-the-Art Volume, pp 225–290

Peck RB (1969) Advantages and limitations of the observational method in applied soil mechanics. Geotechnique 19(2):171–187. ICE, London

Sagaseta C (1987) Evaluation of surface movements above tunnels: a new approach. Colloque ENPC Interaction Sols-Structures, Paris, pp 445–452

Schmidt B (1989) Consolidation settlements due to soft ground tunnelling. In: 12th International Conference on Soil Mechanics and Foundation Engineering, Rio, pp 797–800

Verruijt A, Booker JR (1996) Surface settlements due to deformation of a tunnel in an elastic half plane. Geotech 46(4):753–756

Part IV
Ground Improvement Techniques for Transportation Geotechnics

A Comparative Study of Design and Construction Practice of Stone Column

Suprit Jakati, Anirudha Joshi and Yashwant A. Kolekar

Abstract Stone column is a proved ground improvement technique used for the enhancement of bearing capacity of soft soil and to accelerate the consolidation effect. The design criteria and the construction technique of the stone column vary according to the type of soil, soil drainage conditions, and the type of project involved. In most of the ground improvement projects, due to lack of knowledge and poor practice in construction technique, the time and cost of an overall project gets adversely affected. The present study involves different methods of analyzing the effectiveness of stone column. The present work also includes a comparative study of the standard codes for the design and construction of stone column of different countries and organisations. The effects of the difference in calculation of basic parameters, design considerations, and installation techniques have been studied, and an attempt is made to provide the best possible procedure for the design and construction of stone column.

Keywords Stone column · Ultimate load analysis · Settlement analysis · Material standards

1 Introduction

In the developing countries like India, the increasing value of land demands modern techniques for the ground improvement of the weak soil deposits. Among many ground improvement techniques, ground improvement by installing stone columns has been practically and economically effective. Stone column installation primarily

S. Jakati (✉) · A. Joshi · Y. A. Kolekar
Department of Civil Engineering, College of Engineering Pune, Pune, India
e-mail: jakatisuprit@gmail.com

A. Joshi
e-mail: anirudha.arj@gmail.com

Y. A. Kolekar
e-mail: yak.civil@coep.ac.in

R. Sundaram et al. (eds.), *Geotechnics for Transportation Infrastructure*,
Lecture Notes in Civil Engineering 29,
https://doi.org/10.1007/978-981-13-6713-7_28

enhances the bearing capacity of the soft soil and accelerates the consolidation effect. The stone columns are capable of dissipating excess pore water pressure, reducing void ratio in zone of influence and helps to achieve greater slope stability. According to Aljanabi et al. (2013), some of the field measurements prove the fact that stone columns improve the shear strength and compressibility parameters of the soft grounds, on which highway and railway embankments are constructed. The stone columns provide an effective drainage path to ensure rapid consolidation which results in a quick gain in shear strength of in situ soils. Hence, the stone column method of ground improvement accelerates the overall construction schedule and helps in the completion of the project well within the stipulated time. Hence, the stone column technique of ground improvement is encouraged in the construction of highway and railway embankment, shipbuilding facilities, sewage treatment plants, storage tanks in oil and gas refineries, and many projects which cover a vast land area.

The present paper attempts to understand the basics of different methods of ultimate load analysis and settlement analysis of stone columns. Also, the different construction practices, specifications of material used for construction, and different types of test during and after the construction of stone columns are discussed.

2 Design Considerations of Ultimate Load Capacity

Different researchers have proposed the theories for the estimation of ultimate load capacity of stone column. Generally, the load capacity of stone column is controlled by the passive resistance of the soft soil and the friction angle of the granular material used.

2.1 Cavity Expansion Theory

The idea that the stresses in the stone column exists in state of triaxial state, and both the stone column and surrounding soil are about to fail, which is the essential assumption made to provide analytical solutions. In these methods of solutions, the ultimate passive resistance of the surrounding soil is equated to the lateral confining stress σ_3. From the classical plastic theory, the ultimate vertical stress, σ_1, is equal to the coefficient of passive pressure of the stone column, k_p, times the lateral confining stress. Hence,

$$\sigma_1/\sigma_3 = (1 + \sin \Phi_s)/(1 - \sin \Phi_s) = k_p \tag{1}$$

where Φs = angle of internal friction of the stone column.

The cavity expansion theory suggests that the passive resistance developed by the surrounding soil can be modeled as an infinitely long cylinder which expands

about the axis of symmetry until the ultimate passive resistance of the surrounding soil is developed. Thus, the behavior of lateral bulging of stone column can be imitated for the study and compared to the expanding cylindrical cavity. Considering the elastic–plastic theory given by Gibson and Anderson (1961), for a frictionless material and infinitely long expanding cylinder cavity, the expression for ultimate lateral stress σ_3 is given by:

$$\sigma_3 = \left\{ \sigma_{ro} + c \left[1 + \log_e \frac{E}{2c(1+\mu)} \right] \right\} \tag{1a}$$

Considering q_{ult} as σ_1 and substituting Eq. 1a in Eq. 1, we get

$$\sigma_{ult} = \left\{ \sigma_{ro} + c \left[1 + \log_e \frac{E}{2c(1+\mu)} \right] \right\} (1 + \sin \Phi_s)/(1 - \sin \Phi_s) \tag{2}$$

where

q_{ult} ultimate stress that can be applied to the stone column
σ_{ro} total in situ lateral stress (initial)
E elastic modulus of the soil
C undrained shear strength
μ Poisson's ratio
Φ_s angle of internal friction of the stone column.

Further, Vesic's (1972) extended the above theory and accounted the friction of the soil into the theory. According to this theory, the ultimate stress that can be applied to stone column is given by:

$$q_{ult} = \left[c\, F'_c + q\, F'_q \right] (1 + \sin \Phi_s)/(1 - \sin \Phi_s) \tag{3}$$

where

c cohesion
q mean stress measured in all direction at equivalent failure depth
F'_c, F'_q Vesic's cavity expansion factors.

The Vesic's cavity expansion factors are function of angle of internal friction, poisons ratio, and cohesion of the surrounding soil. The following table suggests the values of equivalent modulus of elasticity to be considered with respect to certain soil quality.

Type of soil	Equivalent modulus of elasticity
Non-organic (soft to stiff)	11 times of cohesion(11C)
Organic or very soft soil with plastic index > 30	5 times of cohesion(5C)

For a good analysis, the crushed stones with angle of internal friction 42°–45° and gravel with angle of 38°–42° should be considered.

The cavity expansion theory can be used to estimate both the short- and long-term ultimate capacity of the stone column.

2.2 Indian Standard Code Method

According to Indian Standard Code IS 15284 part 1 (2003), for determination of ultimate bearing capacity of stone column the code assumes triaxial state of stress in the stone column, and both the column and surrounding soil are at verge of failure. Hence, Eq. (1) holds good for this theory too. Load capacity of the treated ground is obtained by summing up the bearing capacity resulting from the resistance offered by the surrounding soil against its lateral deformation (Q_1), resistance offered by the soil due to surcharge over it (Q_2), and the bearing support provided by the intervening soil between the columns (Q_3).

Therefore, the overall safe load (Q) on each column and its tributary soil is given by:

$$Q = Q_1 + Q_2 + Q_3. \tag{4}$$

2.2.1 Estimation of Q_1

The bearing capacity resulting from the resistance offered by the surrounding soil against its lateral deformation (bulging) is given by:

$$Q_1 = (\sigma_v \pi / 4D^2)/\text{F.S} \tag{5}$$

And

$$\sigma_v = (\sigma_{ro} + 4C_u)\text{Kp}_{col} \tag{6}$$

where

σ_v limiting axial stress in the column when it approaches shear failure due to bulging
D diameter of stone column
σ_{ro} initial effective radial stress

$$\text{Kp}_{col} = \tan^2(45^\circ + \Phi/2) \tag{6a}$$

F.S factor of safety.

2.2.2 Estimation of Q_2

The surcharge load may be due to the application of sand blanket and sand pad. Due to this load, consolidation takes place and the strength of the soil increases. Hence, the increase in the soil strength reduces the bulging of the stone column. Hence, this additional increase can be calculated by using the relation:

$$\Delta\sigma_{\mathrm{ro}} = \frac{q_{\mathrm{safe}}}{3}(1 + 2\,K_{\mathrm{o}}) \tag{7}$$

where

$$q_{\mathrm{safe}} = C_{\mathrm{u}}\mathrm{Nc}/2.5 \tag{7a}$$

Cu undrained cohesion
Ko at rest lateral earth pressure.

The bearing capacity generated due to resistance offered by the soil due to surcharge over it can be calculated by the formula:

$$Q_2 = (\mathrm{Kp}_{\mathrm{col}}\Delta\sigma_{\mathrm{ro}}A_{\mathrm{s}})/\mathrm{F.\ S.} \tag{8}$$

2.2.3 Estimation of Q_3

The bearing support provided by the intervening soil between the columns can be calculated by the formula:

$$Q_3 = q_{\mathrm{safe}}A_{\mathrm{g}} \tag{9}$$

where

A_{g} area of the intervening soil for each column and its tributary soil
$\mathrm{A_g}$ $0.866\ \mathrm{S}^2 - (\pi D^2/4)$…for triangular pattern of installation
$1.0\ S^2 - (\pi D^2/4)$…for square pattern of installation.

D and S are diameter and spacing of the stone columns.

3 Settlement Analysis of Stone Column

The methods available for the settlement analysis of stone column can be broadly classified under two categories:

1. Simple approximate methods, depending on certain assumptions.
2. Complex methods, involving fundamental behavior which requires finite element methods to obtain the solutions.

3.1 Equilibrium Method

The equilibrium method is a very simple method based on stress concentration factor n and the replacement ratio a_s. Though simple calculations are involved, the theory provides satisfactory settlement results when compared in reality. As the vertical stresses generated are inversely related to stress concentration factor n and replacement ratio a_s, the lower values of these factors provide a safer estimate in the settlement analysis.

The following assumptions are used by Barksdale and Bachus (1983) in developing the equilibrium method: (1) The idealization of unit cell holds good; (2) depending on the stress concentration ratio n of the stone column and its tributary soil, the total vertical load applied to the unit cell is shared between the stone column and the tributary soil in the unit cell; (3) there is a equal amount of displacement in the stone column and its tributary soil due to external loading; and (4) a uniform vertical stresses due to external loading exist throughout the length of the stone column.

The applied stress, σ, is shared between the columns and the surrounding soft ground in proportion to the relative stiffness of the two materials, the cross-sectional area of the columns, and their spacing.

The sharing of applied load between the soil and stone column is determined from the following formulae:

$$\sigma_g = \frac{\sigma}{1+(n-1)a_s} \quad \sigma_s = \frac{n\sigma}{1+(n-1)a_s} \tag{10}$$

or

$$\sigma_g = \mu_g \sigma \quad \sigma_s = \mu_s \sigma \tag{11}$$

where

σ applied stress
σ_g vertical stress in surrounding ground
σ_s vertical stress in compacted columns.

The consolidation settlement of the composite (treated) soil S_t is given by:

$$S_{t,} = m_v \sigma_g H \tag{12}$$

$$= m_v \mu_g \sigma H \tag{12a}$$

where

m_v modulus of volume decrease of soil and
H thickness of treated soil.

3.2 Design Charts for Settlement Analysis

3.2.1 Priebe Method

The unit cell model of stone column is considered for estimating settlement in ground treated with stone column. The assumptions made in the analysis also include the triaxial state of stress within the unit cell and the generation of uniform pressure in the entire unit cell.

Priebe formulated the curves which related the ratio of settlement of untreated to treated ground S/S_t, the area replacement ratio a_s, and angle of internal friction of the stone Φ_s.

3.2.2 Greenwood Method

The empirical charts were given by Greenwood (1975), which primarily established the relation between the settlement reduction in ground due to stone column, the spacing of stone column, and undrained soil strength in the unit cell.

The manual of ground improvement for highways of Federal Highway Administration can be referred for the details and applications of the design curves suggested by the above two methods.

3.3 Finite Element Methods

In the modern day where digital computers are easily accessible, the behavior of the ground improved by stone column can be easily studied using finite element methods. These methods consider more amounts of natural characteristics of the materials and their behavior. During the analysis of stone column using finite element method based software, the materials can be modeled as elastic or plastic and their settlements may be linear or non linear. During the analysis of stone column using finiteelement method based software, the materials can be modeled as elastic or plastic and theirsettlements may be linear or non linear.

For the best estimate, settlement should be taken as being the average of simple approximate methods and complex finite element methods. Generally, equilibrium methods yield more settlement, and finite element method yield less settlement compared to actual ground settlement.

4 Subsurface Investigation and Testing of the Unimproved Ground

As a preliminary work in any construction project, ground investigation plays a major role which decides required resource, cost, and completion of the project.

A successful ground investigation can clearly suggest the need of the ground improvement and a suitable, effective method to overcome the problem.

A detailed survey of the existing neighboring projects can be helpful in deciding the parameters used in ground improvement technique. The study of geological conditions and major events in the past at the site shall be valued during the investigation.

According to Barksdale and Bachus (1983), the following points provide a helping hand for the better planning and execution for the subsurface investigation of the unimproved soil. The Subsurface investigation guidelines mentioned in NHBC standard helps in better subsurface investigation.

1. A detailed study of subsurface exploration includes sampling, establishing the depth of bore hole and spacing of test borings.
2. Generally, the upper earth's crust is made up of loose and weak soil; hence, it is important to have a detailed and rigorous investigation till this depth. If the depth of treatment and the depth of stone column are calculated, then the bore holes should be extended to the depth equal to that of stone column. Generally, subsurface investigations are terminated after reaching the firm hard strata.
3. A number of penetration tests have to be conducted on the sites. The vane shear test provides better results of undrained cohesive strength of the soil. The standard penetration test and Dutch cone penetration test shall be used depending on the type of soil. The code of practice associated with the location of the sites shall be practiced to know the quantity and depth of samples to be taken.
4. The piezometers should be installed in selected boreholes to observe the variations in groundwater level.
5. For the area with peat deposits, open test pits shall be dug for investigations.

4.1 Tests on Soil

General tests to determine index properties and engineering properties shall be conducted to have a preliminary data for the design and construction of stone columns. The following guidelines suggest mandatory and frequently conducted tests:

1. The index properties of the soil have to be established with help of test like liquid limit, plastic limit, water content, and specific gravity. Further triaxial test may be conducted to find the elastic modulus of soil. Any established relations between the soil properties and elastic modulus may also help. The above properties are must required when numerical based software is used for the analysis of the stone column.
2. The field vane tests have to be conducted in the soft cohesive soils to know the value of the undrained shear strength. Also, undrained shear strength has to be calculated from shear test in the laboratory and has to be compared with the results available from field tests.

3. To determine settlement characteristics of the cohesive soils, one should perform a one-dimensional consolidometer test. Since soil behavior cannot be predicted accurately, more number of samples must be subjected to the consolidation test. Barksdale suggests a minimum number of ten samples to be subjected to the consolidation tests for weak strata.
4. Permeability tests have to be conducted in the laboratory with more number of samples to get an average value of coefficient of permeability. On field, pumping test can be made to know the in situ permeability of the soil. This coefficient of permeability factor plays a very important role in evaluation of settlement and determining bearing capacity of the treated ground.

5 Material Standards

5.1 Stone

The crushed stone (gravel) for column backfill shall be well graded. To minimize the risk of failure of stone column, the crushed stone should be hard, unweathered stone free from organics, trash, or other deleterious materials. The stones should not react chemically with the existing ground properties thus leading to complications. The gradation, specific gravity, density of loose stone, and density of compacted stone should be as per design requirement. The crushed stones of nominal size 20–75 mm are normally accepted.

5.2 Sand

As the sand blankets are used for providing uniform loading on the site to be improved, the material should have identical properties with respect to hardness and the source it is made up from. Well-graded sand shall be used with a mean diameter of at least 0.2 mm. The sand shall contain less than 15% passing through 75 micron sieve of Indian Standard.

5.3 Water

Water available from the local source can be used for the construction of stone column given it does not chemically react with materials used and deteriorate the strength of stone column.

6 Conclusion

In this paper, a comparative study is made for the design and construction practices for stone columns, which are followed generally worldwide. The technical inputs of the present paper are discussed after studying various standard codes, manuals, and construction reports on the design and construction of stone column.

In considering design analysis of ultimate load capacity, various methods are available depending on the interactive behavior and load transfer between the stone fill and its tributary soil. The best design should be provided considering one's design philosophy with actual site conditions. The settlement analysis should be calculated using simple hand calculation techniques as well as from the complex finite element analysis. The average of both the results is generally considered as best solutions for settlement analysis. Further, some guidelines are provided for the subsurface investigations of unimproved sites, tests to be performed, and material standards that must be used for the construction of stone column.

References

Aljanabi QA, Chik Z, Kasa A (2013) Construction of a new highway embankment on the soft clay soil treatment by stone columns in Malaysia. J Eng Sci Technol 8(4):448–456.

Barksdale RD, Bachus RC (1983) Design and construction of stone columns, vol I. Federal Highway Administration, Washington, D.C.

Design and construction for ground improvement—Guidelines, Part 1: Stone columns. IS 15284-1 (2003)

Gibson RD, Anderson WF (1961) In-situ measurements of soil properties with pressure meter. Civ Eng Public Works Rev 56(658)

Greenwood DA (1975) Vibroflotation: rationale for design and practice. In: Bell FG (ed) Methods of treatment of unstable ground. Newness-Buttersworth, London, pp 189–209

NHBC Standards (2010) Part 4: foundations

Vesic's AS (1972) Expansion of cavities in infinite soil mass. J Soil Mech Found Eng Div, ASCE 98(SM3):265–290

An Elastic Visco-Plastic Model for Soft Soil with Reference to Radial Consolidation

Pankaj Baral, Buddhima Indraratna and Cholachat Rujikiatkamjorn

Abstract The time-dependent stress–strain behaviour of soft soil due to its viscous nature affects its long-term settlement and pore water dissipation. A novel mathematical model developed using the Peaceman–Rachford ADI scheme (P–R FD Scheme) can describe the visco-plastic behaviour of soft clay with a non-Darcian flow function; this model is a combination of the basic radial consolidation equation developed by Barron and Bjerrum's time-equivalent (Bjerrum in Geotechnique 17:81–118, 1967) concept that incorporates Yin and Graham's (Can Geotech J 26:199–209, 1989b) visco-plastic parameters. The settlement and excess pore water pressure obtained from this model are then compared with preexisting models such as a *Class C* prediction for the Ballina trial embankment at National Field Testing Facility (NFTF). This elastic visco-plastic model provides better results in terms of settlement and pore water pressure with the field data, although the excess pore water pressure that did not dissipate after one year is mainly due to the piezometers becoming biologically and chemically clogged in terrain with acid sulphate soil (ASS).

Keywords Visco-plastic · Soft soil · Peaceman–Rachford ADI · Class C prediction

1 Introduction

The use of vertical drains in soft soil saves a huge amount of time and money because they accelerate the dissipation of pore water and reduce the time needed to reach post consolidation settlement (Bergado et al. 1996; Indraratna et al. 2012; Chu et al. 2000). The dissipation of excess pore water pressure (EPWP) and the rate of settlement are directly influenced by the visco-plastic behaviour of soft clay

P. Baral (✉) · B. Indraratna · C. Rujikiatkamjorn
Faculty of Engineering and Science, School of Civil, Mining and Environmental Engineering, University of Wollongong, Wollongong, NSW 2522, Australia
e-mail: pbaral@uow.edu.au

R. Sundaram et al. (eds.), *Geotechnics for Transportation Infrastructure*, Lecture Notes in Civil Engineering 29,
https://doi.org/10.1007/978-981-13-6713-7_29

(Qu et al. 2010; Degago et al. 2011), despite not having an elastic visco-plastic model for radial consolidation that can describe the real behaviour of clay. This paper considers a novel analytical model that will describe the visco-plastic behaviour of soft clay with reference to radial consolidation. This model incorporates the elastic visco-plastic behaviour of soft soil into a consolidation equation derived for the *r*- and *z*-directions of a vertical drain and also considers the non-Darcian flow of fluid parameters during radial consolidation. An alternating direction implicit (ADI) finite-difference (FD) method called the Peaceman–Rachford (P–R) method is used to solve the complex partial differential equation and to calculate the settlement and dissipation rate of excess pore water pressure.

2 Elastic Visco-Plastic Model that Considers Non-Darcian Fluid Flow

2.1 Assumptions

The governing equation for radial consolidation with elastic visco-plastic behaviour is based on the non-Darcian flow of fluid and the visco-plastic constitutive relationship by Yin and Graham (1989a), and it captures the Bjerrum time-equivalent constant. The finite-difference (FD) technique is then used to solve the complex nonlinear partial differential equation from which the following assumptions are made:

(1) The soil is fully saturated and homogeneous.
(2) The applied load is uniformly distributed and all the compressive strain within the soil element occurs in the radial and vertical directions.
(3) The drain's zone of influence is assumed to be circular and axisymmetric.
(4) The permeability of the drain is infinite compared to the soil.
(5) The flow of pore water through the soil follows the non-Darcian flow law.

2.2 Derivation

A differential soil element around a vertical drain in a cylindrical coordinate system (as shown in Fig. 1) is considered where the movement of pore water is only allowed in radial and vertical directions (*r*- and *z*-directions), and there is no flow in the Ω-direction. In order to satisfy the flow continuity equation, the rate of volume change must be equal to the net flow rate, where $\partial V/\partial t$ is given by,

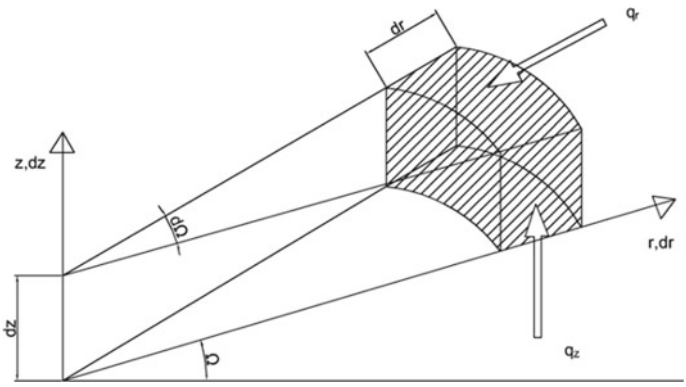

Fig. 1 Coordinates in the *r*- and *z*-directions

$$\frac{\partial V}{\partial t} = \Delta q = \frac{\partial q_r}{\partial r}\mathrm{d}r + \frac{\partial q_z}{\partial z}\mathrm{d}z \tag{1}$$

$$q_r = v_r(r\mathrm{d}\Omega\mathrm{d}z) \tag{2}$$

$$q_z = v_z(r\mathrm{d}\Omega\mathrm{d}r) \tag{3}$$

where q_r and q_z are the net flow rate in the *r*- and *z*-directions, and v_r and v_z are the flow velocities in the *r*- and *z*-directions.

The incremental volume change of the soil element ∂V is given by,

$$\partial V = -(\varepsilon_r + \varepsilon_\Omega + \varepsilon_z)(r\mathrm{d}\Omega\mathrm{d}r\mathrm{d}z) \tag{4}$$

where $\varepsilon_r, \varepsilon_\Omega,$ and ε_z are the strains of the element in the *r*-, Ω- and *z*-direction, respectively. By substituting (2), (3), and (4) into Eq. (1),

$$\frac{\partial \varepsilon_v}{\partial t} + \frac{\partial v_r}{\partial r} + \frac{v_r}{r} + \frac{\partial v_z}{\partial z} = 0 \tag{5}$$

The non-Darcian flow relationship proposed by Hansbo (1960) consists of exponential and linear parts, but for simplicity, the power law for the curve is used in this analysis, and it is given by:

$$v = \alpha_c i^\beta \tag{6}$$

where

v	the flow velocity,
i	the hydraulic gradient and,
α_c and β	flow constants depending on the type of soil.

The r- and z-components of velocity are given below:

$$v_r = \alpha_c |i_r|^{\beta} = \alpha_c \left| \frac{1}{\gamma_w} \frac{\partial u}{\partial r} \right|^{\beta} \tag{7}$$

$$v_z = \alpha_c |i_z|^{\beta} = \alpha_c \left| \frac{1}{\gamma_w} \frac{\partial u}{\partial z} \right|^{\beta} \tag{8}$$

Substituting (7) and (8) into (5),

$$\frac{\partial \varepsilon_v}{\partial t} + \frac{\alpha_c \beta}{{\gamma_w}^{\beta}} \left[\left| \frac{\partial u}{\partial r} \right|^{\beta-1} \left\{ \frac{\partial^2 u}{\partial r^2} + \frac{1}{r} \frac{\partial u}{\partial r} \right\} + \left| \frac{\partial u}{\partial z} \right|^{\beta-1} \frac{\partial^2 u}{\partial z^2} \right] = 0 \tag{9}$$

Equation (9) is the governing equation for radial consolidation.

According to the Yin–Graham EVP model (Yin and Graham 1989b), strain at any given effective stress is:

$$\varepsilon_z = \varepsilon_{z0}^{\mathrm{ep}} + \frac{\lambda}{V} \ln \frac{\sigma'_x}{\sigma'_{z0}} + \frac{\psi}{V} \ln \frac{t_0 + t_{\mathrm{e}}}{t_0} \tag{10}$$

where $\varepsilon_{z0}^{\mathrm{ep}}$ is the strain at the reference point, (ψ/V) is determined from the slope of creep strain plotted against $\ln(t_{\mathrm{e}})$, and t_{e} is the equivalent time.

From Eq. (10), the equivalent time can be calculated by

$$t_{\mathrm{e}} = -t_0 + t_0 \exp \left[\left(\varepsilon_z - \varepsilon_{z0}^{\mathrm{ep}} \right) \frac{V}{\psi} \right] \left(\frac{\sigma'_x}{\sigma'_{z0}} \right)^{-\frac{\lambda}{\psi}} \tag{11}$$

According to the creep model given by Bjerrum (1967) (see Fig. 2):

The incremental strain rate $\frac{\partial \varepsilon_z}{\partial t}$ based on this figure can be written as:

$$\frac{\partial \varepsilon_z}{\partial t} = \frac{\kappa}{V \sigma'_z} \frac{\partial \sigma'_z}{\partial t} + \frac{\psi}{v} \frac{1}{t_0 + t_{\mathrm{e}}} \tag{12}$$

By substituting Eq. (11) into Eq. (12), the elastic visco-plastic model can be obtained as:

$$\frac{\partial \varepsilon_z}{\partial t} = \frac{\kappa}{V \sigma'_z} \frac{\partial \sigma'_z}{\partial t} + \frac{\psi}{t_0 V} \exp \left[-\left(\varepsilon_z - \varepsilon_{z0}^{\mathrm{ep}} \right) \frac{V}{\psi} \right] \left(\frac{\sigma'_x}{\sigma'_{z0}} \right)^{\frac{\lambda}{\psi}} \tag{13}$$

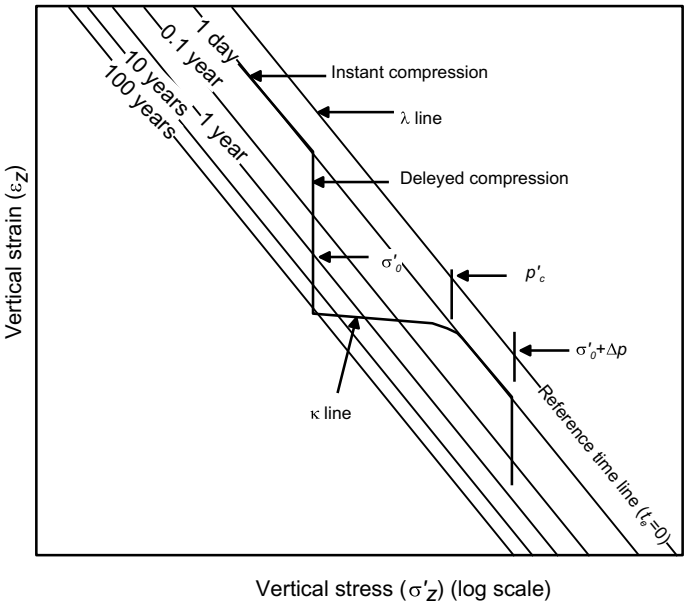

Fig. 2 Bjerrum time equivalent concept (after Bjerrum 1967)

Equation (13) can be rewritten in terms of excess pore pressure by:

$$\frac{\partial \varepsilon_z}{\partial t} = \frac{\kappa}{V(\sigma_z - u)} \frac{\partial(\sigma_z - u)}{\partial t} + \frac{\psi}{t_0 V} \exp\left[-\left(\varepsilon_z - \varepsilon_{z0}^{ep}\right) \frac{V}{\psi}\right] \left(\frac{(\sigma_x - u)}{\sigma'_{z0}}\right)^{\frac{\lambda}{\psi}} \tag{14}$$

where σ_z is the total vertical stress.

If the total vertical stress is constant and ε_{z0}^{ep} is assumed to be zero, then Eq. (14) becomes:

$$\frac{\partial \varepsilon_z}{\partial t} = -m_v \frac{\partial u}{\partial t} + g(u, \varepsilon_z) \tag{15}$$

where $g(u, \varepsilon_z)$ is a visco-plastic constant term and given by,

$$g(u, \varepsilon_z) = \frac{\psi}{t_0 V} \exp\left[-(\varepsilon_z) \frac{V}{\psi}\right] \left(\frac{(\sigma_x - u)}{\sigma'_{z0}}\right)^{\frac{\lambda}{\psi}}$$

Combining (9) with (15)

$$m_v \frac{\partial u}{\partial t} - g(u, \varepsilon_z) = \frac{\alpha_c \beta}{\gamma_w{}^{\beta}} \left[\left| \frac{\partial u}{\partial r} \right|^{\beta - 1} \left\{ \frac{\partial^2 u}{\partial r^2} + \frac{1}{r} \frac{\partial u}{\partial r} \right\} + \left| \frac{\partial u}{\partial z} \right|^{\beta - 1} \frac{\partial^2 u}{\partial z^2} \right] \tag{16}$$

2.3 FD Solution of Axisymmetric Equation

The Peaceman–Rachford alternating direction implicit (ADI) (Murray and Lynn 1965) is a two-step finite-difference method used to solve Eq. (16). In step one, the implicit differentiation is applied in the r-direction and the explicit differentiation in the z-direction gives the predictor; in step two, the implicit differentiation is applied in the z-direction and the explicit differentiation in the r-direction gives the corrector. An intermediate time step $t + \Delta t/2$ has been defined for the predictor and corrector, and it lies between t and $t + \Delta t$ (Fig. 3a).

The finite-difference grid for this solution is shown in Fig. 3b, where i is the variable along the x-direction which represents the r-coordinates that vary from $i - 1$, i, and $i + 1$. Similarly, j is the variable along the y-direction which represents the z-coordinates that vary from $j - 1$, j, and $j + 1$. The pore water pressure is calculated at each node of the grid using the P–R ADI scheme.

To simplify Eq. (16), $\left(\frac{\partial u}{\partial r}\right)^{\beta-1}$ and $\left(\frac{\partial u}{\partial z}\right)^{\beta-1}$ are defined at the last time step and continue the iteration process along with the Peaceman–Rachford ADI scheme.

$$\omega_{i,j}^{t} = \left(\frac{u_{i+1,j}^{t} - u_{i,j}^{t}}{2\Delta r}\right)^{\beta-1} \tag{17}$$

$$\varphi_{i,j}^{t} = \left(\frac{u_{i,j+1}^{t} - u_{i,j}^{t}}{2\Delta z}\right)^{\beta-1} \tag{18}$$

Equation (16) is derived to incorporate the elastic visco-plastic behaviour for soft soil that consists of a linear and nonlinear part of $\left(\frac{\partial u}{\partial r}\right)$ and $\left(\frac{\partial u}{\partial z}\right)$. This combination of a linear and nonlinear part in a partial differential equation means it cannot be solved in one step so an iterative method for the nonlinear part is applied to the nonlinear flow portion to solve the equation correctly.

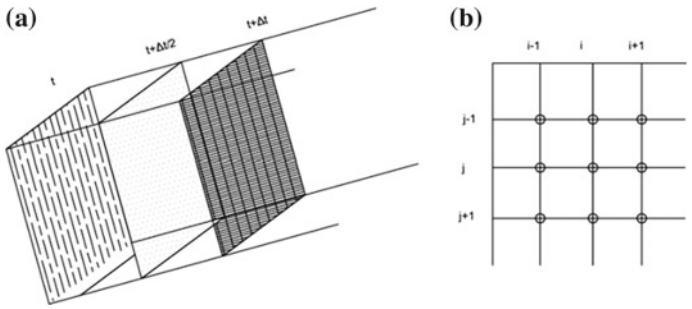

Fig. 3 **a** Time steps for P–R ADI scheme and **b** FD nodes at a given time

The form of equation that should undergo FD-ADI scheme is

$$\frac{\partial u}{\partial t} = \frac{\alpha_c \beta}{\gamma_w{}^{\beta} m_v} \left[\left| \frac{\partial u}{\partial r} \right|^{\beta-1} \left\{ \frac{\partial^2 u}{\partial r^2} + \frac{1}{r} \frac{\partial u}{\partial r} \right\} + || \frac{\partial u}{\partial z} |^{\beta-1} \frac{\partial^2 u}{\partial z^2} \right] + \frac{1}{m_v} g(u, \varepsilon_z) \tag{19}$$

Applying the FD method to Eq. 19 gives us the predictor and corrector in matrix form:

For each j, the predictor matrix is given by

$$u_{i,j}^{t+\frac{\Delta t}{2}} = C^{\mathrm{I}} + C^{\mathrm{II}} u_{i+1,j}^{t+\frac{\Delta t}{2}} + C^{\mathrm{III}} u_{i-1,j}^{t+\frac{\Delta t}{2}}$$

Similarly, for each i, the corrector matrix is given by

$$u_{i,j}^{t+\Delta t} = C^{\mathrm{I}} + C^{\mathrm{II}} u_{i,j+1}^{t+\Delta t} + C^{\mathrm{III}} u_{i,j-1}^{t+\Delta t}$$

By using the pore water pressure at a different time at each node, the vertical strain at each node can be calculated using the following equation:

$$(\varepsilon_z)_{i,j,t+\Delta t} = (\varepsilon_z)_{i,j} - m_{vi,j,t} \left(u_{i,j,t+\Delta t} - u_{i,j,t} \right) + \Delta t g(u, \varepsilon_z)_{i,j} \tag{20}$$

This entire computation is carried out using a finite-difference technique by adopting forward, backward, and central difference techniques. For this purpose, a user-friendly program is written into MATLAB in a tri-diagonal matrix form and executed with settlement and pore water pressure as an output.

3 Validation and Discussions

This elastic visco-plastic model has been validated using a *Class C* (Lambe 1973) prediction exercise from the Ballina Embankment. A *Class A* prediction of the Ballina embankment was carried out before construction, and a *Class C* prediction was carried out after field data became available. The *Class A* Prediction based on industry standard data and large-scale consolidometer (350 mm large specimen: see Fig. 4) matches the initial rate of settlement and ultimate settlement quite accurately, although a large error arose due to the absence of a creep model in our *Class A* prediction method. The inclusion of visco-plastic behaviour (i.e. creep) made the prediction more accurate and is thus defined as a *Class C* prediction. The same case history is utilised in this paper to validate the novel mathematical model.

A 3-m-high embankment with a 80 m long × 15 m wide crest has been constructed with a 1.5H: 1V side slope. There is a 95 m long × 25 m wide × 1 m high working platform on the existing ground surface to provide top drainage and facilitate drain installation. This embankment has three sections: Two sections are 30 m long and contain conventional PVD wick drains and biodegradable jute

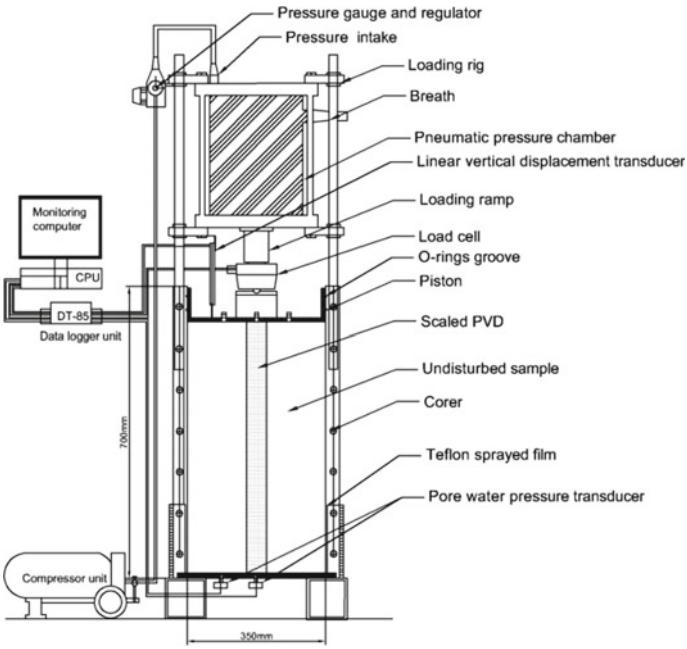

Fig. 4 Large-scale consolidometer (modified after Indraratna and Redana 2000)

drains, while the third section is 20 m long and contains conventional PVD drains with a geotextile layer instead of a sand drainage layer. A suite of instruments such as inclinometers, magnetic extensometers, settlement plates, vibrating wire piezometers, and hydraulic profile gauges has been installed to monitor embankment behaviour (see Fig. 5). This embankment was constructed in stages over a 60-day period. The compacted bulk density of the sand drainage layer (0.6–1 m thick) is 15.9 kN/m^3 while the compacted density of the above fill is 20.6 kN/m^3; this results in a total surcharge load of 59.8 kN/m^3. The vertical drains are 14–15 m deep; they were installed using a rectangular mandrel with a 120 mm × 60 mm

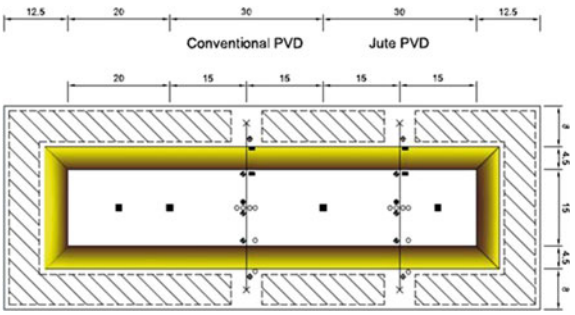

Fig. 5 Layout of embankment

cross section and an 80 t drain stitcher. There are 190 mm × 90 mm rectangular plates attached to the tip of the mandrel to act as drain anchors while the drains were installed in a square pattern at 1.2 m spacing.

The sub-soil profile consists of an almost 0.2 m thick layer of organic material (decomposing sugar cane plants), below which there is a 1 m thick layer of sandy clayey silt, and a very plastic 8.8 m thick layer of silty clay. Beneath these layers, there is a 4-m-thick transition zone consisting of large amounts of sand, followed by a 5 m thick layer of fine sand (see Fig. 6). This deposit can be classified as highly compressible marine clay with very low permeability and high plasticity (CH). At most depths of the upper Holocene layer, the natural water content is very close to their liquid limits.

All the soil parameters and drain parameters needed to solve the elastic visco-plastic model are listed in Table 1. When they are input into a MATLAB-coded interface of EVP-FDM model (Indraratna et al. 2018), the behaviour of embankment in terms of settlement and excess pore water pressure is obtained as an output. The staged construction of the embankment, the surface settlement, and the excess pore water pressure at 6 m depth are plotted in Fig. 7.

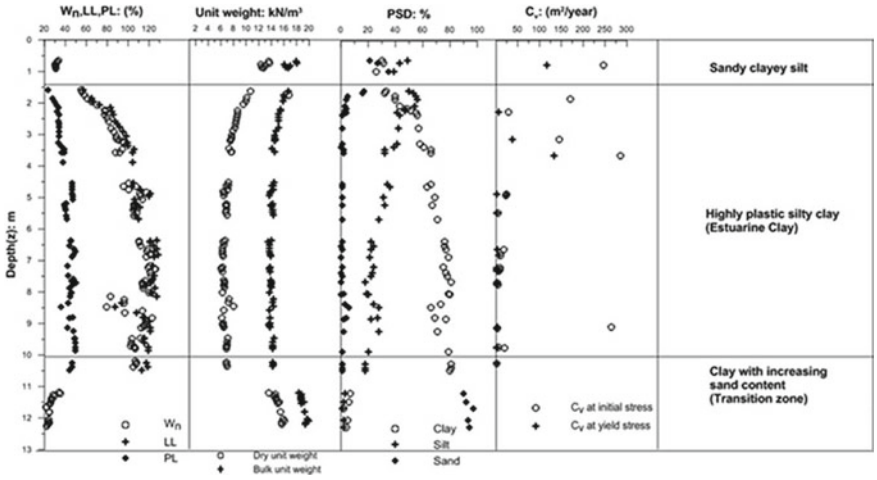

Fig. 6 Basic soil properties of Ballina clay (modified from Pineda et al. 2016)

Table 1 Soil and drain properties used for the predictions

Thickness (m)	κ/v	λ/v	ψ/v	e_0	α_c (m/s) × 10^{-10}	p_c'
2.7	0.034	0.148	0.003	3.1	5.28	46.3
3.0	0.062	0.156	0.004	2.8	4.95	27.2
3.0	0.098	0.192	0.004	2.8	4.86	44.1
3.0	0.107	0.138	0.004	2.8	5.45	50.8
3.3	0.047	0.180	0.003	2.7	6.16	65.6

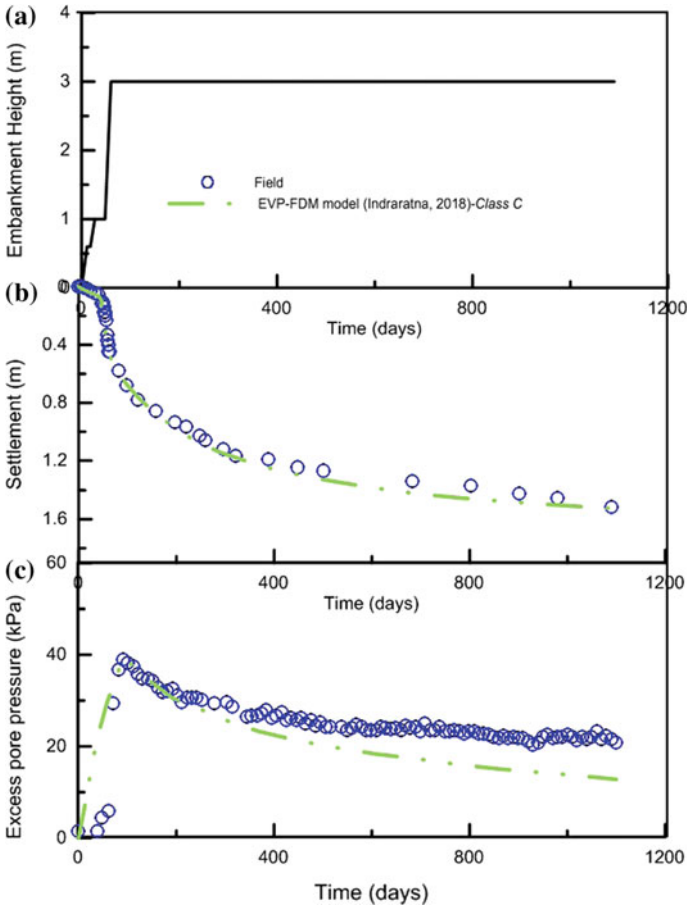

Fig. 7 Settlement and EPWP prediction with field data (modified from Indraratna et al. 2018)

As Fig. 7 shows, the *Class C* prediction using an EVP-FDM model yields better predictions in terms of surface settlement, whereas the excess pore pressures are still at much higher levels than the predicted values, especially after 1–1.5 years, due to the piezometer tips becoming biologically and chemically clogged in highly prone ASS terrain (Indraratna et al. 2017). In acid sulphate floodplains, piezometers are influenced by tidal intrusion and flooding (they must be corrected when determining the excess pore water pressure), filter corrosion or chemical alteration in acidic groundwater, armouring by minute rust particles (i.e. precipitated iron oxide), the formation of biomass due to acidophilic bacteria, and associated gas cavitation, as well as potential physical clogging by very fine (dispersive) particles over time. Embankments constructed in acid sulphate soil floodplains with a large

organic content may experience climatic and biological (bacterial) factors that cause vibrating wire piezometers to become inaccurate over time because their filters cannot be flushed after installation, unlike standpipes that can be maintained.

4 Conclusion

To summarise, the elastic visco-plastic (EVP) model could capture the non-Darcian fluid flow in radial consolidation based on Yin and Graham's EVP parameters and Bjerrum's time equivalent concept, while the two-step finite-difference method known as Peaceman–Rachford (P–R) was applied to the governing equations of radial consolidation to make the solution more accurate by performing the calculations consecutively using predictor and corrector. This approach means that embankment behaviour in terms of surface settlement and excess pore water pressure has been predicted very accurately using the proposed EVP-FDM model. The minor discrepancy while predicting excess pore water pressure is inevitable which is due to chemical and biological clogging of piezometer tips after almost a year especially in acid sulphate soil (ASS) terrain where oxidisable pyrite layers are present within relatively shallow depths of the upper Holocene clay. Further research on biological chemical clogging of piezometer tips in ASS terrain through industry linkages is now underway to identify the types of bacteria causing potential clogging of ceramic filters over time and to identify the possible benefit of using other materials as a filter tip to develop technically sound and cost-effective corrective measures for piezometers at University of Wollongong.

Acknowledgements The authors would like to thank the Centre of Geo-mechanics and Railway Engineering (CGRE), University of Wollongong, for providing a scholarship for the first authors' Ph.D. study. The efforts of university technicians (Cameron Neilson, Ritchie Mclean, and Alan Grant) during fieldwork and laboratory setup are gratefully acknowledged, as is the dedication provided by Dr. Richard Kelly and Prof. Scott Sloan as they managed the Ballina trial embankment project.

References

Bergado D, Anderson L, Miura N, Balasubramaniam A (1996) Soft ground improvement in lowland and other environments. ASCE

Bjerrum L (1967) Engineering geology of Norwegian normally-consolidated marine clays as related to settlement of buildings. Geotechnique 17:81–118

Chu J, Yan SW, Yang H (2000) Soil improvement by the vacuum preloading method for an oil storage station. Geotechnique 50:625–632

Degago SA, Grimstad G, Jostad HP, Nordal S, Olsson M (2011) Use and misuse of the isotache concept with respect to creep hypotheses a and b. Geotechnique 61:897–908

Hansbo S (1960) Consolidation of clay, with special reference to influence of vertical sand drains. Proc Swed Geotech Inst 18:160

Indraratna B, Redana I (2000) Numerical modeling of vertical drains with smear and well resistance installed in soft clay. Can Geotech J 37:132–145
Indraratna B, Rujikiatkamjorn C, Kelly RB, Buys H (2012) Soft soil foundation improved by vacuum and surcharge loading. Proc Inst Civ Eng Ground Improv 165:87–96
Indraratna B, Baral P, Ameratung J, Kendaragama B (2017) Potential biological and chemical clogging of piezometer filters in acid sulphate soil. Aust Geomech J 52(2):79–85
Indraratna B, Baral P, Rujikiatkamjorn C, Perera D (2018) Class A and C predictions for Ballina trial embankment with vertical drains using standard test data from industry and large diameter test specimens. Comput Geotech 93:232–246
Lambe TW (1973) Prediction in soil engineering. Geotechnique 23:149–202
Murray W, Lynn M (1965) A computer-oriented description of the Peaceman–Rachfordadi method. Comput J 8:166–175
Pineda J, Suwal L, Kelly R, Bates L, Sloan S (2016) Characterisation of Ballina clay. Géotechnique 66(7):556–577
Qu G, Hinchberger S, Lo K (2010) Evaluation of the viscous behaviour of clay using generalised overstress viscoplastic theory. Geotechnique 60:777–789
Yin JH, Graham J (1989a) General elastovisco plastic constitutive relationship for 1-d straining in clays. In: 3rd international symposium on numerical models in geomechanics, Niagara Falls
Yin JH, Graham J (1989b) Viscous-elastic-plastic modelling of one dimensional time-dependent behaviour of clays. Can Geotech J 26:199–209

Bioenzymatic-Lime Stabilization of Different Soils

Amit Joshi and C. H. Solanki

Abstract Soil stabilization in modern era is a prime need as the availability of good land is not possible everywhere. By modifying the properties of soil like the bearing capacity, strength characteristics can be enhanced to meet the design requirements for pavement construction. The conventional methods are time-consuming and are not economically feasible. Hence, there is a need to discover the other possible ways to satisfy the performance as well as economic criteria. Stabilization of soil with bioenzyme along with lime is a very new method to improve the geotechnical properties of the soil. In the present work, the effect of stabilization of two different soils with bioenzymes along with lime has been studied. Locally, available soils are taken, and experimental investigation is carried out. One of the soils is found to be expansive, and another is non-expansive but having very low strength characteristics, so both the soils are fall in category of problematic soil. Optimum dose of bioenzyme and various amount of lime (2, 4, 6, 8%) both used together for stabilization. Appropriate curing period of one, two, and four weeks is provided. The tests are carried out to determine the consistency limits, compaction characteristics, unconfined compressive strength (UCS), California bearing ratio (CBR), Free swell index and mineralogical test is also carried out. The laboratory test results show promising results in terms of strength of the stabilized soil. Strength characteristics like unconfined compressive strength (UCS) and CBR value were improved by 14 times and 8 times to its initial value, respectively, and the soil which was highly expansive became low expansive after treatment. More than 5 times reduction is recorded in FSI value. XRD analysis is also carried out that also justifies the stabilization.

Keywords Bioenzyme · Lime · Stabilization · Black cotton soil · Yellow soil · XRD

A. Joshi (✉) · C. H. Solanki
Department of Applied Mechanics, SVNIT, Surat, Gujarat, India
e-mail: a.amit843123@gmail.com

C. H. Solanki
e-mail: chandresh1968@yahoo.co.in

R. Sundaram et al. (eds.), *Geotechnics for Transportation Infrastructure*,
Lecture Notes in Civil Engineering 29,
https://doi.org/10.1007/978-981-13-6713-7_30

1 Introduction

Soil is an indispensable thing of this nature. It is attached to everyone in several ways. All the basic needs of life, whether it is related to food, clothes, and house, are completed by the soil. Without soil, it is not possible to think about life on this earth. The growing metropolitan cities want a number of good lands for both construction and road development. This is the major issue for the construction industry since most of the good lands have already been constructed.

Many areas of India having soils with high silt and clay contents, low strengths, less bearing capacity and high swelling and shrinkage properties. These negative soil characteristics are generally due to the nature and quality of the fines present in the material. Some soils are having very low strength characteristics and will not sustain any construction if build upon that. On the other hand, expansive soils are also problematic. Expansive soils show swell–shrink behavior with the variation in moisture content due to the presence of some swelling clay minerals like montmorillonite.

Expansive soils mostly present in the arid and the semiarid region of the world and are in abundance where the average annual evaporation is more than the precipitation. They are commonly termed as black cotton soils in India.

These soils cover almost more than twenty percent of the total area in India. These soils are residually made from gneisses, volcanic ash, and sedimentary rocks containing calcareous shale, lime, slates, and sand stones. Most of the central part of India is found with expansive black cotton soil. Black cotton soil poses serious construction problems both to structures and highways.

In such conditions, soil stabilization is best option to modify the soil properties and make soil ready for construction. The stabilizers used for this purpose are bioenzyme and lime. Bioenzymes are organic molecules that catalyze specific chemical reactions. They are basically used in low concentrations. Bioenzyme additives attach with large molecules and that are attracted to the clay mineral's negative surface charge. To reduce the amount of bioenzyme, for obtaining the same degree of improvement, the idea of mixing bioenzyme with lime is taken, and it may be greatly advantageous for purpose as working principles of both bioenzymes and lime can be substituted to each other, and since lime and enzyme use the same mechanism of cation exchange to improve soil properties, the idea of adding both lime and enzyme together in the soil and to investigate the alterations in soil properties seemed feasible.

2 Literature Review

A lot of studies have been done on stabilization of soils with bioenzyme and lime both when they are used separately and also the lime with different solid chemicals. Lime stabilization is used from the time of roman, while bioenzymes are existing

from more than decades. Attempt is made to study the effect when both mixed together. Central Road Research Institute (India) (2003) has done laboratory tests on three different soils, Cuddalore soil, marine clay, and Pondicherry soil, stabilized with TerraZyme which is a kind of bioenzyme. Marine clay had liquid limit of 70%, plasticity index of 30%, and clay portion of 62% with 24% silt. It had optimum moisture content (OMC) of 24.5% and dry density (MDD) of 1.55 Mg/m^3. TerraZyme is added with soil at dose of one liter per 0.5 m^3 of soil. The soil was tested for swelling index, unconfined compression strength, CBR, and indirect tensile strength. It is concluded that there is a good improvement in CBR after four weeks of curing as value goes from 1.2 to 4.5%. 104% increment is gained in unconfined compressive strength after stabilization with TerraZyme and 4 weeks of curing. The indirect tensile strength of the marine clay also gives an improvement after curing of four weeks upon treatment with TerraZyme.

Tewodros (2010) has done study in Ethiopia on expansive soils. He constructed the test sections on a road with expansive subgrade in the Chancho Ginchi road. Different methods of soil stabilization were used (mechanical, chemical stabilization, and lime). The expansive subgrade was mechanically stabilized by adding non-plastic gravel with a 50% proportion by volume, and then, it was compacted for required density. The expansive soil was treated with semi-processed lime using 10% by weight, and then, the expansive subgrade was treated with a combination of TerraZyme and hydrated lime. Nine trial sections were constructed by using different materials. This comparative study on different trial sections exposed that TerraZyme stabilization gives good results.

The idea behind mixing bioenzyme and lime together is that there are many salts that have been used with lime for stabilization. Also, bioenzymes alone are used a lot for stabilization. There is no significant work done on this combination. Although Eujine et al. (2016) conducted a study on the alteration of CBR values in soft soils using enzymatic lime. Natural soil samples were treated and cured with enzyme, lime, and enzyme and lime together. The treated samples were subjected to different laboratory tests. The optimum dosages were obtained based on the results of unconfined compressive strength (UCS) tests. After that, samples were treated with optimum dosages and compacted in Proctor molds and then subjected to CBR tests for different periods of curing. More improvement was noticed in enzymatic lime stabilization of soils instead of lime stabilization and enzyme stabilization of soils. CBR tests were also conducted by altering the percentage of clay in the soil samples. In all tests, enzymatic lime stabilization of soils yields more improvement in properties. Enzymatic lime stabilization of soils can be used for improving the bearing capacity of the subgrade, with noticeable savings on both aggregate and disposal charges. Exposure to water has significantly reduced the CBR of all treated soils, with enzyme treated soil being affected the most. CBR of enzymatic lime-treated soils has improved by more than 450% in unsoaked condition as compared to untreated soils.

3 Materials

Soil
Two types of soil are used for carrying out the investigation. One soil sample is collected from Tapi River Bank near Piplod area of Surat city. This soil is named as black cotton soil (BCS), while other soil samples that are named as yellow soil (YS) are collected near the applied mechanics department (AMD) of SVNIT, Surat. Several tests are performed on both the soils for obtaining their properties and suitability for present work.

Bioenzyme
A commercially available bioenzyme under the trade name TerraZyme is used for the present study. TerraZyme was obtained from Nature Plus Inc., USA, through Avijeet Agencies, Ahmedabad. 200 ml of solution is used to carry out the present work.

3.1 Dosage

Based on the research studies and information given by supplier, a dosage may be taken as ml/m^3 of soil (volume in milliliter is needed to treat 1 m^3 of soil). The baseline dosage for medium to mild plastic soil (PI = 4–12) will be 1 l of TerraZyme for 8–12 m^3 of soil. For this work, three dosages are selected as follows (Table 1).

Lime
Lime is purchased from the local market in form of hydrated lime in packets of 5 kg. The CaO content of lime is 65%, and it is obtained by the test conducted in the laboratory.

Table 1 Dosage of TerraZyme

Dosage	ml/m^3 of soil	Curing period in days
1	200 ml/2.5 m^3	0 day, 7 days, 14 days, 28 days
2	200 ml/2.0 m^3	
3	200 ml/1.5 m^3	

4 Experimental Investigations

Untreated soil is tested for laboratory tests like gradation (sieve and hydrometer analysis), Atterberg limits, moisture content, maximum dry density (MDD), optimum moisture content (OMC), specific gravity, free swell index (FSI), unconfined compressive strength (UCS), and California bearing ratio test (CBR) as per IS code. The finding is tabulated below in Table 2.

5 Test Results of Treated Soil and Discussions

Laboratory tests are done on soil samples after mixing of bioenzyme, and the optimum dose of bioenzyme is decided on the basis of laboratory testing, and then, the various percentage of lime (2, 4, 6, 8) are mixed with that optimum dose of bioenzyme.

Three dosage of bioenzyme alone mentioned in Table 1 are given to each sample, and curing period given is 0 day, 7 days, 14 days, and 28 days. It is found that the highest dose of bioenzyme yields high results; hence, that dose is taken as optimum for bioenzyme. After that, both soil samples are tested with that highest

Table 2 Properties of untreated soils

S. No.	Property	Values	
		Black cotton soil	Yellow soil
1	Specific gravity	2.34	2.70
2	Grain size analysis		
	Gravel (%)	0	0
	Sand (%)	10	13
	Silt (%)	58	70
	Clay (%)	32	17
3	Consistency limits		
	Liquid limit	58	38
	Plastic limit	26	25
	Plasticity index	32	13
4	IS soil classification	CH	MI
5	Optimum moisture content (OMC)	23.92	22.62
	Maximum dry density (MDD) in g/cc	1.578	1.74
6	Unconfined compressive strength (UCS) in KPa	138	173
7	California bearing ratio (CBR) (unsoaked)	3.8	5.3
	Soaked	1.83	3.29
8	Free swell index (FSI)	70.4	20.2

bioenzyme dose along with the various percentage of lime; hence, four dosages are made. Now, again all the tests are done for these total seven dosages. Laboratory testing is done to find the properties like UCS, CBR, and FSI.

Unconfined Compressive Strength (UCS)

From the figure, it can be noticed that the effect of stabilizers is very much significant on UCS value, but the addition of lime yields better results. On the zero day of curing, the results are somewhat limited, but after a period of seven days, the effect is something extraordinary as values get boosted. Expansive soil gets 311% improvement on 7 days curing with dose 3. The initial value which is 138 kPa changes to 568 kPa (Fig. 1).

It is observed that 7 days of curing with bioenzyme recorded some considerable results, but when samples tested for dosage of lime-added bioenzyme, something extraordinary happened. Lime effect is so significant that on 7 days of curing only, 520% increment on initial value is recorded. The best result obtained corresponding to the 6% of lime added after that value again decreased. For higher curing periods that are 14 days and 28 days, the trend of improvement is also similar. At 28 days of curing, bioenzyme dose alone gives almost 1066 kPa value for black cotton soil and 1866 kPa when used with 6% of lime. So for black cotton soil which is expansive soil the UCS value increased from 138 to 1866 kPa which is quite a satisfactory result. In UCS value for black cotton soil, more than 1250% increment is seen which mean initial value becomes more than 13 times (Fig. 2).

Now for another soil, which is a yellow soil more or less same trend is followed just in case of previous soil but here the overall improvement is less in comparison to black cotton soil. The bioenzyme and 4% of lime give more than 30% improvement in the UCS value on zero day of curing only. Further increase in lime decreases the result. If we talk about the final improvement, then the maximum value occur is 1365 kPa in comparison to 173 kPa which is a quite tremendous

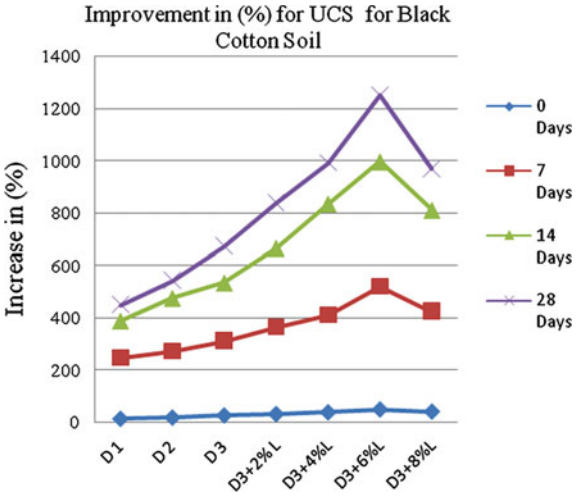

Fig. 1 Improvement in UCS for black cotton soil

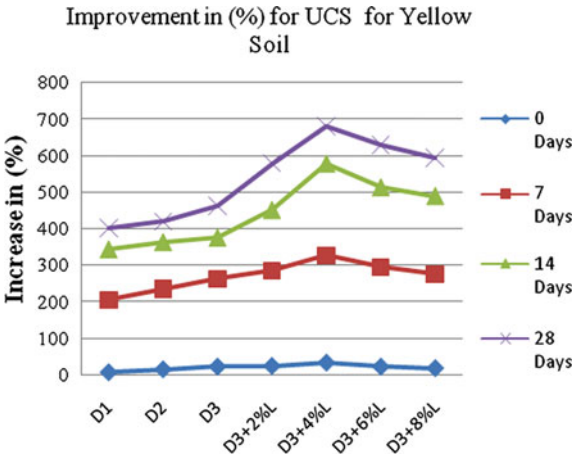

Fig. 2 Improvement in UCS for yellow soil

result and that is obtained with 4% lime used with bioenzyme. 682% of improvement is gained in this case of yellow soil.

It is clearly seen from the results that the initial improvement supposes to happen in both soil samples. For the highest increment in terms of how many times the initial value is changed in first 7 days for both soils, it is observed from Fig. 3 that the gap between the two curves for zero day to 7 days is widest among all curves which shows that here the increment is highest. The gap between 7 and 14 days is good and more or less same as previous gap between curves of zero day to 7 days which shows that here also good increment is recorded. Now from 14 days to 28 days curing, the gap of curves is very narrow which shows that there is an improvement, but it is not that great, but still it is considerable. The rate of improvement is greatly reduced in 14–28 days of curing. Such trends are followed for both the soils, but it is seen that bioenzyme is working almost same with both type of soils, but the overall improvement is something different for both soils as black cotton soil records 14 folds to initial value, while yellow soil shows highest improvement as 8 times only. One thing that is also different for both the soils that is black cotton soil is improved maximum with bioenzyme and 6% of lime, so it is its optimum dose, while yellow soil improves with bioenzyme and 4% of lime; hence, this is its optimum dose. So there is the difference in optimum dosage in two soils when they are treated with bioenzyme and lime both.

California Bearing Ratio (CBR)

For pavement sub base and base course stabilization, CBR is one of the most important parameter as it directly governs the thickness of pavement, so a higher value of CBR is very much desired. The results of untreated soils indicate that CBR values for both soils are quite low, and they need to be increased for any construction work.

The soil samples are prepared, and they are given the particular curing and soaking. In this study, the first set of testing is done after giving samples 3 days of

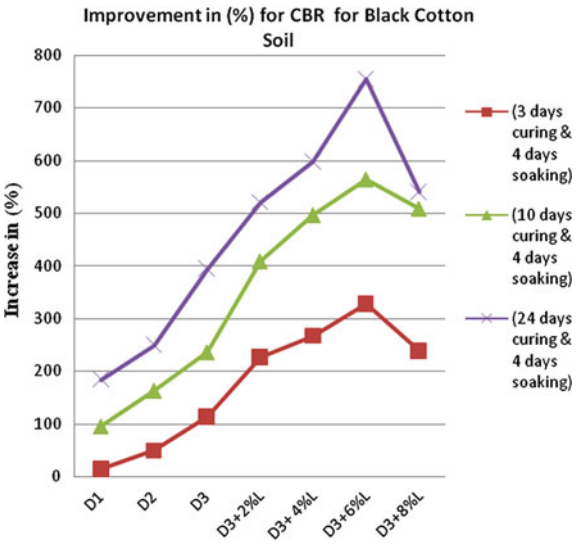

Fig. 3 Improvement in CBR for black cotton soil

curing and then 4 days of soaking, the second set is given 10 days of curing and 4 days of soaking, and for the last set of testing, 24 days of curing and 4 days of soaking are given in particular sequence. On the zero day of curing, CBR value of BC soil for the dose 3 which is the highest dose yields highest improvement, and it is 114% of the initial value. Taking dose 3 as optimum dose of bioenzyme, lime is again added as 2–8%. Now, the lime-added bioenzyme yields some better results than only enzyme as it does for all previously tested properties. Here, the highest improvement comes by bioenzyme with 6% of lime as CBR goes to a value of 7.84 and 329% improvement is recorded. The second set of testing is done for 10 days of curing and then 4 days of soaking. The results obtained here for bioenzyme dosage are quite satisfactory as 236% improvement in CBR value is obtained. For lime-added dosage, CBR reaches to 12.18 from initial value of 1.83 which is a fine result. After that, 24 days of curing and 4 days of soaking are done for the last set of testing. Here, the rate of increase of CBR value is greatly reduced as compared to previous increases, but still it is considerable. For bioenzyme dose, the value is reached to 9.06. The overall a maximum gain in CBR value for black cotton soil is 15.65 from 1.83. The final improvement percentages for lime-added bioenzyme dosage are 521, 598, 755, and 540% for lime 2, 4, 6, and 8%.

Now for the second soil which is yellow soil, the untreated soil has CBR of 3.29. On curing of 3 days and soaking of 4 days, the bioenzyme dose 3 yields maximum gain in CBR value. For the bioenzyme and lime mix dosage, the results obtained are even better as with 4% of lime and enzyme, result improved by 252%. After 4% of lime, if we further increase the percentage of lime, then it starts to reduce the CBR value; hence, 4% lime with enzyme is said to be optimum dose for yellow soil. Now, for second set of testing which means for 10 days of curing and 4 days of soaking, the bioenzyme dosage alone gives results as 7.89, 8.68, and 9.44 for three

dosages. Now, here the improvements in percentage are up to 186%. With addition of lime to enzyme, this improvement goes to 317% and CBR reaches to 13.73. For the final set of testing, the 24 days of curing and then 4 days of soaking are adopted in same manner as mentioned earlier. For that particular set of testing, some great results are noticed as with bioenzyme dosage the initial value of CBR 3.29 reaches to 13.13 which is 300% improvement. So it is observed that the initial value of CBR becomes almost 4 times. Lime and enzyme dosages for this period give CBR value which is maximum among all dosage and curing periods. 397% improvement is recorded in yellow soil for CBR (Fig. 4).

If we summarize the CBR test results, then we have some important points to discuss. If we see the above figures which show the improvement with the help of lines, then we can see that for black cotton soil treated with bioenzyme only, the initial improvement rate for 3 days curing and 4 days soaking is almost same as of yellow soil. Dose 3 of bioenzyme shows almost equal improvement for both soils. But after that period, we can observe that black cotton soil has more overall improvement than yellow soil, and the rate of increment in black cotton soil is also greater than yellow soil. One thing that is common for both the soils is that the rate of improvement for bioenzyme dosage is same for all curing periods which means that the gap between curves is almost of same up to bioenzyme dosage alone, but for lime-added enzyme, this rate is higher in black cotton soil. Coming to optimum dosage for both soils, the bioenzyme dose 3 yields maximum results which is highest dose also for lime-added enzyme dosage; we get different dosage for both soils as optimum. In case of black cotton soil, enzyme with 6% lime yields maximum results, and beyond 6% lime, the values are reduced, while in case of yellow soil, lime 4% is coming out to be optimum dose as beyond that values are

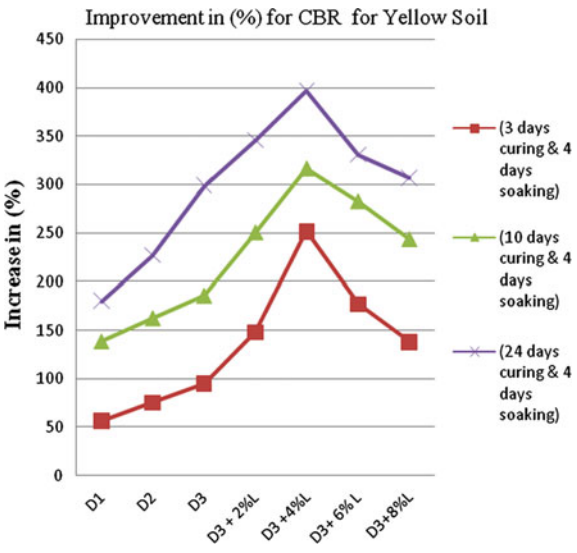

Fig. 4 Improvement in CBR for yellow soil

continually decreasing. Now, we talk about overall improvement; then, it is more in black cotton soil as it gives 750% increment, while in yellow soil, the improvement is restricted up to 400% only.

Free Swell Index (FSI)

Free swell index test is one of the real measures of swelling potential; hence, for expansive soil sample, it is essential to do this test for having the knowledge of swelling characteristics. This test is done on both soils, and it is found that BC soil is having high swelling potential, whereas yellow soil has low swelling potential. Now, again after treatment of soil, free swell index test is done again for both soil samples, and we have got some great results regarding expansive sample. Black cotton soil which initially has FSI value 70% is treated with different dosage and tested for different curing periods. The effect of bioenzyme on FSI value just after mixing is somewhat very limited as we can observe from table also that on zero day curing the maximum reduction is also near to 8% only and even lower dosage unable to show any reduction in value, but the dosage mixed with lime means bioenzyme along with lime show satisfactory results as value comes down to 53 which means 20% reduction happened. After seven days of curing, dose 3 which is highest dose for bioenzyme gives more than 30% reduction in FSI value which is quite a good result. Now, for lime-added enzyme dosage again here 8% lime is giving maximum reduction as 70% of FSI comes to only 30% in just seven days of curing. Here, the difference among the dosage is also quite significant as improvement level is differing by a long margin which is not seen before for other properties. So here also, for zero day to seven day, the rate of improvement is great. Now, for 14 days and 28 days of curing, the rate of improvement is reduced, but still a significant reduction in FSI value is observed. If we talk about the maximum reduction in FSI value, then it is 12 from 70, so 80% reduction is observed which is a great result, but from 14 days to 28 days, the reduction is only 40% (Fig. 5).

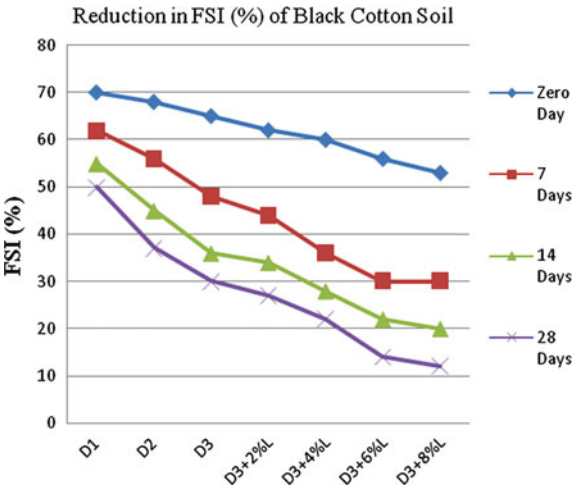

Fig. 5 Reduction in FSI for black cotton soil

Now, if we shift to discussion on yellow soil which has initially the FSI value 20%, then the results obtained are also satisfactory. Initially, there is no or very little improvement as FSI is already not that much high and soil is low expansive only, but lime-added dosage of bioenzyme on curing of seven days reduces the value near to 12% which is a satisfactory result. The further decrement in FSI is not seen after this point

Mineralogical Study

The X-ray diffraction analysis is done on both type of soils and with each bioenzyme and bioenzyme with lime dosage. As we obtained best engineering results for both soils as per of dose 3 of bioenzyme and later it was decided as optimum dose of bioenzyme for these soils, hence Dose 3 treated soils with curing periods of 28 days is taken for XRD analysis as 28 days curing yields maximum results. Now, for bioenzyme with lime dosage, the two soils give different doses as their optimum dose so that the optimum dose of each soil with 28 days of curing again is selected for XRD testing. Which means for black cotton soil dose 3 of bioenzyme along with 6% of lime and for yellow soil dose 3 of enzyme with 4 and of lime was taken. Thus, total of four samples are given for XRD analysis to study the microstructure changes in treated soils.

We know that due to treatment with lime, three major cementations compounds are formed and these are the calcium silicate hydrate (CSH) [$CaO–SiO_2–H_2O$], calcium aluminates hydrates (C–A–H) [$CaO–Al_2O_3–H_2O$], and calcium aluminum silicate hydrate (CASH).

The other compounds present are quartz and montmorillonite, which were originally present in the untreated soil. However, the peaks of these elements also show reduction. The appearance of some new peaks at d-spacing of 4.18–4.26 in both types of soils shows that there is formation of cementations compounds which ultimately governs the development of strength and reducing the swelling behavior. The basal spacing or d-spacing of calcium silicate hydrate (CSH) lies near to 3.04 and 1.82 Å according to the literature available, while the compound calcium aluminum silicate hydrate (CASH) has d-spacing near to 2.250 and 1.988 Å. The reason behind the development of these cementitious compounds is hydration and pozzolanic reaction.

Stabilization with bioenzyme leads to formation of calcium silicate hydrate (CSH) and which can be seen by the appearance of new peaks. Treatment with the bioenzyme and with lime, we get some better results as per of only bioenzyme as here more cementation compounds are formed, and these are the calcium silicate hydrate (CSH), calcium aluminates hydrates (C–A–H), and calcium aluminum silicate hydrate. The formation of new peaks confirms the development of these compounds, and their presence justifies the improvement in soils with these stabilizers.

6 Conclusion

The behavior for strength characteristics through UCS and CBR is predicated, and it is recorded that these values are significantly improved. Although there are variations in the trends of improvement, both stabilizing techniques work for both soils, but black cotton soil shows more improvement. Bioenzyme dosages yield good results, but mixing of lime along with bioenzyme again brings great results. In UCS test, bioenzyme along with lime shows tremendous results as in case of black cotton soil the value becomes 14 times to initial value, while yellow soil shows highest improvement as 8 times. In case of CBR testing overall improvement in black cotton soil as it gives 750% increase while yellow soil improvement is restricted up to 400% only. Expansive characteristics of black cotton soil sample are recorded by FSI value, and there is a great reduction of 80% which brings sample low expansive. Mineralogical study by X-ray diffraction methods also suggests that there are formations of cementation compounds through generation of new peaks.

References

Eujine GN, Chandrakaran S, Sankar N (2016) Alteration of CBR values in soft soils using enzymatic lime. In: indian geotechnical conference (IGC) 2016, IIT Madras

Tewodros A (2010) Experimental treatment options for expansive soils on unpaved roads in Ethiopia. In: ABABA 1st AF road practitioners conference, Central Laboratory Ethiopian Road Authority, 23–25 Nov 2010

Contact Pressure Distribution in Geocell Reinforced Rural Roads

Vijay Kumar Rayabharapu and Sireesh Saride

Abstract About 60 and 95% of the road network comprised of rural roads in United States and India, respectively. Everyday rural roads are being constructed by the engineers all around the world to meet the traffic needs, for which, the traditional pavement design and construction practices require high-quality materials for fulfillment of construction standards. Quality materials are unavailable or short of supply in many parts of the world. Design engineers are often forced to seek alternatives using substandard materials, commercial construction aids, and innovative design practices to improve the structural support to the pavement structure when weak subgrades are encountered. In this research, results from a series of large-scale laboratory tests on a simulated rural road consisting of a reinforced and unreinforced dense base/sub-base layer overlying weak subgrade were considered. A series of large-scale laboratory testing were conducted on geocell reinforced rural road under traffic loading conditions. The base/sub-base and weak subgrades were prepared at 75 and 30% relative densities, respectively, by pluviation technic in a large steel tank. An equivalent single axle wheel load (ESAL) of 550 kPa was considered which was applied through a circular steel plate using dynamic hydraulic actuator of 100 kN capacity. Several earth pressure cells were placed at the interface of the dense base/sub-base and weak subgrade layers to measure the contact pressure transmitted on to the weak subgrade. Results indicated that the pressures exerted by the traffic loads can be reduced to about 60% by introducing geocell mattress in base/sub-base layers over weak subgrades.

Keywords Contact pressure · Geocell · Rural roads

V. K. Rayabharapu (✉)
Department of Civil Engineering, B V Raju Institute of Technology, Narsapur 502313, India
e-mail: vkraya@gmail.com

S. Saride
Department of Civil Engineering, Indian Institute of Technology Hyderabad,
Hyderabad 502285, India
e-mail: sireesh@iith.ac.in

R. Sundaram et al. (eds.), *Geotechnics for Transportation Infrastructure*,
Lecture Notes in Civil Engineering 29,
https://doi.org/10.1007/978-981-13-6713-7_31

1 Introduction

A low volume road (LVR), also known as rural road in India and farm to market (FM) road in the United States, can be defined as a road in which the average annual daily traffic (AADT) is about 500 commercial vehicles per day (Behrens 1999; Keller and Sherar 2003). (AASHTO) LVRs are defined as roads with 0.7–1 million Equivalent Single Axel Loads (ESALs) for a given performance period (Mallick and Veeraragava 2010). Generally LVRs are designed as paved or unpaved roads, which depend on the purpose and subgrade soil conditions. Unpaved roads are preferred if the subgrade soils are strong. However, the performance of LVRs can be improved by surfacing the unpaved roads (Muench et al. 2004; Pinard 2006). Generally, rural roads consist of either a base/sub-base layers. The thickness of these layers always depends on the support extended by the underlying subgrades.

The total road network of India covers over 4.2 million kilometers, out of which, village and other roads (LVR) share is about 80% (MORTH 2011). It was estimated United States is comprised of about 60% LVRs. The construction, maintenance, and rehabilitation of these roads are a major task and involve about 54% of the total annual investment of transportation systems in USA (Praticò et al. 2011).

The Ministry of Rural Development (MORD) of legislature of India propelled the "Pradhan Mantri Gram Sadak Yojana (PMGSY)"—a Prime Minister's Rural Road Program in year 2000 to associate with every single climate street all residences with populace more than 500 (250 in bumpy, deserts, and inborn areas) in the primary example. The PMGSY targets incorporate new availability to around 1,78,000 homes including development of around 3,75,000 km of streets separated from overhauling of 3,72,000 km of existing country streets which are in poor condition (Saride and Umashankar 2010; Praticò et al. 2011).

These figures plainly exhibit that the streets are a critical part of the universes' transportation foundation and economy, in this manner calling for feasible plans and development procedures to guarantee advanced asphalt development (Saride and Umashankar 2010). The execution of the LVRs can be enhanced by embracing appropriate adjustment methods (Bushman et al. 2005; Croft 1967), receiving optional materials and novel development methods, for example, incorporation of geosynthetic support in base/sub-base layers or feeble subgrades (Little 1995).

Fifty years prior, out of the blue, geocell support for asphalt applications were begun by US Army Corps of Engineers for enhancing the bearing limit of inadequately evaluated sand by utilizing it as a parallel control (Webster 1979). Sidelong control, expanded bearing limit, and tensioned layer impact are primary support instruments for geocell fortification (Giroud and Noiray 1981; Dash et al. 2001; Han et al. 2008). Pokharel (2010) examined substantial scale cyclic stacking tests on geocells and watched that the geocells have enhanced the quality, expanded the level of versatile twisting and life of the unpaved street segments over frail subgrade. Saride et al. (2013, 2015) watched that the perpetual misshapenings were diminished by 8 overlap, and TRBs were expanded to 45 for the instance of

sleeping cushion estimate $h/D = 1$, $b/D = 4$ against the unreinforced bed at 5% plate settlement under rehashed movement stacking.

Han et al. (2008) detailed by that the situation of geocell from the surface of stacking is likewise urgent. In opposite, the arrangement profundity of geocell ought to be kept up at around 1–5% of the width of the stacking zone in static load tests as seen in Dash et al. (2001) and Sitharam and Saride (2005).

However, literature study reveals that the quantification of performance of the geocell reinforced granular base/sub-base layers in terms of reduction in contact pressure over weak subgrades supporting LVRs has not well documented. In this study, an attempt has been made to quantify the contact stress reduction over weak subgrades due to provision of geocell mattress in base/sub-base layers through dynamic earth pressure cells.

2 Experimental Program

In this study, the dry sand placed at its 30% relative density has been considered as weak subgrade supporting low volume roads. A granular base/sub-base of the LVR was formed, over the weak subgrade, at 75% relative density of sand.

Dry sieve analysis gave the soils distribution of particles as seen in Fig. 1 and is stated as poorly graded sand denoted by SP according to the Unified Soil Classification System (USCS).

The physical properties of sand such as G, e_{max} and e_{min} were determined according to the ASTM standards and given as 2.63, 0.74, and 0.51. The angle of

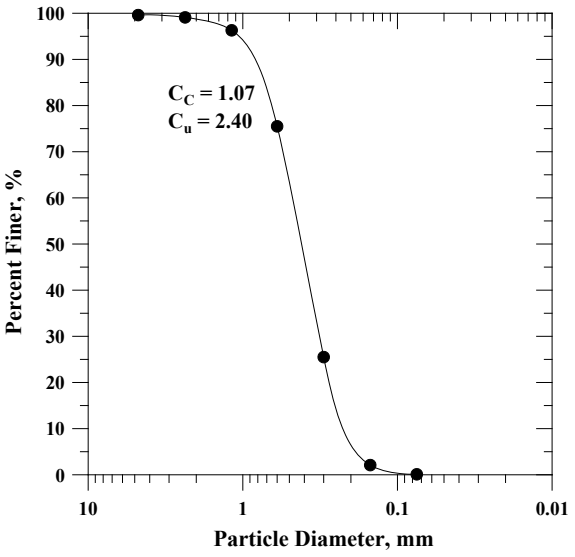

Fig. 1 Particle size distribution curve for sand

Table 1 Properties of geocell

Properties	Values			
Material composition	Polymer—High-Density Polyethylene (HDPE)			
Density (g/cm^3)	0.935–0.965			
Weld spacing (mm)	356			
Cell depth (mm)	75	100	150	200
Min. cell seam strength (N)	1050	1400	2100	2800
Cell size (±10%) (mm)	259 × 224			
Cell area (±4%)	290			

shearing resistance of sand at its 75% relative densities was determined to be 37° by conducting shear tests on plain sand in a box with 100 mm × 100 mm × 30 mm sizes.

Geocell mattress is made of ultrasonically Welded high density polyethylene (HDPE) Which is strong, light weight, 3D cellular confinement system. These strips were placed and spread on the weak sand subgrade to prepare a geocell reinforced granular (sand or aggregate) mattress. The geocell is manufactured from a polymer of HDPE material with a density ranging between 0.935 and 0.965 g/cm^3 having a weld at regular intervals of 356 mm which is used in the present study. The properties of the geocells are listed in Table 1.

3 Test Setup

Weak subgrade overlying reinforced stiff geocell reinforced sand beds with 30 and 75% relative density were prepared in a tank. The inner dimensions of test tank are 1 m × 1 m × 1 m (length × width × height). To apply a repeated traffic loading on the sand subgrades, a rigid steel plate of diameter 150 mm and thickness 15 mm was used in the experiment. The dimension of the tank and diameter of loading plate were determined based on the literature. Chummar (1972) has found that the failure wedge, stretched around 2–2.5D on either side of the footing and to a depth of around 1.1D from the bottom of the footing which is below footing plate on a sand bed, where D is the diameter of the footing. Edil et al. (2009) were adopted similar kind of test tank and plate diameter in their laboratory experiments on geosynthetic reinforced pavements. The schematic of the test bed and experimental setup used in the present study has been shown in Figs. 2 and 3.

Strain-type soil earth pressure transducers were used to check the boundary effects on the experimental results from reinforced test beds. The pressures were measured during the repeated load tests by pacing them at the boundaries of the tank. Minimal pressures (less than 1% of the applied pressure) were recorded confirming the influence of the boundary on the test results is negligible. Loading

Fig. 2 Experimental test setup

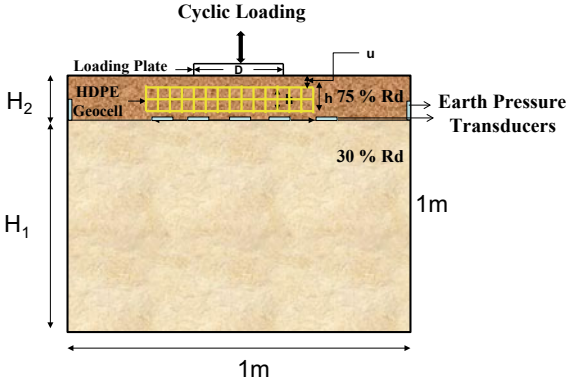

Fig. 3 Schematic of test bed

was given by graphical user interfaced multi-purpose test software along with the help of hydraulic power unit, hydraulic service manifold, and sophisticated double acting linear dynamic 100 kN capacity actuator which is attached to a 3.5 m high, 200 kN capacity reaction frame.

4 Testing Procedure

All figures and tables shall be numbered sequentially and cited with discussion in the main body of the paper.

4.1 Sand Bed Preparation

Sand raining or sand pluviation is a technic used to maintain the relative density of the sand in the test tank. The subgrade was prepared with sand placed at 30% relative density until the height H_1 in all the tests. A 75% relative density of sand was used as a granular base/sub-base layer over the weak subgrade to a thickness of H_2 in all the tests. The height, H_2, depends on the height of the geocell mattress, h and the depth of placement of geocell mattress from surface, u and sand cushion maintained between the dynamic earth pressure cells and the mattress. By taking samples at different depths during the pluviation, the density of the test bed was frequently monitored. The densities were well within the range of 2% error. A total of nine (9) dynamic earth pressure cells were placed right at the interface of weak subgrade and stiff granular base/sub-base layer to measure the pressure transmitted to the subgrade through the base/sub-base layer during the repeated load test. Out of nine earth pressure cells, five were placed right at the center line of the loading across the width of the base/sub-base layer. Rest of the four earth pressure cells were placed at four boundaries of the test tank to measure the pressure transmitted to the boundaries.

After filling the test tank with the sand up to the desired height, the fill surface was leveled and the loading plate was placed on a predetermined alignment such that the loads from the actuator applied would be transferred concentrically to the footing. To facilitate this, a recess was made into the loading plate at its center to accommodate a ball bearing through which vertical loads were applied to the plate. In the case of reinforced beds, upon ceasing the pluviation at predetermined depth, the geocell was positioned and stretched on the leveled subgrade and continued the sand pluviation to fill the geocell mattress with mentioned relative density.

4.2 Repeated Load Tests (RLT)

The repeated load tests were completed with a most extreme heap of 550 kPa (ESAL) and at least 55 kPa (10% of the greatest weight) utilizing a PC controlled servo pressure driven actuator with a persistent haversine stacking design as appeared in Fig. 4 at a recurrence of 1.0 Hz as portrayed in Saride et al. (2015) and Rayabharapu and Saride (2019).

The loading was picked such that it repeats the moving activity on the asphalt. Multi-reason test product programming was set up to control and gain the connected

load information and in addition the distortion information. The stacking example of the repeated load test and relating contact pressures is found in Figs. 4 and 5.

A typical Contact pressure with time and number of cycles is shown in Fig. 5. The pressures are obtained from the pressure cells placed at the interface for unreinforced and geocell reinforced bed under cycling loading conditions. It can be

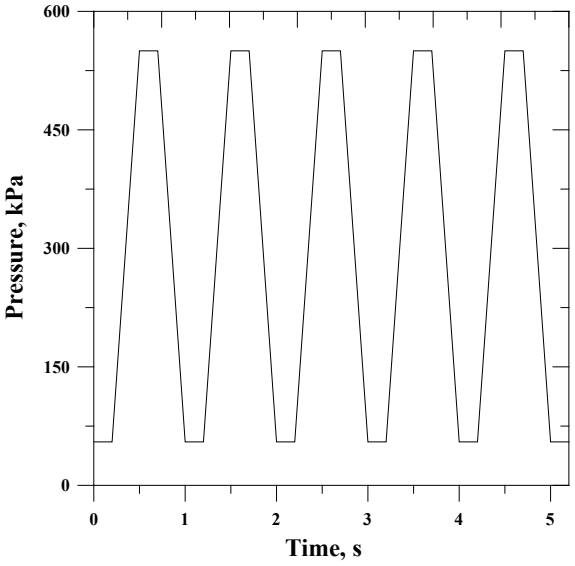

Fig. 4 Loading pattern used for RLT

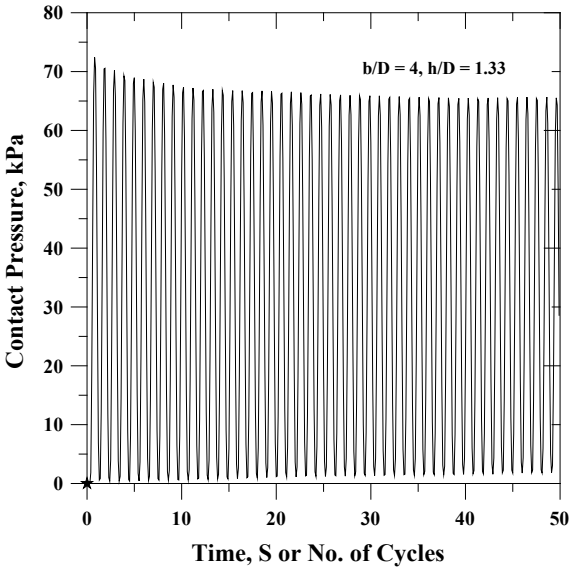

Fig. 5 Typical pressure–time pattern of RLT

Table 2 Test series done in this study

Test series	Description	Constant parameters	Variable parameters
A	Un reinforced bed	H_1 = 75% R_D, H_2 = 30% R_D	H_1 = 0.25 m, H_2 = 0.65 m H_1 = 0.20 m, H_2 = 0.65 m H_1 = 0.15 m, H_2 = 0.65 m H_1 = 0.125 m, H_2 = 0.65 m
B	Geocell reinforced bed	H_1 = 75% R_D, H_2 = 30% R_D, h/D = 1.33, u/D = 0.1	b/D = 2, b/D = 3.25, b/D = 4
C	Geocell reinforced bed	H_1 = 75% R_D, H_2 = 30% R_D, b/D = 4, u/D = 0.1	h/D = 0.5, h/D = 0.67, h/D = 1.0, h/D = 1.33

noticed that the pressures are little higher for the initial loading cycles which are considered to be the initial data acquired to set, while their magnitude attenuates thereafter.

To verify the efficiency of the geocell layers in the base/sub-base layers, a series of repeated load model tests were conducted to reduce the stresses coming on to the weak subgrade as listed in Table 2. The height and width of geocell mattress are expressed in terms of normalized ratios with respect to the diameter of the loading plate as h/D and b/D, respectively. The model tests include unreinforced tests, single geocell layers with different sizes (width and height) with respect to the plate diameter.

5 Results and Discussion

The pressures at the subgrade have reduced as the amount of geocell reinforcement increases, against the unreinforced subgrade for which pressures are higher. Pressure cells are placed at a distances of 1, 1.5. 2.0 times the width of the loading plate on either sides of the loading plate at the interface.

To quantify the reduction in contact pressures and the efficacy of geocell, the contact pressures of each configuration at 1, 5, 50, 75, and 100 cycles are considered and presented from series B of testing in Figs. 6, 7 and 8. It is clearly evident that the contact pressures of geocell reinforced beds are reducing with increase in the geocell width. The pressures reduced from 160 kPa in case of h/D = 1.33, b/D = 4 to almost 100 kPa in case of h/D = 1.33, b/D = 2 which is a reduction of about 40% between the least and highest reinforced case in this series.

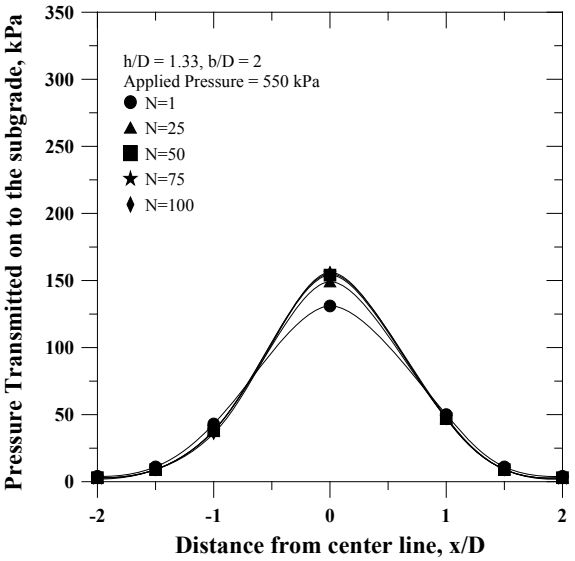

Fig. 6 Pressure transmitted for h/D = 1.33, b/D = 2

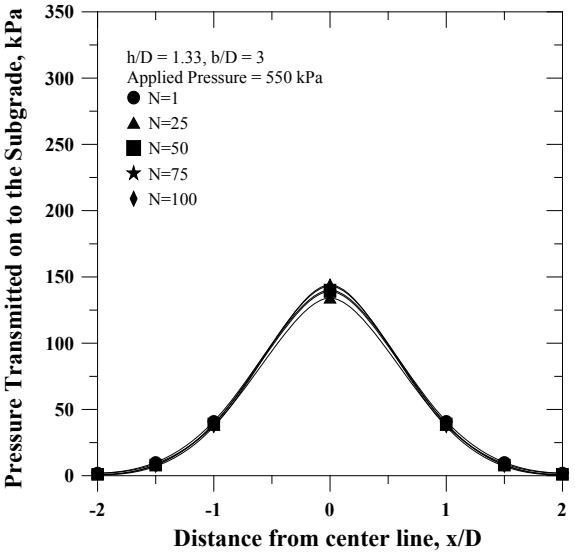

Fig. 7 Pressure transmitted for h/D = 1.33, b/D = 3

Figures 6, 7, and 8 show the variation of the pressures transmitted on to the subgrade with distance from center line corresponding to the geocell reinforced sections of h/D = 1.33 and b/D = 2, 3.5, 4 for various cycles, respectively. From the figures, it is evident that, the pressures transmitted on to the subgrade with distance from center line in a geocell reinforced are reduced compared to the

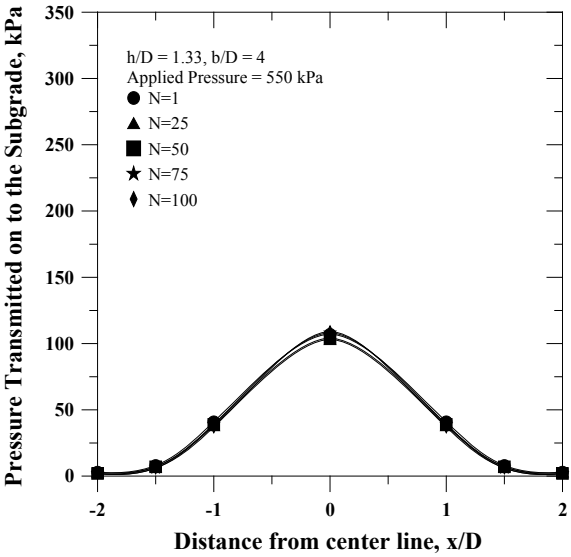

Fig. 8 Pressure transmitted for $h/D = 1.33$, $b/D = 4$

unreinforced for the same applied pressure. In reinforced beds as the width of the geocell reinforcement increases, the pressure transmitted on to the subgrade is reduced at the center and the pressure transmitted on to the either sides of the loading plate increased. This is because as the width of the reinforcement increases number of cells in the geocell increases which yields to more all-round confinement preventing the lateral spreading of the infill material.

Hoop stresses within the geocell walls and earth pressures in the adjacent cells are mobilized when the vertical loads are applied which reduces the lateral deformation of the infill material. This increases the stiffness and the load deformation behavior of the soil. The soil geocell layer with increased stiffness acts as a stiff mat resulting in the vertical pressures distribution spreads across the area of the subgrade soil by redistributing the applied pressures away from the center and reducing the pressures transferred at the center below the loading plate.

The contact pressures of each configuration from series C as discussed earlier are presented in Figs. 9, 10, 11 and 12. The contact pressures of geocell reinforced beds are reducing with increase in the geocell height. The pressures reduced from 350 kPa in case of $b/D = 4$, $h/D = 0.5$ to almost 100 kPa in case of $b/D = 4$, $h/D = 1.33$ which is a reduction of about 70% between the least and highest reinforced case in this series.

Figs. 9, 10, 11 and 12 show the variation of the pressures transmitted on to the subgrade with distance from center line corresponding to the geocell reinforced sections of $b/D = 4$ and $h/D = 0.5$, 0.67, 1.0, 1.33 for various cycles. From the figures, it is seen that, as the height of the geocell reinforcement increases, the pressure transmitted on to the subgrade is reduced. The pressures transmitted on to the subgrade with distance from center line in a geocell reinforced bed are lesser

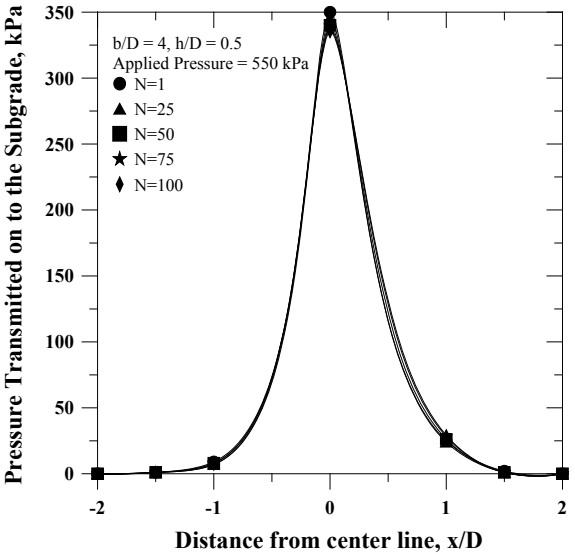

Fig. 9 Pressure transmitted for $b/D = 2$, $h/D = 0.5$

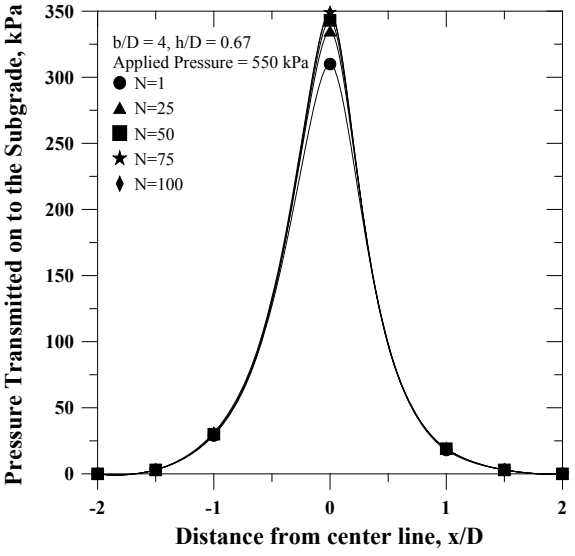

Fig. 10 Pressure transmitted for $b/D = 2$, $h/D = 0.67$

compared to the unreinforced for the same applied pressure. The pressures transmitted are higher for lesser height of the geocell reinforced beds compared to the widths of the geocell as the heights of the dense bed are lesser by which the pressure is directly transferred below the center plate as in case punching failure. The pressures transmitted on to the either sides of the loading plate increased with heights. This is attributed to the flexural rigidity of the geocell reinforced beds for

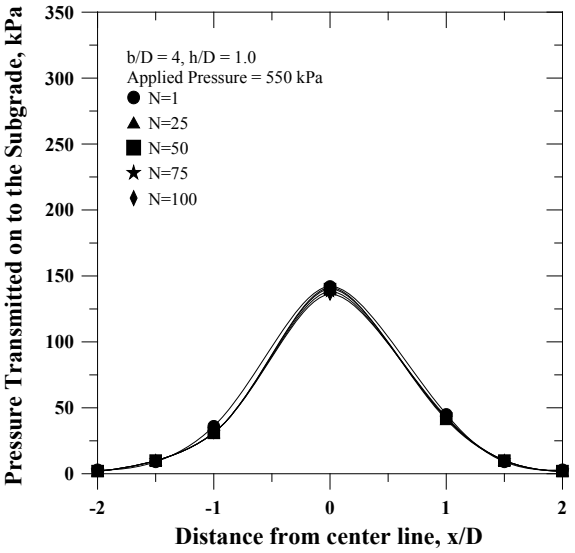

Fig. 11 Pressure transmitted for $b/D = 2$, $h/D = 1.0$

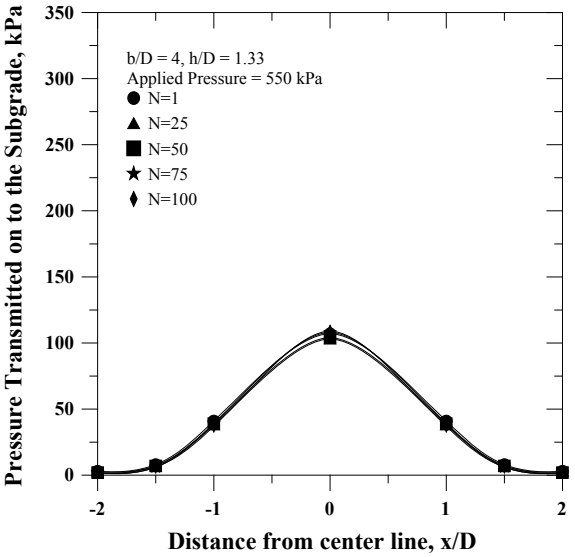

Fig. 12 Pressure transmitted for $b/D = 2$, $h/D = 1.33$

higher heights resulting in transmitting less pressure at the center and more pressures away from the center by redistributing the applied pressures on to the subgrade. Vertical loading of the geocell reinforced sections creates a semi-rigid slab or beam effect. This distributes loads evenly, reduces settlement, and reduces surface degradation resulting in less rutting, potholes, and distortions, means less wear and tear on vehicles, tires, and drivers.

To further quantify the contact pressures of the beds under repeated loading, a parameter contact pressure reduction (CPR), expressed in percentage, for different cases studied as per Table 2 is introduced. CPR is the ratio between contact pressure of the unreinforced bed and geocell reinforced bed difference to that of the unreinforced bed for a pressure applied. Hence, CPR for the particular pressure applied can be expressed as:

$$(\mathrm{CPR}) = \left(1 - \frac{\text{Contact Pressure}_{\text{rein}}}{\text{Contact Pressure}_{\text{unrein}}}\right) \times 100$$

Results from test series A show that the unreinforced test beds could not sustain any number of loading cycles before they reach the prescribed plate settlement of 20%. Hence, the pressures in increments are applied until its failure and the pressure corresponding are noted. In all cases, the bed failed even before reaching the pressure applied on the reinforced cases, i.e., 550 kPa. The data are then extrapolated to get the contact pressure on the subgrade for all the unreinforced cases for the corresponding pressure applied.

All contact pressure reduction (CPR) were analyzed from the series of experiments. The variation of CPR with *b*/*D* ratios and *h*/*D* ratios for different geocell configurations from the testing considered in this study of series B and series C are demonstrated in Figs. 13 and 14.

From Fig. 13, the pressures transmitted on to the subgrade of an unreinforced and reinforced bed at the center for a particular pressure applied are considered. CPR is calculated for varying *b*/*D*'s and given as 29, 35 and 50%, respectively, for

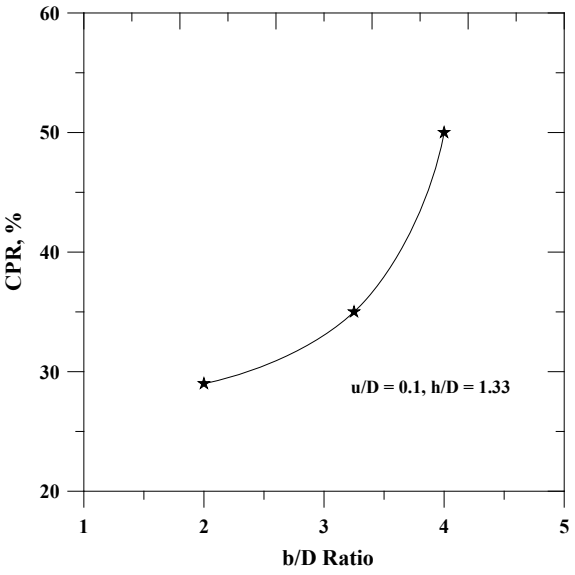

Fig. 13 Variation of CPR with *b*/*D* ratio—Series B

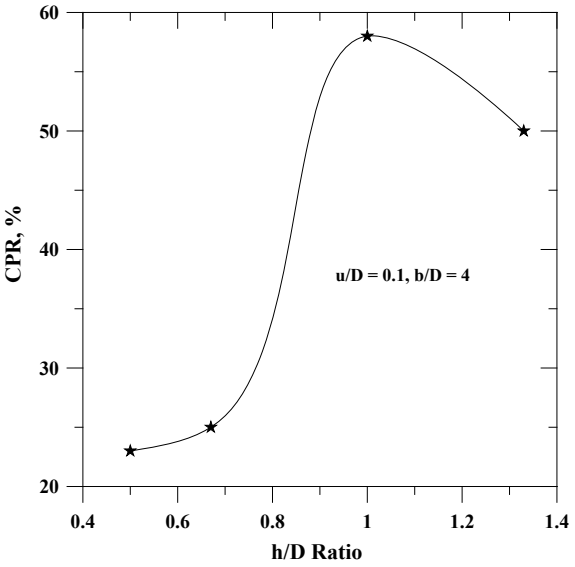

Fig. 14 Variation of CPR with *h*/*D* ratio—Series C

h/*D* = 1.33, *b*/*D* = 2, 3, 4. From the figure, it is clear that the maximum reduction in pressures coming on to the subgrade is 50% in the case of *h*/*D* = 1.33, *b*/*D* = 4 case of geocell reinforcement.

From Fig. 14, the pressures transmitted on to the subgrade of an unreinforced and reinforced bed at the center for a particular pressure applied are considered. CPR is calculated for varying *h*/*D*'s and given as 23, 25 58 and 50%, respectively, for *b*/*D* = 4, *h*/*D* = 0.5, 0.67, 1.0, 1.33. From the figure, it is clear that the maximum reduction in pressures coming on to the subgrade is 58% in the case of *b*/*D* = 4, *h*/*D* = 1.0 case of geocell reinforcement.

Hence, it can be summarized that the geocell of sufficient size (*b*) and thickness (*h*) will provide a higher contact pressure reduction for a given level of traffic loading conditions.

Further study is required to understand the optimal benefits from the critical geocell geometry. It is also important to determine the depth of this kind of reinforcement and number of layers of reinforcement for optimum performance.

6 Conclusions

From a large-scale cyclic model tests on unreinforced and geocell reinforced beds, following conclusions can be drawn:

1. Geocell can be used as reinforcement in pavement subgrade layers to increase the stiffness of the subgrade.

2. Contact pressures of geocell reinforced beds reduced with increase in the geocell widths. The pressures reduced from 160 kPa in case of h/D = 1.33, b/D = 4–100 kPa in case of h/D = 1.33, b/D = 2 which is a reduction of about 40% between the least and highest reinforced case.
3. Contact pressures of geocell reinforced beds reduced with increase in the geocell height. The pressures reduced from 350 kPa in case of b/D = 4, h/D = 0.5–100 kPa in case of b/D = 4, h/D = 1.33 which is a reduction of about 70% between the least and highest reinforced case.
4. Contact Pressure Reduction (CPR) for varying b/D's are 29, 35, and 50%, respectively, for h/D = 1.33, b/D = 2, 3, 4.
5. Contact Pressure Reduction (CPR) for varying h/D's are 23, 25, 58, and 50%, respectively, for b/D = 4, h/D = 0.5, 0.67, 1.0, 1.33
6. The maximum reduction in pressures coming on to the subgrade is 58% in the case of b/D = 4, h/D = 1.0 case of geocell reinforcement. Hence, it is important to choose an optimum size geocell for higher structural support for a given traffic loading system.
7. Further systematic study is required to completely understand the geocell material in pavement layers such as base and sub-base layers with aggregate infill.

Acknowledgements The authors would like to express their appreciation to STRATA Geosystems India Pvt. Ltd. for providing the geocell material for this research.

References

Behrens ILC (1999) Overview of low-volume roads. Transportation research record 1652. Transportation Research Board, pp 1–4

Bushman WH, Freeman TE, Hoppe EJ (2005) Stabilization techniques for unpaved roads, vol 1936. Transportation Research Board, pp 28–33

Chummar AV (1972) Bearing capacity theory from experimental results. J Geotech Eng ASCE 98 (12):1311–1324

Croft JB (1967) The structures of soils stabilized with cementitious agents. Eng Geol 2(2):63–80

Dash SK, Krishnaswamy NR, Rajagopal K (2001) Bearing capacity of strip footings supported on geocell-reinforced sand. Geotext Geomembr 19(4):235–256

Edil TB, Fratta D, Shuettpelz CC (2009) Development of testing methods to determine interaction of geogrid-reinforced granular material for mechanistic pavement analysis. Wisconsin DOT and FHWA project report

Giroud JP, Noiray L (1981) Geotextile-reinforced unpaved road design. J Geotech Eng Div 107 (GT9):1233–1254

Han J, Yang XM, Leshchinsky D, Parsons RL (2008) Behavior of geocell-reinforced sand under a vertical load. J Transp Res Board (2045):95–101

Keller G, Sherar J (2003) Low-volume roads engineering—best management practices field guide. USDA, Forest Service

Little ND (1995) Stabilization of pavement subgrades and base courses with lime. Kendall/Hunt Publishing Co., Dubuque, Iowa

Mallick RB, Veeraragava A (2010) Sustainable pavements in India—the time to start is now. New Build Mater Constr World (NBM&CW) Mag 16(3):128–140

Ministry of Road Transport and Highways (MORTH) (2011) Annual report on Indian roads 2010–11. Government of India

Muench ST, White GC, Mahoney JP, Pierce LM, Sivaneswaren N (2004) Long-lasting low-volume pavements in Washington state. In: International symposium on design and construction of long lasting asphalt pavements. International Society for Asphalt Pavements, Auburn, AL, pp 729–773

Pinard M (2006) New approaches to sustainable provision of low volume sealed roads. In: International workshop, Bamako, Mali, 18–19 Jan 2006

Pokharel SK (2010) Experimental study on geocell-reinforced bases under static and dynamic loading. Ph.D. thesis, University of Kansas, USA

Praticò F, Saride S, Puppala AJ (2011) Comprehensive life cycle cost analysis for the selection of subgrade stabilizers for better performance of low volume roads. Transportation research record 2204, TRB, National Research Council, Washington D.C., pp 120–112

Rayabharapu VK, Saride S (2019) Geocell reinforced dense sand bases overlying weak sand sub-grades under repeated loading. In: Ground improvement techniques and geosynthetics, lecture notes in civil engineering, vol 14. pp 285–294

Saride S, Umashankar B (2010) Towards green pavements in India. In: First US-India workshop on global geoenvironmental engineering challenges, New Delhi, India, 7 Nov 2010

Saride S, Vijay KR, Suraj V, Anand JP (2013) Repeated load tests on geocell reinforced sand subgrades. In: Proceedings of the geosynthetics international conference, Long Beach, CA, vol 3, no 4, pp 537–549

Saride S, Rayabharapu VK, Vedpathak S (2015) Evaluation of rutting behaviour of geocell reinforced sand subgrades under repeated loading. Indian Geotech J 45(4):378–388

Sitharam TG, Saride S (2005) Behaviour of embedded footings supported on geocell reinforced foundation beds. ASTM Geotech Test J 28:452–463

Webster SL (1979) Investigation of beach and trafficability enhancement using sand-grid confinement and membrane reinforcement concepts. Report GL-79-20, US Army Engineer Waterways Experiment Station, Vicksburg, MS, USA

Development of Freeze-Thaw Water Retention Test Apparatus for Coarse Granular Materials

Tomoyuki Aoyagi, Jiaqiang Yang, Shingo Matsutani, Tatsuya Ishikawa, Takahisa Nakamura and Yoshitsugu Momoya

Abstract With time passing, the performance of railway ballasted track and road pavement gradually degrades along with the degradation in railroad ballast and base course layer. However, the Japanese design standard does not consider the age-related deterioration of ballasted track and asphalt pavement. To establish a rational maintenance method of aged ballasted track and road pavement, this study focused on the water retentivity. In this paper, a water retention test apparatus was newly developed to carry out water retention test for coarse granular materials subjected to freeze-thaw. The test samples are Toyoura sand, clean and fouled ballast, and new and aged crusher runs. First, the performance of the newly developed test apparatus was examined by comparing the test results of water retention tests of this paper with the past researches. Second, the influence of age-related degradation for coarse granular materials on the water retentivity was discussed by comparing the test results for aged test samples with the new ones. As a result, the following findings were obtained: (a) The developed test apparatus can

T. Aoyagi (✉) · J. Yang · S. Matsutani
Graduate School of Engineering, Hokkaido University, Sapporo 0608628, Japan
e-mail: aotomo.blue-goat@softbank.ne.jp

J. Yang
e-mail: jq-yang@eis.hokudai.ac.jp

S. Matsutani
e-mail: sabasaba@eis.hokudai.ac.jp

T. Ishikawa
Faculty of Engineering, Hokkaido University, Sapporo 0608628, Japan
e-mail: t-ishika@eng.hokudai.ac.jp

T. Nakamura · Y. Momoya
Railway Technical Research Institute, Tokyo 1858540, Japan
e-mail: nakamura.takahisa.19@rtri.or.jp

Y. Momoya
e-mail: momoya.yoshitsugu.29@rtri.or.jp

R. Sundaram et al. (eds.), *Geotechnics for Transportation Infrastructure*,
Lecture Notes in Civil Engineering 29,
https://doi.org/10.1007/978-981-13-6713-7_32

carry out highly accurate water retention tests in a wide suction range and greatly shorten the testing time. (b) SWCC is seriously affected by the intrusion of fouling materials, regardless of the sample.

Keywords Water retention · Age-related deterioration · Coarse granular materials

1 Introduction

Railway ballasted tracks and road pavements are used all over the world and are indispensable in everyday life. With time passing, the performance of railway ballasted tracks and road pavements gradually degrades along with the degradation in railroad ballast and subbase course layer. For example, at ballasted tracks in cold regions constructed over 20 years ago, the fine fraction increases with the particle crushing of coarse granular materials caused by repeated traffic loads and the intrusion of roadbed and subgrade materials, thereby resulting in the frost heave phenomenon (Aihara et al. 2003). However, the Japanese design standard does not consider the age-related deterioration of ballasted track and asphalt pavement. To establish a rational maintenance method of aged ballasted track and road pavement in cold regions, this paper focused on the water retentivity which was closely related to the mechanical behavior of unsaturated fouled ballast and aged subbase course. However, it takes a lot of testing time for the water retention test of coarse granular materials, which is a big problem when conducting the test. Also, an accurate measurement is difficult for a wide range of suction. In this paper, a water retention test apparatus, which adopts a suction method and a pressure method, was newly developed to deal with these problems and to carry out water retention tests for coarse granular materials subjected to freeze-thaw. Initially, the performance of the newly developed test apparatus was examined by comparing the results of water retention tests performed in this paper with the past researches. After that, the influence of age-related degradation for coarse granular materials on the water retentivity was discussed by comparing the test results for aged test samples with the new ones.

2 Test Apparatus

A newly developed water retention test apparatus is shown in Fig. 1. The test apparatus has the following features. (1) It can be used for the water retention test based on the Japanese testing standard JGS 0151-2009. (2) The testing time is shortened by reducing the specimen size and setting two drainage paths. (3) It is

possible to carry out the water retention tests by using the suction method and the pressure method. (4) Before performing the water retention test, the freeze-thaw test can be carried out by changing the cap. The specimen size is 150 mm in diameter and 100 mm in height. In this test apparatus, since the cap is a perforated loading plate, both the cell pressure and the pore air pressure of the specimen are equal. However, since the side part of the specimen is surrounded by a rigid collar, the cell pressure acts as an upper load and is compressed one-dimensionally. The overburden pressure is mechanically controlled using a BF cylinder. The two drainage paths in the pedestal part are designed to be capable of handling a wide range of suction by using a Versapor membrane on one side and a ceramic disk on the other side. A schematic drawing of the pedestal is shown in Fig. 2. Measurement of the drainage volume is performed by using an electronic balance in the suction method, while a double-tube buret and a differential pressure gauge are used in the pressure method. The freeze-thaw test starts after replacing the cap. The freezing cap and the pedestal have a circulation path of antifreeze, and by using a constant temperature water tank, it is possible to freeze the specimen one-dimensionally from the bottom of the specimen.

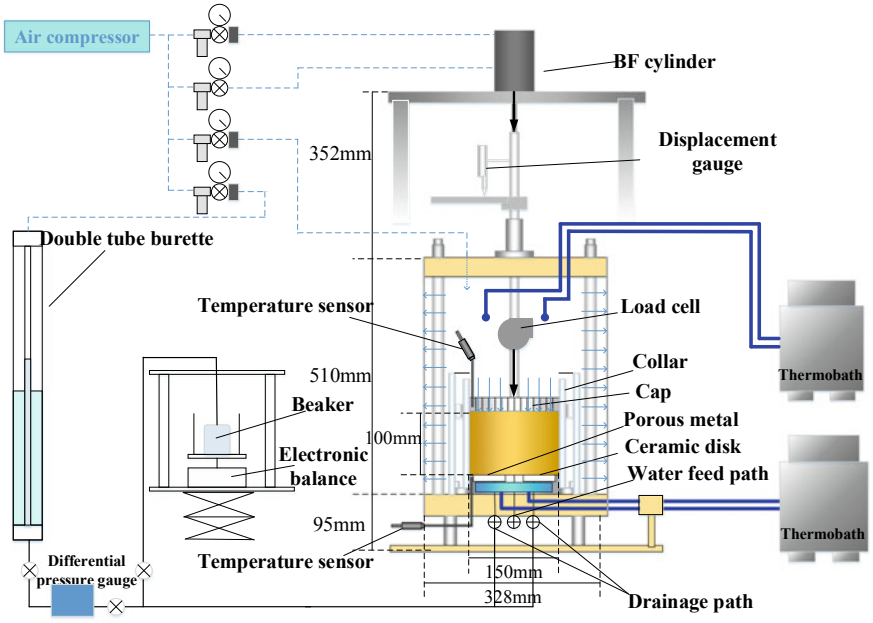

Fig. 1 Water retention test apparatus

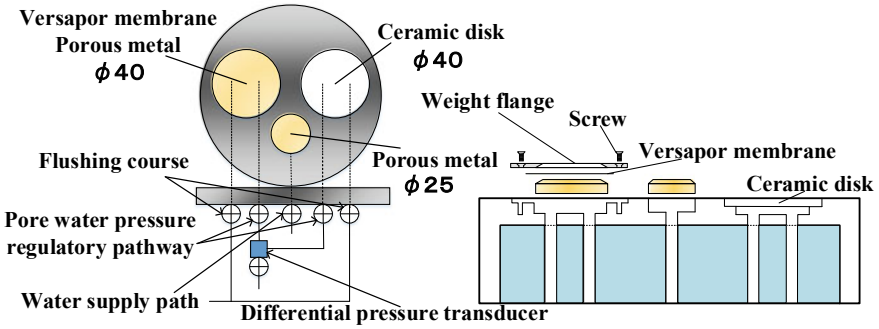

Fig. 2 Pedestal part

3 Test Method

3.1 Sample

At first, in order to evaluate the validity of the newly developed test apparatus, the test was conducted with Toyoura sand, which has comparatively abundant past data. After that, the test was conducted using the clean and fouled ballast, and new and the aged crusher runs, to evaluate the applicability of the test apparatus coarse granular materials and to discuss the influence of aged deterioration on water retentivity. The physical property of each sample is shown in Table 1 ($\boldsymbol{\rho_s}$: soil particle density, $\boldsymbol{\rho_{dmax}}$: maximum dry density, $\boldsymbol{w_{opt}}$: optimum moisture content, $\boldsymbol{D_{50}}$: mean grain size, $\boldsymbol{U_c}$: uniformity coefficient, $\boldsymbol{F_c}$: fine fraction content). The grain size distribution curve is shown in Fig. 3.

Table 1 Physical property of each sample

Sample	ρ_s (g/cm^3)	ρ_{dmax} (g/cm^3)	w_{opt} (%)	D_{50} (mm)	U_c (mm/mm)	F_c (%)
Toyoura sand	2.650	1.651	14.3	0.18	1.30	0
1/2CB	2.730	1.652	3.3	21.4	1.42	–
1/2FB	2.727	2.176	7.6	20.3	–	15
1/1CB	2.000	1.682	3.0	40.7	1.33	–
1/1FB	2.818	2.185	7.8	30.0	–	14.5
1/2FB(50%)	2.620	2.104	5.3	19.8	–	7.8
NewC-40	2.642	2.192	5.8	8.4	38.7	1.1
AgedC-40	2.642	2.055	5.5	8.1	–	4.4

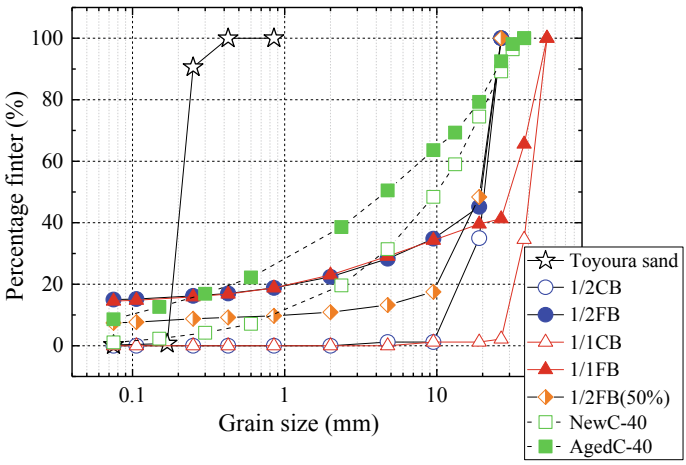

Fig. 3 Grain-size distribution curve

3.1.1 Railroad Ballast

Clean ballast was prepared which was used for actual railway track, and fouled ballast was an artificial mixed soil composed of railroad ballast, gravel (C-30) and kaolin mixture (6:3:1 mixture in weight ratio), which has the same grain size distribution with the fouled railroad ballast at the site. In order to compare with the triaxial compression test which was carried out in the past (Matsutani et al 2017), these tests were carried out with the clean ballast of 1/2 similarity grain size (1/2CB), the fouled ballast by cutting the gravel more than 26.5 mm (1/2FB) and each full-scale ballast (1/1CB and 1/1FB). In addition, a test was conducted using a sample in which the fine grain content of 1/2FB was halved [1/2FB (50%)]. This is to examine the difference in water retentivity in accordance with the degree of age-related deterioration.

3.1.2 Crusher Runs

Crusher run (C-40) commonly used for lower roadbed material was used in this study as well. Tests were carried out with the new C-40 used on the site (NewC-40) and age-related deterioration C-40 (AgedC-40). AgedC-40 was made by abrading NewC-40 at a rotational speed of 33 rpm for 10 min with a Los Angeles testing machine in accordance with JIS A 1121 (JIS 2007).

Table 2 Test conditions of each sample

Sample	Water content	σ_c' (kPa)	ρ_{dc} (g/cm^3)	D_c (%)	S_r (%)	S_{r0} (%)
Toyoura sand	Saturated	49	1.48	89.3	91.3	5.5
1/2CB	Saturated	20	1.47	89.0	86.4	5.7
1/2FB	Saturated	20	1.78	81.7	91.2	40.2
1/1CB	Saturated	20	1.35	89.0	84.4	4.1
1/1FB	Saturated	20	1.87	85.5	96.9	40.7
1/2FB(50%)	Saturated	20	1.62	84.7	88.3	25.1
NewC-40	Saturated	10	1.83	86.9	97.9	32.8
AgedC-40	Saturated	10	1.81	93.5	94.9	31.0

3.2 Preparation of Test Specimens

The test conditions of each sample are shown in Table 2 ($\boldsymbol{\rho_{dc}}$: dry density after consolidation, $\boldsymbol{D_c}$: degree of compaction, $\boldsymbol{S_r}$: degree of saturation, $\boldsymbol{S_{r0}}$: residual degree of saturation).

3.2.1 Toyoura Sand

As for Toyoura sand, a cylindrical specimen was prepared using the air pluviation method with an air-dried sample (w = 1.6%), so that the initial relative density of the specimen would be equal with reference to the experimental conditions in the previous study (Tokoro 2011; Mori 2016). For the saturation, water was added from the bottom end of the specimen. Following the saturation, the consolidation was carried out isotropically under a prescribed overburden pressure of 49 kPa in order to compare with the past study (Tokoro 2011).

3.2.2 Railroad Ballast

A specimen was prepared using an air-dried sample (1/2CB: w = 1.69%, 1/2FB: w = 1.8%, 1/1CB: w = 1.8%, 1/1FB: w = 3.0%). Initially, to make a uniform specimen with a small variation in density, each of the two layers (50 mm in thickness) was compacted by a vibrator in 5 min with constant compaction energy so as to attain the degree of compaction of 90%. As for the saturation, water was added from the bottom end of the specimen. The consolidation was carried out isotropically under a prescribed overburden pressure of 20 kPa in order to compare with the past study (Matsutani et al. 2017).

3.2.3 Crusher Runs

In the same way as mentioned above using air-dried samples (NewC-40: w = 1.043%, AgedC-40: w = 0.958%), a cylindrical specimen was also prepared by applying the vertical vibration with a specified compaction energy at each layer into a cylindrical mold. The saturation was also carried out as above. Considering the overburden pressure (2.64 kPa) of the road pavement and the possibility of frost heave of the specimen, the consolidation was carried out isotropically under a prescribed overburden pressure of 10 kPa referring to JGS 0172-2009.

3.3 Water Retention Test

A water retention test was conducted using a suction method and a pressure method.

3.3.1 Suction Method

As the initial state, the water level of the beaker is aligned to the electronic balance with the top of the specimen. By lowering the position of the electronic balance from that state, a certain amount of suction is applied. The drainage is carried out to the beaker on the electronic balance from the drainage path on the Versapor membrane side. At that time, since both the inside parts of the cell and the chamber are open to the atmosphere, the pore air pressure is the same as the atmospheric pressure. The overburden pressure does not changed and remains constant in each sample. Suction is applied in the range of 0.1–5.0 kPa (0.1, 0.35, 0.5, 1.0, 2.0, 3.0, 4.0, 5.0 kPa).

3.3.2 Pressure Method

After the suction method was completed, the pore water pressure is set to 195 kPa, and the pore air pressure is 200 kPa, which means the applied suction is 5.0 kPa. For the drainage, using both the Versapor membrane path and the ceramic path up to the suction 20 kPa, and for the suction 20 kPa or more, only the ceramic path is used because the suction exceeds the air entry value of the Versapor membrane. The drained water flows to the double-tube buret. At that time, the cell pressure is the same as the pore air pressure and the overburden pressure is kept unchanged. The pore water pressure is gradually lowered, and a predetermined suction is given by the difference between the pore air pressure and the pore water pressure. Suction is applied in the range of 5.0–100 kPa (5.0, 7.0, 10, 15, 20, 30, 50, 75, 100 kPa).

3.4 Freeze-Thaw Process

The freeze-thaw process was carried out with reference to Kawabata et al. (2013), which was based on JGS 0172-2009. Figure 4 shows the circulation path diagram, and Fig. 5 shows the temperature change graph of the constant temperature water bath. The anti-freezing fluid is circulated by using constant temperature water baths, and the temperature of the pedestal and the cap is controlled independently. At first, both the cap and the pedestal are kept at 0 °C for 6 h. Subsequently, anti-freezing fluid at 0.3 °C is circulated in the cap during freezing. As for the pedestal, in order to avoid supercooling, the specimen was frozen by applying a thermal shock to circulate the anti-freezing fluid at −15 °C. The thermal shock is finished after confirming that the temperature rise due to latent heat, the pedestal temperature reaches −3 °C, or after 10 min pass. After the thermal shock, the initial freezing temperature is adjusted to −0.5 °C and the temperature is lowered at a rate of −0.15 °C/h. When it is confirmed that the suction and drainage to the specimen and stop of the axial displacement are confirmed, the freezing is finished. Also, in order to keep the temperature of the inner cell at constant, water at 2 °C is circulated between the outer cell and the inner cell. Finally, the temperature baths are controlled at a constant temperature of 10 °C and 24 h was given to thaw the specimen.

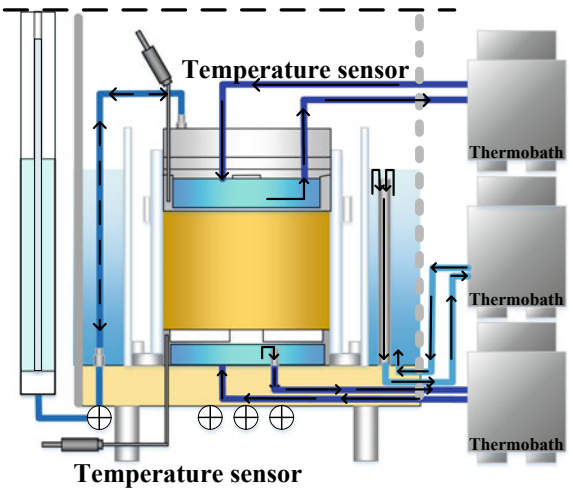

Fig. 4 Cap and circulation route during freeze-thaw

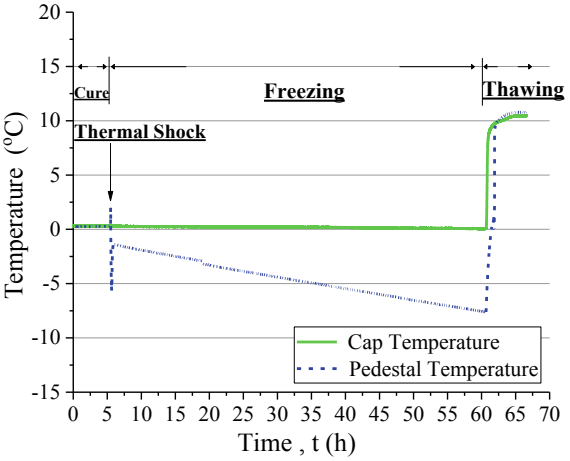

Fig. 5 Temperature change of constant temperature

4 Results and Discussion

4.1 Toyoura Sand

In this study, fitting was applied to measured values of soil–water characteristic curve using Fredlund and Xing's Eq. (1) (Fredlund and Xing 1994).

$$S_e = C(s)\left[\frac{1}{\mathrm{In}\{e+(s/a)^n\}}\right]^m \tag{1}$$

Here, S_e is effective saturation and s is suction. And, a, m, n are parameters; $C(s)$ is 1. The effective saturation is shown in Eq. (2).

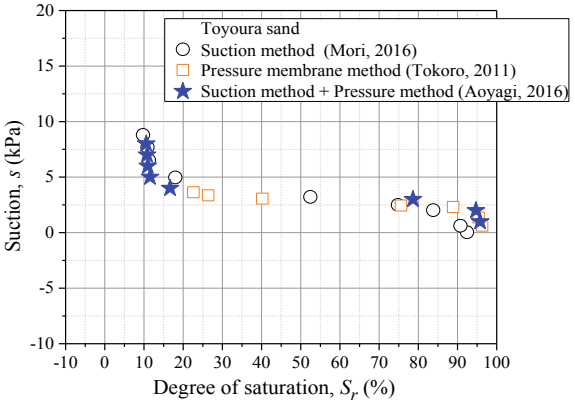

Fig. 6 Soil–water characteristic curve (Toyoura sand)

$$S_e = \frac{\theta - \theta_r}{\theta_s - \theta_r} \tag{2}$$

Here, θ is the moisture content by volume, θ_r is the water ratio in the residual, and θ_s is the water ratio in the saturation. In Eq. (1), both θ_r and θ_s are parameters and are determined by fitting.

In order to confirm the validity of the newly developed test apparatus, Fig. 6 shows the comparison of the soil–water characteristic curve (SWCC) of Toyoura sand obtained in this study and the past studies. Tokoro (2011) tested using the pressure membrane method, and Mori (2016) tested using the suction method. In comparison with the past study, the shape and position of the SWCC are almost the same. In addition, the air entry value is 2.32 kPa for the result of Tokoro (2011), 2.52 kPa for the result of Mori (2016) and 2.56 kPa for this study; therefore, the test accuracy seems to be satisfactory. From the above observations, it can be judged that the water retention test apparatus is functioning appropriately applying both the suction method and the pressure method.

4.2 Railroad Ballast

In order to discuss the influence of the fine grain content on water retentivity after confirming the validity of the test apparatus for coarse granular material, Fig. 7 shows SWCC of the railroad ballast according to the test result of this study with that of the past study (Matsutani et al. 2017). The shape and position of the SWCC show similarity to the past study. Although the water retention test was carried out with the specimen with a height of 1/3 as compared with the past study, the test results are similar. It is considered that there is almost no influence of the size of the specimen on the grain size. Moreover, even if comparing the results of 1/1 ballast and 1/2 ballast,

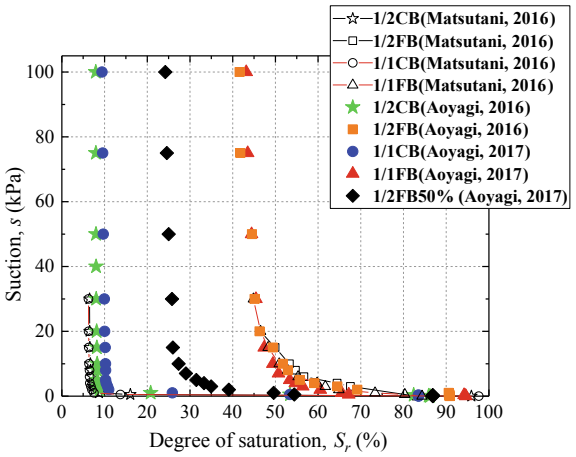

Fig. 7 Soil–water characteristic curve (railroad ballast)

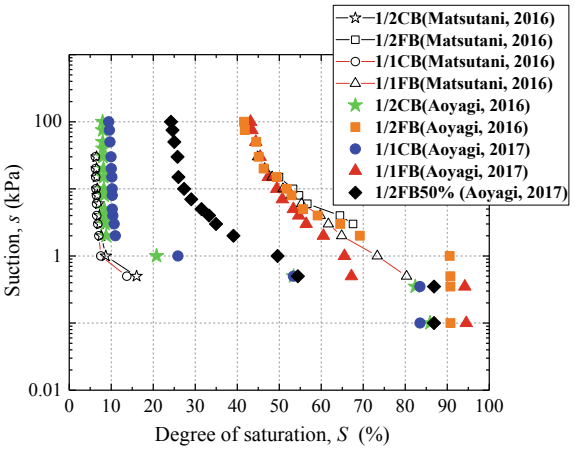

Fig. 8 Logarithmic axis graph in Fig. 7

there is no big difference in the test result. From this result, it is suggested that the test which carried out using 1/1 ballast at the specimen height of 10 cm and the test which carried out using 1/2 ballast at the specimen height of 5 cm are equivalent results. As long as the particle diameter is about 1/2 ballast, it is considered that the test can be conducted even at the specimen height of 5 cm. From the above observations, it was confirmed that the validity of the newly developed test apparatus for coarse-grained material is high.

Focusing on precision, since previous studies can only be tested with the pressure membrane method, it is difficult to control the pressure of 0.1 units, and the reliability of the data in the low suction region is doubtful. Thus in the past study, it is impossible to confirm the air entry value. On the other hand, in this test result, using the suction method in the low suction region, as shown in Fig. 8, the air entry

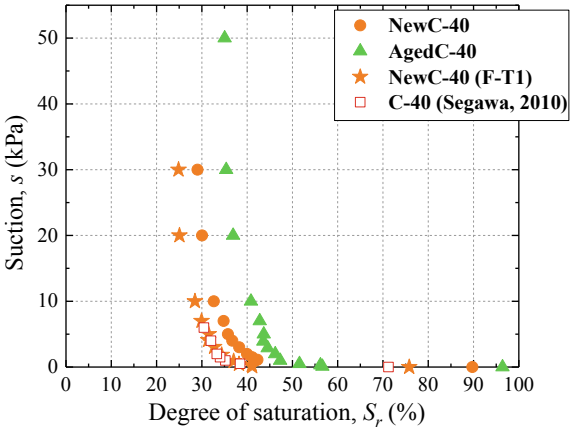

Fig. 9 Soil–water characteristic curve (C-40)

value in FB was confirmed and therefore the measurement accuracy improved compared with the past study.

As can be seen from the test results of 1/2CB, 1/2FB, 1/2FB (50%), the water retention becomes higher as the fine particle content increases. As for 1/2FB (50%), SWCC passes almost midway between 1/2CB and 1/2FB, and it is conceivable that the fine fraction content and the water retentivity have a positive correlation. Therefore, it can be judged that an increase in the fine fraction has a very significant effect on water retentivity.

4.3 *Crusher Run*

In order to discuss the inference of age-related degradation on water retentivity, Fig. 9 shows SWCC of the crusher run according to the test result of this study with that of the past study (Segawa et al. 2010). For NewC-40 that gave freeze-thaw [NewC-40(F-T1)], Fig. 10 shows the axial displacement of the specimen and drainage during freeze-thaw, the drainage graph. First, it can be seen that AgedC-40 has higher saturation at each suction and higher water retentivity than NewC-40. This can be judged that age-related degradation has a great effect on water retentivity.

Comparing the results of the previous study with NewC-40, NewC-40(F-T1) in this study, SWCC is almost the same shape. Slightly, NewC-40 saturation is high,

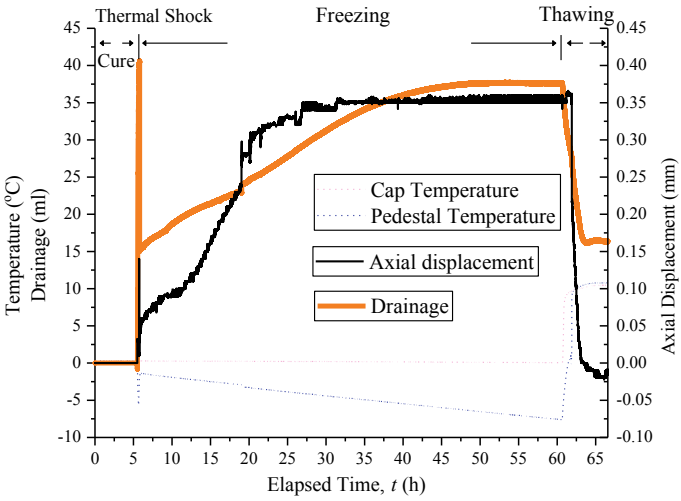

Fig. 10 Axial displacement and drainage during freeze-thaw

but this seems to be due to insufficient saturation of the porous metal and the ceramic disk at the preparation stage. With regard to NewC-40(F-T1), since the expansion coefficient at freeze-thaw was 0.34% and the frost heaving speed was 0.019 mm/h, which was less than 0.1 mm/h and which is the judgment criterion without frost-susceptible, frost heave was not confirmed. Therefore, it was found that the influence of the freeze-thaw on the water retentivity of the new lower roadbed material is almost nothing. In the future, it is necessary to carry out a water retention test with AgedC-40 subjected to freeze-thaw and consider how much the age-related degradation will be affected by freeze-thaw.

4.4 Test Time

In the past study, water retention tests of railroad ballast were carried out by the pressure membrane method using the medium-size triaxial apparatus, and the test time was about 1 week. On the other hand, the test in this paper was completed on 3 or 4 days using the new developed apparatus. This is a result of the drastic reduction of the time for each suction sequence by reducing the size of the specimen and constructing two kinds of drainage paths.

5 Conclusion

As a result, the following findings were obtained:

(a) The developed test apparatus can carry out highly accurate water retention tests in a wide suction range and greatly shorten the testing time.
(b) Soil–water characteristic curves are seriously affected by intrusion of fouling materials, regardless of the test sample.
(c) The age-related degradation has a great influence on water retentivity.
(d) The new lower roadbed material is not affected by freeze-thaw.

Therefore, the newly developed freeze-thaw water retention test apparatus is useful for evaluating water retentivity. In addition, it was found that the water retentivity of the coarse-grained material is greatly affected by the increase in fine grain content and age-related degradation.

References

Aihara H, Tsunashima K, Haraguchi M, Akagawa S (2003) The effect of fines content in the ballast frost heave. In: Japan Society of Civil Engineers 2013 annual meeting, III-382, pp 763–764

Fredlund DG, Xing A (1994) Equations for the soil-water characteristic curve. Can Geotech J 31:521–532

Japanese Geotechnical Society Standards Laboratory Testing Standards of Geomaterials, vol 1 (2009), pp 162–169

Japanese Industrial Standards (JIS) (2007) Method of test for resistance to abrasion of coarse aggregate by use of the Los Angeles machine

Kawabata S, Ishikawa T, Toyota K, Yamauchi S, Kameyama S (2013) Influence of freezing condition and specimen size on evaluation of frost-susceptibility. J JSCE E1 69(3)

Matsutani S, Ishikawa T, Aoyagi T, Nakamura T, Momoya Y (2017) Effect of grain size on deformation-strength characteristics of unsaturated railroad ballast. In: 57th technical report meeting, Hokkaido Branch, Japanese Geotechnical Society, Japan, pp 67–74

Mori A (2016) Development of unsaturated permeability test apparatus using approximated profile method. Hokkaido University

Segawa H, Ishikawa T, Miura S, Tokoro T (2010) Development of medium-size triaxial apparatus for the evaluation of mechanical behavior of unsaturated granular base coarse materials. In: 52th technical report meeting, Hokkaido Branch, Japanese Geotechnical Society, Japan, pp 27–34

Tokoro T (2011) Development of evaluation method for hydraulic properties of the soils subjected to freeze-thaw action. Ph.D. thesis, Hokkaido University

Effect of Bagasse Ash Admixture on Geotechnical Properties of Shedi Soil in Addition with Lime and Sodium Salts

N. Chethan, H. N. Ramesh and S. Nethravathi

Abstract Shedi soil (Lithomargic clay) is the name given to the locally available whitish, pinkish or yellowish silty soil underlying lateritic soil densely deposited along west coast of India. Lithomargic soil is considered as weaker soil as it does not possess any desirable engineering property, so strength behaviour of Shedi soil under varying moisture content is major problem for construction projects in this region. This paper brings out the effect of lime and sodium on various geotechnical properties such as the index properties, compaction characteristics and strength characteristics of Shedi soil admixture with bagasse ash. The tests on index properties, compaction characteristics and strength have been carried out for Shedi soil replaced with various percentages of bagasse ash (BA), lime and sodium salts for different moulding water contents and curing period. It has shown that the plasticity index of soil increases with increase in BA-lime concentration and maximum dry density decreases with increase in Optimum Moisture Content (OMC). Though the plasticity index of soil increases and Maximum Dry Density decreases (MDD), Unconfined Compressive Strength (UCS) of Shedi soil increases significantly from 227 to 2311 kPa when treated with bagasse ash-lime and sodium salt with curing period and moulding water content.

Keywords Shedi soil · Bagasse ash · Lime · Index properties · UCS strength

N. Chethan (✉)
Department of Civil Engineering, Guru Nanak Institute of Technology, Khanapur, Hyderabad 501506, India
e-mail: chethan.72658@gmail.com

H. N. Ramesh
Department of Civil Engineering, University Visvesvaraya College of Engineering, BUB, Bengaluru 560001, India
e-mail: rheddur@yahoo.com

S. Nethravathi
Department of Civil Engineering, R.V. College of Engineering, Bengaluru, Karnataka 560059, India
e-mail: nethravathis@rvce.edu.in

R. Sundaram et al. (eds.), *Geotechnics for Transportation Infrastructure*,
Lecture Notes in Civil Engineering 29,
https://doi.org/10.1007/978-981-13-6713-7_33

1 Introduction

Considerable length of roads planned to be constructed in India under various programmes require large quantities of highway material and underground structures like tunnels, deep excavations and caverns are increasingly constructed in all type of soils including lithomargic soils. The suitability of existing soil as sub-base or sub-grade course depends on soil characteristics and strength. The lithomargic soil strata exist at considerable depths below ground level. This layer formed from lateritic soil by some chemical action of groundwater (water table). Therefore, in the present work, strength analysis of lithomargic soil and possible additions of suitable chemicals to improve the quality of the lithomargic soil needs further exploration. The research work involves study on Engineering behaviour of lithomargic soil of west coast of India especially in Bhatkal area with field and laboratory investigation; study of erosions of lithomargic soil strata along slopped cuttings and underground caverns using additives, chemicals and sodium salts, etc. and evolving methodology for their construction in lithomargic soil stratum.

1.1 Objective of the Study

In the present work, tests been done to examine strength behaviours of Shedi soil, which is quite problematic, abundantly available in the west coast region of Karnataka state, India. Roads constructed on this type of soil sub-grade will not have good stability and durability. During monsoon, one can see difficulties for design, construction and maintenance of most of the rural roads in these regions.

The main objectives of the present study are as follows:

- To improve the strength of locally available weak sub-grade soil (i.e. Shedi soil), by varying the percentage of bagasse ash with addition of lime and sodium salts and analysing the suitability.
- To evaluate the influence of bagasse ash on the OMC and MDD, UCS and Consistency limits.

1.2 Scope of the Work

The main scope of the work was to study the index and compaction properties and strength characteristics of Shedi soil with the addition of various percentages of bagasse ash to arrive at the optimum percentage and intended to compare the change in geotechnical properties of natural soils.

2 Experimental Studies

2.1 Materials

Shedi soil (SS) obtained was from an industrial site of Bhatkal, Mangalore, and were collected in plastic cement bags, transported to the laboratory, and spread on flat trays of size, 1500 mm × 900 mm. The lumps were broken down using rammers, and the soil was sun-dried for 10 days, until the weight of soil on the trays found to be constant, indicating that the soil is moisture-free. The Shedi soil fractions were then intermixed 5 times using the technique of quartering. The basic Geotechnical properties of soil were determined. After the soil is sun-dried, then sieve analysis is undertaken. Thus, soil passing through 425 μm IS sieve used for this investigation and is utilized in the experimental work. The admixture used in study is bagasse ash (BA). BA obtained from Mandya Sugar factory, Mandya district, Karnataka state, located 100 km from Bangalore. The ash burnt in muffle furnace at 500 °C for two hours to remove the unburnt carbon content. The physical and chemical properties of Shedi soil and bagasse ash are presented in Tables 1 and 2.

Chemically pure hydrated lime and sodium salts bought from Vaasu Scientific chemicals Lab private limited (Avenue Road) Bangalore, India has been used in this investigation.

Table 1 Physical properties of Shedi soil and bagasse ash

Properties	Shedi soil	Bagasse ash
Colour	Yellowish pink	Pale grey
Specific gravity	2.47	1.8
Grain size distribution		
Coarse sand fraction (%)	5.4	0
Fine sand fraction (%)	22.6	77.2
Silt size (%)	53.4	22.8
Clay size (%)	18.6	
Atterberg's limit		
Liquid limit (%)	43	63
Plastic limit (%)	26	NP
Plasticity index (%)	17	NP
Shrinkage limit (%)	19	
Unified classification	MH-OH	–
Compaction characteristics		
Maximum dry density (kN/m^3)	15.7	10.59
Optimum moisture content (%)	20	45
Unconfined compressive strength (kPa)	180	N/C

N/C = Not conducted

Table 2 Chemical properties of Shedi soil and bagasse ash

Chemical composition	Shedi soil (%)	Bagasse ash (%)
Silicon dioxide (SiO_2)	57.60	55.80
Alumina (Al_2O_3)	29.90	25.80
Iron oxide (Fe_2O_3)	3.00	10.60
Calcium oxide (CaO)	0.23	0.12
Magnesium oxide (MgO)	0.17	0.08

2.2 Methodology

Experiments have carried out by mixing Shedi soil with the bagasse ash and chemicals. The replacement of Shedi soil with bagasse ash content varied gradually as 10, 20, 30, 40, 50 and 60% by weight of total mix. The properties of the different mixes with varying bagasse ash content and chemicals were examined for laboratory prepared specimens for different mounding water content and curing of 7 and 30 days. The properties including Atterberg's limits (LL, PL and SL), MDD and OMC and Unconfined Compressive Strength were determined.

3 Result and Discussion

3.1 Atterbeg's Limits

3.1.1 Liquid Limit

The liquid limit is the water content corresponding to the arbitrary limit between liquid and plastic state of consistency of soil. The liquid limit of clays primarily controlled by: (i) the shearing resistance at the particle level, and (ii) the thickness of diffused double layer. Liquid limit tests been carried out, and the effect of BA on Shedi soil in addition to lime and sodium salts has been studied. Variation of liquid limit of Shedi soil treated with bagasse ash, lime and sodium salts represented in Fig. 1 and values given in Table 3. Liquid limit tests been carried out by adding various percentages of bagasse ash to Shedi soil. The liquid limit of Shedi soil with bagasse ash increases initially and then decreases. It was observed that, Shedi soil treated with different percentages of bagasse ash, up to 60% replacement of the combination liquid limit increases from 45 to 59% of the immediate testing. This may be due to effects of fine particles of bagasse ash and water-holding capacity of bagasse ash, with increasing curing period the liquid limit reduces. In addition, this may be due to the effect of coarser particles that makes the mixture more frictional; hence, a reduction in the thickness of the diffuse double layer leads to decrease in the water holding capacity. Likewise, with the optimum percentages (by UCS strength) of bagasse ash and lime, Shedi soil treated with 1% of sodium salts (NaOH and NaCl).

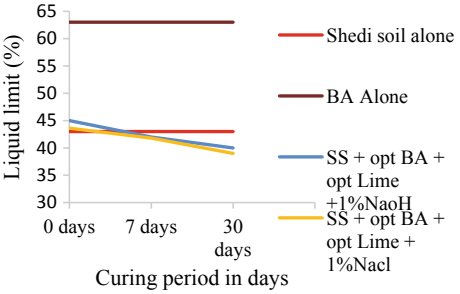

Fig. 1 Variation of liquid limit of Shedi soil treated with optimum of BA, lime and 1% sodium salts

Table 3 Variation of liquid limit of Shedi soil treated with optimum of BA, lime and 1% sodium salts

Combination	Liquid limit (%)		
	Curing period in days		
	0	7	30
Shedi soil alone	43	43	43
BA alone	63	63	63
SS + opt BA + opt Lime + 1% NaOH	45	42	40
SS + opt BA + opt Lime + 1% NaCl	43.6	41.8	39

3.1.2 Plastic Limit

The plastic limit is the minimum water content at which the plasticity of the soil particles must be able to move one another to take up a new position and retain the new equilibrium position. The plastic limit of Shedi soil alone found to be 26%. Immediate testing of the treated Shedi soil shows no variation in the plastic limit of the soil. This is due to the reason that BA initially acts on the non-plastic material, because of less bonding capacity. On the other side by adding the lime and sodium salts to the soil in the presence of the optimum BA that is again decreasing the plastic limit of the treated soil because of the decrease in the diffused double layer thickness. Present in the soil, making them to work to alter the properties of the soil (Fig. 2; Table 4).

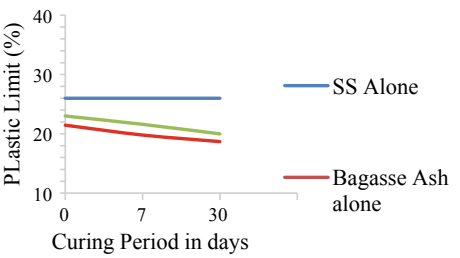

Fig. 2 Variation of plastic limit of Shedi soil treated with optimum of BA, lime and 1% sodium salts

Table 4 Variation of plastic limit of Shedi soil treated with optimum of BA, lime and 1% sodium salts

Mixture	Plastic limit (%)		
	Curing period in days		
	0	7	30
SS alone	26	26	26
Bagasse ash alone	Non-plastic		
SS + 15% BA +1 % Lime	23	21.6	20
SS + 15% BA + 2% Lime	21.45	19.8	18.7
SS + 15% BA + 3% Lime	Non-plastic		
SS + 15% BA + 4% Lime			
SS + 15% BA + 5% Lime			

3.1.3 Shrinkage Limit

The resistance offered against volume change in the test for shrinkage limit is an indicator of shear resistance that can be mobilized between the particle contacts for any given tension force. The greater the shear resistance offered between the particle contacts, greater is the resistance against volume change of the particles and vice versa. Therefore, shear resistance is a function of the frictional properties of the material, electrical attractive and repulsive forces and the normal forces acting between the particles and/or at particle contacts. The shrinkage limit of Shedi soil alone is found to be 19% and of BA, lime and sodium salts are non-shrinkable. As the percentage of BA, lime and 1% of sodium salts increases, the shrinkage limit of the soil increases. This behaviour may be due to the predominance of the non-plastic nature of BA, and the increase in shrinkage limit is mainly due to an expansion of diffuse double layer thickness (Fig. 3; Table 5).

3.2 Compaction Characteristics

Compaction is a process through which densification is attained by removal of air voids at a constant water content of soil mass. For achieving this soil compaction, majority of the field activities adopt the results of laboratory compaction tests like standard or modified proctor or mini compaction tests. In case of fine-grained soils,

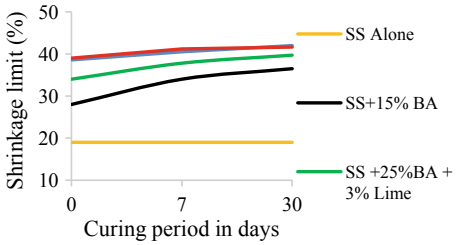

Fig. 3 Variation of shrinkage limit of Shedi soil treated with optimum of BA, lime and 1% sodium salts

Table 5 Variation of shrinkage limit of Shedi soil treated with optimum of BA, lime and 1% sodium salts

Mixture	Shrinkage limit (%)		
	Curing period in days		
	0	7	30
SS alone	19	19	19
SS + 15% BA	28	34	36.5
SS + 25% BA + 3% Lime	34	37.8	39.7
SS + 15% BA + 3% Lime + 1% NaOH	38.6	40.5	42
SS + 15% BA + 3% Lime + 1% NaCl	39	41.2	41.65

compaction process is quite complex as the soil consists of both active and relatively inactive clay minerals. Compaction test results are expressed in a graphical representation between dry density and water content. Majorly, two significant compaction characteristics are optimum moisture content (OMC) and maximum dry density (MDD). The maximum dry density of Shedi soil and bagasse ash alone was found to be 15.7 and 10.7 kN/m^3, respectively, with optimum moisture content of 20 and 45%. Addition of various percentages of bagasse ash to the Shedi soil, the maximum dry density continuously decreases and the moisture content increases up to 60%. The optimum content obtained by conducting UCS for the combination is found to be 15%. This decrease in the maximum dry density is due to the low specific gravity and low density of bagasse ash and high optimum moisture content, i.e., 45%. Moreover, increase in optimum moisture content is due to increasing demand for water by various captions and the clay mineral particles to undergo hydration reaction. This may be due to the formation of more gelatinous compounds, which can retain high moisture content, as there was no much time elapsed after mixing sodium salts (Fig. 4; Table 6).

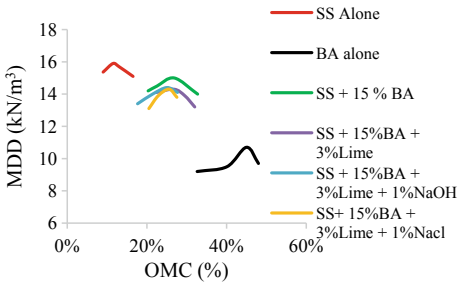

Fig. 4 Variation of compaction characteristics of Shedi soil treated with optimum of BA, lime and 1% sodium salts

Table 6 Variation of compaction characteristics of Shedi soil treated with optimum of BA, lime and 1% sodium salts

Mixture	Maximum dry density (kN/m^3)	Optimum moisture (%)
SS alone	15.7	20
BA alone	10.7	45
SS + 15% BA	14.72	27
SS + 15% BA + 3% Lime	14.12	27
SS + 15% BA + 3% Lime + 1% NaOH	14.12	25
SS + 15% BA + 3% Lime + 1% NaCl	14.02	26

3.3 Role of Moulding Water Content on the Strength Properties (UCS)

The strength of the soil depends on density and compactive effort of soils, which are highly susceptible to erosion, on mixing with bagasse ash and curing for a sufficient period, not only become resistant to erosion, also there is increase in strength. The strength properties is studied at the dry of optimum, optimum and wet of optimum conditions for immediate as well as with various curing periods of Shedi soil treated with optimum percentage of lime, bagasse ash and sodium salts. Generally, it found that 1% sodium salts have an optimum effect. Optimum amount of bagasse ash and lime added to Shedi soil is determined by unconfined compression strength test. As observed from test, the unconfined compressive strength of Shedi alone on immediate testing was 180 kPa, respectively. On addition of 10–60% of bagasse ash to Shedi soil, the strength increases up to 15% of bagasse ash addition on immediate testing as well as with curing periods due to pozzolanic reaction, agglomeration between the soil and bagasse ash in presence of water and flocculation of the clay particles. Addition of various percentages of lime to Shedi soil treated with optimum percentage of bagasse ash the strength increases up to 3% addition of lime, there after strength further increases lightly with the increase in percentage of lime on immediate testing and curing period. By observing the percentage increase of the unconfined compressive strength, at 3% we can find the greater increase of the strength. Hence, 3% of lime to Shedi soil and 15% bagasse ash mixture has chosen as the optimum content of the mixture. It is the well-known fact that for untreated soils, the strength of soils compacted at dry of optimum is more than when compacted at the wet of optimum. However, the wet of optimum condition is used for construction of earthen dams, tailing dams, highway and embankments. Hence, this proposed study focuses on the effect of moulding water content on the strength behaviour of Shedi soil (lithomargic clay) with additives. The strength of soil varies with the moulding water contents. However, in addition of additives strength may increase depending on the pozzolanic property with curing periods. The dry density and water content at dry of optimum, optimum and wet of optimum conditions have selected based on compaction test results of the

respective combinations. The unconfined compressive strength of Shedi soil is 213 kPa at dry of optimum, 180 kPa at optimum and 169 kPa at wet of optimum conditions on immediate testing. The strength of Shedi soil and optimum lime and bagasse ash mixture increased from 332 to 1024 kPa at dry of optimum, 282–940 kPa at optimum and 254–681 kPa at wet of optimum conditions at 30 days curing period. This was due to flocculation of particles on dry side of the optimum and development of pozzolanic reaction compounds within the available water the strength increases. On addition of 1% sodium salts, i.e., NaOH to the lime-treated Shedi soil and bagasse ash mixtures, the increase in the UCC strength takes place from 281 to 2311 kPa in dry of optimum, 253–2212 kPa in optimum and 227–2164 kPa in wet of optimum from 0 to 30 curing days testing. Figures 5, 6, 7 and Table 7 will show the variation of UCS for optimum mixture for moulding water content.

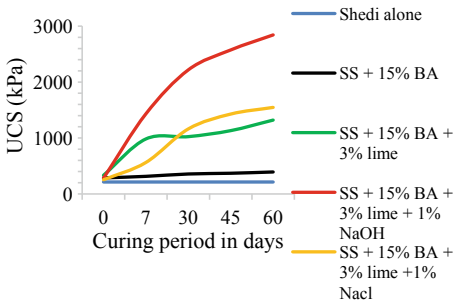

Fig. 5 Variation of unconfined compressive strength of dry of optimum percentage of Shedi soil, lime, bagasse ash mixture treated with 1% sodium salts with different curing periods

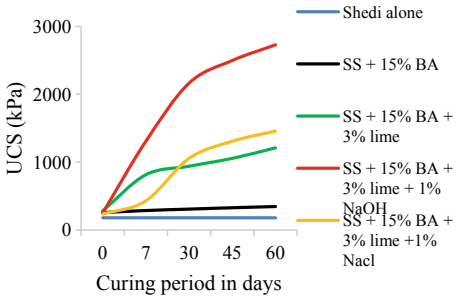

Fig. 6 Variation of unconfined compressive strength of optimum percentage of Shedi soil, lime, bagasse ash mixture treated with 1% sodium salts with different curing periods

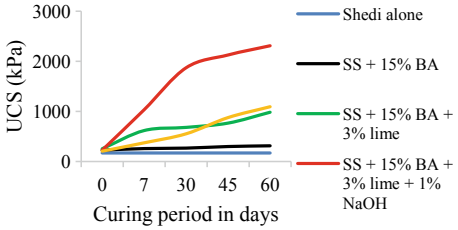

Fig. 7 Variation of unconfined compressive strength of wet of optimum percentage of Shedi soil, lime, bagasse ash mixture treated with 1% sodium salts with different curing periods

Table 7 Variation of unconfined compressive strength of Shedi soil treated with bagasse ash, lime and sodium salts at dry of optimum, optimum and wet of optimum conditions at various curing period

Mixture	Unconfined compressive strength in kPa								
	Dry of optimum			Optimum			Wet of optimum		
Curing period in days	0	7	30	0	7	30	0	7	30
Shedi soil alone	213	213	213	180	180	180	169	169	169
BA alone	Non-plastic								
SS + 10% BA	241	287	306	210	219	229	193	206	211
SS + 15% BA	286	314	356	259	287	308	227	258	267
SS + 20% BA	210	232	237	219	228	249	181	292	201
SS + 30% BA	197	211	222	209	219	228	176	183	196
SS + 40% BA	183	194	207	199	206	217	169	173	191
SS + 50% BA	177	190	198	197	206	217	157	169	179
SS + 60% BA	166	184	191	187	200	207	151	166	170
SS + 15% BA + 1% Lime	326	624	637	292	500	591	242	410	479
SS + 15% BA + 2% Lime	310	721	762	266	627	729	266	482	534
SS + 15% BA + 3% Lime	332	983	1024	282	815	940	254	618	681
SS + 15% BA + 4% Lime	320	1023	1123	275	863	983	262	636	739
SS + 15% BA + 5% Lime	342	1046	1233	285	875	999	272	648	794
SS + 15% BA + 3% Lime + 1% NaOH	281	1432	2311	253	1308	2212	227	1034	2164
SS + 15% BA + 3% Lime + 1% NaCl	254	563	1162	235	430	1055	206	372	1092

4 Conclusions

The results obtained from the above-discussed experimental work, following conclusions are drawn:

- In consideration to Atterberg's limits, liquid limit and plastic limit of Shedi soil increases with increase in percentages of bagasse ash content for immediate testing. As the curing period increases, the plastic limit marginally decreases. Decrease in the plastic limit of Shedi soil treated with 15% bagasse ash and increase in lime with and without curing periods was due to high reactive silica content leading to formation of higher quantity of CSH gel promotes pozzolanic reactions and with increased duration of curing.
- Addition of 1% NaCl and 1% NaOH to optimum percentage of Shedi soil, bagasse ash, lime mixtures, both liquid limit and plastic limit decreases both with and without curing.
- Shedi soil treated with BA, lime and 1% sodium salts show decrease in shrinkage limit for with and without curing.
- MDD of Shedi soil decreases and OMC increases with increases in BA, lime and 1% sodium salts for with and without curing. This is due to decrease in

repulsive pressure of soil, which resists compactive effort, consequently soil particles become closer with lower water absorption capacity.

- Shedi soil replaced with 15% BA content and treated with 3% lime shows greater strength, 180–259 and 282 kPa for immediate testing and 308 and 940 kPa for 30 days of curing, respectively, based on UCS. Addition of 1% NaOH and 1% NaCl increases to 2212 and 1055 kPa for 30 days of curing compare to untreated soil due to pozzolanic reaction. However, NaOH treated samples exhibit more strength compared to NaCl treated samples.
- In India, we design the flexible pavement using IRC 37-2012. As code suggests higher the strength of subgrade, lesser will be the thickness of pavement. Hence, higher strength will be obtained from a mixture of optimum percentages with curing period, and this mixture will be adapted for subgrade for designing highway pavement in this region.

References

Allamaprabhu (2012) Geotechnical characteristics of lithomargic clay blended with marine clay as landfill liner material. Int J Earth Sci 05(06):01

ASTM Standard D698 (2000) Standard test methods for laboratory compaction characteristics of soil using standard effort. ASTM, WC, PA

Gandhi KS (2012) Expansive soil stabilization using bagasse ash. Int J Eng Res Technol (IJERT) 1 (5):2278–0181

IRC 37-2012 guidelines for the design for the flexible pavements (third revision)

Kumar PSP, Rajasekhar K (2009) Laboratory investigation of Shedi soil stabilized with pond ash and coir. In: Indian geotechnical conference (IGC), Guntur, India

Mu'azu MA (2007) Evaluation of plasticity and particle size distribution characteristics of bagasse ash on cement treated lateritic soil. Leonardo J Sci 10(1):137–152

Mu'azu MA (2007) Influence of compactive effort on bagasse ash with cement treated lateritic soil. Leonardo Electron J Practices Technol 10(1):79–92

Ramakrishnegowda C, Yaji R, Shivashankar R, Sivapullaiah PV (2011) Geotechnical properties of Shedi soil affected by alkali contamination. Int J Environ Prot 1(4):45–52

Sarvade PG, Nayak S (2014) Studies on the utilization of quarry dust to improve the geotechnical properties of lithomargic clay. Int J Adv Struct Geotech Eng 3(1):54–59

Sivapullaiah PV, Sridharan A (1985) Liquid limit of soil mixtures. Geotech Test J 8(3):111–116

Sridharan A, Nagaraj HB, Prasad PS (2000) Liquid limit of soils from equilibrium water content in one-dimensional normal compression. Proc Inst Civ Eng Geotech Eng 143(3):165–169

Effect of Granular Layer Strength and Thickness on Jute Geotextiles Reinforced Rural Road

Souvik Patra and Ashis Kumar Bera

Abstract In the present study, a 3D finite element (FE) analysis has been carried out to study the stress and strain response of Jute Geotextiles (JGT) reinforced rural road by static analysis. In the rural road, JGT has been placed in between top granular layer and subgrade soil with a thin layer of sand above and below of JGT as Sand-JGT-Sand (SJS) reinforcement. SJS reinforced rural road has been modelled and analysed by using the commercial FE software package ABAQUS 6.12. Two types of reinforced rural road section have been developed to simulate the effect of degradation of JGT. Nonlinear behaviour of the road materials has been taken into account for top granular layer, sand and for subgrade soil, JGT has been discretized using membrane element. Results of FE analysis indicate a significant improvement in the service life of SJS reinforced rural road section, before and after degradation of JGT over unreinforced rural road section. Only a small fraction of the tensile strength of JGT has been mobilized in SJS reinforced rural road sections. Maximum percentage utilization of JGT tensile strength has been found as 4.76 and 2.38% for thin and thick top granular layer, respectively.

Keywords FE analysis · Rural road · Jute geotextiles · Service life · Tensile strength

1 Introduction

Construction of pavement on soft subgrade foundation by use of geotextiles is quite common practice today. Recent concerns on environmental awareness also increase the use of natural geotextiles in place of manmade synthetic geotextiles. The main

S. Patra · A. K. Bera (✉)
Department of Civil Engineering, Indian Institute of Engineering Science and Technology, Shibpur, Howrah 711103, India
e-mail: ashis@civil.iiests.ac.in

S. Patra
e-mail: souvik4rmjgec@gmail.com

R. Sundaram et al. (eds.), *Geotechnics for Transportation Infrastructure*, Lecture Notes in Civil Engineering 29,
https://doi.org/10.1007/978-981-13-6713-7_34

differences between these two types of geotextiles are that natural geotextile poses low strength and degrades with time. Recent studies also notified that the degradation does not affect the use of natural geotextile, especially in pavement foundation. Incomparative view of cost, natural geotextiles such as Jute, Coir are cheaper than the manmade synthetic geotextiles. Ramaswami and Aziz (1989) showed that JGT is an effective solution to strengthen the road subgrade especially in low volume roads and on haul roads. In India, low volume roads which carries a design traffic of 10,000–1,00,000 for design period of 10 years also known as Rural roads (IRC SP 72: 2015). The purpose of the rural road is to connect the rural area for economic and social uplift and to provide an all-weather access. Further research work on the application of JGT by Basu et al. (2009) shows the effectiveness of JGT in road application. Khan et al. (2014) carried out extensive field investigation on JGT reinforced rural road in Bangladesh and reported that JGT can provide the beneficial effect like other synthetic geotextiles.

In the present study, an attempt has been made to study the effect of strength and thickness of the top granular layer on the extension of the service life for JGT reinforced rural road system. In the present paper, an attempt has been also made to study the utilization of strength of JGT in the rural road system. Critical pavement responses such as vertical compressive subgrade strain developed at the subgrade soil layer, tensile stress and tensile strain developed at JGT has been observed. In the present analysis, the extension in the service life of rural road due to JGT has described in terms of traffic benefit ratio (TBR).

2 Plan for FE Analysis

To conduct a parametric study and to consider the effect of degradation of JGT in the present work, four types of rural road sections have been considered. These rural road sections are unreinforced rural road (UR), JGT reinforced rural road section before degradation (RJ) and JGT reinforced rural road section after degradation (DJ). Detail of the rural road sections has been presented later. In the present FE analysis in each model series, the strength and thickness of top granular layer have been varied to study the influence of granular layer strength and thickness on the stress and strain values of the rural road sections considered in the present study. The thickness of the top granular layer (h) has been taken as 0.15 and 0.4 m. The strength condition of the top granular layer has been varied as a weak and a strong granular layer based on the California bearing ratio (CBR) of the top granular layer (CBR_{GL}). In weak granular layer, it has been assumed that the layer is made of granular sub-base material (CBR_{GL} = 20%) and in case of the strong granular layer, it has been considered that the layer is made of gravel base material (CBR_{GL} = 80%) (IRC SP 72: 2015). Two types of subgrade soil condition based on subgrade CBR (CBR_{SG}) has been taken as very poor (CBR_{SG} = 2.0%) to fair (CBR_{SG} = 5%) to check the effect of road foundation on the compressive strain values over subgrade soil of JGT reinforced rural road and on the utilization of JGT strength in the rural road. Detail plan for the present FE analysis has been presented in the Table 1.

Table 1 Plan for FE analysis

Model series	Reinforcement type	Model name	h (m)
UR	–	UR 150	0.15
	–	UR 400	0.4
RJ	JGT	RJ 150	0.15
	JGT	RJ 400	0.4
DJ	Degraded JGT	DJ 150	0.15
	Degraded JGT	DJ 400	0.4

3 Rural Road Sections

Generally, rural roads are comprised of subgrade soil and the top granular layer above it with or without thin bituminous surface coating (IRC: SP: 20 2002). In rural roads, bituminous surface coating acts as a non-structural layer and hence neglected in the present study. In the present investigation, the rural road has been considered as an unpaved road system.

3.1 Unreinforced Rural Road Section (UR)

In the present investigation, the unreinforced rural road sections have been considered as an unpaved road system with subgrade soil and top granular fill layer above it. In general, rural roads are single lane road comprises of 3.75 m carriageway and shoulders on both sides of the carriageway. In this series (UR) of the model, CBR_{SG} has been kept at 2.0 and 5.0%.

3.2 Rural Road Section Reinforced with JGT (RJ)

This model series contains the SJS reinforced rural road system before degradation of JGT and named as RJ. In this type of model, a unit of JGT with thin sand layers (25 mm thick) on each side of it has been placed as a Sand-JGT-Sand (SJS) reinforcement layer in between subgrade soil and top granular layer. Presence of sand layers on both side of JGT (SJS unit) also enhances the durability and increase the puncture resistance (Midha et al. 2017). In this series of the model, CBR_{SG} has been kept as 2.0 and 5% as in case of UR sections. Figure 1 shows a general configuration of an SJS reinforced rural road before degradation of JGT.

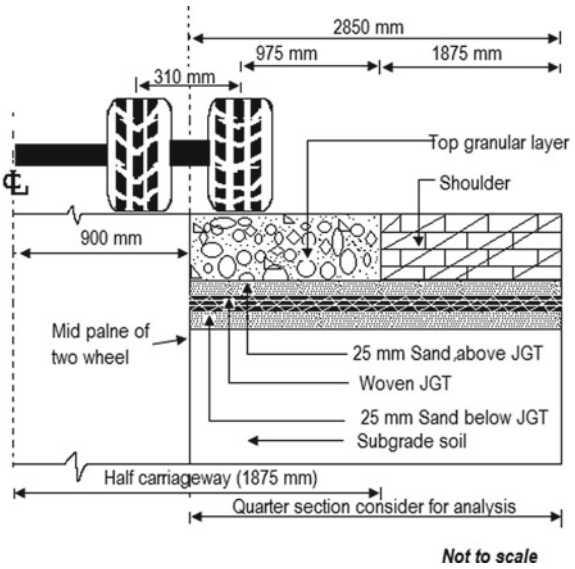

Fig. 1 Schematic sketch of general configuration of an SJS reinforced rural road and area considered for analysis

3.3 Rural Road Section Reinforced with Degraded JGT (DJ)

These types of model series describe the condition of SJS reinforcement in the rural road after degradation of JGT and called in the DJ series. This condition has been accomplished by considering an increased CBR_{SG} and a sand layer of 50 mm without JGT in between top granular fill layer and subgrade soil. Usually, untreated JGT takes about one year for 50% degradation (Saha et al. 2012). In the present analysis, it has been assumed that in one-year subgrade strength has been increased about 1.25 times of its initial CBR_{SG} (Patra and Bera 2017). The subgrade CBR value for degraded reinforced rural road sections is enhanced by 1.25 times, respect to the subgrade CBR values of UR and RJ series of rural road section, i.e. CBR_{SG} of 2.5 and 6.25%.

4 FE Response Model

Development of a suitable FE response model requires to define the soil behaviour in the form of a material constitutive relationship, and it is also a need to simplify the geometry and boundary conditions of the SJS reinforced and unreinforced rural road without compromising the reliability of the output results. A detail description of the consideration of the present FE response model developed in ABAQUS environment has been presented.

4.1 Load and Geometry

In the present paper, the geometry of the unreinforced and SJS reinforced rural road system has been considered as a 3D problem (Cho et al. 1996). In the present investigation, only quarter of the pavement section has been considered to take advantage of the symmetry. It is vital to select a proper domain size for the FE analysis which will provide the most precise response of the rural road structure and the computational cost should be manageable. The size of the FE model for rural road section has been taken as 2.85 m in width (X-direction), 3 m along the length (Y-direction) and a subgrade depth of 3 m. The depth of the subgrade soil layer has been considered based on a sensitivity analysis carried out by observing the change in compressive strain at the top of subgrade soil with the change in depth of subgrade soil layer. In the present 3D FE modelling of rural road section, the load contact area has been assumed as an equivalent rectangular contact area with a standard axle load of 80 kN (8160 kg or 18 kips) and for a wheel load of 20 kN. In the present paper, a uniformly distributed tyre contact pressure (P_c) of 550 kPa has been considered (Perkins et al. 2012). In the present study, the dimension of the tyre contact area of a wheel load of 20 kN has been taken as 225 mm in length and 160 mm in breadth which involves an area of 36,000 mm^2.

4.2 Materials

Selection of material models to simulate the pavement layers behaviour plays an important role on the results of FE analysis. ABAQUS provides the flexibility to adopt different material models such as linear elastic, porous elastic, plastic, visco-elastic, etc. Generally, in the unpaved road system, the pavement layers pose nonlinear material behaviour. In the present work subgrade soil, top granular layer and sand have been modelled as an elasto-plastic material. JGT and shoulder have been considered as a linear elastic material. In the present analysis, the elastic modulus of woven JGT has been determined based wide width tensile strength test in accordance with ASTM D4595 (2001) in the Geotechnical Engineering Laboratory at IIEST, Shibpur. The elastic modulus has been taken as secant modulus obtain at peak. Perkins et al. (2012) reported to consider a Poisson's ratio (v) of 0.25 for geotextiles. In the present study, Poisson's ratio of JGT has been taken as 0.25. Material parameters used for sand have been determined based on static triaxial compression test carried out in the Geotechnical Engineering Laboratory at IIEST, Shibpur. The elastic modulus of sand has been taken as the initial tangent modulus at low confining pressure. Details of the materials parameter considered in the present FE analysis have been presented in Table 2.

In the present FE modelling, plasticity has been defined using Drucker-Prager plasticity model (DP). Drucker-Prager failure surface is defined by the following Eq. (1)

Table 2 Materials parameters for present FE analysis

Pavement layer	CBR (%)	Linear elasticity		Plasticity	
		M_R (MPa)	v	β (°)	d (kPa)
Weak GL	20	88.43	0.35	50.19	20.78
Strong GL	80	134.03	0.35	58.56	29.25
Shoulder	–	75	0.4	–	–
Sand	–	48.88	0.35	57.57	1.97
JGT	–	100	0.25	–	–
Subgrade (Poor)	2	20	0.4	16.27	155.77
Subgrade (Fair)	5	50	0.4	37.67	397.73

GL Granular Layer

$$F_S = q - p\tan\beta - d = 0 \tag{1}$$

where 'p' is the mean normal stress, 'q' is the principal stress difference, 'β' is the material's angle of friction, i.e., the angle of the yield surface in p–q stress space and 'd' is its cohesion, i.e., the intercept at the ordinate by the yield surface in p–q stress space. In the present study, the resilient modulus of the top granular soil layer ($M_{R-\mathrm{GL}}$) has been determined by using Eq. (2) which was adopted by Giroud and Han (2004).

$$M_{R-\mathrm{GL}} = 30\,\mathrm{MPa} \times \mathrm{CBR}_{\mathrm{GL}}^{0.3} \tag{2}$$

Similarly, the resilient modulus of subgrade soil ($M_{R-\mathrm{SG}}$) has been determined based on its soaked CBR value using Eq. (3) (IRC: 37 2012).

$$M_{R-\mathrm{SG}}(\mathrm{MPa}) = 10 \times \mathrm{CBR}_{\mathrm{SG}}[\mathrm{for}\,\mathrm{CBR}_{\mathrm{SG}} \leq 5\%] \tag{3}$$

In the present analysis, undrained cohesion (c_u) of the subgrade soil layer has been calculated using Eq. (4), proposed by Giroud and Han (2004).

$$c_u(\mathrm{kPa}) = 30 \times \mathrm{CBR}_{\mathrm{SG}}(\%) \tag{4}$$

4.3 Boundary Conditions and Analysis

Selection of proper boundary condition has a significant effect on the responses obtained from FE analysis. In the present analysis, the bottom nodes of the model have been considered as fixed support. The vertical sides at the mid of two wheels and mid-plane of a single wheel have been assumed as X-symmetric plane and Y-symmetric plane, respectively. Along the line of symmetry horizontal displacements are restricted and the nodes are allowed to move freely in the Z-direction. The vertical faces away from the wheels have been defined by roller support.

In the present analysis, all the connecting interfaces of pavement layers have been simulated using tie constraints followed by the selection of master and slave surfaces (Hibbitt et al. 2012). A similar type of interaction between pavement layers has been adopted successfully earlier by Abu-Farsakh et al. (2014). In the present paper, the analysis procedure has been considered as static analysis.

4.4 Discretization

Meshing criteria is one of the most important considerations in FE analysis. The results of the analysis can change significantly based on element type, shape and size. As the loading on the pavement surface is localized, finer mesh near the loading area and coarser mesh away from the load area has been adopted. In the present study, C3D8R, an 8-node linear brick element with reduced integration scheme, has been used to discretize the top granular layer, shoulder, sand and subgrade soil layer. Previous researchers, Taherkhani and Jalali (2017), have also reported that C3D8R is a stable and a suitable element for FE analysis on pavement system. Kuo and Chou (2004) simulate the geogrid reinforcement by the use of a layer of membrane element. In the present analysis, JGT has been considered as a membrane type material and JGT has been discretized using 4-noded membrane element (M3D4R) with reduced integration scheme from ABAQUS element library. In this present study, the thickness of the membrane element has been taken as 1.46 mm. In the present FE modelling, an element size of 0.04 mm $\times$ 0.04 mm $\times$ 0.04 mm has been used at the loading area, based on the mesh convergence study. A similar discretizing technique has been adopted earlier in Patra and Bera (2016).

4.5 Validation of the Present FE Model

Before proceeding to the further analysis to study the effect of strength and thickness of the top granular layer on SJS reinforced rural road, it is necessary to validate the model with existing acceptable results. For this purpose, results obtained from FE model developed in the present study have been compared with results presented in Gupta et al. (2015). The validation has been carried out in terms of vertical compressive subgrade strain at the top of subgrade soil layer. For this purpose, UR400 section has been taken and a uniform tyre pressure of 0.56 MPa has been applied on rectangular tyre contact areas. Two type of tyre contact area has been consider as Imprint-1, having dimensions of 225 mm $\times$ 160 mm according to the present study, and Imprint-II having a dimension of 200 mm $\times$ 180 mm as per Gupta et al. (2015). Linear elastic and nonlinear material parameters have been taken from Gupta et al. (2015). From the analysis, it has been seen that the results obtained in the present study are close to Gupta et al. (2015). The difference

between the strain values is about 8.94 and 6.16% for tyre Imprint-I and imprint-II. Hence, the developed FE model of the rural road section in ABAQUS can be expected acceptable to conduct an FE analysis of unreinforced and SJS reinforced rural road sections.

5 Results and Discussions

In the present FE analysis, a detail investigation has been carried out on vertical compressive subgrade strain (ε_z) at the top of subgrade soil and on development of tensile stress and tensile strain in JGT. In the present study, the effect of strength of top granular layer has been described in terms of modulus ratio (R_M). Modulus ratio has been determined as in Eq. 5 (Giroud and Han 2004).

$$\text{Modulus ratio}(R_M) = \frac{M_{R-GL}}{M_{R-SG}} \tag{5}$$

The beneficial effect of SJS reinforced rural road has been evaluated in terms of TBR and presented in Fig. 2. Figure 3a, b present the percentage (%) of JGT tensile strength utilized with modulus ratio for the top granular layer thickness of 0.15 and 0.4 m, respectively. Table 3 shows the TBR values obtained for both the SJS reinforced section before and after degradation of JGT. In Table 4, tensile stress (σ_1) and tensile strain (ε_1) developed in JGT for the SJS reinforced section before degradation of JGT has been presented. Based on the results obtained from the present FE analysis, a discussion has been made on the following points.

- Vertical compressive subgrade strain (ε_z) and TBR.
- Strength mobilization in JGT.

5.1 Vertical Compressive Subgrade Strain (ε_z) and TBR

Vertical compressive subgrade strain (ε_z) is the most important parameter in design of flexible pavement system with thin surface coating. Various pavement design authority such as Asphalt Institute, Indian Road Congress (IRC) also relate this parameters to compute the allowable load repetitions of a pavement structure for a particular limiting rut depth. Qiu et al. (2000) suggested a limiting rut value of 25 mm for low volume roads. In the present study, failure of a rural road has been taken as a limiting rut of 25 mm. Gupta et al. (2014) proposed a mechanistic design criteria for rut depth of 25 mm in case of unreinforced low volume roads, considering nonlinearity in both top granular and in subgrade soil, as in the Eq. (6). Here, $N_{25\,mm}$ is the number of load repetitions which causes a surface rut of 25 mm. Equation (6) can be modified to obtain allowable load repetitions for a limiting rut

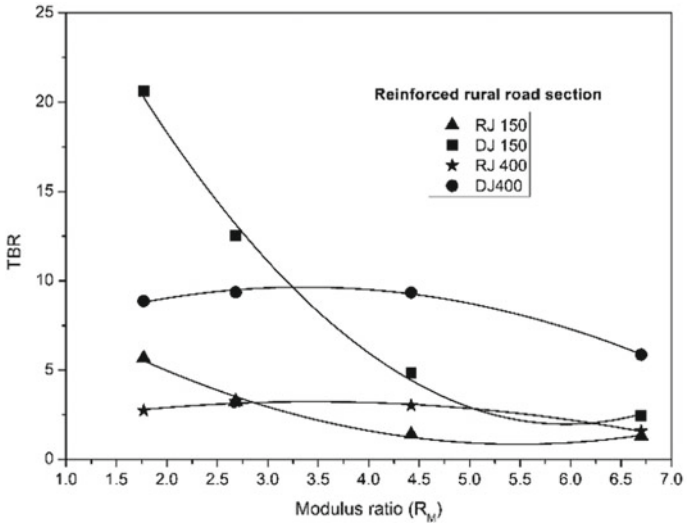

Fig. 2 Plots between TBR (TBR_{RJ} and TBR_{DJ}) and modulus ratio of the rural road structure

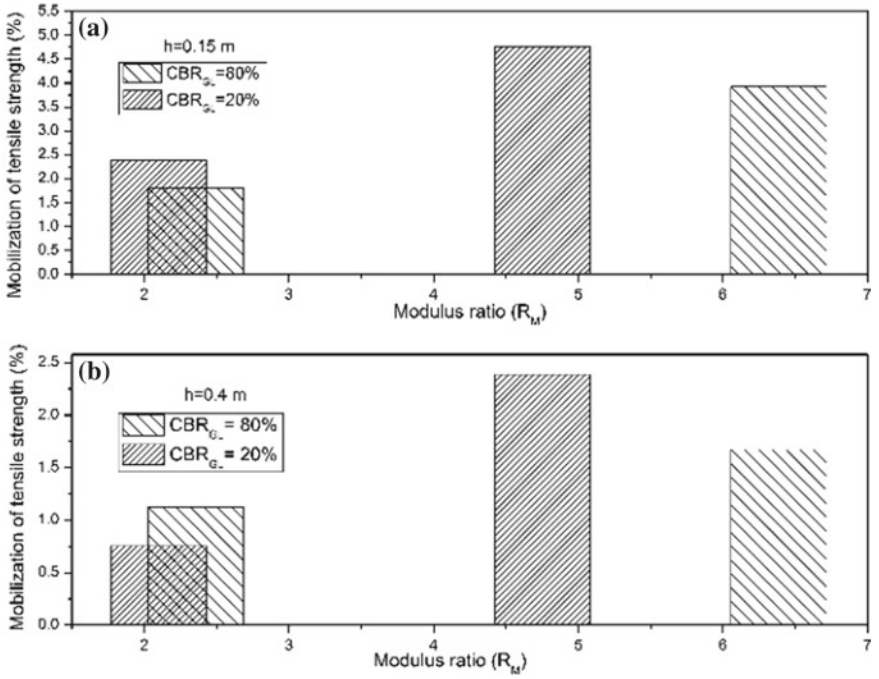

Fig. 3 Percentage of JGT tensile strength mobilized with modulus ratio for **a** top granular layer thickness of 0.15 m and for **b** top granular layer thickness of 0.4 m

Table 3 TBR_{RJ} and TBR_{DJ} values obtained for SJS reinforced rural road sections

CBR_{GL} (%)	CBR_{SG} (%)	TBR_{RJ}		TBR_{DJ}	
		h = 0.15 m	h = 0.4 m	h = 0.15 m	h = 0.4 m
20	2	1.41	3.03	4.82	9.34
20	5	5.68	2.74	20.61	8.87
80	2	1.32	1.58	2.46	5.87
80	5	3.25	3.24	12.53	9.36

Table 4 Tensile stress and strain developed in the JGT

CBR_{GL} (%)	CBR_{SG} (%)	Thickness of granular layer (h)			
		0.15 m		0.4 m	
		σ_1 (kPa)	ε_1 (%)	σ_1 (kPa)	ε_1 (%)
20	2	562.82	0.442	282.46	0.223
20	5	281.40	0.216	89.36	0.107
80	2	464.52	0.375	197.85	0.157
80	5	213.93	0.170	133.56	0.071

depth of 25 mm as in Eq. (7). Equation (7) has been applied for all the rural road sections considered in the present study.

$$\varepsilon_z = 0.0058 \times N_{25\,\mathrm{mm}}{}^{-0.171} \tag{6}$$

$$N_{25\,\mathrm{mm}} = 8.329 \times 10^{-14} \times \left(\frac{1}{\varepsilon_z}\right)^{5.848} \tag{7}$$

In the present study, the reduction in 'ε_z' due to SJS reinforcement at the top subgrade soil has been presented in terms of TBR. Chandra et al. (2008) determined TBR with the help of vertical compressive subgrade strain 'ε_z'. In the present study TBR, for both the SJS reinforced rural road sections, before and after degradation of JGT has been determined using Eq. (8) and using Eq. (9), respectively.

$$TBR_{RJ} = \left(\frac{\varepsilon_{z-RJ}}{\varepsilon_{z-UR}}\right)^{-5.848} \tag{8}$$

$$TBR_{DJ} = \left(\frac{\varepsilon_{z-DJ}}{\varepsilon_{z-UR}}\right)^{-5.848} \tag{9}$$

where TBR_{RJ}, and TBR_{DJ} are the TBR values for the SJS reinforced rural road section before degradation of JGT and the TBR values for the reinforced section after degradation of JGT, respectively. 'ε_{z-UR}', 'ε_{z-RJ}', and 'ε_{z-DJ}' are the 'ε_z' measured at the top of subgrade soil for the unreinforced, SJS reinforced, and

reinforced section after degradation of JGT, respectively. From Fig. 2, it has been seen that as the modulus ratio between the top granular layer and subgrade soil is increasing and the TBR values are decreasing. Figure 2 also revealed that the nature of decreasing of TBR values with increase in modulus ratio is influenced by the thickness of the top granular soil. It has been also found that for lower thickness of top granular layer (0.15 m), there is a continuous decrease in TBR values with increase in modulus ratio, i.e., as the subgrade strength is decreasing lower, TBR_{RJ} and TBR_{DJ} values have been obtained depending on the strength of the top granular layer.

Whereas in case of a rural road section with a higher top granular layer thickness (0.4 m) shows an optimum value of TBR_{RJ} and TBR_{DJ} values are higher for a particular 'R_M'. This notified that the maximum benefit due to SJS reinforcement in the rural road can be achieved for a particular range of modulus ratio. In the present study, from the Fig. 2, for 0.4 m of the top granular layer, it can be said that maximum values of TBR_{RJ} and TBR_{DJ} will be achieved at a modulus ratio around 3.75 and 4.25, respectively. From Table 3, it has been observed that for poor subgrade soil condition, a decrease in top granular layer strength leads to increase both TBR_{RJ} and TBR_{DJ}. A decrease in top granular layer strength from CBR_{GL} of 80–20% leads to increase the TBR_{RJ} and TBR_{DJ} values in the range of 1.07–1.91 times and 1.93–2.38 times, respectively. In case of fair subgrade soil (CBR_{SG} = 5%), a decrease in top granular layer strength leads to increase the TBR_{RJ} and TBR_{DJ} values for the lower thickness of top granular layer (0.15 m). Whereas in the case of the higher thickness of the top granular layer (0.4 m), a decrease in top granular layer strength leads to decrease the TBR_{RJ} and TBR_{DJ} values with strong subgrade soil foundation. The reason is that with higher thickness and strong subgrade soil foundation makes the rural road structure less dependent on SJS reinforcement before and after degradation of JGT. Hufenus et al. (2006) also reported that the inclusion of reinforcement in unpaved road system is effective for $CBR_{SG} \leq 3\%$ and when $h \leq 0.5$ m. In the present study, it has been seen that TBR_{DJ} values are higher than the TBR_{RJ} values which imply that the increment in subgrade strength leads to a higher benefit. It is due to that the vertical compressive subgrade strain is also related to the bearing capacity of the subgrade soil. In the present study, it has been also noticed that for the soft subgrade soil condition, an increase in top granular layer thickness from 0.15 to 0.4 m results in an increase in TBR_{RJ} values for weak and strong top granular layer of 2.16 times and 1.20 times, respectively. Similarly, TBR_{DJ} values have been increased 1.59 times and 1.96 for weak and strong top granular layer, respectively. In case of strong subgrade soil, it has been observed that an increase in top granular layer thickness leads to decrease both TBR_{RJ} and TBR_{DJ} values.

5.2 Strength Mobilization in JGT

In the present mechanistic analysis, an attempt has been also made to study the utilization of tensile strength of JGT in SJS reinforcement. For this purpose, maximum stresses (σ_x, σ_y and τ_{xy}) developed in the JGT under the wheel load has measured for the SJS reinforced rural road section before degradation of JGT. Similar strain measurement has been performed in the JGT under the tyre pressure of 0.55 MPa. The major principle stress (σ_1) developed in the JGT, which corresponds to the tension of the geotextile has been calculated using Eq. (10) (Bhandari and Han 2010).

$$\sigma_1 = \frac{(\sigma_x + \sigma_y)}{2} + \sqrt{\left(\frac{\sigma_x - \sigma_y}{2}\right)^2 + \tau_{xy}^2} \tag{10}$$

The tension developed in the JGT under the wheel loading has been calculated using Eq. (11)

$$T_{MJ} = \sigma_1 \times t_J \tag{11}$$

where, 'T_{MJ}' in kN, is the tension mobilized at JGT in SJS reinforcement and 't_J' (m) is the thickness of JGT.

Figure 3a, b shows the mobilization of the tensile strength of JGT used in the present study. Table 4 presents the values of principal stress and strain, i.e., tensile stress and tensile strain developed in JGT for SJS reinforced section (before degradation of JGT) considered in the present study. From Table 4, it has been seen that the tensile strain developed in the JGT is in the range of 0.167–0.442% and 0.071–0.375% for weak and strong granular layers, respectively. Figure 3 presents the mobilization of tensile strength (%) in JGT at different modulus ratio for weak and strong granular layers. From Fig. 3, it has been observed that in case soft subgrade soil (CBR_{SG} = 2%), a decrease in top granular layer strength from CBR_{GL} of 80–20% leads to increase in strength mobilization of JGT from 3.93 to 4.76% and 1.67 to 2.39% for thin (0.15 m) and thick (0.4 m) granular layer, respectively. In case strong subgrade soil (CBR_{SG} = 5%), an increase in top granular layer thickness from 0.15 to 0.4 m results in a reduction in strength utilization of JGT from 1.81 to 1.13%. From Fig. 3, it has been also found that a reduction in top granular layer thickness from 0.4 to 0.15 m leads to an increase in strength utilization of JGT is in the range of 1.60 times to 3.15 times. Similarly, an increase in strength of top granular layer from CBR_{GL} of 20–80% results in a reduction in tensile strength mobilization of JGT which is in the range of 0.67 times to 1.42 times.

6 Conclusion

In the present paper, a series of FE simulations have been carried out to investigate the benefits of SJS reinforcement in rural roads. Efforts have been also made to study the influence of top granular layer strength and thickness in the extension of service life of the rural road section and to determine the strength utilization in SJS reinforcement. Based on the present FE modelling, results of analysis and based on the discussion made earlier, following conclusions have been drawn:

- For poor subgrade soil condition, a decrease in top granular layer strength from CBR_{GL} of 80–20% leads to increase both the TBR_{RJ} and TBR_{DJ} values.
- In case of soft subgrade soil foundation, an increase in top granular layer thickness, the values of TBR_{RJ} and TBR_{DJ} are increasing for both weak and strong top granular layer, respectively.
- TBR_{RJ} and TBR_{DJ} values have found to be falling with an increase in top granular layer thickness for strong subgrade soil (CBR_{SG} = 5%).
- The TBR_{RJ} and TBR_{DJ} values are found within the range of 1.32–5.68 and in the range of 2.46–20.61, respectively, under study.
- A small fraction of the tensile strength of JGT has been mobilized in SJS reinforced rural road sections. Maximum percentage utilization of JGT tensile strength has been found as 4.76 and 2.38% for thin (0.15 m) and thick (0.4 m) top granular layer.

References

Abu-Farsakh MY, Gu J, Voyiadjis GZ, Chen Q (2014) Mechanistic–empirical analysis of the results of finite element analysis on flexible pavement with geogrid base reinforcement. Int J Pavement Eng 15(9):786–798

American Society for Testing and Materials (2001) ASTM D4595: 2001. Standard test method for tensile properties of geotextiles by the wide-width strip method

Basu G, Roy AN, Bhattacharyya SK, Ghosh SK (2009) Construction of unpaved rural road using jute–synthetic blended woven geotextile—a case study. Geotext Geomembr 27(6):506–512

Bhandari A, Han J (2010) Investigation of geotextile-soil interaction under a cyclic vertical load using the discrete element method. Geotext Geomembr 28(1):33–43

Chandra S, Viladkar MN, Nagrale PP (2008) Mechanistic approach for fiber-reinforced flexible pavements. J. Transp Eng 134(1):15–23

Cho YH, McCullough B, Weissmann J (1996) Considerations on finite-element method application in pavement structural analysis. Transp Res Record J Transp Res Board 1539:96–101

Giroud JP, Han J (2004) Design method for geogrid-reinforced unpaved roads. I. Development of design method. J Geotech Geoenviron Eng 130(8):775–786

Gupta A, Kumar P, Rastogi R (2014) Mechanistic–empirical approach for design of low volume pavements. Int J Pavement Eng 16(9):797–808

Gupta A, Kumar P, Rastogi R (2015) Critical pavement response analysis of low-volume pavements considering nonlinear behavior of materials. Transp Res Rec J Transp Res Board 2474:3–11

Hibbitt D, Karlsson B, Sorensen P (2012) ABAQUS user's manual: 2012. Dassault Systèmes Simulia Corp

Hufenus R, Rueegger R, Banjac R, Mayor P, Springman SM, Brönnimann R (2006) Full-scale field tests on geosynthetic reinforced unpaved roads on soft subgrade. Geotext Geomembr 24 (1):21–37

Indian Road Congress 37 (2012) Guidelines for the design of flexible pavements. New Delhi, India, pp 370–380

IRC SP 20: 2002 Indian Road Congress (2002) Manual for route location, design, construction and maintenance of rural roads. New Delhi, India

IRC SP:72 (2015) Guidelines for the design of flexible pavements for low volume road. Indian Road Congress, New Delhi, India

Khan AJ, Huq F, Hossain SZ (2014) Application of jute geotextiles for rural road pavement construction. Ground Improv Geosynthetics 370–379

Kuo CM, Chou FJ (2004) Development of 3-D finite element model for flexible pavements. J Chin Inst Eng 27(5):707–717

Midha VK, Joshi S, Kumar SS (2017) Performance of chemically treated jute geotextile in unpaved roads at different in situ conditions. J Inst Eng (India) Ser E 1–8

Patra S, Bera AK (2016) Field and numerical investigation on time dependent behaviour of jute geotextile (JGT) reinforced rural road. In: Indian geotechnical conference, Chennai, India

Patra S, Bera AK (2017) Time dependent field CBR and its regression model. Int J Civil Eng Technol 8(1):82–88

Perkins SW, Christopher BR, Lacina BA, Klompmaker J (2012) Mechanistic-empirical modeling of geosynthetic-reinforced unpaved roads. Int J Geomech 12(4):370–380

Qiu Y, Dennis N, Elliott R (2000) Design criteria for permanent deformation of subgrade soils in flexible pavements for low-volume roads. Soils Found 40(1):1–10

Ramaswami S, Aziz M (1989) Jute geotextile for roads. In: International workshops on geotextile, India, pp 137–143

Saha P, Roy D, Manna S, Adhikari B, Sen R, Roy S (2012) Durability of transesterified jute geotextiles. Geotext Geomembr 35:69–75. https://doi.org/10.1016/j.geotexmem.2012.07.003

Taherkhani H, Jalali M (2017) Investigating the performance of geosynthetic-reinforced asphaltic pavement under various axle loads using finite-element method. Road Mater Pavement Des 18 (5):1200–1217

Elasto-Plastic Analysis of a Tunnel Strengthened by Grouting

M. Vinothkumar and R. Malathy

Abstract Design and analysis of tunnels and underground structures are challenging areas of Geotechnical Engineering. The soil/rock in tunnelling areas is often strengthened by grouting. This improves the properties of soil/rock and enhances the stability. In the present study, a two-dimensional analysis that explains the properties of soil/rock strengthened by grouting is carried out. Initially, the settlement behaviour of grouted soil mass with different curing periods of 7, 14 and 28 days was studied by the plate load laboratory model test, and the settlement behaviour of grouted soil mass was compared with ungrouted soil mass. The experimental results reveal that the settlement of the grouted soil mass is comparatively reduced with respect to increase in curing period. The analysis was carried out using PLAXIS 2D software, a two-dimensional indirect finite element programme which facilitates elastic/elasto-plastic analysis of underground excavations. The distribution of stress and deformation under different loading conditions is visualized from the analysis. Based on the results, critical locations for failure were identified. Then, the grouting was applied to the soil mass. Comparison of the mechanical properties of the grouted and ungrouted soil mass brings out the effectiveness of the grouting in improving the stability of the tunnel.

Keywords Underground structures · Grouting · PLAXIS 2D · Stress distribution

M. Vinothkumar (✉) · R. Malathy
Department of Civil Engineering, Sona College of Technology,
Salem 636005, Tamil Nadu, India
e-mail: vinothkumarksr29@gmail.com

R. Malathy
e-mail: malathycivil@sonatech.ac.in

R. Sundaram et al. (eds.), *Geotechnics for Transportation Infrastructure*,
Lecture Notes in Civil Engineering 29,
https://doi.org/10.1007/978-981-13-6713-7_35

1 Introduction

Poor-quality soils, because of their low bearing capacity, need to be improved by implementing ground improvement techniques (GIT). Especially in granular soils, the ground improvement technique is essentially needed to improve the shear strength of the soil (Daykar et al. 2012). It can be achieved through various methods and techniques like vibro-flotation, grouting, etc. Selection of right method is based on various factors like condition of the soil, degree of the compaction, type of structures need to be supported, depth of compaction, as well as site considerations like sensitivity of adjacent structures. For many of the foundation problems, compaction of the soil is the effective solution, and it is useful for reducing the settlement. However, up to 20 m depth only, the dynamic compaction will be effective if any water is present at shallow depth (Yilmaz et al. 2008). But the grouting will improve the bonding and cohesive capacity of the soil (Anagnostopous 2005). Nowadays the grouting process is carried out widely to strengthen the soil mass and to improve the bearing capacity of the soil mass (Daykar et al. 2012). Grouting is an effective method to improve the physical and mechanical properties of the soil (Sayaehv and Kalantari 2012). The improved properties give rise to better load bearing capacity and stability of the soil (Kumar et al. 2011). The application of grouting will reduce the liquefaction process during periods of dynamic loading (Sayaehv and Kalantari 2012), and the resistance of the soil can be improved without altering the physical structure. The application of grouting will reduce the void space and increase the density of the soil mass which alters the engineering properties such as strength, stiffness, etc. (Kumar et al. 2011). A brief overview of significant literature is presented. Different kinds of grouting material are described. Stepwise procedure for grouting by making use of various equipments is prescribed (Lowe and Standford 1982; Schwarz and Krizek 1992; Lovly 1998). Permeation grouting is an effective method to enhance the bearing capacity of the soil and to decrease the void ratio of the soil mass without disturbing the structure of the soil; in this way, the permeability of the soil can be reduced to a great extent, and the groundwater movement can be controlled (Daykar et al. 2012). This study describes the improvement attained in the strength of unconsolidated sand bed after permeation cement grouting. The permeation grouting method is employed to disperse the grouting material uniformly into the soil mass (Glory and Abraham 2001). Today, the grouting operations are carried out based on empirical rules only. A proper finite element modelling will give appropriate ideas for the implementation of grouting. But to identify the behaviour of the soil after grouting at the earliest, a proper numerical analysis should be carried out before implementation of the grouting. The numerical analysis tool of PLAXIS 2D software facilitates to carry out the elastic/elasto-plastic analysis. This analysis is very much helpful to identify the behaviour of the soil with respect to the load in elastic and elasto-plastic states.

Table 1 Cement properties

Properties	Values
Grade	PPC
Specific gravity	3.04
Consistency (%)	32
Fineness (%)	98
Initial setting time (Min)	30
Bulk density (kg/m^3)	1360

2 Materials Used

As per the ASTM and BIS classifications, river sand was used. It was graded into fine particles (74–425 μm), medium (425–2 μm) and coarse (2–4.75 mm).

Ordinary Portland cement-43 grade was used as grouting material. The properties of the cement are tabulated in Table 1 (Table 2).

Soil sample was analysed, and their physical properties are presented in Table 2.

3 Experimental Set-up

3.1 Plate Load Test

As per IS: 1904-1978, the plate load test was carried out to assess the strength improvement of the grouted soil mass. It was carried out in grouted as well as ungrouted soil masses.

Table 2 Soil sample properties

Properties	Values
Specific gravity	2.3
Coarse sand (%)	22
Medium sand (%)	68
Fine sand (%)	10
Normal density (kN/m^3)	17.42
Saturation density (kN/m^3)	19.92
Friction angle φ	30
Poisson ratio	0.2
Young's modulus (E_{50})	20,000

Fig. 1 Plate load test arrangement for soil sample in ungrouted state

3.1.1 Plate Load Test for Ungrouted Sand

In the first stage, the soil was taken in a box of dimensions 25 cm × 25 cm 25 cm. A steel plate of one-fifth size of the box was placed over the surface of the soil sample. Then, the load was applied at gradual increments on the plate. The density and void ratio of the sand in a loose state were 17.8 and 0.69 kN/m^3, respectively. On applying the load, the soil began to settle down. This setting was measured using a dial gauge. The test arrangement is shown in Fig. 1.

3.1.2 Plate Load Test for Sand in with Grout State

Initially, cement was mixed with water, and the consistent cement slurry was prepared. Pipes with micro-holes on the surface were inserted into the soil at four corners. The mixed cement slurry was injected through the pipes into the soil by applying pressure. It gushed out the holes and dispersed into the soil. This type of grouting is known as permeation grouting. After completion of grouting the model was cured for 7, 14 and 28 days. Plate load test was conducted for the grouted sample after 7, 14 and 28 days of curing. The applied loads and corresponding settlement were noted in each trial (Fig. 2).

Arora stated Eq. 1 to calculate the settlement of sandy soil

$$S_f = S_P \left[\frac{(B_f(B_P + 0.3))}{(B_p(B_f + 0.3))} \right]^2 \quad (1)$$

Fig. 2 Plate load test arrangement of grouted soil sample

Arora stated Eq. 2 to calculate the ultimate bearing capacity of sandy soil

$$q_u(f) = q_u(p) \times \left(\frac{B_f}{B_P}\right) \tag{2}$$

where $q_u(p)$ = ultimate bearing capacity of plate, $q_u(f)$ = ultimate bearing capacity of foundation, B_f = width of foundation, S_f = settlement of foundation, S_p = settlement of plate, B_p = width of plate.

3.2 Permeability Test

Permeability test was carried out by using the permeability test apparatus. It was conducted in two states; the permeability values for grouted and ungrouted soil samples were determined and compared.

4 Elasto-Plastic Analysis

Generally, when a load is applied, soil undergoes three kinds of phase, namely elastic, elasto-plastic and plastic. Elastic state can be identified from a plot of stress–strain values obtained from laboratory tests. Elasto-plastic state denotes a condition/zone lying between elastic and plastic zones. This is known as yield line Huang (2013). In the present study, the PLAXIS 2D software was used to identify the elasto-plastic behaviour of the soil (grouted and ungrouted) under different loading conditions. Initial experiments were conducted in the laboratory, and the properties

of the sand were determined. Then, a model was created using the PLAXIS 2D software for both cases of grouted and ungrouted states, and then, the analysis process was carried out.

4.1 Model Generation

A Mohr–Coulomb model was derived from the PLAXIS 2D software which functions on the principles of finite element analysis. Initially, the boundary conditions were created based on the requirement, and then, the geometry of the NATM tunnel was introduced into the boundary conditions. Then, the soil parameters were entered into the boundary, and a real field condition was generated within the boundary.

4.1.1 Ungrouted and Grouted Soil Model generation

Initially, the model was tested in ungrouted state, and the deformation and stress distribution behaviour were studied. From the plate load test, the stress–strain behaviour of the soil during the grouted and ungrouted state was constantly monitored with respect to the loading. From the stress–strain behaviour, the Young's modulus value of the soil was identified in both cases. Keeping the same model, the change of E value, permeability value of the soil was entered in grouted soil model, and the behaviour of the soil with respect to the load was analysed in

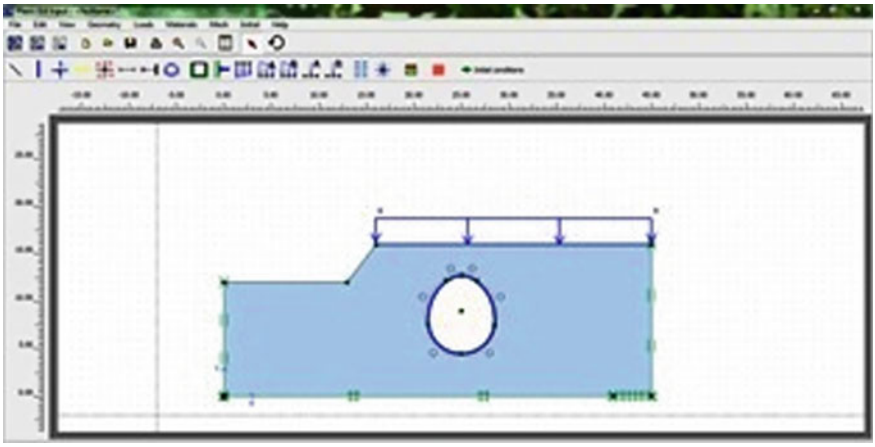

Fig. 3 Generated soil model for ungrouted and grouted soil mass

both cases. The maximum deformation with respect to the loading was recorded. The critical point was identified from the stress–strain distribution pattern. The deformation and stress distribution patterns in respect of ungrouted and grouted models were compared. The strength improvement due to grouting was determined. Figure 3 shows the generated model for with and without grouting.

5 Results and Discussion

The results of the above conducted tests (plate load test, permeability test and elasto-plastic analysis output) are discussed below.

5.1 Plate Load Test Results

Plate load test was carried out to determine the strength improvement in the sandy soil after grouting. Grouted soil sample after different periods of curing of 7, 14 and 28 days was tested. The settlement of the soil was relatively reduced in the case of grouted soil sample with increasing periods of curing. Figure 4 shows the load versus the settlement behaviour of the grouted and ungrouted sand for different periods of curing. The increased Young's modulus was observed after curing of grouted sample.

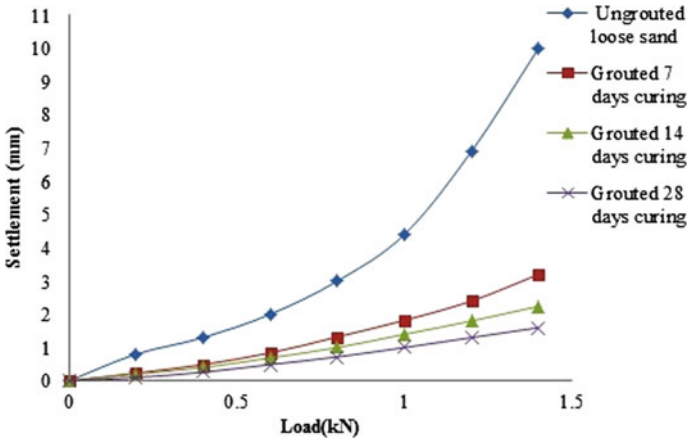

Fig. 4 Load settlement behaviour of grouted and ungrouted soil mass under different curing periods

5.2 Permeability Test Result

The permeability of grouted and ungrouted soil mass was 0.0083 and 0.0169 cm/s, respectively. From the observed results, it is found that the permeability of the soil after the grouting stage is comparatively reduced.

5.3 Elasto-Plastic Analysis Output

The Mohr–Coulomb model was generated. The numerical finite element analysis was carried for the generated model, and the stress distribution and deformation behaviour of the soil mass were predicted. The critical locations in the stress distribution were recorded. Figure 5 shows the stress distribution and maximum deformation rate in ungrouted soil state. In Fig. 5, the stress distribution critical locations are located on the sloped corner, the surface of the soil mass and the right side face of the tunnel section. As such, it is necessary to strengthen and improve the stability of these areas.

After introducing the Young's modulus value of grouted soil mass, due to the increase in E value and decrease in permeability value after the grout state, the critical locations in the soil mass were reduced, and uniform stress distribution was attained. By the process of grouting, the deformation of the soil mass was comparatively reduced (Fig. 6).

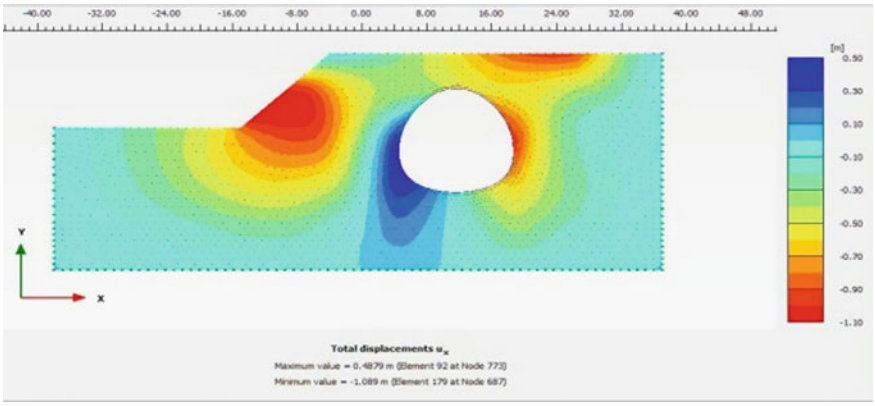

Fig. 5 Stress distribution in ungrouted soil mass

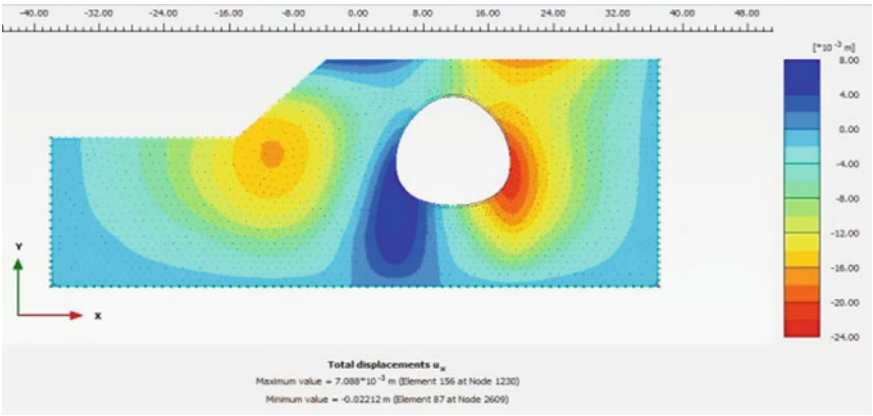

Fig. 6 Stress distribution in grouted soil mass

6 Conclusions

From the experimental results of plate load test, it is observed that the settlement of the grouted soil was reduced with respect to the load as compared to the ungrouted soil sample. Especially an increase in curing period reduced the settlement. After 28 days of curing, the settlement was highly reduced as compared with the ungrouted sample. From the permeability test, it is found that the permeability value of the soil was comparatively reduced due to grouting; it is possible that this reduction in permeability will restrict the movement of groundwater. From the numerical analysis, it is summarized that deformation of the soil mass can be reduced, and uniform stress distribution of the soil mass can be realized by eliminating the critical points in the ungrouted state by means of grouting. By using Eq. 1, the settlement of the soil was calculated in both grouted and ungrouted stage. The 40–48% of settlement is reduced in after grout stage. From Eq. 2, the bearing capacity of the soil was calculated in both cases, it was observed that the 12.5–20% of bearing capacity was increased in grouted stage. After the cement grouting for proper curing the settlement is decreases gradually with respect to curing period. From the plate load test, the Young's modulus of the grouted sample was increased in after grouted stage. The cement grouting in sandy soil with increasing curing period is reducing the settlement of soil. The novelty of this study is the NATM tunnel section which was introduced in the sandy soil strata and analysed stress distribution, deformation in grouted and ungrouted states. This study is carried out to overcome the difficulty during the process of tunnel construction because in some areas, the sandy soil layer may be interrupted during the process of tunnel construction.

References

Anagnostopous CA (2005) Laboratory study of an injected granular soil with polymer grouts. Tunn Undergr Space Tech 20:525–533

Daykar P, Venkat Raman K, Raju KV (2012) Study on permeation grouting using cement grout in sandy soil. IOSR J Mech Civil Eng 4:5–10

Glory J, Abraham BM (2001) Improvement of bearing capacity of sandy soils by grouting. In: IGC 2001, The New Millennium conference, Indore, pp 14–16

Huang F (2013) The effect of weak interlayer on the failure pattern of rock mass around the tunnel-scaled model test and numerical analysis. Tunn Undergr Space Technol 35:207–218

Kumar TGS, Abraham BM, Sridharan A (2011) Bearing capacity improvement of loose sandy foundation soils through grouting. Int J Eng Res Appl 2248–2296

Lovly KM (1998) Effect of admixture on cement grout. In: Indian geotechnical conference, New Delhi

Lowe J, Standford TC (1982) Special grouting at Tarbela dam project. In: Proceedings of conference on grouting, New Orleans, ASCE, New York, pp 152–172

Sayaehv S, Kalantari B (2012) Use of grouting method to improve soil stability against liquefaction—a review. EJGE 17:1559–1566

Schwarz LG, Krizek RJ (1992) Effect of mixing on rheological properties of micro fine cement. In: Proceedings of the conference on grouting, soil improvement and geosynthetics, New Orleans, ASCE, New York, pp 512–525

Yilmaz D, Babuccu F, Batmaz S, Kavruk F (2008) Liquefaction analysis and soil improvement in beydagdam. Geotech Geol Eng 26(2):211–224

Experimental Study on Flyash-Stabilized Expansive Soil

Sanjivani D. Nigade-Saha and B. V. S. Viswanadham

Abstract About 51.8 million hectares of India are covered with expansive black cotton soils. The expanding road network has compelled engineers to build roads over these weak soils. Constructing pavements on expansive subgrades involves a threefold problem of a poor supporting strata, heavy vehicular loading and lastly, scarcity of good-quality aggregate. Roads constructed on expansive soils incur large capital costs and maintenance costs. Flyash produced in several thermal power plants is largely unutilized. It can be used as a stabilizing material in the road pavements, as an alternative to replacement of locally available (substandard) materials, thereby reducing the problems associated with disposal of flyash, and also leading to economical constructions. Laboratory investigations were undertaken to study the stabilizing effect of locally available Class F-type flyashes, when used in combination with lime. Index tests to determine free swell index, linear shrinkage and pH along with detailed tests to determine UCS, CBR and heave were performed. The free swell and linear shrinkage were significantly reduced. UCS improved consistently with time. The soaked CBR test of LFA-treated samples indicate excellent improvement in strength and reduction in volume-change behaviour. The performance of the LFA treatment was largely affected by the type of flyash.

Keywords Expansive soil · Flyash-stabilized flexible pavements · Linear shrinkage · CBR · UCS · Heave

S. D. Nigade-Saha (✉) · B. V. S. Viswanadham
Department of Civil Engineering, Indian Institute of Technology Bombay, Powai 400076, India
e-mail: sanjivaniphd@gmail.com

B. V. S. Viswanadham
e-mail: viswam@civil.iitb.ac.in

R. Sundaram et al. (eds.), *Geotechnics for Transportation Infrastructure*, Lecture Notes in Civil Engineering 29,
https://doi.org/10.1007/978-981-13-6713-7_36

1 Introduction

In India, about 51.8 million hectares of the land area (i.e. 16.6% of the total geographical area of the country) are covered with expansive black cotton soil. Almost 90% area of the two central states, viz., Maharashtra and Madhya Pradesh, and significant portions of adjoining states like Karnataka, Telangana, Gujarat and Rajasthan are covered with deposits of this expansive soil. These soils are unsuitable for construction either as fill material or as a subgrade as, in the presence of moisture, they exhibit undesirable engineering properties like low shear strength, low bearing capacity and very low penetration resistance. In addition, they also exhibit extensive volumetric changes. Due to their low strengths, such subgrades will require very thick pavement crusts. Also, pavements on such soils undergo large distress during service life, thereby requiring frequent maintenance. Thus, roads on expansive subgrades are problematic during the construction stage as well as the service life of the pavement, thereby incurring huge capital and maintenance costs.

The increased demands of electrical energy and availability of sufficient coal reserves have led to rise in number of coal-fired thermal power plants in the country. Indian coal has an ash content of 30–45%, thereby generating a very huge amount of flyash. In comparison with countries like Germany, Belgium and the Netherlands, where more than 95% of flyash generated is reportedly used, the level of utilization of flyash in India is low, thereby leading to large-scale accumulation of flyash. The unutilized flyash causes water and air pollution and also requires large areas of land for its disposal. As per report of Central Electrical Authority (CEA) New Delhi 2016, during the first half of the year 2015–16, about 83.64 million ton of flyash was generated, of which only 46.87 million ton flyash was utilized. The data regarding the modes in which flyash was utilized indicates that the percentage utilization was about 42% for manufacture of cement, 12.85% in flyash-based building products, 11.21% for land-reclamation, 10.91% for mine filling, etc., and only 4.87% in the construction of roads and embankments. There is a large potential of fly ash utilization in the road sector. Utilization of flyash in the road sector shall lead to savings of precious natural resources.

Beeghly (2003) has reported about 50% savings in construction costs due to reduction in material cost and 20% savings in maintenance costs due to permanent improvement of subgrade strength due to lime flyash (LFA) stabilization of the subgrade. 100% reduction in pavement costs against the option of undercutting and replacement of local soil has also been reported. The stabilizing effect of four different flyashes in stabilizing a highly expansive soil has been studied. All the Class F flyashes, when used in combination with lime, were effective in significant strength gain and reduction in volume-change behaviour of the expansive soil.

2 Materials

It is necessary to characterize the materials as the degree of improvement of subgrade strength is highly dependent on the physical and chemical properties of the treated soil and the stabilizer used. The physical and chemical properties of the untreated subgrade soil, various flyashes and activators used are presented in the following paragraphs.

2.1 Expansive Soil

The expansive soil for the present study is a black cotton soil that has been procured from a locality near Pune in the state of Maharashtra. The specific gravity of the soil sample was found to be 2.685. The activity of the untreated soil is 0.6. The free swell index was found to be 110%. Atterberg limits of the untreated soil were determined as per IS 2720 (Part V). The soil exhibited a liquid limit of 80% and plastic limit of 35%. Thus, the soil has a very high value of plasticity index of 45%. Since the plasticity index of the soil is greater than 35%, as per the recommendations of Little and Nair (2009), the soil will need treatment with any of the following stabilizers, viz.

(a) Lime
(b) Lime + cement
(c) Class F flyash + lime
(d) Class C flyash + lime

The grain size distribution curve is presented in Fig. 1. The soil can be classified as a clayey soil with very high plasticity (CH). The soil has more than 60.5% particles finer than 75 μm. Hence is unsuitable for being used as base material and can be used as a subgrade material only. The high value of free swell index indicates large volume changes in the presence of water, thereby posing threat of structural failure of the pavements laid on it.

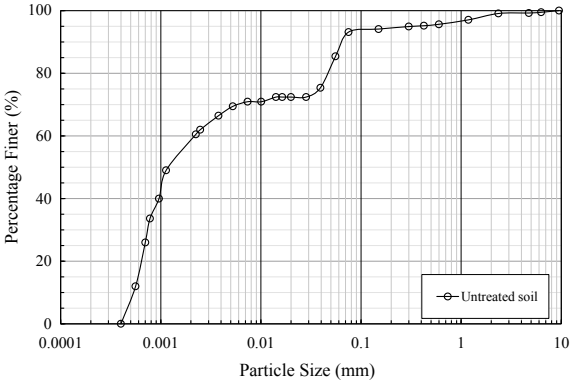

Fig. 1 Grain size distribution of untreated soil

Table 1 Properties of expansive soil

Property	Untreated soil
Liquid limit (%)	80
Plastic limit (%)	35
Plasticity index (%)	45
Gravel (>4.75 mm)	0.76%
Sand (0.075–4.75 mm)	6.11%
Silt (0.002–0.075 mm)	32.63%
Clay (<0.002 mm)	60.5%
Free swell index (%)	110

The index properties, swell characteristics, etc., of the untreated soil are summarized in Table 1.

The compaction characteristics of the black cotton soil were found by conducting a standard proctor test on the soil. As the soil was highly expansive, the soil was mixed with water and kept for 24 h prior to conducting the test. The untreated soil has OMC and MDD values of 35.5% and 12.66 kN/m^3. The soil was soaked at OMC and kept for 24 h and then compacted at MDD in the CBR mould. The soil has an unsoaked CBR value of 6.1% and a soaked CBR value of 1.5%. It is thus a weak subgrade.

2.2 Flyash

Pulverized fuel ash (PFA) is a waste product of thermal power plants. PFA extracted from the fuel gases by any suitable process like cyclone separation or electrostatic precipitation is called flyash. ASTM C 618-15 specifies two categories of flyash, viz. Class C and Class F. The Class F flyash is produced by the combustion of bituminous coal or anthracite. It contains less than 10% of CaO and hence possesses only pozzolanic properties. The Class C flyash is produced by the combustion of sub-bituminous coal or lignite. It contains more than 10% of CaO and possesses cementitious properties as well as pozzolanic properties.

Indian flyashes are generally of the Class F type. The flyashes available from the plants at Nashik, Dahanu, Ratnagiri and Surat were procured for the present study and are denoted as Flyash N, Flyash D, Flyash R and Flyash S, respectively. The physical characteristics of these flyashes are summarized in Table 2, and their grain size distribution curves are presented in Fig. 2.

Significant variation in the specific gravity, colour and physical appearance of flyash has been observed with change in source. Flyash D is a well-graded silty clay, light in colour and with small-sized soft lumps. Flyash N is a gap-graded sandy silt, grey in colour, with significant amount of black particles of unburnt coal, but without any lumps. Flyash R is light in colour and without any lumps. Flyash S is very dark in colour, with large-sized hard lumps. Both Flyash R and Flyash S are uniformly graded silty soils.

Table 2 Physical properties of flyash

Parameter	Flyash D	Flyash N	Flyash R	Flyash S
G_s	2.065	2.054	2.125	2.430
C_u	8	2.5	3.1	2.8
C_c	0.8	1.1	1.3	0.4
Fine sand (%)	17.4	40.2	6.0	14.2
Silt (%)	40.6	51.8	73.1	75.5
Clay (%)	42.0	7.8	20.8	10.0

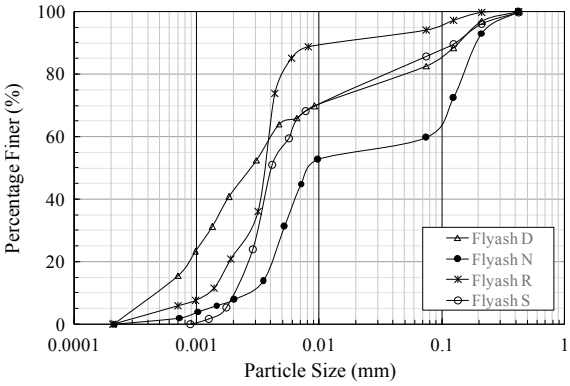

Fig. 2 Grain size distribution of flyashes

Flyash D and Flyash N show very low specific gravity of 2.065 and 2.054, respectively. A high value of specific gravity of 2.430 is observed for Flyash S, indicating the presence of heavy minerals.

The stabilizing effect of flyash is greatly affected by its' chemical composition. The chemical composition of the flyashes as determined by the XRF/ICP-AES technique is presented in Table 3. All flyash samples used in the present study were found to be of Class F type.

Table 3 Chemical composition of flyash

Parameter	Flyash D	Flyash N	Flyash R	Flyash S
CaO (%)	0.14	0.37	1.35	1.18
SiO_2 (%)	54.80	58.12	43.56	48.44
Al_2O_3 (%)	22.00	12.52	20.51	21.44
Fe_2O_3 (%)	10.80	13.22	12.50	12.18
MgO (%)	0.01	0.03	0.24	0.14
CaO/SiO_2 ratio	0.003	0.006	0.031	0.024
$SiO_2 + Al_2O_3 + Fe_2O_3$	87.60	83.85	76.57	82.05

A higher value of CaO indicates the presence of lime, thereby increasing the cementitious reactions. Flyash R and Flyash S have almost 1% higher lime content than Flyash D and Flyash N. The highest value of the CaO/SiO_2 ratio is found for Flyash R and is followed by Flyash S. Flyash D and Flyash N show very poor values of the CaO/SiO_2 ratio. Flyash D has the lowest values of CaO content and the highest value of combined content of $SiO_2 + Al_2O_3 + Fe_2O_3$.

2.3 Lime

Laboratory-grade quicklime was used. The lime is available in a fine-powdered form. The specific gravity of lime was found to be 2.070.

3 Test Procedures

Details of the tests like formulation of sample mix, procedure for preparing, storing and curing of samples and the various tests conducted are presented in following paragraphs.

3.1 Mix Design

The literature reviewed indicates that the amount of flyash used for stabilizing soils is generally up to 25%. Mishra et al. (2005) and Senol et al. (2006) have varied the percentage of flyash up to 20%. Cokca (2001) has reported the optimum percentage of flyash as 20%. Therefore, the percentage of flyash in the present study has been adopted as 20%.

The pH of the stabilized soil has been specified as 12.4, for sustaining the long-term pozzolanic reactions that result in strength gain and permanent improvement in stability. The optimum lime content, which is the lowest percentage of lime in soil that gives a pH of 12.4, was found on the basis of the pH procedure developed by Eades and Grim (ASTM D 6276-99a).

The pH of untreated soil was found to be 7.5. The results of the pH test as shown in Fig. 3 indicate that the optimum lime content of the soil is about 4%. It is decided to use a lesser percentage of lime in combination with the flyashes. Eight trial combinations with four different flyashes and 0% or 2% of lime as indicated in Table 4 were formulated and tested.

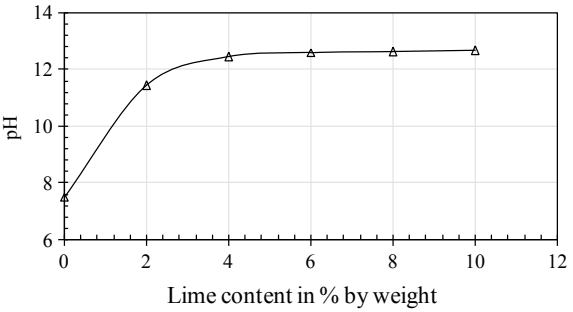

Fig. 3 Optimum percentage of lime from pH test

Table 4 Trial mix for laboratory tests

Proportion of soil:flyash:lime	Flyash D	Flyash N	Flyash R	Flyash S
80:20:0	D20	N20	R20	S20
78:20:2	D20L2	N20L2	R20L2	S20L2

3.2 Sample Storage and Curing

For uniform mixing of the stabilizers in powder form to the highly expansive soil, it was necessary that the moisture in the soil was uniformly distributed. Also during curing, the water content of the samples needs to be controlled. Therefore, special precautions were taken in preparation of the samples and their storage during the curing period. The amount of water as much close to the required moisture content as possible was added to the oven-dried soil and mixed thoroughly. The moist soil was then allowed to stand overnight in airtight polythene bags. The required quantity of stabilizer was then added to the soil and hand-mixed for about 8–10 min. Care was taken to break the clods/lumps that were formed during this process. The soils so prepared were immediately transferred to airtight bags to prevent loss of moisture. Blending of mix materials and casting of samples were done alternately to maintain constant time lag between blending and compaction.

After casting of samples, they were immediately transferred to airtight polythene bags and kept in a humid enclosure, as shown in Fig. 4. Storage and curing were done as per the protocol mentioned in the NCHRP report. Samples for UCS tests were prepared and cured in above-mentioned manner. Samples for CBR tests were compacted in CBR moulds immediately after adding stabilizers. The moulds were then placed in airtight polythene bags for required curing period. Samples for linear shrinkage tests were mixed and cured as mentioned above but cast into the moulds after required curing period. For free swell index tests, the stabilized soil was mixed and cured as mentioned earlier and then oven-dried.

Fig. 4 Storage of samples for curing

3.3 Test Programme

The test programme has been decided on the basis of ASTM D 4609-94, 'Standard Guide for Evaluating Effectiveness of Chemicals for Soil Stabilization'. The free swell test and the linear shrinkage tests are indicators of improvement in the volume-change characteristics. The UCS and CBR tests were conducted to assess the improvement in strength. The results of the soaked CBR tests show the effect of stabilization on moisture susceptibility.

4 Results and Discussion

Results of various tests conducted to assess the suitability of the different flyashes and LFA mix are discussed in the following paragraphs.

4.1 Free Swell Index and Linear Shrinkage

The potential of the expansive soil to expand on exposure to water can be assessed by the free swell index which is the increase in the volume of a soil, without any external constraints, on submergence in water. It can be determined as per IS: 2720 (Part XL). Linear shrinkage is the decrease in one dimension of a soil mass, expressed as a percentage of the original dimension, when the water content is reduced from the liquid limit to the shrinkage limit. The potential of expansive soils to shrink due to loss of water can be assessed by conducting the linear shrinkage test as per IS 2720 (Part XX). Table 5 lists the free swell index and linear shrinkage of the eight trial combinations.

Table 5 Free swell index and linear shrinkage of stabilized soil

Mix	Free swell index (%)	Linear shrinkage (%)
Untreated soil	110.0	21.1
D20	111.8	20.7
D20L2	88.9	14.3
N20	116.7	20.1
N20L2	50.0	13.9
R20	100.0	20.3
R20L2	80.0	13.5
S20	111.1	19.4
S20L2	80.0	12.3

The untreated soil showed a FSI of 110 indicating a critical degree of severity. However, on treatment with different types of flyash, the FSI increased slightly except for Flyash R, where a 10% reduction was noted. On treatment with LFA, the free swell index reduced by 20–30% approximately. In case of the LFA treatment with Flyash N, there was a very significant decrease in FSI, indicating the effect of its coarser particle size.

The linear shrinkage of untreated soil was 21.12%. After the test, the untreated soil samples were found in a crumbled state. The flyash-treated samples were warped longitudinally and exhibited significant linear as well as radial shrinkage. LFA-treated samples showed least distortion.

Treatment with all four types of flyash showed little reduction in linear shrinkage. However, in case of treatment with LFA, the linear shrinkage values reduced to 12.3–14.1%, which is a reduction of almost one-third of that of the untreated soil. Both the free swell index test and the linear shrinkage test indicate that LFA is an effective stabilizer to control volume change of expansive soil. The least effect in controlling the volume-change behaviour of the expansive soil was shown by the LFA treatment with flyash D.

4.2 Compaction Characteristics

The strength of the untreated as well as stabilized soil is assessed by conducting tests on the laboratory samples compacted to the in situ field conditions. Determination of the optimum moisture content and maximum dry density is therefore necessary. The addition of lime causes a change in the mineralogical structure of an expansive soil. It is reported that the OMC increases generally by 2–4% and even greater in case of highly expansive clays. The MDD has been reported to decrease typically by about 48–80 kg/cum on addition of lime. However, no general statement can be made about the modified relation between OMC and MDD of flyash-treated soils. The compaction characteristics of the treated and the untreated soil samples were determined as per IS: 4332 (Part III).

The untreated soil has OMC and MDD values of 35.5% and 12.66 kN/m^3, respectively. The soil treated with LFA showed a reduction in both MDD and OMC. The OMC and MDD of the LFA-treated soil were found to be 33.0% and 12.2 kN/m^3, respectively. For the flyash-treated soil, the OMC and MDD values were obtained as 31.0% and 13.35 kN/m^3, respectively.

4.3 Unconfined Compressive Strength

To assess the effectiveness of a stabilizer, various agencies have notified the unconfined compressive strength criteria. An improvement of 345 kPa has been specified in ASTM D4609-94. UCS samples of size 50 mm in diameter and 100 mm in height were cast at the optimum moisture content and maximum dry density using compression device and then were allowed to cure for duration of 7 days. Three samples each of every soil mix were tested in a UTM at a strain rate of 1.25 mm/min. The untreated soil showed ductile failure with bulging. The samples treated with flyash showed slight bulging at mid-height. The failure plane was well defined and inclined. The LFA-treated soil showed brittle failure with wide vertical cracks at the ends of the samples. The failure strain of the untreated soil reduced from 6.2% to about 1–1.5% in case of treated soil. The elastic parameters are listed in Table 6.

An improvement of 130–170 kPa above the strength of the untreated soil is achieved for flyash-treated soils, except for Flyash N, where a strength gain of 280 kPa was achieved due to stabilization The improvement in the UCS has been about 230 kPa for the LFA mix with Flyash R, whereas it is about 300–490 kPa in case of the LFA mix with other flyashes. The initial tangent modulus of the untreated soil improved from 3.3 MPa to about 25–40 MPa for the flyash-treated soil and to about 40–55 MPa for LFA-treated soil.

Table 6 Elastic parameters of flyash-/LFA-treated soil

Mix	σ_f (MPa)	Elastic modulus (MPa)		
		E_i	E_s	E_f
Untreated soil	0.098	3.29	3.18	1.58
7D20	0.25	38.80	24.80	20.34
7D20L2	0.40	55.23	39.57	42.45
7N20	0.38	36.80	33.49	25.13
7N20L2	0.44	53.31	40.82	35.16
7R20	0.24	25.12	22.31	18.76
7R20L2	0.33	38.78	31.36	29.26
7S20	0.27	24.15	18.75	17.58
7S20L2	0.59	56.52	46.38	37.31

Note The prefix '7' indicates 7 days of curing

In comparison with the flyash-treated soils, the LFA-treated soils have shown a very significant increase in the elastic parameters, which is in the range of the required strength gain, as specified in D 4609-94. It is therefore decided to carry further tests with LFA-treated soil.

Mishra et al. (2005) have reported retardation in the strength after 14 days of curing. Therefore, the improvement in the UCS over increased durations of curing was monitored. Samples were cured for 14 and 28 days with uniform conditions of humidity maintained for the entire duration of curing. The stress–strain plots of samples tested after 14 and 28 days of curing were compared with those cured for 7 days as shown in Figs. 5, 6, 7 and 8. A consistent increase in the failure stress values as well as the initial tangent modulus, with increase in duration of curing, is observed.

The UCS of the LFA-treated soil with Flyash D increased from 400 to 510 kPa and that of LFA-treated soil with Flyash N increased from 440 to 560 kPa. For the LFA-treated soil with Flyash R, the UCS value has increased from 330 to 630 kPa. The LFA-treated soil with Flyash S has shown the highest strength gain from 320 to 800 kPa. Thus, the soils treated with 2% lime and 20% of the four flyashes provide a 28-day UCS value between 0.51 and 0.8 MPa, which is adequate for a stabilized subgrade. After 28 days of curing, the initial tangent modulus was found in the range of 75–95 MPa as against 3.29 MPa of the untreated soil. The 1% secant modulus was obtained in the range of 45–65 MPa as against 3.18 MPa of the untreated soil. The failure strain for LFA-treated soils with either flyash N or Flyash R varied in the range of 0.75–1.25%. The LFA-treated soil with Flyash D showed lower failure strains varying between 0.65 and 0.95%. The LFA-treated soil with Flyash S failed at slightly higher strain values varying between 1.45 and 1.55%. Table 7 summarizes the elastic parameters.

The maximum UCS value is exhibited by the LFA-treated soil with Flyash S. The LFA-treated soil with Flyash R shows the highest values of 1% secant modulus and failure modulus. Flyashes with higher CaO content have shown better performance.

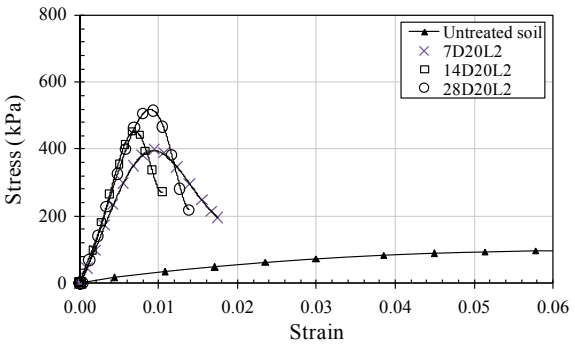

Fig. 5 Improvement in UCS of LFA-treated soil with Flyash D

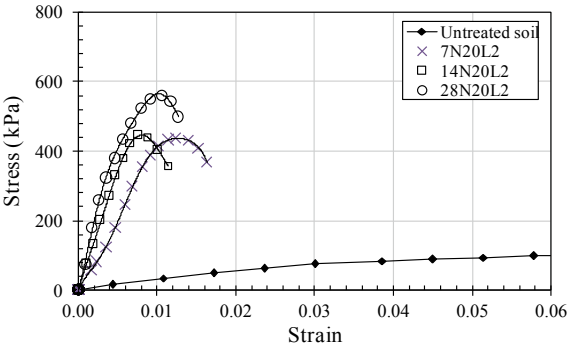

Fig. 6 Improvement in UCS of LFA-treated soil with Flyash N

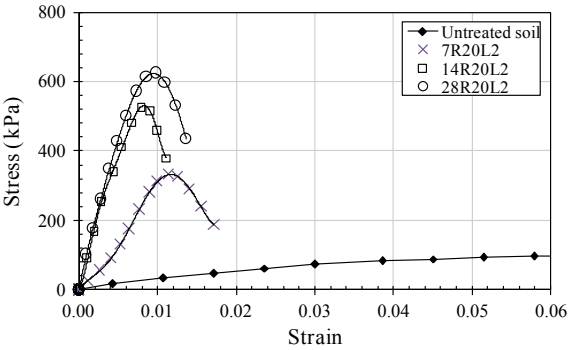

Fig. 7 Improvement in UCS of LFA-treated soil with Flyash R

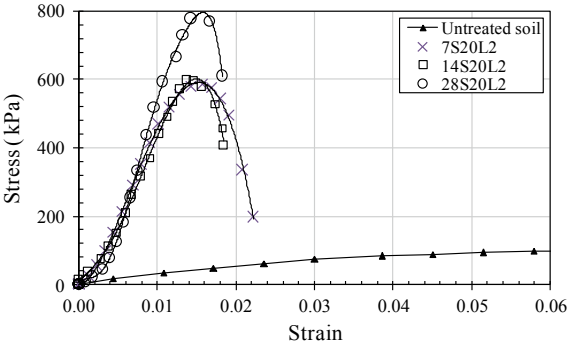

Fig. 8 Improvement in UCS of LFA-treated soil with Flyash S

4.4 California Bearing Ratio

The California bearing ratio is a very useful parameter in designing of flexible pavements. The LFA-treated samples were cured for 7 days and then soaked for 4 days with standard surcharge. The soaked CBR values and the % heave are listed in Table 8.

Table 7 Improvement in elastic parameters of LFA-treated expansive soil with curing

Mix	σ_f (MPa)	Elastic modulus (MPa)		
		E_i	E_s	E_f
7D20L2	0.40	55.23	39.57	42.45
28D20L2	0.51	74.27	48.91	55.25
7N20L2	0.44	53.31	40.82	35.16
28N20L2	0.56	93.15	55.67	52.62
7R20L2	0.33	38.78	31.36	29.26
28R20L2	0.63	82.04	62.26	63.90
7S20L2	0.59	56.52	46.38	37.31
28S20L2	0.80	81.39	55.15	51.80

σ_f: Stress at failure; E_i = initial tangent modulus; E_s = secant modulus at 1% strain; E_f = elastic modulus at failure

Table 8 CBR and heave of LFA-treated samples

Mix	CBR (%)	Heave (%)
Untreated soil	1.5	5.18
7D20L2	25.40	0.01
7N20L2	20.88	0.02
7R20L2	38.18	0.04
7S20L2	38.25	0.05

The LFA-treated soils with Flyash D and Flyash N gave a soaked CBR value between 21 and 25%. A very high value of CBR of 38% was obtained for both Flyash R and Flyash S. With longer duration of curing, the stabilizing effects are expected to be more prominent. The LFA treatment has reduced the heave from 5.25% to less than 0.05%, thereby reducing the moisture susceptibility.

5 Conclusions

Following conclusions can be drawn from the study:

- Class F-type flyashes are effective in stabilizing highly expansive soils only when used in combination with lime. The effectiveness of a flyash depends on its specific gravity, CaO content and CaO/SiO_2 ratio. Free swell index tests and linear shrinkage tests can be conducted to assess the effectiveness of various stabilizers.
- With LFA treatment of expansive soil, the UCS can be improved from 100 kPa to the range of 500–800 kPa, whereas the initial tangent modulus can be improved from 3 MPa to the range of 75–95 MPa. However, the failure strains are reduced to 1.0–1.5%.

- The heave of a soaked CBR sample is a better criterion than the free swell index to assess the swelling potential of a stabilized subgrade.
- The LFA treatment improved the soaked CBR values from 1.5% to the range of 20–40% and restricted the heave to 0.05%, thereby proving its suitability in treating expansive subgrades.

References

ASTM C 618-15 Standard specification for coal flyash and raw or calcined natural puzzolana for use in concrete

ASTM D 4609-94 Standard guide for evaluating effectiveness of chemicals for stabilization

ASTM D 6276-99a Standard test method for using pH to estimate the soil-lime proportion requirement for soil stabilization

Beeghly JH (2003) Recent experiences with lime-flyash stabilization of pavement subgrade soils, base and recycled asphalt. In: International ash symposium, University of Kentucky, Paper 46, pp 1–18

Central Electrical Authority, New Delhi (2017) Report on flyash generation at coal/lignite base thermal power stations and its utilization in the country for the 1st half of the year 2016–17 (Apr 2016–Sept 2016)

Cokca E (2001) Use of Class C fly ashes for the stabilization of an expansive soil. J Geotech Geo-Environ Eng ASCE 127(7):568–573

IS 2720(Part XX):1987 Methods of test for soils: determination of linear shrinkage. Bureau of Indian standards, New Delhi

IS 2720(Part XL):1977 Methods of test for soils: determination of free swell index of soils. Bureau of Indian standards, New Delhi

IS 4332(Part III):1967 Methods of test for stabilized soils: test for determination of moisture content-dry density relation for stabilized soil mixtures. Bureau of Indian standards, New Delhi

IS 4332(Part V):1970 Methods of test for stabilized soils: determination of unconfined compressive strength of stabilized soils. Bureau of Indian standards, New Delhi

Little DN, Nair S (2009) Recommended practice for stabilization of subgrade soils and base material. NCHRP Project 20-07 Final report, Transportation research board

Mishra A, Biswas D, Upadhyaya S (2005) Physico-mechanical behavior of self-cementing class C fly ash–clay mixtures. Fuel 84:1410–1422

Senol A, Edil TB, Bin-Shafique MS, Acosta HA, Benson CH (2006) Soft subgrades stabilization by using various fly ashes. Resour Conserv Recycl 46:365–376

Ground Improvement Using Industrial Waste Materials

G. Reshmi and Anirban Mandal

Abstract Black cotton soil offers a weak foundation for any structure made on it due to its swelling and shrinkage characteristics and inherent low strength. Roads constructed on these black cotton soils often suffer from early failures like rutting. An attempt have been made in this research to modify the black cotton soil as a subgrade material using some industrial waste materials like copper slag, fly ash and cement kiln dust. Tests like standard proctor test, unconfined compressive strength (UCS) test and California bearing ratio (CBR) tests were conducted on all soil-industrial waste combinations. CBR and UCS value of original soil sample was less which later got improved after addition of the above waste materials. Finally a flexible pavement design was done for the initial subgrade and for improved subgrades formed. Percentage reduction in pavement thickness due to subgrade improvement was also calculated. Such an attempt of using waste materials helps both in proper waste disposal and creation of improved subgrades.

Keywords Copper slag · Fly ash · Cement kiln dust · UCS test · CBR test

1 Introduction

Ground improvement incorporates various methods employed for modifying the properties of the soil to improve its engineering performance. Ground improvement techniques are used for a variety of engineering works like the construction of roads, bridges, air field pavements or on any other civil construction. If some industrial waste materials can be used for the modification, it will be highly economical. India produces large amounts of waste materials from different types of

G. Reshmi (✉) · A. Mandal
Department of Civil Engineering, Visvesvaraya National Institute of Technology, Nagpur 440010, India
e-mail: reshmi10592@gmail.com

A. Mandal
e-mail: amandalthesis@yahoo.com

R. Sundaram et al. (eds.), *Geotechnics for Transportation Infrastructure*,
Lecture Notes in Civil Engineering 29,
https://doi.org/10.1007/978-981-13-6713-7_37

industries. Their disposal is a matter of serious concern nowadays. These materials are non-decaying and remain in our environment for longer periods. So they have to reuse for some purposes, and one such application is weak subgrade improvement incorporating these waste materials. Different types of waste materials are produced by industries like fly ash, blast furnace slags, cement kiln dusts, lime kiln dusts, red mud, copper slag, steel slag, etc.

Copper slag (CS) is produced during pyrometallurgical production of copper from copper ores and contains materials like iron, alumina, calcium oxide, silica, etc. For every tonne of metal production, about 2.2 tonnes of slag is generated (Gorai et al. 2003). Dumping such huge quantity of slag produces environmental and space problems. Various studies have been conducted by various investigators and copper producing units all over the world to explore possible utilization of copper slag. Toxicity test conducted on slag leachate proved it as a non-hazardous material (Das et al. 1982). So it can be safely reused.

In India, production of fly ash is very high. Annual generation of fly ash has increased tremendously. India produce 300–400 Million tons of fly ash per year, so the consumption has to be increased subsequently (Haque 2013). Fly ash can provide divalent and trivalent cations that promote flocculation of dispersed clay particles. Thus, expansive black cotton soils can be potentially stabilized by cation exchange using fly ash (Cokca 2001).

Cement kiln can be used as an alternative to conventional stabilizers like cement and lime. They have self-cementing characteristics when they react with soil in a manner similar to Portland cement. Cement kiln dusts (CKD) have approximately one-third of the amount of cement oxides present in Portland cement (Ismail and Balal 2016).

Black cotton soils are highly clayey soils and are expansive which possess high swelling and shrinkage properties. Black cotton soil is hard when it is dry and it loses its stability when it becomes wet. Then, when it becomes dry, it shows a lot of cracks on its surface. Thus, such soils show considerable volume changes due to moisture fluctuations. Black cotton soils are found in states like Maharashtra, Gujarat, Madhya Pradesh, Tamil Nadu, Andhra Pradesh and Karnataka. The pavements constructed over black cotton soils should be of increased thickness due to inherent low CBR strength and suffer from early failures. In this study, an attempt was made to improve the subgrade characteristics of black cotton soil using some industrial waste materials like copper slag, fly ash and cement kiln dust. Apart of individual usage of waste materials, combined mixing technique was adopted.

Various mixtures of copper slag, fly ash and soil were evaluated for use in different layers of road pavement by conducting different geotechnical tests. The suitability of using copper slag in bituminous mixes was also evaluated. The copper slag–fly ash mix and copper slag–soil mix was found to have use as embankment fill material. They were also proved to be used as subgrade and sub-base materials in pavement (Havanagi et al. 2007). Copper slag has the capability of increasing CBR and UCS strengths when mixed with soils (Lavanya et al. 2011). As per a study, as copper slag concentration increases in soil, MDD increases due to high specific gravity of copper slag and OMC decreases due to increased sand sized

particles. California bearing ratio and unconfined compressive strength value was found increasing (Tandel and Patel 2009).

Dhawan et al. (1994) explored the feasibility of ash utilization in bulk for road construction. They considered three types of ashes as fly ash, bottom ash and pond ash admixed with different types of soil. The result indicated that improvement of California bearing ratio values of the soil with the coal ash from thermal power station and fly ash can be used as sub base materials, subgrade and embankment. (Prabakar et al. 2004) studied influence of fly ash on soils and reported that the addition of fly ash reduced the dry density of the soil due to the low specific gravity and unit weight of soil and improved the shear strength. Kumar and Singh (2008) evaluated the strength parameters of four locally available materials for their use in the sub-base course of a pavement.

Cement kiln dust has cementing capabilities similar to Portland cement. Various studies were conducted for evaluating the efficiency of cement kiln dust in subgrade improvement. A study was conducted to study the effect of curing time on strength development of black cotton soil stabilized by combined quarry dust and cement kiln dust admixture (Amadi and Osu 2016). Results indicated that a general increase in unconfined compressive strength values with increasing cement kiln dust content as well as the curing time for all soil mixtures. Improvement in UCS values ranged from 1.5 to 5 times higher than those tested immediately after preparation.

2 Materials

2.1 Soil Sample

Black cotton soil obtained from VNIT campus was used for the study. Various tests were conducted on the soil sample using various IS Codes. The values obtained for various tests are shown in Table 1. As per IRC-SP-72-2015, the soil was a 'Very Poor' subgrade material

Table 1 Properties of soil

Properties	Remarks
Specific gravity	2.54
Optimum moisture content (%)	23.25
Maximum dry density (g/cc)	1.54
Plasticity index	33
Soaked CBR value (%)	2.11
Unconfined compressive strength (kN/m^2)	166.6
AASHTO Soil classification system	A-7-6
Unified soil classification system	CH

2.2 Copper Slag (CS)

Copper slag used for the study was obtained from Blastech enterprises, Mumbai. Copper slag is a black, glassy and granular natured material whose self-weight is relatively high. The properties of copper slag are shown in Table 2.

2.3 Fly Ash (FA)

Fly ash used in the study was bought from National Thermal Power Corporation, Raipur. The properties of ash varies depending on the type and source of coal used, method and degree of coal preparation, cleaning and pulverization, type and operation of power generation unit, ash collection, handling and storage methods. Therefore, the properties of fly ash vary from plant to plant and even within the same plant. The properties of fly ash used are given in Table 3.

2.4 Cement Kiln Dust (CKD)

Cement kiln dust used for the present study was obtained from Chanda Cement Works, ACC Limited, Chandrapur. Properties of cement kiln dust are also not constant, and they vary from plant to plant. The properties of cement kiln dust used are shown in Table 4.

Table 2 Properties of copper slag

Properties	Remarks
Specific gravity	3.621
Colour	Black, glassy
Grain shape	Angular, multifaceted
Particle size	100% sand sized particles

Table 3 Properties of fly ash

Properties	Remarks
Specific gravity	1.95
Liquid limit	33
Plastic limit	Non plastic
Colour	Grey

Table 4 Properties of cement kiln dust

Properties	Remarks
Colour	Off white
Liquid limit	30
Plastic limit	16
Specific gravity	2.62

3 Methodology

Initially all the properties of original soil sample like specific gravity, Atterberg limits, free swell index, standard proctor test, soaked California bearing ratio test and unconfined compressive strength was determined as per relevant IS codes. Then, copper slag was added to soil at increments of 10% from 0 to 50% and tests like standard proctor test, unconfined compressive strength test and soaked California bearing ratio test was conducted on all soil–copper slag combinations. Then, an optimum soil–copper slag combination was obtained. Then, to incorporate some cementation or binding property, fly ash and cement kiln dust was added to it. Initially fly ash was added to optimum soil–copper slag mix at increments of 4% from 0 to 16%. An optimum mix was obtained. Then, cement kiln dust was added to optimum soil–copper slag mix at increments of 4% from 0 to 16%. Standard proctor test, unconfined compressive strength (UCS) test and soaked California bearing ratio (CBR) test were conducted on the above two mixes also. Grain size distribution of all the materials used is shown in Fig. 1.

UCS test was done on soil–copper slag–fly ash mix and soil–copper slag–cement kiln dust mixes on 0, 7, 14, 28 days of curing to study strength development which occurs over ages. CBR test on the optimum mixes of the above two combination was also done by 7-day curing followed by 7-day soaking. The various mixes used for the study is shown in Table 5. In the improved subgrades obtained as a result of stabilization, pavement design was done using IRC-SP-72-2015. Percentage reduction in pavement thickness and material savings obtained as a result of subgrade stabilization was calculated.

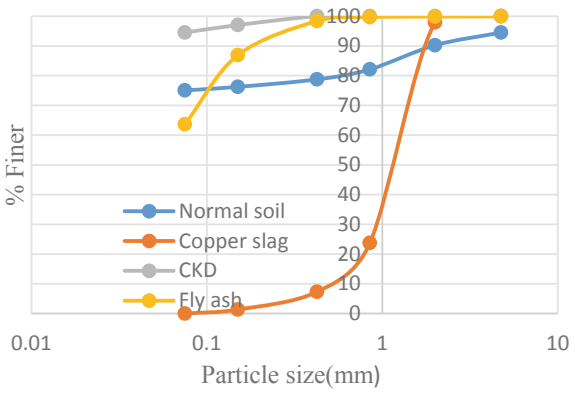

Fig. 1 Grain size distribution of various materials used in study

Table 5 Soil-industrial waste combinations tested

S. No.	Combination
1	100% soil sample
2	90% soil + 10% copper slag
3	80% soil + 20% copper slag
4	70% soil + 30% copper slag
5	60% Soil + 40% copper slag
6	50% soil + 50% copper slag
7	96% (soil–copper slag) + 4% fly ash
8	92% (soil–copper slag) + 8% fly ash
9	88% (soil–copper slag) + 12% fly ash
10	84% (soil–copper slag) + 16% fly ash
11	96% (soil–copper slag) + 4% CKD
12	92% (soil–copper slag) + 8% CKD
13	88% (soil–copper slag) + 12% CKD
14	84% (soil–copper slag) + 16% CKD

4 Results and Discussion

4.1 Soil–Copper Slag Combination

Copper slag (CS) was mixed to soil at increments of 10% from 0 to 50%.

4.1.1 Effect on Compaction

Standard proctor test was conducted on all soil–copper slag combinations. It was observed that as copper slag concentration increased, MDD increased and at 50% of copper slag addition it got reduced and OMC went on reducing. Increase in MDD is due to high specific gravity of copper slag. A reduction in OMC was observed due to increase in concentration of sand sized particles which has lesser dependency towards water. Compaction curves obtained are shown in Fig. 2.

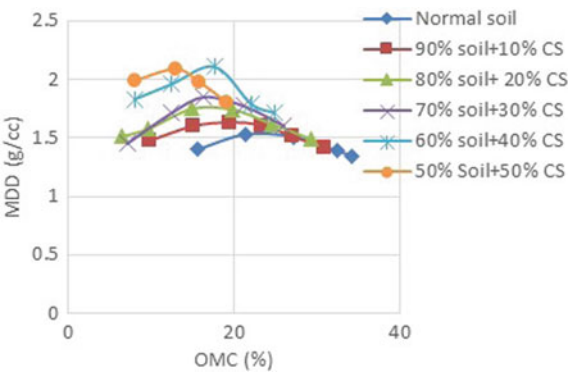

Fig. 2 Compaction curves of soil–copper slag mixes

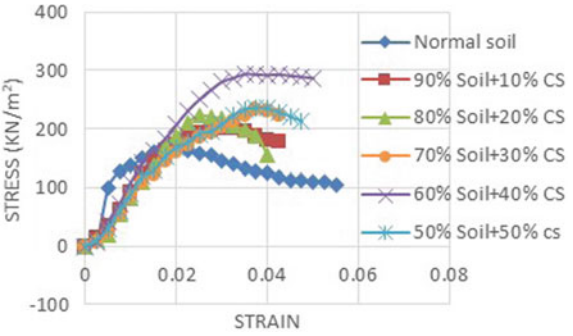

Fig. 3 Stress–strain graph of soil–copper slag mixes

4.1.2 Effect on Unconfined Compressive Strength Test

When copper slag was added to soil at increments of 10% from 0 to 50%, UCS value increased till 40% addition of copper slag and later it got reduced. UCS value increases initially due to mechanical stabilization of the mix. Angle of internal friction of copper slag is high which also contributed to increase in strength. After a particular point of copper slag addition, that is 50% in this study, due to high concentration of sand sized particles bonding between soil and copper slag will be lost which leads to further reduction in strength. The graphs obtained are shown in Fig. 3.

4.1.3 Effect on Soaked California Bearing Ratio Test

Copper slag is a granular material whose angularity and friction angle is very high. Addition of copper slag to soil enhances density of the mix. Thus, addition of copper slag helps in enhancing stability and load bearing capacity. So when this copper slag was added to black cotton soil in increments of 10%, CBR value went on increasing. The graph is shown in Fig. 4.

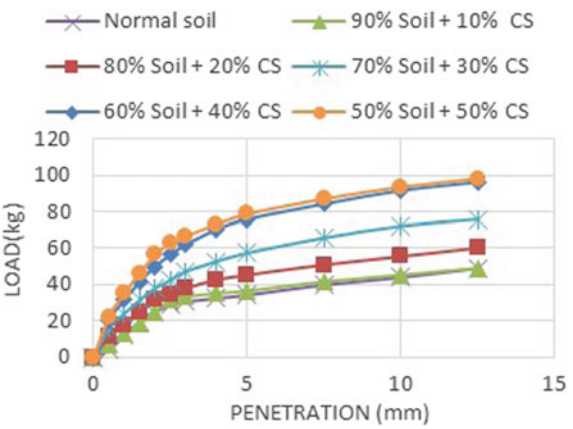

Fig. 4 Load-penetration graphs of soil–copper slag mixes

UCS strength decreased after 40% addition of copper slag, but CBR value increased till 50% addition of copper slag. Maximum density was obtained at 40% addition of copper slag. So 60% Soil + 40% copper slag mix was taken as optimum.

4.2 Soil–Copper Slag–Fly Ash Mix

To optimum soil–copper slag mix, fly ash was added at increments of 4% from 0 to 16%.

4.2.1 Effect on Compaction

When fly ash was added to optimum soil–copper slag mix subsequently MDD decreased, OMC decreased and then increased. Decrease in MDD may be due to replacement of a portion soil and copper slag by fly ash whose specific gravity is less as compared to the other two. The compaction curves obtained are shown in Fig. 5.

4.2.2 Effect on Soaked California Bearing Ratio Test

Soaked CBR test was conducted to simulate worst field conditions possible. When fly ash was added to optimum soil–copper slag mix at increments of 4% from 0 to 16%, CBR value increased till 12% addition of fly ash and later it got reduced. To study effect of strength development which occurs in curing, CBR test was conducted on soil–copper slag mix with 12% fly ash addition by 7-day curing followed by 4-day soaking. Only a marginal improvement in CBR was obtained as compared to normal soaked CBR test. The value obtained was 7.72. The graphs obtained for various combinations are shown in Fig. 6.

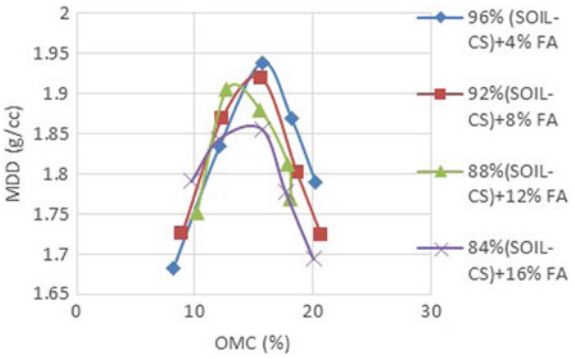

Fig. 5 Compaction curves of soil–copper slag–fly ash mixes

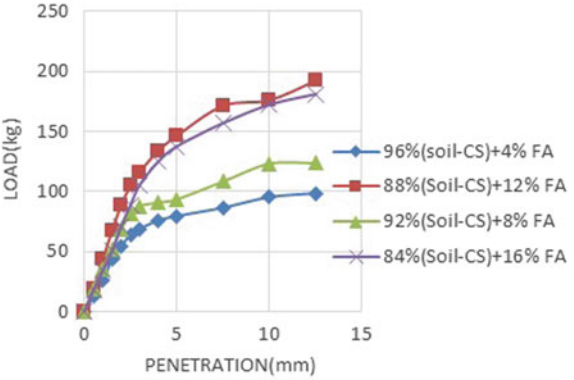

Fig. 6 Load penetration graphs of soil–copper slag–fly ash mixes

4.2.3 Effect on Unconfined Compressive Strength Test

UCS tests on soil–copper slag–fly ash mixes were done after 0, 7, 14, and 28 days of curing to study strength development which take place over ages. The samples were safely covered using polythene covers to prevent loss of moisture. Fly ash contains siliceous and aluminous materials and also certain amount of lime. When mixed with black cotton soil, it reacts chemically and forms cementitious compounds.

It can be seen that, increase in the value of UCS is gradual and relatively small for smaller curing periods of 7 and 14 days. The improvement in the UCS is comparatively better for a longer curing period of 28 days. Within that time a strong matrix of soil, copper slag and fly ash is formed. After 12% fly ash addition, UCS value got reduced which may be due to reduction in the amount of copper slag which contributed much in improvement of UCS. The variation of UCS values is shown in Fig. 7.

From UCS and CBR test results, it can be observed that strength decreased after 12% addition of fly ash, so 88%(Soil-CS) + 12% FA combination was taken as optimum. A comparative study was conducted between 88% (Soil-CS) + 12% FA combination and 88% Soil + 12% FA combination to verify whether copper slag

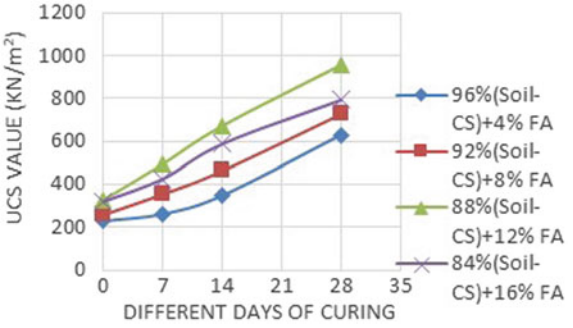

Fig. 7 Variation of UCS value of soil–copper slag–fly ash mixes

addition was beneficial. From standard proctor tests, it was understood that using copper slag, soil–fly ash mix can be compacted to increased densities at lower moisture contents. UCS values obtained by soil–copper slag–fly ash mix was high as compared to soil–fly ash mix at increased curing periods. Also CBR values obtained by soil–copper slag–fly ash mix was high as compared to soil–fly ash mix.

4.3 Soil–Copper Slag–Cement Kiln Dust Mixes

Cement kiln dust was added to optimum soil–copper slag mix at increments of 4% from 0% to 16%.

4.3.1 Effect on Compaction

When cement kiln dust was added to soil–copper slag mix at 4% increments, OMC decreased and MDD increased. Increase in MDD occurred due to cement kiln dust particles occupying every voids within the mix. The specific gravity of cement kiln dust is high as compared to soil. The compaction curves obtained are shown in Fig. 8.

4.3.2 Effect on Unconfined Compressive Strength Test

From the test results, it was observed that UCS value increases with increasing percentages of CKD and with increasing curing period. Based on these results, it is obvious that curing time exerts a strong effect on the development of strength of the BC soil–copper slag mixture stabilized with CKD. It is due to pozzolanic reactions and formation of cementitious products and is therefore identified as a major variable affecting the strength development of the stabilized soil mixtures. The variation of UCS value is shown in Fig. 9.

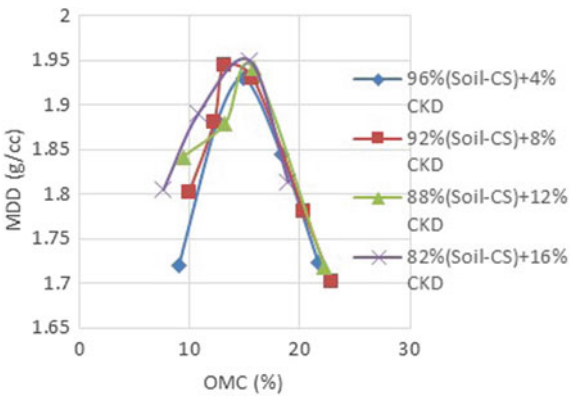

Fig. 8 Compaction curves of soil–copper slag–CKD mixes

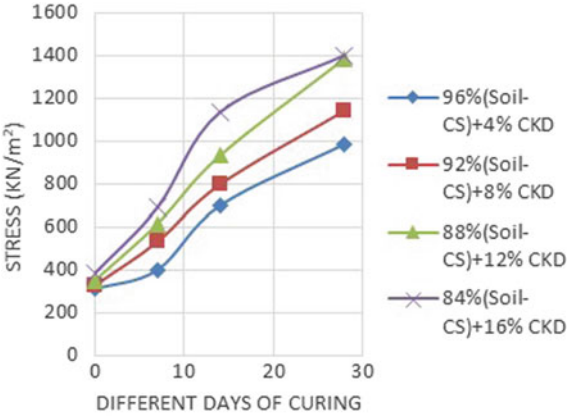

Fig. 9 Variation of UCS value of soil–CS–CKD mixes

4.3.3 Effect on Soaked California Bearing Ratio Test

When cement kiln dust was successively added to optimum soil–copper slag mix, soaked CBR value went on increasing. The graphs obtained are shown in Fig. 10.

From UCS and CBR test results, it became clear that as CKD percentage increases, strength increases. At 16% addition of CKD, CBR value obtained was 6.36 which satisfied the need that road subgrade should be above 5%. So 84% (Soil-CS) + 16% CKD is taken as the optimum combination. CBR test on optimum mix was also done by 7-day curing followed by normal soaking for 4 days to study if some strength improvement occurs over ages. Only a marginal increase in CBR was obtained which was 6.69.

A comparative study was conducted between 84%(Soil-CS) + 16% CKD mix and 84% soil + 16% CKD combination to verify whether copper slag addition was beneficial.

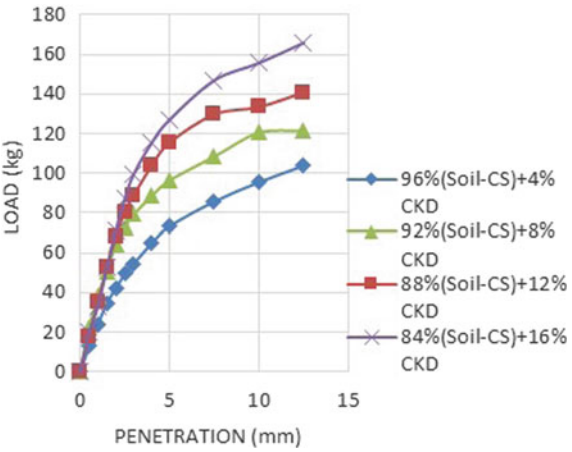

Fig. 10 Load penetration graphs of soil–CS–CKD mixes

Standard proctor test results indicated that using copper slag, soil–cement kiln dust mix can be compacted to more density at less moisture contents. UCS test results indicated that copper slag contained mix developed more strength for all curing days. Also CBR results indicated that copper slag contained mix developed much higher CBR values as compared to other.

From UCS and CBR test results, it became clear that as CKD percentage increases, strength increases. At 16% addition of CKD, CBR value obtained was 6.36 which satisfied the need that road subgrade should be above 5%. So 84% (Soil-CS) + 16% CKD is taken as the optimum combination. CBR test on optimum mix was also done by 7-day curing followed by normal soaking for 4 days to study if some strength improvement occurs over ages. Only a marginal increase in CBR was obtained which was 6.69. A comparative study was conducted between 84% (Soil-CS) + 16% CKD mix and 84% soil + 16% CKD combination to verify whether copper slag addition was beneficial. Standard proctor test results indicated that using copper slag, soil–cement kiln dust mix can be compacted to more density at less moisture contents. UCS test results indicated that copper slag contained mix developed more strength for all curing days. Also CBR results indicated that copper slag contained mix developed much higher CBR values as compared to other.

5 Pavement Design

When subgrade CBR is less, thickness of overlying pavement layers will be high to reduce stresses coming from traffic load which reaches the subgrade. So when CBR increases, thickness of overlying pavement layers can be reduced. Pavement design is done using IRC-SP-72-2015. In this study, initial soaked CBR value of soil was 2.11 making it a 'Very poor' subgrade material. Soil mixed with 40% copper slag yielded a CBR value of 4.13 making it a 'Poor' subgrade material. 88% (soil–copper slag) + 12% Fly ash yielded a CBR value of 7.64 making it a 'Good' subgrade material. 84% (soil–copper slag) + 16% Cement kiln dust combination yielded a CBR value of 6.36 making it a 'Fair' subgrade material.

For pavement design, traffic category on rural roads is classified to 9 classes based on Cumulative ESAL (Equivalent single axle load) applications which will come on the pavements during design its design life.

So in this study, as subgrade CBR increased due to addition of industrial waste materials, pavement thickness reduces when compared to pavement on initial unimproved subgrade. The pavement thickness reduction obtained is shown in Table 6. Thus, if thickness of overlying pavement layers reduces to subgrade improvement, huge quantity of materials which are to be used in different layers can be reduced. That can lead to huge cost savings.

Table 6 Pavement thickness reduction obtained as a result of subgrade improvement

CBR value	2.11	4.13	7.64	6.36
Traffic category	Total pavement thickness over subgrade (mm)			
TI	300	200	150	175
T2	325	275	175	250
T3	375	325	225	275
T4	425	375	275	300
T5	475	425	300	325
T6	550	475	325	375
T7	650	525	375	425
T8	650	575	425	525
T9	725	575	425	475

6 Conclusions

- Using industrial waste materials like copper slag, fly ash and cement kiln dust, subgrade characteristics of expansive soil can be improved which can result in pavement thickness reduction and material consumption reduction in various layers of pavement leading to huge cost savings.
- Apart from using these materials alone, a combined stabilization method was found better, that is Soil + Copper slag + Fly ash combination was better than Soil + Fly ash combination and Soil + Copper slag combination. Similarly Soil + Copper slag + Cement kiln dust combination was better than Soil + Cement kiln dust combination and Soil + Copper slag combination.
- The strategy of using the industrial waste materials in subgrade improvement helps in both pollution reduction and creation of improved pavements.

References

Amadi AA, Osu AS (2016) Effect of curing time on strength development in black cotton soil-Quarry fines composite stabilized with cement kiln dust (CKD). J King Saud Univ Eng Sci

Cokca E (2001) Use of class c fly ashes for the stabilization of an expansive soil. J Geotech Geoenviron Eng 127:568–573

Das BM, Tarquin AJ, Jones AD (1982) Geotechnical properties of a copper slag. Transp Res Record 941

Dhawan PK, Swami RK, Mehta HS, Bhatnagar OP, Murty (1994) Bulk utilization of coal ashes from road works. Indian Highways 22(11):21–30

Gorai B, Jana RK, Premchand (2003) Characteristics and utilization of copper slag—a review. Resour Conserv Recycl 39:299–313

Haque ME (2013) Indian fly-ash: production and consumption scenario. Internat J Waste Res 3 (1):22–25

Havanagi VG, Mathur S, Prasad PS, Kamaraj C (2007) Feasibility of copper slag-fly ash-soil mix as a road construction material. J Transp Res Board No. 1989. 2:13–20

IRC:SP:72-2015 Guidelines for the design of flexible pavements for low volume rural roads. First revision

Ismail AIM, Balal ZL (2016) Use of cement kiln dust on the engineering modification of soil materials, Nile Delta, Egypt. Geotech Geol Eng 34:463–469

Kumar P, Singh SP (2008) Fiber-reinforced fly ash subbases in rural roads. J Transp Eng ASCE 134(4):171–180

Lavanya C, Sreerama Rao A, Darga Kumar N (2011) A review on utilization of copper slag in geotechnical applications. In: Proceedings of Indian geotechnical conference, Kochi (Paper no. H-212)

Prabakar J, Dendorkar N, Morchhale RK (2004) Influence of fly ash on strength behavior of typical soils. Constr Build Mater 18(263):267

Tandel YK, Patel JB (2009) Review of utilization of copper slag in highway construction. Aust Geomech 44

Use of Jute Fiber in Improving Geotechnical Properties of Soil

Parvesh Kumar and Fayaz Ahmad Mir

Abstract Soil improvement is used in the field of geotechnical engineering in order to increase the engineering properties of soil. Various soil improvement techniques have been developed which are very effective in the geotechnical engineering. Soil improvement by adding natural fiber is a common practice used nowadays. In this soil improvement technique, natural fibers are mix randomly in soil. Natural fibers like Jute, coir, bamboo, etc. are easily available and are very cheap as compared to synthetic fibers. These natural fibers are eco-friendly and have no harmful effects on environment. They can easily mix with soil and act as a reinforcing material. In this paper, discussion is made on the enhancement of the properties of soil when Jute fiber is added to soil. Natural Jute fiber after cutting into a certain aspect ratio is mixed with soil. For the present study, the soil sample is taken from NIT Srinagar college campus. From the results, it can be concluded that addition of Jute fiber in soil has significant effects on soil properties.

Keywords Soil · Reinforcing material · Natural fiber · Aspect ratio

1 Introduction

Due to rapid growth of urbanization and industrialization, soil improvement is major concern in the construction activities. The process in which the index properties and other engineering characteristics of soil are improved by using different techniques is called soil improvement. Soil is used as a construction material

P. Kumar (✉)
Department of Civil Engineering, Delhi Technological University, Bawana Road, Delhi, India
e-mail: parvesh.kaushal2@gmail.com

F. A. Mir
Department of Civil Engineering, National Institute of Technology, Srinagar, Jammu & Kashmir, India
e-mail: fayazamir@yahoo.co.in

R. Sundaram et al. (eds.), *Geotechnics for Transportation Infrastructure*, Lecture Notes in Civil Engineering 29,
https://doi.org/10.1007/978-981-13-6713-7_38

in several fields such as buildings, roads, irrigation, and structure. Soil improvement is required when the mechanical properties and strength of the soil are weak. Soil needs to be improved according to the requirement which varies from site to site. Synthetics nets were used for the first time in civil engineering application work in 1962. Then in 1969, nonwoven fabrics were used as a filter in the upstream face of an earthen dam. Singh and Bagra (2013a, b), performed experimental tests on the soil reinforced with Jute fiber. From the results, it was concluded that with an increase in the quantity of Jute fiber, there is an increase in the CBR value of soil. Md. Akhtar Hossain, Md. Shakhawat Hossain, Md. Kamrul Hasan conducted a study on soil reinforced with Jute fiber. From the results, it was concluded that if the amount of Jute fiber increases in the soil, the optimum moisture content increases and maximum dry density decreases. From the results, it can also be concluded that with an increase in the length of Jute fiber there is an increase in the CBR value. Praveen Aggarwal and Bajinder Sharma, in 2011, conducted a study to analyze the effect of Jute on subgrade characteristics of soil. The soil sample is taken from a depth of 60 cm. Jute fibers of different diameters (2–8 mm) and lengths are mixed in the subgrade in different percentages (.2–1%) to find out the optimal quantity. It was observed that inclusion of Jute fiber reduces the maximum dry density from 1.88 to 1.80 gm/cc and the OMC increases from 13.5 to 15.5%. Dharmendra Kumar, Sudhir Nigam, Abhinav Nangia, and Shailendra Tiwari, in 2015, conducted a study on reinforcing the soil properties by using Jute fiber. For that, five soil samples were taken to study the effect of Jute fiber on CBR value of soil. The result shows that the CBR value increases with fiber content both in soaked and unsoaked conditions. Pankaj Dhemla et al., in 2015, conducted a study to determine the increment in the CBR value with the addition of Jute fibers in Rajasthan. The Jute is used in different proportions of 0.25%, 0.5% of weight of different lengths 20 mm, 40 mm. The CBR value before addition of Jute fiber at 2.5 mm penetration is 5% and when we add 0.50% Jute fiber of its weight then the CBR value increased by almost 50%. During the study, the effect of length of fiber used in the CBR was observed and it is concluded that there is an increase in the strength of soil.

2 Materials and Methodology

2.1 Soil

This study is conducted on soil sample collected from National Institute of Technology Srinagar campus. The soil sample is collected from a depth of 1.5 m. The soil sample is then pulverized and kept for drying. After 24 h oven-drying process, the various properties of soil such as index properties, compaction properties, unconfined compressive strength, and CBR value of soils in soaking and unsoaking conditions were find out in the laboratory.

2.2 Reinforcement Material

Natural Jute fiber is selected as the material for reinforcement purpose in this study. Jute fiber is purchased from the market. Then, it is cut down in a certain aspect ratio and that aspect ratio is kept constant throughout the study. The length of the Jute fiber is kept 25 mm, and the diameter is kept 1 mm. Then, these natural fibers are mixed properly in soil in order to enhance the properties of the soil. The properties of Jute fiber are shown in Table 1 (Fig. 1 and Table 2).

Table 1 Properties of Jute fiber

Specific gravity	1.4
Water absorption	13%
Tensile strength	400–600 MPa
Young modulus	50–60 MPa
Specific modulus	35–40 MPa

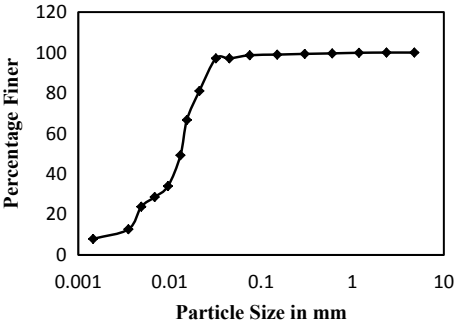

Fig. 1 Particle-size distribution curve of college soil sample from hydrometer test

Table 2 Geotechnical properties of NIT Srinagar campus soil

Property	Value
Specific gravity	2.613
Liquid limit	33.8%
Plastic limit	25.305%
Coefficient of uniformity (C_U)	7.5
Coefficient of curvature (C_C)	2.13
Optimum moisture content	20.5%
Maximum dry density	1.76 gm/cc
Cohesion	.55 kg/cm^2
Angle of internal friction	19°
Unconfined compressive strength	1.0107 kg/cm^2
CBR value under unsoaked conditions	4.01%
CBR value under soaked conditions	2.84%

2.3 Methodology

Soil used in this study is taken from National Institute of Srinagar, Jammu, and Kashmir college campus. Soil is taken from college campus at a depth of 1.5 m from the ground surface. After the process of drying, various tests were carried out on the oven-dried soil sample and its basic properties such as compaction characteristics, unconfined compressive strength, California bearing ratio under both soaked and unsoaked conditions were determined. Then, Jute is used as a reinforcing material in the soil. Jute is added to soil in different percentages which vary from .25 to 1%. Again same tests were conducted on soil and the change in the properties of soil on the inclusion of Jute fiber is determined.

3 Results and Discussion

3.1 Effect on Compaction Characteristics of Soil with Addition of Jute Fiber

To determine the effect of addition of Jute fiber on compaction characteristics, various light compaction tests were conducted on campus soil in unreinforced and reinforced conditions. Based on the average values of maximum dry density and optimum moisture content, following graphs were obtained.

From these graphs, we can conclude that the value of optimum moisture content will increase with increase in Jute fiber content and the maximum dry density of soil will decrease on the inclusion of Jute fiber. It is also noticed that if length and the thickness of the Jute fiber increases there is an relative increase in the optimum moisture content and reduction in maximum dry density. From the graphs, it may be concluded that the inclusion of Jute fibers decreases the maximum dry density and there is an increase in the optimum moisture content (Figs. 2 and 3).

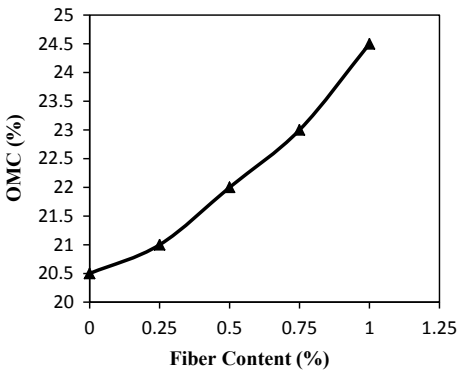

Fig. 2 Variation in optimum moisture content with fiber content

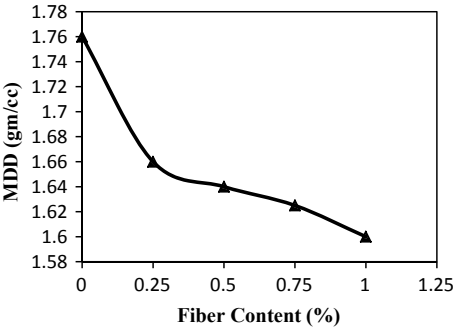

Fig. 3 Variation in maximum dry density with increase in fiber content

3.2 Effect on Unconfined Compressive Strength of Soil with Increase in Fiber Content

To determine the unconfined compressive strength, around 15 tests were conducted on college campus soil. For compressive strength of unreinforced soil, soil specimen is prepared in a standard cylindrical split mold of 38 mm diameter and 76 mm long. After determining the compressive strength of unreinforced soil sample, the Jute fiber is added to soil in different percentages (.25–1%) and the average value of unconfined compressive strength is determined for different percentages of Jute fiber which is shown in Fig. 4.

Based on the above graph, it can be concluded that there is an increase in unconfined compressive strength value of soil with the inclusion of Jute fiber.

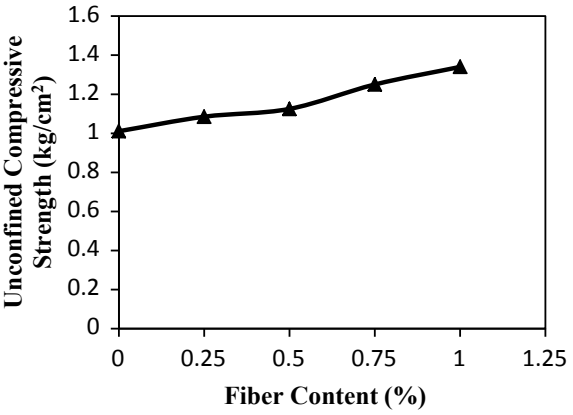

Fig. 4 Variation in unconfined compressive strength with addition of Jute

3.3 Effect on CBR Value Under Unsoaked Conditions

California bearing ratio tests were conducted on soil sample. The CBR tests were initially conducted on unreinforced soil sample, and CBR value in terms of percentage is determined for unreinforced soil sample. After determining the CBR value of plain soil, the Jute fiber is added to soil as a reinforcing material. Initially, the CBR value of soil sample under unsoaked conditions was 4.014%. With the addition of Jute, the CBR value of soil increases up to 8.759%. The maximum increase is experienced at 1% Jute content. The maximum increase in CBR value was found to be more than 118% as compared to the plain soil under unsoaked conditions. After conducting California bearing ratio tests on college soil, following graph can be obtained which clearly show that there is an increase in CBR value in terms of percentage when Jute is added to the unreinforced soil sample in different percentages (Fig. 5).

Based on the above graph, it may be concluded that CBR value increases with increase in fiber content. The CBR value is maximum at 1% Jute content, i.e., 8.759%.

3.4 Effect on CBR Value Under Soaked Conditions

After conducting California bearing ratio tests on college soil under soaked conditions, following graph can be obtained (Fig. 6).

Based on the above graph, it may be concluded that CBR value increases with increase in fiber content. Initially, the CBR value of soil sample under soaked conditions was 2.846%. With the addition of Jute, the CBR value of soil increases up to 6.350%. The CBR value is maximum at 1% Jute content, which is more than 123% over that of plain soil in soaked conditions.

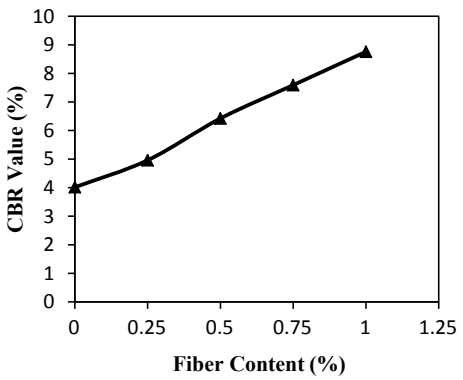

Fig. 5 Variation in CBR value at different Jute fiber contents under unsoaked conditions

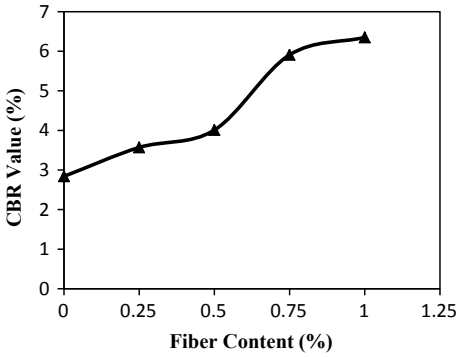

Fig. 6 Variation in CBR value at different Jute fiber contents under soaked conditions

4 Conclusion

After the completion of the study, following results can be summarized.

1. From the results, it is concluded that there is a change in maximum dry density and optimum moisture content with addition of Jute fiber. The value of maximum dry density decreases from 1.76 to 1.60 gm/cc and optimum moisture content increases from 20.5 to 24.5% with the inclusion of .25–1% Jute fiber in soil.
2. The UCS value of plain soil sample increases from 1.0107 to 1.34 kg/cm^2 on inclusion of Jute from .25 to 1%.
3. Under unsoaked conditions, the CBR value of plain soil sample increases from 4.014 to 8.759% on inclusion of Jute. Under soaked conditions, the CBR value increases from 2.846 to 6.350% when the Jute is added from .25 to 1%.

References

Aggarwal P, Sharma B (2011) Application of jute fiber in improvement of sub grade characteristic. ACEEE Int J Transp Urban Dev 01(1)

Bairagi H, Yadav RK, Jain R (2014) Effect of jute fibers on engineering characteristics of black cotton soil. Int J Eng Sci Res Technol

Gray DH, Ohashi H (1983) Mechanics of fiber reinforcement in sands. J Geotech Eng 109(3):335–353

Hasan R, Rayyaan R (2014) Effect of fiber geometry on the tensile properties of thermoset jute fiber composites. Int J Sci Res Publ 4(10)

Hossain MA, Hossain MS, Hasan MK (2015) Application of jute fiber for the improvement of sub grade characteristics. Am J Civ Eng 3(2):26–30

Kumar D, Nigam S, Nangia A, Tiwari S (2015) Improvement in CBR values of soil reinforced with jute fiber. Int J Eng Tech Res 3(5)

Mali S, Singh B (2014) Strength behavior of cohesive soils reinforced with fibers. Int J Civ Eng Res 5(4):353–360

Singh HP, Bagra M (2013) Improvement in CBR value of soil reinforced with jute fiber. Int J Innov Res Sci Eng Technol 2(8)

Singh HP, Bagra M (2013) Strength and stiffness response of Itanagar soil reinforced with jute fiber. Int J Innov Res Sci Eng Technol 2(9)

Improving the Performance of Ordinary Stone Column by Geotextile Encasement

Anil Kumar Choudhary, Binex Kunjumon and Jagadanand Jha

Abstract Marine clay usually possesses low shear strength coupled with high compressibility. These undesirable features make marine clay a problem either as a foundation material or a material for construction. Out of many methods to stabilize soft soils, stone column is one of the best preferred options. In soft soil, the effectiveness of ordinary stone column is low as the confining stress by surrounding soil is very less but such their performance can be substantially improved by providing a geotextile encasement around the column. The paper presents the results of series of laboratory model tests carried out with encased stone columns formed in marine clay. The effect of shear strength, (*s*/*d*) ratio, and seam strength of geotextile on load-carrying capacity was studied. The experiment is modeled in finite element analysis using PLAXIS. The experimental results were compared with those obtained from PLAXIS, and they showed very close resemblance. Ferrochrome slag which is a major waste material from stainless steel industry was used as the fill material which provides an ideal solution for effective waste management. The load settlement curves indicate that there is a great improvement in the load-bearing capacity of the stone column by geotextile encasement.

Keywords Flyash · Ferrochrome slag · End-bearing piles · Floating piles

A. K. Choudhary (✉) · B. Kunjumon
Department of Civil Engineering, National Institute of Technology, Jamshedpur, India
e-mail: drakchoudharycivil@gmail.com

B. Kunjumon
e-mail: binexk@gmail.com

J. Jha
Muzaffarpur Institute of Technology, Muzaffarpur 842003, Bihar, India
e-mail: jagadanand@gmail.com

R. Sundaram et al. (eds.), *Geotechnics for Transportation Infrastructure*,
Lecture Notes in Civil Engineering 29,
https://doi.org/10.1007/978-981-13-6713-7_39

1 Introduction

India has over 6000 km coastline which mainly consists of marine clay which poses several challenges to geotechnical engineers. Due to rapid urbanization and industrialization of coastal India, it is necessary to find out the ways and means to use such problematic soils for large civil Engineering projects.

Of the several techniques available for improving soft soil, granular piles/stone columns have been found to be promising. However, use of traditional stone columns consisting of natural aggregates is found be increasingly unsustainable and expensive because of non-availability of these aggregates. It is therefore necessary to look for some substitutes in the form of Industrial wastes which shall not only be cheaper but also solve the problem of their disposal to great extent.

One such promising industrial waste is ferrochrome slag coming out of the steel industries in large quantities and at present it is being disposed on land occupying huge space as well as a major source of pollution. When crushed, it resembles dark-colored aggregate with high angularity and therefore its use in granular piles as a substitute to natural aggregates may provide an economically viable and environment-friendly solution for gainful utilization of this waste material.

Further, geosynthetic encasement of such granular piles shall not only increase the stiffness of the granular pile by restraining bulging under externally applied loads but also reduce the resulting settlements.

An asymmetrical 15-noded geometry with the dimensions of tank is made and analyzed using finite element software PLAXIS. The pattern and the load at failure were determined and further analyzed. A comparison was done with PLAXIS, and experimental results show very good resemblance.

2 Literature Review

Use of laboratory model load tests for evaluating the beneficial effects of geosynthetic encasement in load-carrying capacity of granular piles in soft clay has been found in several publications. The performance of regular granular column over geosynthetic-encased granular column is evaluated by studying the load-carrying capacity and settlement characteristics of model granular column under a model footing.

Hughes and Withers (1974) carried out series of model load tests on granular columns in normally consolidated clay. The test results indicated that the ultimate capacity of granular column was governed primarily by the maximum radial reaction of the soil against the bulging. Load-carrying capacity of granular pile is highly dependent on frictional properties of the granular mass and magnitude of the passive earth pressure developed due to the bulging effect of the column. However, in soft clays, the passive resistance offered by clay is very less. This problem can be overcame by providing a geosynthetic encasement to the granular column.

Malarvizhi and Ilamparuthi (2004) conducted laboratory model load tests on stone column and reinforced stone column embedded in clay. Tests were conducted with different slenderness ratios and different encasing materials. They observed that settlement decreased with increase in stiffness of the encasement. In 2010, they studied the mechanism of geogrid-encased stone column by numerical analysis. In this study, model load tests were conducted in the laboratory on stone columns and encased stone columns were simulated numerically using PLAXIS FE code and results were compared with experimental results.

Murugesan and Rajagopal (2010) conducted numerical investigation on the performance of geosynthetic-encased stone columns. In this study, the qualitative and quantitative improvement in load capacity of the stone column by encasement was studied through a comprehensive parametric study using the finite element analysis. In 2010, they conducted laboratory model load tests on ordinary and encased granular columns for both single as well as group columns. They found that the encased granular column exhibited a stiffer response, whereas the ordinary columns showed significant strain-softening behavior.

3 Test Materials

3.1 Marine Clay

Marine clay required for the study was collected at a depth of 6 m from Mangalore in Karnataka. The clay was air dried and transported to Jamshedpur in sealed bags.

3.2 Ferrochrome Slag

The ferrochrome slag for the study was collected from Tata Steel plant in Jamshedpur. The crushed slag passing through 10-mm sieve and retained on 4.75-mm sieve was used in the study. Figure 1 shows the grain-size distribution curves for ferrochrome slag and marine clay used in the study. Tables 1 and 2 summarize the physical properties of marine clay and ferrochrome slag, respectively.

3.3 Geotextile

A woven polypropylene geotextile manufactured by Tencate was used in the study. Table 3 summarizes the mechanical properties of geotextile used in the study.

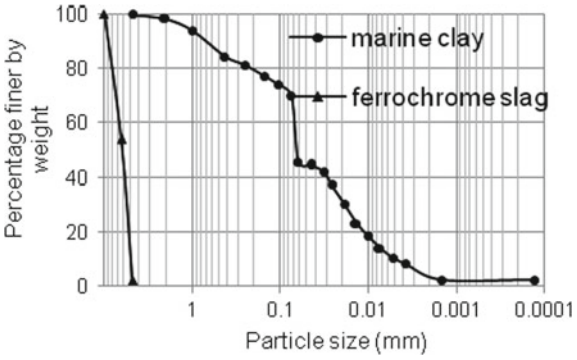

Fig. 1 Grain-size distribution of ferrochrome slag and marine clay used in the study

Table 1 Properties of marine clay

Property	Value
Specific gravity	2.49
Gravel content (%)	Nil
Sand content (%)	30
Silt content (%)	49
Clay content (%)	21
Liquid limit (%)	56
Plastic limit (%)	23
Soil classification as per ISSCS	CH
Free swell index	Nil

Table 2 Properties of ferrochrome slag

Property	Value
Specific gravity	2.67
Crushing strength (%)	16.60
Impact strength (%)	16.40
Angularity number	18.00
Coefficient of uniformity, C_u	1.36
Coefficient of curvature, C_c	0.89
Soil classification as per ISSCS	GP
Maximum dry unit weight (kN/m^3)	17.00
Minimum dry unit weight (kN/m^3)	13.40
Peak friction angle at 80% relative density (°)	44.00
Cohesion, c (kPa)	Nil

Table 3 Properties of geotextile used

Property	Value
Material of geotextile	Polypropylene
Type of geotextile	Woven
Tensile strength (kN/m)	30.00
Tensile elongation (%)	15.00
CBR puncture strength (kN)	3.00
Opening size, O_{90} (mm)	0.35
Water flow rate, Q_{50} (l/m^2/s)	100.00

4 Test Setup

Steel cylindrical tank of height 300 mm was used as model tank. The inner diameter of the tank was taken as the diameter of unit cell as per IS 15284 (Part-1) for triangularly laid granular columns. All tests were conducted with a granular column of diameter 60 mm. Assuming triangular pattern and spacing-to-diameter ratios (*s*/*d*) as 2, 3, and 4, three different model tanks with inner diameters 126, 189, and 252 mm were fabricated. All tests were conducted with the length-to-diameter ratio (*l*/*d*) of granular column as 4. Hence, clay was placed for a height of 240 mm in which the granular column was installed at the center. By using a 60-mm-diameter steel model footing, vertical load was applied over the diameter equal to that of granular column. Surrounding footing, sand layer of 30 mm height was placed on the clay surface. The load was applied at a constant strain rate of 1.2 mm/min. The applied load was noted by a calibrated load cell and the deformation by means of a LVDT. The data was logged through a digital data logger. Figure 2 presents the schematic view of the experimental setup.

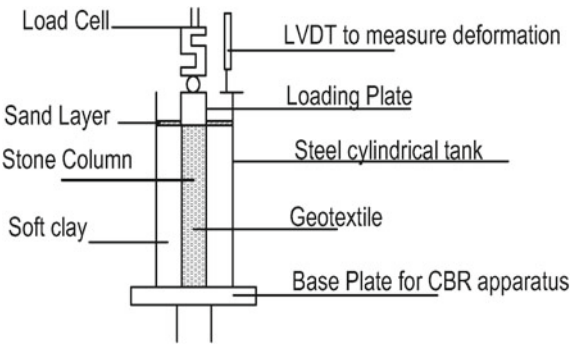

Fig. 2 Test apparatus used in the experimental study

4.1 Preparation of Test Specimen

4.1.1 Preparation of Clay Bed

Lubricating grease was applied inside the tank to reduce any friction between soil and the walls of cylinder. Air-dried clayey soil was first pulverized and sieved through 1-mm sieve. The pulverized clay was dried in oven for 24 h. Oven-dried clay was mixed with predetermined amount of water and mixed thoroughly. In order to allow uniform moisture distribution, the moist soil was kept in airtight containers for a week. To prepare the test bed, the moist soil was placed in the cylinder and compacted in 3-cm-thick layers till the desired height was reached. For each layer, the required amount of soil to achieve a desired bulk density was weighted out and placed in the cylinder using a metal scoop. The soil was then gently leveled out and compacted to proper depth by placing a circular wooden board on the surface and hitting the board with a drop hammer. Through a series of trials, the amount of soil, water content of soil, height of fall, and number of blows of the drop hammer required to achieve the desired density for each lift were determined in prior. By carefully controlling the water content and compaction, a fairly uniform test condition was achieved throughout the test program. Each layer was compacted uniformly so as to achieve a uniform density in all the test beds. In order to verify the uniformity of the test bed, undisturbed samples were collected from different locations in the test bed to determine the in situ unit weight, moisture content, and vane shear strength of the clay soil. The clay bed was filled to a total height of 240 mm. Upon filling, the surface was leveled with a sharp-edged ruler. Great care was taken, so that the density at the top surface was not affected.

4.1.2 Construction of Granular Column

The granular column is constructed by replacement method. A seamless pipe made of stainless steel with inward-beveled-sharpened edge was fabricated. The pipe was driven into the clay at its center up to bottom of the tank. The clay within the pipe was scooped out using a special scoop. To prevent aggregates from drawing out moisture from clay bed, the aggregates were soaked in water for 24 h. The aggregates were then surface dried using a towel. Surface-dried aggregates of size 4.75–10 mm were charged into the hole in layers of 50 mm each. In order to ensure that the results of this test have a practical significance it was important that the granular fill has a realistic relative density. Thus, a relative density of 80% was selected. For each layer, the required amount of aggregates to produce a desired bulk density was weighed and placed in the pipe giving uniform compaction using a tamping rod. The marking on the inner side of the cylinder was used as a reference for levels. Casing pipe was raised in stages ensuring a minimum of 5 mm penetration below the gravel placed.

For constructing geosynthetic-encased granular column, the geotextile was rolled into a tube of 60 mm diameter and a height of 240 mm. The tube was stitched along the seam. A geotextile strap was stitched at the bottom end of the geotextile tube to anchor the geotextile against granular fill. After driving the casing pipe and removal of soil, the geotextile tube was placed inside the pipe with geotextile smoothly touching the walls of the pipe. Aggregates were charged into the pipe and compacted as previously. The casing pipe was raised in stages. Since the aggregates were charged over the strap attached in the geotextile tube, it prevented the encasement from sliding and rising along with the casing pipe.

4.2 Testing Methodology

Upon preparation of clay bed and construction of granular column, the cylinder was sealed in a polythene sheet to prevent loss of moisture and left for 24 h. This ensured contact between clay and granular column as well as gain in strength of disturbed clay. After 24 h, waiting the model footing was placed on the granular column with precise alignment such that the load on the column was concentric. A 30-mm sand bed was placed around model footing to jacket it from tilting. Load was applied at a constant rate of 1.2 mm/min. The applied load on the column was measured through a calibrated load cell. The settlement was measured using a calibrated LVDT attached to the cylinder. The test was stopped when failure occurred within the granular column or at the predefined amount of displacement. After the completion of load test, samples were collected from clay bed to determine the moisture content and dry density, thus to ensure standardized conditions were maintained throughout the investigation.

4.3 Test Variables

Three different series of tests (i.e., A, B, and C) were carried out. Test series A was carried out on regular granular column, and Test series B was carried on single-seam geosynthetic-encased granular column, and Test series C was carried on double-seam geosynthetic-encased granular column. All tests were carried on clay bed with 45% moisture content and compacted to dry density 12.0 kN/m^3. The undrained shear strength of clay as determined by vane shear test was 6 kPa. Under each test series, the spacing-to-diameter ratio (s/d) is varied as 2, 3, and 4. The paper presents the results of a total of six model load tests carried out in the present investigation.

5 Results and Discussion

The load intensity versus settlement responses observed from two test series of tests are presented in Figs. 3 and 4

From the results presented in Fig. 3, it can be observed that load-carrying capacity of ordinary granular column increases with reduction in spacing-to-diameter (*s*/*d*) ratio. Closely spaced granular columns have better load-carrying capacity due to increased confinement. Increased confinement increases the passive resistance toward bulging. Regular granular columns exhibit bulging failure.

Results presented in Fig. 4 show that geotextile encasement significantly increases load-carrying capacity of the granular column. The columns do not show any signs of bulging.

In general, shear strength of clay influences the vertical load capacity of stone column. As per IS code, vertical capacity of stone column mainly depends on the shear strength of clay, bulging of stone column and stone column material. However, in the present case, marine clay that was used in the investigation having very low shear strength; therefore, only the effects of stone column material and bulging were considered.

Also, it was interesting to note that when encased with geotextile, shear strength of clay had almost no influence on the load-carrying capacity, and the load-carrying capacity appears to be independent of shear strength of surrounding clay.

As per IS 15284: Part-1 (2003), bulging of stone column needs to be considered up to 2*D*; where *D* is the stone column diameter. Figure 5 presents the amount of bulging for various cases, and it is seen that bulging is greatly reduced by geotextile encasement. This reduction in bulging is due to the confinement provided by the geotextile which restricts the radial movement of stones.

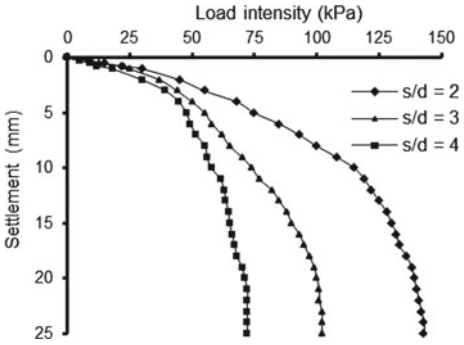

Fig. 3 Load intensity versus settlement curves with varying *s*/*d* for ordinary granular column (Test series A)

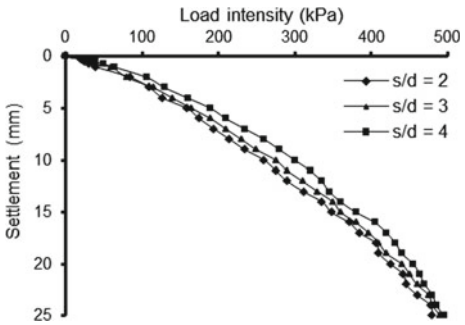

Fig. 4 Load intensity versus settlement curves with varying *s/d* for geosynthetic-encased granular column (Test series B)

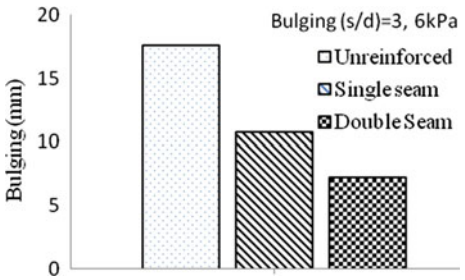

Fig. 5 Bulging of stone column with geotextile encasement

6 Conclusions

1. The load-carrying capacity of the ordinary granular column is significantly increased by geotextile encasement. Geotextile-encased granular column exhibits greater stiffness.
2. Load-carrying capacity of granular column is dependent on spacing-to-diameter ratio. With the increase in the spacing-to-diameter ratio, the load capacity of ordinary granular column decreases; while in case of geotextile-encased stone columns, it is independent of spacing-to-diameter ratio.
3. The load capacity of ordinary granular columns is highly dependent on shear strength of surrounding soil. However, in case of encased granular columns, the shear strength of surrounding soil has almost negligible influence on the load-carrying capacity.
4. Regular granular column fails by bulging and exhibit strain-softening. However, the amount of bulging can be greatly reduced by geotextile encasement.

References

Hughes JMO, Withers NJ (1974) Reinforcing of soft cohesive soils with stone columns. Ground Eng 7(3):42–49

IS 15284: Part-1 (2003) Design and construction for ground improvement—guidelines, Part-1: stone colums. Indian Standards, Bureau of Indian Standards, New Delhi

Malarvizhi SN, Ilamparuthi K (2004) Load versus settlement of clay bed stabilized with stone and reinforced stone columns. In: Proceedings. Asian regional conference on geosynthetics, GeoAsia, pp 322–329

Murugesan S, Rajagopal K (2010) Studies on the behavior of single and group of geosynthetic encased stone columns. J Geotechn Geoenviron Eng 136(1):129–139

Influence of Lime and Fiber on Strength and Consolidation Characteristics of Expansive Soil

Monowar Hussain and Subhradeep Dhar

Abstract This research article presents the strength and consolidation characteristics of expansive soils stabilized with lime and fiber. The initial phase of the experimental program includes the unconfined compressive strength (UCS) test of soil specimens prepared at three different percentages of lime (i.e., 3, 5, and 9% by dry weight of soil) and four different percentages of polypropylene (PP) fiber (i.e., 0.5, 1, 1.5, and 2% by dry weight of soil). From the test results, it is found that lime content, fiber content, and curing duration have significant influence on the compressive strength of lime-stabilized-fiber-reinforced soil. The maximum improvement of strength is found at 5% lime and 1.5% fiber. In the second phase, the effect of lime and fiber on consolidation behavior of expansive soil is evaluated. The consolidation tests are conducted at optimum lime (i.e. 5%) obtained from UCS test and with different percentages of PP fiber. It is observed that the addition of lime and fiber on expansive soil reduces the compression index (c_c), coefficient of volume compressibility (m_v), and increases coefficient of consolidation (c_v). The improvement of these parameters reduces the excessive settlement, i.e., rutting, cracking, and unevenness in pavement. Therefore, lime-stabilized-fiber-reinforced expansive soil can be used as pavement material.

Keywords Lime · Fiber · Expansive soil · Strength · Consolidation

M. Hussain (✉) · S. Dhar
Department of Civil Engineering, National Institute of Technology, Silchar 788010, Assam, India
e-mail: monowarhussain@gmail.com

S. Dhar
e-mail: subhradeep24@gmail.com

R. Sundaram et al. (eds.), *Geotechnics for Transportation Infrastructure*, Lecture Notes in Civil Engineering 29,
https://doi.org/10.1007/978-981-13-6713-7_40

1 Introduction

Expansive soils are generally problematic soil that contains montmorillonite-rich clays and are spread out in large area of the world. In India, these soils cover about 20% of the total landmass, which mostly includes Uttar Pradesh, Madhya Pradesh, Chennai, Rajasthan, Gujarat, Maharashtra, and Andhra Pradesh. Expansive soil absorbs water causing heaving during the wet periods and during dry periods they exhibit shrinkage due to evaporation of water from them. These alternate swelling and shrinkage movements due to different seasonal cycles cause severe damage to the civil engineering structures such as pavement, foundation, sewage pipes, embankments, and retaining wall. The damage cost exceeds several billions of dollars per annum over the whole world (Miller and Rifai 2004). Problem of expansive soil is not solely limited to swelling and shrinkage, low strength and poor bearing capacity are also equally responsible. Due to scarcity in quality soil, material engineers are frequently required to construct road over such problematic soil and are continually challenged by the problems of such poor quality soil.

Roads are considered the most preferred transportation system for trade and commerce, and in developing countries like India, road transport system is considered as the backbone of the growth of nation's economy. Therefore, efficient and well-established roads should be constructed with utmost care. The performance of a road depends on the quality of its subgrade soil. Subgrade acts as foundation to the road pavement structure under all traffic and weather conditions. The formation of waves, corrugations, rutting, and shoving in flexible pavements and the phenomenon of pumping, blowing, and consequent cracking of cement concrete pavements are generally attributed to the poor soil subgrade conditions (Khanna and Justo 2015). Therefore, building a stable subgrade is essential for constructing an effective and long-lasting pavement system. The subgrade is designed in such a way that it can support more load before reaching a critical deformation value and prevent excessive permanent deformation (Army Corps of Engineers 1984). Generally, traditional treatments like compaction, surcharge loading, and replacement technique are used to modify the weak subgrade soil. But they are found to be quite expensive and lead to long construction period. Therefore, various ground improvement techniques such as soil stabilization and reinforcement are carried out for the improvement of strength and compressibility behavior of soft subgrade soil.

Over the last few decades, several chemical treatment methods are used to stabilize expansive soil by using the admixtures such as cement, lime, and fly ash. This chemical stabilization alters the chemical and physical properties of the soil, improves the strength, and controls the volume-changing potential of soil. Among the various chemical treatment methods, lime stabilization is the most effective one which stabilizes the soil by replacing the very active sodium ions found in montmorillonite with less active calcium ions and is generally proven to be cost-effective treatment on expansive soil. It is widely used in different civil engineering and earth structures because of its economy and simplicity of construction (Wilkinson et al.

2010). Several research articles focused the beneficial effect of lime in enhancing the performance of clay soil (Bell 1996; Dash and Hussain 2012). The addition of lime to expansive soil promotes cation exchange reaction between the surface of clay mineral and calcium ions. As the calcium ions (Ca^{2+}) are released from the lime (CaO), it reacts with the silica (SiO_2) and alumina (Al_2O_3) that exist in the clay soil mineral and forms calcium silicate hydrates (CSH) and calcium aluminate hydrates (CAH), which coat the soil particles and subsequently crystallize to bond them (Bell 1996). Lime stabilization helps to enrich the strength and bearing capacity of soils. The compressibility and swelling potential are also reduced after lime treatment (Cai et al. 2006). IRC-51 recommended lime stabilization techniques for improving quality of soft subgrade soil. The Texas Highway Department, along with highway builders, has been using lime to stabilize subgrades whenever encountered with clay. However, the results of Dash and Hussain (2012) reveal that an excessive lime treatment reduced the strength gain due to excessive formation of cementation gel. Further, brittle failure occurred in lime-stabilized soil and causes great loss of strength after failure. To overcome these deficiencies in lime treatment, geotechnical engineers introduced high tensile element called fibers to stabilize the high-plasticity clayey soil.

Concept of fiber reinforcement in soil has been used since ancient time. Historical monuments like Great Wall of China and ziggurats are some examples of ancient earth reinforcement technique. In the modern era of soil reinforcement, randomly distributed fiber-reinforced techniques are much preferred than continuous planar inclusions (geotextiles and geogrids) because of its strength isotropy and absence of localized weak planes (Maher and Gray 1990). Gray and Ohashi (1983) reported that during shear, tensile force is mobilized in fiber and it is divided into two components, i.e., vertical and tangential to shear plane. The vertical component increases the confining stress, and tangential component directly resists the shear of fiber–sand matrix. Fiber reinforcement significantly improves strength and stiffness, ductility, and the crack reduction capacity of the soil composite (Kumar and Gupta 2016). A notable increase in compressive and tensile strength of fiber-reinforced cohesive soil has been reported in the scientific literature (Cai et al. 2006; Anggraini et al. 2015). Further, swelling, compressibility, and volume change of soil are also found to decrease when fiber is added to soil (Phanikumar and Singla 2016).

Recently, the fiber reinforcement technique is satisfactorily used in road construction projects. Lindh and Eriksson (1990) have conducted a pilot experiment in two pavement test stretches by incorporating a 100-mm layer of sand mixed with short plastic fibers (48 mm) at 0.25 and 0.5% fiber contents. It is found that fiber-reinforced sand performed better than the unreinforced sand with no rutting of the road surface during the first 2 years of traffic use. Santoni et al. (2001) showed that the sand-fiber stabilization of a sand subgrade supported over 1000 passes of a C-130 tyre load with less than 51 mm of rutting. Tingle et al. (2002) concluded that fiber-stabilized sands can be used as an alternative to traditional road construction material for rural roads.

Although good numbers of literatures are available on both lime and fiber-reinforced soil separately, there is still necessary knowledge of strength and

consolidation characteristics of lime-stabilized-fiber-reinforced expansive soil. In this research work, an experimental investigation is carried out to address the effect of discrete polypropylene fiber on the strength and consolidation characteristics of lime-stabilized expansive soil.

2 Materials and Methodology

2.1 Expansive Soil

The soil used in this study is commercially available bentonite. It is predominantly fine-grained consisting of approximately 96% soil. The specific gravity, liquid limit, and plastic limit of the soil are 2.6, 316.2, and 266.28%, respectively. As per Unified Soil Classification System (USCS), the soil is classified as clay with high plasticity (CH) and A-7-5 according to the AASHTO classification system.

2.2 Lime

Laboratory reagent-grade quick lime (CaO) is used as chemical stabilizer in this investigation. Its molecular weight and minimum assay are found to be 56.08 and 95%, respectively.

2.3 Fiber

The fiber used in this study is commercially available monofilament polypropylene fiber (PP). The physical and engineering properties of PP fiber are given in Table 1.

Table 1 Physical and engineering properties of fiber used

Property	Value
Type	Polypropylene
Average length (mm)	6 mm
Average diameter (mm)	0.034
Aspect ratio (*L*/*d*)	176
Breaking tensile strength (MPa)	350
Modulus of elasticity (MPa)	3500
Fusion point	165 °C
Burning point	590 °C
Acid and alkali resistance	Very good

2.4 Sample Preparation

In the present investigation, a series of tests are carried out under systematic planned scheme to study the strength and volume change behavior of lime-stabilized-fiber-reinforced expansive soil. Three different percentages of lime (i.e., 3, 5, and 9% by weight of dry soil) and four different percentages of PP fiber (i.e., 0.5, 1, 1.5, and 2% by weight of dry soil) are used in this research. Effect of lime on the strength and consolidation characteristics of soil is determined under test series 1. The combined effect of lime and fiber on strength and consolidation behavior is evaluated in test series 2.

For sample preparation, different lime and fiber contents are mixed with soil manually by hand and proper care is taken to obtain a homogenous mixture. After mixing, water is added according to the requirement and resulted wet mixing is done in non-permeable dish to avoid the water loss.

According to the road authorities in Australia and Department of Highways (DOH) and Rural Roads, Thailand, and other countries, the unconfined compressive strength (UCS) test is considered as the critical design parameter for subgrade construction. UCS test is carried as per ASTM D 2166 (2006) to evaluate the strength improvement of expansive soil due to lime-fiber treatment. For preparing the lime-treated soil samples, lime is mixed with expansive soil in dry state and then required quantity of water is added. An additional amount of water equal to 32% of the mass of lime is added to the mixture to take into account slacking of lime and loss due to evaporation. For lime-fiber-treated soil, required percentage of fiber is added in small increments to soil–lime mixture and they are mixed manually. Care is taken such that no lump of fiber is formed. After achieving a homogeneous mixture, required water is added to it. The required quantity of material is then compacted in MDD–OMC sample preparation in three layers inside a split mold of size 38 mm in diameter and 76 mm in length. The inside surface of the mold should be coated with a lubricant in order to reduce the chance of fracturing during the extraction. Compacted specimens after extracting from the mold are kept in the airtight polythene bags and stored in desiccators at room temperature for curing periods of 7, 14, and 28 days. After curing, the specimens are sheared under a constant strain rate of 1.2 mm/min.

In order to evaluate the effect of lime and fiber inclusion on compressibility characteristics of expansive soil, 1-D consolidometer test is carried out as per IS: 2720 (Part XV-1986). The compressibility characteristics, such as compression index (c_c), coefficient of volume compressibility (m_v), and coefficient of consolidation (c_v), are used to determine the magnitude of settlement and the rate of settlement. The amount of dry soil required for producing proctor MDD in the oedometer ring with soil specimen of 60 mm diameter and 20 mm height is weighed out. With this soil, the required quantity of lime and fiber is added and prepared in the same way as described in UCS.

3 Results and Discussions

3.1 Strength and Consolidation Behavior of Lime-Stabilized Soil

3.1.1 Effect of Lime on the Unconfined Compressive Strength of Soil

Figure 1 shows the variation in UCS with lime content and curing period. It can be observed that the UCS gradually increases with the percentage of lime content up to 5% of lime beyond that it is found to decrease with further addition of lime. The UCS of lime-stabilized soil further increased with increase in the curing period. With addition of 5% lime at 28 days of curing period, UCS enhanced to 788 kPa, which is threefold improvement compared to untreated soil. It is also observed that for all curing, UCS attains maximum value at 5% of lime content. Therefore, 5% lime is the optimum lime content to improve the strength of expensive soil. Addition of lime to the soil creates a strongly basic environment (i.e., pH > 12) in pore fluid, whereas silica (SiO_2) and alumina (Al_2O_3) present in the soil are progressively dissolved. The dissolved silica and alumina form cementitious gel (like CSH and CAH) which coat the coarser particles and subsequently strongly bond between them, leading to increase in strength and brittleness of the material. Thus, lime-stabilized expansive soil can be used in sub-base as it achieves the strength higher than 700 kPa as per IRC-51. However, with further increases in lime, a reduction in strength occurred because lime has neither appreciable friction nor cohesion; therefore, excessive lime decreases the strength (Bell 1996).

3.1.2 Effect of Lime on the Compressibility Characteristics of Soil

The compression index (c_c) is extremely useful for determination of the settlement in the field, which shows the amount of compression undergone by a particular sample with the increase in applied pressure. Higher the c_c value, larger is the resulting vertical deformation in clay. The slope of the linear virgin compression part of the e-$\log_{10}\sigma_v$ curve is termed as compression index (c_c). From Table 2, it is

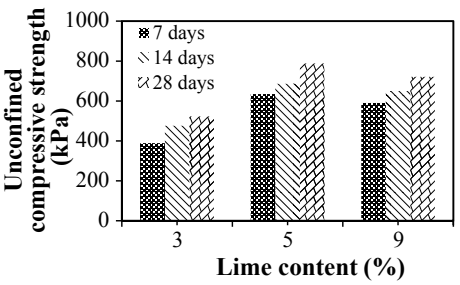

Fig. 1 Unconfined compressive strength of lime-stabilized expansive soil at different curing periods

Table 2 Summary of consolidation parameters of lime-stabilized expansive soil

Lime content (%)	c_c	m_v (m^2/kN) (10^{-05})	c_v (cm^2/s) (10^{-03})	k (cm/s) (10^{-09})
0	0.172	7.23	0.03	0.23
3	0.039	1.61	1.17	1.84
5	0.025	1.18	1.23	1.42
9	0.016	0.66	1.54	1.00

Note: c_c, m_v, c_v, k determined at stress level 400–800 kPa

observed that addition of lime drastically reduces the compression index (c_c) and coefficient of volume change (m_v). Lime addition causes flocculation and aggregation of clay particles, thus producing card-house type of structure in the clay–lime matrix (Hussain and Dash 2015). These structures effectively resist the vertical stress, hence decreasing the compressibility. The decrease in compressibility is also due to the cementation gel products formed in the second phase of reaction between lime and soil. The coefficient of consolidation (c_v) for treated and untreated expansive soils is calculated by using Casagrande logarithm of time-fitting method. Coefficient of consolidation (c_v) increases with increase in lime content; thus, the time required to achieve primary consolidation decreases for lime-stabilized soil for a particular degree of consolidation and a drainage path. The coefficient of permeability (k) is determined indirectly from the one-dimensional consolidation test result. The coefficient of permeability (k) can be obtained indirectly using the expression, $k = m_v c_v \gamma_w$, where m_v is the coefficient of volume change, c_v is the coefficient of consolidation, and γ_w is the unit weight of water. The coefficients of permeability (k) of lime-stabilized expansive soil are found in 10^{-9} cm/s range, which resembles practically impermeable drainage characteristic. Thus, suitable drainage provision is advisable during construction of pavements to prevent moisture accumulation on pavement and to facilitate quick runoff of surface water (IRC-37). However, little increase in the value of k is observed at 3% lime content, due to flocculation process which increases the void ratio of the soil–lime mixture, thereby creating the drainage path in the stabilized soil. This improvement in permeability after lime treatment is I agreement with the IRC–SP-77. But at 5 and 9% lime, the k value decreases due to formation of cementitious gel which fill ups the void spaces. Thus, it makes the stabilized soil less permeable at higher lime content.

3.2 *Strength and Consolidation Behavior of Lime-Stabilized-Fiber-Reinforced Soil*

3.2.1 Effect of Lime and Fiber on the Unconfined Compressive Strength of Soil

Variation in unconfined compressive strength with fiber and lime content for lime-stabilized-fiber-reinforced soil at 28 days of curing is depicted in Fig. 2. Data of fiber-treated sample are also plotted for comparison purpose. As expected, the UCS of lime-stabilized fiber-reinforced soil increases with increases in fiber content up to 1.5%, beyond which it declines. However, the value of UCS for any fiber content increases up to 5% of lime and after that decreases at 9% of lime. Similar behavior is observed for 7 days and 14 days of curing period. When lime is added, due to cation exchange reaction, the soil particles undergo flocculation and form aggregates (Bell 1996). These aggregate particles are harder compared to those of raw soil particles. These hard particles punched the fiber surface leading to improved interlocking and bonding in the modified soil–fiber matrix. Moreover, the cementitious gel formed after lime treatment filled all the pores of the soil and gives a denser matrix and causes more effective fiber reinforcement (Cai et al. 2006). The UCS is also found to be increase with increase in the curing period, which is attributed to the long-term pozzolanic reactions of lime with the soil leading to an increase in strength (Rajasekaran and Rao 1996). Similar behavior is observed at lime content of 3 and 9%. The maximum UCS value is found for the combination of 5% lime + 1.5% fiber content at 28 days of curing, which is 1452 kPa; it increases by 6 times than that of the untreated specimen (i.e., 243 kPa). The improvement in compressive strength of soft soil after lime-stabilized fiber-reinforced technique has very important practical significance in road performance. The addition of randomly distributed fibers to lime-stabilized soil ensures that instead of a catastrophic brittle failure, a structure is still able to bear load, sometimes increasing load after the first crack. Thus, it enhances the service life of a pavement structure.

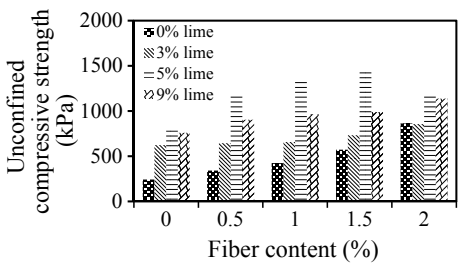

Fig. 2 Variation in unconfined compressive strength with fiber and lime content at 28 days of curing

Table 3 Summary of consolidation parameters of lime-stabilized fiber-reinforced expansive soil

Fiber content (%)	c_c	m_v (m^2/kN) (10^{-05})	c_v (cm^2/s) (10^{-03})	k (cm/s) (10^{-09})
0	0.025	1.18	1.23	1.42
0.5	0.027	1.05	1.72	1.77
1	0.030	1.15	1.94	2.16
1.5	0.025	0.92	2.57	2.31
2	0.020	0.63	3.75	2.32

Note: c_c, m_v, c_v, k determined at stress level 400–800 kPa

3.2.2 Effect of Lime and Fiber on the Compressibility Characteristics of Soil

Effects of lime-stabilized fiber-reinforced technique on consolidation behavior of expansive soil are evaluated at optimum lime content (i.e., 5%) obtained from UCS test and with different percentages of PP fiber. The results are shown in Table 3. It is observed that the compression index increases with inclusion of polypropylene fibers up to 1% and thereafter it decreases. Reduction in coefficient of volume compressibility (m_v) of lime-stabilized fiber-reinforced soil is observed with the increase in fiber content. The reduction in c_c and m_v might be attributed to the fact that the cementitious products formed after lime treatment bind the fiber–soil particle together and provide compact matrix structure, thus effectively resisting soil to compression. The study of coefficient of consolidation indicates that fiber inclusion in the lime-stabilized soil increases the c_v value. The k values in case of lime-fiber-treated soils show an increasing trend with increase in fiber content. The increase in k values might be attributed to the increase in void ratio resulting from the addition of fiber to the lime-treated soils. Increase in k value provides good drainage and can prevent internal flooding, thus ensuring long and trouble-free service of all forms of pavements.

4 Conclusions

In this study, a series of experiments have been carried out to study the influence of lime and PP fiber on strength and consolidation characteristics of expansive soil. From this investigation, the following conclusion can be made.

Amendments of lime in expansive soil enhanced the UCS up to 5% of lime, beyond which the improvement of strength decreases. The increase in compressive strength is about threefold in comparison with parent soil. The gain in strength is due to the production of cementitious products such as CSH and CAH and the pozzolanic reactions occurring during the curing time. Thus, it is advantageous to use lime for improvement in the strength of soft subgrade soil.

Addition of lime to the expansive soil reduces the compression index (c_c) and coefficient of volume change (m_v). Lime stabilization causes flocculation and pozzolanic reaction on the expansive soil, thus effectively resisting the vertical stress and decreasing the compressibility. Increase in coefficient of consolidation (c_v) after lime treatment results in decrease in the time requirement to achieve primary consolidation. Little increase in the value of permeability (k) is observed after lime treatment due to flocculation which creates the drainage path in the resultant soil matrix.

The inclusion of fiber reinforcement within lime-stabilized soil caused an increase in the compressive strength. The maximum unconfined compressive strength is obtained for the combination of 5% lime and 1.5% fiber at 28 days of curing, which is 6 times that of the untreated soil.

The combined treatment of lime-fiber increases the compression index (c_c) up to 1%, thereafter it decreases. Coefficient of volume compressibility (m_v) decreases and coefficient of consolidation (c_v) as well as permeability (k) increases with increase in fiber content. The reduction is due to the cementitious products which bind the fiber–soil particle and provide compact matrix structure, thus effectively resisting volumetric changes of soil. The increment in k, provides good drainage to pavement foundation.

Based on the results, it can be recommended that lime-stabilized fiber-reinforced technique can be used as a good quality pavement material in subgrade/sub-base for improving strength and mitigating the excessive settlement, i.e., rutting, cracking, and good drainage in pavement.

References

Anggraini V, Asadi A, Huat KBB, Nahazanan H (2015) Effects of coir fibers on tensile and compressive strength of lime treated soft soil. Measurement 59:372–381

Army Corps of Engineers (1984) Engineering and design-airfield flexible pavement-mobilization construction, Engineering Manual, Department of the Army Corps of Engineers Office of the Chief of Engineers, Washington, DC, USA, 1110, pp 3–141

ASTM D 2166 (2006) Standard test method for unconfined compressive strength of cohesive soil. ASTM International, West Conshohocken, PA

Bell FG (1996) Lime stabilization of clay minerals and soils. Eng Geol 42(4):223–237

Cai Y, Shi B, Ng CWW, Tang C (2006) Effect of polypropylene fibre and lime admixture on engineering properties of clayey soil. Eng Geol 87(3):230–240

Dash SK, Hussain M (2012) Lime stabilization of soils: reappraisal. J. Mater Civ Eng 24(6):707–714

Gray D, Ohashi H (1983) Mechanics of fiber reinforcement in sand. J Geotech Eng 335–353

Hussain M, Dash SK (2015) The influence of lime on the compaction behavior of soils. Environ Geotech. http://dx.doi.org/10.1680/envgeo.14.00015

IRC SP-77 (2008) Manual for design construction and maintenance of gravel roads. Indian Road Congress

IRC-37 (2001) Guidelines for the design of flexible pavements. Indian Road Congress

IRC-51 (1992) A guideline for the use of soil-lime mixes in road construction. Indian Road Congress

IS 2720-15: Methods of test for soils, determination of consolidation properties. Bureau of Indian Standards

Khanna SK, Justo CEG (2015) Highway engineering. Roorkee, Nemchand & Brothers Publications, India

Kumar A, Gupta G (2016) Behavior of cement-stabilized fiber-reinforced pond ash, rice husk ash-soil mixtures. Geotext Geomembr 44:466–474

Lindh E, Eriksson L (1990) Sand reinforced with plastic fibers—a field experiment. In: Proceedings of the international reinforced soil conference. British Geotechnical Society, Glasgow, pp 471–473

Maher MH, Gray DH (1990) Static response of reinforced with randomly distributed fibers. J Geotech Eng 116(11):1661–1677

Miller CJ, Rifai S (2004) Fiber reinforcement for waste containment soil liners. J Environ Eng 130 (8):981–985

Phanikumar BR, Singla R (2016) Swell-consolidation characteristics of fibre-reinforced expansive soils. Soils Found 56(1):138–143

Rajasekaran G, Rao NS (1996) Lime stabilization technique for the improvement of marine clay. Soils Found 37: 94–104

Santoni RL, Tingle JS, Webster SL (2001) Engineering properties of sand–fibre mixtures for road construction. J Geotech Geoenviron Engg ASCE 127(3):258–268

Tingle JS, Santoni RL, Webster SL (2002) Full-scale field tests of discrete fibre-reinforced sand. J Transp Eng ASCE 128(1):9–16

Wilkinson A, Haque A, Kodikara J, Adamson J, Christie D (2010) Improvement of problematic soils by lime slurry pressure injection: case study. J Geotech Geoenviron Eng 136(10):1459–1468

Liquefaction Countermeasures for Soil Supporting Existing Structures: A Review

Adyasha Swayamsiddha Amanta and Satyanarayana Murty Dasaka

Abstract Liquefaction of ground is a very common problem in geotechnical field. And for this problem, there are enough countermeasures to improve our grounds against liquefaction. However, most of these measures deal with the improvement of open ground against liquefaction. But there are many important structures standing which were designed without considering liquefaction. Majority of the liquefaction cases reported are due to earthquake, but few other sources of dynamic load are traffic load, vibrations from blasting, etc., which may lead to the generation of excess pore pressures. With the growing population and advancement of technology, the loads on the existing railway and road embankments are also increasing in the form of high-speed trains and heavily loaded traffic. This may lead to the generation of higher vibrations, which these embankments are not designed for. It is very difficult to use the existing countermeasures to improve the soil supporting these structures. This study mainly provides a review on the methods available to countermeasure liquefaction for soils supporting existing structures.

Keywords Liquefaction · Countermeasures · Existing structures

1 Introduction

When a loose saturated granular soil is subjected to a dynamic or static load, it shows a tendency to densify, which leads to the generation of excess pore pressures. In case of sudden dynamic loading like earthquake loading or other dynamic loading, the pore water will not get drained in a less time and behave as undrained. This generation of excess pore pressure decreases the effective stress in the soil.

A. S. Amanta (✉) · S. M. Dasaka
Department of Civil Engineering, Indian Institute of Technology Bombay, Powai, Mumbai 400076, India
e-mail: adyasha@iitb.ac.in

S. M. Dasaka
e-mail: dasaka@civil.iitb.ac.in

R. Sundaram et al. (eds.), *Geotechnics for Transportation Infrastructure*, Lecture Notes in Civil Engineering 29,
https://doi.org/10.1007/978-981-13-6713-7_41

When the effective stress becomes zero, soil looses all its strength and stiffness and starts behaving like a liquid. This phenomenon is known as soil liquefaction.

When a soil liquefies, because of loss of strength, it can no longer support the structures standing on it. As a result, the liquefaction-induced damage is very severe on constructed facilities. So the mitigation measure for this liquefaction is very important. Majority of the liquefaction cases reported are due to earthquake, but few other sources of dynamic load are traffic load, vibrations from blasting, etc., which may lead to the generation of excess pore pressures.

There are many important structures standing which were designed without considering liquefaction. With the growing population and advancement of technology, the loads on the existing railway and road embankments are also increasing in the form of high-speed trains and heavily loaded traffic. This may lead to the generation of the higher vibrations, which these embankments are not designed for.

Many researchers worked in the field of liquefaction and developed many techniques like solidification, densification, drainage, deep mixing, injection method, and desaturation to countermeasure liquefaction. However, most of these measures deal with the improvement of open ground against liquefaction. It is very difficult or seldom possible to use many of these techniques for existing structures. This study mainly discusses the available methods to countermeasure liquefaction for soils supporting existing structures.

2 History of Countermeasures for Liquefaction

The phenomenon of "liquefaction" is known long ago, but it drew the attention after 1964 Niigata Earthquake and 1964 Alaska Earthquake where the structure witnessed severe damages due to liquefaction (Yasuda 2007). After 1964, different mitigation measures were developed that improve the ground to prevent liquefaction and strengthen structures to prevent or minimize damage if the ground liquefies.

Many oil tanks underwent extensive settlements as a result of liquefaction, during the 1964 Niigata Earthquake. But, very few tanks whose foundation ground had been compacted by vibro-floatation reported no such settlements. Here for the first time, the compaction of ground was perceived to be effective against liquefaction. Keeping this in view, the foundation of few tanks at a factory in Hachinohe City was improved (Watanabe 1966). Later, the 1968 Tokachi-oki Earthquake confirmed the effectiveness of this method again (Ohsaki 1970).

In 1950s and 1960s, the sand compaction pile (SCP) method was applied against liquefaction. The effectiveness of this method was shown in Ishihara and Koga (1981). Different methods of solidification and drainage against liquefaction, i.e., lattice-type deep mixing (DM) technique and the gravel drain (GD) technique, were developed in 1970s and 1980s, respectively (Yasuda and Harada 2014). Later on, methods like pre-mixing, use of artificial materials, and injection techniques were developed.

Though many researchers worked in this field and developed many techniques to countermeasure the liquefaction, many existing important structures were built without considering liquefaction. It is very difficult to use these methods for strengthening foundation soil supporting structures against liquefaction. This study mainly deals with the liquefaction countermeasures for soil supporting existing structures.

Considering the aforementioned problem, some researchers started working in this field. A few methods were presented in Yasuda (2007) which could be applied as a countermeasure to the problem. Though it is reported that few of them are in practice in Japan, their application is very difficult. Schematic representation of some of these techniques is shown in Fig. 1.

Although from the above-mentioned study it seems like a number of solutions are there to the considered problem, the studies reported till now are restricted to a very few techniques. The reported studies are mostly based on model studies. These can be categorized under the following headings.

2.1 Countermeasure by Drainage

Buildup of excess pore pressure under undrained loading condition is the key or the gateway to the initiation of liquefaction. By providing drainage, one can prevent or reduce the generation of excess pore pressures, and hence, drainage acts as a

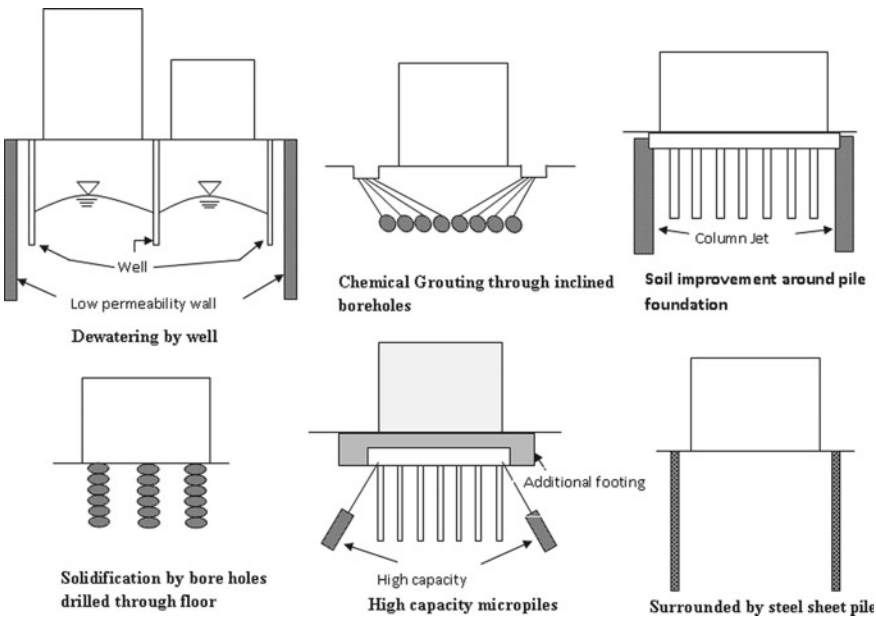

Fig. 1 Remediation methods for existing structures (Yasuda 2007)

countermeasure against liquefaction. Even the installation of drain system does not create much noise or vibration. Hence, this method is preferable in the constructed sites. To serve the purpose of drainage, different materials are reported to be used.

According to Orense et al. (2003), "a material to be used for above-mentioned drain must have sufficiently high permeability for liquefaction remediation and a high resistance against liquefaction." Several researchers have conducted tests to investigate the effect of drains on liquefaction process.

Tokimatsu and Yoshimi (1980) and Sasaki and Taniguchi (1982) performed model tests to evaluate the effect of gravel drain on the liquefaction potential of the foundation soil under existing structure. Both the studies reported the reduction in the structure uplift after the countermeasure. Later, Masakatsu et al. (1992), Orense et al. (2003), and Towhata et al. (2015) investigated the use of these drains for the prevention of buried pipelines during liquefaction by performing shake table tests. The three studies considered three different materials for their studies. Masakatsu et al. (1992) used two types of drains, i.e., gravel wall and gravel pile, where the gravel pile is found to be very sensitive to its spacing; Orense et al. (2003) introduced the use of recycled concrete crushed stoned as wall-type gravel drain sand; Towhata et al. (2015) investigated the use of vertical drain pipe to protect existing underground lifelines from liquefaction. The vertical pipes proposed can be installed along with the buried structure at particular intervals without any excavation. All these studies confirmed that the use of drains reduces generation of excess pore pressure and reduces the uplift of the underground structures. In addition, the effects of spacing of drainage pipe, width of the drain walls, and particle size of the drain material were also reported to affect the efficiency of the method. It is reported that though by the introduction of drains uplift of the structures reduced, still some uplift in the structure was observed (Orense et al. 2003).

2.2 *Countermeasure by Confinement*

One of the main causes of liquefaction-induced settlement of structure is lateral flow of the foundation soil in its liquefied state. Keeping this in view, many researchers investigated the effectiveness of the confinement of the foundation soil as a liquefaction countermeasure. Different confinement methods proposed are the use of sheet pile walls, use of secant pile walls, etc. Sáez and Ledezma (2015) proposed the use of secant pile wall for confinement. Studies by Zheng et al. (1996), Mizutani and Towhata (2001), etc. considered sheet pile wall as confinement method.

Sáez and Ledezma (2015) developed numerical models to evaluate the effectiveness of a foundation perimeter wall as the mitigation for the effects of liquefaction in a 64 m-diameter reinforced concrete water tank. The foundation perimeter was considered as a secant pile wall. The study concluded that with the proposed measure, liquefaction-induced settlements did not eliminate, but the settlements were relatively more homogeneous in nature leading to lesser structural damage.

Zheng et al. (1996) carried out finite element modeling to evaluate the use of sheet pile rings under oil tank sites, while Mizutani and Towhata (2001) carried out shake table model study to investigate the use of sheet pile wall for the protection of the river dikes against liquefaction by installing sheet pile wall at two different positions of the dike, i.e., installation of sheet piles at the toe of the dike and at the top of the dike. However, both the studies report similar behavior, i.e., reduction in settlement and reduction in the excess pore water pressure. But this measure does not seem efficient enough to nullify settlements completely.

All these studies concluded that confinement method alone can reduce the subsidence of soil to some extent, but they cannot completely eliminate the settlements. Further to improve this, the effect of different factors like stiffness of the sheet piles, depth of the groundwater table, length of sheet pile walls, and sheet pile walls equipped with drains was evaluated in further studies, which are discussed below.

2.3 Countermeasure by Confinement Combined with Other Technique

Although confinement method does not allow the lateral flow of soil, it cannot even reduce or stop the generation of excess pore water pressures. So, the fact is the soil is getting liquefied, but in a confined area. The soil grains post-liquefaction get rearranged; this might be the reason that confinement method alone did not completely eliminate the settlements. To overcome this, many researchers have tried combination of different methods with confinements like use of drains with sheet pile wall and lowering of GWL with sheet pile wall.

To examine the capability of utilizing sheet pile walls against foundation liquefaction on overlying highway embankments, Adalier et al. (2004) conducted a series of dynamic centrifuge model tests to evaluate the use of the gravel surcharge berm with sheet pile wall under highway embankments. A number of combinations based on the placement of the gravel berm and the position of the sheet pile wall were tried. Figure 2 shows the points considered for the observation of deformation, and the deformation profiles are presented in Table 1. Among them, the case with sheet pile along with toe area gravel berm was proposed to eliminate cracking and lateral spreading of the embankment, but the settlement still persists.

Motohashi et al. (2011) and Rasouli et al. (2015) carried out 1-g model tests to study the effects of sheet pile walls on the liquefaction-induced settlement of existing structures with length of sheet piles and groundwater level (GWL) as variables. Both the studies showed similar behavior (shown in Fig. 3). Later, Rasouli et al. (2016) even introduced drains along with sheet pile walls as a liquefaction countermeasure. The lowering of GWL and installation of drains reduce the settlement to a great extent. The orientation of drains along with sheet pile adopted by Rasouli et al. (2016) is shown in Fig. 4.

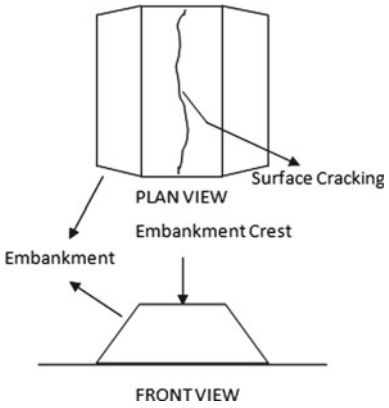

Fig. 2 Diagram showing the embankment crest and surface cracking (Adalier et al. 2004)

Table 1 Deformation profiles of model embankments (Adalier et al. 2004)

Model description	Embankment crest settlement	Surface cracking
No remediation	1.55 m	1.3 m wide, 2.5 m deep
With sheet pile	0.75 m	0.15 m wide, 1 m deep
Sheet pile + gravel surcharge berm	0.55 m	No visible surface cracking
Sheet pile + gravel surcharge berm + drainage	0.59 m	No visible surface cracking

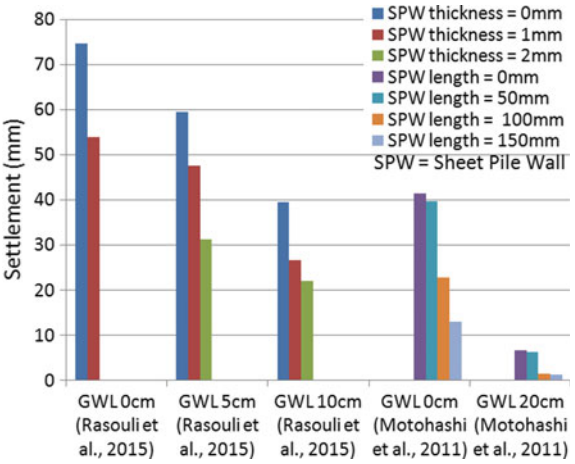

Fig. 3 Structure settlement with varying lengths of sheet pile wall, thickness of sheet pile wall, and GWL

2.4 Countermeasure by Structural Support

Few studies proposed introduction of certain structural support to the overlying structure to reduce its settlement. Mitrani and Madabhushi (2005) evaluated the use of grout micropile as a liquefaction countermeasure for existing structures by performing a series of centrifuge tests, which did not seem to be much effective. Towhata et al. (2015) proposed use of chemical grouting method and connection with pavement by stiff bars (namely, horn structure method), schematically shown in Fig. 5, to protect existing underground lifelines from liquefaction.

The horn structure method proposed could be executed with a partial excavation of backfill soil, and the chemical grout solidifies the surrounding soils by injecting it into the ground through the tubes. The injection of chemical grouts can be installed without any excavation. In this study, 1-g shaking model tests were performed to check the effectiveness of these methods against liquefaction and the results reported the methods as an effective countermeasure.

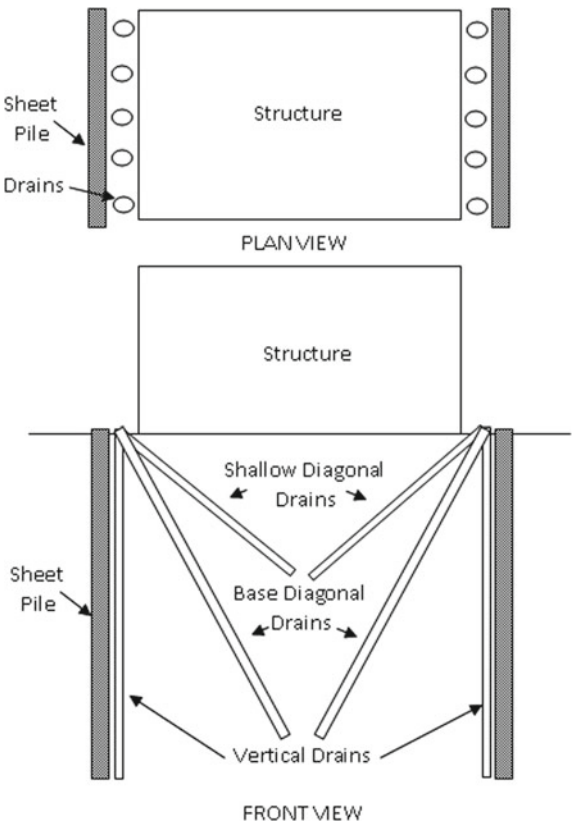

Fig. 4 Schematic diagram of a typical experiment and position of sensors and drains (Rasouli et al. 2016)

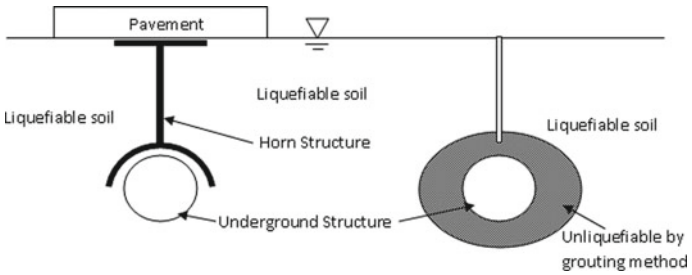

Fig. 5 Mitigation measures for existing underground structures: horn structure (left) and chemical grouting method (right) (Towhata et al. 2015)

2.5 Countermeasure by Inducing Desaturation by Air Injection

The liquefaction is caused by monotonic, transient, or repeated disturbance of the saturated cohesionless soil in undrained condition (Kramer 1996). Desaturation of soil is hence proposed as a liquefaction countermeasure. This desaturation of soil is achieved by different methods. Some studies proposed direct air injection methods to desaturate the ground, whereas some reported indirect methods like microbial method and electrolysis method to induce desaturation.

Okamura et al. (2003) observed that during the installation of SCP, air bubbles get injected into the soil. To confirm if the soil is getting desaturated by this process, they collected undisturbed soil samples by ground freezing method from three different sites that were improved by SCP within a month. From this, they confirmed that this desaturation retains for about a month. Later, Okamura and Teraoka (2006) collected samples from three other sites and reported that the air bubble injected had survived for 26 years.

Later, many researchers evaluated the effectiveness of the air injection method as a liquefaction countermeasure. Ishihara et al. (2003) carried out centrifuge test to investigate the extent of area desaturated by air injection in natural saturated ground. They observed that the improved area increases almost concentrically with the increase in the air injection pressure. Later, Okamura and Teraoka (2006) studied the effect of air bubble injection under shallow foundation using shake table test. They found that this method is more effective at the greater depth and not that much effective for shallow depths. Later, Marasini and Okamura (2015) and Zeybek and Madabhushi (2017) also investigated the response of air-injected partially saturated soils beneath existing structures by using centrifuge model test. Both the studies reported that the air injection reduces settlement and decreases the generation of excess pore pressure. In addition, they also reported the increase in the structural acceleration after the desaturation.

As it is difficult to desaturate ground homogeneously, Nagao et al. (2007) proposed the use of microbubbles of diameter around 10–100 μm to overcome this. But the process was not much effective. Yasuhara et al. (2008) investigated the rate,

magnitude, and distribution of desaturation by air injection method. From their study, they observed that the ultimate magnitude of air volume trapped in a particular volume of soil after the air supply ceases was independent of the air injection pressure.

Besides these model studies, Okamura et al. (2011) carried out in situ desaturation test and evaluated it through field monitoring by 3D electric resistivity tomography. They reported that air injection desaturates the soil, and degree of saturation of unsaturated specimens was in the range of 88–94%. The time of stay of the injected air in the soil depends on the soil properties and ground condition. Though all these studies confirmed the effectiveness of this method, they did not confirm much about the long-term existence of this induced desaturation.

Apart from direct air injection method, few researchers proposed some other methods to induce desaturation in soil. Mostly, natural soil deposits are non-homogeneous in nature, and to attain a uniform desaturation by air injection method in such soils is very difficult. Yegian et al. (2007) proposed two methods which can introduce uniform desaturation, i.e., electrolysis and drainage-recharge method. In the first method, two electrodes were separated by soil and electrolysis process was carried out. The process resulted in the production of hydrogen gas at the cathode, and this induced desaturation to the soil. The method of drainage-recharge involved drainage of a saturated soil sample and again refilling the sample with the collected drained water. The test setups for the two methods proposed are presented in Fig. 6. Both the methods successfully desaturated the samples. Later, He et al. (2016) proposed a microbial method for the desaturation of the soil. They reported the use of anaerobic bacteria and nutrients to introduce desaturation to the soil. They reported through computed tomography images that desaturated soil contains small pockets of gas bubbles. Both the studies confirmed the effectiveness of the methods against liquefaction.

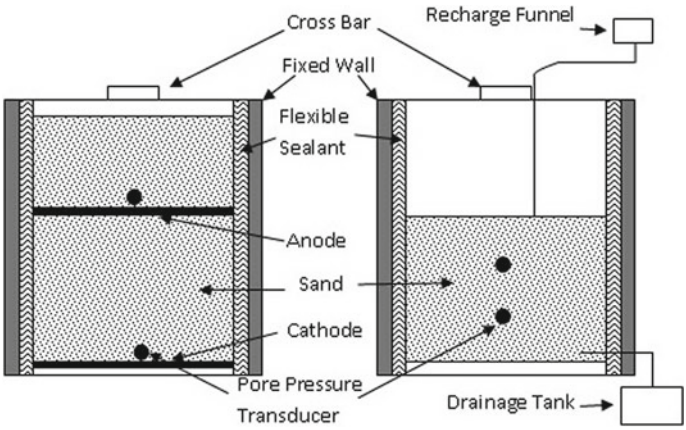

Fig. 6 Test setup for electrolysis (left) and drainage-recharge (right) method of desaturation (Yegian et al. 2007)

Though the effectiveness of the desaturation of soil by air injection method against liquefaction was confirmed by many, the long-term behavior of desaturation is studied by very few. Yegian et al. (2007) and He et al. (2016) carried out some experimental programs for the same. For both the cases, the desaturation persisted for long time when the water is static. But in water flow condition, the soil gets saturated very fast.

3 Case Studies

There are few case studies which report the improvement of the ground against liquefaction in the constructed areas. Yasuda and Harada (2014) reported a case study to improve the residential areas after the 2011 Great East Japan Earthquake. The study reported mechanism of the liquefaction-induced damage to houses and appropriate countermeasures, which were discussed in a technical committee chaired by the author in the Kanto Branch of the Japanese Geotechnical Society (JGS).

Koseki et al. (2015) presented a case study on damage to the houses after Minami-Kurihashi, Kuki City, during the 2011 off the Pacific Coast of Tohoku Earthquake, Japan, due to the sand boiling and liquefaction.

Both the case studies concluded that the groundwater-lowering method is the most promising countermeasure available for the concerned problem.

Another study by Rasouli et al. (2016) reported a case where the runway and the ground around the common ducts of Fukuoka International Airport were improved by application of silica stabilizers without affecting the serviceability of the runway. This study reported the use of newly developed controlled curved drilling.

4 Summary

The main problem which a structure faces due to the foundation soil liquefaction is the settlement of the foundation, which is mostly differential in nature. So a method proposed to countermeasure liquefaction under existing structure must be able to eliminate this settlement.

Again due to the space constraints in the constructed areas, the methods should not use large areas for the machinery setup. Out of the different methods discussed in the previous sections, very few methods are feasible, which can be practically used for the purpose. There is a need for an economic solution for improving liquefaction resistance of soil supporting structures.

References

Adalier K, Pamuk A, Zimmie TF (2004) Earthquake retrofit of highway/railway embankments by sheet-pile walls. Geotech Geol Eng 22(1):73–88

He J, Chu J, Wu S, Peng J (2016) Mitigation of soil liquefaction using microbially induced desaturation. J Zhejiang Univ Sci A 17(7):577–588

Ishihara K, Koga Y (1981) Case studies of liquefaction in the 1964 Niigata earthquake. Soils Found 21(3):35–52

Ishihara M, Okamura M, Oshita T (2003) Desaturating sand deposit by air injection for reducing liquefaction potential. In: Pacific conference on earthquake engineering

Koseki J, Wakamatsu K, Sawada S, Matsushita K (2015) Liquefaction-induced damage to houses and its countermeasures at Minami-Kurihashi in Kuki City during the 2011 Tohoku Earthquake, Japan. Soil Dyn Earthq Eng 79:391–400

Kramer SL (1996) Geotechnical earthquake engineering. Prentice Hall

Marasini NP, Okamura M (2015) Air injection to mitigate liquefaction under light structures. Int J Phys Model Geotech 15(3):129–140

Masakatsu M, Masaho Y, Masaru K (1992) Small scale tests on countermeasures against liquefaction for pipelines using gravel drain system. In: Proceedings of 4th US–Japan workshop on earthquake resistant design of lifeline facilities and countermeasures against soil liquefaction, Buffalo, NY

Mitrani H, Madabhushi SPG (2005) Centrifuge tests investigating inclined grout micro-piles as a method of liquefaction remediation for existing buildings. In: Proceedings of the sessions of the geo-frontiers 2005 congress, ASCE

Mizutani T, Towhata I (2001) Model tests on mitigation of liquefaction-induced subsidence of dike by using embedded sheet-pile walls. In: Proceedings of 4th international conference of recent advances in geotechnical earthquake engineering and soil dynamics, San Diego, USA

Motohashi Y, Yasuhara K, Komine H, Murakami S (2011) Mitigation of existing structure settlement by sheet pile walls when liquefaction. Geo-Frontiers 2011, ASCE, pp 1815–20

Nagao K, Azegami Y, Yamada S, Suemasa N, Katada T (2007) A mirco-bubble injection method for a countermeasure against liquefaction. In: Proceedings of the 4th international conference on earthquake geotechnical engineering, Thessaloniki, pp 25–28

Ohsaki Y (1970) Effects of sand compaction on liquefaction during the Tokachioki Earthquake. Soils Found 10(2):112–128

Okamura M, Teraoka T (2006) Shaking table tests to investigate soil desaturation as a liquefaction countermeasure, Geotechnical Special Publication 145, ASCE, pp 282–293

Okamura M, Ishihara M, Oshita T (2003) Liquefaction resistance of sand deposit improved with sand compaction piles. Soils Found 43(5):175–187

Okamura M, Masaya T, Katsuji N, Nao F, Motoharu J, Takehiko I, Hideaki Y, Emiko N (2011) In-situ desaturation test by air injection and its evaluation through field monitoring and multiphase flow simulation. J Geotech Geoenviron Eng 137(7):643–652

Orense RP, Morimoto I, Yamamoto Y, Yumiyama T, Sugawara K (2003) Study on wall-type gravel drains as liquefaction countermeasure for underground structures. Soil Dyn Earthq Eng 23(1):19–39

Rasouli R, Towhata I, Hayashida T (2015) Mitigation of seismic settlement of light surface structures by installation of sheet-pile walls around the foundation. Soil Dyn Earthq Eng 72:108–118

Rasouli R, Towhata I, Rattez H (2016) Shaking table model tests on mitigation of liquefaction-induced distortion of shallow foundation. In: Proceedings of geotechnical hazards from large earthquakes and heavy rainfalls, pp 463–477

Sáez E, Ledezma C (2015) Liquefaction mitigation using secant piles wall under a large water tank. Soil Dyn Earthq Eng 79:415–428

Sasaki Y, Taniguchi E (1982) Shaking table tests on gravel drains to prevent liquefaction of sand deposits. Soils Found 22(3):1–14

Tokimatsu K, Yoshimi Y (1980) Effects of vertical drains on the bearing capacity of saturated sand during earthquakes. In: Proceedings of the international conference on engineering for protection from natural disasters, Bangkok

Towhata I, Otsubo M, Uchimura T, Shimura M, Liu B, Hayashida T, Taeseri D, Cauvin B (2015) Shaking model tests on liquefaction mitigation of embedded lifeline. In: Perspectives on earthquake geotechnical engineering. Springer, pp 311–41

Watanabe T (1966) Damage to oil refinery plants and a building on compacted ground by the Niigata earthquake and their restoration. Soils Found 6(2):86–99

Yasuda S (2007) Methods for remediation of existing structures against liquefaction. In: Proceedings of the 4th international conference on earthquake geotechnical engineering, Keynote Lecture

Yasuda S, Harada K (2014) Measures developed in Japan after the 1964 Niigata earthquake to counter the liquefaction of soil. In: 10th U.S. national conference on earthquake engineering

Yasuhara H, Okamura M, Kochi Y (2008) Experiments and predictions of soil desaturation by air-injection technique and the implications mediated by multiphase flow simulation. Soils Found 48(6):791–804

Yegian MK, Eseller-Bayat E, Alshawabkeh A, Ali S (2007) Induced-partial saturation for liquefaction mitigation: experimental investigation. J Geotech Geoenviron Eng 133(4):372–380

Zeybek A, Madabhushi SPG (2017) Influence of air injection on the liquefaction-induced deformation mechanisms beneath shallow foundation. Soil Dyn Earthq Eng 97(2):266–276

Zheng J, Suzuki K, Ohbo N, Prevost JH (1996) Evaluation of sheet pile-ring countermeasure against liquefaction for oil tank site. Soil Dyn Earthq Eng 15(6):369–379

Model Tests to Determine Lateral Load Capacity of Helical Piles Embedded in Sand

Shweta Dave and Mohit Soni

Abstract Helical piles are used in civil engineering practice to provide stability against tension, compression, and lateral loads. Present research paper highlights the parametric study of helical piles under lateral loads, through an experimental investigation on model piles embedded in dry sand. Series of lateral load tests were performed with helical piles of diameter 19 mm with number of helices 1 and 2 of embedment ratios 12, 16, and 20, respectively, and the results were compared with plain piles. This research aimed to study the response of helical piles under horizontal loading. Test results revealed that the lateral capacity of helical piles is greater than that of plain shaft piles, and the increase in number of helical plates also increases the capacity of helical piles. The embedment ratio, number of helixes, diameter of helixes, their position on the pile shaft, and soil properties determine the lateral capacity of helical piles. The experimental results are also compared with theoretical model suggested previously for helical pile.

Keywords Helical pile · Lateral loads · Anchors

1 Introduction

Helical piles extensively used in engineering applications consist of one or more helical-shaped circular plates welded to a central steel shaft at a particular spacing ratio. The speedy installation, reusability, instantaneous use against uplift, compressive and lateral loads, and overturning moments are special features over the conventional pile systems. Helical pile is a deep foundation system used for

S. Dave (✉)
Government Engineering College, Gandhinagar 382028, India
e-mail: sdave_1966@yahoo.co.in

M. Soni
Geotechnical Engineering, Applied Mechanical Department, L.D. College of Engineering, Ahmedabad 380015, India
e-mail: mohitsoni250693@gmail.com

R. Sundaram et al. (eds.), *Geotechnics for Transportation Infrastructure*,
Lecture Notes in Civil Engineering 29,
https://doi.org/10.1007/978-981-13-6713-7_42

structures such as pipelines, power transmission towers, monopoles, residential houses, offshore structures, aircraft mooring, tunnels, and suspension bridges. Although the use is increasing, the proper design and effect of helix parameters on the ultimate lateral loads are still under investigation. Figure 1 shows the typical laboratory test setup of helical pile.

Puri et al. (1984) developed a theoretical model to estimate the lateral load capacity of helical anchor pile–soil system; they concluded that lateral load capacity of helical anchor pile is controlled almost exclusively by extension shaft for depths greater than 3–5 times the critical relative stiffness factor R or T. In the theoretical model, they incorporated the modified model of Matlock and Reese (1960) to yield lateral deflections at ultimate lateral loads as determined from the test data in sands and clays. They validated their model by comparing the results with those of previously published full-scale lateral load tests.

Prasad and Narasimha Rao (1996) performed laboratory tests on helical piles with 2 and 4 helices inserted in saturated clay. They proved that lateral capacity of helical piles increases from 1.2 to 1.5 times that of plain shaft pile, and it increases with embedment depth and shear strength of the soil. Narasimha and Prasad (1993) proved that the load-carrying capacities of the helical anchors in clays are controlled by the spacing of the helical plates. They reported the need for laterally loaded helical piles.

Mittal et al. (2010) performed an experimental investigation on laterally loaded screw anchor pile in dry sand with a different number of helices in continuation and lateral load applied at different heights from the soil surface. The embedment length also varied, and static lateral load is applied on screw anchor piles. A theoretical model is developed for predicting lateral load capacity of screw anchor piles in sand. The test is also validated by means of field test. The author proved that lateral load increases as the number of helices and embedment depth increases.

Abdrabbo and El Wakil (2016) performed lateral load test on helical piles with different helix diameters, numbers, and spacing. They proved that lateral load capacity is dependent upon soil properties, the helix diameter, number, and spacing. They reported that most economic number of helices is 2 and the most effective spacing ratio is 3.

Fig. 1 Laboratory test setup

To study the parametric behavior of helical pile under lateral loads, an experimental investigation has been conducted on small-scale model piles of mild steel embedded in dry sand. The tests are performed on plain shaft piles, single-helix piles, and double-helix piles at a spacing ratio 3 (*S*/*d* ratio, spacing between helical plate/diameter of plain shaft). The lateral load is applied at an eccentricity 100 mm above the soil surface. The embedment ratio (*L*/*d ratio*, embedment length/diameter of pile shaft) is 12, 16, and 20. The experiment results are also compared with the empirical equation developed by Mittal et al. (2010).

2 Experimental Investigation

2.1 Test Program

A total of nine lateral load tests were conducted on model piles in sand at a relative density of 60%.

2.2 Test Setup

Model pile load tests were conducted on sand in the Geotechnical Laboratory, Applied Mechanics Department, L.D. College of Engineering, Ahmedabad. The experimental tests are performed on model piles in a cylindrical test tank with 600.0 mm diameter and 650.0 mm height. The tank dimensions were taken more than three times the diameter of the helix plates to avoid the boundary condition effect. A pile holding assembly is used to facilitate the horizontal loading at the top of model pile. The assembly is also connected with proving ring, and simultaneously, a mechanical jack is connected horizontally to the loading frame as shown in Fig. 2. The lateral load is applied by using mechanical jack. Two dial gauges of accuracy 0.01 mm are supported on the steel plate of pile holding assembly to measure the horizontal displacement.

2.3 Properties of Sand

The sand used was locally available in Madhumati River in Gandhinagar. The soil was poorly graded sand SP as per IS soil classification system. The index and engineering properties of sand used for the study are shown in Table 1. For all tests, the sand was compacted at the unit weight of 17.4 kN/m^3 (60% relative density). To achieve uniform density, the surface vibration technique, with the surface vibrator device, was used. The soil bed was prepared by compacting the dry sand in layers, each 50 mm thick up to 650 mm height.

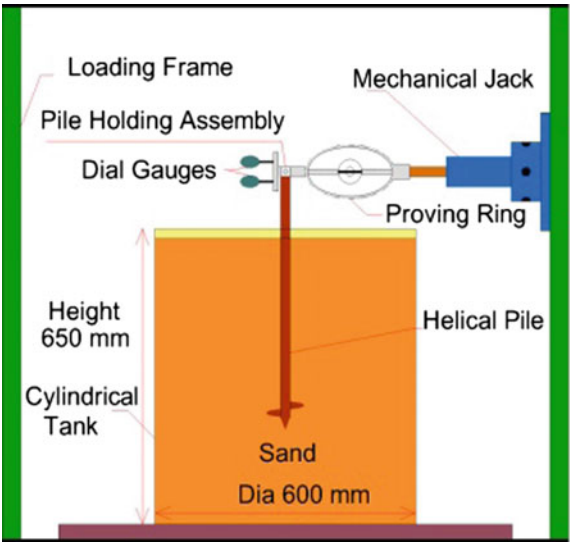

Fig. 2 Schematic diagram of test setup

Table 1 Physical properties of sands

Test	IS code	Determination
Soil classification as per IS	IS: 2720 (Part 4) 1983	C_u = 2.90 C_c = 1.117 ***SP***
Specific gravity (G)	IS: 2720 (Part 3) 1980	G= 2.67
Relative density I_d	IS: 2720 (Part 14) 1983	I_d = 60% $\gamma_{dmin.}$ = 14.8 kN/m^3 $\gamma_{dmax.}$ = 19.6 kN/m^3
Direct box shear (C and $\varphi°$)	IS: 2720 (Part 13) 1986	C = 0 $\varphi°$ = 31

2.4 Model Pile and Instrumentation

Mild steel helical piles with 19 mm diameter shaft and 50.5 mm diameter of helix (Fig. 3) were used in the experiment. The helixes were fabricated from steel plates of thickness 2 mm. The helixes are machined to give external diameter of D 50.5 mm with a fixed pitch, p, equal to the pile diameter, d, 19 mm. The helixes are welded accurately to the pile. The pile lengths considered are 328 mm, 404 mm, and 480 mm corresponding to embedment ratios (L/d ratio) of 12, 16, and 20, respectively, so a total of 9 pile samples, 6 helical piles, and 3 plain shaft piles are prepared. The lateral load is applied at an eccentricity (e) of 100 mm from the soil surface. The tests are performed

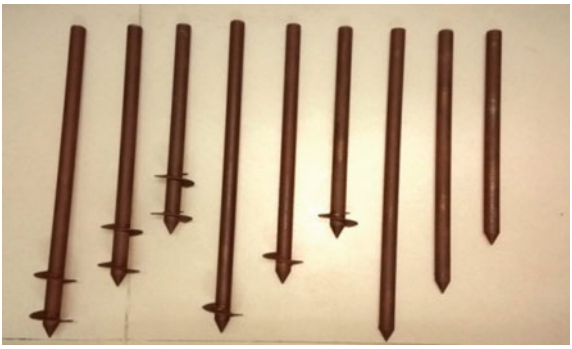

Fig. 3 Model piles

on plain shaft piles, single-helix piles, and double-helix piles at a spacing ratio (*S*/*d* ratio) 3, which is 57 mm. All the piles had a conical end of an apex of 60°.

2.5 Pile Installation

After the soil bed had been prepared, the pile was slowly screwed into the soil bed with enough downward force until the required depth of embedment was achieved. The verticality of the pile was checked with a plumb after every 50 mm of penetration. The pile head was free and kept 100 mm above the sand surface to make the provision for application of lateral load. The pile lengths of 328, 404, and 480 mm were driven at depths of 228, 304, and 380 mm, respectively, from the sand surface.

2.6 Test Procedure

The lateral load was applied at the top of the pile embedded in the sand by rotating the mechanical jack. These loads were applied in increments. The observation of mechanical dial gauges was recorded when there was no further increase in lateral displacement corresponding to the applied load. The ultimate lateral load was calculated at 12 mm displacement.

3 Test Results and Discussions

A series of lateral load tests were carried out on plain shaft pile, single-helix pile, and double-helix pile. Typical load–displacement curves for the single-helix pile $n = 1$ is shown in Fig. 4. These curves correspond to three embedment ratios (*L*/

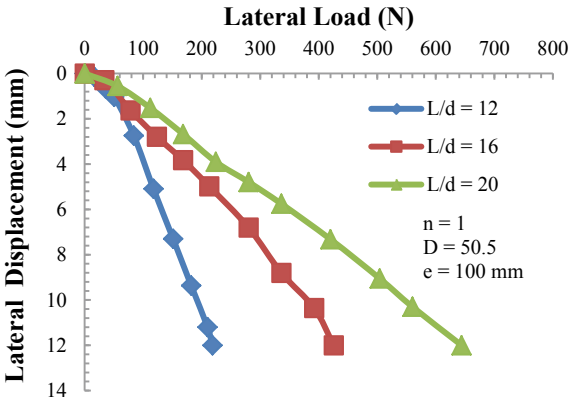

Fig. 4 Load displacement curve for variable *L/d*

d = 12, 16, and 20), and the ultimate capacities were 218.4, 425.6, and 644 N, respectively, at an eccentricity of 100 mm.

It has been clearly observed that the ultimate lateral load capacity of pile increases with the addition of helical plates.

The ultimate lateral load is considered at the point where displacement attained by the pile head is 12 mm. Typical load displacement curves are plotted for the pile at a different number of helical plates (*n* = 1,2) and plain shaft pile at an eccentricity (*e* = 100 mm). The embedment length of pile for (*L/d* = 12) was 228.0 mm. The corresponding ultimate lateral capacities were 156.8, 218.4, and 296.8 N as shown in Fig. 5. The embedment length of pile for (*L/d* = 16) was 304.0 mm. The corresponding ultimate lateral capacities were 322.0, 425.6, and 518.0 N as shown in Fig. 6. The embedment length of pile for (*L/d* = 20) was 380.0 mm. The corresponding ultimate lateral capacities were 546.0, 644, and 716.8 N as shown in Fig. 7 (Table 2).

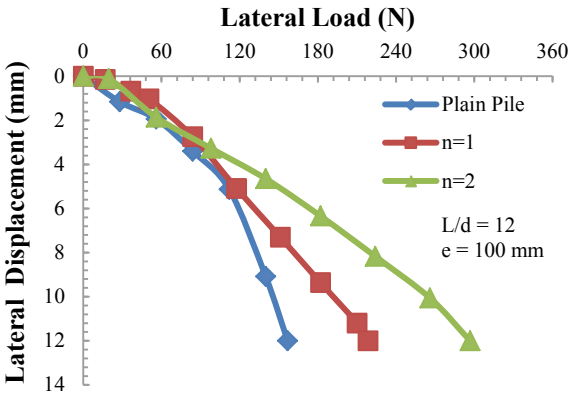

Fig. 5 Load displacement curve showing variation for number of helixes (*n*) at *L/d* = 12

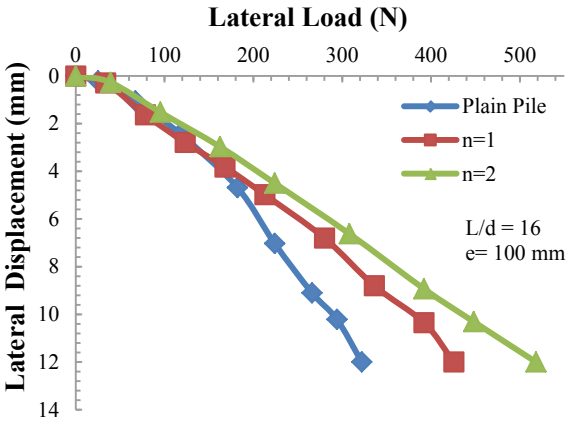

Fig. 6 Load displacement curve showing variation for number of helixes (n) at L/d = 16

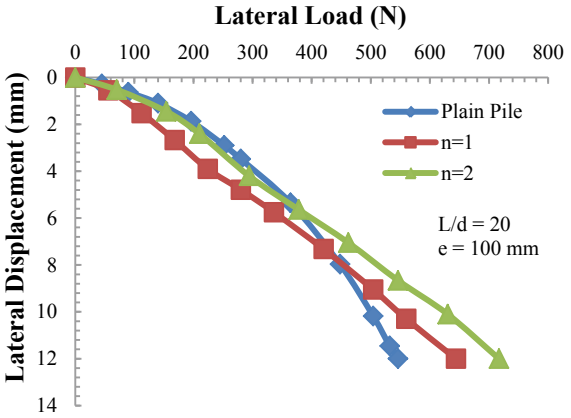

Fig. 7 Load displacement curve showing variation for number of helixes (n) at L/d = 20

Table 2 Ultimate lateral load for helical pile

e = 100 mm	Ultimate lateral load (N)		
	No. of helical plates (n)		
L/d	0	1	2
12	156.8	218.4	296.8
16	322.0	425.6	518.0
20	546.0	644.0	716.8

It is observed that with an increase in embedment ratio, i.e., increase in embedment length, the ultimate lateral load capacity of helical pile increases. The percentage increase in lateral load capacity for increase in embedment ratio (L/d) from 12 to 16 is more than the percentage increase in lateral load capacity for increase in

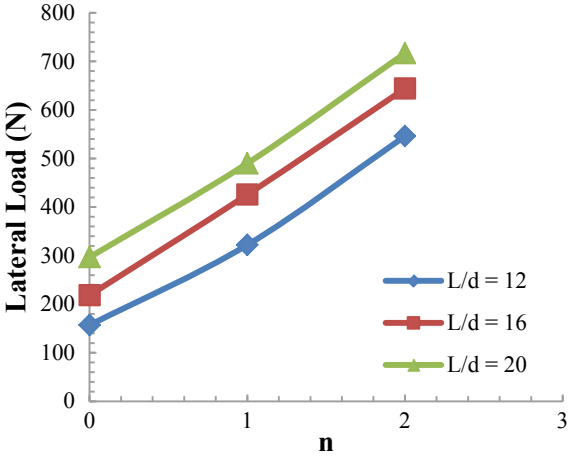

Fig. 8 Ultimate lateral load versus number of plates (*n*)

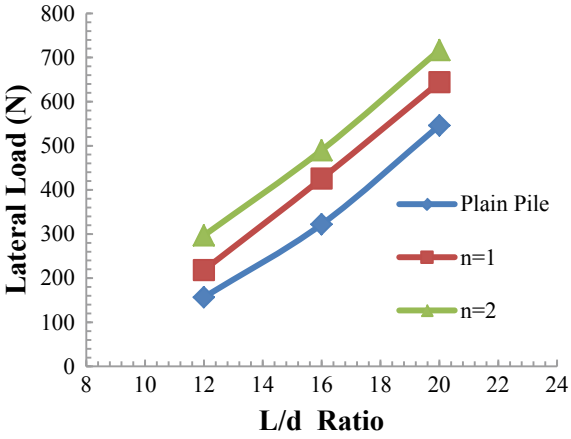

Fig. 9 Ultimate lateral load versus embedment ratio (*L*/*d*)

embedment ratio (*L*/*d*) from 16 to 20 as is demonstrated in Fig. 8. From the plotted relationship, it is also observed that although the embedment length increases, helix had no increase in the lateral capacity as it gives small embedment length.

With an increase in number of helical plates (*n*), the lateral load capacity of helical pile increases. Further, it is observed that the percentage of increase in lateral load capacity for increase in *n* from 0 to 1 is more than the percentage of increase in lateral load capacity for increase in *n* from 1 to 2 as is demonstrated in Fig. 9.

Table 3 Comparison of lateral load capacities from experimental results with the predicted results of empirical equation

e = 100 mm	Ultimate lateral load (N)		
	No. of helical plates		
L/d		n = 1	n = 2
12	Exp.	218.4	296.8
	Theor.	163.48	198.99
16	Exp.	425.6	518.0
	Theor.	329.0	400.0
20	Exp.	644.0	716.8
	Theor.	565.96	688.90

4 Theoretical Approach

Mittal et al. (2010) have developed an empirical equation for calculating the ultimate lateral load capacity of helical pile. The equation is used for comparison between experimental results and theoretical results. Experiment results are found to be quite high as shown in Table 3.

$$\frac{Q_1}{\gamma d^3} = A \times \left(\frac{L}{d}\right)^{2.431} \times (n)^{0.2836} \times \left(\frac{H_{\text{ag}}}{B}\right)^{-0.6284}$$

A constant from regression process (A = 5.007),
Q_1 ultimate lateral load (kN),
γ unit weight of soil (N/mm^3),
d diameter of pile shaft (mm),
B diameter of helical plate (mm),
L embedded length of pile (mm),
n number of helical plates, and
H_{ag} height above ground (mm).

5 Conclusion

- From the present investigation on helical piles in sand, the following conclusion can be drawn.
- Helical pile capacity is more than plain pile, and as the number of helical plates increases, the capacity of helical pile also increases.
- The capacity of helical pile increases as embedment length increases up to a particular length after which it increases moderately.

- When embedment length is less, then the influence of helical plate on lateral capacity is more, but as embedment length increases, then the same size of helical plate influence reduces on lateral capacity.

Acknowledgements The authors are highly thankful to Dr. Satyendra Mittal, B. Ganjoo, and Sunny Shekhar for providing theoretical approach to laterally loaded screw anchor piles.

References

Abdrabbo FM, El Wakil AZ (2016) Laterally loaded helical piles in sand. Alexandria Eng J 55:3239–3245 (Elsevier)

Matlock H, Reese LC (1960) Generalized solutions for laterally loaded piles. ASCE J Soil Mech Found Div 86(SM5):63–91

Mittal S, Ganjoo B, Shekhar S (2010) Static equilibrium of screw anchor pile under lateral load in sand. Geotech Geol Eng 28:717–725

Narasimha S, Prasad Y (1993) Estimation of uplift capacity of helical pile anchors in clay. J Geotech Eng ASCE 119(2):352–357

Prasad YVSN, Narasimha Rao S (1996) Lateral capacity of helical piles in clays. J Geotech Eng 122(11):938–941

Puri VK, Stephenson RW, Dziedzic E, Goen L (1984) Helical screw anchor piles under lateral loading. Laterally Loaded Deep Foundations: Analysis and Performance, ASTM STP 1013:194–213

Overcoming Geotechnical Challenges in Rail and Metro Projects Using Ground Improvement

Jonathan Daramalinggam and Madan Kumar Annam

Abstract In rail and metro construction, a variety of encountered geotechnical challenges need to be overcome. These arise from ground conditions, the presence of nearby structures and the choice of construction technique. Often, ground improvement techniques can be employed effectively to address these challenges. Using examples from India, Australia, Malaysia, and Singapore, this paper will demonstrate the use of a variety of ground improvement techniques adopted in transportation infrastructure projects. Examples include the use of compaction grouting to facilitate the construction of a NATM tunnel though partially loose soils in the New Delhi metro project, compensation grouting to limit and prevent damage to overlying structures during TBM tunneling works in the Perth metro project, rock fissure grouting in limestone to limit water ingress into excavation pits during metro construction in Kuala Lumpur, Malaysia, and the use of deep soil mixing and jet grouting as part of a cut-and-cover tunnel construction in Singapore.

Keywords Ground improvement · Compaction grouting · Compensation grouting · Rock fissure grouting · Deep soil mixing · Jet grouting

1 Introduction

Modern rail and metro projects face a variety of challenges. For new inter-city rail projects, the track alignments encounter a variety of ground conditions, inevitably some of which are unfavorable. Combined with the more stringent track settlement

J. Daramalinggam (✉)
Keller Asia Pacific Limited, 72 Anson Road, #11-03, Anson House, Singapore 079911, Singapore
e-mail: jonathan@kellersing.com.sg

M. K. Annam (✉)
Keller Ground Engineering India Pvt. Ltd., 7th Floor, Centennial Square, 6A, Dr. Ambedkar Road, Kodambakkam, Chennai 600024, India
e-mail: madankumar@kellerindia.com

R. Sundaram et al. (eds.), *Geotechnics for Transportation Infrastructure*, Lecture Notes in Civil Engineering 29,
https://doi.org/10.1007/978-981-13-6713-7_43

tolerances required by modern high-speed trains, settlement control in difficult ground conditions becomes critical. Nowadays, older tracks are being upgraded for higher speed trains, and in some instances, the ground needs to be strengthened while keeping the existing trains in service. In urban metro projects, challenges include underground construction, tunneling, deep excavations, proximity to existing utilities and buildings, soft or permeable soils, existing underground structures, and obstructions. For some of these geotechnical challenges, ground improvement techniques provide an optimal solution.

Ground improvement (also known as ground modification or soil improvement) refers generally to any technique or process that improves the engineering properties of the soil mass (Raju and Daramalinggam 2012). Primarily, engineers are interested in improving the shear strength, stiffness, or permeability of the soils via ground improvement. Sometimes, however, engineers aim to directly induce or prevent movements on structures using ground improvement, for example, using compensation grouting.

Ground improvement usually uses the following principles.

1. Chemical modification, e.g., permeation grouting, deep soil mixing, jet grouting
2. Densification (or compaction), e.g., vibro compaction, dynamic compaction, compaction grouting, impact rolling
3. Reinforcement, e.g., vibro stone columns, rigid inclusions, dynamic replacement columns
4. Consolidation, e.g., prefabricated vertical drains, vacuum consolidation, vibro stone columns.

Kirsch and Bell (2012) provide more details on various ground improvement techniques.

A very interesting case study of how ground improvement techniques was used in a large inter-city rail project is Malaysia's Ipoh-Padang Besar Double Tracking project. The project involved the double tracking and electrification of 329 km of rail line, bridge construction, stations, road-over-bridges, and various other ancillary works. With differing ground conditions and stringent track settlement requirements, different ground improvement methods were adopted in this project. Lee et al. (2013) describe some of the ground improvement methods that were adopted in this project. These included driven piles at transition zones, the use of vibro stone columns, installation of prefabricated vertical drains, the use of geotextiles for basal reinforcement, and removal and replacement of soft soils.

This paper presents four selected case histories from Asia and beyond, illustrating how ground improvement, and in particular grouting techniques have been used to overcome various challenges in metro projects.

2 Case Histories

2.1 *Compaction Grouting for NATM Tunnel Construction, New Delhi Metro*

The compaction grouting technique uses displacement of the in situ soil to improve its engineering properties. This involves slow injection of low-mobility grout into the loose ground, displacing the soil particles laterally, hence compacting the overall soil mass. An appreciable increase in overall density can be achieved by correctly spacing grout points and controlling the grouting process. This method is normally used to improve non-cohesive deposits and improve load bearing behavior of the soil. Sometimes, it is also used to lift and reinstate structures that have settled excessively. The grout material comprises of cement mortar (cement, water, and sand) mixed at a batching plant and delivered to site. The slump of this "compaction grout" is normally in the range of 120–150 mm. The process of compaction grouting is shown in Fig. 1 and involves three major steps.

- Installation of the grout pipe
- Injecting the compaction grout, forming bulbs
- Staged grouting to achieve uniform compaction.

As part of Phase 2 of the New Delhi Metro, a NATM tunnel was planned near Saket Station. The crown of the tunnel was about 9 m below ground, but the presence of overlying loose sandy silt complicated the process. The alignment ran under, an abandoned nallah channel that had been excavated and filled in with locally available sandy silt (Fig. 2). This resulted in inconsistent SPT N values ranging from 4 to 17.

The NATM tunnel was supposed to be excavated through silty sands of SPT N values ranging from 20 to 30 (Fig. 3). The loose overlying soils were not

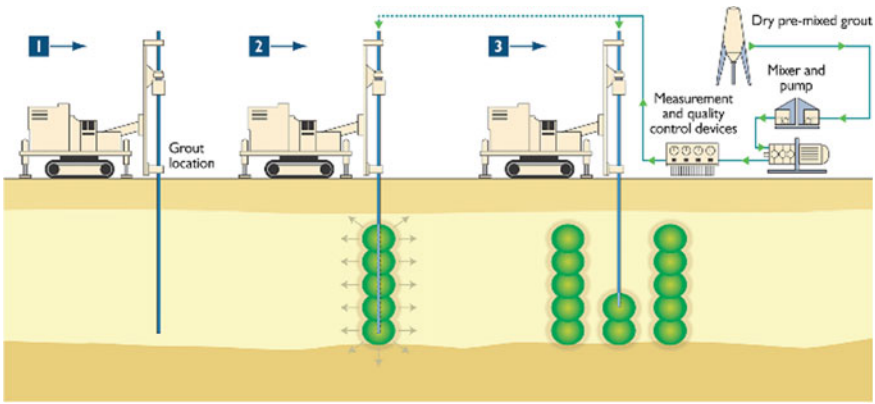

Fig. 1 Process of compaction grouting

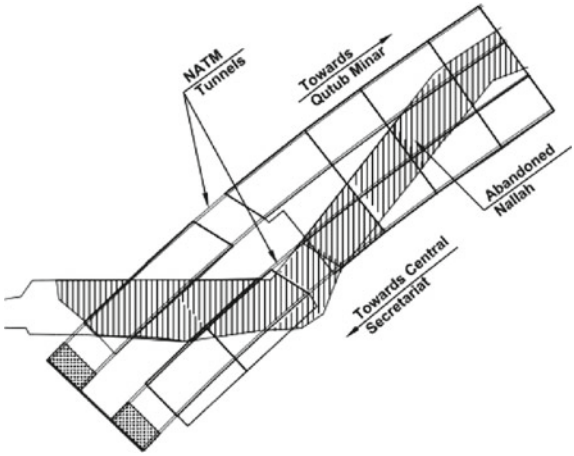

Fig. 2 Proposed NATM tunnel alignment

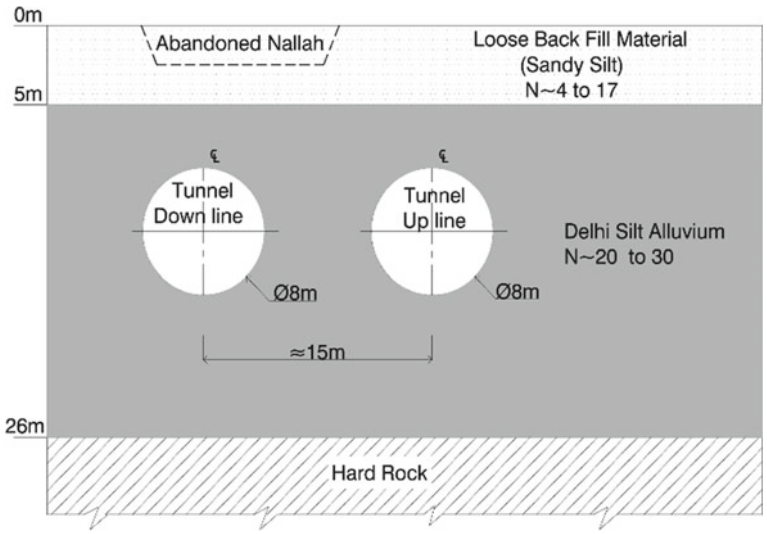

Fig. 3 Typical cross section of the twin tunnels

considered adequate for the NATM method, potentially causing collapse during tunneling. Thus, compaction grouting was employed to increase the density and strength of the sandy silt.

Stinger rods were drilled into the ground down to approximately 8 m, just below the bottom of the stratum to be improved. Then, the low-slump grout was pumped slowly, under pressure. The grout consists of cement, water, sand, bentonite, and a

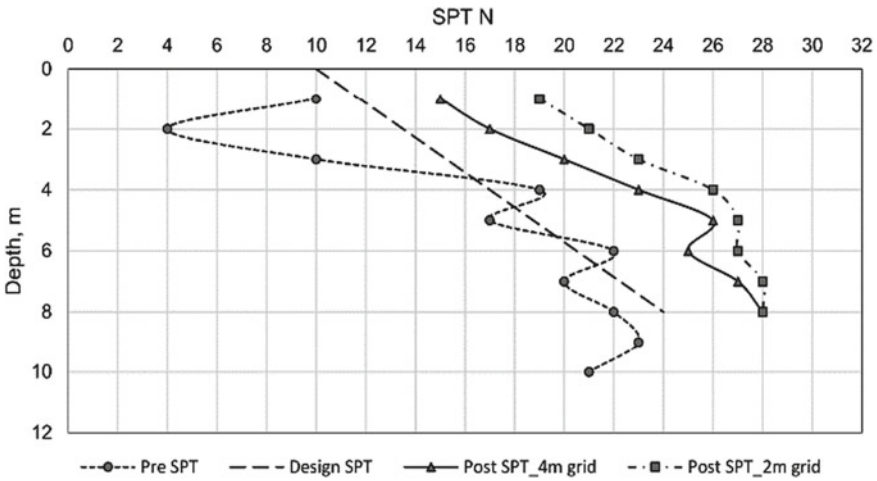

Fig. 4 Confirmatory testing through pre- and post-SPTs

plasticizer. A low water cement ratio of 0.5 is used. The target was to create a grout bulb with a diameter of 0.4–0.5 m. In the main works, about 400 m^3 of grout was pumped into the ground.

Pre- and postinvestigation with boreholes (for SPT) were drilled to assess improvement and SPT N values indicated satisfactory results as illustrated in Fig. 4. The project was completed successfully, and metro rail line is operational.

2.2 Compensation Grouting for a Metro Project in Perth, Australia

One of the most challenging processes in urban metro construction is tunneling beneath existing buildings. Tunnels are necessary because of space constraints in built-up urban environment, and it is not always possible to align the tunnel along a road. Sometimes, the crown of the tunnel comes close to the foundations of a building, with the risk of inducing settlement and damaging the buildings. Older buildings are particularly susceptible to such damage.

When the city of Perth (Australia) was building its metro system, one portion of the tunnel drive called for tunneling directly under a ground of four existing buildings with a total footprint of about 200 m^2. The four buildings (along William Street, at a busy shopping area) were founded on loose-to-medium dense sand and had different structural systems (reinforced concrete, brick, timber frames, steel frames). This cluster of buildings was predicted to experience a maximum of 25-mm settlement during the two tunnel drives. This magnitude of settlement (some of it differential) would induce unacceptable cracks on the structures.

Compensation grouting was selected as the preferred method of protecting the buildings from excessive settlements. The goal of the compensation grouting scheme was to.

- Limit settlements of individual footings to 10 mm
- Limit differential settlements across any building to 1:500
- Limit heave to 5 mm.

Compensation grouting utilizes TAMs (tube-a-manchette), pipes with grout holes at selected intervals, with rubber sleeves, to repeatedly inject cement-bentonite grout to firstly pre-heave the structure slightly and subsequently actively heave the ground as the tunnel drive is ongoing. The objective was to compensate any settlements induced by the tunneling. By using a double packer, grout is injected through a specific set of grout holes, closest to the point of interest. Because the grout tends to fracture the soil matrix, the process is sometimes known as "Soilfrac."

The TAMs were installed from two 4-m-diameter access shafts in the middle of William Street (Fig. 5). A total of 57 TAMs were installed between July and October in 2005, ranging in length from 23 to 50 m (Fig. 6).

Various instruments (building settlement markers, surface settlement markers, wireless electrolevels, and optical prisms with automatic total stations) were used to provide feedback to the grouting and tunneling crews.

As normal with compensation grouting, the works were divided into two distinct phases. In the pre-conditioning phase, the objective was to heave the structures about 3 mm. The grouting was carried out in several passes until no significant relaxation is observed. This implies that the ground is "tight" and will respond properly during the active grouting phase. Usually, a high level of redundant grout holes is kept, in case of any blocked holes. In this project, during the pre-conditioning phase, only 1 out of 4 holes were used.

In the active phase lasting two weeks (i.e., during the tunnel drives), grouting was done through selected points, based on the feedback from the instruments. At the end of both TBM drives, building settlements were kept to within 5 mm. Additional details about this project can be found in Williams and Nobes (2007).

2.3 Rock Fissure Grouting for the Klang Valley MRT, Kuala Lumpur, Malaysia

2.3.1 Introduction

The Sungai Buloh–Kajang line of the Klang Valley Mass Rapid Transit (KVMRT) runs partly though a meta-sedimentary formation called "Kenny Hill" and partly through Kuala Lumpur Limestone. About 9.5 km of the 51 km line is underground, passing through the heart of Kuala Lumpur. Construction in the limestone

Fig. 5 Access shafts in the middle of William Street. The fan of TAMs spreads from the shaft to the left of the photograph

formation poses the greater challenge. Tan (2005) summarizes the characteristics of Kuala Lumpur Limestone as well as the challenges posed by the formation. Interestingly, Tan (2005) lists various sinkhole incidents in Malaysia and notes that most were triggered by construction activities. Using experience gained from previous tunneling works (Raju and Yee 2006), engineers were able to plan grouting programs to minimize the negative impact of the tunneling and excavation activities. The main activities that were of concern in the KVMRT project were

- Station box excavation
- Cutter-head interventions
- Escape shaft excavations
- Tunneling close to sensitive structures with low rock overburden.

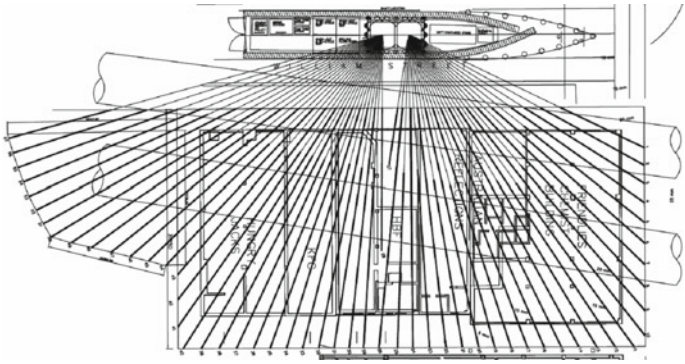

Fig. 6 "Fan" of TAMs starting from the access shaft, spreading out to cover the footprint of the four buildings

A variety of ground improvement techniques were employed in the KVMRT project. These included jet grouting, compaction grouting, and deep soil mixing. Only rock fissure grouting is described in here. Sreenivas et al. (2016) provide more details on the other grouting schemes.

2.3.2 Geotechnical Challenges

Kuala Lumpur Limestone is characterized not only by underground cliffs, overhangs, and pinnacles but also interconnected solution channels and some areas of fractured rock. The overburden soil is typical loose silty sand or soft silty clays. The groundwater table is generally high, often just 1–3 m from ground surface.

The presence of solution channels and cavities means that as an excavation proceeds (with the soil retained by a secant pile wall or deep soil mixing wall), groundwater will be drawn down from the surroundings and enter into the excavation pit, both causing problems for the excavation works and resulting in settlement of the ground surrounding the pit. While simply pumping the water out might be a solution for the excavation itself, a drawdown of the water table will result in damage to neighboring properties unacceptable in Kuala Lumpur.

The same ground profile also means that tunnel boring activities, particularly cutter-head interventions, pose a risk of sinkhole creation or slurry "blowouts" at ground surface.

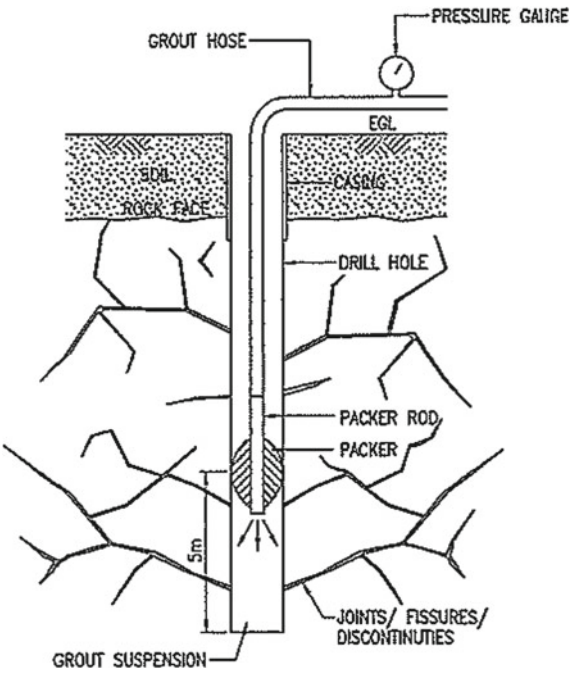

Fig. 7 Grouting through a single packer

2.3.3 Rock Fissure Grouting as a Solution

The process of rock fissure grouting in Kuala Lumpur Limestone can be summarized as follows:

- Drilling through the overburden soil with conventional wash boring, and setting a steel casing down to the rock head.
- Drilling through the rock, usually with a down-the-hole-hammer.
- Setting a single packer and grouting (usually with cement-bentonite) in 5 m ascending stages (Fig. 7).
- Grouting is stopped when either (a) a pre-determined maximum pressure is reached for a particular duration, with a reduced flow rate, or (b) a pre-determined volume of grout has been pumped, without pressure building up.

During drilling in the event that fractured and unstable rock is encountered before reaching the target depth, drilling is suspended at the rock mass is grouted. The grout is allowed to set for 24 h before drilling resumes.

For the KVMRT job, rock fissure grouting was used to (a) form a grout "curtain" around an excavation pit, (b) form a grout "plug" at the base of an excavation (Fig. 8), or (c) form a grout "block" for a cutter-head intervention (Fig. 9).

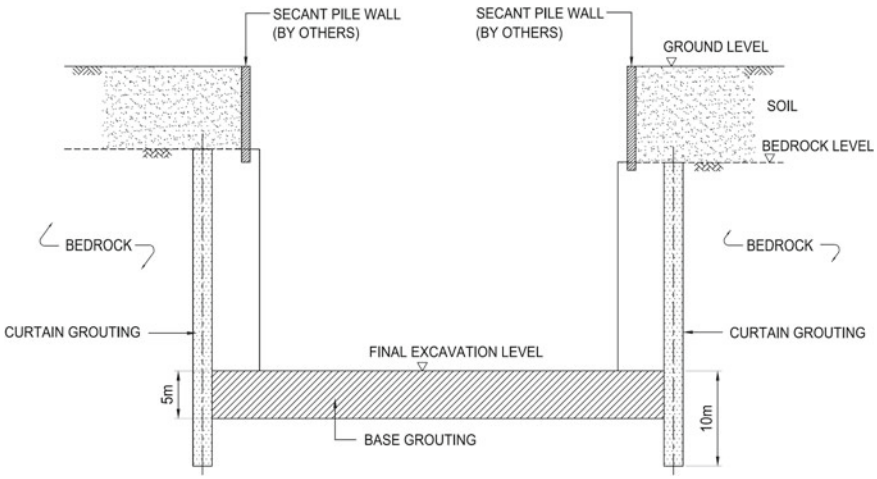

Fig. 8 Base grouting to form a grout "plug"

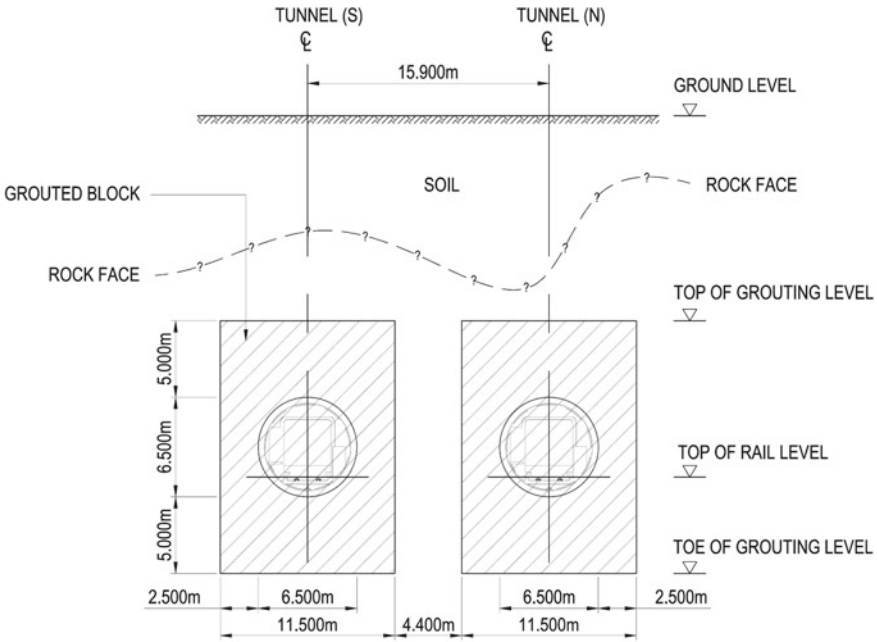

Fig. 9 Grout "block" for cutter-head interventions

The "closure" method was used to provide a balance between robustness of the grouting method and cost of the solution (Fig. 10). For a grout curtain, primary holes were drilled 4 m apart, down to 10 m below final excavation level. The "curtain" is set 5 m behind the retaining wall and excavation face (Fig. 11).

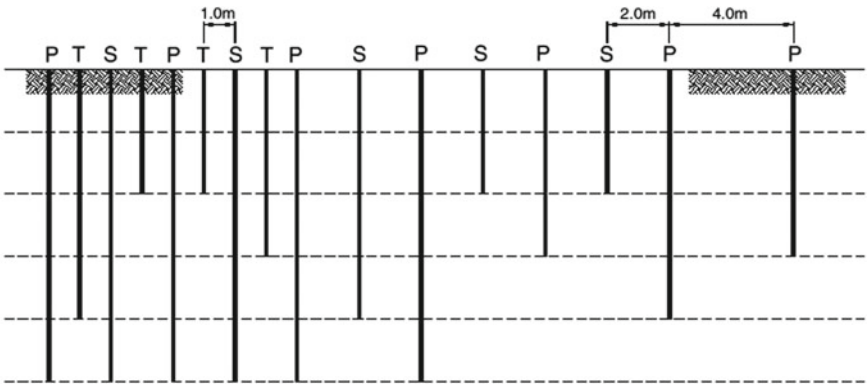

Fig. 10 Closure method—primary, secondary, and tertiary grouting points

Fig. 11 Drilling rig setting up 5 m behind retaining wall

Grouting proceeds upwards until all the limestone is grouted. As grouting proceeds, grout volumes are monitored closely. If grout takes are high, it indicates the presence of solution channels. Secondary holes are drilled between the primary holes (meaning the hole-to-hole spacing becomes 2 m), and grouting is carried out. If grout takes are still high, a set of tertiary holes are drilled. This progressive approach to drilling and grouting results in the identification and treatment of areas with fractures and solution channels, slowly closing off any pathways water might have into the excavation.

For a grout "plug" at the base of an excavation, primary holes are drilled on a wide 10 m × 10 m grid, and grouting carried out from 5 m below the final excavation level up till just above the final excavation level. As with a grout curtain, secondary

Fig. 12 Ariel photo of Tun Razak Exchange station in construction, after rock fissure grouting

and tertiary points are added according to the measured grout takes. There are occasions where cavities or large fissures (rather than solution channels) are intercepted. This is usually identified by very high grout takes. Here, engineers might vary the thickness of the grout mix, perhaps switching to a thick mortar-like mix.

Keller conducted rock fissure grouting for two station boxes, namely Cochrane Station (21 m wide, 176 m long, 35 m deep) and Tun Razak Exchange Station (30 m wide, 168 m long, 45 m deep), after which other construction activities could proceed (Fig. 12). Rock fissure grouting for cutter-head interventions was carried out in a similar way. For a typical tunnel diameter of 6.5 m, a grout "block" 11.5 m wide, 16.5 m high was created (Fig. 9).

2.4 Deep Soil Mixing and Jet Grouting for an Overrun Tunnel in Singapore

2.4.1 Introduction

For the extension of Singapore MRT network, a large portion of which is underground, numerous excavations were made. Kumarasamy (2014) outlines the geology of Singapore along one of the major metro lines and its impact on choice of construction method, particularly the type of earth retention system. Some of these excavations were made in Singapore's Kallang Formation, which consists of a thick deposit of marine clay overlying fluvial and cemented sands or silts.

The Marina Bay South station is situated in reclaimed land at the southern tip of the island. At this location, the ground consists of about 12–13 m of loose silty sand (reclamation fill), 7–8 m of soft marine clay, follow generally by stiff to hard sandy

silts. As the final station on the North–South line, an overrun tunnel was required for safety and operational reasons. The tunnel was to be constructed by a cut-and-cover method, supported by 52-m-deep diaphragm walls and struts.

2.4.2 Geotechnical Challenge

Because the excavation was partly in the reclaimed fill and partly in the soft marine clay, diaphragm wall bending moments in the soft clay was excessive. To reduce the bending moments and control lateral deflections, the consultants specified a 5-m-thick layer of improved soil to act as a strut (Fig. 13).

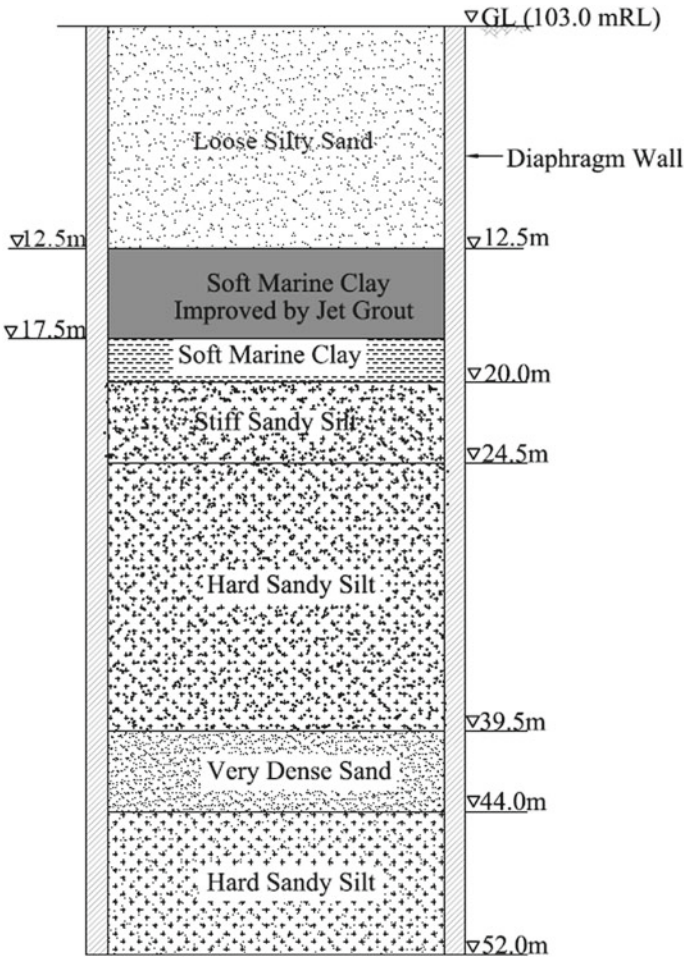

Fig. 13 Schematic of soil improvement

The contract for the soil improvement was split between several contractors, with Keller being awarded a 40 m × 20 m portion in plan.

In order to create an effective strut, the soil improvement slab had to be generally continuous, formed of overlapping columns, and connected fully with the diaphragm walls. Work was made more complicated at this area of the site because of two old trial sections of deep soil mixing, existing jet grout columns, and the presence of a 1.8-m diameter test pile.

2.4.3 Deep Soil Mixing and Jet Grouting Solution

The way to economically create this slab of improved soil was to utilize a combination of 0.9–1.3 m diameter jet grout columns (to form good contact with the diaphragm walls, the test pile, existing deep soil mixing, existing jet grouting) and twin 0.85-m-diameter deep soil mixing (DSM) columns. In theory, it would be possible to do the entire slab using jet grouting. However, due to the generation of spoil and the amount of cement used in the jet grouting process, the cost of producing a cubic meter of jet grouting in marine clay was about double the cost of producing a cubic meter of deep soil mixing. Initially, the plan was to create about 80% of the slab volume of deep soil mixing, utilizing about 20% jet grouting only to make the "contact" with the existing soil improvement and the diaphragm walls. However, due to breakdowns to the DSM rig, about 50% of the slab had to be done with jet grouting (Fig. 14).

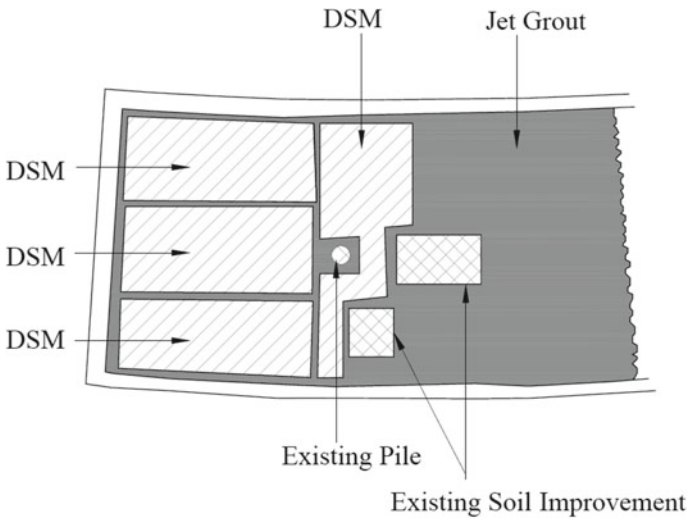

Fig. 14 DSM and jet grouting layout

Fig. 15 Deep soil mixing rig with overlapping twin paddles

Key operational parameters for deep soil mixing (Fig. 15) are summarized below:

- Column diameter: 0.85 m
- Water/cement ratio of grout mix: 1.0–1.5
- Grout density: 1.36–1.5 (checked with a hydrometer)
- Target average cement content: Greater than or equals to 280 kg/m^3
- No. of mixing cycles: 3
- Grout pressure: 4–5 bars.

Key operational parameters for jet grouting (Triple fluid system, Fig. 16) are summarized below:

- Column diameter: 0.9, 1.2, and 1.3 m
- Water/cement ratio of grout mix: 0.65–0.80
- Grout density: 1.59–1.68
- Water pressure: 360–420 bars
- Grout pressure: 10–15 bars
- Air pressure: 1–3 bars.

Fig. 16 Triple-fluid jet grouting

2.4.4 Quality Control and Testing

Quality was controlled by monitoring and testing during construction as well as post-construction testing. Key QA steps during construction are as follows:

- Ensuring positional tolerance of column
- Monitoring of grout density
- Inspection of grout batching records
- Control of key operational parameters
- Inspection of rig construction records.

EN 14679:2005 provides more details of quality control of deep soil mixing works and EN 12716:2001 provides more details of quality control of jet grouting works.

Post-construction testing for both deep soil mixing and jet grouting was done in accordance with the Land Transport Authority's contract specifications. The key QC requirements are summarized below.

- After 28 days full-length vertical coring at the center of the column and outer ring of the column, or at the overlap between columns, minimum total core recovery (TCR) required was 85%
- Cores should have a minimum diameter of 50 mm
- For DSM, 1 core should be taken every 1,000 linear meters. For jet grouting, 4 cores should be taken for every 1,000 m^3 of soil improvement
- Unconfined compressive tests (UCS) showing an equivalent undrained shear strength, cu, greater than of equals to 300 kPa (i.e., UCS value of 600 kPa) and a Young's Modulus of 150 MPa.

In addition, for soil improvement performed by jet grouting, additional boreholes with SPT were required.

The test results are summarized below:

- For the DSM areas, 5 full-length cores were drilled, with average core recovery of 92%. A total of 20 UCS tests were carried out, with the average UCS value 2.4 MPa and average Young's Modulus value of 546 MPa.
- For the jet grouting areas, 10 full-length cores were drilled, with average core recovery coincidentally of 92%. A total of 28 UCS tests were carried out with an average UCS value of 2.1 MPa and an average Young's Modulus value of 428 MPa.

This extensive test program gave confidence that the design parameters for the soil improvement slab were exceeded. Works were completed successfully, and the station has been in operation for several years.

3 Summary and Conclusions

Four geotechnical problems associated with rail and metro projects were presented, with their associated ground improvement solutions. Firstly, in the New Delhi Metro project, the problem of NATM tunneling with a portion of loose overburden was solved with the use of *compaction grouting*. In the Perth Metro project, the challenge of twin TBM drives under existing buildings was met by resorting to *compensation grouting*. In Kuala Lumpur, the difficulties associated with deep excavations in cavity-prone limestone were overcome by *rock fissure grouting*. Finally, in Singapore, problem of a deep excavation in reclamation fill overlying soft clay was surmounted by the installation of a soil improvement "strut" using *deep soil mixing* and *jet grouting*. Over the years, ground improvement techniques have proven themselves to be very useful in solving complex geotechnical problems.

References

EN 12716:2001 Execution of special geotechnical works. Jet Grouting. European Committee for Standardization, Brussels

EN 14679:2005 Execution of special geotechnical works. Deep Mixing. European Committee for Standardization, Brussels

Kirsch K, Bell A (2012) Ground improvement, 3rd edn. CRC Press

Kumarasamy J (2014) Geology along circle line and its effect on choice of construction methods. In: Underground Singapore 2014, pp 36–46

Lee PT, Tan YC, Gue SS (2013) Ground treatment for electrified double track railway in the northern part of Peninsular Malaysia. In: Leung CF, Goh SH, Shen RF (eds) Advances in geotechnical infrastructure, 18th SEAGC cum inaugural AGSSEA conference, Research Publishing, Singapore, pp 107–113

Raju VR, Daramalinggam J (2012) Ground improvement: principles and applications in Asia. In: Proceedings of the Institution of Civil Engineers, Ground Improvement, vol 165, May 2012, Issue GI2, pp 65–76

Raju VR, Yee YW (2006) Grouting in limestone for SMART tunnel project in Kuala Lumpur, Malaysia. In: International conference and exhibition on tunneling and trenchless technology, Kuala Lumpur, Malaysia, March 2006

Sreenivas P, Chang JHK, Prasad PVSR (2016) Grouting in limestone for KVMRT tunnel project in Kuala Lumpur. In: Chan SH, Ooi TA, Ting WH, Chan SF, Ong D (eds) Proceedings of 19th SEAGC and 2nd AGSSEA, Kuala Lumpur, pp 499–504

Tan SMS (2005) Karstic features of Kuala Lumpur limestone, Jurutera, No. 6 June 2005. In: Mah S (ed) The Institution of Engineers Malaysia, Kuala Lumpur, pp 6–11

Williams M, Nobes C (2007) Soilfrac compensation grouting for building protection. In: Proceedings of the seminar on new MetroRail city project, Australasian Tunnelling Society, Engineers Australia, Perth

Performance Analysis of PLAXIS Models of Stone Columns in Soft Marine Clay

M. Vinoth, P. S. Prasad and U. K. Guru Vittal

Abstract The behavior of stone columns in soft marine clay under a cement concrete road pavement was examined through PLAXIS 2D. It is a well-known fact that modeling in 2D will require less computational effort compared to a full 3D analysis. The main difficulty with regard to PLAXIS 2D modeling of stone columns is the conversion of the stone column grid to a 2D stone trench structure. Different approaches (enhanced soil parameter, embedded beam element and equivalent column method) are available in modeling of stone column in PLAXIS 2D. However, not much literature is available for choosing the proper approach in PLAXIS 2D modeling of stone column in soft marine clay. The aim of this paper is to establish the suitable approach which provides better results with minimal effort for modeling in PLAXIS 2D. A case study, of work carried out at Mumbai for the road pavement between Wadala Depot and Chembur, provides the basis for PLAXIS 2D modeling. The sub-soil profile in this stretch comprises of soft marine clay, and the ground below cement concrete pavement had been treated with stone column prior to construction of rigid pavement. The results of the PLAXIS 2D models were then validated by examining the main characteristics of cement concrete pavement deformation within the column grid.

Keywords PLAXIS 2D · Stone column · Soft marine clay

M. Vinoth (✉) · P. S. Prasad · U. K. Guru Vittal
CSIR—Central Road Research Institute, CRRI (PO), New Delhi 110025, India
e-mail: vinothm.27@gmail.com

P. S. Prasad
e-mail: pulikanti@gmail.com

U. K. Guru Vittal
e-mail: vittal.crri@gmail.com

R. Sundaram et al. (eds.), *Geotechnics for Transportation Infrastructure*,
Lecture Notes in Civil Engineering 29,
https://doi.org/10.1007/978-981-13-6713-7_44

1 Introduction

Installation of stone columns in soft marine clay is very common as it increases the load carrying capacity of the foundation soil as well as provides the free drainage path for water to travel to the ground surface and reduces the post-construction settlements. In order to assess stone column performance through numerical modeling, designer has to go through one of the complex tasks, which is the conversion of the stone column grid to a two-dimensional (2D) stone trench structure. Earlier researchers have proposed several methods to convert the axisymmetric unit cell to the equivalent plane-strain model for the purpose of 2D numerical modeling of multi-drain field applications Hird et al. 1992; Indraratna and Redana 1997. These conversion methods involved the derivations of the equivalent plane-strain permeability or the equivalent plane-strain geometry based on the matching of axisymmetric and plane-strain consolidation analytical solutions. Numerical modeling by using finite-element software PLAXIS 2D 2015 provides three different approaches (enhanced soil parameter (ESP), embedded beam element (EBE) and equivalent column method (ECM)) for modeling stone column. Each one of these approaches has been separately used by various researchers Tan et al. (2008); Ng and Tan (2015) for modeling stone column, but a comparative study to bring out the best-suited method for this type of problems is not addressed. So, in the present study, performance of the three different approaches, were assessed using the field data obtained from the case history carried out at Mumbai for the road pavement between Wadala Depot and Chembur. The finite column permeability and smear effects are excluded from this study.

2 Case History Details

The soil profile considered for the present study is from the case history of Mumbai monorail project, Mumbai Prasad et al. (2016). The width of the six-lane concrete road is 11 m. The surcharge loading considered for the analysis is 44 kN/m^2 (including the dead load of pavements). Typical soil profile in this stretch is given in Table 1.

Table 1 Typical soil profile

Type of soil	Layer Thickness	SPT 'N' value
Fill Soil	0.5–4.5	5–8
Soft Clay	0.5–12	3–6
Stiff Clay	7.5–16.5	5–45
CWR	13.5–16.5	>50
MWR	>10	>100

CWR—Completely weathered rock
MWR—Moderately weathered rock

The ground water level in the boreholes varied from 1.1 to 1.7 m from natural ground level (NGL). The stone columns are arranged in a triangular pattern. The diameter and spacing of stone columns are 0.9–2.5 m c/c, respectively. Depth of stone column from ground surface varies from 9 to 12 m. Six borehole data (BH-01, BH-02, BH-03, BH-04, BH-05, and BH-06) were considered for the comparative study.

3 Formulation of Equivalent Stiffness and Permeability

For ECM and EBE, the equivalent stiffness was arrived based on the approach proposed by Tan and Oo (2005). Priebe (1995) approach was used in arriving at the equivalent stiffness for ESP method. Permeability for all the three cases was arrived based on the approach suggested by Tan and Oo (2005). These approaches are reviewed here.

As per Tan and Oo (2005) approach, equal flow path length normal to the column perimeter can be obtained by considering the column width of plane-strain case equal to the axisymmetric column diameter, i.e.,

$$b_c = r_c \tag{1}$$

as shown in Fig. 1a,b. Similarly, Indraratna and Redana (2000) used this type of geometrical transformation in their permeability-matching approach for the plane-strain conversion of vertical drains. So, the equivalent plane-strain width B can be taken equal to the radius of drainage zone R [Fig. 1a,b], i.e.,

$$R = B \tag{2}$$

In general, this geometry conversion method is a very easy one since the transition between plane-strain meshed geometry and axisymmetric can be derived from the same basic (2D) input geometry.

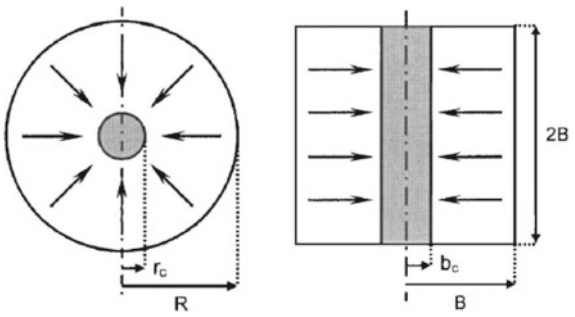

(a) Axisymmetric (b) Plane Strain

Fig. 1 Cross sections of unit-cell stone column and plane-strain conversions

Accordingly, material properties of plane-strain also need to be adjusted to account for the geometrical changes. By matching the column-soil composite stiffness, the following relationship can be used to arrive at the plane-strain material stiffness

$$E_{\text{composite}} = E_{c,ax}a_{s,ax} + E_{s,ax}\left(1 - a_{s,ax}\right) \tag{3}$$

where $E_{\text{composite}}$ and E_s = elastic moduli of the composite material and the surrounding soil, respectively, and subscript ax denote axisymmetric conditions. Area replacement ratio $a_s = A_c/(A_c + A_s)$, where A_c and A_s = cross-section areas of the column and the surrounding soil, respectively. The composite stiffness obtained from Eq. (3) gives the average stiffness of the axisymmetric unit cell. The relevant stiffness of the stone column and the surrounding soil of the plane-strain model are computed by using the composite stiffness of the axisymmetric unit cell ($E_{\text{composite}}$) obtained from Eq. (3). The relation for computation of stiffness of materials in the plane-strain unit cell is given by:

$$E_{\text{composite}} = E_{c,pl}a_{s,pl} + E_{s,\text{pl}}\left(1 - a_{s,pl}\right) \tag{4}$$

For simplicity, $E_{s,pl} = E_{s,ax}$, has been considered in this study. Hence $E_{c,pl}$ can be determined from Eq. (4). The soil permeability was matched by using the following equation as derived by Tan and Oo (2005):

$$\frac{k_{h,pl}}{k_{h,ax}} = \frac{F(N)_{pl}}{F(N)_{ax}}\left[\frac{m_{vs}m_{vc}(1-a_s)}{m_{vc}(1-a_s)+m_{vs}a_s}\right]_{pl}\left[\frac{m_{vc}(1-a_s)+m_{vs}a_s}{m_{vs}m_{vc}(1-a_s)}\right]_{ax}\frac{B^2}{R^2} \tag{5}$$

where k_h = coefficient of soil permeability in horizontal direction; α_{vc} and α_{vs} = coefficients of compressibility of the column and the surrounding soil, respectively. $F(N) = \left[\frac{N^2}{(N^2-1)}\right]\ln(N) - \frac{\left(3N^2-1\right)}{4N^2}$; diameter ratio $N = R/r_c$ for axisymmetric condition, whereas $N = B/b_c$ for plane-strain condition; $m_{vs} = \alpha_{vs}/(1 + e_s)$; $m_{vc} = \alpha_{vc}/(1 + e_c)$; and e_c and e_s = void ratios of the columns and the surrounding soil, respectively. As, the influence of soil permeability in vertical direction $k_{v,pl}$ is negligible when compared to horizontal, it is assumed that plane-strain vertical flow to be same as axisymmetric condition, $k_{v,pl} = k_{v,ax}$.

Priebe (1995) proposed improvement factors for soil improved through installation of stone columns. Improvement factors are evaluated on the assumption that the column material shears from the beginning while the surrounding soil reacts elastically. Furthermore, the soil is assumed to be displaced already during the column installation to such an extent that its initial resistance corresponds to the liquid state: i.e., the coefficient of earth pressure amounts to $K = 1$. The result of the evaluation is expressed as basic improvement factor n_0.

$$n_0 = 1 + \frac{A_c}{A}.\left[\frac{1/2 + f(\mu_s, A_c/A)}{K_{aC}.f(\mu_s, A_c/A)} - 1\right] \tag{6}$$

where $f(\mu_s, A_c/A) = \frac{1-\mu_s^2}{1-\mu_s-2\mu_s^2}.\frac{(1-2\mu_s).(1-A_c/A)}{1-2\mu_s+A_c/A}$; μ = Poisson's ratio;$K_{aC} = \tan^2\left(45^\circ - (\varphi_c/2)\right)$; A = area of unit cell, A_c = cross-sectional area of single stone column. The columns materials are still compressible. This compressibility of the stone column material can be addressed by using a reduced improvement factor n_0. This can be arrived from the formula developed for the basic improvement factor n, when the given reciprocal area ratio A/A_c is increased by an additional amount of $\Delta(A/A_c)$.

$$n_1 = 1 + \frac{\overline{A_c}}{A}.\left[\frac{1/2 + f\left(\mu_s, \overline{A_c/A}\right)}{K_{aC}.f\left(\mu_s, \overline{A_c/A}\right)} - 1\right] \tag{7}$$

where $\frac{\overline{A_c}}{A} = \frac{1}{A/A_c + \Delta(A/A_c)}$; $\Delta(A/A_c) = \frac{1}{(A_c/A)_1} - 1$;

$$\left(\frac{A_c}{A}\right)_1 = -\frac{4.K_{ac}.(n_0-2)+5}{2.(4.K_{aC}-1)} \pm \frac{1}{2}.\sqrt{\left[\frac{4.K_{ac}.(n_0-2)+5}{4.K_{aC}-1}\right]^2 + \frac{16.K_{aC}.(n_0-1)}{4.K_{ac}-1}}$$

The stone columns are better supported laterally with increasing overburden and, therefore, can provide more bearing capacity. Therefore, in order to consider this effect, depth factor f_d is calculated based on following equation and suitably applied to the improvement factor,

$$f_d = \frac{1}{1 + \frac{K_{oc} - W_s/W_c}{K_{oc}}.\frac{W_c}{p_c}} \tag{8}$$

where $p_c = \frac{p}{\frac{\overline{A_c}}{A} + \frac{1-\overline{A_c/A}}{p_c/p_s}}$; $\frac{p_c}{p_s} = \frac{1/2 + f\left(\mu_s, \overline{A_c/A}\right)}{K_{aC}.f\left(\mu_s, \overline{A_c/A}\right)}$; $W_c = \sum(\gamma_c.\Delta d)$; $W_s = \sum(\gamma_s.\Delta d)$; $K_{oC} = 1 - \sin\varphi_c$; p = surcharge pressure, d = thickness of soil layer, γ_s and γ_c denote bulk densities of soil and column. In order to counter simplifications and approximations, compatibility controls have to be performed. This is to guarantee that the settlement of the stone columns resulting from their inherent compressibility does not exceed the settlement of the surrounding soil resulting from its compressibility by the loads which are assigned to each. So using the following equation, upper limit of improvement factor can be obtained,

$$n_{Gr} = 1 + \frac{A_c}{A}.\left(\frac{D_c}{D_s} - 1\right) \tag{9}$$

where D_c and D_s are Young's moduli of stone column and soil, respectively. Final improvement factor is given by

$$n_2 = f_d \times n_1 \tag{10}$$

Therefore, enhanced stiffness of soil will be equal to existing soil stiffness multiplied by improvement factor n_2. Similarly, shear resistance from friction of the composite system can be calculated using the below equations:

$$\tan \bar{\varphi} = m'.\tan \varphi_c + (1 - m').\tan \varphi_s \tag{11}$$

$$c' = (1 - m').c_s \tag{12}$$

where $m' = (n-1)/n$; n = improvement factor, φ_c and φ_s are the angles of internal friction of column and soil, respectively, c' = Cohesion of unimproved soil.

4 Settlement Calculation

Theoretical settlement was calculated by using Terzaghi's (1925) one-dimensional consolidation equation.

$$S_c = \sum_{i=1}^{n} \frac{C_{\mathrm{ci}} H_{\mathrm{oi}}}{1 + e_{\mathrm{oi}}} \log\left(\frac{\sigma_{v'fi}}{\sigma_{v'\mathrm{oi}}}\right) \tag{13}$$

where C_{ci} = compression Index of respective layer, H_{oi} = thickness of respective layer, $e_{0\mathrm{i}}$ = initial void ratio of respective layer, $\sigma_{v'\mathrm{fi}}$ = final vertical effective stress of respective layer, $\sigma_{v'\mathrm{Oi}}$ = initial vertical effective stress of respective layer.

As per the reduced stress method, settlement reduction factor due to stone column installation was determined using the following equation,

$$\mu_g = \frac{n}{1 + (n-1)a_s} \tag{14}$$

where $n = \sigma_s/\sigma_g$; σ_s and σ_g are vertical stress in compacted columns and surrounding ground.

5 Numerical Modeling

Three different finite-element models of the stone column-improved soil section were considered: enhanced soil property, equivalent beam method and equivalent column method. The plane-strain modeling was chosen as the road spanned a

distance of about 8.5 km with almost uniform cross-sectional geometry in the direction normal to the plane. The plane-strain models were developed using 15-node triangular elements in PLAXIS 2D version 2015. For EBM and ECM, the width of stone columns was considered as 0.9 m, same that of axisymmetric condition. A spacing of 2.5 m was uniformly considered in all the embankment models. Self-soil weight was taken into account by applying the gravity effect, assuming the default gravity acceleration, g, is 9.810 m/s^2, and the direction is with the negative y-axis. Default unit weight of the water is 10 kg/m^3. In order to minimize the boundary effects, the overall geometry of the model was kept more than 5 times and 2.5 times the width of road in X-direction and Y-direction, respectively. During mesh generation stage, fine refinement was used so that more number of elements will be generated for obtaining more precise results. In order to simulate the dead load (self-weight of pavement layers) and live load at top a line load with an intensity of 44 kPa was applied. Parameters used for the analysis of BH-01 borehole data are listed in Table 2, where γ = bulk density; φ' = angle of internal friction; c' = cohesion; E = Young's modulus or stiffness; μ = Poisson's ratio; k_h and k_v are coefficients of permeability in vertical and horizontal directions, respectively.

The soft soils were modeled as undrained material in PLAXIS. Stone column for ECM was idealized as a homogeneous drained material having certain characteristics of stiffness and strength parameters. The elastic modulus of column material was taken as ten times that of soil. The compression index c_c, swell index c_s and initial void ration e_0 of soft clay are 0.59, 0.144 and 1.973, respectively. The compression index c_c, swell index c_s and initial void ration e_0 of stiff clay is 0.38, 0.125 and 1.438, respectively. Permeability in horizontal direction for soft clay is taken as twice of vertical direction. In order to avoid numerical complications, a small nonzero value has been considered for the strength parameters.

Plane-strain model parameters considered for both ECM and EBM are same, and the stiffness for both the method was determined using Eqs. (3) and (4). Permeability for all the three methods for modeling in PLAXIS 2D 2015 has arrived from Eq. (5). Shear parameters and stiffness values for embedded beam were selected as layer-dependent. Stiffness parameters for ESP method Eqs. (6)–(10) were used and shear parameter is used using Eqs. (11) and (12).

5.1 Simulation Procedures

The project involved the installation of stone columns and construction of six-lane concrete road over it was simulated as follows. The stone columns were first installed by partial soil replacement for ESP and ECM but for EBM embedded beam row is activated. Next-stage surcharge load (including the dead load of pavements) is activated. Last-stage consolidation process is carried out till the excess pore water pressure reduces to 1 kPa, and once this value is reached the analysis stops.

Table 2 Material properties of all models—BH-01

Material	Model	Drain Type	γ (kN/m^3)	γ_{sat} (kN/m^3)	Φ' (°)	C' (kPa)	E (kPa)	μ	k_v (m/day)	k_h (m/day)
Fill Soil#	HSM	Drained	18	18.75	29	0.1	11,500	0.3	8.64	8.640
Soft Clay[a]	SSM	Undrained (A)	15.6	15.6	1	13.5	3100	0.4	0.069	0.165
Stiff Clay[b]	SSM	Undrained (A)	16.6	16.6	1	22.5	6000	0.4	0.102	0.177
MWR	HSM	Undrained (B)	19.5	20.5	33	3500	1.43E + 07	0.25	0.1	0.033
Stone Column	MC	Drained	19	20	42	0.1	12,200	0.33	1	1.000
Embedded Beam	–	–	19	Layer Dependent	12,200	Layer Dependent				

Values are only for ECM and EBM; corresponding for ESP model, E = 21,487 kPa

[a]Values are only for ECM and EBM; corresponding for ESP model, E = 6107 kPa and 8106 for above water table and below water table, respectively

[b]Values are only for ECM and EBM; corresponding for ESP model, E = 15,134 kPa

HSM Hardening Soil Model; *SSM* Soft Soil Model; *MC* Mohr Coulomb

6 Results and Discussions

Analysis for all the six boreholes was done using all the three methods (i.e., ESP, EMB and ECM). Typical maximum settlement obtained from the analysis carried out using BH-01 has been shown in Fig. 2a–c. Theoretical settlements were calculated using Eqs. (13 & 14). All the analysis results along with theoretical and field values [obtained through leveling by Mumbai Mono Rail Development Authority in October 2010 and February 2015. This level difference as reported varies from 250 to 550 mm at different chain ages, Prasad et al. (2016)] are tabulated in Table 3.

From Table 3, it can be seen that out of three methods embedded beam method has better results than other two methods. One of the other interesting things we can notice is that theoretical predictions also vary with field values in the range of 16–56%. This variation is also erratic because in some cases it has over-predicted and in others underestimated. In cases where theoretical predictions are on higher end may be because the top fill layers would have dissipated the surcharge, leading to lower load intensity transferred to the soft soil layers and resulting in lesser settlement. Reason for under prediction may be the fill thickness is less than those considered for settlement calculation.

Except one borehole in all the other cases, ESP has underestimated settlement in the range of 40–90%. In EBM except for last borehole location in all other location, it has predicted settlement with just 25% variation. In ECM, constantly in all locations it has underestimated the settlement in the range of 50–90%.

It can be noted that for BH-05 and BH-06, all the methods including theoretical approach have underestimated the settlement. So this shows that actual thickness of fill and soft soil varies at site than what is considered for the study.

In order to explain the huge variation of settlement prediction among the three methods, each model's material stress state at the end of the analysis was studied. Figures 3a–c and 4a–c shows the elastic points and plastic points, respectively, at the end of simulation. It can be seen that EBM has very little elastic points and some plastic yielding in the surrounding region of the column material. It is clearly indicated by numerous plastic stress points that are concentrated within and slightly beyond the column periphery. The yielding pattern of the other two methods is almost the same but with less scatter beyond the column periphery and more plastic points; this explains the differential responses of the other two methods. The plastic yielding in the EBM allows itself to simulate the settlements of actual field case, while the other model's elasticity gives a stiffer response leading to a lower final settlement. The sustained elastic behavior in the ECM and ESP may be due to its larger cross-sectional column area with higher elastic capacity in both shearing and bending.

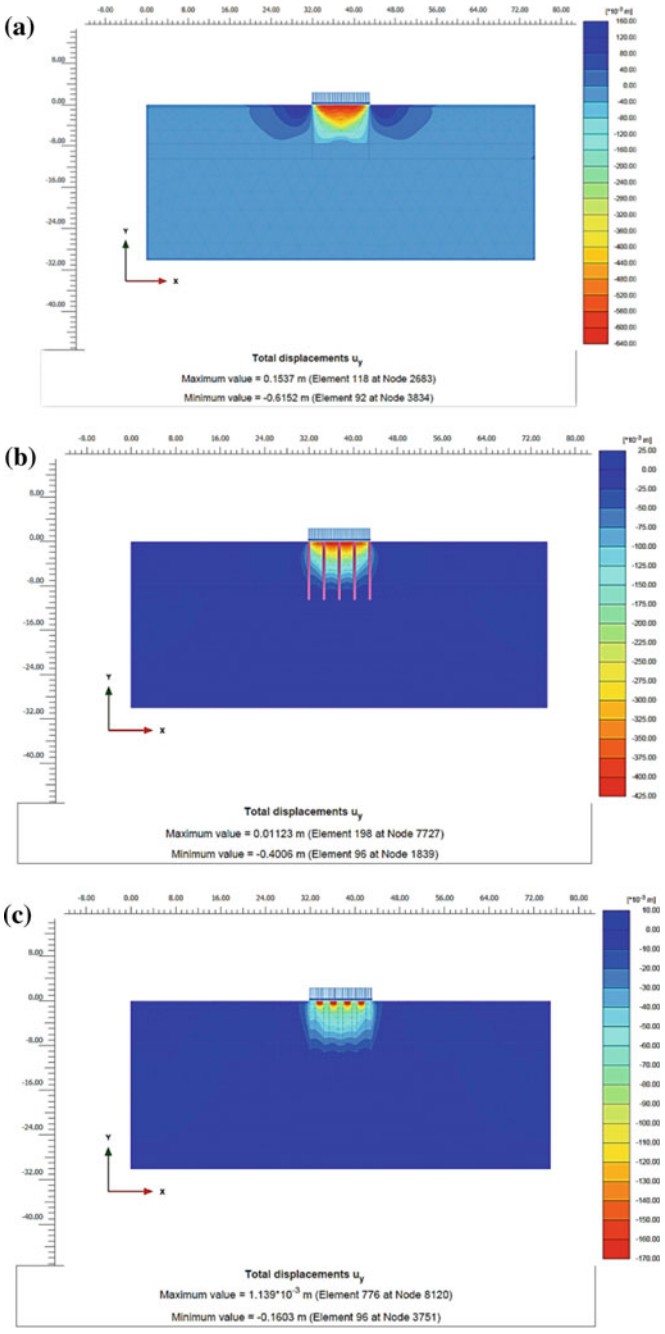

Fig. 2 **a** Displacement—ESP. **b** Displacement—EBM. **c** Displacement—ECM

Table 3 Settlement comparison

Borehole	Theoretical	PLAXIS			Field[a]
		ESP	EBM	ECM	
BH-01	455.6	615.2	400.6	160.3	325
BH-02	349.0	147.1	209.3	100.8	300
BH-03	317.6	137.1	222.2	124.1	250
BH-04	390.9	181.2	226.1	76.52	300
BH-05	289.4	166.1	233.7	106.8	450
BH-06	258.1	39.55	103.6	41.22	450

[a]Prasad et al. (2016)

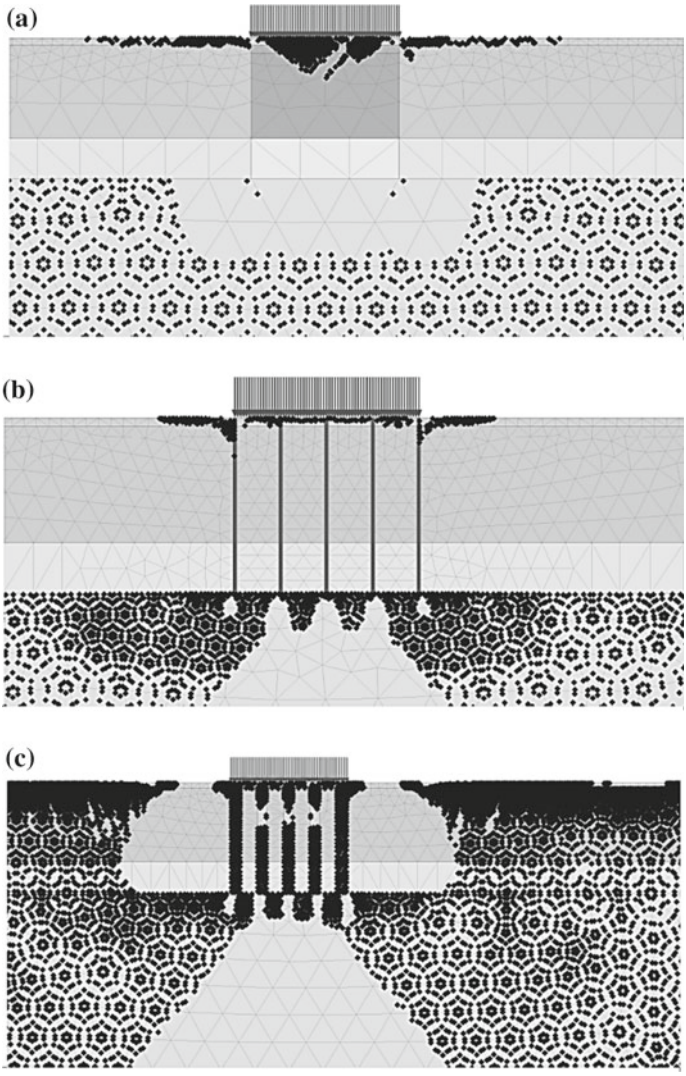

Fig. 3 **a** Elastic Points—ESP. **b** Elastic points—EBM. **c** Elastic points—ECM

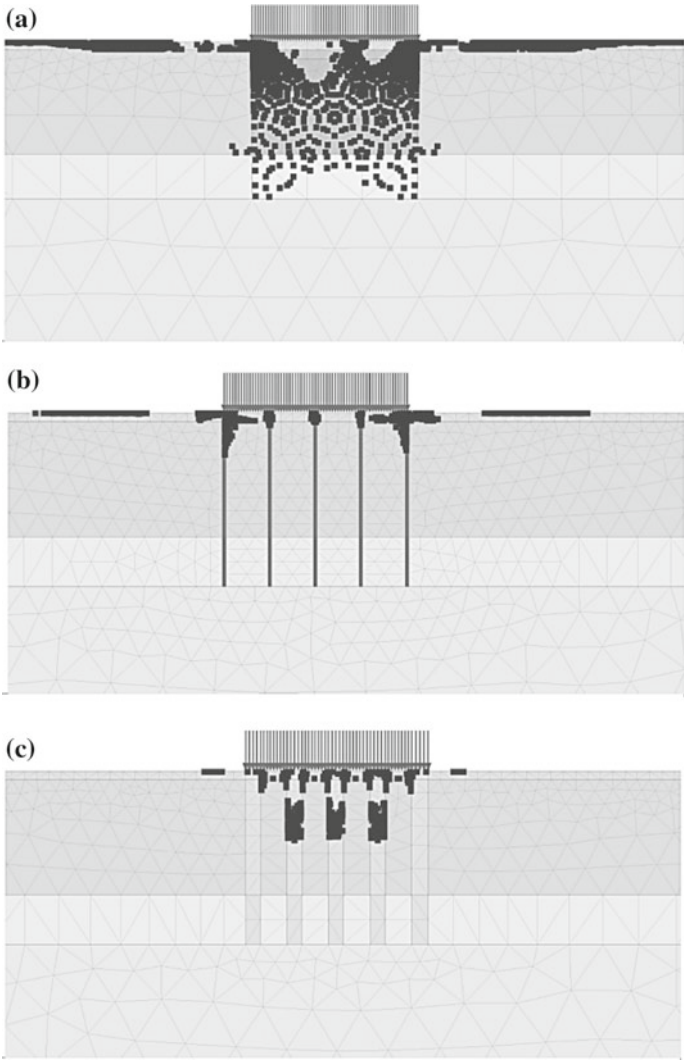

Fig. 4 **a** Plastic points—ESP. **b** Plastic points—EBM. **c** Plastic points—ECM

7 Conclusion

This paper presents a comparative performance study of three different approaches (i.e., enhanced soil parameter, embedded beam element and equivalent column method) available in PLAXIS 2D 2015 version for assessing the settlement performance of stone column, by comparison with the field data, from a case history carried out at Mumbai for the road pavement between Wadala Depot and Chembur. Six borehole data were considered for the comparative study.

Stiffness and permeability of axisymmetric condition were converted into equivalent plane-strain values using Tan and Oo (2005) approach. Enhanced shear parameters of soil were also determined using Priebe (1995) approach. Theoretical settlement was calculated using Terzaghi's (1925) one-dimensional consolidation equation and settlement reduction factor due to stone column installation was determined using reduced stress method.

With all these data, analysis was carried out in PLAXIS 2D 2015. Following points can be brought out from the analysis results:

1. Out of three methods, embedded beam method has better results than other two methods. Except for the last borehole location in all other location, it has predicted settlement with just 25% variation.
2. Except one borehole in all the other cases, ESP has underestimated settlement in the range of 40–90%.
3. ECM constantly in all locations has underestimated the settlement in the range of 50–90%.
4. The plastic yielding in the EBM allows itself to simulate the settlements of actual field case, while the other model's elasticity gives a stiffer response leading to a lower final settlement. The sustained elastic behavior in the ECM and ESP may be due to its larger cross-sectional column area with higher elastic capacity in both shearing and bending.

Thus, embedded beam method is the preferred method for carrying out numerical modeling for elasto-plastic materials.

References

Hird CC, Pyrah IC, Russell D (1992) Finite element modelling of vertical drains beneath embankments on soft ground. Geotechnique 42(3):499–511

Indraratna B, Redana IW (1997) Plane-strain modeling of smear effects associated with vertical drains. J Geotech Geoenviron Eng 123(5):474–478

Indraratna B, Redana IW (2000) Numerical modeling of vertical drains with smear and well resistance installed in soft clay. Can Geotech J 37(1):132–145

Prasad PS, Guru Vital UK, Sitaramanjaneyulu K, Madhav MR (2016) Remedial measures for upheaval of PQC panels adjacent to piers of Mumbai Monorail in Mumbai, 5th ICFGE-2016, Bangalore, India, pp 366–377

Priebe HJ (1995) The Design of vibro replacement, Ground Engineering, Dec 1995, pp 31–37

Tan SA, Oo KK (2005) Stone column FEM modeling—2D and 3D considerations illustrated by case history. In: Proceedings of international symposium on tsunami reconstruction with geosynthetics, ACSIG, Bangkok, Thailand, pp 157–169

Tan SA, Tjahyono S, Oo KK (2008) Simplified plane-strain modeling of stone-column reinforced ground. J Geotech Geo-Environ Eng, ASCE 134(2):185–194

Ng KS, Tan SA (2015) Simplified homogenization method in stone column designs. Jpn Geotech Soc, Soils Found 55(1):154–165

Terzaghi K (1925) Erdbaumechanik and bodenphysikalischer grundlage, Deuticke, Lpz

Terzaghi K, Peck RB, Mesri G (1996) Soil mechanics in engineering practice, Third Edition, Part II, Theoretical soil mechanics, John Wiley & Sons Inc, New York

Strengthening Low Plastic Soils Using MicroFine Cement Through Deep Mixing Methodology

Parth Shah, Manish Shah and Abhay Gandhi

Abstract The objective of the research work was to evaluate the settlement trait, modulus of subgrade reaction, elasticity, and shear strength of low plastic soil strengthened using Cement Deep Mixing technique. This is accomplished by performing modeled Plate Load and Unconfined Compression Test, respectively. For achieving the objective, a tank of size 75 cm × 75 cm × 75 cm was fabricated in which soil was compacted at different degree of saturation as 80 and 100% of optimum moisture content and using deep mixing assembly, soil–cement columns of different lengths as 100 and 200 mm were drilled and grouted. The assembly created comprised of cutter blade at the base of a solid pipe for facilitating drilling of the hole into the soil, and perforations all around the pipe facilitates grouting action during withdrawal. Filz theory (Geo-Front Congr ASCE 162(1):1–13, 2005) was adopted for deep mixing. Five columns of 5 cm diameter each out of which four columns at a spacing of 25 cm c/c and one under the footing were formed. Microfine cement slurry with water: cement ratio of 1.2 was used for grouting. Low plastic soil treated with microfine cement showed an appreciable reduction in the settlement as compared to untreated soil and was found to be adequate.

Keywords Cement deep mixing · Modulus of subgrade reaction · Modulus of elasticity · Shear strength

P. Shah · M. Shah (✉) · A. Gandhi
Applied Mechanics Department, L.D. College of Engineering, Ahmedabad 380015, India
e-mail: mvs2212@yahoo.co.in

P. Shah
e-mail: parthshah080695@gmail.com

A. Gandhi
e-mail: abhayrgandhi@gmail.com

R. Sundaram et al. (eds.), *Geotechnics for Transportation Infrastructure*, Lecture Notes in Civil Engineering 29,
https://doi.org/10.1007/978-981-13-6713-7_45

1 Introduction

Deep soil mixing (DSM) technique is an in situ soil strengthening technique which delivers cement and/or other additives in either dry or slurry form using blades which lead to formation of soil–cement columns in different configurations. The aim of DSM technique was to minimize the settlement of soft ground, provide seismic resistance to soil against liquefaction, and reduce compressibility of soil and many more (CDIT 2002). There is a difference between jet grouting of the soil and DSM technique. Both the methods deal with penetrating the binder either in slurry or in dry form, but in case of jet grouting the main phenomena effecting its application is the pressure head which is created during injection of the slurry, whereas in case of DSM technique, static and the rotational head are the parameters that has an influence on the efficacy of the technique. DSM technique deals with penetrating the assembly into soil and filling up the hole with some suitable binder like cement, lime, flyash (Probaha 1988) during the withdrawal with the help of rotary motion of assembly; on the other hand, jet grouting deals with sealing up the hole with suitable binder at a certain higher injection pressure. DSM can be broadly classified as wet deep mixing method (WDMM) and dry deep mixing method (DDMM), the former being used for moisture content below 40% and the latter for moisture content above 60%. DSM technique mainly includes 23 different techniques. Cement deep mixing (CDM) is one among them which involves use of cements in either slurry or powder form to be used as a binder to be mixed with soil. CDM is further categorized in two different methods, namely CDM and CDM-LODIC method; the installation pattern of soil–cement column was adopted as suggested by Kitazume and Tersahi (2015). Ismail et al. (2002) suggested that Ordinary Portland Cement is best suited for the use as a binder material. Farouk and Shahein (2013) studied the effect of cement dosage, curing time, water-to-cement ratio on strength as well as the interaction between footing and soil. Carasca (2016) studied the strength characteristics of made up soil. The present research emphasizes on computing the settlement trait and shear strength of low plastic soil, subjected to variation in degree of saturation as 80 and 100% of optimum moisture content and at 90% of maximum dry density, soil–cement column length as 10 and 20 cm were strengthened using cement deep mixing technique. For shear strength test of deep mixed soil–cement, quantity was decided on the basis of method suggested by Federal Highway Administration Design Manual (2013), whereas for modeled Plate Load Test, CDM-LODIC method was employed which deals with replacing equivalent weight of soil by weight of cement at desired water-to-cement ratio.

2 Deep Mixing Assembly

The assembly created for facilitating the drilling of hole and its filling with cement slurry mainly comprised of a cutter blade whose width was so fixed that it drilled hole of exactly 50 mm in diameter. This blade was attached at the base of a solid pipe 25 mm in diameter; the main reason behind using solid pipe was from its stability point of view, so as it does not fail to meet its requirement. Filling of the hole by cement slurry was commenced during the withdrawal of the assembly. The assembly consisted of an inlet at the top and perforations over the circumference of the solid pipe, and these proved to be advantageous in achieving the desired mixing between the soil and the cement.

2.1 Working of Deep Mixing Assembly

As can be seen from Fig. 1, top portion of the solid pipe is reduced to a diameter of 125 mm, the reason behind this is the top portion of reduced diameter gets fixed into the hand drill, and the hand drill facilitates the rotating of the assembly during drilling as well as during the withdrawal. Two-way drill machine was employed to achieve two-way movement of the assembly during drilling and withdrawal, i.e., if the assembly was rotated clockwise during the drilling operation, it would be rotated anticlockwise during the withdrawal and vice versa. The speed of the assembly during penetration as well as during the withdrawing operation plays an important role in achieving the purpose of the work. Higher rotation speed was employed during withdrawing than that during penetration, the reason for this was to cause cement slurry to flow to the maximum distance during withdrawal and to cause minimum disturbance to the soil during penetration.

3 Investigation of Shear Strength of Soil

There are various factors affecting the shear strength of soil among which one being degree of saturation of soil. To investigate the effect of the same on shear strength, low plastic clay was selected as type of soil. The soil was compacted at different degree of saturation as 80 and 100% of optimum moisture content keeping the cement dosage same as obtained using the guidelines provided in FHWA-HRT 13-046 and water-to-cement ratio as 1.2. Microfine cement was used as binder in order to prevent the disintegration of soil particles as well as for the proper interaction between the finer soil particles and the cement. FHWA consists of standard curve of relation between the desired Unconfined Compression Strength and Total water-to-binder ratio, and thus for the desired strength of soil, the total water to

Fig. 1 Deep mixing assembly

binder ratio can easily be obtained from the plot. After obtaining the total water to binder ratio, the equations which facilitate the determination of the dosage of cement as per FHWA are as follows:

$$\gamma_{d,\text{slurry}} = \frac{G_b \times \gamma_w}{1 + (w : b)G_b} \tag{1}$$

$$\text{VR} = \frac{w \times \gamma_{d,\text{soil}}}{(w_T : b - w : b) \times \gamma_{d,\text{slurry}}} \tag{2}$$

$$\text{VR} = \frac{\alpha}{\gamma_{d,\text{slurry}}} \tag{3}$$

3.1 Physical Properties of Soil

Prior to commencing the preparation of soil specimen, the physical properties of the soil were evaluated by conducting laboratory tests. Laboratory tests were conducted as per the Indian Standards. The soil was classified as low plastic clay as per IS classification method.

Table 1 Physical properties of soil

Properties	Results
Specific gravity	2.7
Liquid limit (%)	32
Plastic limit (%)	21
Soil classification (IS)	CL
Free swell index (%)	9
Cohesion (kg/cm^2)	0.5
Angle of internal friction (°)	23
Optimum moisture content (%)	13
Maximum dry density (kN/m^3)	19.5

3.2 Sample Preparation and Testing Procedure

Field efficiency as in DSM technique is 50–80% of the laboratory (EuroSoilStab 2002) and hence fixing the desired shear strength of soil on field and taking its equivalent shear strength to be achieved in the laboratory, total water-to-binder ratio is obtained from the standard curve and cement dosage is then worked out using Eqs. (1), (2), and (3) mentioned above. The cement dosages obtained for degree of saturation as 80 and 100% of optimum moisture content are provided in Table 1. The desired unconfined compression strength test on field was fixed to be 250 kPa, and hence, on the basis of efficiency standards suggested by EuroSoilStab (2002), laboratory strength to be achieved was kept to be 400 kPa. The samples were prepared with the obtained cement dosages at a water cement ratio of 1.2 in mold of 40 mm diameter and 80 mm in length. These samples were cured for 28 days in sealed plastic bags at room temperature, and the strength was evaluated by performing unconfined compression strength test at a strain rate of 1.5 mm/min (Table 2).

4 Investigation on Settlement Trait of Strengthened Soil

One of the main advantages of CDM technique is the reduction in settlement of strengthened soil, this research deals with evaluating the percentage reduction in settlement of low plastic soil compacted at different degree of saturation and strengthened using different soil–cement column lengths. To achieve the objective

Table 2 Cement dosages at different degree of saturation

Degree of saturation (%)	$\gamma_{d,\text{slurry}}$ (kN/m^3)	VR	α (kg/m^3)
80	6.6	10^{-1}	65.6
100	6.6	1.3×10^{-1}	85.3

of the study, a deep mixing assembly comprising of cutter blade and perforations all around was created. Cutter blade was attached to base of solid pipe which facilitated drilling of hole in the soil and perforations all around the pipe facilitated filling of cement slurry in hole so created by rotational motion of the assembly during its withdrawal. The width of blade was so set that it exactly facilitated in drilling the hole which is 5 cm in diameter and of the desired length. Four columns were formed at a distance of 25 cm c/c and one exactly beneath the footing.

4.1 Test Setup

4.1.1 Preparation of Soil-Cement Columns

On the basis of trial and error, a water to cement ratio of 1.2 was found to be producing a workable mixture. Hence, a water-to-cement ratio of 1.2 was used and cement dosages for studying the settlement trait were fixed on basis of CDM-LODIC method which mainly involves replacing the weight of soil excavated from the hole by equivalent weight of cement. The soil–cement columns were installed in a steel tank of dimension 75 cm × 75 cm × 75 cm using deep mixing assembly by the procedure as described by Filz (2005). Deep mixing assembly was penetrated into the soil up to the desired depth and during its withdrawal slurry of microfine cement was poured in the inlet provided at the top of assembly, once the assembly was filled up with the slurry the assembly was rotated in the direction opposite to that during penetration. Due to higher rotating speed, cementious particles got well mixed with the soil particles, thus improvising the soil. Four columns each of diameter 50 mm and spaced at 250 mm c/c and one exactly under the footing of the same dimension. The replacement area ratio defined as the ratio of total cross-sectional area of column to the area loaded by steel plate. Replacement area ratio of 8.7% was kept fixed and degree of saturation of soil and soil–cement column length was varied to evaluate their combined effect on the percentage reduction in settlement (Fig. 2).

4.1.2 Preparation of Soil Bed

The soil bed was prepared in a steel tank supported on a loading frame specially fabricated for this purpose. The steel tank had internal dimensions of 750 mm 750 mm × 750 mm. In order to prohibit the movement of the tank as well as frame during the preparation of the soil bed and when during the installation of soil–cement columns, both the frame and the tank were fixed on a rigid support. The tank was also stiffened by diagonally placed angles to avoid its movement under the load. The soil was compacted at density corresponding to 90% of the maximum dry density with moisture content varying as 80 and 100% of optimum moisture content. In order to execute modeled plate load test on the treated as well as the untreated soil, a

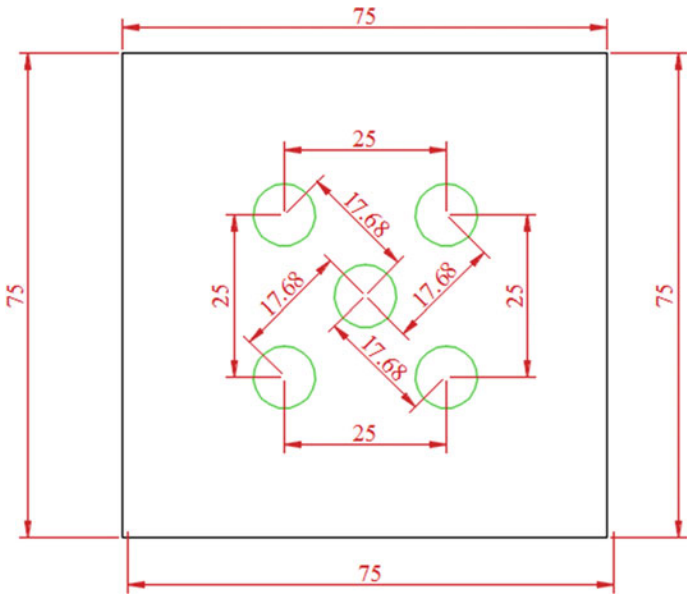

Fig. 2 Schematic plan of arrangement soil–cement columns

strip footing of size 150 mm × 150 mm (i.e., one fifth of the tank dimensions) was fabricated. The entire setup is schematically shown below in Fig. 3.

4.2 Testing Procedure

The test was initially commenced on untreated soil and latter on the strengthened soil in order to evaluate the percentage reduction in settlement of soil after strengthening. Strip footing of size 15 cm × 15 cm was loaded using a mechanical jack, and load was applied in equal increments. To ensure that footing model is subjected to a concentrated load, the rod is fixed at its base with the help of a cap having the same internal diameter as that of the rod. The rod is connected to the proving ring which in turn is attached to the mechanical jack. The settlement was recorded by mechanical dial gauge. Two dial gauges were installed at 180° in order to obtain average settlement. The loading was continued up to settlement of 25 mm or when the soil stops taking the load, whichever is earlier.

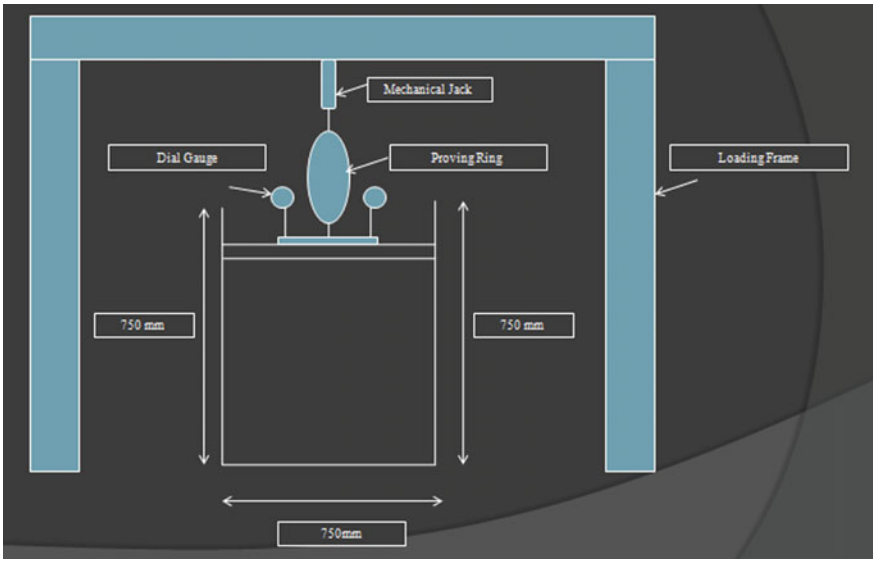

Fig. 3 Schematic diagram of modeled plate load test setup

4.3 Extracted Soil–Cement Columns

After completion of the modeled plate load test, soil–cement columns were extracted in order to check the extent up to which the cement particles grab the soil particles. On extraction it was found that cement particles were able to grab the soil particles in the range of about 3.5 times the diameter of column. Figure 4 shows the extracted soil–cement columns which depicts the influence zone of 3.5 times the diameter of column which nearly simulates the influence zone that is achieved in the field.

Fig. 4 Extracted soil–cement columns

5 Analysis and Discussion of Results

5.1 Strength of Treated Soil

The shear strength of untreated as well as treated soil was evaluated by performing unconfined compression strength test. The soil was compacted at 90% of maximum dry density with varying degree of saturation as 80 and 100% of optimum moisture content and was treated with cement dosages as obtained by employing the procedure given in FHWA. Since for unconfined compression strength test, the length-to-diameter ratio of specimen must vary between 2 and 2.5, and the diameter of soil–cement column was fixed as 50 mm, the effect of soil–cement column length was not being undertaken in evaluating the shear strength of strengthened soil. The results achieved for degree of saturation as 80 and 100% of optimum moisture content are presented in Table 3. The results clearly depict that although the cement dosage was fixed taking the desired strength value as 400 kN/m^2, in place of 250 kN/m^2, taking into account guidelines provided in EuroSoilStab, as the moisture content approaches toward the optimum the strength reduces although the cement dosage is fixed based on that particular moisture content. Thus, deep soil mixing technique is more preferable when the soil is compacted at the dry side of optimum. It can be clearly seen from the results presented in Table 3 that as the moisture content of soil approaches optimum moisture content, the strength of soil reduces even below the desired strength on the field. An increase in the moisture content of soil by 20% tends to reduction in strength by 10–15%. Thus, wet deep mixing method (WDMM) is more feasible when soil is compacted at dry side of its optimum; however, dry deep mixing method (DDMM) might turn out to be feasible at higher moisture content of soil, since it involves use of binder in dry form. It can be observed from the below tabulated values that with rise in the cement dosage strength reduces reason for which can be given as, since the cement dosage is entirely dependent on degree of saturation of soil and with the increase in degree of saturation the strength is reducing, it follows the same trend with cement dosage as well.

The stress–strain curve for samples at degree of saturation as 80% and 100% of optimum moisture content is presented in Fig. 5.

The values of unconfined compression strength obtained at 80 and 100% of optimum moisture content are compared graphically as shown in Fig. 6.

Table 3 Unconfined compression strength for different degree of saturation

Degree of saturation (%)	Unconfined compression strength test (kPa)			Average unconfined compression strength (kPa)
	1	2	3	
80	254.4	253.7	291	266.4
100	193	242.3	272	235.7

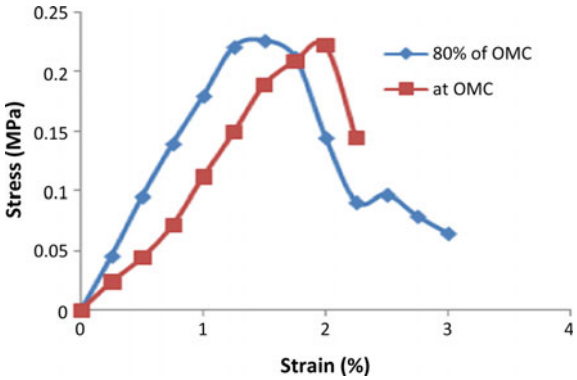

Fig. 5 Stress strain relationship at 80 and 100% of optimum moisture content

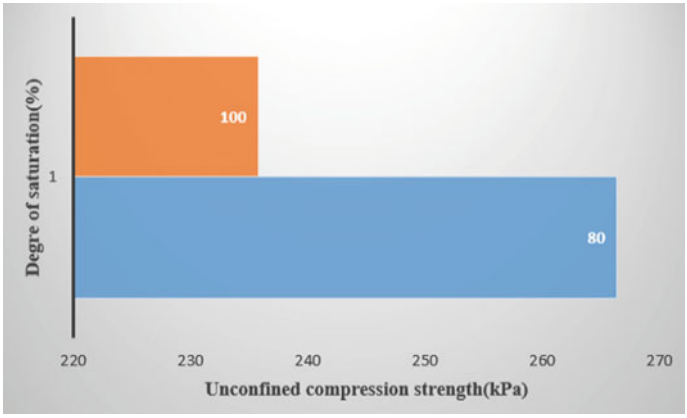

Fig. 6 Comparison between unconfined compression strength at 80 and 100% of optimum moisture content

5.2 Settlement Trait of Treated Soil

5.2.1 Effect of Degree of Saturation

The effect of degree of saturation on settlement trait of strengthened soil for soil–cement column length of 100 and 200 mm is illustrated in Figs. 7 and 8, respectively. As expected, for a given length of soil–cement column, the soil compacted on dry side of optimum showed about 10–15% greater reduction in the settlement as compared to those compacted at optimum moisture content.

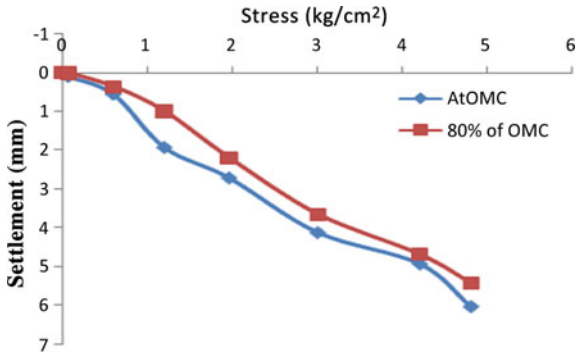

Fig. 7 Stress–settlement curve for 100 mm soil–cement column length at different degree of saturation

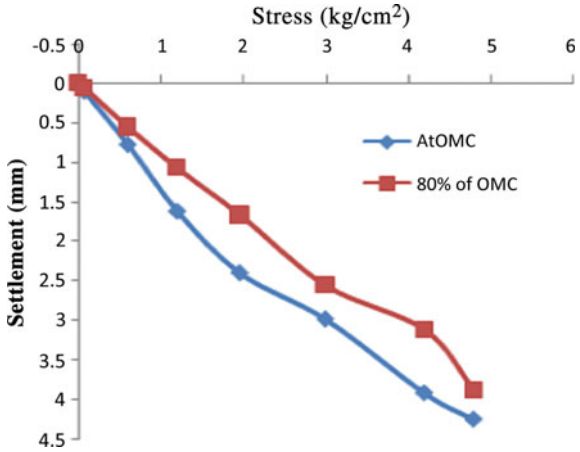

Fig. 8 Stress–settlement curve for 200 mm soil–cement column length at different degree of saturation

5.2.2 Effect of Soil–Cement Column Length

Figures 9 and 10 depict the settlement trait of soil for different length of soil–cement column length for soil compacted at 80 and 100% of optimum moisture content, respectively. For a given degree of saturation, increasing the column length showed about 35% more reduction in settlement.

5.2.3 Stress–Settlement Curves for Untreated and Strengthened Soil

The stress–settlement curve for untreated soil as well as for the soil treated with different soil–cement column lengths and compacted at different degree of saturation as 80 and 100% of optimum moisture content and treated with different soil–cement column lengths as 100 and 200 mm are illustrated in Fig. 11. Figure clearly depicts that under the same load untreated soil undergoes a settlement of 29.9 mm, whereas treated soil undergoes a maximum settlement of 6 mm.

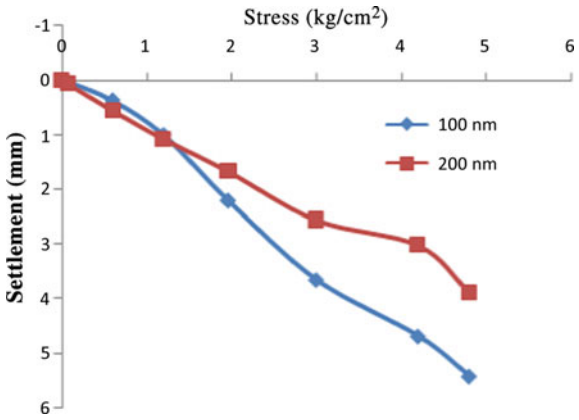

Fig. 9 Stress–settlement curve for soil compacted at 80% of OMC with different soil–column length

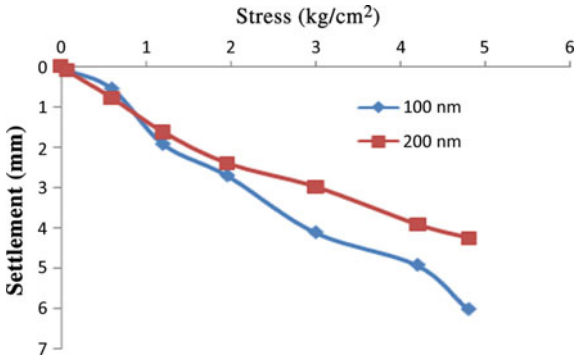

Fig. 10 Stress–settlement curve for soil compacted at OMC with different soil–column length

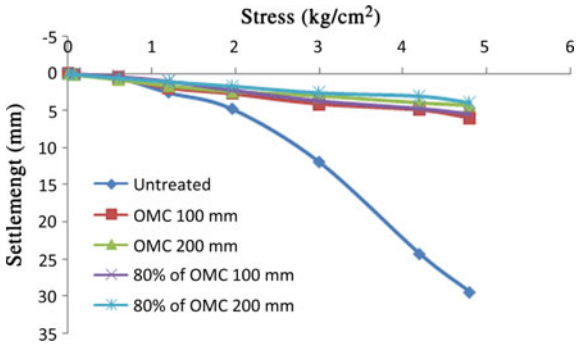

Fig. 11 Stress–settlement curve for untreated and treated soil

5.3 Modulus of Subgrade Reaction and Modulus of Elasticity

The stress–settlement curve obtained after commencement of the modeled plate load test helps in determining the modulus of subgrade reaction of the soil. The modulus of subgrade reaction was worked out corresponding to a settlement of 1.25 mm as well as to load of 0.7 kg/cm^2.

$$k = \frac{p}{0.125} \text{ kg/cm}^2/\text{cm} \tag{4}$$

$$k = \frac{0.70}{d} \text{ kg/cm}^2/\text{cm} \tag{5}$$

Equations (4) and (5) represent the equation employed for evaluating the modulus of subgrade reaction corresponding to settlement of 1.25 mm and an average displacement d (in cm), respectively. After applying corrections for the plate size, degree of saturation and for the load settlement curve, least of the above two values is taken as the modulus of subgrade reaction for the soil.

From the relation available between the modulus of elasticity and modulus of subgrade reaction of the soil as given by Eq. (6), modulus of elasticity of the treated as well as the untreated soil was worked out.

$$k = \frac{0.65E_s}{B(1-\mu^2)} \sqrt[12]{\frac{B^4E_s}{EI}} \tag{6}$$

FHWA (2013) suggests that the ratio of modulus of elasticity to unconfined compression strength at 28 days varies as 75–300; this relation is presently used to validate the experimental results. The ratio of experimentally obtained modulus of elasticity of treated soil to unconfined compression strength test of deep mixed soil at 28 days works out to be 146 (<300) for 80% degree of saturation, and 162 (<300) for 100% degree of saturation. It can be observed from the values of modulus of subgrade reaction and modulus of elasticity tabulated in Table 4 that there is a drastic improvement in their values as compared to untreated soil as well as when the degree of saturation is varied from 100 to 80% at a particular soil–cement column length.

Table 4 Modulus of subgrade reaction and modulus of elasticity of treated and untreated soil

Degree of saturation (%)	Soil-cement column length (mm)	Modulus of subgrade reaction; k (kg/cm^2/cm)	Modulus of elasticity; E (kg/cm^2)
At OMC (Untreated)	0	4.44	161.01
80% of OMC (Treated)	100	7.4	258.01
	200	7.7	267.65
At OMC (Treated)	100	5.0	179.67
	200	5.3	189.6

6 Conclusion

The important conclusions that can be derived from this study are listed below:

- As the moisture content of the soil approaches the optimum moisture content, strength of the treated soil reduces.
- For a given degree of saturation of the soil, with the increase in the soil–cement column length about 30–35% more reduction in settlement was observed.
- For a given soil–cement column length, with the increase in the degree of saturation of soil, the percentage reduction in settlement was recorded to decline by 10–15%.
- At same degree of saturation, with the increase in the soil–cement column length modulus of subgrade reaction was found to increase by 5–7%.
- For the same column length, with decrease in degree of saturation modulus of subgrade reaction was found to increase by 45–50%.
- At same degree of saturation, with the increase in the soil–cement column length modulus of elasticity of soil was found to increase by 4–6%.
- For the same column length, with decrease in degree of saturation modulus of elasticity of soil was found to increase by 45–50%.

It can thus be concluded that cement deep mixing (CDM) technique when applied on low plastic soils subjected to variation in degree of saturation gives satisfactory results. Use of microfine cement as a binder for low plastic soils was found to be adequate for a suitable water to cement ratio selected. Various assumptions regarding the length of soil–cement column were made in the study due to lack of ample amount of Indian Codal guidelines on CDM technique, the assumptions made provided adequate results, thus indicating the feasibility of CDM technique as a modern ground improvement technique for low plastic soil.

Acknowledgements The authors are thankful to Dr. G. P. Vadodaria for providing all the facilities required for the successful accomplishment of this research work.

References

Carasca O (2016) Soil improvement by mixing: techniques and performances. Energy Proc 85:85–92

Coastal Development Institute of Technology (CDIT) (2002) The deep mixing method: principle, designed construction

EuroSoilStab (2002) Design guide soft soil stabilization, CT97-0351

Farouk A, Shahein MM (2013) Ground improvement using soil-cement columns: experimental investigation. Alexandria Eng J (Elsevier) 52:733–740

Federal Highway Administration Design Manual: Deep Mixing for Embankment and Foundation Support (2013) FHWA-HRT-13-046

Filz GM et al (2005) Standardized definitions and laboratory procedures for soil-cement specimens applicable to wet method of deep mixing. Geo-Front Congr ASCE 162(1):1–13

Ismail MA et al (2002) Effect of cement type on shear behavior of cemented calcareous soil. ASCE 128(6):520–529

Kitazume M et al (2015) Applicability of molding procedures in laboratory mix tests for quality control and assurance of the deep mixing method (Elsevier) 55:761–777

Probaha A (1988) State-of-the-art in deep mixing technology, Part I: basic concepts and overview of technology

Study on Strength and Volume Change Behavior of Expansive Soil Using Non-traditional (Bio-enzyme) and Traditional (Lime and Bagasse Ash) Stabilizers

Srinivas F. Chitragar, Chandrashekhar B. Shivayogimath and Raviraj H. Mulangi

Abstract Roads are vital for the economic growth of a country. Keeping balance between performance and cost of the roads and at the same time fulfilling the environmental regulations is becoming a challenge for engineers to design road with poor engineering properties of soils like expansive soils. Present research work is focused on the study on strength and volume change behavior of soft soil using non-traditional stabilizer bio-enzyme and traditional stabilizers lime and bagasse ash. Recently, bio-enzymes have emerged as a new agent for soil stabilization. These enzymes have been proven to be effective, economical, and environmentally friendly. One such bio-enzyme, terrazyme, is selected to study its effect of Free Swell Index (FSI) of the soil with different dosages of bio-enzyme (i.e., 0, 100, 200, and 300 ml/cum of soil). Further, the effect of combination of traditional stabilizer like lime and bagasse ash with bio-enzyme is carried out. The study shows that the optimum dosage of stabilizers (i.e., terrazyme 300 ml/cum + bagasse ash 3% + lime 3%) gave significant increase in CBR value and significantly decreased in FSI values. Based on the laboratory tests, it can be concluded that the combination of additives can be considered as a potential stabilizers for expansive soils.

Keywords Expansive soils · Free Swell index · California bearing ratio · Terrazyme

S. F. Chitragar (✉) · C. B. Shivayogimath
Department of Civil Engineering, Basaveshwar Engineering College (Autonomous), Bagalkot 587102, Karnataka, India
e-mail: fc.srinivas@gmail.com

C. B. Shivayogimath
e-mail: cbsmath15@gmail.com

R. H. Mulangi
Department of Civil Engineering, National Institute of Technology Karnataka (NITK), Suratkal, Karnataka, India
e-mail: ravirajsdni@gmail.com

R. Sundaram et al. (eds.), *Geotechnics for Transportation Infrastructure*, Lecture Notes in Civil Engineering 29,
https://doi.org/10.1007/978-981-13-6713-7_46

1 Introduction

The growth of the vehicular population has created a need for better and economical vehicular population which requires good highway having proper geometric design, pavement condition, and maintenance. The highways have to be maintained so that comfort, convenience, and safety can be provided to the commuters according to Ravishankar et al (2009). The Indian road network is over 54,72,144 km long as per 2015 statistics of which less than 50% are paved. Qualitatively, India's roads are a mix of modern highways and narrow unpaved roads and are in need of drastic improvements according to the study done by Venica and Vaishnava (2015).

The black cotton soil (BC soil) covers considerably large area, nearly one-third of Indian land. This BC soil occurs mostly in North Karnataka, Maharashtra, Gujarat, and Madhya Pradesh. In North Karnataka region, the land under cultivation is mostly of BC soil. It is inorganic clay of medium-to-high compressibility. It is characterized by high shrinkage and swelling properties, and hence, the BC soil has been challenging to the highway engineers. This soil is very hard in dry state but loses its strength completely when it is in wet condition. We often face the problem to construct the road in such soil, which does not posses sufficient strength to support subbase and the super imposed loads coming on it during service life of the pavement, this soil will also undergo large volumetric change which reflects the unevenness in the pavement surface

Soil stabilization is a process in which weak soil has been modified to the required physical property and strength by means of mechanical compaction or by using some additives which is known as soil stabilization. A study done by Prasad and Sen (2015) shows that soil stabilization can be achieved by improving gradation of particle size to some extent and further improvement can be achieved by using pozzolanic and cementitious materials like cement fly ash and lime. According to study carried out by Agarwal and Kaur (2014) and Lekha et al. (2012), properties of soil which are modified to engineers' requirement are strength, compressibility, permeability, and volume stability. The laboratory tests followed by field tests may be required in order to determine the engineering and environmental properties. Laboratory tests results will help in deciding the choice of stabilizer and amounts.

Saurabh and Mishra (2008) reported the use of terrazyme in India. They found that it has been used to construct a low-volume roads constructed under PMGSY and few state highway on black cotton soil in Nasik, Maharashtra. Public Works Department has constructed two roads using terrazyme, and a cost reduction of 18–26% is reported. Some trial roads are also constructed in states of Tamil Nadu, Kerala, and Karnataka, and in Maharashtra by using terrazyme.

2 Laboratory Investigate

The following laboratory investigations were carried out to study the behavior of black cotton soil.

2.1 Free Swell Index (FSI) Test

Free Swell Index is an indicator of expansive behavior of the soil, which is determined in accordance with IS: 2720 Part-40. To determine FSI, two soil samples of oven dry and passing through 425-μm IS sieve of 10 gm each is taken and mixed one with 100 ml water and another with 100 ml kerosene in a measuring jar and stirred properly. It is allowed to settle, and after 24 h final volume of soil in each cylinder is recorded. FSI is determined by using Eq. 1 given below.

$$\text{FSI} = \frac{V_\text{d} - V_\text{k}}{V_\text{k}} \times 100 \tag{1}$$

where

V_d volume of soil specimen reading from the graduated cylinder containing distilled water, and

V_k volume of soil specimen reading from the graduated cylinder containing kerosene (Fig. 1).

2.2 California Bearing Ratio (CBR) Test

The CBR test was conducted in the laboratory on the prepared specimen in mold. The laboratory apparatus consists of mold of 150 mm dia. With base plate and collar, a loading frame with cylindrical plunger of 50 mm dia. And dial gauge for measuring the penetration values of causing a cylindrical plunger of 50 mm dia. To penetrate pavement component materials at 0.625 mm/min., the load values to

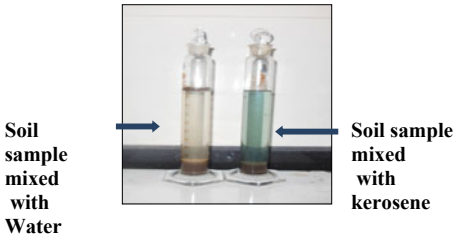

Fig. 1 FSI test apparatus

Fig. 2 CBR test apparatus

cause 2.5–5 mm are recorded. The surcharge weight was placed under the plunger of loading frame. The load values were noted corresponding to penetrate values of 0.0, 2.5, and 5 mm, etc. The load penetration graph was plotted against penetration values. The CBR value at 2.5 mm penetration, which is higher than that 5 mm, is reported as the CBR value. If the CBR value obtained from the test at 5 mm penetration is higher than 2.5 mm, then test should be repeated for checking. If check test again give similar results than higher value obtained at 5 mm penetration is reported as the CBR value. The CBR test apparatus is shown in Fig. 2

3 Objectives

i. Evaluate effects of additive on Free Swell Index of soils by addition of different dosages of terrazyme (i.e., 0, 100, 200, 300 ml/cum of soil)
ii. To study the volumetric change in soil by Free Swell Index due to addition of different dosage of terrazyme with 3% bagasse ash and 3% lime.
iii. To study the strength behavior of black cotton soil by CBR test by addition of different dosage of terrazyme with 3% bagasse ash and 3% lime.

4 Experimental Program/Methodology

In this study, the black cotton soil is collected from the village Naragund which is in Gadag District of Karnataka state, India. According to the HRB classification, the soil is identified as A-7-5-type soil which is inorganic fat clay of high plasticity (CH) as per unified soil classification system (USCS). The detailed characterization of soil has been done, and further, it is continued to study the strength and Free Swell Index (FSI) of the soil by using traditional and non-traditional stabilizers.

To study the swelling behavior of soil, FSI test of the soil is carried out with four different dosages of terrazyme (i.e., 0, 100, 200, and 300 ml/m^3 of soil) and addition of 3% lime and 3% bagasse ash are also carried out. Further, to determine the change in behavior of strength, CBR test is carried out only with non-traditional stabilizer terrazyme of dosage 300 ml/m^3 and the mixture of terrazyme with 3% lime and 3% bagasse ash is also done. The results were analyzed. Physical characteristics of these soils are summarized in Table 1.

4.1 Non-traditional Stabilizer Terrazyme

Terrazyme is a liquid enzyme which is organic in nature and is formulated from the vegetable and fruit extract. Terrazyme is an ionic surface-active agent which changes the hydrophilic nature of clay and lime materials to hydrophobic. Its application not only assists in the expulsion of water from soils, but also aids the lubrication of soil particles and increases the compatibility of many soils. The reaction of terrazyme on these materials is particularly effective because of the ion-exchange capacity of clay minerals the property that clay minerals have of absorbing certain ions such as the terrazyme molecule, thereby changing its physical properties. Properties of the terrazyme are shown in Table 2.

$$H_2O + \text{clay} \longrightarrow \text{terrazyme Calcium Silicate Hydrates}$$

Table 1 Physical properties of soil used in this study

Property	Results	IS codes
Specific gravity	2.12	IS 2720(Part-3)-2002
Liquid limit (%)	64.7	IS 2720 (Part 5)-2006
Plasticity Index (PI, %)	30.2	IS 2720 (Part 5)-2006
HRB classification	A-7-5	HRB classification
USCS classification	CH	ASTM D 2487
Maximum dry unit weight (kN/m^3)	14.6	IS: 2720(Part 7)-2011
Optimum moisture content (%)	28.72	IS: 2720(Part 7)-2011
Free Swell Index	93.16	IS: 2720(Part 40)-2002
CBR (%)	1.12	IS: 2720(Part 16)-2002

Table 2 Properties of terrazyme

Properties description	Values
Specific gravity	1.05
pH value	3.50
Appearance or odor	Dark brown and non-obnoxious
Total dissolved solids	9.7 ppm
Cation exchange capacity	3.87%
Hazardous content	None
Boiling point	212F
Evaporation rate	Same as water
Solubility in water	Complete
Melting point	Liquid
Reactivity data	Stable

Source info@avijeetagencies.com

5 Result and Discussion

Table 3 and Fig. 3 show the variation of FSI % with addition of terrazyme and with the addition of combination of additives. The maximum reduction in FSI is seen in the combination of additives, i.e., terrazyme 300 ml/cum with 3% lime and 3% bagasse ash which is almost 3.25 times reduction in FSI value, whereas the soil with the addition of terrazyme gave 1.77 times reduction. It is shown that the combination of additives gave better reduction in FSI.

The study is carried out in determining the strength parameter of expansive soil by CBR test. Variation of CBR % with addition of terrazyme and with the addition of combination of additives has been carried out. The maximum increased CBR value is seen in combination of additives, i.e., terrazyme 300 ml/cum with 3% lime and 3% bagasse ash, which is more than six times compared with the initial CBR of untreated soil, whereas the soil with the addition of terrazyme gave nearly two-times increase in CBR value. It is shown that the combination of additives gave better increase in strength of the expansive soil. The same has been represented in Table 4 and in Fig. 4

Table 3 FSI values of different mixes of soil

Terrazyme (ml/cum)	FSI (%) soil + terrazyme	FSI (%) soil + terrazyme + lime 3% + bagasse ash 3%
0	93.16	93.16
100	62.7	48.48
200	59.45	33.45
300	52.52	28.60

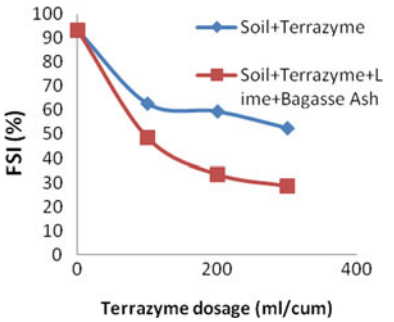

Fig. 3 FSI of soil without and with additive

Table 4 CBR of different mixes of soil

Additives and dosages	Average CBR values (%)
Untreated soil	1.12
Soil + terrazyme (300 ml/cum)	2.08
Soil + terrazyme (300 ml/cum) + bagasse (3%) + lime (3%)	7.21

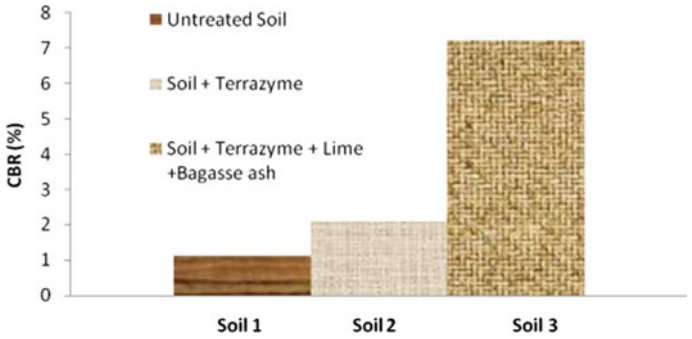

Fig. 4 CBR of soil without and with additives

6 Conclusions

From the above investigation, the following conclusions can be drawn:

i. The black cotton soil is tested with all the physical parameters, with the Atterberg limits; the soil is classified as **clay loam** soil as per textural classification.
ii. As per the Highway Research Board classification, it is classified as A-7-5 properties.

iii. The CBR value of the BC soil increases from 1.12 to 7.21% with the addition of terrazyme + bagasse ash + lime. The increase in CBR value is an indication of higher compressive strength of a soil, better for construction of subgrade of the pavement by stabilizing the expansive soil.
iv. Swelling potential of the BC soil decreases drastically from 93.16 to 28.6% with combination of terrazyme, bagasse ash and lime, which gives the better performance of subgrade soil.

Based on the different laboratory performance tests, it can be concluded that terrazyme + bagasse ash + lime can be considered as a potential stabilizers for clay and silty soils like black cotton soil. It helps to improve compressive strength of soil, in addition to decrease in swelling potential of soils.

Acknowledgements Author would like to thank the undergraduate students Mr. Vinay Y. G., Miss. Pallavi Tuppad, Mr. Vinaykumar W., and Mr. Siddalinga Reddy who helped in the experimentation work of the above study. Author would also like to thank suppliers for their help in providing materials and additives; the author has no intension to promote any commercial products used in the present study.

References

Agarwal P, Kaur S (2014) Effect of bio-enzyme stabilization on unconfined compressive strength of expansive soil. Int J Res Eng Technol 3(5):30–33

ASTM D2487-11 Standard practice for classification of soils for engineering purposes (unified soil classification system)

IS 2720 (Part III)-2002 Determination of specific gravity of soil

IS 2720 (Part VII)-2011 Determination of water content-dry density relation using light compaction

IS 2720 (Part IV)-2006 Grain size analysis

IS 2720 (Part V)-2006 Determination of liquid and plastic limit

IS 2720 (Part XVI)-2002 Laboratory determination of California bearing ratio

IS 2720 (Part XL)-2002 Determination of free swell index of soil

Lekha BM, Sarang G, Ravi Shankar AU (2012) Laboratory investigation on black cotton soil stabilized with non-traditional stabilizer. IOSR J 7–13 (e-ISSN: 2272-1684 p-ISSN: 2320-334X)

Prasad J, Sen J (2015) Stabilization of black cotton soil using bio-enzyme for a highway material. 4(12)

Ravi Shankar AU, Rai HK, Mithanthaya R (2009) Bio-enzyme stabilized lateritic soil as a highway material. J Indian Road Congress 143–151

Saurabh BG, Mishra CB, Umrigar NF (2008) Sub grade soil stabilization using terrazyme

Venica S, Vaishnava P (2015) Soil stabilization by using terrazyme. Int J Adv Eng Technol 8:566–573

Use of Dynamic Compaction in Constructing Subgrades Over Reclaimed Fills

Saptarshi Kundu and B. V. S. Viswanadham

Abstract In recent times, rapid urbanization coupled with an acute shortage of suitable lands for construction of transportation infrastructures have opened up arenas for finding means of utilizing existing weak subgrades by adopting eco-friendly ground improvement technologies. In this context, dynamic compaction (DC) has evolved as a viable option in view of the simplicity, cost-effectiveness and low-carbon footprint associated with this technique. In the present paper, an attempt has been made to investigate the effectiveness of DC in facilitating construction of pavements and road subgrades over loose reclaimed fills and engineered MSW landfills post their design life. The primary objective is to assess and identify the various geotechnical parameters guiding the efficiency of the mechanism depending upon the road functionality and traffic expectations. Five influencing factors that need to be considered in the field are discussed in this respect, wherein the first factor involves consideration of the deformation modulus of the weak subgrade illustrated through construction of a moderately large road project over a reclaimed island of 198,000 m^2 extent consisting of extremely loose silty sand deposits. Pressuremeter tests conducted post DC revealed substantial improvement in the upper 7 m of stratum with an increase of about 4 times the average deformation modulus of soil. The next factor is the liquefaction susceptibility of the fill material, which is demonstrated through a case study involving improvement of liquefiable flood-plain site by heavy tamping, resulting in significant reduction in liquefaction susceptibility of the remediated ground. The third criteria considered is the initial moisture content of the fill material related to placement of a road embankment foundation over a marshy land by DC associated with sand-drain installation, which resulted in significant improvement in the dry density and cohesion of the in situ soil. The fourth factor is the energy level involved in compaction process, the importance of which is demonstrated through a

S. Kundu · B. V. S. Viswanadham (✉)
Department of Civil Engineering, Indian Institute of Technology Bombay, Mumbai 400076, India
e-mail: viswam@civil.iitb.ac.in

S. Kundu
e-mail: saptarshikundu123@gmail.com; kundusaptarshi@iitb.ac.in

R. Sundaram et al. (eds.), *Geotechnics for Transportation Infrastructure*, Lecture Notes in Civil Engineering 29,
https://doi.org/10.1007/978-981-13-6713-7_47

project involving extensive treatment of a hydraulic fill consisting of primarily compressible clays by DC for future infrastructural constructions. The fifth parameter discussed is the effect of DC on long-term settlements of infrastructures observed during reclamation of a MSW site by high-energy DC methodology for constructing highway embankments and road utilities. Based on these compilations, a relationship between tamper mass and height of fall adopted in the field is suggested in this paper, and the depth of improvement and surface settlements incurred during DC in case of reclaimed fill materials are evaluated for optimizing the process of foundation design in the field.

Keywords Dynamic compaction · Reclaimed fills · MSW landfills

1 Introduction

In recent times, rapid urbanization coupled with population explosion in and around the cities have created acute scarcity of suitable construction sites to accommodate the growing industrial and social needs. This has led to renewed interest in finding suitable means of improving the geotechnical characteristics of existing problematic soils to facilitate construction on these sites. Further, possibilities of reclamation of fills and waste disposal sites are also coming to the forefront in the current global scenario. However, the engineering properties of the reclaimed fills and problematic soils need to be improved prior to their use in construction of road subgrades and foundation support for infrastructural facilities. Although substantial work has been carried out in the context of dealing with problematic soil types, the challenges associated with construction on reclaimed fills are yet to be addressed and documented. The following section summarizes the potential problems associated with reclaimed lands and suggests suitable ground improvement methods for dealing with those problems.

1.1 Problem Formulation

A major problematic soil type encountered in the field include man-made fills, which are heterogeneous by nature and do not exhibit consistent or reliable engineering properties. In urban areas, infilling of built areas is occurring at an increased rate, and as municipalities struggle to accommodate the increasing population level, the leftover sites are targeted for development. Such sites often require extensive remedial measures including massive excavation and replacement or mass-scale disposal. The fill materials existing in these sites can be of three different types; engineered fill, dumped fill or hydraulically deposited fill, out of which, engineered fill is most widely used for the purpose of supporting structures. It consists of granular materials or select subgrade soils compacted in thin lifts to a minimum

level of compaction. When properly constructed and monitored, engineered fill can be relied on for subgrade construction with acceptable bearing capacity. Hydraulic fill is placed typically using water either through stream or river action, or by land reclamation in water bodies. Dumped fill is by nature the most variable fill type encountered in the field, and the typical response is to remove and either re-engineer it back in place, or, to replace it with approved engineered fill soils. In general, the fill materials possess high compressibility characteristics, generating large and often unexpected settlements. This can yield disastrous consequences for structures unwittingly built on such deposits. Fills placed in a relatively dry state are likely to induce major post-construction settlements in the form of volumetric soil collapse, whereas, fill placed in a wet condition undergo considerable consolidation but less collapse. Thus, for a particular fill, the amount, type and even the rate of settlement will depend on a variety of factors, including fill depth, moisture and compaction characteristics, and groundwater conditions prevailing in the site after fill placement. Accordingly, one should keep large settlements in mind when designing transportation infrastructures on recently reclaimed fills.

1.2 Methodology Adopted

In order to overcome the problems associated with existing weak subgrades, various ground improvement methods are adopted in the field related to mechanical and hydraulic modification, physical and chemical stabilization, modification by inclusions or a combination of the above. The selection of a particular method depends on the type and degree of improvement required, soil type existing in the field and road functionality and traffic expectations within the proposed subgrade. Among the available ground improvement techniques, Dynamic compaction (DC) has gained popularity as an effective improvement technique for geomaterials over the past few decades, in view of its simplicity, low-environmental impact and cost effectiveness. The low carbon footprint associated with this ground remediation method addresses the adverse ecological threats imposed on the environment and society due to unsustainable geotechnical engineering practices encountered in the face of rapid urbanization. In addition, DC enables reclamation of MSW sites for future infrastructure projects including construction of highway embankments and major road utilities Swain and Holt (1987) and Lewis and Langer (1994). Drawing parallel to the above, an attempt has been made in the present paper to investigate the effectiveness of DC in facilitating construction of pavements and road subgrades over loose reclaimed fills and in engineered MSW landfills post their design life. Five different field case studies have been discussed in this respect, and the increase in deformation modulus and relative density of existing weak subgrade under the impact of DC has been investigated. Further, the various design parameters influencing the process in the field are discussed briefly, and the final depth of improvement achieved post DC is evaluated to facilitate an understanding of the depth of foundation to be adopted in such reclaimed fills.

2 Influence of Various Field Conditions

The various design parameters affecting the performance of DC in reclaimed fills need to be assessed to ensure an effective planning and execution of the process in the field. In this regard, five typical field cases pertaining to the implementation of DC on a wide variety of reclaimed soil types have been discussed in subsequent sections.

2.1 Deformation Modulus of Weak Subgrade

The deformation modulus of the existing fill material and that expected in the remediated ground are crucial parameters which need to be addressed while evaluating the design aspects of DC. Drawing parallel to the above, a typical case is discussed in this section related to construction of a moderately large road project over a reclaimed island of 198,000 m^2 extent consisting of extremely loose silty sand deposits. The island, referred to as Marjan island or Coral Island is the first manmade group of islands of its kind that was undertaken in the northern emirate of Ras Al Khaimah in the United Arab Emirates. As per the database of Hamidi et al. (2011a, b, 2012), geotechnical investigation of the study area indicated the presence of a heterogeneous fill consisting of very loose to medium dense sand in the top 7 m, whereas, the next stratum extending up to 16 m was composed of medium dense to very dense silty sand with occasional interbedded pockets of sandy silt. The fines content in general varied from 13 to 30%, and Pressuremeter test (PMT) data indicated a deformation modulus as low as 70 kPa in the vicinity of the fill material. The above geotechnical parameters measured at the site indicated possibility of large differential settlements during the proposed land reclamation due to the self-weight of the soil. Structural and traffic loads further increased the risks of failure due to excessive ground deformations and insufficient bearing capacity. In view of the above, DC was implemented at the site by transmitting high energy impacts to the underlying fill with a pounder of mass 170–200 kN from a drop height of 20 m by imparting 5–8 blows at each print location. In the ironing or light dynamic compaction phase, a 120 kN pounder was dropped from 17 m height. Based on the road functionality, the ground improvement design criteria were specified as 25 mm under a uniform load of 20 kPa on the road area, whereas the maximum differential settlement between any two pints on the roadway was selected as 1:500. The above design criteria were verified in the remediated ground post DC by assessing the deformation modulus through PMT tests. The results indicated an increase of 4 times the value of average deformation modulus of the weak subgrade, and that the maximum improvement was achieved at an influence depth of about 8 m as presented in Fig. 1.

In addition, the corresponding settlements incurred at salient testing points were observed to be only 2.2 mm, which is substantially less than the acceptable

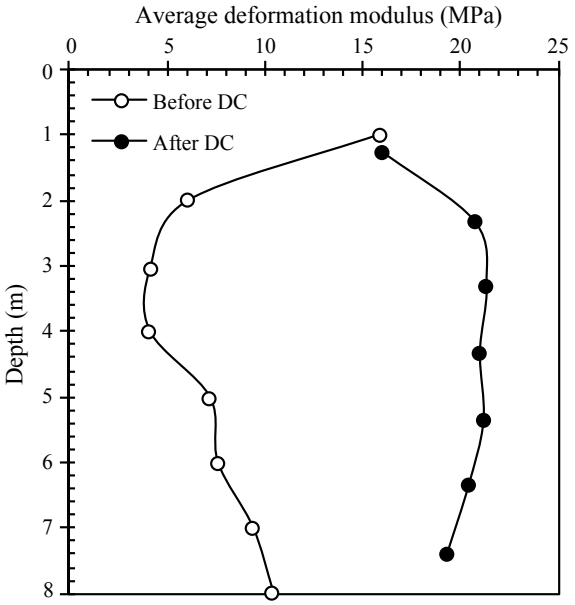

Fig. 1 Improvement in deformation modulus of weak subgrade after DC. Modified after Hamidi et al. (2012)

settlement between two points. The above study hereby demonstrates the efficacy of DC in land reclamation projects with especial emphasis on the importance of deformation modulus of the fill material in deciding verification of design criteria.

2.2 Liquefaction Susceptibility of the Fill

Another important design criterion to be considered while undertaking DC projects in reclaimed fill areas is the liquefaction susceptibility of the in situ ground. In such cases, conventional DC procedure adopted in the field as outlined previously may not be sufficient to meet the design criteria related to construction of transportation infrastructures. A typical example of such a case is described in this section through improvement of a flood-plain site consisting of loose sand deposits extending up to a depth of 22 m, which are highly susceptible to liquefaction Kumar and Puri (2001). Preliminary subsurface investigation techniques revealed the existence of a thin layer of fill comprising of primarily weathered shale and silty clay underlain by a thick deposit of floodplain alluvium. The presence of low density saturated sands within the liquefiable site eventually prompted the use of heavy tamping technique coupled with additional stone column installation measures to counteract major seismic events. In this case, for achieving the project goals, initially a tamper of 170 kN weight was made to fall from a height of 21 m in phases on a grid pattern over the entire fill expanse. Standard Cone Penetration (SPT) tests conducted at the site post DC indicated that the maximum improvement zone due to densification

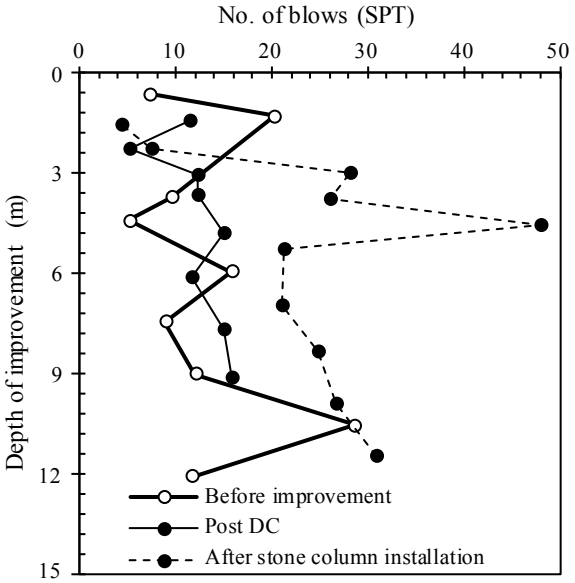

Fig. 2 SPT data before and after DC. Modified after Kumar and Puri (2001)

occurred at 6–9 m below the ground surface as illustrated in Fig. 2, which was much less than the depth of the existing liquefiable stratum.

In order to increase the effective depth of compaction, the top 1.5 m of fine grained soil strata was removed for construction of short stone columns. The tamper mass, number of drops, and drop height selected during installation of stone columns were reported to be in the range of 170 kN, 10 and 21 m respectively. It was observed that the stone columns facilitated dissipation of the excess pore water pressure generated due to DC, thereby accelerating the process and affecting the soil improvement up to a larger depth of 12 m, as evident from Fig. 2. The above case study highlights the importance of taking into account the liquefaction potential of weak subgrades, and on possible remedial measures to counteract the same. Further, it can be concluded that heavy tamping in association with stone column installation within the reclaimed flood plain site was successful in facilitating constriction of shallow foundations for transportation facilities, thereby reducing the overall project cost attributed to pile foundations.

2.3 Initial Moisture Content of Fill Material

The importance of selecting the appropriate ground modification methodology at the site in the context of presence of considerable moisture content of the in situ fill material is discussed in this section. In this regard, the placement of a road embankment foundation over a marshy land consisting of a 41 m deep gully

formation is considered, and the results of DC are compared with those obtained from compaction by rolling. After field testing and repeated trials, DC was employed at the site to treat the wet soft marshy fill having an initial water content of 7–19% by imparting vibration waves of around 2000 kN-m energy per drop. The entire process was executed in three different stages, and the degree of compaction of the improved ground was evaluated. As reported by Zou et al. (2005), majority of the test samples which were compacted by rolling failed to meet the design criteria of 90% compaction, whereas, for all the sample points taken within the zone of DC, the compaction degree exceeded 90%, and met the compaction requirement of the road embankment. However, the test results post DC indicated that the influence depth was less than 5 m, which did not meet the design requirement of 7 m. In addition, the initial high moisture content of the fill material coupled with heavy rainfall during the compaction process resulted in a water content of about 24% of the foundation layer. Hence, to accelerate the consolidation process of the soft foundation soil, fabric-enclosed sand drains of 0.1 m diameter were installed at a spacing of about 3 m, which resulted in larger influence depth and reduction in soil compressibility. At the same time, significant improvement was noted in the dry density and cohesion of the in situ soil. The results derived from the present field study hereby indicate that DC can be applied in a much larger range of water content of the fill material as compared to rolling process, and that during rainy season, it is difficult to guarantee a suitable water content of filled soil for compaction by rolling. Further, the above case study highlighted that the moisture content adopted during DC in fills placed in wet condition at the site should be close to the optimum moisture content, which was observed to be between 11 and 15% in the present case.

2.4 Energy Level Involved in Compaction

The energy level involved in compaction process plays a crucial role in guiding the efficiency of DC. The same is discussed in this paper through a project involving extensive treatment of a hydraulic fill by DC for coastal reclamation purposes. The fill material at the site consisted of primarily compressible soft clays with an average grain size starting from 200 mm and exceeding 800 mm, as per the reports of Feng et al. (2010). In view of the above, high energy levels of about 8000 kN-m were adopted for remediation of the hydraulic fill by DC, as owing to the differences in the improvement mechanism between low and high energy compactions, it would be inappropriate to apply the design method and experiences of low energy DC in projects dealing with coarse-grained materials. The other important influencing factors taken into consideration at the site included the mass of the tamper, the height of fall, the number of passes, the sequence of drop points, the time delay between passes, the grid spacing etc. The above parameters were so designed that post DC, the desired ground bearing capacity and improvement depth could reach the design requirements of not less than 120 kPa and 10 m

respectively. The entire process of DC was executed in three stages, and in the first and second passes, a 400 kN pounder was dropped from a height of 20 m, resulting in a high impact energy level of 8000 kN m per drop. For the third pass, a lower impact energy of 2000 kN m per drop was simulated, equivalent to a 200 kN pounder dropping from a height of 10 m. During monitoring of the remediated ground, it was observed that no notable ground heave occurred under an impact energy level of 8000 kN-m, whereas, substantial heave was observed at the ground surface when the impact energy level was about 3000 kN-m. The radius of influence was also observed to increase proportionally with higher energy of tamping. Further, subsurface investigation techniques like SASW performed at the site indicated that the depth of improvement post DC was not less than 10 m, and existence of weak layers were not reported. In addition, plate load test data clearly signified that he bearing capacity of the improved ground met the allowable design capacity of 120 kPa. The above project hereby highlights that during reclamation of fill areas consisting of primarily coarse-grained materials, high-energy DC process should be adopted in the field, as the improvement extends to greater depths and higher ground bearing capacities can be achieved in this case.

2.5 Effect of DC on Long-Term Settlements

The fifth parameter considered is the effect of DC on long-term settlements of infrastructures, demonstrated through a case study related to monitoring of the performance of highway embankments having 3–9 m in height, constructed over an existing municipal solid waste (MSW) landfill site. The typical depth of the landfill material varied from about 1.8 to 7.4 m, and it consisted of approximately 45% organic material. High-energy DC was subsequently adopted at the site to reduce post construction settlements of the highway structures Lewis et al. (2004). In this case, a 180 kN weight was dropped from a height of 24.4 m, and two solid steel weights of varying cross sections were used for imparting the drops. The first tamper consisted of a 1.8 m square weight while the other was a 2.1 m diameter circular weight. The weights were made to fall for a maximum of five to ten times at each print location, until no substantial increase in crater depth was observed. In addition, preloading technique was used over a separate portion of one of the highway embankments by constructing a 1.5 m high surcharge loading for comparing the effectiveness of the above two methods. The settlement profile of the constructed highways was monitored for both sections of the embankments. The results indicated that the roadway embankment constructed over landfill material treated by DC performed better with respect to that treated by surcharge as far as primary settlements were concerned. In a similar manner, the secondary settlements monitored for a period of 12 years signified much slower rate of settlements in the zone treated by DC, accompanied by reduced differential settlements by about 50% as compared to that observed in the surcharge area.

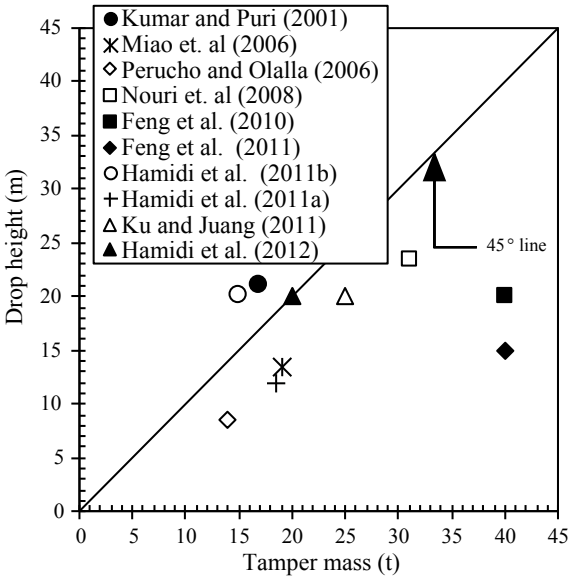

Fig. 3 Correlation between the drop height and tamper mass adopted during DC of reclaimed fills

3 Correlation of Tamper Mass and Drop Height

The relationship between tamper mass and drop height adopted at the site during DC on reclaimed fill materials is illustrated in Fig. 3.

The compilation is based on the values reported in the field by several researchers including Kumar and Puri (2001), Miao et al. (2006), Perucho and Olalla (2006), Nouri et al. (2008), Feng et al. (2010, 2011), Hamidi et al. (2011a, b, 2012) and Ku and Juang (2011). As can be observed from Fig. 3, the drop height adopted in the field usually lies between 10 and 20 m, with majority of the points being clustered around 20 m. In a similar manner, the tamper mass is observed to lie in the range of 15–40 tonnes, which is a much wider range as compared to that of the height of fall. In general, the data points presented in Fig. 3 are widely scattered around the 1V:1H line, thereby indicating that the drop height and tamper mass are seldom equivalent in the field, and in almost all the cases considered, the latter exceeds the former substantially in magnitude.

4 Calculation of Depth of Improvement

The design strategy and application of DC process at the site are largely empirical in nature, and till date, the execution methodology relies heavily on the designer's experience and judgment. In this regard, a simplified empirical relationship was

suggested by Menard and Broise (1975) for a preliminary estimation of the depth of improvement due to DC as presented in Eq. (1):

$$d_{\max} = n\sqrt{WH} \tag{1}$$

where $d_{\max}$ is the improvement depth (m), W is the tamper weight (tonnes), H is the drop height of tamper (m) and n is an empirical constant. Several researchers have calibrated the original equation Eq. (1) based on available data from various DC sites to arrive at typical values of the parameter 'n'. Mayne et al. (1984) and Lukas (1986) have suggested that the value of n usually varies from 0.30 to 0.80 in case of granular soils. However, till date, limited research has been carried out for estimating the depth of improvement in reclaimed fills. In this regard, the data points obtained on the basis of compiled field case histories as discussed above are plotted in Fig. 4, wherein the abscissa represents the energy level applied in the field, and the ordinate depicts the corresponding influence depth achieved at the site.

As evident from Fig. 4, by adopting the method of curve-fitting to Eq. (1), the lower and upper limits of the empirical parameter n comes out to be 0.30 and 0.60 respectively, with the mean value located at 0.45. Hence, Fig. 4 can be used to get a preliminary idea about the expected depth of improvement in the field in case of reclaimed fills subjected to DC. This, in turn, enables the designer to assess the potential of DC to the particular project depending upon design requirements, and aids in optimizing the process of foundation design in the field.

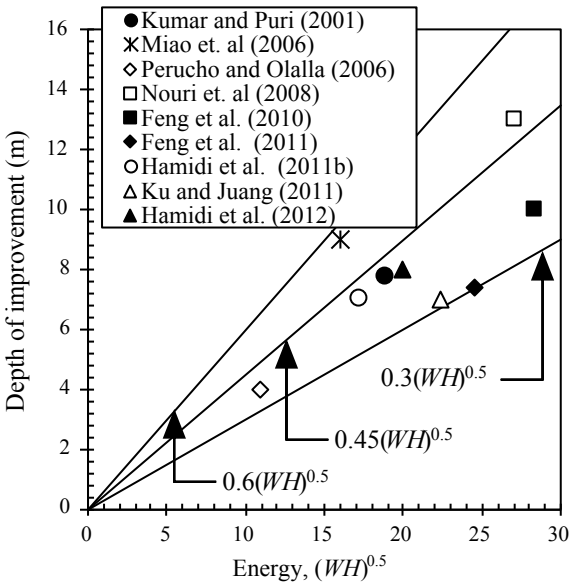

Fig. 4 Prediction of improvement depth in reclaimed fills subjected to DC

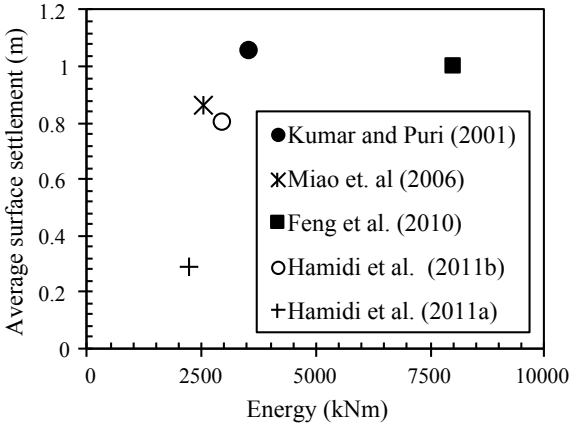

Fig. 5 Prediction of average settlement within reclaimed fills subjected to DC

5 Prediction of Average Settlement Induced by DC

In addition, the average settlement induced at the ground surface during DC on reclaimed fills is presented in Fig. 5, based on the database of Kumar and Puri (2001), Miao et al. (2006), Feng et al. (2010) and Hamidi et al. (2011a, b). Figure 5 indicates that the enforced subsidence under DC typically lies in the range of 0.80–1.0 m. Hence, Fig. 5 can be utilized at the site to develop an understanding about the reduction in post-construction settlements in the ground remediated by DC.

6 Conclusions

The present paper highlights the various design parameters affecting the performance of DC in reclaimed fill areas through illustration of typical field cases. In this respect, the significance of the deformation modulus of the fill material was discussed in deciding verification of design criteria related to construction of a moderately large roadway within a marine reclamation project. In the next case, the aspect of considering liquefaction susceptibility of the existing weak subgrade was highlighted in connection with construction of stone columns alongside heavy tamping through improvement of a flood-plain site. This was followed by a discussion on the initial moisture content of the fill material, and the fact that DC can be applied in a much larger range of water content as compared to rolling process was established with respect to placement of a road embankment foundation over marshy lands. Further, the study revealed that the moisture content adopted during DC in fills placed in wet condition at the site should be close to the optimum moisture content, which in this case was between 11 and 15%. The fourth parameter investigated was the energy involved in the field during DC process. In this regard, a case study was discussed including treatment of a hydraulic fill by DC for coastal

reclamation purposes related to construction of future infrastructural projects. The study signified that in case of coarse-grained materials, high-energy DC process should be adopted in the field to facilitate greater improvement depths and higher ground bearing capacities. In addition, the efficiency of DC was compared with that of surcharge loading while discussing the settlement profiles encountered at a highway embankment site constructed over an existing MSW landfill. The long-term settlements monitored in the field indicated that the secondary settlements reduced by 50% on an average for the roadway embankment treated by DC with respect to that treated by surcharge. Finally, based on the compilation of the above discussed field results, the relationship between tamper mass and drop height was suggested in the paper, which indicated that the optimum drop height usually adopted in the field is about 20 m, while that of tamper mass is between 15 and 40 tonnes. It was further observed that in almost all the cases investigated, the tamper mass was substantially higher as compared to the height of fall. In the next stage, an empirical constant was evaluated for predicting the depth of improvement in reclaimed fills subjected to DC, which exhibited a range of 0.30–0.60, with the mean located at 0.45. The value thus obtained corroborates fairly well with the earlier findings of researchers related to improvement in granular soils, where values in the range of 0.30–0.80 were suggested. The empirical equation suggested in the present study enables the designer to ascertain the applicability of DC at the site depending upon design requirements. Finally, the average settlement induced at the ground surface during DC on reclaimed fills was studied, and a value of 0.80–1.0 m was arrived at for majority of the field cases investigated. The magnitude of enforced settlements thus obtained indicate tentatively the reduction in post-construction settlements in the ground remediated by DC. However, further studies are warranted in this regard by adopting various energy levels and by incorporating the effect of heterogeneity of the fill material for economizing and optimizing the process of foundation design in the field.

References

Feng SJ, Shui WH, Gao LY, He LJ, Tan K (2010) Field studies of the effectiveness of dynamic compaction in coastal reclamation areas. Bull Eng Geol Env 69(1):129–136

Feng SJ, Shui WH, Tan K, Gao LY, He LJ (2011) Field evaluation of dynamic compaction on granular deposits. J Perform Constructed Facil 25(3):241–249

Hamidi B, Varaksin S, Nikraz H (2011a) Predicting Menard modulus using dynamic compaction induced subsidence. In: Proceedings of the international conference on advances in geotechnical Engineering (ICAGE), Perth, Australia, 7–9 Nov 2011, pp 221–226

Hamidi B, Nikraz H, Varaksin S (2011b) The treatment of a loose submerged subgrade using dynamic compaction. Int J Pavement Res Technol 4(2):124–130

Hamidi B, Nikraz H, Varaksin S (2012) The application of dynamic compaction on Marjan Island. In: Proceedings of the 11th Australian-New Zealand conference on geomechanics (ANZ 2012), Melbourne, Victoria, 15–18 July 2012, pp 1202–1207

Ku CS, Juang CH (2011) Variation of CPTU parameters and liquefaction potential at a reclaimed land induced by dynamic compaction. J GeoEng 6(2):89–98

Kumar S, Puri VK (2001) Soil improvement using heavy tamping—a case history. ISET J Earthq Technol 38(2–4):123–133

Lewis PJ, Langer JA (1994) Dynamic compaction of landfill beneath embankment. Vertical and horizontal deformations of foundations and embankments, ASCE, GSP 40, New York, pp 451–461

Lewis PJ, Mansfield J, Ashraf S, Zicko K (2004) Performance of a highway embankment constructed over landfill material. In: Proceedings of the fifth international conference on case histories in geotechnical engineering, New York, 13–17 Apr 2004, pp 1–7

Lukas RG (1986) Dynamic compaction for highway construction, design and construction guidelines, vol 1. Rep. No. FHWA/RD-86/133, U.S. Federal Highway Administration, Washington, DC, pp 204–219

Mayne PW, Jones JS, Dumas JC (1984) Ground response to dynamic compaction. J Geotech Eng 110(6):757–774

Menard L, Broise Y (1975) Theoretical and practical aspects of dynamic consolidation. Géotechnique 25(1):3–18

Miao L, Chen G, Hong Z (2006) Application of dynamic compaction in highway: a case study. Geotech Geol Eng 24(1):91–99

Nouri HR, Ali-Elahi H, Jalili M, Hosseininia ES (2008) Evaluation of empirical relationships for dynamic compaction in liquefiable reclaimed silty sand layers using pre/post cone penetration tests. In: 6th international conference on case histories in geotechnical engineering, Arlington, VA, 11–16 Aug 2008, pp 1–8

Perucho A, Olalla C (2006) Dynamic consolidation of a saturated plastic clayey fill. Ground Improv 10(2):55–68

Swain A, Holt DN (1987) Dynamic compaction of a refuse site for a road interchange. In: Proceedings of ICE on building on marginal and derelict land, Thomas Telford, London, pp 339–357

Zou WL, Wang Z, Yao ZF (2005) Effect of dynamic compaction on placement of high-road embankment. J Perform Constructed Facil 19(4):316–323

Use of Geosynthetics in Mitigating the Effects of Mud Pumping: A Railway Perspective

Mandeep Singh, Buddhima Indraratna and Cholachat Rujikiatkamjorn

Abstract In Australia, where the major network of railways traverses along the coastal regions, millions of dollars are spent on track maintenance annually to mitigate track differential settlement. One of the recurring problems faced with ballasted tracks on estuarine soils is mud pumping. Mud pumping is a complex phenomenon involving the migration of fine soft subgrade particles into the coarser ballast/sub-ballast layer. The problem has been widely reported and is of interest among the railway engineers over the last couple of decades. The migration of fines causes excessive settlements and track degradation leading to track instability, thereby incurring excessive maintenance costs. The primary objective of this paper was to assess the existing remediation measures for mud pumping reported. The current mitigation techniques range from the in situ mixing of additives to the use of geosynthetics to separate the layers in a track structure. On the other hand, the use of geosynthetics has proven to act as a separator between the track layers; their effectiveness is highly dependent on the type of subgrade soil. The comprehensive study reveals the probable causes of mud pumping and a better understanding of the phenomenon.

Keywords Track maintenance · Mud pumping · Geosynthetics · Triggers

M. Singh (✉) · B. Indraratna · C. Rujikiatkamjorn
Centre for Geomechanics and Railway Engineering, School of Civil Mining and Environmental Engineering, University of Wollongong, Wollongong, NSW, Australia
e-mail: ms579@uowmail.edu.au

B. Indraratna
e-mail: indra@uow.edu.au

C. Rujikiatkamjorn
e-mail: cholacha@uow.edu.au

R. Sundaram et al. (eds.), *Geotechnics for Transportation Infrastructure*,
Lecture Notes in Civil Engineering 29,
https://doi.org/10.1007/978-981-13-6713-7_48

1 Introduction

Railways have become one of the predominant modes of transportation in several countries, carrying goods and commuters from one place to another. With the increasing demand for faster and heavy-haul trains, the responsibility lies with the rail industries to provide lucrative and efficient services. Further, the economic aspect of the track construction and operations is also to be taken into account. For example, the track maintenance costs are estimated around 14–15 million dollars in the state of New South Wales alone (Hussaini et al. 2012). The identification of the localised track-bed problems and providing a cost-effective and efficient remediation measure is a twofold problem for the rail engineers.

One such localised track-bed problem is the formation of wet spots or bog holes (Fig. 1), which can occur when soft saturated subgrade soils are subjected to repetitive rail loading and result in the development of mud pumping. With the subsequent passage of trains over the wet spots, the fines squeeze into the coarser upper layers and foul the ballast. This phenomenon is known as mud pumping. It causes severe track deterioration and forms pockets of ballast under the sleeper. As the trains pass over these locations, the sleepers interact with the ballast and form cracks on the sleeper base. Upon successive passes of the train, the rough angular surface of the ballast rubs and leads to the more rounded ballast. The ballast loses the interlocking thereby compromising on track stability. In Australia, where the majority of the eastern rail corridor was built on soft subgrade soils, such as silty clays, the problem of mud pumping is widespread. Many case studies present in the literature report of the mechanism behind mud pumping (Alobaidi and Hoare 1999;

Fig. 1 Mud pumping prone site in New South Wales, Australia

Aw 2007; Hayashi and Shahu 2000) but predominantly they propose measures for mitigating the effects of mud pumping (Alobaidi and Hoare 1998; Aw 2007; Ayres 1986; Duong et al. 2014; Hudson et al. 2016). This paper summarises the reported occurrences of mud pumping in the literature and reviews the existing remediation measures for mud pumping. The main objective of this article was to discuss the triggers that cause the pumping of fines. Also, it makes an effort to understand the phenomenon of mud pumping in the context of railway engineering.

2 Critical Review of the Existing Literature

From the past studies, soils prone to mud pumping lies around the zone of fine, inorganic silts and clays (Table 1). The plasticity of the soils is shown in Fig. 2. It is noteworthy that most of the problematic subgrade soils comprise of inorganic clays with low to medium plasticity.

Table 1 Reported studies on mud pumping

References	PI	LL (%)	USCS	Remarks
Chawla and Shahu (2016)	5	25.5	ML	—Delhi silt —Model tests —Geosynthetic layer
Duong et al. (2014)	11	27	CL	—70% sand + 30% Kaolin clay Soil —Pumping occurred on saturated subgrade —Formation of 'interlayer'
Trinh et al. (2012)	24	57.8	MH	—Sénissiat, France —Highly plastic with >50% fines —Influence of water content
Voottipruex and Roongthanee (2003)	21	43	CL	—Railway embankment in Thailand —Remediation by fly ash and type I Portland cement —Strengthening of soil to reduce pore pressure build-up
Hayashi and Shahu (2000)	–	–	SW	—Shirasu soil, Japan —Propose fluidisation as governing mechanism —Provision of weep holes to mitigate mud pumping
Alobaidi and Hoare (1999)	26	49	CL	—Keuper Marl soil —Unit cell tests with spherical sub-base particles —High permeable geotextile may cause erosion of the subgrade
Ayres (1986)	24	44	CL	—Overconsolidated marine deposited calcareous clay —Classifies mud pumping by two types of erosion failures

2.1 Liquefaction Susceptibility

Liquefaction of soils is a well-established theory in the field of soil dynamics. Soils tend to liquefy when the effective stresses in the reach near zero due to an increase in pore pressure. Duong et al. (2014), while conducting large-scale triaxial tests on subgrade soil observed the excess pore pressures in the subgrade soil rose to values higher than the minimum applied cyclic loading, thereby, reducing the effective stresses to zero after a certain number of cycles. Liquefaction criterion proposed by Bray and Sancio (2006) is imposed on the existing pool of soil data (Fig. 3). The approach considers the water content of the soils in addition to the Atterberg limits (Plasticity Index and Liquid Limit) to quantify liquefaction susceptibility. It can be seen from Fig. 3 that the liquefaction criterion is not applicable to soils that are prone to mud pumping.

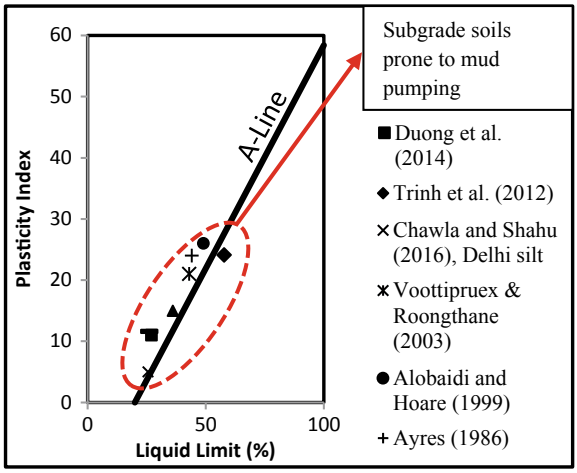

Fig. 2 Plasticity chart of the soils reported at the mud pumping sites

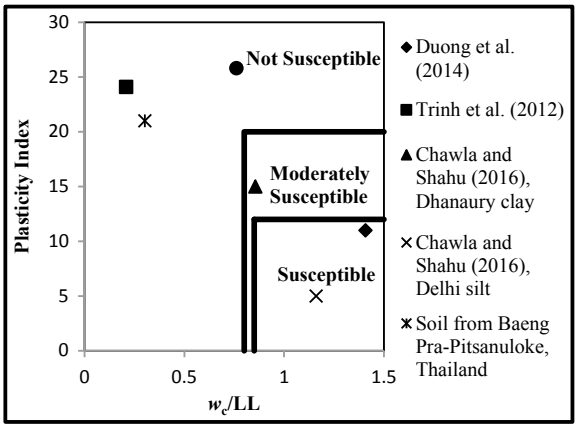

Fig. 3 Liquefaction susceptibility of soils prone to mud pump

2.2 Mitigation Measures for Mud Pumping

There are various remediation methods widely used in industry, and they can be categorised into the following:

i. Track realignment and ballast addition

Realignment of the rail track provides a cheap yet ineffective solution to mud pumping. The train driver visually reports the undulations on the railroad, and then, the extensive manual surveys notify the affected sites. Heavy machinery is used to either raise the rails or remove them and fill the track with fresh ballast. It is, however, a short-term solution as the problem of pumping is not resolved but alleviated. An additional granular capping layer between the subgrade and the ballast can act as a filter by preventing the migration of subgrade into the ballast (Ayres 1986).

ii. Subgrade improvement

The inclusion of geosynthetic layers in the track substructure is known to increase the strength of the track (Chawla and Shahu 2016). The geosynthetics layers may be placed at the interface of the ballast and the capping layer. It provides a uniform distribution of the load coming from the rail and increases the longevity of the track. However, the rails and the sleepers are to be removed entirely to lay the geosynthetics in the existing track, thereby increasing the maintenance time. Another popular method of stabilisation involves the mixing of cementitious elements to the soil. The use of fly ash and Portland cement mix to strengthen the soil provides an alternative to the ground improvement by geosynthetics. The use of cementitious materials reduces the pore pressure build-up in the rail subgrade (Voottipruex and Roongthanee 2003). But these cementitious lumps may induce stress concentration zones in the subgrade layer and assist in the intermixing of subgrade soil.

iii. Track monitoring

Track monitoring methods include manual (e.g. displacement/settlement pegs) and the automated measurements (e.g. geophones and digital image correlation). These monitoring methods are useful to observe the long-term behaviour of the track. The use of dynamic piezometers can indicate the changes in pore water pressures in the subgrade with subsequent passage of trains (Aw 2007). It indicates the probable causes of failure rather than prevent them.

2.3 Experimental Investigations

The pumping of subgrade soils, in the context of pavement engineering, has been investigated in the late 1950s (Yoder 1957). However, in the context of railway

engineering, the problem of mud pumping garnered gradual interest since the 1980s (Ayres 1986). It is suggested that with an increase of frequent passenger services at higher speeds, the use of geotextiles, shows an early promise of static filtering, and does not quite live up to the expectation under dynamic rack conditions. The inspected trenches conducted at old and new tracks suggest that the track movement was severe even when the subgrade had higher strength (Ayres 1986). The precedent of a track prone to pumping is that slurry may exist at or above the base of the sleeper level (similar to Fig. 1). The upward pumping of subgrade fines is termed as the erosion pumping failure (EPF) while the deposits in the upper ballast layer due to wind-blown deposits, attrition of ballast, coal is termed as dirty ballast pumping failure (DBPF). Ayres (1986) conducted experimental tests by sandwiching the geotextile layer between 25 mm of undisturbed soil and 25 mm of gravel, saturated to the top surface. The set-up is transferred to a pulsator apparatus, which can operate at a frequency of 3 Hz. The gradient of the plot of the vertical displacement versus the square root of the number of cycles is used to determine the efficiency of the geotextiles. The ratio of the weight of the eroded subgrade to the number of cycles was used as a practical measure of the applicability of the geotextile. Geotextiles successfully act as a separator by inhibiting the rate of rising of the slurry. However, it is crucial to identify the type of the failure of the track before selecting the geosynthetics for mitigation measure.

Alobaidi and Hoare (1998) conducted a series of pumping tests to quantify the use of geocomposites to mitigate mud pumping. The researchers define soil contamination value as the ratio of the subgrade soil mass passing through the geotextile to the area of the geotextile. To simulate the coarser particles, a sub-base plate made of hemispherical steel balls applies the load onto the subgrade soil in a triaxial pumping apparatus (Alobaidi and Hoare 1994). The amount of fines passing through the geotextile was measured at the end of each test. It is noteworthy that the rate of fines migration decreases with the number of loading cycles predominantly due to the reduction in the contact stress of the sub-base particle with the subgrade, and the percentage of precipitated fines increases with the number of cycles. The predictions from the finite element show a high hydraulic gradient near the interface (Alobaidi and Hoare 1996). The selection criteria are as follows: (i) high vertical compression modulus, (ii) low cyclic flexural movement, (iii) uniform distribution of concentrated load and (iv) act as a separator and restrict the flow of water (Alobaidi and Hoare 1998). Alobaidi and Hoare (1999) proposed that the subgrade soil weakening occurs due to the saturation of unloaded zone at the surface and shear failure due to high contact cyclic stresses occurring under the contact areas. Having a highly permeable geotextile could be the reason for the rapid water outflow during loading-unloading cycles. There is a 'mixing' of the subgrade soil into the subbase particles due to the plastic flow of the soil. To study the physical migration of fines from the subgrade layer into the ballast, Duong et al. (2014), designed a 550-mm Perspex triaxial cell and observed the formation of an 'interlayer'. The cell consisted of an artificial mix of soil (70% crushed sand and 30% kaolin clay by dry weight) compacted in layers, and a 160-mm ballast was placed atop the subgrade. The pumping of fines did not occur when the subgrade was

unsaturated. In contrast, the cyclic loading led to the penetration of the ballast forcing the fine particles upward, also the pore pressure dissipation caused the fines to migrate into the ballast. The cyclic pore pressure generation could well be the governing mechanism for the pumping of soils.

Hayashi and Shahu (2000) believe that fluidisation is the apparent cause of mud pumping as it involves scouring and gradual loss of particles. 'Fluidization is the operation by which fine solids are transformed into a fluid-like state through the contact with a gas or liquid' (Kunii and Levenspiel 2013). It is proposed that upon the passage of the train, there is a rise in the pore water pressure of the base soil that increases the seepage velocity and leads to fluidisation of the soil particles. The effusion of water and the soil leads to mud pumping. To simulate the phenomenon of pumping in a laboratory environment, the researchers designed model set-up to represent the soil beneath the invert and walls of the tunnel. The main aim was to achieve the optimum location of the weep holes in the geometry design under various hydraulic gradients and loading frequencies. It is seen that the loading frequency had little to no effect on the amount of fines pumped, which depend mainly on the hydraulic gradient. The researchers also point out that there is a likelihood of clogging of the geotextile under long-term loading.

Geotextiles serve numerous functions, viz. reinforcement, filtration, drainage and separation. Geotextiles have the prospective to remediate the pumping problem on rail tracks when used at the interface of the sub-ballast and subgrade (Chawla and Shahu 2016). A series of 15 model tests were conducted on a full-panel model track with a similitude ratio of one-third. The efficiency of geotextiles and geogrids was investigated by placing them at the interface between sub-ballast and subgrade. The results from the monotonic and cyclic tests indicate that the reinforcement causes a stable behaviour by inducing a uniform distribution of the stresses. Further, typical silty soils are more prone to pumping because of low plasticity making it easier to dislodge with increasing pore water pressure. This is also consistent with Fig. 2 where most of the soils prone to pumping have low plasticity. Chawla and Shahu (2016) recommend the use of geogrid as a remediation measure for clay type of subgrade soils as they reduce the tie displacements, strains in the ballast and sub-ballast and subgrade displacement in comparison to the geotextile. However, the provision of both geogrid and geotextile provides the combined advantage of either reinforcement.

2.4 Field Studies

A conventional method of soil stabilisation, mixing fly ash and Portland cement, was reported for remediating a mud pumping site in Thailand (Voottipruex and Roongthanee 2003). While the optimum soil–cementitious mix proportion was found by comparing the unconfined compressive strengths, there was a significant reduction in the stresses in the subgrade soil. It is concluded that this method resulted in lesser excess pore pressure water, thereby reducing mud pumping.

However, long-term benefits of the proposed solution are yet to be seen because the cementitious lumps may form an 'interlayer' (Duong et al. 2014) and could cause more intermixing of soils instead of providing a permanent solution.

Aw (2007) introduced a low-cost wireless monitoring platform for monitoring the data for settlements, accelerations, seasonal temperature variations and long-term variation in pore pressures. Hudson et al. (2016) reported field remediation of a track site showing recurring signs of severe mud pumping. The wet bed area was reinforced with a microporous filter sandwiching the geotextiles to separate the slurried sub-ballast from the ballast. The track was monitored using digital image correlation (DIC) technique and geophones. The site showed significant reductions in the sleeper deflections after five months of site monitoring, indicating the efficiency of the geotextile.

3 Discussion

It is evident that the problem of mud pumping is prevalent in the context of railway engineering. The findings of the earlier study lead to classifying the possible triggers that initiate mud pumping. A trigger may act individually or in conjunction with the others and lead to the migration of subgrade fines. The possible triggering mechanisms are (in no particular order):

- High cyclic excess pore pressures upon the passage of trains.
- Dynamic fluidisation of the low plastic soil particles under high hydraulic gradient.
- Intermixing of the subgrade and the ballast layer to form an 'interlayer'.
- Improper drainage in the track substructure causes the presence of free water on the surface.

The use of fault chart approach by Usman et al. (2015) which takes into account the typical subgrade failure mechanisms can provide a plan for track maintenance but it cannot predict the occurrence of mud pumping a priori. In addition, the use of geosynthetics, as inclusions to the track substructure, can inhibit the migration of the fines and increase the longevity of the track. The underlying problem of facilitating drainage under cyclic loading may be solved by the application of prefabricated vertical drains (PVDs). PVDs are extensively used in cohesive soil deposits to assist in consolidation by providing a shorter radial drainage path. Experimental studies undertaken at the University of Wollongong (Indraratna et al. 2009) indicate that PVDs not only assist in consolidation the soft soil but assist in controlling the excess pore pressure build-up under cyclic loading (Fig. 4). This suggests that the PVDs have a stabilising effect when the soft soil is subjected to repeated loading. In addition to that, PVDs continue to dissipate the pore pressures during the rest periods, so that during the next loading cycle, the cyclic pore pressures do not rise to a substantial value. The field predictions carried out at

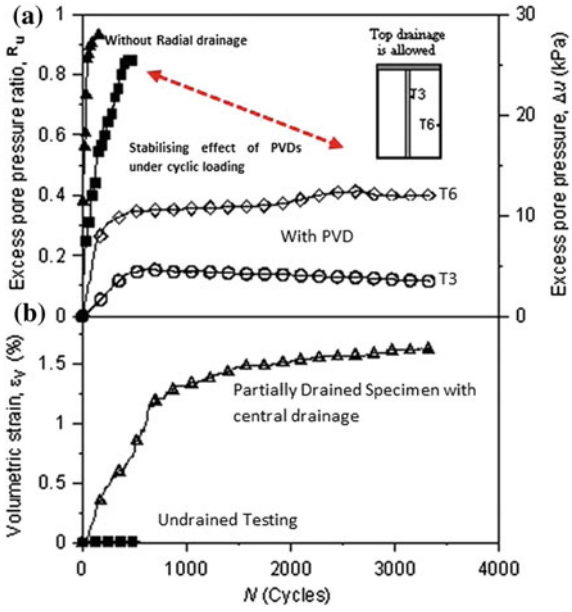

Fig. 4 **a** Cyclic excess pore pressures developed with and without PVD; **b** volumetric compressive strains generated under cyclic loads with PVD (Indraratna et al. 2009) (with permission from ASCE)

Sandgate show promising results of the use of short vertical drains under the railway track (Indraratna et al. 2010). The use of PVDs can also prevent the failure of soft subgrade under high-speed rail conditions. (Ni et al. 2013). Thereby, the role of PVDs can be accounted for even during the post-construction phase.

4 Conclusion

The paper highlights mud pumping under track environment. The sightings of mud pumping sites indicate that the soils prone to mud pumping are primarily low plasticity silty clays. The triggers causing mud pumping are described as a result of combined factors to initiate the complex phenomenon of fines migration. The inclusion of geosynthetics into the track design prevents the squeezing of fines, and to an extent mitigates the excess pore pressure generation by providing a reinforcing effect. The use of a geosynthetic is site specific and depends on the in situ soil properties. However, further geotechnical studies are recommended to investigate the governing mechanism of mud pumping. The use of prefabricated vertical drains may provide a viable alternative to prevent mud pumping by dissipating the cyclic excess pore pressures.

Acknowledgements This research was supported (partially) by the Australian Government through the Australian Research Council's Linkage Projects funding scheme (project LP160101254).

References

Alobaidi I, Hoare DJ (1994) Factors affecting the pumping of fines at the subgrade–subbase interface of highway pavements: a laboratory study. Geosynthetics Int 1(2):221–259

Alobaidi I, Hoare DJ (1996) The development of pore water pressure at the subgrade–subbase interface of a highway pavement and its effect on pumping of fines. Geotext Geomembr 14 (2):111–135

Alobaidi I, Hoare DJ (1998) Qualitative Criteria for anti-pumping geocomposites. Geotext Geomembr 16:221–245

Alobaidi I, Hoare DJ (1999) Mechanisms of pumping at the subgrade–subbase interface of highway pavements. Geosynthetics Int 6(4):241–259

Aw ES (2007) Low cost monitoring system to diagnose problematic rail bed: case study at a mud pumping site. Doctor of Philosophy, Massachusetts Institute of Technology, Cambridge, MA, USA

Ayres DJ (1986) Geotextiles or Geomembranes in track? British Railways' experience. Geotext Geomembr 3:129–142

Bray JD, Sancio RB (2006) Assessment of the liquefaction susceptibility of fine-grained soils. J Geotech Geoenviron Eng 132(9):1165–1177

Chawla S, Shahu JT (2016) Reinforcement and mud-pumping benefits of geosynthetics in railway tracks: model tests. Geotext Geomembr 44:366–380

Duong TV, Cui Y-J, Tang AM, Dupla J-C, Canou J, Calon N, De Laure E (2014) Physical model for studying the migration of fine particles in the railway substructure. Geotech Test J 37(5):1–12

Hayashi S, Shahu JT (2000) Mud pumping problem in tunnels on erosive soil deposits. Géotechnique 50(4):393–408

Hudson A, Watson G, Le Pen L, Powrie W (2016) Remediation of mud pumping on a ballasted railway track. Paper presented at the 3rd international conference on transportation geotechnics

Hussaini SKK, Indraratna B, Vinod JS (2012) Performance of geosynthetically-reinforced rail ballast in direct shear conditions. Paper presented at the 11th Australia–New Zealand conference on geomechanics: ground engineering in a changing world, Australia

Indraratna B, Attya A, Rujikiatkamjorn C (2009) Experimental investigation on effectiveness of a vertical drain under cyclic loads. J Geotech Geoenviron Eng 135(6):835–839

Indraratna B, Rujikiatkamjorn C, Ewers B, Adams M (2010) Class A prediction of the behaviour of soft estuarine soil foundation stabilized by short vertical drains beneath a rail track. J Geotech Geoenviron Eng 136(5):686–696

Kunii D, Levenspiel O (2013) Fluidization engineering. Elsevier

Ni J, Indraratna B, Geng X-Y, Carter JP, Rujikiatkamjorn C (2013) Radial consolidation of soft soil under cyclic loads. Comput Geotech 50:1–5

Trinh VN, Tang AM, Cui Y-J, Dupla J-C, Canou J, Calon N, Schoen O (2012) Mechanical characterisation of the fouled ballast in ancient railway track substructure by large-scale triaxial tests. Soil Found Jpn Geotech Soc 52(3):511–523

Usman K, Burrow M, Ghataora G (2015) Railway track subgrade failure mechanisms using a fault chart approach. Procedia Eng 125:547–555

Voottipruex P, Roongthanee J (2003) Prevention of mud pumping in railway embankment. A case study from Baeng Pra-Pitsanuloke, Thailand. J KMITB 13(1):20–25

Yoder EJ (1957) Pumping of highway and airfield pavements : technical paper. Retrieved from Purdue University, Lafayette, Indiana

Utilization of Waste Plastic Shreds for Stabilization of Soil

Shwetha Prasanna

Abstract When soil available for construction is not suitable for the intended purpose, then soil stabilization is required. In this study, two soil samples were collected from Margoa, Goa State and were reinforced with waste plastic shreds. These plastic shreds were obtained from plastic packaging waste which would cause a major disposal problem for the environment. Waste plastic shreds were added in varying percentages like 2, 4, 6, 8, and 10% to the soil samples as a reinforcement material. From compaction test, maximum dry density (MDD) and optimum moisture content (OMC) were determined and shear strength parameters (cohesion and friction) were obtained from box or direct shear test. For the first soil sample, there was a decrease in MDD, OMC, and cohesion and a slight increase in friction with an increase in the percentage of reinforcement. For the second sample also, almost the same results were obtained that means decrease in MDD, OMC, and cohesion and a slight increase in friction with increase in the percentage of reinforcement. The decrease in maximum dry density of soil must be due to low specific gravity of plastic shreds. Also it has been observed that adding beyond 10% of plastic waste would not vary much in MDD value. The present work concluded that the stabilized soil could be utilized for roadways, parking areas, site development projects, airports, and many other situations where subsoils are not suitable for construction.

Keywords Soil · Stabilization · Plastic waste

S. Prasanna (✉)
Department of Civil Engineering, Don Bosco College of Engineering, Fatorda 403602, Goa, India
e-mail: shwethaprasanna@gmail.com

R. Sundaram et al. (eds.), *Geotechnics for Transportation Infrastructure*, Lecture Notes in Civil Engineering 29,
https://doi.org/10.1007/978-981-13-6713-7_49

1 Introduction

If the engineering properties of soil are undesirable and not suitable for construction purposes, then soil stabilization is required. Soil stabilization process improves the shear strength parameters and controls the shrink–swell properties of a soil. So it helps to enhance the physical properties and load-bearing capacity of a soil. It is mainly used to increase bearing capacity of a subgrade soil to support pavements and foundations. In earth structures, it is used to reduce permeability and compressibility of the soil mass. So overall it is the process of alteration or preservation of one or more soil properties to improve the engineering characteristics and performance of a soil. In this process, a special soil, cementing material, or other chemical materials are added to a natural soil to improve its properties. It can be achieved by mechanically mixing the natural soil and stabilizing material together so as to achieve a homogeneous mixture. Otherwise by adding stabilizing material to an undisturbed soil deposit and obtaining interaction by letting it permeate through soil voids (Perloff 1976). Reinforced soil is the one in which soil fill is strengthened by a variety of tensile inclusions. These tensile inclusions are in many forms ranging from strips and grids to discrete fibers and woven and nonwoven fabrics.

Nowadays the volume of plastic material in municipal solid waste generated across the world has grown because of the widespread increase of single-use plastics in day-to-day consumer applications. More than 50% of the discarded plastics come from packaging applications. So, waste plastic becomes the main problem in many areas, especially in landfills. These waste plastics are not a biodegradable material, hence, may cause serious environmental pollution also, Siddiqui (2009). In the past few decades, the rate of production of plastic waste has been increased tremendously in almost all parts of the world due to population growth, industrialization, and technological development. The conventional waste disposal methods are found to be inadequate. In this regard, a small attempt has been made in this research work to use waste plastic as a reinforcing material to improve the strength of soil.

The usage of plastic waste for soil stabilization was studied in research programs from around the world. Khedari et al. (2005) developed a new type of soil–cement block using coconut coir with low thermal conductivity. They considered various mixture ratios and fabricated five specimens per sample using local handmade manufacturing process. In their study, thermal conductivity, compressive strength, weight, and bulk density of specimens were investigated, and they concluded that the use of coconut fiber as an admixture can reduce the block thermal conductivity and weight. Babu and Vasudevan (2008) studied strength and stiffness response of coir fiber-reinforced tropical soil. They reported that the strength and stiffness of tropical soil were increased with the inclusion of about 1–2% discrete coir fibers by weight. Subaida et al. (2009) carried out research on laboratory performance of unpaved roads reinforced with woven coir geotextiles. Their test results indicated that the inclusion of coir geotextiles enhanced bearing capacity of thin sections.

Placement of geotextile at the interface of the subgrade and base course increased load-carrying capacity significantly at large deformations. Also they found that considerable improvement in bearing capacity when coir geotextile was placed within the base course at all levels of deformations. The plastic surface deformation under repeated loading was greatly reduced by the inclusion of coir geotextiles within the base course irrespective of base course thickness. Muntohar (2009) investigated the strength of stabilized clay soil reinforced with randomly distributed discrete plastic waste fibers by carrying out unconfined compressive strength and tensile-split strength test. In their study, the clay soil was stabilized with lime and rice husk ash mixtures. The effect of the fiber length and content on the compressive and split tensile strength was investigated. Their laboratory investigation results showed that inclusion of the plastic waste fiber increased unconfined strength and tensile-split strength of the stabilized clay soil significantly. Dasaka and Sumesh (2011) reported that varying the length of coir fibers and content in soil results in an improvement in the strength characteristics. Hejazi et al. (2012) reviewed the use of natural and synthetic fibers as construction and building materials and reported that fiber reinforcement improves the strength and stiffness of composite soil. Azzam (2013) studied behavior of modified clay microstructure using polymer nanocomposites technique. They illustrated the application of using polymer stabilization in creating a new nanocomposite material with clay soil. Their experimental results showed that the resulting nanocomposites acted as nanofiller materials which decreased the plasticity and compressibility parameters of the treated clay. Gupta and Sharma (2016) studied black cotton soil modification by the application of waste materials. They presented an approach of improvement in the various geotechnical properties of black cotton soil, by blending it with waste materials such as river sand, fly ash, and marble dust. They observed that the impact effect of waste materials on the environment was reduced mainly due to optimum utilization of these waste materials in the improvement of various properties of black cotton soil. Prasanna and Kumar (2017) carried out a research on soil reinforcement using coconut shell ash as waste material for Indian soil. By comparing all the results, they observed that Atterberg's limits such as maximum liquid limit was achieved at 2% and maximum plastic limit was at 10% coconut shell ash reinforcement. Then regarding compaction, they concluded that by adding at 0.8% of waste achieved maximum improvement of MDD and OMC. From direct shear test results, they concluded that angle of internal friction and cohesion was achieved at the range of 0.4–0.8%.

A very few literatures are available on stabilization of sandy soils with shredded plastic wastes for the coastal region of Goa, India. This article is the one which provides various properties of soil and explains how the properties of soil can be stabilized using shredded plastic wastes for the region under consideration. The main objectives of this study are to: To carry out physical test on soil without reinforcement, to carry out physical test on soil with reinforcement (shredded plastic waste) in varying percentages, to analyze the specimen for shear strength and compaction, to compare results of the test conducted on ordinary soil and soil with reinforcement.

2 Materials and Methodology

The soil samples used in this study were obtained as undistributed samples along the coastal region of Goa. The study area falls under the district of South Goa in the Taluka of Salcete in India. The samples were taken from Fatorda village falling in the above said region. The samples were of sandy-textured soil. The shredded plastic wastes (Fig. 1) were collected from plastic packaging industry. In this project work, experimental study was conducted with shredded plastic waste as reinforcing material to increase the strength of soil. Different tests were conducted on soil sample with varying percentage of shredded plastic waste. The samples were subjected to different laboratory tests, such as moisture content, bulk density, specific gravity, particle size distribution, Atterberg limits, compaction, and direct shear test.

3 Results and Discussion

Undisturbed samples were collected from the field and different laboratory tests were conducted. Moisture content and specific gravity of the sample 1 was found to be 13.41 and 2.76%, respectively. Sieve test was performed on sample 1 and identified soil as sandy soil. Then Atterberg's limit (liquid limit and plastic limit) test was performed on sample 1. The values of liquid limit (LL), plastic limit (PL), and plasticity index (PI) obtained were 26.3, 9.69, and 16.51%, respectively. Reinforcement analysis was done only for compaction and direct shear tests with different percentages of shredded plastic wastes. After that, optimum moisture content (OMC) and maximum dry density (MDD) were found by compaction test. The following results were observed for the sample 1. OMC was found to be 19.5% and MDD was 2.05 g/cm^3. After addition of shredded plastic wastes as reinforcement in various percentages, the following changes were obtained. For addition of 2% of shredded plastic wastes, OMC and MDD were decreased to 19.1% and 1.86 g/cm^3. Again after addition of another 2% that is a total of 4% shredded plastic wastes, OMC and MDD were 17.5% and 1.76 g/cm^{3,} respectively. Here also OMC and MDD reduced slightly. For 6% of shredded plastic wastes, OMC and MDD again decreased by 16.82% and 1.72 g/cm^{3,} respectively. At 8%, OMC and MDD was 15.45% and 1.7 g/cm^{3,} respectively. Again OMC and MDD were decreased to 14.3% and 1.54 g/cm^3 with addition of 10% of shredded plastic wastes. From this, it could be observed that with the addition of shredded plastic wastes as reinforcement, optimum moisture content, and maximum dry density were decreased. The results are shown in the following Table 1. Figure 2 shows the results of OMC and MDD with different percentages of shredded plastic waste for sample 1.

For sample 2 also, similar tests were conducted. Moisture content and specific gravity were 15.22 and 2.42%, respectively. From the sieve test, it was found that

Fig. 1 Plastic shredding machine and shredded plastic

soil belongs to sandy soil. Atterberg's limit, i.e., LL was 32.4%, PL was 16.41%, and PI was 15.99. Then compaction test was carried out and found OMC (23.52%) and MDD (1.50 g/cm^3) without adding waste material. For this sample also, similar trend was observed that is with the addition of shredded plastic wastes as reinforcement, optimum moisture content, and maximum dry density were decreased. At 2%, OMC and MDD were 23% and 1.49 g/m^3, at 4% OMC (21.93%) and MDD (1.48 g/m^3), at 6% OMC (21.60%) and MDD (1.47 g/m^3), at 8% OMC (21.40%)

Table 1 Optimum moisture content (OMC) and maximum dry density (MDD) with different percentages of wastes for sample 1 and 2

% of plastic waste (%)	Sample 1	Sample 2
0	OMC = 19.50% MDD = 2.05 g/cc	OMC = 23.52% MDD = 1.500 g/cc
2	OMC = 19.10% MDD = 1.86 g/cc	OMC = 23.00% MDD = 1.50 g/cc
4	OMC = 17.50% MDD = 1.77 g/cc	OMC = 21.93% MDD = 1.48 g/cc
6	OMC = 16.82% MDD = 1.72 g/cc	OMC = 21.60% MDD = 1.47 g/cc
8	OMC = 15.45% MDD = 1.70 g/cc	OMC = 21.40% MDD = 1.43 g/cc
10	OMC = 14.30% MDD = 1.54 g/cc	OMC = 20.40% MDD = 1.39 g/cc

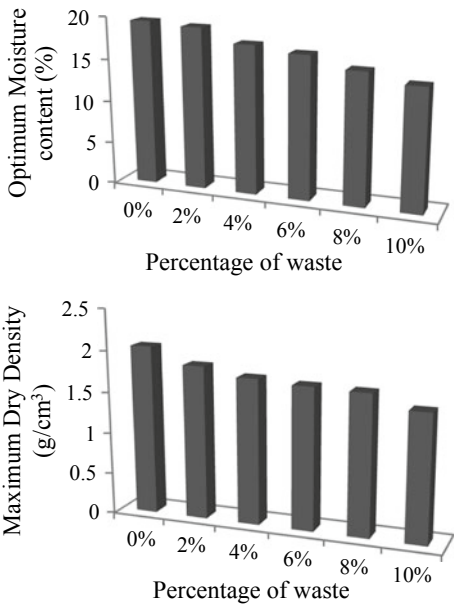

Fig. 2 Optimum moisture content (OMC) and maximum dry density (MDD) with different percentages of wastes for sample 1

and MDD (1.43 g/m^3), and at 10% OMC (20.4%) and MDD (1.40 g/m^3), respectively. This result shows that there was a slight reduction in MDD and OMC values with increase in the percentage of reinforcement. It has been observed that mixing beyond 10% of plastic waste would not vary much in MDD value. The results are shown in Table 1. Figure 3 shows the results of OMC and MDD with different percentages of shredded plastic waste for sample 2.

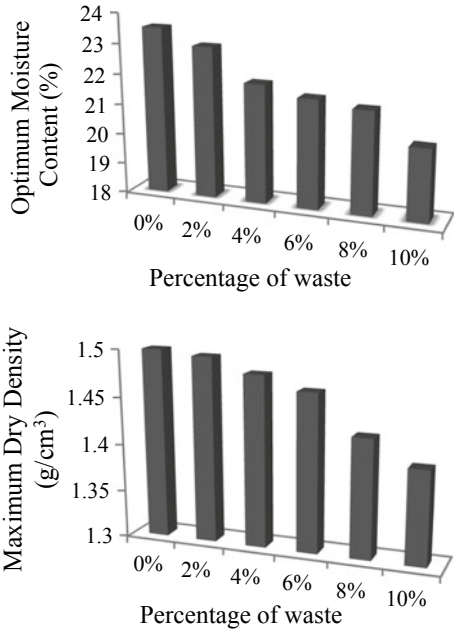

Fig. 3 Optimum moisture content (OMC) and maximum dry density (MDD) with different percentages of wastes for sample 2

Then shear strength parameters of soil, i.e., cohesion (c) and angle of friction (ϕ) were determined using direct shear test. First for sample 1, unreinforced test was conducted; a shredded plastic waste was not used. The following $c = 0.195$ kg/cm^2 and $\phi = 8°$ values were obtained. Generally, higher the friction and cohesion values better are the shear strength of the soil and also the stability of the slope. Then soil was reinforced with shredded plastic waste in different percentages. With 2% of shredded plastic waste as reinforcement, the following $c = 0.1$ kg/cm^2 and $\phi = 8°$ values were obtained. In this case, cohesive value decreased exponentially, but the angle of internal friction remained the same. At 4%, $c = 0.085$ kg/cm^2 and $\phi = 9°$. Here cohesion decreased and friction increased slightly. At 6%, $c = 0.1$ kg/cm^2 and $\phi = 10.5°$. Here both cohesion and friction were increased slightly. At 8%, $c = 0.095$ kg/cm^2 and $\phi = 12°$ slight increase in friction value. At 10%, angle of internal friction remained constant ($\phi = 12°$) and cohesion increased to 0.14 kg/cm^2. Here it could be observed that an angle of internal friction increased exponentially, but the cohesive value is reduced slightly. Further at 4, 6, 8, and 10% cohesion value was varying but not linear in nature. The angle of internal friction was increased as the percentage of reinforcement was increased. Figure 4 shows the comparison of friction and cohesion values with different percentages of shredded plastic waste for sample 1. Table 2 shows the results of direct shear test for sample 1 and 2.

For sample 2 also, direct shear test was conducted and found cohesion and friction values. For unreinforced soil, i.e., without adding shredded plastic waste, the following $c = 0.24$ kg/cm^2 and $\phi = 11°$ values were obtained. When reinforced with shredded plastic waste, at 2%, $c = 0.15$ kg/cm^2 and $\phi = 13°$, here cohesion

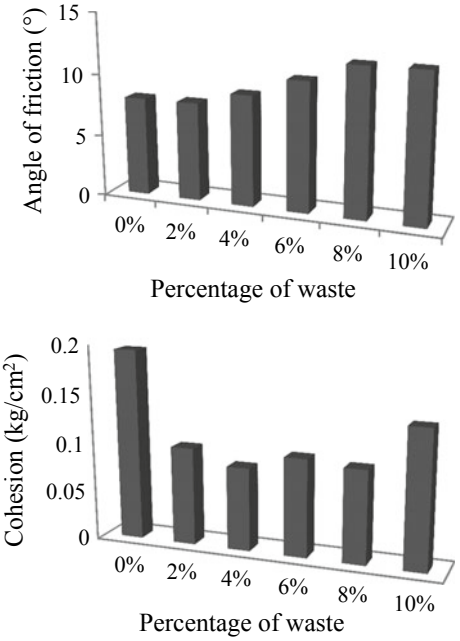

Fig. 4 Angle of internal friction (ϕ) and cohesion (c) with different percentages of waste for sample 1

Table 2 Angle of internal friction (ϕ) and cohesion (c) with different percentages of wastes for sample 1 and 2

% of plastic waste (%)	Sample 1	Sample 2
0	c = 0.195 kg/cm^2 ϕ = 8°	c = 0.24 kg/cm^2 ϕ = 11°
2	c = 0.10 kg/cm^2 ϕ = 8°	c = 0.15 kg/cm^2 ϕ = 13°
4	c = 0.09 kg/cm^2 ϕ = 9°	c = 0.12 kg/cm^2 ϕ = 14°
6	c = 0.10 kg/cm^2 ϕ = 10.5°	c = 0.13 kg/cm^2 ϕ = 19°
8	c = 0.095 kg/cm^2 ϕ = 12°	c = 0.09 kg/cm^2 ϕ = 19°
10	c = 0.14 kg/cm^2 ϕ = 12°	c = 0.10 kg/cm^2 ϕ = 22°

was decreased slightly but friction was increased. At 4%, c = 0.12 kg/cm^2 and ϕ = 14°, again cohesion deceased and friction increased. At 6%, c = 0.13 kg/cm^2 and ϕ = 19°, here cohesion value decreased slightly but friction value increased drastically. At 8%, c = 0.09 kg/cm^2 and ϕ = 19°. At 10%, c = 0.10 kg/cm^2 and ϕ = 22°. For both 8 and 10% cohesion value decreased and friction value increased. So for this sample also the same conclusion was drawn that means the angle of internal friction increases as the percentage of reinforcement increases. The results are shown in Table 2 and Fig. 5.

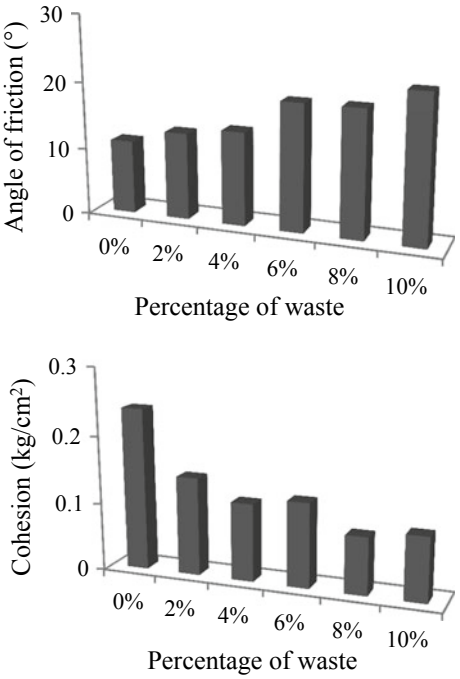

Fig. 5 Angle of internal friction (ϕ) and cohesion (c) with different percentages of waste for sample 2

4 Conclusions

Shredded plastic waste can be considered as an eco-friendly material for soil stabilization. It has lower carbon content than cement or other hydraulic binders. In this study, considerable results were obtained by mixing soil with various percentages of waste shredded plastic. An addition of shredded plastic waste decreased the maximum dry density and optimum moisture content of the soil. The angle of internal friction (ϕ) increased and cohesion (c) decreased considerably with inclusion of different percentages of shredded plastic waste in both soil samples. This study suggests that if shredded plastic is properly mixed and applied, then it could be used as an economical soil stabilization material. And also it eradicates the disposal problem of plastic waste. Further research in this field may shed light on the application of plastic material for stabilization of soil. Finally, this study concluded that shredded plastic waste could be used as one of the waste materials for soil reinforcement in the region under consideration.

Acknowledgements Author thanks the anonymous referees for their valuable suggestions. And also Rituja Tari, Pooja Naik, Shriya Usgaonker, Dhanada Mayeker, Rajeshwari Palni and Radhiya Chodnekar for their help in conducting the experiments related to this project.

References

Azzam WR (2013) Behavior of modified clay microstructure using polymer nanocomposites technique. Alexandria Eng J Fac Geoeng 12:143–150

Babu S, Vasudevan K (2008) Strength and stiffness response of coir fiber-reinforced tropical soil. J Mater Civ Eng ASCE 20:571–577

Chayan G, Ravi KS (2016) Black cotton soil modification by the application of waste materials. Periodica Polytech Civ Eng 60:479–490

Dasaka SM, Sumesh KS (2011) Effect of coir fibre on the stress–strain behavior of a reconstituted fine-grained soil. J Nat Fibre 8:189–204

Hejazi SM, Sheikhzadeh M, Abtahi SM, Zadhoush A (2012) A simple review of soil reinforcement by using natural and synthetic fibers. Constr Build Mater 30:100–116

Khedari J, Watsanasathaporn P, Hirunlabh J (2005) Development of fiber-based soil–cement block with low thermal conductivity. Cem Concr Compos 27:111–116

Muntohar AS (2009) Influence of plastic waste fibers on the strength of lime-rice husk ash stabilized clay soil. Civ Eng Dim 11:32–40

Perloff WH (1976) Soil mechanics, principals and application. Wiley, New York

Sherwood P (1993) Soil stabilization with cement and lime, state of the art review. Transport Research Laboratory, HMSO, London

Shwetha P, Prasanna Kumar N (2017) Soil reinforcement using coconut shell ash: a case study of Indian soil. J Civ Eng Constr 6:73–78

Siddiqui MN (2009) Conversion of hazardous plastic wastes into useful chemical products. J Hazard Mater 167:28–35

Subaida A, Chandrakaran E, Sankar N (2009) Laboratory performance of unpaved roads reinforced with woven coir. Geotext Geomembr 27:204–210

Utilization of Class 'C' Fly Ash in Flexible Pavement System—A Review

Amruta R. Joshi, Satyajit Patel and Jagdish Telangrao Shahu

Abstract Class *C* fly ash is a by-product of combustion of lignite or subbituminous coals having higher CaO content than Class *F* fly ashes. Class *C* fly ash possesses self-cementing properties; hence, its utilization as stabilizing agent for road material appears to be one of the most efficient solutions for dealing with critical problem of fly ash disposal. When clayey soils are stabilized with fly ash, mechanical properties of soil relevant to highway design and construction are found to be significantly improved. A review of literature for effect of use of Class *C* fly ash on California bearing ratio (CBR), resilient modulus (M_R) and unconfined compressive strength (UCS) of soil is done and reported in this paper. With increase in fly ash content and curing period of soil samples, UCS, CBR and M_R values for fly ash-treated soils are significantly improved when compared with those for untreated soils. These improved values on fly ash addition place the treated soils in the category of good to excellent for pavement base course, subbase course and subgrade applications. This paper also reviews some of the key advances in improving our understanding about clayey soils stabilized with Class *C* fly ash. The practical and research needs in order to enhance effectiveness of soil stabilization using Class *C* fly ash are addressed through discussion.

Keywords Class *C* fly ash · Flexible pavement · Stabilization

A. R. Joshi (✉) · S. Patel
Applied Mechanics Department, Sardar Vallabhbhai National Institute of Technology, Surat 395007, Gujrat, India
e-mail: joshiamruta89@gmail.com

S. Patel
e-mail: spatel@amd.svnit.ac.in

J. T. Shahu
Department of Civil Engineering, Indian Institute of Technology, New Delhi 110016, India
e-mail: shahu@civil.iitd.ac.in

R. Sundaram et al. (eds.), *Geotechnics for Transportation Infrastructure*,
Lecture Notes in Civil Engineering 29,
https://doi.org/10.1007/978-981-13-6713-7_50

1 Introduction

The disposal of fly ash produced from combustion of coal in thermal power plants is one of the major global challenges. In thermal power plants, fly ash is obtained as a by-product of the combustion of pulverized coal. The amount of fly ash collected from furnaces is about several tons per minute.

Fly ash is a material that can be widely used for manufacturing cement, replacing cement partially in concrete, manufacture of bricks, blocks, tiles, etc. It can be used for embankment construction and, filling of underground as well as open mines, reclamation of low-lying areas and degraded/waste lands, etc., and hence effectively used as geotechnical material. The pozzolanic property of fly ash along with lime reactivity is ideal for cementitious applications. Due to its geotechnical properties and reasonably close physical and chemical properties to that of common soils, fly ash can be considered as a good substitute of soil. It is acceptable for sintered applications due to the presence of silica, alumina, iron oxide, etc., in required amount. Very low levels of heavy metals, toxic elements and radio nuclides make fly ash suitable and safe for various applications.

Nowadays, improving the engineering properties of locally available soils are a critical issue in engineering projects. Improving the characteristic of unsuitable soil is a major geotechnical concern in some cases. Pavement structures on poor soil subgrades show early distress causing the premature failure of the pavement. Clayey soil usually have the potential to demonstrate undesirable engineering behaviour, such as low bearing capacity, high shrinkage and swell characteristics and high moisture susceptibility. Stabilization of these soils is a usual practice in which a stabilizing agent is added to the soils in order to improve their engineering performance. (Moghal 2017).

Use of Class *C* fly ash for stabilization is beneficial because it acts as drying agent. Class *C* fly ash hydrates rapidly in presence of water and hence being water consumer can be effectively used for stabilizing wet soils. Addition of fly ash dilutes swelling effect in clayey soils; hence, it can work efficiently against volume changes in clayey soils. Pozzolanic properties of fly ash aids in long-term strength gain of stabilized soils (Parsons and Kneebone 2005).

1.1 Classification of Fly Ash

Based on chemical composition and type of coal burned, two major Classes of fly ashes are identified in ASTM C618-15 (2017). These are designated as Class *F* and Class *C*. Incineration of fresher lignite or subbituminous coal results in Class *C* fly ashes. These are naturally pozzolanic, exhibiting self-cementing abilities. In the presence of water, these ashes harden and gain strength over time. Class *F* fly ashes are generated by the incineration of older, harder bituminous and anthracite coals. These fly ashes are pozzolanic in nature. These fly ashes contain very less amount

of CaO and lack the self-cementing properties. According to ASTM C618-15, for a Class *C* fly ash, the sum of Al_2O_3 + SiO_2 + Fe_2O_3 should be in the 50–70%, whereas for a Class *F* fly ash, the sum of Al_2O_3 + SiO_2 + Fe_2O_3 should be greater than 70% (Moghal 2017).

1.2 Soil Stabilization Effect Due to Fly Ash Addition

Class *C* fly ash is the self-pozzolanic fly ash having considerable amount of CaO in comparison with Class *F* fly ash. The reactive silica and lime in Class *C* fly ash produce cementitious products in presence of water. The stabilization effect due to addition of Class *C* fly ash to soil can be explained with following equations (Moghal 2017);

$$2(3CaO.SiO_2) + 6H_2O \rightarrow 3CaO.\,2SiO_2.3H_2O + 3Ca(OH)_2 \quad (1)$$

$$\text{Hydrolysis} : Ca(OH)_2 \rightarrow Ca^{++} + 2(OH^-)_2 \quad (2)$$

The hardening process of soil–Class *C* fly ash mixture is synergistic effect of short-term and long-term strength gain. The short-term effect is due to cation exchange process and takes place immediately as fly ash is blended with soil. The long-term effect is result of hydration of cementitious material and pozzolanic reaction in presence of high quantities of CaO, SiO_2 and Al_2O_3 (Kang et al. 2014).

Accordingly, the use of pozzolanic fly ashes for improvement of soils' engineering properties can provide viable solutions to environmental issues and curtail the cost of soil stabilization projects. A wealth of the literature shows that lime and fly ash are a good combination for stabilizing both silty and sandy soils because they considerably enhance the stiffness of the final product (Arora and Aydilek 2005; Puppala 2016).

1.3 Utilization of Class C Fly Ash in Pavement Stabilization

Pavements are the major application in which fly ash can be effectively used and result in significant savings in land-filling costs. Relying on Class *C* fly ash in the presence of lime, Bergeson and Barnes 1998 developed design guidelines for determining the structural layer coefficient for the base layer of flexible pavement. Their study revealed that the required base layer thickness decreases with the addition of these additives. Figure 1 shows typical cross section of flexible pavement. It is clear that reduction in thickness of any layer will require less material and hence will be cost-effective.

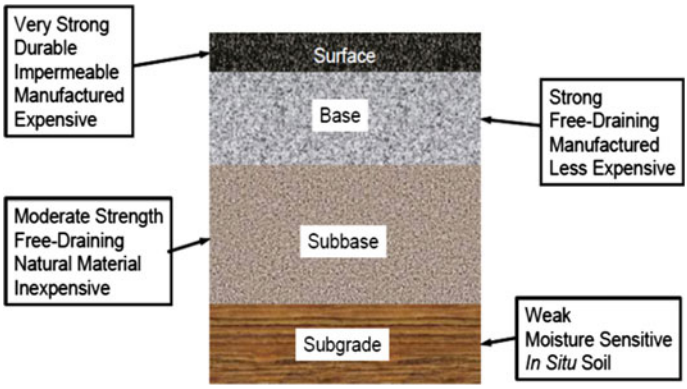

Fig. 1 Typical cross section of flexible pavements (FHWA_NHI_05_037)

2 Effects of Fly Ash Stabilization on Soils for Pavement Applications

The Class *C* fly ash can be effectively used for base, subbase and subgrade courses of flexible pavement system. The studies oriented towards use of Class *C* fly ash as a stabilizing agent with respect to application in pavement layers are discussed herewith;

2.1 Compaction Parameters

It is found that at low fly ash content addition weak soils show increased maximum dry density. Gain in maximum dry density may be attributed to packing of fine fly ash particles in voids of relatively larger soil particles during compaction (McManis and Arman 1989; Zia and Fox 2000). The optimum moisture content increases with increase in fly ash content in soil—fly ash mixtures. With the increased number of finer particles in mixture, specific surface of the mixture increases (Zia and Fox 2000; Shon et al. 2010). Due to this, the progressive hydration of soil–fly ash mixture is accelerated and more water is consumed (Zia and Fox 2000). In long term, pozzolanic products induced from hydration process of fly ash may fill in voids and in turn densify soil (Kang et al. 2015). Due to self-cementitious nature, Class *C* fly ash can be directly added to soil as stabilizing agent. But in the presence of additives such as $CaCl_2$, soil–Class *C* fly ash-$CaCl_2$ produces high maximum dry density at low optimum moisture content which in turn leads to increased strength, dimensional stability and reduced permeability of treated soils (Shon et al. 2010).

2.2 Unconfined Compressive Strength (UCS)

Figure 2 shows the variation in UCS values before and after addition of Class *C* fly ash to soil studied by various authors. UCS value of soil–fly ash mixture is affected by fly ash content, curing period, water content and soil type.

Addition of Class *C* fly ash results in stiffer and stronger material. Stiffness of sample treated with fly ash is greater than untreated samples. This is helpful in judging mechanical characteristic with respect to subgrade application (Misra 1998). The bridging and aggregation of soil–fly ash particles due to formation of hydration gel alters the stress–strain response at macro-scale (Kang et al. 2014). The amount of fly ash added to soil–fly ash mixture affects the rate of strength gain to a greater extent. The higher the fly ash content added to soil–fly ash mixture, the strength gain is the faster. But ultimate strength of soil–fly ash mixture in not governed by fly ash content. As the curing time for soil–fly ash mixture specimen was increased, UCS value increased gradually. But at the end of 28 days curing, all the samples reached highest UCS value. This means that the sample stiffening speed is increased as the fly ash content is increased. The soil–fly ash mixtures at any fly ash content are cured for sufficient time, all mixtures can gain approximately same highest UCS value (Kang et al. 2015). At greater fly ash content, shrinkage cracks may form in the soilfly ash specimen due to accelerated hydration and reduction in water content at greater rate. Hence, the amount of fly ash for soil stabilization should be determined carefully.

UCS of stabilized dredged material increased with increasing fly ash content and curing time. For a given curing time, UCS increased linearly with increasing fly ash content. The improvement in UCS increased significantly as curing time increased. The effect of curing time on UCS for specimens with higher fly ash content was more significant than for specimens with lower fly ash content. Strength of the stabilized dredged material after 12 freeze–thaw cycles decreased by an average of only 4.7%, indicating that stabilized dredged material in this study is resilient to freeze–thaw cycling (Yu et al. 2017). Addition of fly ash to the organic soils resulted in significant increase in UCS relative to that for unstabilized soils at very wet condition (Tastan et al. 2011).

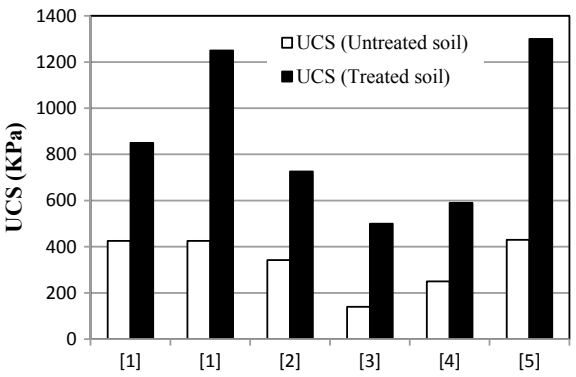

Fig. 2 Variation in UCS for untreated and Class *C* fly ash-treated soils (Misra 1998; Zia and Fox 2000; Kang et al. 2014; Sridharan et al. 1997; Yu et al. 2017)

2.3 California Bearing Ratio (CBR)

Figure 3 shows the variation in CBR values before and after addition of Class *C* fly ash to soil studied by various authors. Variation in CBR value of Class *C* fly ash-treated soils depends upon fly ash content, curing period, water content and soil type.

The California bearing ratio of stabilized dredged material increased with increasing FA content and curing time. The CBR of dredged material stabilized using Class *C* fly ash is comparable to the CBR of compacted silty sand or sand and places the material in a category of fair to good for pavement subgrade applications (Yu et al. 2017).

For loess–fly ash mixtures, maximum CBR value was obtained at 10% fly ash addition and on further fly ash addition the mixture showed strength loss (Zia and Fox 2000). Incorporation of Class *C* fly ash to weak soils improves strength and stiffness quickly. Also no deterioration in subgrade strength with respect to age was observed for Class *C* fly ash-treated subgrades (Parsons and Kneebone 2005). Hence, stabilizing weak soils with Class *C* fly ash can be effective with respect to both short-term and long-term strength and durability of soil–fly ash mixture.

For soft fine-grained subgrade soils treated with Class *C* fly ash, increase in fly ash content causes gain in CBR value of soil–fly ash mixture. As the compaction water content increases, the CBR value of soil–fly ash mixture decreases. For organic soils, low CBR values are obtained as a result of inhibition of hydration of cementitious binders due to organic matter (Edil et al. 2006; Tastan et al. 2011). CBR value increases appreciably in inorganic soils on Class *C* fly ash addition (Edil et al. 2006).

On the basis of improved dynamic cone penetration value for soil–fly ash mixture, it is clear that stiffness of the soil is improved on Class *C* fly ash addition (Shon et al. 2010).

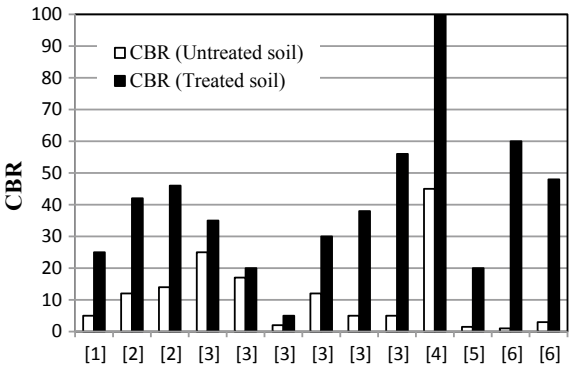

Fig. 3 Variation in CBR values for untreated and Class *C* fly ash-treated soils (Zia and Fox 2000; Parsons and Kneebone 2005; Edil et al. 2006; Shon et al. 2010; Yu et al. 2017; Bin-Shafique et al. 2004)

For natural soils, Edil et al. 2006 formulated equation for estimating resilient modulus from CBR value as follows;

$$M_R = 3\ CBR \tag{3}$$

2.4 Resilient Modulus (M_R)

Figure 4 shows the variation in resilient modulus values before and after addition of Class *C* fly ash to soil studied by various authors. Effect of fly ash addition on resilient modulus value depends upon fly ash content, curing period, water content and soil type.

Resilient modulus of soil–fly ash mixtures increases with increase in fly ash content as well as curing period (Edil et al. 2006; Tastan et al. 2011; Kang et al. 2014).

Resilient modulus is the property relevant to long-term performance under service loads, and soil–fly ash mixtures are expected to gain strength with increasing curing time (Edil et al. 2006; Kang et al. 2014). Hence, Kang et al. 2014 formulated relationship between resilient modulus and curing time based on experimental data. The expression is as follows;

$$M_R = a.T^b \tag{4}$$

where a—improved M_R on 1 day curing; T—curing time; b—exponential rate of improvement.

Further, Kang et al. 2014 formulated relationship between resilient modulus and permanent strain, as permanent strain is closely related to rut resistance which is parameter of prime importance while designing flexible pavement. The relationship is as follows;

$$M_R = A.\varepsilon^B \tag{5}$$

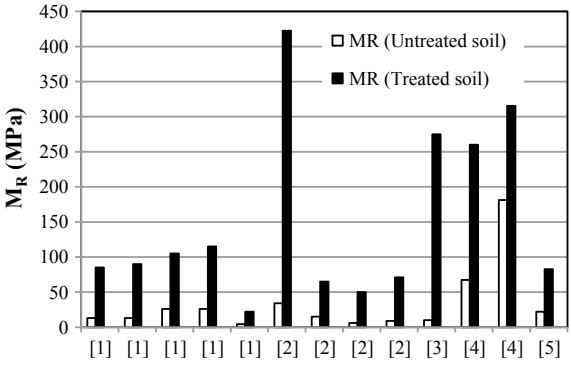

Fig. 4 Variation in resilient modulus for untreated and Class *C* fly ash-treated soils (Tastan et al. 2011; Edil et al. 2006; Shon et al. 2010; Kang et al. 2014; Yu et al. 2017)

where A and B—regression coefficients; ε—permanent strain.

When permanent strain induces at rapid rate, MR value decreases. Hence, the above equation is important for estimating permanent deformation based on MR value.

The resilient modulus of stabilized dredged materials increased significantly as the fly ash content is increased. The M_R values for stabilized dredged materials were comparable to gravel or crushed stone and places the material in a category of good to excellent for pavement subgrade applications (Yu et al. 2017). The soil stabilization using Class *C* fly ash produced significant improvement in resilient modulus such that very soft soil with no fly ash was brought to medium-stiff subgrade consistency on fly ash addition (Tastan et al. 2011). M_R value increases appreciably in inorganic soils on Class *C* fly ash addition. For organic soils, Class *C* fly ash addition had very small effect on M_R value (Edil et al. 2006).

Rosa et al. 2017 studied effect of freeze and thaw (F-T) cycles on resilient modulus values of Class *C* fly ash stabilized geomaterials. It was found that strength of fly ash stabilized soils after F-T cycles was at least three times greater than that for unstabilized soils. On exposure to F-T cycles, reduction in resilient modulus in soil–fly ash mixture samples was attributed to deceleration of pozzolanic reactions caused by freezing temperature. Clay stabilized with Class *C* fly ash shows large decrease in M_R during F-T cycles. Change in MR on F-T cycles is depending on CaO content of fly ash and not the amount of fly ash added to soil. Greater reduction in MR with F-T cycles was observed for soil–fly ash mixture with low CaO fly ash (Rosa et al. 2017).

3 Concluding Remarks

- Incorporating Class *C* fly ash into subgrade soils results in significant improvement in the strength and stiffness of the pavement section very quickly. This is beneficial as the subgrades are subjected to heaviest loads during construction of the road and the development of related properties.
- Increase in strength by Class *C* fly ash addition is attributed to chemical reactions and reduction in water content due to addition of dry solids. But the type of fly ash and soil governs the significance of the reactions taking place within the mixtures.
- The unconfined strength of soil stabilized with Class *C* fly ash increases as the fly ash content and curing time increase.
- CBR value of soil–Class *C* fly ash mixtures increases with increment in fly ash content and curing period. Class *C* fly ash effectively stabilized inorganic soils compared to organic soils. CBR values for soils stabilized with Class *C* fly ash place them in category of good-to-excellent subgrade formation.

- Resilient modulus value increases with fly ash addition to the soil and the curing of soil–fly ash mixture. The fly ashes having more CaO content show greater improvement in terms of MR on stabilization.
- The strength of the pavement system contributed by improved subgrade and results in reductions in thickness of pavement layers which in turn leads to cost-effective design of pavement.

Although it is concluded that weak soils specifically clayey soils are effectively stabilized using Class *C* fly ash for subgrade application, effect of organic content of clayey soils on fly ash addition and subsequent strength behaviour needs to be focused. Hence detailed study towards stabilization of organic soils using Class *C* fly ash can be carried out to determine effects of composition of fly ash and contents of organic soils on long term strength of soil.

References

ASTM C618-17 (2017) Standard Specification for coal fly ash and raw or calcined natural pozzolan for use in concrete, ASTM International, West Conshohocken, PA

Arora S, Aydilek AH (2005) Class *F* fly-ash-amended soils as highway base materials. J. Mater Civ Eng, ASCE, 17(6):640–649

Bergeson KL, Barnes AG (1998) Iowa thickness design guide for low volume roads using reclaimed hydrated Class *C* fly ash bases (No. ISU-ERI-Ames Report 98401), Engineering Research Institute, Iowa State University

Bin-Shafique S, Edil TB, Benson CH, Senol A (2004) Incorporating a fly-ash stabilised layer into pavement design. Proc Inst Civ Eng-Geotech Eng 157(4):239–249

Edil TB, Acosta HA, Benson CH (2006) Stabilizing soft fine-grained soils with fly ash. J Mater Civ Eng, ASCE, 18(2):283–294

Kang X, Kang GC, Chang KT, Ge L (2014) Chemically stabilized soft clays for road-base construction. J Mater Civ Eng 27(7):04014199

Kang X, Ge L, Kang GC, Mathews C (2015) Laboratory investigation of the strength, stiffness, and thermal conductivity of fly ash and lime kiln dust stabilized clay subgrade materials. Road Mater Pavement Des, Taylor & Francis, 16(4):928-945

McManis K. L., and Arman A. (1989) Class *C* fly ash as full or partial replacement for Portland cement or lime, Transportation Research Record 1219. Transp Res Board, Washington, DC, 68–81

Misra A (1998) Stabilization characteristics of clays using class *C* fly ash. Transportation Research Record: J Transp Res Board, (1611):46-54

Moghal AAB (2017) State-of-the-art review on the role of fly ashes in geotechnical and geoenvironmental applications. J Mater Civ Eng, ASCE, 29(8):04017072

Parsons RL, Kneebone E (2005) Field performance of fly ash stabilized subgrades. Proc Inst Civ Eng-Ground Improv 9(1):33–38

Puppala AJ (2016) Advances in ground modification with chemical additives: From theory to practice. Transp Geotech, Elsevier, 9:123-138

Rosa MG, Cetin B, Edil TB, Benson CH (2017) Freeze–Thaw performance of fly ash–stabilized materials and recycled pavement materials. J Mater Civ Eng, ASCE, 29(6):04017015

Shon CS, Saylak D, Mishra S (2010) Combined use of calcium chloride and fly ash in road base stabilization. Transp Res Rec: J Transp Res Board 2186:120–129

Sridharan A, Prashanth JP, Sivapullaiah PV (1997) Effect of fly ash on the unconfined compressive strength of black cotton soil. Proc Inst Civ Eng-Ground Improv 1(3):169–175

Tastan EO, Edil TB, Benson CH, Aydilek AH (2011) Stabilization of organic soils with fly ash. J Geotech Geoenviron Eng, ASCE, 137(9):819–833

Yu H, Yin J, Soleimanbeigi A, Likos WJ (2017) Effects of curing time and fly ash content on properties of stabilized dredged material. J Mater Civ Eng, ASCE, 29(10):04017199

Zia N, Fox P (2000) Engineering properties of loess-fly ash mixtures for road base construction. Transp Res Rec: J Transp Res Board 1714:49–56

Variation of CBR Values of Laterite Soil Mixed with Jarofix and Lime

G. Santhosh and K. S. Beena

Abstract Road networking is one of the vital indicators of development of any country. Presently, scarcity of good subgrade soil is one of the major problems for improving road network. At the same time, handling and disposal of waste is one of the main problems of industrialization. Jarofix which is a waste material from zinc industry is one with limited utilization nowadays. So, the present study is an investigation on the effect of lime and Jarofix when mixed with soil, by conducting unsoaked CBR tests. Initially, the CBR values were evaluated by adding 10, 20, 30, 40, and 50% of Jarofix mixed with soil and the values were found to be decreasing as the percentage of Jarofix increases. The long-term effects of the same mixes were studied after 7, 14, 28, 56, and 90 days and CBR values found to be increasing with age. For further improvement, the tests were done with the addition of 2.5, 5, 7.5, 10, and 12.5 percentage of lime for the same soil–Jarofix combinations. The CBR values were improving with percentage of lime and age, and the optimum percentage of lime was found to be 7.5% which showed an increase of more than 100% in CBR.

Keywords Jarofix · Waste utilization · Ground improvement

1 Introduction

India has a road network of more than 33 lakhs km which is the second largest road connecting system in the world. Most of the passenger traffic is carried by the roads. Roads are one of the strongest measures of economic activity and the development of any nation. The quality of pavement depends on the strength of its subgrade. The main function of the subgrade is to provide adequate support to the

G. Santhosh (✉) · K. S. Beena
School of Engineering, CUSAT, Kochi, Kerala, India
e-mail: santhoshg@scmsgroup.org

K. S. Beena
e-mail: beenavg@gmail.com

R. Sundaram et al. (eds.), *Geotechnics for Transportation Infrastructure*,
Lecture Notes in Civil Engineering 29,
https://doi.org/10.1007/978-981-13-6713-7_51

pavement and for this the subgrade should possess sufficient stability under adverse climate and loading condition. The properties of the subgrade soil are important in deciding the thickness requirement of pavements. If the natural soil is very soft and weak, it needs some improvement for use as subgrade (Chakraborty et al. 2014). Generally, ground improvement techniques are recommended in this situation. Improvement of soil could be achieved by soil modification or stabilization, or both. Soil modification is mainly the addition of a modifier like cement, lime, fly ash, cement klin dust, bagasse ash, rice husk, etc., to the soil. (Beena and Santhosh 2013). Also, scientists all over the world are searching for alternate materials for the conventional materials in various areas of construction for reducing the cost for improvement.

Industrialization and urbanization have good and bad impacts. On the negative side, there is great concern about the various pollutions due to it. All over world, huge quantities of hazardous wastes are generated during different industrial processes. Improper management of solid wastes causes adverse effects on the ecology which may lead to cause possible outbreak of diseases and epidemics, which is a threat to human community everywhere. Now, dumping the wastes over the useful land has been the main option available for the disposal. This has created non-utilization of large area of land and causes other environmental problems also. In India, approximately 960 million tonnes of solid waste is being generated annually as by-products during industrial, mining, municipal, agricultural, and other processes. Of which, 4.5 million tones are considered as hazardous in nature (Rathore et al. 2014).

The utilization of these industrial wastes in any of the civil engineering field is one of the best solutions to dispose the waste (Muntohar et al. 2013). Jaroste is one of such solid wastes from zinc industries. It is acidic in nature. Due to the presence of toxic substances like zinc, lead, cadmium, copper, and other metallic and non-metallic oxides, it is susceptible to leaching and which may cause adverse or chronic effects on environment and human health (Rathore et al. 2014). Hence all over the world, its disposal has become a major environmental concern in all zinc industries. When Jarosite is mixed with lime and cement, the resulting stable material is called Jarofix (Sinha et al. 2015). So, the best way to solve the disposal problem of Jarosite like other wastes is to decrease the quantity for disposal by bulk utilization in various civil engineering fields.

Lime is a safe and economic stabilization agent. Lime, (CaO or CaOH2) is a burned by-product of lime stone (CaCO3), is one of the oldest developed construction material. When solid waste added to soil found to be ineffective and if it can be effectively used along with lime for soil improvement, it will also be beneficial to handle the problems of waste disposal. (Dash and Hussain 2012). Research is going in and around the world for the utilization of various wastes for ground improvement.

Raj et al. (2014) have studied the variation of Atterberg's limits and swelling characteristics of bentonite Jarofix mixtures, and it shows a decreasing trend when the percentage of Jarofix increases. Sinha et al. (2013b) have evaluated the geotechnical characteristics of Jarosite and its utilization for road construction.

Sinha et al. (2013a) have studied the different properties like grain-size distribution, Atterberg's limits, Proctor compaction tests, UCC tests, CBR tests, consolidation tests, and direst shear tests on Jarofix, bottom ash, local soil–Jarofix–bottom ash mixtures and Jarofix–soil mixtures. Joysha and Syam (2016) have conducted laboratory tests on black cotton soil in combination with Jarofix. Results reveal that when Jarofix is added to soil the Atterberg's limits were found to be varying. Free swelling of black cotton soil decreases to 0% when 50% of Jarofix is added and the maximum dry density decreases with increase in percentage of Jarofix. 10% Jarofix is found to be optimum. Both soaked and unsoaked CBR obtained maximum value when 10% Jarofix added to the soil. Rachel and Ramya (2017) have studied the effect of Jarofix on Cochin marine clay. They found that the maximum dry density of cochin marine clay decreases, whereas the optimum moisture content and CBR values increases as the percentage of Jarofix increases.

So, in this study, the effect of Jarofix when added to the soil and the optimum lime required to be added to soil–Jarofix mixture, to obtain maximum strength were studied.

2 Materials

2.1 Soil

Soil sample used in this study is laterite soil, which are most commonly observed soil type in Kerala and which is reddish in color due to the presence of iron. Laterite is rich in iron and aluminum. The soil sample used in this study was taken from a depth of 2 m from ground level at a site nearly 5 km from the Aluva, Ernakulam district, Kerala by machine excavation after clearing 1 m top soil. Samples were air dried, and the lumps were broken by pulverizing between the fingers and thumb, and it was stored in a large tank. The grain-size analysis reveals that the soil consists of 11% gravel, 85.4% sand, and 3.6% silt and clay fraction. As per the IS classification, the soil can be named as SW.

2.2 Jarofix

Jarosite is the major by-product at Binani Zinc Ltd, Binanipuram., Kochi, Kerala which is a major zinc manufacturing company in Kerala. Jarosite is a toxic material, and its utilization is restricted due to Kerala Pollution Control Board regulations. Jarosite is converted into Jarofix by adding cement and lime at source itself, so as to keep the material inert in the dumping yards, which is dumbed over a large area inside the company.

Table 1 Geotechnical properties of Soil and Jarofix

Properties	Soil	Jarofix
Specific gravity	2.52	2.31
% of Gravel (>4.75 mm)	11	0
% of Sand (4.75–0.075 mm)	85.4	3.62
% of Silt and clay (<0.075 mm)	3.6	96.38
IS classification	SW	MH
Liquid limit (%)	47	61
Plastic limit (%)	27	44
Plasticity index (%)	20	17
Shrinkage limit (%)	21	32
Optimum moisture content (%)	18.5	48.3
Maximum dry density (kN/m^3)	17	11.6
UCC (kN/m^2)	272.1	63.8
Unsoaked CBR	23.5	12.6
Soaked CBR	11.51	4.97
Angle of internal friction	12	1
Cohesion (kN/m^2)	27.7	32.1

Jarofix which is used in the study is collected from there and is brought to laboratory in polythene bags. The physical appearance of the material is fine powder, light brown in appearance, and the lumps were broken by pulverizing between the fingers. After air drying and pulverizing, the Jarofix samples were transferred to plastic bags and stored in airtight containers at room temperature. The grain-size analysis shows that the material consists of mainly fine particles, and the silt and fine fraction comes to be 96.38% and remaining 3.62% is sandy fraction. As per IS classification, the material belongs to MH. The geotechnical properties of soil and Jarofix were determined as per IS standards and are as shown in Table 1. The chemical characteristics of Jarofix are shown in Table 2.

Table 2 Chemical characteristics of Jarofix*

Chemical components	Range (%)
SO_3	19–31
CaO	4–18
SiO_2	3–12
Al_2O_3	<12
Fe_2O_3	18–36
Na_2O	<4
Cadmium	<0.08
Lead	<5.5
Zinc	<3.5

*As supplied by Binani Zinc Ltd, Binanipuram.,Kochi, Kerala

2.3 Lime

Lime is a calcium-containing inorganic material in which carbonates, oxides, and hydroxides predominate. Lime was obtained in the form of shells from local shops. The sample was sprinkled with water and let to rest for a day, after which powered form of lime was obtained, and it was sieved through 425 microns before the tests are conducted. To reduce the carbonation effect due to humidity, the lime was kept in an airtight plastic container.

3 Experimental Studies

All the samples used in this study were air dried because oven dry may cause the variation of properties. The purpose of this work is the utilization of Jarofix for soil modification along with lime and thereby reducing the problems created due to dumping of Jarofix in zinc manufacturing industries. The load-carrying capacity of pavements mainly depends on the strength of subgrades. One of the main tests for finding the strength of subgrade is CBR test. So, for checking the suitability of Jarofix as subgrade material, the unsoaked CBR tests were conducted on parent soil samples and the soil mixed with 10, 20, 30, 40, and 50% of Jarofix, and the results were analyzed. All the materials used were weighted properly as per the required mix and mixed in a tray fully on dry weight basis for all the tests. All the samples were prepared at their respective optimum moisture content obtained from compaction test. Also, the CBR tests of these mixes were conducted after 7, 14, 28, 56, and 90 days without losing its mixing water content. Then for studying the effect of lime on the soil–Jarofix mixture and to find the optimum percentage of lime in each soil–Jarofix mixture, the CBR tests were done with varying percentage of lime. The different percentages of lime added were 2.5, 5, 7.5, 10, and 12.5. Also, the tests were done after 7, 14, 28, 56, and 90 days of mixing. The samples kept in airtight plastic bags and containers, and, care had been taken not to lose moisture content for the durability test. In this paper S, J, and L stands for soil, Jarofix, and lime, respectively.

4 Effect of Jarofix on Unsoaked CBR Values

Subgrade of a pavement should be strong enough to give adequate support to the pavement and for supporting and distributing the wheel loads. The design and behavior of a flexible pavement depends mainly on the stability of the subgrade soil. CBR test is one of the common tests for evaluating the strength of stabilized

soils. CBR value is the ratio of force per unit area required to penetrate the sample with a standard piston to that required for a corresponding penetration in a standard material. A cylindrical mold having internal diameter 150 mm and height 175 mm is used for preparing the mold. The total weight of the samples taken was corresponding to achieve maximum dry density from Proctor compaction test. It is mixed with water content corresponds to optimum moisture content. It was tested on CBR testing machine having 50 kN capacity, and load is applied at the rate of 1.25 mm/min and the loads were noted for different penetrations.

The load corresponds to 2.5 and 5 mm penetrations were found from graph. The CBR value is normally expressed as percentage comparing with standard material. Generally, the CBR value at 2.5 mm will be greater than that at 5 mm and in such case the former shall be taken as CBR for design purpose. If CBR for 5 mm exceeds that for 2.5 mm, the tests should be repeated and if get the identical results, the CBR value corresponds to 5 mm penetration should be taken for design. The CBR tests were conducted on parent soil and soil mixed with 10, 20, 30, 40, and 50% of Jarofix. The load penetration curves were plotted as shown in Fig. 1. The value for the soil was 23.65% and the value decreases to 15.1% when 50% Jarofix mixed with the soil. The value for the Jarofix is 12.6%. The reduction in CBR value may be due to the addition of Jarofix with a lower CBR value than the parent soil. The variation is as shown in Fig. 2.

To study the variation of CBR values with age, the same soil–Jarofix combinations mixed at respective OMC water content preserved in sealed airtight containers without losing the moisture content for different days. Then, the samples were compacted in the CBR mold after 7, 14, 28, 56, and 90 days and tested.

For every combination of soil and Jarofix, the CBR values increase with age as shown in Fig. 3. But the soil shows the same strength in all the days which indicates that there happens the development of strength when Jarofix present in the soil. The strength gain may be due to pozzolanic reaction, cation exchange, and strength-gaining compounds formed with in the soil–Jarofix mixture in the presence of water due to the chemical components present in the Jarofix. But the results reveal that there is only marginal increase in CBR value when Jarofix alone mixed with the soil. So, to further increase the CBR values, each combination mentioned is mixed again with 2.5.5, 7.5, 10, and 12.5% of lime on dry weight basis, and the

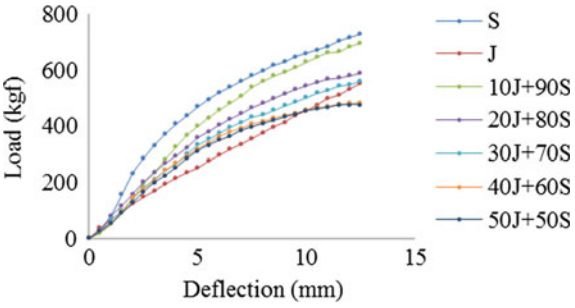

Fig. 1 Load deflection curves Jarofix

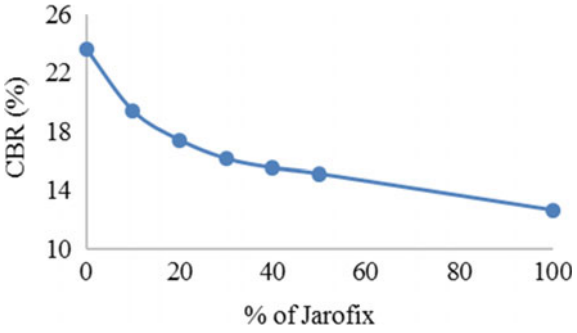

Fig. 2 Variation of CBR values with Jarofix

CBR values were found. Figures 4, 5, and 6 show the variation of the CBR values for the S, J, and 10J+90S, respectively. Similar variations were obtained for 20J +80S, 30J+70S, 40J+60S, and 50J+50S also.

The CBR values of all combinations vary with increase in percentage of lime. In general, as the percentage of lime increases, the CBR value of samples increases up to maximum value and then decreases. Though the maximum CBR value is observed for 10% of lime for J, 20J+80S, and 40J+60S, there is only marginal improvement from 7.5% lime content, which is the optimum percentage for all other combinations. Hence, the optimum percentage of lime can be taken as 7.5%. The maximum percentage of increase in CBR value for S is 127 compared to the value without addition of lime. The same for J is 111%, 10J+90S is 168%, 20J+80S is 178%, 30J+70S is 146%, 40J+60S is 139%, and combination of 50J+50S is 134%.

The increase in CBR value of the soil–Jarofix mixture along with lime may be attributed to the physicochemical phenomena, namely the cation exchange that takes place between the lime and the negatively charged clay particles together with the flocculation–agglomeration mechanism. These take place rapidly and produce immediate improvements in soil properties including uncured strength. In addition, pozzolanic reactions may occur later between the calcium ions and the silica and alumina of the clay minerals. This results in the formation of cementitious products

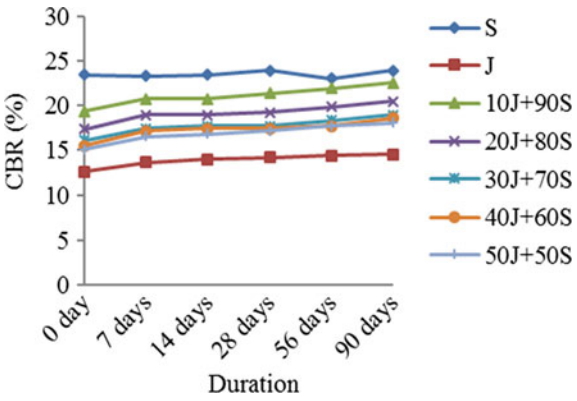

Fig. 3 Variation of CBR values with age

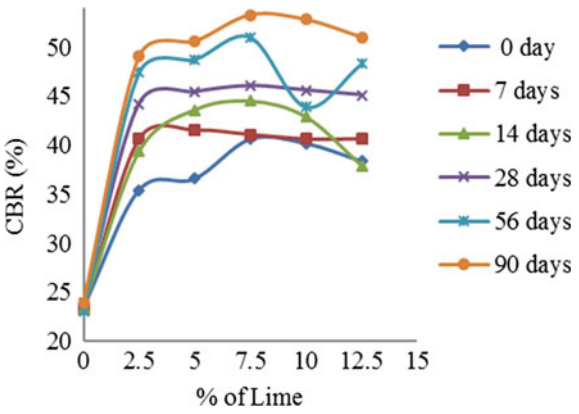

Fig. 4 Variation of CBR value of S with different percentages of lime for different days

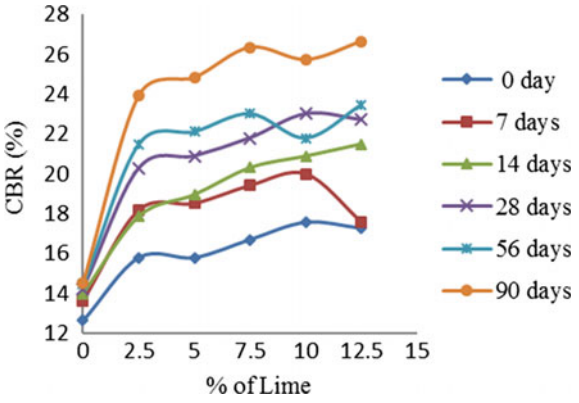

Fig. 5 Variation of CBR value of J with different percentages of lime for different days

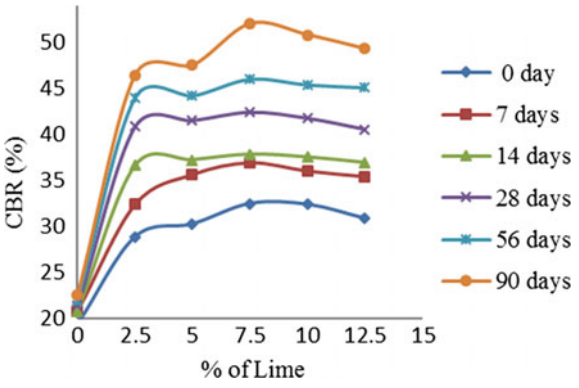

Fig. 6 Variation of CBR value of 10J+90S with different percentages of lime for different days

such as calcium–silicate–hydrates (C–S–H), calcium–aluminate–hydrates (C–A–H), and calcium–aluminum–silicate–hydrates (C–A–S–H) that are also responsible for the strength increase. (Amadi and Okeiyi 2017).

The variations in CBR values also can be represented with age for different percentages of lime. Figures 7, 8, and 9 show the variation of S, J, and 10J+90S on 7, 14, 28, 56, and 90 days. Similar variations were obtained for 20J+80S, 30J+70S, 40J+60S, and 50J+50S. For all combinations, the CBR values increase with age in the presence of lime when tested without losing moisture content.

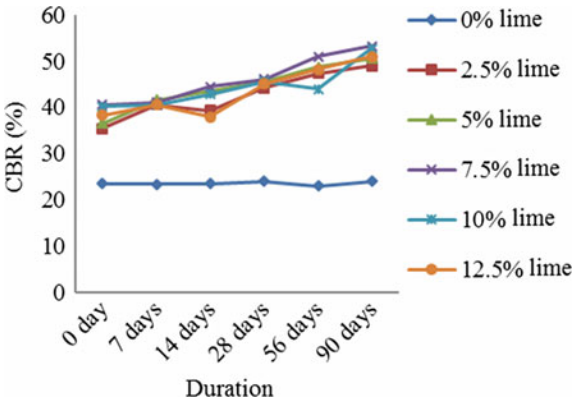

Fig. 7 Variation of CBR values of S with age

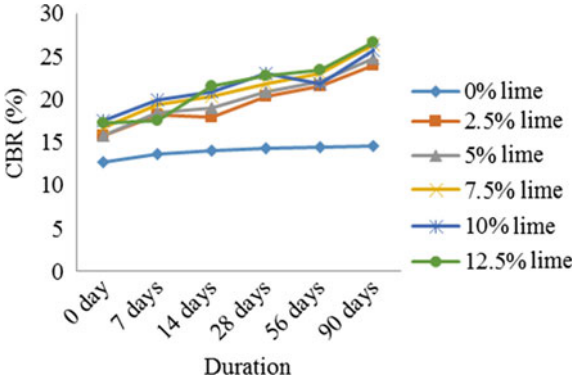

Fig. 8 Variation of CBR values of J with age

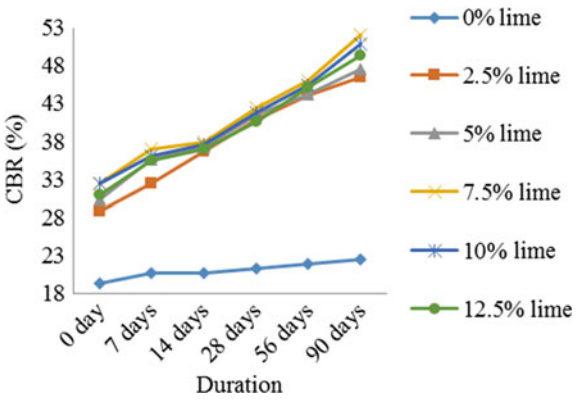

Fig. 9 Variation of CBR values of 10J+90S with age

5 Conclusions

The CBR value of subgrade is one of the main design parameters of flexible pavement. The thickness of the different layers of the pavement depends mainly on this value. In this study, the suitability of Jarofix as subgrade material, which is the waste material from zinc industry has been investigated. The following conclusions were obtained:

- The CBR values were found to be decreasing when the percentage of Jarofix to the virgin soil increases.
- The CBR values of the same soil–Jarofix mixtures were found to be increasing when tested after 7, 14, 28, 56, and 90 days tested without losing its water content at the time of mixing. But the increase was not considerable.
- To further improve the CBR values, 2.5, 5, 7.5, 10, and 12.5% of lime were added to the soil, Jarofix and soil–Jarofix mixtures. From the results, it was found that as the percentage of lime increases the CBR value of the samples increases up to maximum value and then decreases. Considering the cost aspect, the optimum percentage of lime can be taken as 7.5%.
- Also for all percentage of lime, the CBR values were found to be increased with age when tested without losing its moisture content at the time of mixing.

More studies are needed to understand the complete behavior of the soil—Jarofix mixture along with lime, like soaked CBR conditions, and, the studies are continuing in this direction to explore more applications of Jarofix.

References

Amadi AA, Okeiyi A (2017) Use of quick and hydrated lime in stabilization of lateritic soil: comparative analysis of laboratory data. Int j Geo-Eng 1–13

Beena KS, Santhosh G (2013) Studies on strength characteristics of soil mixed with bio-waste. In: Indian geotechnical conference, Roorkee

Chakraborty S, Mukherjee SP, Chakrabarti S, Chattopadhyay BC (2014) Improvement of sub grade by lime and rice husk ash admixturers. Int J Innovative Res Sci, Eng Technol 11.034–11.040

Dash SK, Hussain M (2012) Lime stabilization of soils: reappraisal. J Mater Civ Eng 707–714

Joysha B, Syam D (2016) Study of swelling and strength characteristics of black cotton soil mixed with jarofix. Int J Core Eng Manag, IJCEM 107–115

Muntohar AS, Widianti A, Hartono E, Diana W (2013) Engineering properties of silty soil stabilized with lime and rice husk ash and reinforced with waste plastic fiber. J Mater Civ Eng 1260–1270

Nitisha R, Patil MP, Devendra D (2014) Utilization of jarosite generated from lead-zinc smelter for various applications: a review. Int J Civ Eng Technol, IJCIET 5(11):192–200

Rachel J, Ramya K (2017) A study on the effect of Jarofix on Cochin marine clay. In: International conference on geotechniques for infrastructure projects, Thiruvananthapuram

Raj A, Beena KS, Santhosh G, Santhosh KN (2014) Geoenvironmental characteristics of jarofix mixed soil. In: International conference on energy, environment, materials and safety, CUSAT, Kochi, India

Sinha AK, Havanagi VG, Arora VK (2015) Stress-Strain Behaviour Of Stabilised Jarofix Waste Material. In: 50th Indian geotechnical conference, Pune, Maharashtra, India

Sinha AK, Havanagi VG, Arora VK, Ranjan A, Mathur S (2013a) Characterization of Jarofix waste material for the construction of road. Highway Res J 35–42

Sinha AK, Havanagi VG, Ranjan A, Mathur S, Singh BK (2013b) Geotechnical characterization of jarosite waste material for road construction. In: Indian geotechnical conference, Roorkee

Volume Compressibility and Pore Pressure Response of Kutch Soils with Varying Plastic and Non-plastic Fines

Majid Hussain and Ajanta Sachan

Abstract Effect of fines content (FC) and its nature (*plastic fines and non-plastic fines*) on the volume compressibility and pore pressure response of 32 soils from 10 locations of Kutch (high seismicity region) is studied. Volume compressibility and pore pressure response of soils are studied and analyzed in the context of variations in plastic and non-plastic fines content. Volume compressibility increased with an increase in fines content: Influence of plastic fines is more compared to non-plastic fines. Fines content and nature of fines controlled the magnitude of excess pore water pressure generated within the soil mass. Plastic fines inhibited pore water pressure generation to a greater degree than non-plastic fines. Soils with same fines content but higher plastic fine content exhibited larger volume compressibility and lower pore water pressure evolution. Skempton's pore pressure parameter (A) of these soils indicated similar response as that of liquefiable soils. FC and nature of fines affected the degree of brittleness, which has been evaluated by obtaining undrained brittleness index (I_{B2}) with respect to pore pressure. The correlation between volume compressibility and pore water pressure response exhibited negative value ($R = -0.14$) indicating the opposite effect of FC.

Keywords Compressibility · Pore pressure · Fines content · Plastic fines · Non-plastic fines

M. Hussain (✉) · A. Sachan
Department of Civil Engineering, Indian Institute of Technology Gandhinagar, Gandhinagar, India
e-mail: majid.hussain@iitgn.ac.in

A. Sachan
e-mail: ajanta@iitgn.ac.in

R. Sundaram et al. (eds.), *Geotechnics for Transportation Infrastructure*,
Lecture Notes in Civil Engineering 29,
https://doi.org/10.1007/978-981-13-6713-7_52

1 Introduction

Compressibility and shear strength behavior of soils are largely dependent on density, stress state, and boundary conditions of the soil. Effect of fines on the compressibility of soil is a function of amount and nature of fines present (Rutledge 1947; Lade et al. 2009). Loose silty sands, when subjected to drained and undrained conditions, exhibited contractive response under both the boundary conditions (Pitman et al. 1994). Pore pressure evolution might lead to strength reduction resulting in various types of failures like strain softening (SS), limited strain softening (LSS), and strain hardening (SH) (Castro 1969). The large positive pore water pressure causes spontaneous triggering with large movement and high velocity also known as static liquefaction. Many researchers have explained the mechanism of static liquefaction. Terzaghi (1956), Sladen et al. (1985) and Yamamuro and Lade (1997) articulated collapse of the metastable soil structure during undrained monotonic loading as a possible cause of static liquefaction. The phenomenon has drastic implications when encountered in silty sands. Such type of soils offers minimal resistance to earthquake liquefaction (Ishihara 1993).

Loose silty sands are highly compressible, which creates large excess pore pressure (Δu) during undrained shearing leading to static liquefaction (Yamamuro and Lade 1998; Sladen et al. 1985). The immediate consequences of large volume compressibility (m_v) and large excess pore pressure (Δu) are large deformations and low load-carrying capacity. Factors controlling m_v and Δu such as relative density, fines content, effective confining pressure, stress history, and anisotropy were explored recently by many researchers (Lee and Farhoomand 1967; Lade and Yamamuro 1997; Yamamuro and Lade 1997; Thevanayagam 1998; Yamamuro et al. 2008; Monkul and Yamamuro 2011). Most of these studies were carried out on clean standard sands and silts. Effect of non-plastic fines content was studied by many researchers by controlled and systematic addition of fines to the clean standard host sands (Shen 1977; Kuerbis et al. 1988; Pitman et al. 1994; Vaid 1994; Lade and Yammuro 1997; Yamamuro and Lade 1997; Yamamuro and Lade 1998; Salgado et al. 2000; Papadopoulou and Tika 2008; Sitharam and Dash 2008). Effect of plastic fines was studied by few researchers indicating a significant decrease in undrained strength of sand with an increase in plastic fines (Georgiannou et al. 1990; Georgiannou et al. 1991 and Abedi and Yasrobi 2010). The coupled effect of plastic and non-plastic fines is yet to be explored. While gradation of standard river sands is more or less uniform between particular grain sizes, the gradation of natural sandy soils, silty-sand, and clayey-sand changes with depth as well as horizontal distance. To understand the compressibility behavior and pore pressure response of such deposits, extensive research needs to be carried out under various boundary and loading conditions. In the current experimental study, m_v and Δu of naturally occurring soil samples from 10 locations at different depths from Kutch region are presented. Sitharam et al. (2004) and Ravishankar et al. (2005) studied the dynamic behavior of soil collected from the epicenter of 2001 Bhuj Earthquake. Variations in grain size distribution (GSD), fines content (FC), and nature of fine content

(plastic and non-plastic) were observed. The dependency of volume compressibility and excess pore pressure response of soils was analyzed in the context of variations in plastic fines (clay) and non-plastic fines (non-plastic silt).

2 Material Properties and Specimen Preparation

Soil samples from 3000 km^2 area of Kutch region were collected. Basic geotechnical properties, viz. GSD, Specific Gravity (G_s), and Atterberg Limits, are given in Table 1 (Hussain and Sachan 2017). A series of isotopically consolidated undrained triaxial compression (CIUC) tests were performed (ASTM D4767-04 2004). Figure 1 shows the GSD of the soils used in the current study (Hussain and Sachan 2017). Triaxial tests were performed on cylindrical specimens of 50-mm-diameter and 100 mm height. Specimens were prepared at in situ dry density using moist tamping method at 8% water content. Saturation of the specimens was accomplished by back pressure saturation. It involved flushing the specimens with CO_2 for 45 min followed by water flushing. Water equivalent to 2–3 times the volume of the specimen was pushed through the specimen at low pressure. Following water flushing, backpressure was applied in two saturation ramps to acquire B value larger than 0.95.

3 Results and Discussion

CIUC triaxial tests were analysed in the context of volume compressibility (m_v) and pore pressure response (Δu, A, and I_{B2}) for 32 soils collected from 10 locations of seismically active Kutch region.

3.1 Volume Compressibility of Kutch Soils

Specimens were subjected to isotropic consolidation under the effective confining pressure of 100 kPa, after saturation. Volumetric strains experienced by soil specimens at the end of consolidation varied over a wide range, 1.02–7.84%. The corresponding volume compressibility, m_v, evaluated was found in between 10^{-4} and 7.8×10^{-4} m^2/kN. The volume compressibility of soils is controlled by factors, viz. density and fines content. Further silt (non-plastic) and clay (plastic) fractions have a different effect on the compressibility of soils. In the current study, both variables control the volumetric strains during consolidation. Figure 2 shows volume compressibility of the soils of Kutch Region as a function of FC, silt (non-plastic) content, and clay (plastic) content. Effect of FC, plastic fines, and non-plastic fines on volumetric compressibility of silty-sands and clayey-sands are shown in Fig. 2a. The response of all 32 soils is shown in Fig. 2b. In silty sands, compressibility

Table 1 Geotechnical properties of soils in Kutch region

Soil Name	Depth m	γ_{di} kN/m^3	G_S	GSD				FC %	Atterberg Limits			Soil Class
				G	S	M	C		LL	PL	PI	
				%	%	%	%		%	%	%	
Chang Dam		23°27.591' N		70°24.408' E								
S1 (L1)	0.5	15	2.67	6	78	11	5	16	-	-	-	SM
S2 (L2)	0.5	15.69	2.66	0	82	15	3	18	15.5	NP	NP	SM
S3 (L2)	1.5	15.70	2.68	5	76	17	2	19	20.0	NP	NP	SM
Kharoi		23°28.367' N		70°23.330' E								
S4	0.5	16.01	2.67	0	82	13	5	18	15.7	NP	NP	SM
S5	1.5	16.90	2.67	5	84	9	2	11	13.8	NP	NP	SP-SM
S6	2.5	16.00	2.67	1	86	11	2	13	12.7	NP	NP	SM
Suvai Dam		23°36.428' N		70°29.821' E								
S7	0.5	17.03	2.67	0	72	21	7	28	15.1	NP	NP	SM
S8	1	14.37	2.66	2	74	19	5	24	14.6	NP	NP	SM
S9	1.5	13.55	2.66	1	82	14	3	17	14.8	NP	NP	SM
Fatehgarh Dam		23°41.369' N		70°48.057' E								
S10	0.5	17.17	2.72	0	1	62	37	99	54.0	19.0	35	CH
S11	1.5	15.53	2.67	1	54	42	3	45	19.9	NP	NP	SM
S12	2.5	15.45	2.69	0	78	21	1	22	16.3	NP	NP	SM
Chobari		23°30.722' N		70°20.881' E								
S13	0.5	17.51	2.7	0	56	42	2	44	24.2	14.2	10.0	SC
S14	1.5	16.96	2.71	0	51	42	7	49	26.2	14.8	11.4	SC
S15	2.5	17.57	2.7	0	59	37	4	41	24.6	16.2	8.4	SC
Khadir		23°50.82' N		70°14.39' E								
S16	0.5	15.94	2.66	2	79	17	2	19	16.9	NP	NP	SM
S17	1.5	16.82	2.66	1	74	22	3	25	15.6	NP	NP	SM
S18	2.5	16.96	2.66	2	88	9	1	10	13.7	NP	NP	SP-SM
Tappar Dam		23°15.017' N		70°07.586' E								
S19	0.5	17.36	2.67	0	58	24	18	42	34.1	11.2	22.9	SC
S20	1.5	16.39	2.66	5	66	14	15	29	31.4	10.1	21.3	SC
S21	2.5	17.67	2.68	4	72	14	10	24	22.2	10.5	11.7	SC
Budharmora		23°20.634' N		70°11.501' E								
S22	0.5	17.71	2.68	2	69	21	8	29	23.2	14.6	8.6	SC
S23	1.5	14.27	2.71	1	34	46	19	65	44.3	15.7	28.6	CL
S24	2.5	12.26	2.7	2	18	57	23	80	65.8	26.9	38.9	CH
Banniari		23°24.299' N		70°09.910' E								
S25	0.5	13.37	2.74	0	17	81	2	83	26.4	NP	NP	ML
S26	1.5	14.59	2.75	0	5	68	27	95	47.2	18.6	28.6	CL
S27	2	16.26	2.68	0	68	26	6	32	24.6	11.6	13.0	SC
S28	2.5	17.60	2.69	1	78	13	8	21	28.0	11.7	16.3	SC
Shivlakha Dam		23°24.659' N		70°35.128' E								
S29	0.5	14.43	2.69	0	71	25	4	29	16.8	NP	NP	SM

(continued)

Table 1 (continued)

Soil Name	Depth m	γ_{di} kN/m^3	G_S	GSD				FC %	Atterberg Limits			Soil Class
				G	S	M	C		LL	PL	PI	
				%	%	%	%		%	%	%	
S30	1.5	14.88	2.7	1	88	9	2	11	17.4	NP	NP	SP-SM
S31	2	16.37	2.69	1	74	18	7	25	15.0	NP	NP	SM
S32	2.5	13.40	2.68	0	28	50	22	72	39.0	15.5	23.5	CL

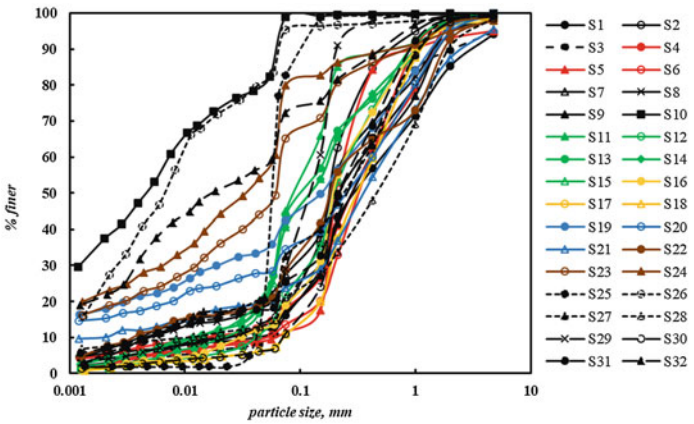

Fig. 1 Grain size distribution of Kutch soils

increased at a higher rate with increase in plastic fines as compared to the similar increase in non-plastic fines. Thevanayagam (2000) and Bandini and Sathiskumar (2009) reported that the effect of silt content on m_v was insignificant, which was aligned with the current study. However, such dependency was not found in other soils. The microstructure of a soil varies with FC and affects the mechanical behavior of the soil. FC of soils in the current study varied from 11 to 99%. FC in the silty sands varied from 11 to 49% with non-plastic fines varying from 9 to 42%. Smaller silt particles create a large number of unstable particle contacts, which exhibit higher compressibility (Yamamuro et al. 2008). As the soils in the current study are having GSD distributed over a wide range, particles with different microstructure tend to collapse and rearrange themselves in different configurations affecting the soil compressibility significantly (Zhao et al. 2013; Zhao and Zhang 2013). Evaluated values of m_v for the soils in the current study implied large settlements and highly contractive response under undrained loading conditions.

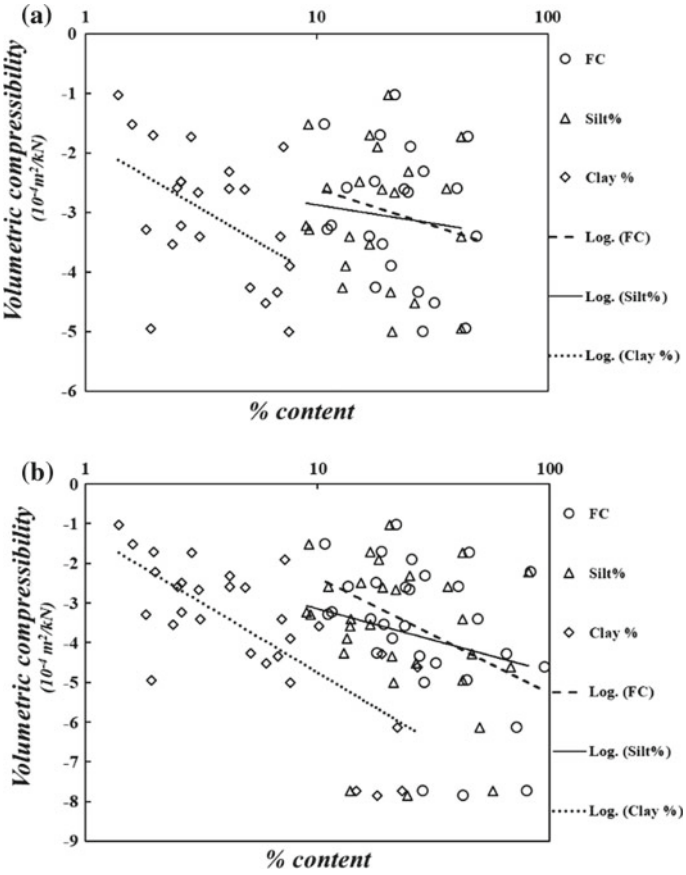

Fig. 2 Variation of volume compressibility, m_v, with FC and nature of fines for Kutch region **a** Silty-sands and clayey-sands, **b** All soils

3.2 *Pore Pressure Response of Kutch Soils with Varying Plastic and Non-plastic Fines*

After the isotropic consolidation was over, specimens underwent undrained shearing. Excess pore pressure evolution (Δu) varied over a wide range with strong dependency on FC and nature of fines present in the particular soil. Soils in the current study exhibited positive pore pressure evolution during undrained shearing varying from 63 to 98 kPa. Excess pore pressure (Δu) evolved at a faster rate during initial stages of loading, $\varepsilon_a < 0.5\%$. Excess pore pressure evolution (Δu) was observed to be greater than 95 kPa for silty sands indicating static liquefaction. It was observed that 50% of final Δu developed at peak stress (Table 2). Higher Δu meant reduced mean effective pressure leading to low load-bearing capacity of soils. Figure 3a, b, c shows the evolution of Δu during undrained shearing of soils collected from Chang Dam,

Table 2 Volume compressibility and pore pressure response of Kutch soils

Soil Name	NF* %	PF† %	FC %	ε_v%	Peak Parameters		Residual Parameters			
					ε_f %	u_f	ε_r	u_r	A_f	I_{B2}
Chang Dam										
S1 (L1)	11	5	16	-	-	-	-	-	-	-
S2 (L2)	15	3	18	2.5	0.45	46	25	96	1.1	0.52
S3 (L2)	17	2	19	3.5	0.42	48	25	96	1.3	0.50
Kharoi										
S4	13	5	18	4.3	0.6	57	25	92	1.6	0.38
S5	9	3	12	3.2	0.5	53	25	96	1.3	0.45
S6	11	2	14	2.6	0.48	52	25	98	1.2	0.47
Suvai Dam										
S7	21	7	28	4.3	0.54	51	23	95	1.4	0.46
S8	19	5	24	2.6	0.48	49	22	89	1.3	0.46
S9	14	3	17	3.4	0.42	45	25	97	1.2	0.53
Fatehgarh Dam										
S10	62	37	99	-	-	-	-	-	-	-
S11	42	3	45	1.7	0.55	51	25	95	1.1	0.46
S12	21	1	22	1.0	0.56	46	19	95	0.7	0.50
Chobari										
S13	42	2	44	5	0.76	53	25	85	1.1	0.37
S14	42	7	49	3.4	0.5	34	25	75	0.7	0.55
S15	37	4	41	2.6	0.5	28	25	76	0.7	0.63
Khadir										
S16	17	2	19	1.7	0.46	50	25	96	1.5	0.48
S17	22	3	25	2.7	0.54	53	25	93	1.4	0.43
S18	9	2	11	1.5	0.38	44	25	90	1.0	0.54
Tappar Dam										
S19	24	18	42	7.8	0.5	35	25	73	0.7	0.52
S20	14	15	28	7.7	0.5	41	25	72	0.7	0.43
S21	14	10	24	3.6	0.5	41	25	80	0.8	0.49
Budhar mora										
S22	21	8	29	5.0	0.5	44	25	90	0.7	0.37
S23	46	19	65	4.3	0.5	20	25	76	0.7	0.74
S24	57	23	80	7.7	0.5	15	25	66	0.5	0.77
Banniari										
S25	81	2	83	2.2	0.56	46	25	97	0.9	0.53
S26	68	27	95	4.6	0.5	21	25	70	0.6	0.7
S27	26	6	32	4.5	0.76	52	25	85	1.2	0.38
S28	13	8	21	3.9	0.7	46	25	85	1.4	0.46
Shivlakha Dam										
S29	25	4	29	2.3	0.47	44	25	96	1.1	0.54
S30	9	2	11	3.3	0.45	48	25	98	0.9	0.51
S31	18	7	25	1.9	0.5	37	25	96	0.7	0.61
S32	50	22	72	6.1	0.5	30	25	75	0.8	0.60

**Non-plastic fines (silt)* *†Plastic fines (clay)*

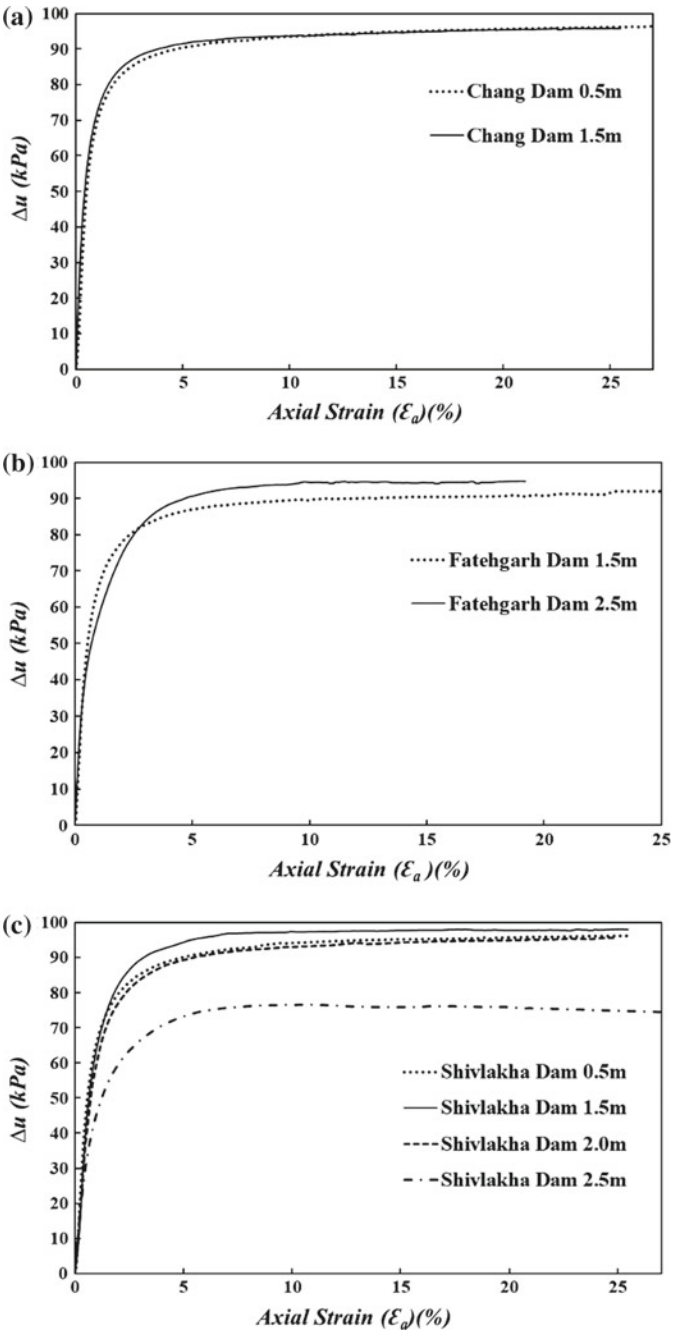

Fig. 3 Pore pressure response of soils from **a** Chang Dam, **b** Fatehgarh Damand, **c** Shivlakha Dam

Fatehgarh Dam, and Shivlakha Dam, respectively. Δu generated was observed to be very close to initial effective confining pressure (100 kPa) leading to the static liquefaction within the soil mass. A large fraction (greater than 0.5) of the ultimate excess pore pressure was observed at strain (ε_f) corresponding to peak stress. FC and nature of fines was observed to impact the excess pore pressure evolution in the natural soil deposits of high seismicity Kutch region.

Figure 4a, b shows the evolution of Δu during undrained shearing for soils collected from Tappar Dam and Chobari, respectively. With higher FC but lower plastic fines, the evolution of Δu of Chobari soils was observed to be similar to that of Tappar Dam soils, which have low FC but significant plastic fines. Lade and Yamamuro (1997), Hazirbaba (2005), Hazirbaba and Rathje (2009), and

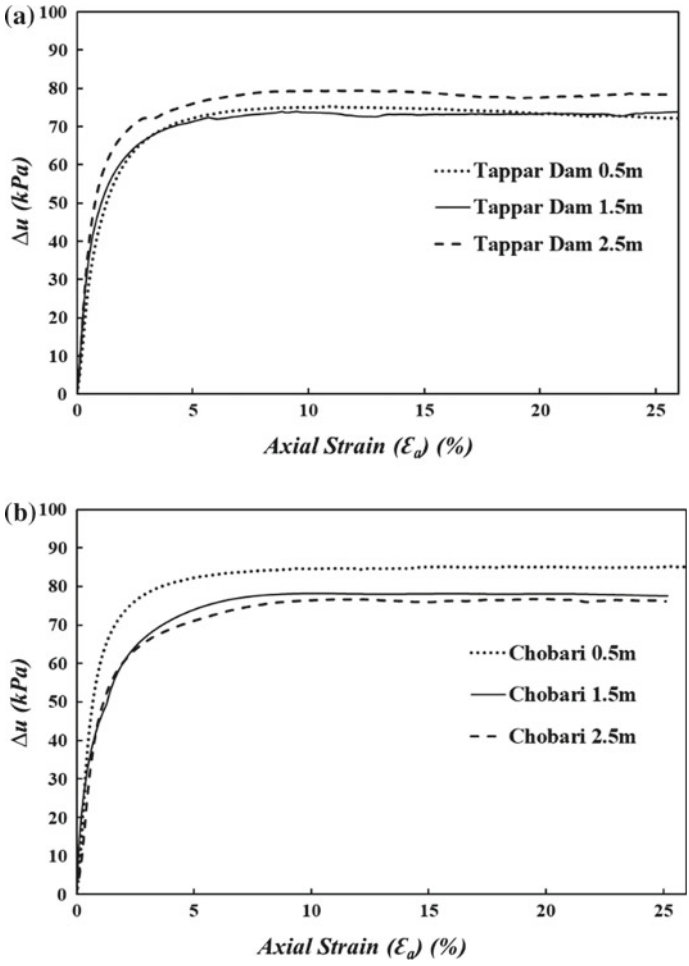

Fig. 4 Pore pressure response of soils from **a** Tappar Dam and **b** Chobari

Thevanayagam et al. (2002) reported similar findings for comparable non-plastic fines content. In the current study at similar non-plastic fines content, Δu is decreased due to the coupled effect of plastic and non-plastic fines. Findings in the current study agree with the study on plastic fines reported by Carraro et al. (2009).

Similar to Δu, Skempton's pore pressure parameter *(A)* at different strain levels was observed to be affected by FC and nature of fines. Figure 5a, b, c shows the evolution of parameter (*A*) for soils from Chang Dam, Fatehgarh Dam, and Shivlakha Dam respectively. Parameter *A* was found to evolve with axial strain. After gradual increase at lower axial strains, parameter A increased sharply due to continuously increasing Δu and reducing deviatoric stress, ε_d. For Fatehgarh Dam (at 2.5 m depth), *parameter A* attained values as high as 94 due to static liquefaction resulting from loss of effective confining stress due to high Δu.

Soils having significant fines and showing significant residual strength, parameter *A* stabilized at a constant value as shown in Fig. 6b. Parameter *A* for soils collected from Chobari was significantly higher as compared to soils from Tappar Dam. This was due to the higher fraction of plastic fines in soils from Tappar Dam. However, total fines content was higher in soils from Chobari.

Similar to undrained brittleness index (I_B) proposed by Bishop (1971), a parameter undrained brittleness index with respect to pore pressure (I_{B2}) was defined to quantify the Δu generation as shown in Eq. 1.

$$I_{B2} = \frac{u_{\text{ultimate}} - u_{\text{yield}}}{u_{\text{ultimate}}} \tag{1}$$

where u_{ultimate} was the Δu at large strains and u_{yield} was Δu at initial peak stress. I_{B2} captured the evolution of Δu before and after yield. I_{B2} of the soils varied from 0.37 to 0.77 in the current study, as shown in Table 2. Figure 7 shows the variation of I_{B2} with FC, non-plastic fines and plastic fines for the silty sands in Kutch region. I_{B2} values for silty-sand soils (non-plastic fines) were observed to be on the lower side. However, higher values were obtained for soils containing significant plastic fines.

Lower I_{B2} corresponds to the higher fraction of ultimate Δu evolving at peak stress indicating softening behavior of soil. This was due to the higher development of Δu at early stages of shearing resulting in reduced mean effective pressure and softening behavior.

In the current study, majority of the soil samples (28 out of 32) had total fines content (FC) greater than 15%, which exhibited large volume compressibility and low shear strength. Typical design CBR values for such type of soil are in the range of 10–20% (Authority 2002). However, the total FC was found to be mainly composed of non-plastic fines. These soils could be used in the design and construction of subgrade and embankments systems by addressing the issues relating to large volume compressibility and pore water pressure. This might require compaction with lower lift thickness. Erodibility and siltation of silty sands can be prevented by using geo-textiles.

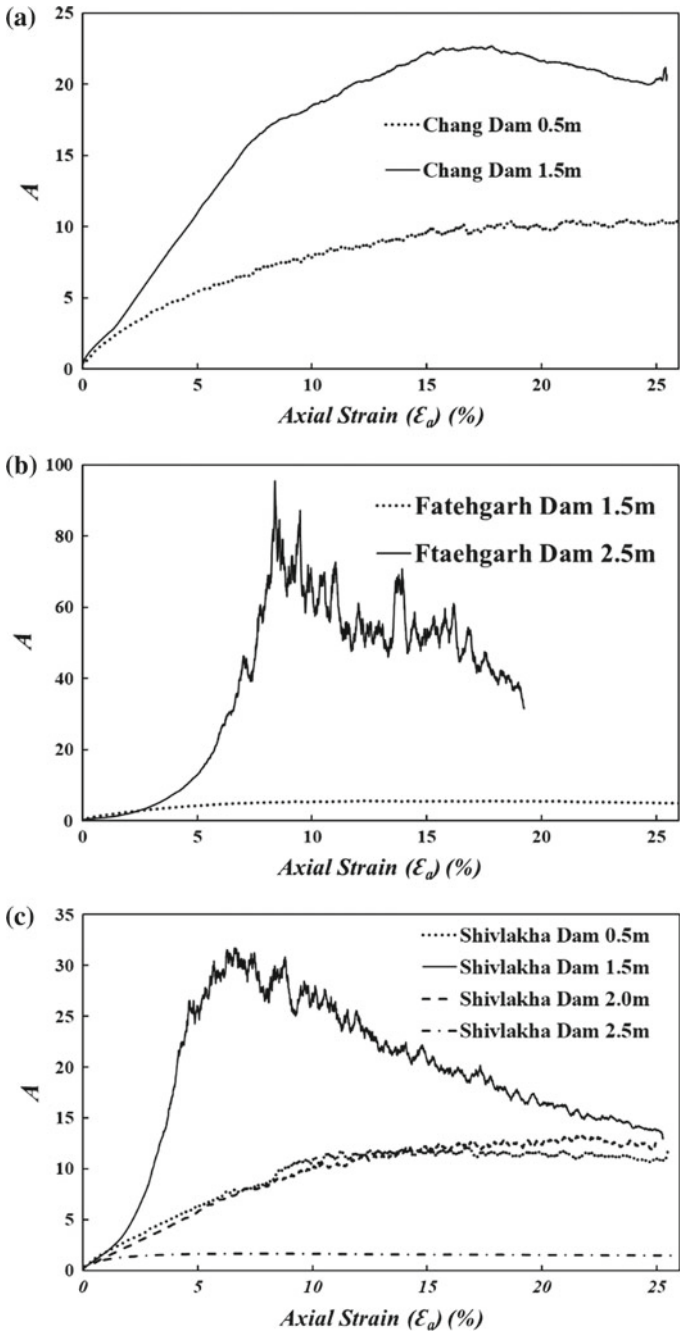

Fig. 5 Evolution of skempton's pore pressure parameter, *A*, for soils from **a** Chang Dam, **b** Fatehgarh Dam and **c** Shivlakha Dam

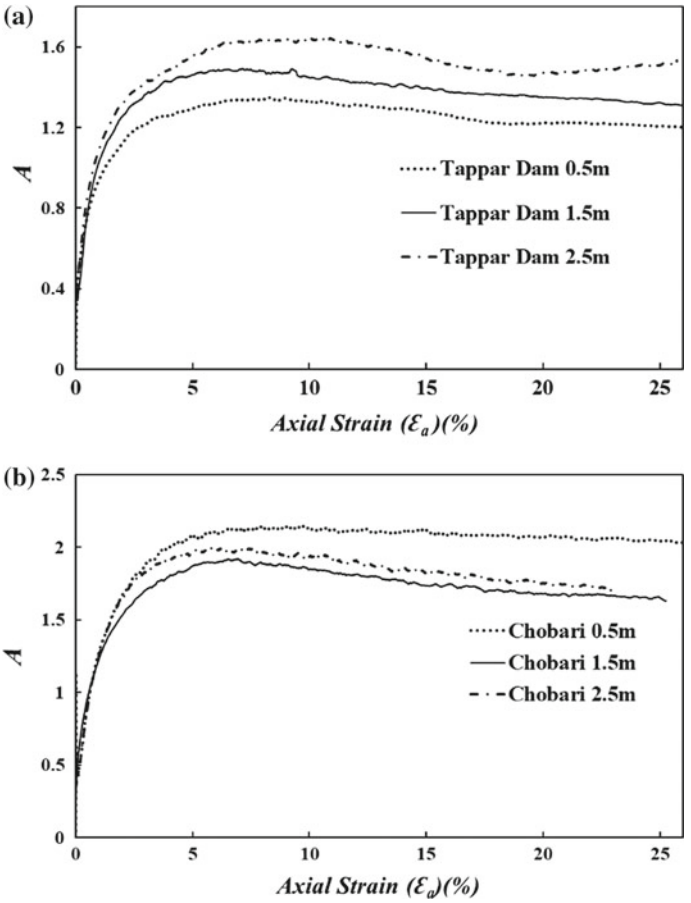

Fig. 6 Evolution of Skempton's pore pressure parameter, *A*, soils from **a** Tappar Dam and **b** Chobari

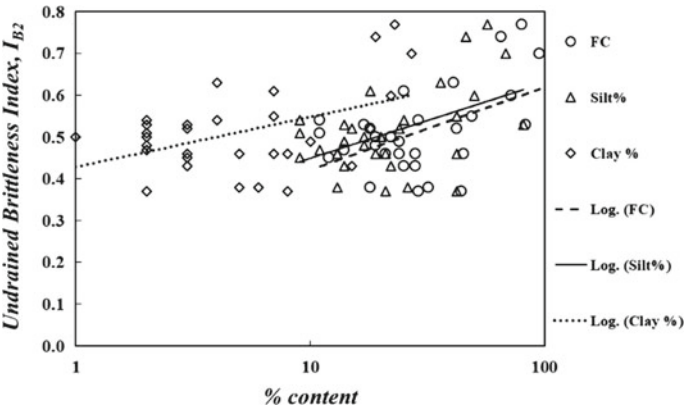

Fig. 7 Variation of I_{B2} with FC and nature of fines for soils in Kutch region

4 Conclusions

Volume and pore pressure response of Kutch soils were explored in the current study. Twenty out of the 32 soil samples classified as SM type soils. The response of silty sands was significantly affected by the FC, which was observed to be controlled by the relative proportion of plastic and non-plastic fines. Volume compressibility and pore pressure response of Kutch soil with varying plastic and non-plastic fines were studied. Key observations are mentioned below.

1. The volume compressibility, m_v, of soils increased with increase in FC. For similar FC, soils with a larger fraction of plastic fines exhibited higher m_v. Large m_v indicated larger consolidation settlement during loading.
2. Pore pressure response was affected by FC and nature of fines. Δu reached 98 kPa in soils with low FC. Soils with higher FC, Δu generation was observed to be controlled by the relative proportion of plastic and non-plastic fines. Plastic fines inhibited pore pressure generation to a higher degree compared to non-plastic fines. The similar response was observed for parameter A.
3. Variation in plastic and non-plastic fines exhibited a subdued effect on undrained brittleness, I_{B2}, with respect to pore pressure. Soils with higher plastic fines content exhibited increased I_{B2} indicating the resistance to pore pressure generation.
4. Large volume compressibility and pore pressure generation of Kutch soils need to be considered in the design of subgrades and embankments to protect them from settlement and shear failure.

References

Abedi M, Yasrobi SS (2010) Effects of plastic fines on the instability of sand. Soil Dyn Earthq Eng 30(3):61–67

ASTM D4767-04 (2004) Standard test method for consolidated undrained triaxial compression test for cohesive soils. ASTM Int., West Conshohocken, Pa

Authority ER (2002) Pavement design manual volume I: flexible pavements and gravel roads

Bishop AW (1971) Shear strength parameters for undisturbed and remoulded soil specimens. In: Stress-strain behaviour of soils (Proceedings of the roscoe memorial symposium), p 47

Bandini P, Sathiskumar S (2009) Effects of silt content and void ratio on the saturated hydraulic conductivity and compressibility of sand-silt mixtures. J Geotech Geoenviron Eng 135 (12):1976–1980

Castro G (1969) Liquefaction of sands. Ph. D. Thesis, Harvard soil mech

Carraro JAH, Prezzi M, Salgado R (2009) Shear strength and stiffness of sands containing plastic or nonplastic fines. J Geotech Geoenviron Eng 135(9):1167–1178

Georgiannou VN, Burland JB, Hight DW (1990) The undrained behaviour of clayey sands in triaxial compression and extension. Geotechnique 40(3):431–449

Georgiannou VN, Hight DW, Burland JB (1991) Undrained behaviour of natural and model clayey sands. Soils Found 31(3):17–29

Hussain M, Sachan A (2017) Evaluation of earthquake liquefaction hazard of Kutch region. J Geotech Transp Eng 3(2):52–61

Hazirbaba K (2005) Pore pressure generation characteristics of sands and silty sands: a strain approach. Ph.D. Thesis

Hazirbaba K, Rathje EM (2009) Pore pressure generation of silty sands due to induced cyclic shear strains. J Geotech Geoenviron Eng 135(12):1892–1905

Ishihara K (1993) Liquefaction and flow failure during earthquakes. Geotechnique 43(3):351–451

Kuerbis R, Negussey D, Vaid YP (1988) Effect of gradation and fines content on the undrained response of sand. In: Hydraulic fill structures, ASCE, pp 330–345

Lee KL, Farhoomand I (1967) Compressibility and crushing of granular soil in anisotropic triaxial compression. Can Geotech J 4(1):68–86

Lade PV, Yamamuro JA (1997) Effects of nonplastic fines on static liquefaction of sands. Can Geotech J 34(6):918–928

Lade PV, Yamamuro JA, Liggio CD Jr (2009) Effects of fines content on void ratio, compressibility, and static liquefaction of silty sand. Geomech Eng 1(1):1–15

Monkul MM, Yamamuro JA (2011) Influence of silt size and content on liquefaction behavior of sands. Canadian Geotech J 48(6):931–942

Pitman TD, Robertson PK, Sego DC (1994) Influence of fines on the collapse of loose sands. Can Geotech J 31(5):728–739

Papadopoulou A, Tika T (2008) The effect of fines on critical state and liquefaction resistance characteristics of non-plastic silty sands. Soils Found 48(5):713–725

Rutledge P (1947) Cooperative triaxial shear research program of the corps of engineers, triaxial shear research distribution studies on soils. Waterways Experiment Station, Vicksburg, Mississippi, pp 1–178

Ravishankar BV, Sitharam TG, Govindaraju L (2005) Dynamic properties of Ahmedabad sands at large strains. Proceedings, Indian geotechnical conference-2005. Ahmedabad, India, pp 369–372

Salgado R, Bandini P, Karim A (2000) Shear strength and stiffness of silty sand. J Geotech Geoenviron Eng 126(5):451–462

Shen CK (1977) The effect of fines on liquefaction of sands. In: Proceedings of the 9th ICSMFE, vol 2. pp 381–385

Sladen JA, D'hollander RD, Krahn J (1985) The liquefaction of sands, a collapse surface approach. Canadian Geotech J 22(4):564–578

Sitharam TG, Govindaraju L, Murthy BS (2004) Evaluation of liquefaction potential and dynamic properties of silty sand using cyclic triaxial testing. Geotech Testing J 27 (5):423–429

Sitharam TG, Dash HK (2008) Effect of non-plastic fines on cyclic behaviour of sandy soils. In: GeoCongress 2008: geosustainability and geohazard mitigation, pp 319–326

Terzaghi K (1956) Varieties of submarine slope failures. In: Proceedings of the 8th Texas Conference on Soil mechanics and Foundation Engineering, Austin

Thevanayagam S (1998) Effect of fines and confining stress on undrained shear strength of silty sands. J Geotech Geoenviron Eng 124(6):479–491

Thevanayagam S (2000) Liquefaction of silty soils—Considerations for screening and retrofit strategies. In: Proceedings 2nd international workshop on mitigation of seismic effects on transportation structures. National Center for Research on Earthquake Engineering, Taipei, Taiwan, pp 314

Thevanayagam S, Shenthan T, Mohan S, Liang J (2002) Undrained fragility of clean sands, silty sands, and sandy silts. J Geotech Geoenviron Eng 128(10):849–859

Vaid YP (1994) Liquefaction of silty soils. ASCE, In Ground failures under seismic conditions, pp 1–16

Yamamuro JA, Lade PV (1997) Static liquefaction of very loose sands. Can Geotech J 34(6):905–917

Yamamuro JA, Lade PV (1998) Steady-state concepts and static liquefaction of silty sands. J Geotech Geoenviron Eng 124(9):868–877

Yamamuro JA, Wood FM, Lade PV (2008) Effect of depositional method on the microstructure of silty sand. Can Geotech J 45(11):1538–1555

Zhao HF, Zhang LM (2013) Effect of coarse content on shear behavior of unsaturated coarse granular soils. Canadian Geotech J 51(12):1371–1383

Zhao HF, Zhang LM, Fredlund DG (2013) Bimodal shear-strength behavior of unsaturated coarse-grained soils. J Geotech Geoenviron Eng 139(12):2070–2081

Part V
Emerging Trends in Transportation Geotechnics of Unsaturated Soils, Macro and Nano Technology, Climate Change and Sustainability

Influence that Osmotic Suction and Tree Roots has on the Stability of Coastal Soils

Pubudu Jayathilaka, Buddhima Indraratna and Ana Heitor

Abstract The contribution made by osmotic suction to unsaturated shear strength analysis has not been considered for the past few decades. Osmotic suction is generated by the salt in pore water, especially in coastal environments, and it can be more significant than matric suction. Tree roots can also induce osmotic and matric suction by continuous transpiration, and when these saline and rooted environments are combined under unsaturated conditions, they can challenge conventional shear strength models. Electrical resistivity can be used as a proper tool to evaluate the properties of soil in a large scale. This review summarizes the historical development of studies related to osmotic suction as well as the present situation of osmotic suction for soil shear strength.

Keywords Osmotic suction · Matric suction · Transpiration · Shear strength · Resistivity

1 Introduction

Over the past few decades, the increase in population in most metropolitan areas has been driving research into new ways of optimizing the development of infrastructure on unsuitable soils. This means that a more sustainable technique for stabilizing soil will be a key parameter. Stabilizing soft soil has proven to be more effective using geo-synthetic liners, pre-fabricated vertical drains, and chemical additives such as lignosulfonate, and while most of them are reasonably effective

P. Jayathilaka (✉) · B. Indraratna · A. Heitor
Center for Geomechanics & Railway Engineering, University of Wollongong, Wollongong, NSW 2522, Australia
e-mail: brpmj808@uowmail.edu.au

B. Indraratna
e-mail: indra@uow.edu.au

A. Heitor
e-mail: aheitor@uow.edu.au

R. Sundaram et al. (eds.), *Geotechnics for Transportation Infrastructure*, Lecture Notes in Civil Engineering 29,
https://doi.org/10.1007/978-981-13-6713-7_53

under saturated conditions, they are not economically feasible. Australia depends heavily on rail tracks, having a large and complex rail network of metropolitan, intrastate, interstate, and haulage totaling about 44,000 km for the railway industry (Fatahi 2007). Due to continuous and cyclic loads from heavy trains, the underlying soil column undergoes uneven settlement, and even more so in a wet environment. Fatahi (2007) reports that the average maintenance cost of the Sydney's rail network exceeded two billion dollars for the last decade, which translates to about 0.55 million dollars per day.

However, since most infrastructures are built and will remain above the groundwater table for most of their service life, the soil remains in an unsaturated condition where the capillary stresses or suction play an important role. The contribution made by soil suction under unsaturated conditions is well documented, and the theoretical framework has been standardized to capture the actual behavior of unsaturated soil (Fatahi 2007; Fredlund 2000;Vanapalli et al. (1996b). While previous studies report that suction governs the shear strength of soil, it is typically associated with the magnitude of matric suction and osmotic suction. Matric suction is the difference between the pore water pressure and pore air pressure, both of which are generally affected by physical factors such as capillarity stresses, relative compaction, particle size, the degree of saturation or water content, and the texture and adsorptive forces of the soil (Fatahi et al. 2015; Fredlund and Rahardjo 1993; Abedi-Koupai and Mehdizadeh 2007). While the influence of matric suction is relatively well established, very few studies focus on osmotic suction. Osmotic suction is the negative pressure between two solutions with identical compositions that are separated by a semi-permeable membrane, such that only one solution can pass through the membrane to be in equilibrium (Krahn and Fredlund 1972). Osmotic suction derives from the salt in pore water (Abhijit et al. 2012; Arifin and Schanz 2009; Sreedeep and Singh 2006; Sreedeep and Singh 2011), and it has a large effect on the shear strength of coastal soils (Barbour and Fredlund 1989; Chien et al. 2009; Kumar et al. 2015; Rao and Thyagaraj 2007).

Engineering applications such as green corridors for railways are quite well established (Indraratna et al. 2006) and here the osmotic component is induced by native vegetation. Most previous studies only report the osmotic influence based on saturated conditions where soil is assumed to be at least at its field capacity, but when tree root reinforcement and the salinity from nutrient uptake are considered, within an unsaturated condition, the behavior of soil becomes much more complex. Moreover, where the physical conditions in which osmotic suction are specific, studies that combine the effect of osmosis, tree root suction, and reinforcement, on the unsaturated shear strength equation are limited. It is therefore important to study this combined effect because there is an increasing interest in using native vegetation for engineering applications.

2 Evolution of the Unsaturated Shear Strength Equation

Terzaghi (1936) introduced the effective stress principle for saturated soil, when the pore space is only filled with water and the water is assumed to be incompressible.

$$\sigma' = \sigma - u_w \tag{1}$$

Bishop (1960) later defined an equation for unsaturated conditions where the air and water phases are considered:

$$\sigma' = \sigma + \chi(u_a - u_w) \tag{2}$$

After Terzaghi's shear strength equation, many other extensions to unsaturated conditions have been proposed over the past few decades, the noteworthy contributions are summarized in Table 1.

Almost all the shear strength equations proposed after Bishop (1960) work include the influence of matric suction, but none of them included osmotic suction when evaluating the shear strength of unsaturated soil. Barbour and Fredlund (1989) proved that when a soil sample is placed into a concentrated salt solution, it causes the osmotic flow, decreases the pore water pressure, changes the volume, and increases its effective strength, whereas Abedi-Koupai et al. (2017) report that an increase in the salinity of pore water reduces cohesion and increases the internal friction angle. Therefore, it is vital to examine in these chemical changes in soil induced by tree roots so that its contribution to the unsaturated shear strength of soil can be quantified.

Table 1 Shear strength equations for unsaturated soils

Author/s	Equation
Bishop (1960)	$\tau' = c' + [(\sigma - u_a) + \chi(u_a - u_w)] \tan \phi'$
Fredlund et al. (1978)	$\tau' = c' + (\sigma - u_a) \tan \phi' + (u_a - u_w) \tan \phi^b$
Lamborn (1986)	$\tau' = c' + (\sigma - u_a) \tan \phi' + (u_a - u_w)\theta_w \tan \phi'$
Lu (1992)	$\tau' = c' + (\sigma - u_a) \tan \phi' + P_s \tan \phi'$
Vanapalli et al. (1996a)	$\tau' = c' + (\sigma - u_a) \tan \phi' + (u_a - u_w)\left(\frac{\theta_w - \theta_r}{\theta_s - \theta_r}\right) \tan \phi'$
Khabbaz and Khalili (1998)	$\tau' = c' + (\sigma - u_a) \tan \phi' + (u_a - u_w)\left[\frac{(u_a - u_w)}{(u_a - u_w)_b}\right]^{\eta} \tan \phi'$
Xu and Sun (2002)	$\tau' = c' + (\sigma - u_a) \tan \phi' + m^{(1-\zeta)}(u_a - u_w)^{\zeta} \tan \phi'$
Lee et al. (2005)	$\tau' = c' + (\sigma - u_a) \tan \phi' + (u_a - u_w)_b \tan \phi' + [(u_a - u_w) - (u_a - u_w)_b)]\Theta^K[1 + \lambda(\sigma - u_a)] \tan \phi'$
Hamid and Miller (2009)	$\tau_f^{'} = c_a^{'} + (\sigma_{nf} - u_{af}) \tan \delta' + (u_{af} - u_{wf}) \tan \delta^b$
	$\tau_f^{'} = c_a^{'} + (\sigma_{nf} - u_{af}) \tan \delta' + (u_{af} - u_{wf})\left(\frac{\theta - \theta_r}{\theta_s - \theta_r}\right) \tan \delta'$
Alonso et al. (2010)	$\tau' = c' + (\sigma - p_g) \tan \phi' + S_r^e s \tan \phi'$
Konrad and Lebeau (2015)	$\tau' = c' + (\sigma - u_a + S_{r,c} s) \tan \phi'$
Zhou et al. (2016)	$\tau' = c' + \left[(\sigma - u_a) + (u_a - u_w)\frac{A_w^{cap}}{A}\right] \tan \phi'$
Wang et al. (2017)	$\tau' = (\sigma - u_a) \tan \phi' + \left[1 + \left(\frac{d_{\omega}(u_a - u_w)}{C_{2\gamma}}\right)^{\frac{C_1}{\log_{10}(C_u)} + 1}\right]^{\frac{-C_1}{C_1 + \log_{10}(C_u)}} * (u_a - u_w)\theta \tan \phi'$

3 Contribution of Osmotic Suction to the Shear Strength

Rao and Thyagaraj (2007) report that osmotic suction in pore water acts like an additional stress component that increases soil stability by reducing the swell potential. Fritz and Marine (1983) report that soils with high cation exchange capacity and low porosities will have a higher osmotic suction that will help to increase the shear strength of expansive clays. Chien et al. (2009) postulate that soil consolidated and stabilized by injecting saline solutions, and that electro-kinetic concentration and zeta potential increase with increasing concentrations of NaCl; they also state that the shear strength of soil is proportional to the zeta potential. Kumar et al. (2015) moreover show experimentally that the unconfined compressive strength of soil increases as the concentration of NaCl increases while Leong and Abuel-Naga (2017) recently mentioned that osmotic suction has almost no effect on the shear strength of compacted low plasticity soil. Merten (1966) proposes the following Eq. (3) for osmotic suction using van Hoff's equation:

$$\Psi_o = R^* T C_m \tag{3}$$

where Ψ_o is the osmotic pressure, R^* is the universal gas constant, T is the absolute temperature, and C_m is the sum of the molar concentration in solution.

Equation 3 is unrealistic because it assumes the pore water is ideal and does not reflect actual field conditions such as a change in pore volume and particle structure, as well as evaporation or transpiration, but it does prove that osmotic suction depends primarily on the concentration of pore water; therefore, osmotic suction is also a function of the change in concentration of pore water and some other related parameters.

Mehdizadeh and Abedi-Koupai (2007) introduced Eq. 4 for the osmotic suction of silty clay soil that is common for Australian coastal areas.

$$\Psi_o = -0.843w + 0.140EC_e + 3.048\sqrt{w} + 0.012w^2 - 0.005EC_e^2 \tag{4}$$

where w is the moisture content and EC_e is the electrical conductivity of the extracted pore water.

Equation 3 is a combination of suction and moisture components, just like a conventional soil water characteristic curve (SWCC). In Mehdizadeh and Abedi-Koupai (2007) study, the change in concentration of the soil sample is practiced but the effect of tree root upon suction is not considered.

4 Contribution of Tree Roots on Shear Strength

Several studies have been carried out to investigate the effect that native vegetation has on the shear strength of soil (Fan and Chen, 2010; Fatahi et al. 2015; Operstein and Frydman, 2000). While most were carried out on slope stabilization (Nawagamuwa et al. 2014; Ni et al. 2018), other applications such as transport infrastructure have been of limited concern.

The additional strength that tree roots generate has been proposed by Waldron (1977) and Wu et al. (1979) under saturated conditions where they postulate that this additional strength can be added directly into a conventional shear strength equation. Fatahi et al. (2015) developed a new model that considers the water uptake by tree roots and its contribution to the variation of the matric suction.

Docker and Hubble (2001) report that larger roots contribute directly to the reinforcement effect while fine roots increase cohesion at the root-soil interface; this is defined as apparent cohesion. Moreover, tree roots imbibe pore water by root water uptake and transpiration, so the moisture content of soil is actually decreasing as the matric suction is increasing. Fatahi (2007) showed that the matric suction variation is larger at the maximum root density rather than the other areas (Fig. 1).

The distribution of root density depends on the tree species and the physical and chemical properties of soil, and since the most common systems are tap roots and fibrous roots trees (Fig. 2), the degree of reinforcement and cohesion will change in accordance with the density of larger roots and fine roots.

Ng et al. (2013) report that the distribution of tree roots depends on the degree of compaction of soil, which means the contribution made by tree roots for reinforcement and suction will vary.

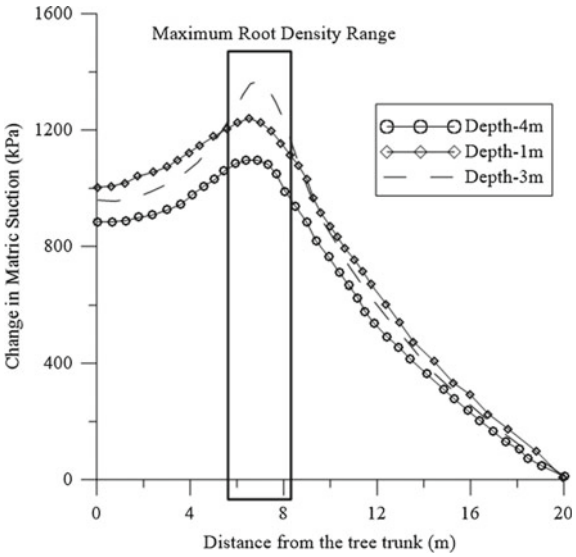

Fig. 1 Change in matric suction (after Pathirage et al. 2017)

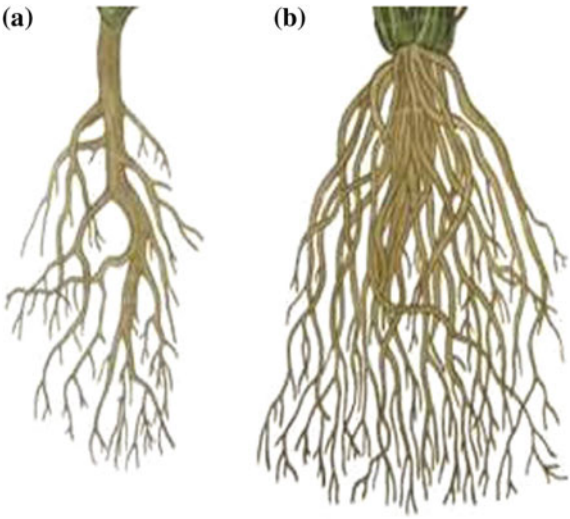

Fig. 2 Common root systems **a** tap rooted and **b** fibrous rooted

5 Combination of Osmotic Suction and Tree Roots on the Shear Strength of Soil

The combined effect of osmotic suction and tree root has not been considered but Pathirage et al. (2017) suggest that osmotic suction influences the tree root suction and the reinforcement of unsaturated soil. Pathirage et al. (2017) also point out that osmotic suction gradually increases close to the tree roots, which means the tree roots generate an additional osmotic effect that reaches its maximum when the root density is at its maximum.

The rate of root water uptake can be modeled using Richard's continuity Eq. (5).

$$\frac{\partial \theta}{\partial t} = \left[\nabla(K\nabla\psi) - \frac{\partial k}{\partial z}\right] - S \tag{5}$$

where S is the sink or sources for water and K is the hydraulic conductivity.

Indraratna et al. (2006) propose an equation for root water uptake or sink term based on root density, potential transpiration, and suction, and then Pathirage et al. (2017) extended the root water uptake function by coupling the osmotic suction (5), with the equation proposed by Indraratna et al. (2006).

$$S = G(\beta(t))F\left(T_p(t)\right)f(\psi(s,\pi)) \tag{6}$$

where $G(\beta(t))$ is the root density factor, $F\left(T_p(t)\right)$ is the potential transpiration factor, and $f(\psi(s,\pi))$ is the soil total suction.

In the root water uptake model (5), an additional matric suction is generated because the moisture content changes such that the osmotic effect from tree roots increases as the concentration gradient between the root and soil interface increases

due to the flow of water. This study therefore proposes a revised total suction equation for unsaturated-rooted-saline environments by Eq. 7.

$$\Psi_T = \Psi_m + \Psi_o + \Psi_{\text{tm}} + \Psi_{\text{to}} \tag{7}$$

where Ψ_m is the matric suction, Ψ_o is the osmotic suction induced by the salinity in pore water, and Ψ_{tm} and Ψ_{to} are the additional matric suction and osmotic suction generated due to root induced transpiration.

The advection dispersion Eq. (8) is used to model the nutrient uptake or solute uptake by tree roots.

$$\frac{\partial(\theta R_e C)}{\partial t} = \nabla\left(\theta D_c \frac{\partial C}{\partial z} - vC\right) - \phi_s \tag{8}$$

where ϕ_s is the sink or sources for solutes, and D_c is the solute dispersion coefficient.

In Eq. 8, the additional osmotic suction induced by root water uptake can be defined so Eq. 4 can be revised to include the total osmotic suction;

$$\psi_o = -0.843w + 0.140EC_e + 3.048\sqrt{w} + 0.012w^2 - 0.005EC_e^2 + \Psi_{to} \tag{9}$$

Figure 3 shows that the change of osmotic suction reaches its maximum when the root density is at its maximum; therefore, tree roots can definitely induce an

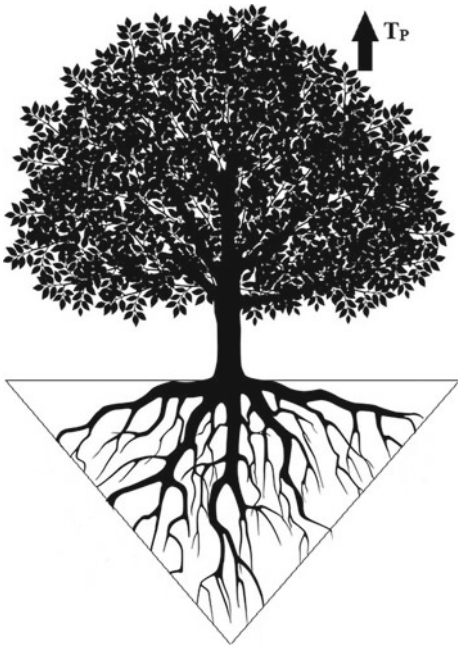

Fig. 3 Root zone

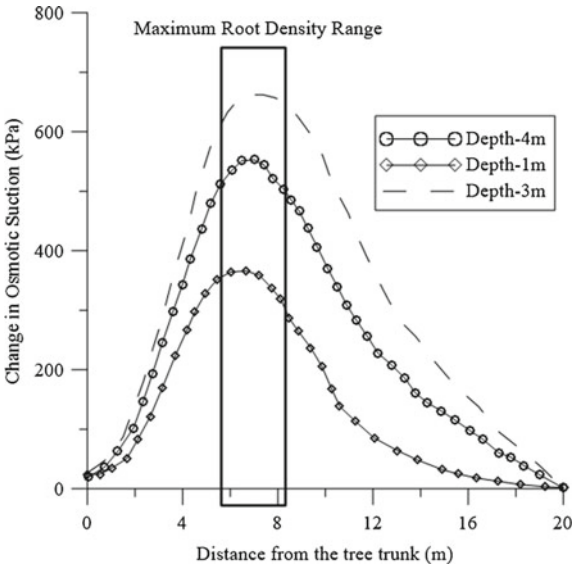

Fig. 4 Change in osmotic suction (after Pathirage et al. 2017)

additional osmotic suction because the continuous transpiration will increase the shear strength of soil (Fig. 4).

6 Revised Shear Strength Equation for Unsaturated-Rooted-Saline Conditions

Fredlund et al. (1978) interpreted an extended Mohr-Coulomb failure criterion for unsaturated soil to include only the matric suction in the model (10).

$$\tau' = c' + \sigma' \tan\ \phi' + (u_a - u_w)\tan\phi^b \tag{10}$$

where u_a is the pore air pressure, u_w is the pore water pressure, σ' is the effective normal stress, c' is the soil cohesion, ϕ^b is the angle with respect to change in matric suction or basic friction angle.

Oloo and Fredlund (1996) report that the characterization of ϕ^b is unrealistic, and therefore, the model proposed by Vanapalli et al. (1996a) is more acceptable (11).

$$\tau' = c' + \sigma' \tan\phi' + (u_a - u_w)\tan\phi' \left(\frac{\theta - \theta_r}{\theta_s - \theta_r}\right) \tag{11}$$

where θ_r is the residual volumetric water content and θ_s is the volumetric water content at saturation.

Waldron and Dakessian (1981) mention that the additional shear strength component ($\Delta\tau_r$) is generated because the root reinforcement can be added directly onto the Mohr-Coulomb equation.

$$\tau' = c' + \sigma' \tan\phi' + (u_a - u_w)\tan\phi'\left(\frac{\theta - \theta_r}{\theta_s - \theta_r}\right) + \Delta\tau_r \tag{12}$$

The osmotic suction generated by impurities in the pore water increase the shear strength ($\Delta\tau_o$), which can then be combined with Eq. 12.

$$\tau' = c' + \sigma' \tan\phi' + (u_a - u_w)\tan\phi'\left(\frac{\theta - \theta_r}{\theta_s - \theta_r}\right) + \Delta\tau_r + \Delta\tau_o \tag{13}$$

An extension for the unsaturated shear strength equation for coupled conditions is yet to be addressed properly so $\Delta\tau_r$ and $\Delta\tau_o$ need further investigation.

7 Theory of Electrical Resistivity on Unsaturated Soil

Herman (2001) concludes that the resistivity of soil will change with the type and properties of material and the resistivity of a good conductor would be approximately $\approx 10^{-8}$ Ωm; therefore, the resistivity of an intermediate conductor such as top soil would be approximately ≈10 Ωm, and of poor conductor, approximately $\approx 10^{8}$ Ωm. As with previous research works, the electrical resistivity of a bulk soil column depends on moisture content or degree of saturation of soil, the degree of compaction, the electrical resistivity of the soil skeleton, the concentration of pore water salt, and the fraction of fines, pore size or porosity and temperature (Abu-Hassanein et al. 1996; Jiao-Jun et al. 2007; Sudduth et al. 2003; Yan et al. 2012). Perez et al. (2009) report that the electrical resistivity is directly proportional to the matric suction, while Hen-Jones et al. (2014) believe that this relationship has an exponential distribution by the experimental data.

Since electrical resistivity is a function of the water content, when a soil is saline the electrical conductivity would vary based on the degree of salinity, so it is better to define electrical resistivity or conductivity as a function of the water content; the matric suction and the amount of impurities such as salt. Furthermore, a fairly realistic model for electrical resistivity of soil can be defined by extending Archie (1942) electrical resistivity model;

$$\rho_{\text{soil}} = f(FF,\ \theta,\ C) \tag{14}$$

where FF is the fine fraction, θ is the volumetric water content, and C is the concentration of pore water.

Electrical resistivity is the reciprocal of electrical conductivity, so Eq. 9 is a specific distribution of Eq. 14 for a particular type of soil. In the field, the soil properties will not remain constant even for a similar soil, so as a bulk range

analysis tool, electrical resistivity is a proper parameter for determining the total suction of soil accurately; it can also be combined with the shear strength analysis.

The electrical resistivity of soil is generally measured with purpose designed electrodes by arranging them in order. Several researchers have introduced configurations (Herman 2001; Jiao-Jun et al. 2007) such as the Wenner configuration, the Schlumberger configuration, and the Dipole–Dipole configuration for bulk scale soil resistivity analysis. Of these configurations, the Wenner configuration is very good for deep analysis, which means the electrical resistivity concepts can be used to determine unsaturated properties such the SWCC of bulk soil.

8 Conclusions

The contribution made by osmotic suction on the shear strength of coastal soil cannot be omitted, and the effect would be even more intense if combined with tree roots.

(a) A realistic equation for osmotic suction has not yet been introduced, so before analyzing its strength, a more representative should be a mandate.
(b) Soil water retention is affected by impurities in the soil, and this would formulate the effect of osmotic suction. Therefore, a new soil water retention curve that includes the influence of salinity could be defined, and where conventional SWCC is invalid.
(c) The salinity of pore water governs the shear strength of unsaturated soil which is why salinity has a greater effect in coastal areas. An observable model is needed for unsaturated shear strength in order to perceive the actual saline conditions of soil, and the contribution of tree roots must be incorporated into the latter model to replicate actual unsaturated-saline-rooted conditions.
(d) Most laboratory experiments were carried out on small samples of disturbed or undisturbed soil, so the results do not replicate actual field conditions; this is why electrical resistivity theories can be useful tools for determining soil suction in complex field environments in order to predict the shear strength of the soil.

Acknowledgements This research has been conducted with the support of the Australian Government Research Training Program Scholarship. The authors would like to acknowledge Dr. Udeni P. Nawagamuwa for the guidance provided for the paper. Also, the authors would like to further acknowledge Dr. Udeshini Pathirage, Dr. Shiran G. Galpathage, and Dr. Muditha Pallewattha for their previous contributions.

References

Abedi-Koupai J, Fatahizadeh M, Mosaddeghi MR (2017) Effect of pore water salinity on mechanical properties of clay soil. JWSS-Isfahan Univ Technol 21(2):119–129

Abedi-Koupai J, Mehdizadeh H (2007) Estimation of osmotic suction from electrical conductivity and water content measurements in unsaturated soils. Geotech Test J 31:142–148

Abhijit D, Malaya C, Srikanth V, Sreedeep S (2012) Comparison of suction measurement technique for class F fly ash. In: Indian geotechnical conference, IIT Delhi, India
Abu-Hassanein ZS, Benson CH, Blotz LR (1996) Electrical resistivity of compacted clays. J Geotech Eng 122(5):397–406
Alonso EE, Pereira J-M, Vaunat J, Olivella S (2010) A microstructurally based effective stress for unsaturated soils. Géotechnique 60:913–925
Archie GE (1942) The electrical resistivity log as an aid in determining some reservoir characteristics. Trans AIME 146(01):54–62
Arifin YF, Schanz T (2009) Osmotic suction of highly plastic clays. Acta Geotech 4(3):177–191
Barbour S, Fredlund D (1989) Mechanisms of osmotic flow and volume change in clay soils. Can Geotech J 26(4):551–562
Bishop AW (1960). The principles of effective stress: Norges Geotekniske Institutt
Chien S-C, Ou C-Y, Wang M-K (2009) Injection of saline solutions to improve the electro-osmotic pressure and consolidation of foundation soil. Appl Clay Sci 44(3):218–224
Docker B, Hubble T (2001) Strength and distribution of casuarinas glauca roots in relation to slope stability. In: Geotechnical engineering (HO KKS and LI KS (eds)). Swets & Zeitlinger, Lisse, pp. 745–749
Fan CC, Chen YW (2010) The effect of root architecture on the shearing resistance of root-permeated soils. Ecol Eng 36(6):813–826
Fatahi B (2007) Modelling of influence of matric suction induced by native vegetation on sub-soil improvement. (Ph.D), University of Wollongong
Fatahi B, Pathirage U, Indraratna B, Pallewattha M, Khabbaz H (2015) The role of native vegetation in stabilizing formation soil for transport corridors: an Australian experience ground improvement case histories, Heinemann, Butterworth, pp 591–628
Fredlund D, Morgenstern NR, Widger R (1978) The shear strength of unsaturated soils. Can Geotech J 15(3):313–321
Fredlund DG (2000) The implementation of unsaturated soil mechanics into geotechnical engineering. Can Geotech J 37(5):963–986
Fredlund DG, Rahardjo H (1993). An overview of unsaturated soil behaviour. Geotech Spec Publ, 1–1
Fritz SJ, Marine IW (1983) Experimental support for a predictive osmotic model of clay membranes. Geochim Cosmochim Acta 47(8):1515–1522
Hamid TB, Miller GA (2009) Shear strength of unsaturated soil interfaces. Can Geotech J 46 (5):595–606
Hen-Jones R, Hughes P, Glendinning S, Gunn D, Chambers J, Wilkinson P, Uhlemann S (2014). Determination of moisture content and soil suction in engineered fills using electrical resistivity: CRC Press/Balkema
Herman R (2001) An introduction to electrical resistivity in geophysics. Am J Phys 69(9):943–952
Indraratna B, Fatahi B, Khabbaz H (2006) Numerical analysis of matric suction effects of tree roots
Jiao-Jun Z, Hong-Zhang K, Gonda Y (2007) Application of Wenner configuration to estimate soil water content in pine plantations on sandy land. Pedosphere 17(6):801–812
Konrad J-M, Lebeau M (2015) Capillary-based effective stress formulation for predicting shear strength of unsaturated soils. Can Geotech J 52(12):2067–2076
Krahn J, Fredlund D (1972) On total, matric and osmotic suction. The emergence of unsaturated soil mechanics, 35
Kumar B, Smitha J, Uday K (2015) Effect of salinity on geotechnical properties of expansive soils. Int J Innov Res Sci Eng Technol (IJIRSET) 4:6008–6015
Lamborn, MJ (1986) A micromechanical approach to modeling partly saturated soils. Texas A&M University
Lee I-M, Sung S-G, Cho G-C (2005) Effect of stress state on the unsaturated shear strength of a weathered granite. Can Geotech J 42:624–631
Leong E-C, Abuel-Naga H (2017) Contribution of osmotic suction to shear strength of unsaturated high plasticity silty soil. Geomech Energy Environ 15:65–73
Lu Z (1992) The relationship of shear strength to swelling pressure for unsaturated soils. Chin J Geotech Eng 14:1–8

Merten U (1966) Desalination by reverse osmosis: The MIT Press
Nawagamuwa UP, Sarangan S, Janagan B, Neerajapriya S (2014). Study on the effect of plant roots for stability of slopes. In: Landslide science for a safer geoenvironment, Springer, pp 153–158
Ng CWW, Leung AK, Woon K (2013) Effects of soil density on grass-induced suction distributions in compacted soil subjected to rainfall. Can Geotech J 51(3):311–321
Ni J, Leung A, Ng C, Shao W (2018) Modelling hydro-mechanical reinforcements of plants to slope stability. Comput Geotech 95:99–109
Oloo S, Fredlund D (1996) A method for determination of φ b for statically compacted soils. Can Geotech J 33(2):272–280
Operstein V, Frydman S (2000) The influence of vegetation on soil strength. Proc Inst Civ Eng-Ground Improv 4(2):81–89
Pathirage U, Indraratna B, Pallewattha M, Heitor A (2017) A theoretical model for total suction effects by tree roots. Environ Geotech, 1–8
Perez N, Garnica P, Landaverde N, Hamza M, Shahien M, El-Mossallamy Y (2009) Measurement of soil suction using soil's resistivity. In: Proceedings of the 17th international conference on soil mechanics and geotechnical engineering: the academia and practice of geotechnical engineering, Alexandria, Egypt, 5–9 October 2009
Rao SM, Thyagaraj T (2007) Swell–compression behaviour of compacted clays under chemical gradients. Can Geotech J 44(5):520–532
Sreedeep S, Singh D (2006) Methodology for determination of osmotic suction of soils. Geotech Geol Eng 24(5):1469–1479
Sreedeep S, Singh DN (2011) Critical review of the methodologies employed for soil suction measurement. Int J Geomech 11(2):99–104
Sudduth KA, Kitchen N, Bollero G, Bullock D, Wiebold W (2003) Comparison of electromagnetic induction and direct sensing of soil electrical conductivity. Agron J 95(3):472–482
Terzaghi KV (1936) The shearing resistance of saturated soils and the angle between the planes of shear. In: Proceedings of the 1st international conference on soil mechanics and foundation engineering
Vanapalli S, Fredlund D, Pufahl D, Clifton A (1996a) Model for the prediction of shear strength with respect to soil suction. Can Geotech J 33(3):379–392
Vanapalli SK, Fredlund DG, Pufahl DE (1996b) The relationship between the soil-water characteristic curve and the unsaturated shear strength of a compacted glacial till. Geotech Test J 19:259–268
Waldron L (1977) The shear resistance of root-permeated homogeneous and stratified soil. Soil Sci Soc Am J 41(5):843–849
Waldron L, Dakessian S (1981) Soil reinforcement by roots: calculation of increased soil shear resistance from root properties. Soil Sci 132(6):427–435
Wang JP, Hu N, François B, Lambert P (2017) Estimating water retention curves and strength properties of unsaturated sandy soils from basic soil gradation parameters. Water Resour Res
Wu TH, McKinnell WP III, Swanston DN (1979) Strength of tree roots and landslides on prince of Wales Island. Alaska. Canadian Geotech J 16(1):19–33
Xu YF, Sun DA (2002) A fractal model for soil pores and its application to determination of water permeability. Physica A 316(1):56–64
Yan M, Miao L, Cui Y (2012) Electrical resistivity features of compacted expansive soils. Mar Georesour Geotechnol 30(2):167–179
Zhou A, Huang R, Sheng D (2016) Capillary water retention curve and shear strength of unsaturated soils. Can Geotech J 53(6):974–987

Influence of Swelling on Flexible Pavements: A Numerical Study

S. N. Thara, Anirban Mandal and Siva Ram Karumanchi

Abstract Expansive subgrades have long been recognised as problematic as they undergo considerable amount of volume changes due to moisture content fluctuations causing considerable distress to the pavement section above it thus making it important to estimate the changes in stresses and displacements in pavement layers. In the present research, swelling and shrinkage effects of expansive subgrade on flexible pavements are studied. Experimental program to find the basic properties of the soils were conducted first. Soil–water characteristic curves of the samples were developed and found to follow the traditional behaviour; soil suction increases as moisture content decreases. Database of soil properties was developed and was used as an input to estimate the stresses and displacements on pavement layers caused by swelling of subgrade using FEM-based software. For 0.8, 2 and 2.9 m water table depths, stresses and displacements were analysed. It was seen that in the swelling stage, water table at 2.9 m showed maximum upward deflection and in the loading stage for 0.8 m GWT, maximum compression was seen followed by 2, 2.9 m. It was inferred that with high ground water table, adequate base clearance should be maintained to minimise the moisture damage and to achieve quality performance of the pavement.

Keywords Matric suction · Swelling · Expansive soils · Stresses · Displacements · SWCC · Ground water table

S. N. Thara (✉) · A. Mandal · S. R. Karumanchi
Department of Civil Engineering, National Institute of Technology Nagpur, Nagpur 440010, Maharashtra, India
e-mail: snthara07@gmail.com

S. R. Karumanchi
e-mail: ram.karumanchi110@gmail.com

R. Sundaram et al. (eds.), *Geotechnics for Transportation Infrastructure*, Lecture Notes in Civil Engineering 29,
https://doi.org/10.1007/978-981-13-6713-7_54

1 Introduction

Subgrade soil is an integral part of the road pavement structure as it provides the support to the pavement from beneath and for this subgrade should possess sufficient stability under adverse climate and loading conditions. The formation of corrugations, waves, rutting and shoving, phenomenon of pumping, blowing and consequent cracking are generally attributed due to the poor subgrade conditions thus making it necessary to study about it before pavement construction. The main problem because of which the subgrade gets affected is due to the influence of moisture. Excess moisture presence in pavement structures usually results in accelerated pavement distresses, particularly when combined with heavy axle load.

Nelson (1992) explained the fact that expansive soils are a worldwide problem as they undergo considerable amounts of volume changes due to moisture content fluctuations. Hence, it is important to appropriately estimate the total volume change potentials of these soils, from both swell- and shrink-related movements, thus enabling us to better characterise the nature of the subsoils, and explore appropriate treatment or modification methods to reduce volume changes of soils. Turki (2015) studied the loss in serviceability of pavements due to swelling. PSI and PCI values are affected due to shrinkage and swelling in pavements. Also, effect of swell can be related to CBR and resilient modulus and empirical relations can be drawn. According to Yang (2005), his study of 'variation of resilient modulus with soil suction for compacted subgrade soils' revealed that among the three factors influencing the variations in the resilient modulus of cohesive subgrades, the moisture content played important role and that deviator stress had a less significant effect.

Hence, the major focus of the current work will be on assessment of stresses and displacements in flexible pavement due to volume change in expansive subgrade caused due to variation in moisture contents in flexible pavements. The rise of the underground water table can result in saturation and weakens the road basement in low-lying areas. The variation in depth of ground water table from 2010 to 2016 for VRCE region from where sample was taken was considered and modelled for three depth variations and stress and displacement in interface of pavement layers were measured using FEM-based ABAQUS Software.

1.1 Objectives of the Study

- To study the potential for swelling and the amount of volume change due to the effect of moisture in the subgrade material.
- To find the maximum pressure required to bring the swelled specimen back to its initial dimension.
- To study the suction characteristics of the subgrade sample.

- To determine soil–water characteristic curves of the samples by studying the suction potential of these soil over a wide range of moisture contents.
- Analysis of stress and displacements in flexible pavement layers due to swelling of subgrade using finite element-based ABAQUS software.
- Analysis of stress and displacements in pavement for different ground water table depth using finite element method.
- To analyse how the variation in ground water table depth effects the moisture content in pavement and consequently swelling of the pavement layers.

2 Literature Review

Moisture movement is generally of two types: saturated flow or partially saturated flow. Theory of moisture movements differ quietly in both of these. Moisture in the saturated region does not vary much and thus contributes less towards swelling phenomenon. In case of pavement structure, the subgrade above water table is in partially saturated stage and subgrade below is in saturated condition. During the variation of water table depth, the portion of soil in the saturated and unsaturated stage also varies thus causing variation in water content and leading to volume change in expansive soils.

2.1 Soil Suction

Suction can be simply stated as 'thirst of soil'. It is the ability to attract and retain water. Suction variable is of great interest in the unsaturated soil mechanics. According to Fredlund (2012), matric suction is the equivalent suction derived from the measurement of the partial pressure of the water vapour in equilibrium with the soil water relative to the partial pressure of the water vapour in equilibrium with a solution identical in composition with the soil water. Nishimura (2000) using modified triaxial apparatus studied that shear strength increases with increase in matric suction. At matric suction exceeding air entry value, shear strength increases. Farouk (2004) studied that shear strength of the sand also show an increase with increasing matric suction though not for entire range of applied matric suction. Zhang (2004)studied how to maintain matric suction under different soil conditions. He concluded that suction cannot be relied upon to provide long-term stability to the slope. However, the infiltration of rainfall in an initially unsaturated soil slope depends not only on the rainfall intensity and duration, but also on the saturated coefficient of permeability, the permeability function and the water storage capacity of the soil.

2.2 Soil–Water Characteristic Curve (SWCC)

An SWCC is J- or S-shaped curve showing the relationship between the soil moisture content and the matric suction. According to Fredlund (2012), the SWCC of the soil depends on the water distribution in pores as well as the soil texture and gradation. The soil–water characteristic curve (SWCC) is one of the most important functions used in assessment of unsaturated soil properties. The study of SWCC conducted by Tinjum (1997) for compacted clays concluded that the shape of the SWCC for desorption of compacted clays depends on plasticity and compaction conditions. Higher air entry suctions are obtained for more plastic soils and when compacting wet of optimum water content or with higher compactive effort. The SWCC is also steeper for compaction wet of optimum and slightly shallower for higher plasticity index. Shape of the SWCC is independent of dry unit weight.

Fredlund (2012) predicted the permeability function for unsaturated soils using the soil–water characteristic curve. It says that predicted curve for the coefficient of permeability is sensitive to the soil–water characteristic curve. Therefore, an accurate description of the soil–water characteristic behaviour is essential to the prediction of the coefficient of permeability.

2.3 Effect of Variation of Ground Water Table

A study conducted by the Murray–Darling Basin Ministerial Council (1999) stated that the lifespan of a road exposed to water logging can be reduced by four times; similarly, in IPWEA (2001), it was pointed out that the pavement serviceability would be significantly reduced if the groundwater level rose to within two metres of the ground surface. The study conducted by Ping (2012) could find that when an adequate groundwater base clearance is not provided, difficulties in constructing the pavement sublayers are often encountered. A full-scale test-pit program and a field experimental program were conducted to evaluate the constructability of pavement compaction in Florida and the experimental results indicated that to ensure constructability, a minimum of three-foot (0.91 m) groundwater base clearance would be suggested for the pavement design and construction. Erlingsson (2013) conducted a study on the influence of groundwater level on the structural behaviour of a pavement structure using FWD. It was concluded that ground water table level had a significant effect on the overall bearing capacity of the pavement and stiffness of pavement unbound layers.

3 Methodology

Sample was collected from VNIT Nagpur campus near Bajaj Nagar girls hostel. The sample was subjected to testing program which included the following tests: grain size distribution by sieve analysis and hydrometer, specific gravity, standard proctor test and Atterbeg limits: liquid limit, shrinkage limit, plastic limit, unconfined compression test, free swell index test. All these tests were carried out according to the procedure followed by Indian Standards 2720. Results of the test are presented in Table 1.

Swelling potential and swelling pressure of the representative sample were found out using conventional oedometer. Three Specimens were prepared and tested at OMC, dry of optimum (1.48 g/cc and 19% Wc) and wet of optimum (28% Wc and 1.48 g/cc).

3.1 Determination of Matric Suction

Test was performed in accordance with ASTM D5298-10. This test method covers laboratory filter paper as passive sensors to evaluate the soil matric suction.

Principle used: The filter paper comes to equilibrium with the soil either through vapour (total suction measurement) or liquid (matric suction measurement) flow. At equilibrium, the suction value of the filter paper and the soil will be equal.

3.1.1 Calibration of Filter Paper

Calibration of filter paper was carried out by controlling the humidity through different salt solutions. In the present study, calibration of Whattman 42 filter paper with NaCl solution of different molalities at 25 °C is done and the same batch is used for measuring soil suction. NaCl solutions were prepared from 0 (i.e. distilled water) to 2.5 molality (i.e. the number of moles of NaCl in mass in 1000 ml of distilled water).

Table 1 Material properties taken from IRC 37:2013

	y	E, kN/m2	υ	K, m/s	e	C	F
Surface	2.1	2,760,000	0.15				
Subbase	2.3	138,000	0.4	0.0018			
Comp-subgrade	1.54	69,000	0.3	10E-8	0.58	40	20
Subgrade	1.4	30,000	0.3	10E-6	0.58	40	20

y—Dry density(kN/m^3) E—Modulus of elasticity, υ—Poisson's ratio,
e—Void ratio, C—Cohesion, K—Coefficient of permeability, F—Friction angle(°)

A 250 ml glass jar was filled with approximately 150 ml of a solution of known molality of NaCl. Two filter papers were put on the plastic support one on top of the other. The glass jar lid was sealed tightly with plastic tapes to ensure air tightness. The filter paper is kept in controlled humidity chamber where it will be maintained at constant temperature with known relative humidity of salt solutions for two weeks and after that water content of filter paper was measured. Once the water content of the filter papers was found, corresponding osmotic suction values were taken from the literature of Bulut (2001). Using these water content and suction values, graph was plotted with suction in log KPa as ordinate and water content in '%' as abscissa. Equation of the calibration curve was found out and this calibration equation is used to find the suction value of soil samples at various moisture contents.

3.2 Numerical Modelling

ABAQUS version 6.14 is used for analysis. The input parameters for the analysis are taken from the above-mentioned experimental procedures.

3.2.1 Pavement Model and Material Characterisation

Pavement model considered in the study is made up of asphaltic surface layer of 0.15 m. Surface layer includes binder course and surface course. Base course and subbase course had been combined in the analysis since both are composed of granular material. 0.3 m thickness is taken for the subbase course. A 0.3 m thick compacted subgrade of highly compressible clay soil is considered beneath the subbase course followed by 5 m thick natural subgrade. Slope of 1.5:1 is considered at the edges.

Along with the material properties, suction at various saturation, swelling potential at various saturations are also inputted in order to describe and analyse the effect of the moisture movement in the soil layers.

3.2.2 Element Type

For top surface, B22 element—a three-noded quadratic beam in a plane was used and for other layers, an eight-noded plane strain quadrilateral (CPE8R), biquadratic displacement, bilinear pore pressure, reduced integration were used. Mesh element size adopted was 0.1 using convergence criteria to get maximum accuracy.

3.2.3 Boundary Condition and Loading

The boundary conditions are applied in such a way that all the movements are restrained at base (i.e. both *x- and y*-displacements are zero) and only *x*-displacements are restrained for left and right boundaries. Boundary conditions were given in terms of negative pore water pressure and swelling too. At the top surface of the ground water table, pore pressure is 0 and at the top of the compacted subgrade maximum negative pore pressure of −500 is given. These conditions are given in negative pore pressure step and kept inactive in swelling, road construction and loading stage. Swelling condition is also given as a boundary value by giving 0 negative pore pressure at the top of the compacted subgrade. Two loads are considered; load due to gravity, i.e. self-weight of the layers of pavement and the static wheel load of standard dimension corresponding to 850 kN/m^2.

3.2.4 Analysis of Stress and Displacements

Analysis had been done for interfaces, between subbase, between compacted subgrade and below natural subgrade. Separate analysis has been done for natural ground and full structure. Analysis had been done to find how stresses and displacements in each layer of pavement are getting affected due to variation of ground water table level. Stress and displacements values for with swell and without swell have been studied and compared. From the water resource information system (WRIS) website, ground water table depth in metres below ground level (mgbl) for VRCE region was obtained and it was observed that in the period 2010–2016, the water table has risen to 0.8 mbgl as a maximum value and 2.9 m mbgl as a minimum value. So, in this study, three variations; 0.8, 2 and 2.9 m are considered for analysis.

4 Results and Discussions

Properties of the representative sample include index and engineering properties of the sample. Sample is found to be highly expansive and classified as CH as per Unified Soil Classification System.

Swelling potential at OMC is 4.14%. Result indicates that sample used has low potential for expansion due to swell. In the case of specimen compacted at dry of optimum, (1.48 g/cc and 19%) the swell potential has increased to 4.54%. This increase is due to the fact that the samples compacted at dry of optimum has high water deficiency and random orientation of particles thus imbibing more water.

Pressure at which the change in volume is 0% is taken as the swelling pressure. Swelling pressure at OMC is 0.8 kg/cm^2. Result indicates that this 0.8 kg/cm^2 pressure is required to bring the swelled specimen back to its original height. Figure below shows the log p versus change in volume curve drawn for the

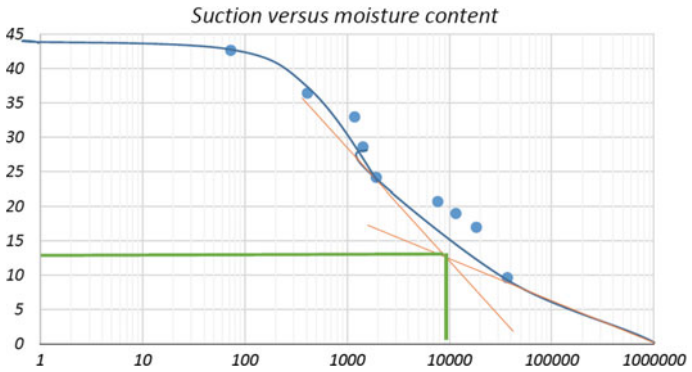

Fig. 1 Soil–water characteristic curve

specimen compacted at OMC. Using the below calibration curve, matric suction values of soil samples compacted at various water contents is obtained and plotted as shown below in the Fig. 1.

This is called soil–water characteristic curve (SWCC). It can be seen that the relation is not perfectly linear and suction increases with decrease in water content.

From Fig. 1, it can be inferred that, all the soil pores are filled with water until the soil specimen reaches the air entry value. After that desaturation starts, the amount of water in the soil decreases significantly with the increase in soil suction. Desaturation stage reaches the residual stage of unsaturation along the desorption portion of a SWCC. Residual water content and residual suction of the given soil sample is 12.5% and 9800 kPa, after 9800 kPa, flow occurs through pores in vapour phase and the volume change in unsaturated soil becomes negligible. Also, air entry occurs at the desaturation stage, in the graph it occurs at 98 kPa.

4.1 Variation of Ground Water Table

4.1.1 Effect in Subgrade

Displacement versus depth below subgrade for-500 pore water pressure compacted at OMC for natural subgrade is plotted for 0.8, 2 and 29 m ground water depth and is as shown in Figs. 2 and 3.

From Fig. 3, it can be seen that in the swelling stage, maximum upward displacement occurs when the GWT is 2.9 m below surface and the deflection value is less for GWT at 0.8 m. This could be because of the fact that suction is more when GWT is very deep and thus the sections above water table has an increase in moisture content and thus producing more swelling effect than when the water table was at 0.8 and 2 m. It was seen that there is no notable variation in stress due to variation of ground water table in swelling stage. Changes in water level above

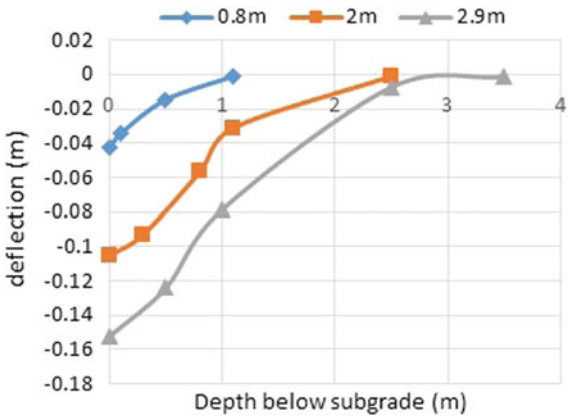

Fig. 2 Negative pore pressure stage

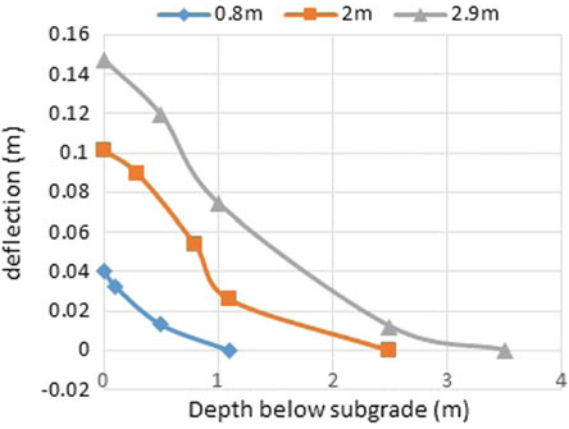

Fig. 3 Swelling stage

ground do not cause changes in effective stresses in the ground below. A rise above ground surface increases both the total stress and the pore water pressure by the same amount, and consequently effective stress is not altered.

From Fig. 3, it can be seen that in the swelling stage, maximum upward displacement occurs when the GWT is 2.9 m below surface and the deflection value is less for GWT at 0.8 m. This could be because of the fact that suction is more when GWT is very deep and thus the sections above water table has an increase in moisture content and thus producing more swelling effect than when the water table was at 0.8 and 2 m.

At each ground water level, the analysis had been done for dry of optimum, OMC and wet of optimum condition. The results obtained are presented below in Figs. 4, 5 and 6.

Maximum positive deflection is seen for the OMC condition followed by wet of optimum and least for the dry of optimum. It was observed that there is no much variation in the stresses for three conditions of dry density. Variation of stress with depth is following the same pattern in all the three cases.

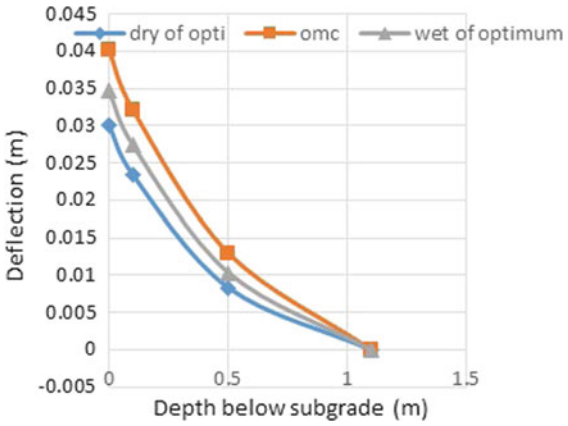

Fig. 4 Swelling effects for 0.8 m GWT

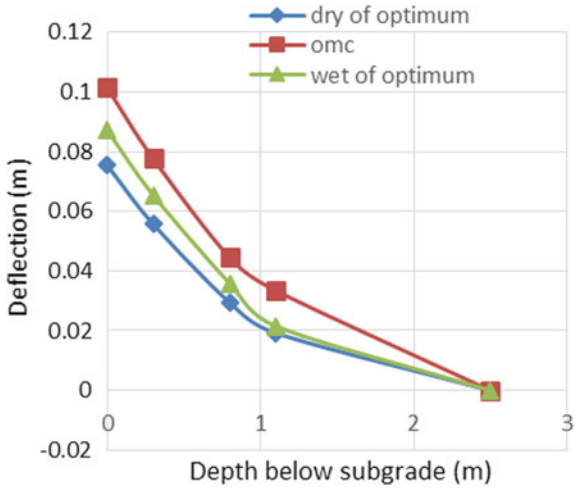

Fig. 5 Swelling effects for 2 m GWT

4.1.2 Effect in Pavement Layers

From Fig. 7, it can be inferred that swelling is maximum in the subbase-compacted subgrade interface and decreases in the subsequent layers below. In the top surface, the heave noticed is less because of the granular subbase below which act as a draining layer. Among the three water table depth, swelling is maximum for 2.9 m GWT because of high matric suction which saturates the soil better when compared to 0.8 and 2 m.

In the load application stage, maximum downward displacement is seen in GWT at 0.8 m and least for GWT at 2.9 m. The point (subbase-compacted subgrade interface) where the upward displacement was maximum has the minimum

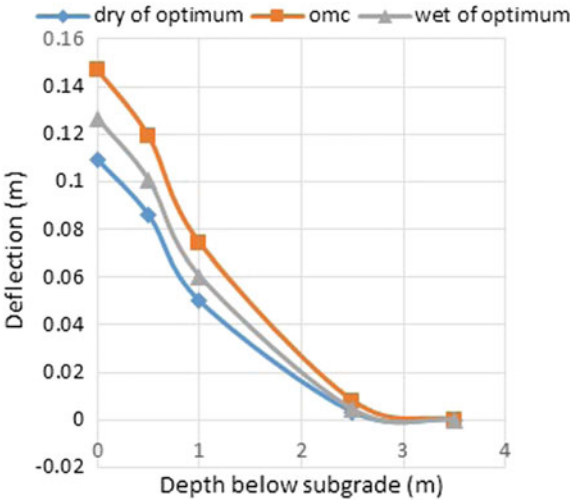

Fig. 6 Swelling effects for 2.9 m GWT

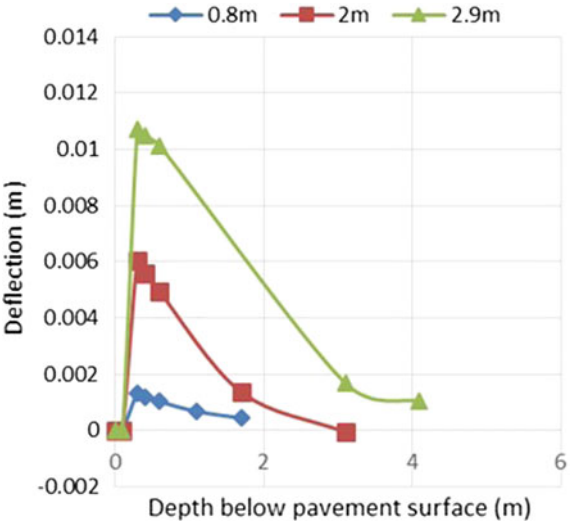

Fig. 7 Deflection in swelling stage

downward displacement. Introduction of water to the material can usually result in reduction in the inter-particle frictional strength and therefore larger resilient and accumulated permanent deformations under traffic loading (Fig. 8).

Variation in stresses was not seen in this case too. When wheel load acts on the surface, the wheel load stresses is maximum on top and gradually decreases as it reaches the subgrade. Due to wheel load, soil or road materials are compressed and the pore air or pore water does not flow out, rather pore air volume is reduced and

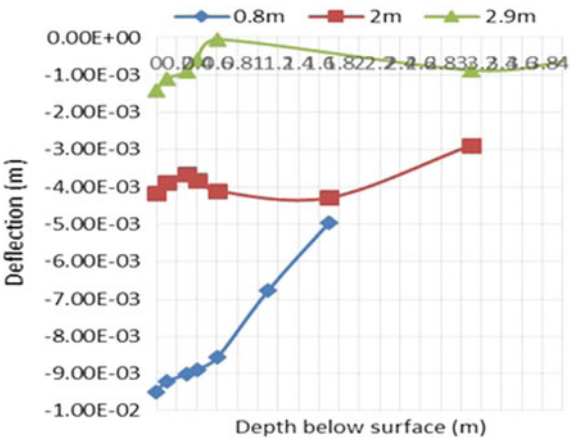

Fig. 8 Deflection in load application

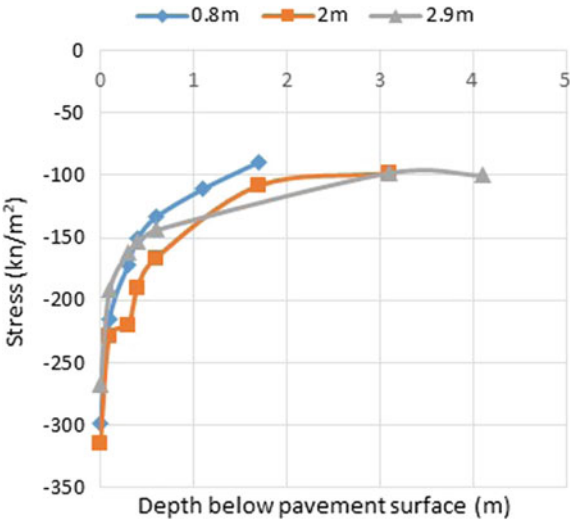

Fig. 9 Stresses in load application stage

pore water pressure has increased. Increased moisture content decreases the effective stress. Since wheel load is very high compared to water pressure, the variation is not seen much here (refer Fig. 9). It was observed that compaction condition has very less effect on the deflection of the pavement layers. Same trend is observed for 2 and 2.9 m ground water table depth. Even the stresses in all the three conditions were exactly coinciding.

5 Conclusions

Swelling is a complex phenomenon associated with the presence of water in the subgrade and pavement layers. Application of ABAQUS proved to be a good tool for analysing the effect of swell in pavement performance. The result obtained using ABAQUS gives the expected behaviour thus validating with the previous literature studies.

The representative soil was found to be highly compressible clayey soil with PI value of 30 and has moderate degree of expansiveness. Swelling pressure and swell potential were found to be maximum for the soils compacted at dry of optimum and least for the one at wet of optimum. Matric suction–moisture content relationship of the focused soil follows the traditional behaviour; soil suction increases as moisture content decreases. Stresses and displacements in the swelled pavement with 90% saturation were seen to be nearly 70% more than unswelled pavement. On comparing the three compaction condition in natural subgrade, maximum swelling is seen for soils compacted at OMC, followed by wet of optimum and dry of optimum. In case of pavement layers, compaction condition has negligible effect. Curves for all the three conditions were nearly coinciding. Variation of pore pressure with depth showed that as height above water table increases, pore pressure decreases. Comparing the ground water table depth, it was seen that in the swelling stage, water table at 2.9 m showed maximum upward deflection and in the loading stage at 0.8 m GWT, maximum compression was seen followed by 2, 2.9 m. With high ground water table, adequate base clearance should be maintained to minimise the moisture damage and to achieve quality performance of the pavement.

References

Bulut RLR (2001) Soil suction measurements by Filter paper. In: Proceedings of geo-institute shallow foundation and soil properties committee sessions at the ASCE 2001 Civil Eng Conference, pp. 243–261

Erlingsson S (2013) The influence of groundwater level on the structural behaviour of a pavement structure using FWD. Sweden: pavement technology department

Farouk A, Lamboj L, Kos J (2004) Influence of matric suction on the shear strength behaviour of unsaturated sand. Acta Polytechnica 7:44

Fredlund DG (2012) Unsaturated soil mechanics in engineering practice. John Wiley & Sons Inc, New York

James M, Tinjum CH (1997) Soil water characteristic curves for compacted clays. J Geotech Geoenviron Eng, 123

Nelson DJJD (1992) Expansive soils-problems and practice in foundation and pavement engineering. Int J Numer Anal Meth Geomech 17:745–756

Nishimura T (2000) Relationship between shear strength and matric suction in an unsaturated silty soil. In: Asian conference on unsaturated soils, Singapore

Ping WBS (2012) The effect of ground water base clearance on constructability of Florida pavements. In: Ninth Asia Pacific transportation development conference, pp 591–598

Shu-Rong Yang W-H (2005) Variation of Resilient modulus with soil suction for compacted subgrade. Transp Res Rec J Transp Res Board, 99–106

Turki (2015) Loss in serviceability of pavements due to expansive subgrades. Environ Eng Geosci, 277–294

Zhang LL, D. (2004) Numerical study of soil conditions under which matric suction can be maintained. Canadian Geotech J, 558–561

Performance of ANN Model in Predicting the Bearing Capacity of Shallow Foundations

Mozaher Ul Kabir, Syed Shadman Sakib, Istiakur Rahman and Hossain Md. Shahin

Abstract This study deals with the performance of the artificial neural networks (ANNs) for predicting the ultimate bearing capacity of shallow foundations on cohesionless soil. From cone penetration tests (CPTs), footing dimensions and other soil parameters were considered as the input variables which have the most significant impact on bearing capacity predictions. The application of artificial neural network was carried out through the following steps; at first, we consider a total of 100 sets of data among which we used 89 sets of data for training to determine a relation between input variables and the bearing capacity of the soil. For testing and validation, other 11 data sets were used. The accuracy of the model was evaluated by comparing the results with conventional bearing capacity equations. Also, high coefficients of correlation, low root-mean-squared errors (RMSEs), and low mean absolute errors (MAE) were the indications to confirm that the ANN-based model predicts with much perfection.

Keywords ANNs · Bearing capacity · RMSE · MAE

1 Introduction

Every foundation setup requires satisfying two imperative criteria: ultimate bearing capacity of confinement and limiting settlement of foundations. Between these two criteria, a complete bearing capacity of confinement is managed by shearing nature

M. U. Kabir (✉) · S. S. Sakib · I. Rahman · H. Md. Shahin
Department of Civil Engineering, Islamic University of Technology, Gazipur, Bangladesh
e-mail: mozaher@iut-dhaka.edu

S. S. Sakib
e-mail: shadmansakib@iut-dhaka.edu

I. Rahman
e-mail: istiakur92@iut-dhaka.edu

H. Md.Shahin
e-mail: shahin@iut-dhaka.edu

R. Sundaram et al. (eds.), *Geotechnics for Transportation Infrastructure*,
Lecture Notes in Civil Engineering 29,
https://doi.org/10.1007/978-981-13-6713-7_55

of the soil and can be evaluated by the theories of Terzaghi (1943), Meyerhof (1963), Vesic (1973), and others. The explanation behind the part of possible theories is the most remote point which adjusted the procedure. In this manner lab results obtained by different researchers were positive. In any case, the trials are generally done on tinier measured models, which are significantly cutback models stood out from real field footings. In this way, various authorities (e.g., (De Beer 1965; Meyerhof 1950)) have prompted that one should be amazingly vigilant while extrapolating disclosures of examinations driven on little footings that have a width of several inches, to the broad evaluated footings. The clarification behind this is credited to the extension in shearing strain along the slip line with the development in width of the foundation and the extent of mean grain size of the soil and the adjust width (Steenfelt 1977). For extensive scale establishments on dense sand, shearing strains demonstrate significant variety along the slip line. The normal assembled point of shearing resistance along the slip line is littler than the greatest estimation of the angle of shearing resistance (φ_{max}) which was obtained via plane strain shear tests.

Henceforth, an ultimate technique is required that gives better gauges of bearing capacity. In the most recent two decades, a few analysts have created successful demonstrating instruments.

One of them is artificial neural networks (ANNs) methodology. In the current past, ANNs have been connected to numerous geotechnical designing issues, including the determination of the bearing capacity of footings, settlement forecasts, liquefaction, and stability of slopes (Shahin et al. 2001). The real preferred standpoint of ANNs is that they reanalyze the old and new information, use the old outline helps or conditions, and additionally propose new conditions (Pande and Shin 2004). This paper shows the relevance of ANN method in building up a compelling nonlinear model for anticipating a definitive bearing capacity of shallow foundations on cohesionless soils. The database, which comprises of load test values of extensive scale footings and smaller estimated demonstrate footings, is utilized to create and check the ANN model. This paper additionally goes for a broad assessment of the ANN model with regression-based models for ultimate bearing capacity using in a total of 100 sets of field data and evaluates their benefits and restrictions. The execution of these models is then occurred to demonstrate the most regularly utilized bearing capacity.

2 Development of Ultimate Bearing Capacity Model

The data used for experimenting and the development of the ANN model were collected from the literatures, which are load test data on real-sized foundations regarding the footing and soil. Among 100 collected field data, 50 are from load tests on large-scale footings and 50 are from small shallow footings. Again from 47 large-scale footing data, 24 were reported by Muhs and Weiß (1971), 11 data by Weiß (1970), 5 of them by Muhs et al. (1969), 2 of them by Muhs and Weiß (1973), 5 of them by Briaud and Gibbens (1999).

One of the challenging initiatives in the model improvement for the prediction of bearing capacity of a shallow foundation is to differentiate parameters those have impact on the bearing capacity, for which a number of the conventional bearing capacity estimation techniques (Terzaghi 1943; Meyerhof 1963; Vesic 1973) are used. In spite of the way that the bearing capacity gotten through these techniques varying abruptly, the fundamental type of condition is the same for every one of the techniques, which is as per the following for establishments in cohesionless soil:

$$q_u = \gamma D N_q S_q d_q + 0.5\gamma B N_\gamma S_\gamma d_\gamma$$

where B—width of footings, D—profundity of footings, c—unit weight of sand (underneath or more the establishment level), N_q, N_γ—bearing capacity factors, S_q, S_γ—shape factors, and d_q, d_γ—depth factors.

Among the parameters identified with the footings, the principle factors influencing the bearing capacity are its width (minimum horizontal measurement, B), footing length (L), depth of the foundation (D), and shape (square, rectangular and round). The depth of the foundation has the most significant impact on the bearing capacity among all the physical properties of the foundation (Meyerhof GG. The bearing capacity of sand. PhD thesis, University of London 1950).

The fundamental parameters with respect to the soil (sand) are its angle of shearing friction and the unit weights of soil layers adjusted to the water table (if available). There are some different factors, for example, compressibility and thickness of the soil layer underneath the foundation which are responsible for a smaller grade. Among the considerable number of properties of soil, the angle of shearing resistance has most noteworthy impact on the bearing capacity, which decreases with the relative thickness of the soil. The unit weight of the soil is depended on the position of water table and proportional to the bearing capacity.

In light of above discussion, the five input factors used for the model encroachment are width of footing (B), depth of footing (D), unit weight of sand (γ), angle of shearing resistance (φ), and ratio of length and width (L/B). By using these five factors, the ultimate bearing capacity (q_u) is the final result.

3 ANN Model Development

In this study, feed-forward multilayer perceptron (MLP) is utilized; the portrayal of which can be found in numerous publications (Zurada 2003; Fausett 1994). The data set was arbitrarily separated into two subsets: training and testing. 87% (or 87 cases) of the information was set for training the model, while the remaining 13% (or 13 cases) was utilized for testing or validation the execution of the proposed ANN-based model. A trial-and-error strategy was used to determine the optimum number of hidden layers in the model which was concluded by using ten hidden

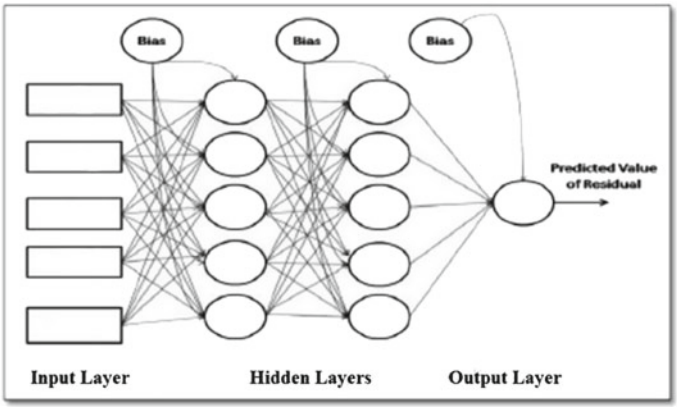

Fig. 1 Architecture of ANN model

layer. Because of five input and one output variable, five nodes were used in the input layer and one in the output layer which is a typical way to deal with problem of overfitting in early stopping (Fig. 1).

This approach includes monitoring the generalization error and stopping training when the minimum validation error is observed. Be that as it may, some care is required when to stop, since the approval mistake surface may have local minima or long flat regions preceding a steep drop-off. To minimize these constraints, Mackay (1991) proposed the use of Bayesian back-propagation neural networks which minimize a combination of squared errors and weights and after that decides the correct combination, in order to create a network which sums up well. This procedure is called Bayesian regularization. In the Bayesian structure, the weights and the biases of the network are assumed to be random variables with indicated appropriation of distribution. The regularization parameters are identified with the unknown variances related to the distribution. These parameters are then evaluated using statistical techniques. In the present investigation, the Levenberg–Marquardt algorithm is utilized under the Bayesian network.

3.1 Multiple-Regression Analysis

To develop a relationship between the single dependent variable, $q_{u,}$ and one or more independent variables c_i, $h_{i,}$ and B, multiple-regression is used, and the prediction of q_u is accomplished by the following equation:

$$q_u = w_1c_1 + w_2c_2 + w_3c_3 + w_4c_4 + w_5h_1 + w_6h_2 + w_7h_3 + w_8B + b$$

Source	SS	df	MS
Model	19083512.9	5	3816702.58
Residual	7649780	83	92166.0241
Total	26733292.9	88	303787.42

Number of obs = 89
F(5, 83) = 41.41
Prob > F = 0.0000
R-squared = 0.7138
Adj R-squared = 0.6966
Root MSE = 303.59

Bearingcapc	Coef.	Std. Err.	t	P>|t|	[95% Conf.	Interval]
Depth	1976.073	221.3357	8.93	0.000	1535.845	2416.301
B	42.20546	94.93179	0.44	0.658	-146.61	231.021
LB	-27.58137	18.34084	-1.50	0.136	-64.06055	8.897819
angleoffriction	86.464	10.51894	8.22	0.000	65.54226	107.3857
unitwt	-21.22461	14.02371	-1.51	0.134	-49.1172	6.667982
_cons	-2833.27	466.6629	-6.07	0.000	-3761.444	-1905.097

Fig. 2 Output result from StataSE 12 for MLR model

where w_i are the regression weights and are processed in a way that limits the aggregate of the squared deviations. Here, b is the y-axis intercept. Multiple-regression is associated with multiple correlation coefficient, which is the variance of the dependent variable explained collectively by all of the independent variables. A multiple-regression model was obtained using Stata SE 12 (Fig. 2).

The following formulas, using the MLR technique, were found to offer the best fitting:

$$q_u = 1976.073D + 86.464h - 2833.27$$

where q_u (kPa) is the bearing capacity, s (m), and h(deg) is the angle of friction.

4 Performance Evaluations and Results

The performance of the model is being evaluated by assessing the degree to which the values obtained from the simulations match actual output. The assessment was performed in this study with various goodness-of-fit or correlation statistics. The values of the performance indices or measures for the three models are summarized in Table 2. The correlation statistic (R), which evaluates the linear correlation between the actual and predicted ultimate bearing capacity, is good for all the models, for calibration as well as validation data. The model efficiency that evaluates the performance of the model in predicting the ultimate bearing capacity

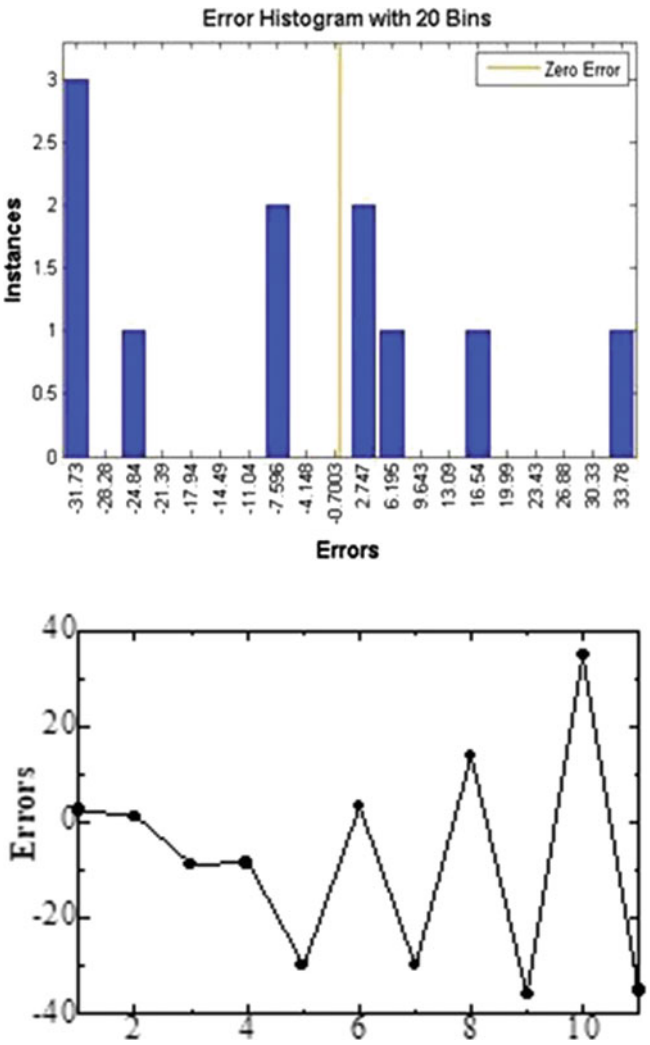

Fig. 3 Distribution of prediction error across different error thresholds

values away from the mean is found to be more than 98% for calibration, and validation data for the ANNs model was close to where it was first referenced (Figs. 3 and 4) (Table 1).

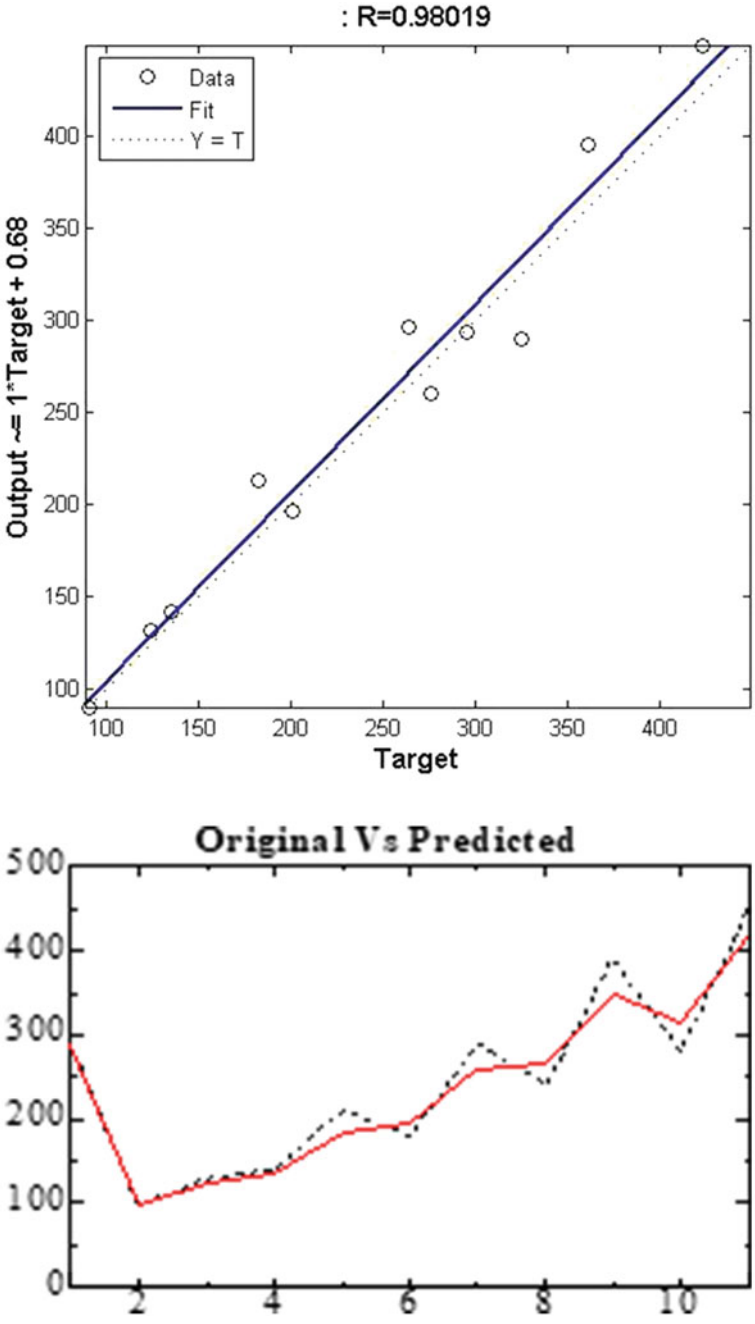

Fig. 4 Measured versus predicted ultimate bearing capacity values

Table 1 Performance evaluation and comparison

Performance index	ANN	MLR	Meyerhof
R^2	0.98019	0.7138	0.648

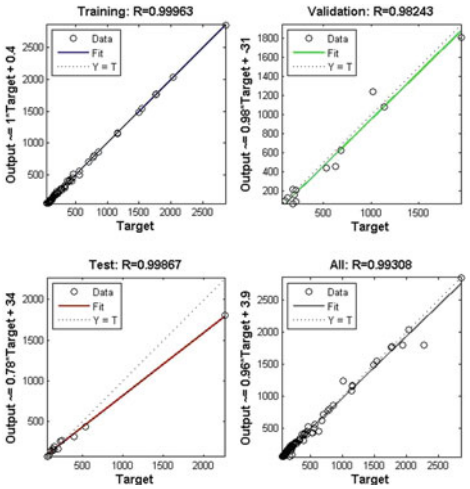

In this study, artificial neural networks (ANNs) and equation developed by the multilinear regression model (MLR) were used to predict the bearing capacity of circular shallow footings on cohesionless soil. The artificial neural network model serves as a simple and reliable tool for the bearing capacity of shallow foundations in sandy soil. The results produced high coefficients of correlation for the trained and testing data sets, and the values are 0.99,308 and 0.98019, respectively, which have much more higher perfection then MLR model. Nevertheless, this study demonstrates that having some known parameters, we can easily be able to have an idea about the ultimate bearing capacity through the ANN model.

References

Briaud JL, Gibbens R (1999) Behavior of five large spread footings in sand. ASCE J Geotech Geoenviron Eng 125(9):787–796

De Beer EE (1965) The scale effect on the phenomenon of progressive rupture in cohesionless soil. In: Proceedings of the 6th international conference on soil mechanics and foundations engineer, s vol. 2 p 13–7

Fausett LV (1994) Fundamentals of neural networks: architectures, algorithms and applications. Prentice-Hall, Englewood cliff s (NJ)

Mackay DJC (1991) Bayesian methods for adaptive models. PhD thesis, California Institute of Technology

Meyerhof GG (1950) The bearing capacity of sand. PhD thesis, University of London

Meyerhof GG (1963) Some recent research on the bearing capacity of foundations. Can Geotech J 1(1):16–26

Muhs H, Weiß K (1971) Untersuchung von Grenztragfa¨higkeitundSetzungsverhalten flachgegru¨ndeter Einzelfundamente im ungleichfo¨rmigennichtbindigen Boden. Deutsche Forschungsgesellschaft fu¨ r Bodenmechanik (DEGEBO), Berlin. HEFT 69

Muhs H, Weiß K (1973) Inclined load tests on shallow strip footings. In: Proceedings of the 8th international conference on soil mechanism and foundation engineering. vol II, p 173–9

Muhs H, Elmiger R, Weiß K (1969) Sohlreibung und Grenztragfa¨higkeit unter lotrecht und schra¨g belasteten Einzelfundamenten. Forschungsgesellschaft fu¨r (DEGEBO), Berlin.HEFT 62

Pande GN, Shin H-S (2004) Artificial intelligence v. equations. In: Proc ICE Civil Eng 157(1):43–6

Shahin MA, Maier HR, Jaksa MB (2001) Artificial neural network applications in geotechnical eng. Austr Geomech 36(1):49–62

Steenfelt JS (1977) Scale effect on bearing capacity factor Nc. Proc. of the 9th international conference on soil mechanism and foundation engineering. vol 1, p 749– 52

Terzaghi K (1943) Theoretical soil mechanics. John Wiley & Sons, New York

Vesic AS (1973) Analysis of ultimate loads of shallow foundations. JSMFD, ASCE 99(1):45–73

Weiß K (1970) Der Einfluß der Fundamentform auf die Grenztragfa¨higkeit flachgegru¨ndeter Fundamente. Deutsche Forschungsgesellschaft fu¨ r Bodenmechanik (DEGEBO), Berlin. HEFT 65

Zurada JM (2003) Introduction to artificial neural systems. Jaico Publishing House